Ph. D. Thesis / Tesis Doctoral

WASTE BIOMASS VALORIZATION FOR THE PRODUCTION OF CELLULOSIC FRACTIONS OF INTEREST IN FOOD PACKAGING APPLICATIONS

VALORIZACIÓN DE RESIDUOS DE BIOMASA PARA LA OBTENCIÓNDE FRACCIONES CELULÓSICAS DE INTERÉS EN APLICACIONES DE ENVASADO ALIMENTARIO

Isaac Benito González / October 2021

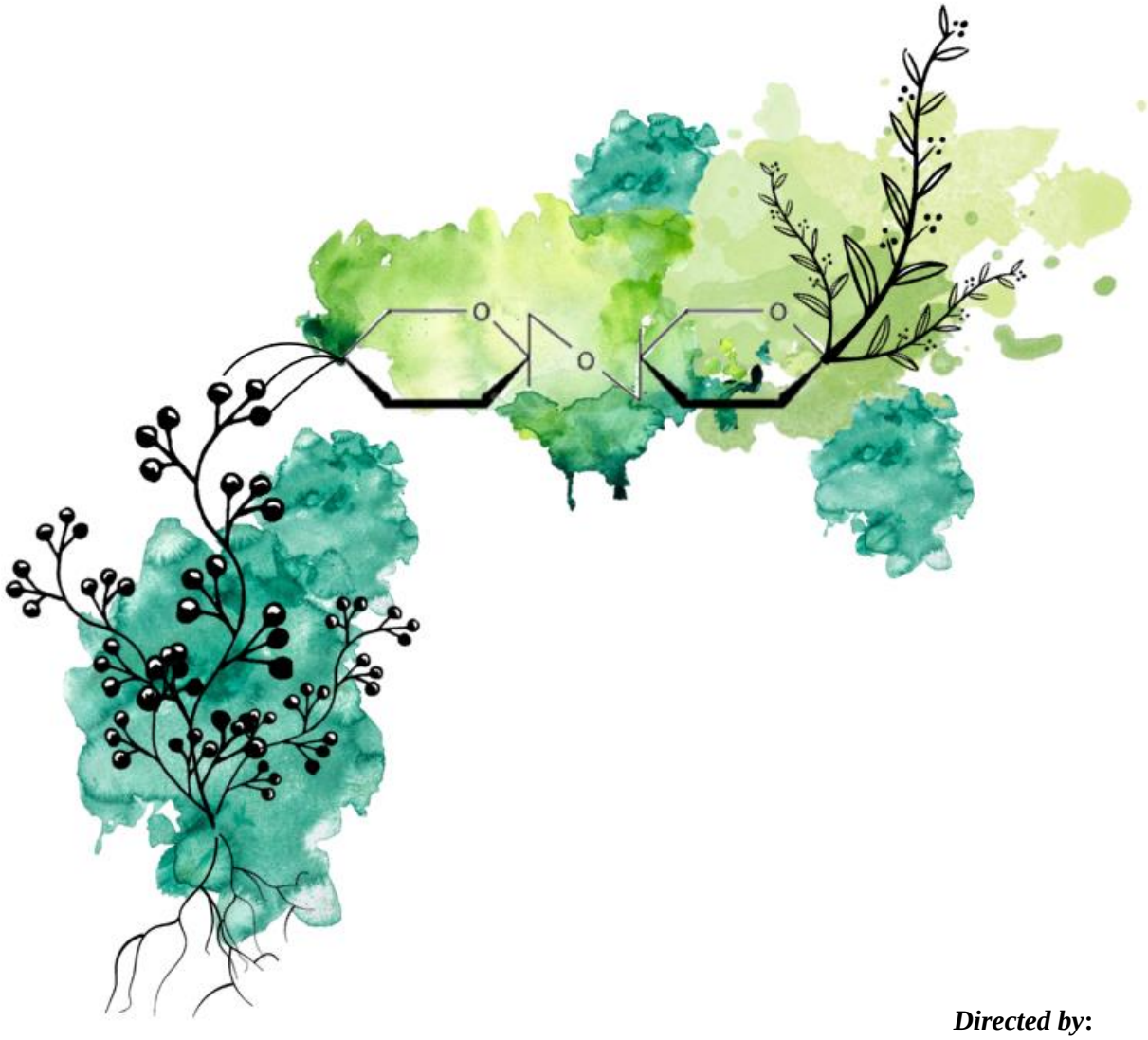

***Directed by*:**

Marta Martínez Sanz

Amparo López Rubio

UNIVERSITAT POLITÈCNICA DE VALÈNCIA

iata
Instituto de Agroquímica y Tecnología de Alimentos

BIOCARB
-4-FOOD

SUSFOOD2

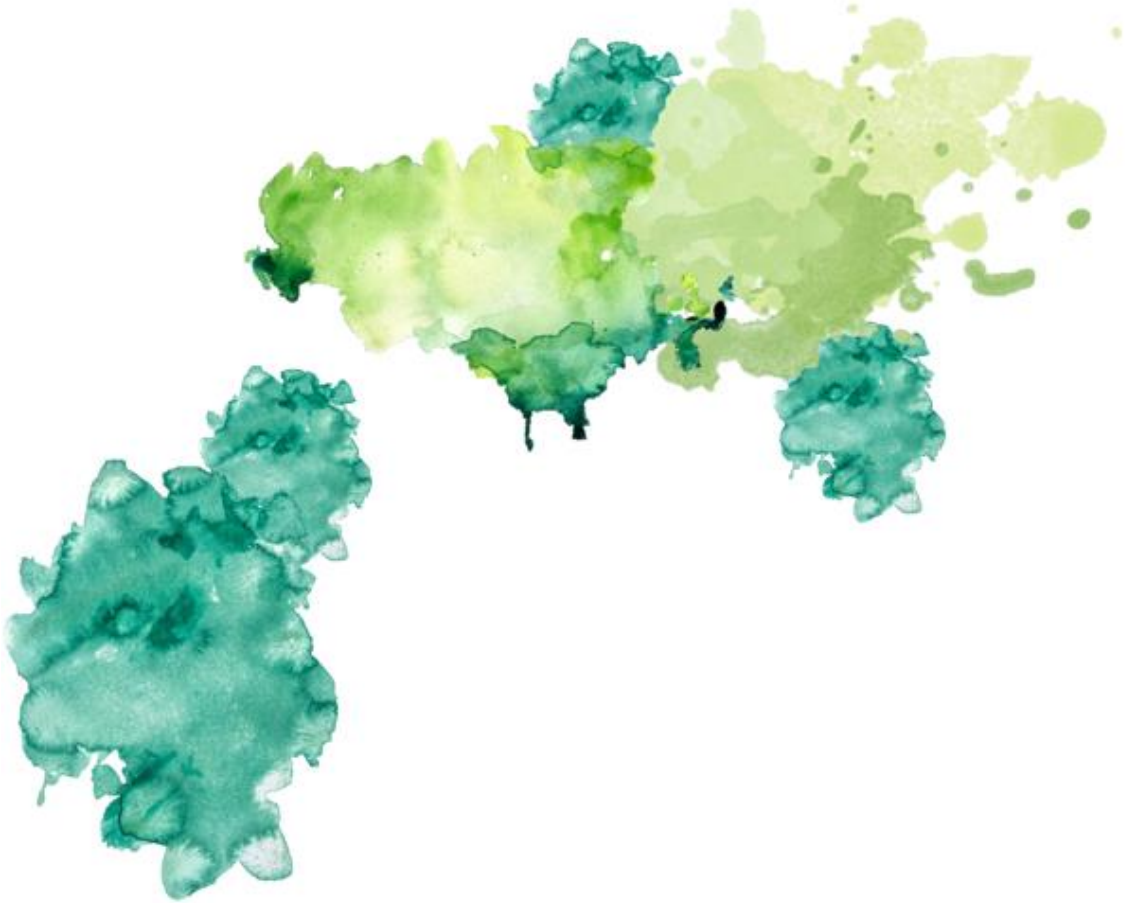

iata
Instituto de Agroquímica
y Tecnología de Alimentos

CSIC
Consejo Superior de Investigaciones Científicas

A mis padres,

porque soy lo que soy

gracias a ellos

"Donde las palabras fallan,

la música habla."

Hans Christian Andersen

Agradecimientos

Me gustaría empezar agradeciendo, como es natural, a mis directoras de tesis Amparo y Marta. Siempre recordaré que, pese a la situación que nos ha tocado vivir, apostasteis por mí para este proyecto en un momento donde muy poca gente lo hacía. Esta aventura científica no existiría si, hace ya algo más de 4 años, no le hubierais dado la oportunidad al chico del TFM de la Posidonia. Por ello os estaré siempre muy agradecido. Además, Amparo, has sido una pieza fundamental para crear el buen ambiente necesario en el labo con tu ya famosa sonrisa, y quién sabe si este final no es sino el comienzo de otro proyecto, a ver qué tal se nos da de empresarios…

A ti Marta, qué decirte. Directora de tesis, compañera de ratos, series, música (ese bajo), hasta un poco madre (compartida con el resto de pupilas) y la gran culpable de que este trabajo haya salido adelante. Un ejemplo para mí y, aunque cada vez las correcciones lleguen con más rojo, una maestra incansable de la que estoy seguro de haber aprendido (casi) todo lo que se. Espero que nunca pierdas esa pasión por lo que haces y sigas transmitiéndola como lo has hecho conmigo.

Por supuesto, a todas mis compañeras de faena que también están embarcadas en aventuras similares (Dani, a ti también guapo). Habéis sido un apoyo fundamental durante este tiempo y en todo momento habéis estado dispuestas a echar una mano con todo lo que fuera necesario sin pedir nada a cambio. Tengo la suerte de, más que compañeras, consideraros mis amigas y siempre me tendréis ahí para lo que necesitéis. Os deseo lo mejor a todas y se que vais a ser unas doctoras estupendas, pues ya lo sois como personas.

No me olvido de las estudiantes que, gracias a sus proyectos, han contribuido además en gran medida a sacar partes del mío adelante. Ojalá en un futuro próximo se os reconozca vuestro trabajo y esfuerzo como se merece, más allá de aparecer en las publicaciones científicas. Sois una pieza clave en este sistema y así se os debería tratar. En otro escalón están Laura, Toni, Agustín, Jaana y MJ cuya ayuda, consejos y oportunidades agradezco también, tanto en las estancias de investigación como en el día a día del labo. Ejemplos de profesionales, aunque ojalá no hiciera falta tanto sudor y trabajo para llegar donde estáis. En cualquier caso, toda una suerte haber podido contar con vosotras. Por último, gracias a todo el personal de IATA que de un modo u otro ha contribuido a que mi periplo aquí haya sido tan agradable, en especial a Ana y Fernando que me han mostrado el lado más humano del instituto.

Por suerte, hay vida más allá del IATA. Una parte importantísima de haberme sentido tan arropado durante estos años se la debo a las amistades que he tenido la fortuna de crear: amigos del MUCIA, Claudia, Anabel, Bou, y muchos más con los que he compartido conciertos, fiestas, deporte, viajes y muchísimos momentos que siempre llevaré en el recuerdo. Y qué decir de Augusto, me abriste las puertas de tu piso siendo un par de “conocidos” y míranos ahora, hasta has conseguido que recupere mi pasión por el violín. En definitiva, ha sido una etapa de mi vida muy bonita y sois los culpables de que me haya enamorado de Valencia, sus rincones e incluso parte de su cultura, habiéndome sentido “com a casa”. Seguro que esta etapa no se cerrará aquí.

Y hablando de casa, la que siempre será la mía. Mi Riojita, donde mi familia siempre ha estado esperándome con los brazos abiertos. Esos abrazos eternos con mi madre al llegar y al despedirnos, donde sin palabras (o con ellas) me decía: "te queremos, sigue así, y cuidado en la carretera". Aunque la distancia no me ha permitido veros todo lo que me habría gustado, cada visita ha sido un soplo de aire fresco para mí. Os quiero mucho. En estos viajes (por suerte compartidos), tenía la difícil tarea de compaginar tiempo con mi familia y con mis amigos. Y aunque "apenas pasaba por casa", siempre había un hueco para visitar a mis tías y primos, así como para el resto de "obligaciones". Y es que tanto mis cucharas como mis bezaringos son mucha tela… y aprecio y disfruto cada minuto bien fresh que paso con ellos. Sin ellos no sabría ni que la posidonia es un alga. Igualmente, aunque la distancia no me permita veros todo lo que me gustaría, sois mis amigos de toda la vida y siempre me tendréis para lo que necesitéis. Por mucho tiempo que pase siempre conseguís que, al minuto de encontrarnos, me sienta como si no hubiéramos estado separados.

Para acabar, me gustaría dedicar unas líneas a mi mayor apoyo durante este periodo. Mi compañera de vida, amiga, confidente, koalo… nadie mejor que tú entiende cómo me siento y las alegrías y contratiempos que me he llevado en esta experiencia, pues los hemos compartido todos. Me siento muy afortunado de tenerte a mi lado y aunque la distancia no haya podido con nosotros, espero que poco a poco podamos reducirla. Estoy seguro de que también vas a ser una doctora maravillosa, y que conseguirás todo lo que te propongas. Te quiero Loli.

En definitiva, GRACIAS de corazón a tantas y tantas personas que, de una manera u otra, me han ayudado a recorrer este camino. Todas sois parte de este trabajo y también de la persona en la que me he convertido. Por muchos años más.

Abstract

The following Ph. D thesis is based on the waste biomass valorization for obtaining cellulose and other relevant compounds aimed to develop food packaging structures.

The massive use of fossil-fuel derived conventional plastics generates an excessive number of residues due to their low degradation rates and inefficient current recycling strategies, which makes them accumulate in both terrestrial and marine ecosystems. In this context, the use of biopolymers (concretely cellulose) plays a key role in offering an abundant, renewable and biodegradable alternative that allows to reduce and even replace the use of these conventional materials.

For this aim, *Posidonia oceanica* (an endemic aquatic plant from the Mediterranean Sea) dead leaves have been selected as the main cellulose source due to their abundance and problematic associated: dead leaves are accumulated in beaches and seashores causing bad odours and must be removed by local authorities without any further use. Thus, the valorization of this residue provides a solution in line with current circular and "zero-waste" economy policies which enables more sustainable exploitation of natural resources. As a result, waste biomass valorization for obtaining cellulose with regards to other more conventional sources is doubly beneficial.

In the first part of the thesis, the potential of *P. oceanica* leaves as a cellulosic source was shown (≈30% cellulose content) after successfully applying a conventional purification protocol. This cellulose, as well as two intermediate cellulosic fractions (with the presence of additional components such as hemicelluloses and/or lignin), were used for developing films both by vacuum filtration and melt mixing and hot pressing in starch composites. In parallel, both cellulose and cellulosic fractions were submitted to acid treatment in order to obtain nanocrystals, being these protocols upscaled at a pilot-plant level for the development of thermoformed trays by injection moulding. Interestingly, the presence of the aforementioned additional components had a positive effect on their performance. Lastly, water-based extracts were successfully obtained from *P. oceanica* dead leaves by ultrasounds and hot-water extraction methodologies, providing a complete valorization of the residue with the aim of minimizing the use of organic solvents.

In a second part, simplified cellulose extraction protocols were applied to other waste sources such as vine shoots, rice straw and rice husks. Both cellulosic fractions and nanocrystals were successfully purified regardless of the source, being the initial composition (holocellulose, lignin, ashes, lipids and proteins) and the monosaccharide profile the key factors which defined the final properties of the materials (evaluated in film form).

In the last part of the thesis, these cellulosic nanocrystals were used for developing aerogels by freeze-drying. In order to overcome their inherent poor mechanical performance and low water resistance, a novel and patented dipping method using polylactic acid (PLA) was designed. These biopolymeric aerogels were broadly characterized by means of several techniques such as Raman and Confocal microscopies. Finally, bioactive aerogels were developed by incorporating some of the most promising *P. oceanica* bioactive extracts (previously obtained and characterized). These aerogels could successfully improve the shelf-life of red meat when used as absorbent pads, significantly diminishing both lipids and oxymyoglobin oxidation.

Then, the following Ph. D. thesis shows the valorization of several waste biomasses by applying simplified protocols for developing food packaging structures. The presence of additional compounds in the resulting materials has been shown not only to reduce associated costs by increasing the total mass yield but also to present improved performance in comparison to more conventional materials, being in line with current circular economy policies. As a result, a more sustainable and viable alternative for the massively used conventional plastics is proposed.

Resumen

La presente tesis doctoral está basada en el aprovechamiento de residuos de biomasa para la obtención de celulosa y otros compuestos de interés con el objetivo de desarrollar estructuras aplicables en el envasado alimentario.

El uso masivo de los plásticos convencionales derivados del petróleo genera una cantidad ingente de residuos debido a su mínima degradabilidad y baja eficacia de las estrategias de reciclaje actuales, provocando así su acumulación en los ecosistemas terrestres y marinos. En este contexto, el uso de biopolímeros (y más en concreto, la celulosa) juega un papel crucial puesto que ofrecen una alternativa abundante, renovable y biodegradable que permite reducir y reemplazar el uso de estos materiales tradicionales.

Para ello, se ha seleccionado como fuente de celulosa los residuos de hojas de *Posidonia oceanica* (planta acuática endémica del mar Mediterráneo) debido a su abundancia y problemática asociada: sus hojas se acumulan en las playas generando mal olor, teniendo las autoridades locales que retirarlas sin un uso específico posterior. Por tanto, además de proponer una solución a un problema de gestión, el aprovechamiento de dicho residuo está en línea con las políticas actuales de economía circular y "residuo cero" que permiten una utilización más sostenible de los recursos naturales. De esta forma, la valorización de residuos de biomasa respecto a otras fuentes tradicionales de celulosa como la madera u otros cultivos específicos es beneficiosa por ambas partes.

En la primera parte de la tesis, se demuestra el potencial de las hojas de *P. oceanica* como fuente de celulosa (≈30% contenido) al purificarse ésta con éxito mediante la aplicación de un protocolo convencional. Dicha celulosa, así como otras dos fracciones celulósicas intermedias (con presencia de componentes adicionales como hemicelulosas y/o lignina) se utilizaron para formar films mediante filtrado a vacío y como aditivos de refuerzo en matrices de almidón comercial mediante mezclado en fundido y prensa. En paralelo, tanto la celulosa como las fracciones celulósicas de interés fueron sometidas a un tratamiento ácido para la obtención de nanocristales. La presencia de compuestos adicionales recalcitrantes tuvo un efecto positivo en las propiedades de estos, cuya obtención fue escalada a nivel planta piloto para la producción de bandejas mediante termoformado de mezclas con almidón. Por último, se obtuvieron extractos bioactivos mediante técnicas en base acuosa (ultrasonidos y calor) para una valorización integral del residuo de hojas de *P. oceanica* con el objetivo de reducir el uso de disolventes orgánicos.

En una segunda parte de la tesis, se aplicaron los protocolos simplificados de extracción de celulosa a otros residuos de biomasa como los sarmientos de vid, la paja de arroz y la cáscara de arroz. Cabe destacar que se purificaron con éxito fracciones y nanocristales celulósicos en todas las biomasas evaluadas, viéndose que las propiedades finales de los materiales (en formato film)

se veían principalmente afectadas por la composición inicial de las biomasas (holocelulosa, lignina, cenizas, lípidos y proteínas) y el perfil de monosacáridos de los residuos de partida. Esto demostró que es posible simplificar los procesos de extracción de celulosa para disminuir costes y aumentar la sostenibilidad de la metodología pese a la posible heterogeneidad de la(s) fuente(s) de partida.

En la última parte de la tesis, estos nanocristales celulósicos se utilizaron como material de partida para la formación de aerogeles mediante un proceso de liofilización. Para paliar la baja resistencia mecánica y al agua de estos materiales, se diseñó un método patentado de inmersión en una disolución de ácido poliláctico (PLA) que recubría el aerogel celulósico mejorando tanto su resistencia mecánica como su resistencia al agua. Estos aerogeles puramente biopoliméricos fueron ampliamente caracterizados mediante distintas metodologías, destacando la microscopía Raman y confocal. Finalmente, se obtuvieron aerogeles bioactivos mediante la incorporación de los extractos de *P. oceanica* más prometedores (previamente obtenidos y caracterizados). Estos aerogeles fueron capaces de aumentar la vida útil de los alimentos empleándose como almohadillas absorbentes bajo carne roja, disminuyendo tanto la oxidación de lípidos como de la oximioglobina.

Por tanto, la presente tesis muestra la valorización de residuos de biomasa mediante protocolos simplificados para el desarrollo de estructuras de envasado alimentario. La presencia de componentes adicionales en los materiales finales ha sido capaz no sólo de reducir los costos asociados y aumentar los rendimientos de extracción, sino también de obtener materiales con propiedades mejoradas en la mayoría de los casos, estando de esta forma en línea con las políticas de economía circular establecidas actualmente. Así, se propone una alternativa sostenible y viable respecto a los plásticos convencionales masivamente utilizados en el mercado actual.

Resum

La present tesi doctoral està basada amb l'aprofitament de residus de biomassa per a l'obtenció de cel·lulosa i altres compostos d'interès amb l'objectiu de desenvolupar estructures aplicables a l'envasat alimentari.

L'ús massiu de plàstics convencionals derivats del petroli genera una quantitat ingent de residus degut a la seua mínima degradabilitat i baixa eficàcia de les estratègies de reciclatge actuals, provocant d'aquesta manera la seua accumlació als eocisistemes terrestres i marins. Dins d'aquest context, l'ús de biopolímers (i més concretament, la cel·lulosa) juga un paper crucial ja que oferix una alternativa abundant, renovable i biodegradable que permet reduir i reemplaçar l'ús d'aquests materials tradicionals.

Per a aquest fet, s'ha seleccionat com a font de cel·lulosa els residus de fulles de *Posidonia oceanica* (planta aquàtica endèmica del mar Mediterrani) degut a la seua abundància i a la problemàtica associada: les seues fulles s'acumulen a les platges generant mal olor i tenint que retirar-les les autoritats locals sense u ús posterior. Per tant, a més de proposar un solució a un problema de gestió, l'aprofitament del residu en qüestió està en la línia de les polítiques actuals d'economia circular i "residu zero" que permeten una utilització més sostenible dels recursos naturals. D'aquesta manera, la valorització de residus de biomassa respecte d'altres fonts tradicionals de cel·lulosa com la fusta i altres cultius específics és beneficiosa per ambdues parts.

En la primera part de la tesi, es demostra el potencial de les fulles de *P. Oceanica* com a font de cel·lulosa (30% del contingut) al purificar-se amb èxit mitjançant l'aplicació d'un protocol convencional. Aquesta cel·lulosa, així com altres dues fraccions cel·lulòsiques intermitges (amb presència de components aditionals com hemicel·luloses o lignina) es van emprar per a formar pel·lícules mijançant mescla en fos i premsa. Paral·lelament, tant la cel·lulosa com les fraccions cel·lulòsiques d'interès van ser sotmeses a un tractament àcid per a l'obtenció de nanocristals. La presència de compostos adicionals recalcitrants va tenir un efecte positiu en les seues propietats. La obtenció resultant va ser escalada a nivell de planta pilot per a la producció de safates a través termoformat de mescla amb almidó. Per últim, es van obtenir extractes bioactius amb tècniques amb base d'aigua (ultrasons i calor) per a la valorització integral del residu de fulles de *P. Oceanica* amb l'objectiu de reduir la utilització de dissolvents orgànics.

En la segona part de la tesi es van aplicar els protocols simplificats d'extracció de cel·lulosa a altres residus de biomasa com els sarments de vinya, la palla d'arròs i la closca de l'arròs. Hem de destacar que es van purificar amb èxit les fraccions i els nanocristals cel·lulòsics en totes les biomasses avaluades. Es va poder veure, conseqüentment que les propietats finals dels materials (amb un format de pel·lícula) es veien principalment afectades per la composició inicial de les biomasses (holocel·lulosa, lignina, cendra, lípids i proteïnes) i el perfil de monosacàrids dels

residus del punt de partida. Es va demostrar que és possible simplificar els procesos d'extracció de cel·lulosa per a disminuir costos i augmentar la sostenibilitat de la metodologia malgrat la possible heterogeneïtat de le(s) font(s) del punt de partida.

En la última part de la tesi, aquestos nanocristals cel·lulòsics es va emprar com a material de partida per a la formació de aerogels mitjançant un procés de liofilització. Per a paliar la baixa resistència mecànica i l'aigua d'aquests materials, es va dissenyar un mètode patentat de immersió en una dissolució d'àcid polilàctic (PLA) que recobria l'aerogel cel·lulòsic millorant tant la seua resistència mecànica com la seua resistència a l'aigua. Aquestos aerogels purament biopolimèrics van ser ampliament caracteritzats a través distintes metodologies, destacant la microscopia Raman i confocal. Finalment, es van obtenir aerogels bioactius mitjançant la incorporació dels extractes de *P. Oceànica* més prometedors (prèviament obtinguts i caracteritzats). Estos aerogels van ser capaços d'augmentar la vida útil dels aliments emplean-se aquesto com coixinets absorbents sota carn roja, disminuint tant l'oxidació de lípids com l'oximioglobina.

Per tant, la present tesi mostra la valoració de residus de biomassa mitjançant protocols simplificats per al desenvolupament d'estructures d'envasat alimentari. La presència de components addicionals en els materials finals ha sigut capaç no només de reduir els costos associats i augmentar els rendiments d'extracció, sinó també d'obtenir materials com propietats millorades en la majoria dels casos, trobant-se d'aquesta forma en línia amb les polítiques d'economia circular establides actualment. Així, es proposa una alternativa sostenible i viable respecte als plásticos convencionals massivament emprades en el mercat actual.

Index

I. Introduction

1. Cellulose

Cellulose is the most abundant biopolymer on Earth, as it represents the major component of plant cell walls [1]. It has been estimated that over 100 billion metric tons of cellulose are synthesized in nature per year [2]. Thus, cellulose is considered as one of the most relevant renewable resources [3] and its exploitation has always generated interest, being traditionally extracted from vegetal resources such as wood, cotton, flax, etc. In particular, the interest in the exploitation of cellulose has enormously grown over the last few years, triggered by the recent regulations which have started restricting the use of conventional polymers (especially for single-use materials) to reduce the massive waste generated as a consequence of their overuse [4, 5]. In this context, the development of cellulose-based materials is regarded as one of the most promising strategies to replace conventional plastics worldwide, with estimated market size of over 8 billion dollars and a growth projection of over 20% in the following years [6].

1.1 Structure

Cellulose is a linear polysaccharide formed by D-glucose units linked together by β(1-4) glycosidic bonds [7]. In nature, cellulose is found forming a very complex hierarchical structure composed of several structural levels. At the simplest structural level, the linear D-glucose chains are assembled forming highly crystalline structures which are commonly known as cellulose nanocrystals (CNC). These crystalline structures are combined with amorphous domains to form the next structural level, known as cellulose microfibrils. The proportion of crystalline cellulose, as well as the morphology of the nanocrystals (cylindrical/parallelepiped shape and cross-section dimensions), depends on the biomass source. While crystalline domains are more recalcitrant due to their higher packing degree and stronger hydrogen bonding, amorphous regions are distributed in a more disordered manner and are more susceptible to degradation under harsh chemical treatments (cf. Figure 1). On the contrary, upon the application of mechanical treatments, amorphous domains are not completely removed resulting in what is commonly known as micro- or nanofibrillated cellulose (MFC or NFC, respectively). It should be noted that although it has been typically assumed that amorphous cellulose domains are interspaced with crystalline domains along the longitudinal axis of cellulose microfibrils, it is known that paracrystalline domains (i.e. regions containing more defective crystals) are also found in the outer regions from the microfibrils [8]. Although CNC and NFC present the same chemical structure, their different morphology (larger sizes are typically observed in NFC) and crystallinity has a strong impact on

the performance properties of these materials. Nevertheless, both nanostructures show outstanding performance for a wide range of applications, as will be further discussed in section 3.

The average diameter of these aforementioned cellulose microfibrils is usually around 10-50 nm, while they may reach several μm in length [9]. However, these cellulose microfibrils cannot be easily found isolated in nature, as they are closely interacting with other structural components. For example, being one of the most abundant components in plant cell walls, cellulose conforms the basis of a more complex organization of structural polysaccharides (hemicelluloses and pectins) and aromatic compounds (lignin), commonly known as lignocellulose. This complex organization, in addition to their interaction with other plant cell wall components such as proteins and lipids, are factors hindering cellulose isolation. Primary cell walls, found in growing tissues, are mainly composed of cellulose, hemicelluloses and pectic polysaccharides. Hemicelluloses are branched polymers of pentose, hexose and acetylated sugars (being xylose derivatives the most representative ones, while mannans, arabinans, galactans and their combinations are also present in many plant cell walls). Although the interaction mechanism of cellulose with hemicelluloses is still not completely understood, it is expected to be different depending on the structure of each particular hemicellulose. For instance, it has been suggested that whereas arabinoxylan interacts with the surface hydroxyl groups from cellulose, xyloglucan can establish interactions with the individual cellulose microfibrils hence leading to the formation of different cellulose–xyloglucan domains [10-12]. Pectic polysaccharides contribute to the wall flexibility and strength of primary cell walls, supporting cell wall expansion and plant growth [13]. Given their predominantly amorphous structure, hemicelluloses and pectins are easily digested when applying mild acid or alkali treatments [14]. After the complete expansion of primary cell walls, a subsequent formation of secondary cell walls may take place, especially in the case of woody tissues which have to withstand large compressive forces. Secondary walls are usually much thicker than primary walls and their composition is adapted to their different structural role. To achieve superior mechanical properties, secondary walls possess a higher content of cellulose microfibrils, which are embedded in a matrix of hemicelluloses and, in most cases, lignin. Lignin takes part as the primary defence in plant cell walls to impede its destruction from microbial attacks. It also helps to decrease their permeability by their structural combination of cross-linked phenolic monomers, whose active groups behave as a protective barrier too [14, 15]. Some of the complex interactions between lignin phenolic groups and cell wall polysaccharides (cellulose and hemicelluloses) are still being understudy as many factors are involved such as molecular weight, degree of esterification or porosity. However, hydrophobic interactions and hydrogen bonds have been shown to play the main role in these kind of interactions and usually define their final structure [16].

It should be highlighted that the intricate hierarchical organization of lignocellulosic biomass presents notable differences between plant species and/or their developmental stage. Some factors such as cellulose crystallinity and dimensions, the amount and chemical composition of other polysaccharides and the presence of lignin should be taken into account to optimize the cellulose extraction protocol for a specific biomass source [17]. Thus, cellulose isolation can be considered as a complex process due to the intricate structural organization of lignocellulosic biomass, which is (as it will be more deeply discussed in the following section) the main natural source of cellulose.

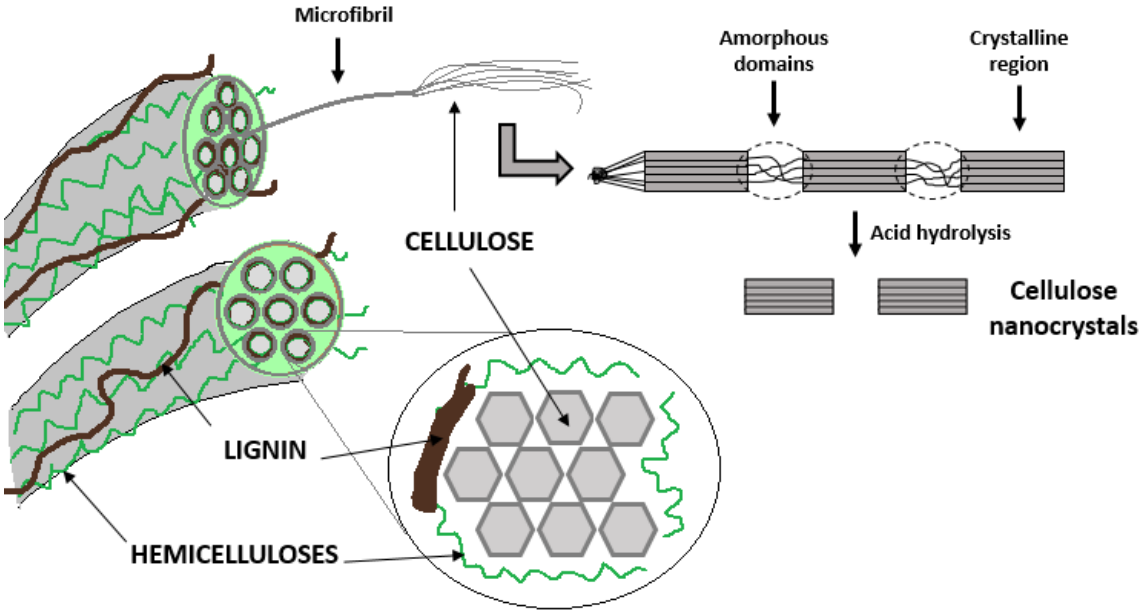

Figure 1. Hierarchical organization of cellulose in vegetal biomass. Figure adapted from *Lee et al* (2014) [14].

1.2 Main sources

As it has been just introduced, cellulose is one of the most abundant biopolymers on Earth and given its physical arrangement, it has a key structural role in many organisms. Thus, it can be extracted from a wide range of sources, such as land crops (e.g. wood [18], cotton [19], sisal [20]), agro-industrial waste (e.g. vine shoots [21], wheat straw [22] or rice husks [23]), marine biomass (e.g. macroalgae [24], aquatic plants [25] and some microalgae [26]) or even synthesized by some bacterial species [27]. Traditionally, cellulose has been mainly extracted from wood, given the high cellulose content in the secondary cell walls from higher plants (40-50% cellulose content) [18] and the extraordinary economic impact derived from the forest industry, which has been extensively exploited during centuries. Cotton has also attracted great attention for the extraction

of cellulose due to its exceptionally high content (>90%), which has been mainly exploited in the textile industry [19]. However, environmental drawbacks derived from their cultivation such as water consumption or the excessive use of pesticides are restricting their production and limiting their application for cellulose extraction nowadays [28]. Other biomass sources which have been extensively cultivated for the extraction of cellulose are sisal (49-61% cellulose) [20], agave (67% cellulose) [29] and bamboo (~40% cellulose) [30]. However, in line with recent zero-waste policies which are being boosted due to environmental reasons, several agro-industrial by-products, are being studied as alternative cellulosic sources. Beyond the most representative examples, banana fibers (~60% cellulose content) [31], rice husks (37%) [23], wheat straw (34-40%) [22], vine shoots (~40%) [21], coconut coir (33%) or sugar cane bagasse (30%) [32] have been successfully used for this purpose.

On the other hand, marine biomass is gaining attraction as a source of cellulose, according to the significant cellulose content in some macroalgae and aquatic plants. Furthermore, the minor amounts (or even absence) of lignin in this type of biomass may facilitate cellulose extraction. Moreover, the rapid growth of seaweeds in comparison with land plants allows reducing harvesting times, which in addition to the much larger and unexploited marine surface (more than 70% of Earth's surface), can reduce the associated costs. Interestingly, marine biomass is known to contain high amounts of diverse bioactive compounds (such as phenolic compounds), thus giving them an additional value in terms of biomass valorization, which may lead to the production of bioactive materials with interest in a wide range of applications [33]. Focusing on cellulose extraction, one of the most representative sources of marine biomass are macroalgae. Several studies have already reported on the extraction of cellulose from green, red and brown algae with yields ranging between 42 and 51% [24]. Marine plants (commonly known as seagrasses), such as *Cymodocea nodosa* (57% cellulose content) [34, 35], *Zostera marina* (57% cellulose) [36] or *Posidonia oceanica* (30% cellulose) [25], have also been recently investigated for the extraction of cellulose. Other marine organisms like tunicates (60% cellulose) have also been explored due to the high aspect ratio and crystallinity of their cellulosic fibres, which makes them optimum for the extraction of high-performance cellulose nanocrystals [37]. Furthermore, microalgae have been also tested for the extraction of cellulose from their cell walls, although their content can differ notoriously among species (20-50%), reaching up to 70-80% in some species such as *Chlorella vulgaris* [26, 38]; however, they are not generally considered as a suitable source since the extraction yields are typically quite low.

Bacterial cellulose (BC) represents one particular case in which cellulose, instead of being combined with other biopolymers, is found in its most pure form. Some bacterial strains such as *Komagataeibacter xylinus* (formerly known as *Acetobacter xylinus*) can transform the glucose (when incubated in a rich-saccharide media) into cellulose, which is produced as a highly hydrated

pellicle in the liquid/air interface. Although BC presents the same chemical structure as plant cellulose, the absence of other components such as lignin or hemicelluloses, as well as its high crystallinity (>86%) and thermal stability [27, 39], make BC an interesting material. However, the high costs associated with the production process are still precluding from the utilization of BC over other sources.

In conclusion, cellulose can be extracted from a wide variety of sources with significant differences in their composition (cellulose content ranging from ~25% up to ~90%) and crystallinity. Moreover, the sources and production strategies used to extract cellulose have been gradually modified according to current needs and knowledge: While conventional sources have been traditionally overexploited, marine biomasses are currently being explored due to their several aforementioned interesting properties. In addition, waste biomass has been shown to represent a feasible and more environmentally friendly cellulose-rich alternative, following current needs and zero-waste policies. As a result, marine organisms and, in particular, their derived waste biomass can be considered as the most innovative and cost-effective sources for obtaining cellulose while minimizing environmental damage. Consequently, this approach will comprise one of the main objectives of this Ph. D. thesis: An effective cellulose extraction by using marine waste biomass as the main source.

Specifically, *Posidonia oceanica (P. oceanica)* is an endemic marine plant from the Mediterranean Sea. During its lifecycle, *P. oceanica* dead leaves detach off their stems and are carried away by marine currents until they are settled in the seashores, being detrimental to the quality of the beaches and representing an additional cost for local authorities to manage their removal [40]. This marine residue is nowadays underutilized, remaining stored for long periods or being composted. Thus, it represents an ideal choice for valorization due to its abundance and interesting composition (30% cellulose content and a significant amount of phenolics and other bioactive compounds, such as chicoric, gentisic and ferulic acids) [25, 41, 42]. Thus, *P. oceanica* dead leaves will be directly collected from local shores and proposed in this Ph. D. thesis for a whole valorization (with the main focus on cellulose extraction) to develop novel food packaging structures following circular economy principles.

2. Methods for cellulose extraction

2.1 Conventional protocols

2.1.1 Cellulose purification

As previously commented, the recalcitrance of lignocellulosic biomass represents the major obstacle to cellulose purification. Due to the high packing degree and strong bonding of the structural components, specific treatments are required to remove structural plant cell wall components and isolate cellulose. In this context, the most conventional protocol for cellulose isolation from vegetal resources consists on three subsequent chemical treatments: (i) a Soxhlet extraction using organic solvent mixtures to remove wax, pigments and oils, (ii) a mild acid bleaching treatment to remove the lignin and (iii) a mild alkali extraction which aims to eliminate the hemicelluloses. The remaining gel-like solid fraction is expected to be pure cellulose [43-47], with a final yield determined by the biomass composition and extraction conditions. This methodology will be applied for the extraction of pure cellulose during the following chapters of the thesis.

Soxhlet extraction using a binary combination of organic solvents (such as toluene, ethanol or chloroform) has been reported to successfully remove lipid compounds (such as waxes) as well as pigments from a wide range of biomasses by direct solubilization due to their polar affinity [48]. Although extraction times might be increased without compromising the effectiveness, most of the lipids are usually extracted after around 3-5 hours. Soxhlet extraction is considered the most effective methodology for the extraction of lipidic compounds for the subsequent purification of cellulose or even to use the extracted biomass for biofuel applications [48].

The subsequent acid bleaching treatment consists on a process where mainly hydronium ions disrupt and attack the bonds between lignin, hemicelluloses and cellulose, solubilizing the non-cellulosic components. It has been extensively reported that a combination of diluted sodium chlorite (~1% w/v) with acetic acid (pH~3) can successfully remove most of the lignin without affecting the structure of cellulose and hemicelluloses. Moreover, no more than 70-80 ºC and 4-5 h are required, being the first hour the most effective one. Additionally, one of the benefits of this process is that hemicellulosic content remains almost unchanged (up to 10% extraction after 4 h) [49], which is beneficial if some cellulose-hemicellulose interactions would be analyzed, as it will be further discussed in the following section.

Finally, alkali treatments, usually applied at mild conditions (below 100 ºC), have been shown to successfully remove hemicelluloses. Mainly, a saponification occurs in the intermolecular ester bonds between hemicelluloses and lignin, and nucleophilic acids substitute these bonds when

alkaline salts are present (like NaOH or KOH) forming a carboxylic salt or alcohol [14, 50]. These processes will not only increase the inner cellulose surface area by the solubilization of hemicelluloses but also make the extracted cellulose more susceptible to further treatment for the isolation of the crystalline fraction, as will be later discussed. It should be considered that this process is typically implemented after diluted acid treatment (as is the case of the conventional protocol followed in this thesis), as hemicelluloses are more exposed to solubilization if lignin has been previously eliminated [14].

Although the most conventional and effective protocol for cellulose extraction has been already mentioned and discussed, other alternative methods which are not based on chemical processes must be also mentioned. The main examples of these alternative methodologies comprise physical treatments (mechanical methods like milling and/or grinding) and biological treatments (enzymatic digestions), as well as their possible combinations. Briefly, physical treatments are known to consume higher amounts of energy while are also considered to be less efficient than chemical treatments. Similarly, enzymatic reactions require longer times and present lower efficiency, thus increasing the associated costs [51-54]. As a result, chemical treatments are considered the most efficient ones for the purification of cellulose in terms of time, effectiveness and cost-efficiency.

2.1.2 Nanocellulose extraction

Once the cellulose microfibrils have already been isolated by the subsequent removal of the other structural components present in the selected biomass source, cellulose nanocrystals or "nanocellulose" can be obtained by removal of the amorphous regions of the cellulose microfibrils. This nanocellulose can easily outperform cellulosic microfibrils for certain applications, as it presents greater crystallinity and surface area. The applications of cellulose and nanocellulose will be discussed in more detail in section 3 of the introduction.

Several approaches can be used for the production of cellulose nanocrystals, but chemical treatments and, in particular, acid hydrolysis, are well-known to be the most effective way of isolating nanocellulose from native cellulose. This process can be affected by several factors, such as the acid concentration, reaction time and temperature [55]. As a result, these parameters must be adjusted according to the composition of the starting lignocellulosic biomass as well as cellulose crystallinity, as has been previously shown in the literature [14, 43, 56]. For example, higher concentrations of sulphuric acid (~50-64% v/v) and longer reaction times (up to 5 days) are often required for highly crystalline cellulose such as bacterial cellulose. On the contrary, milder conditions (~30% v/v and higher cellulose/acid ratio), as well as shorter times (from 1 to

24 h), might be applied for cellulose fibrils derived from lignocellulosic biomass [43, 57, 58]. Thus, the extraction parameters will be adjusted depending on the cellulosic source used along with this Ph. D. thesis and might be slightly modified for different waste biomass sources.

It should be mentioned that there are other alternatives to sulphuric acid hydrolysis, which are also englobed in chemical treatments. One example is the TEMPO oxidation (conversion of cellulose into nanocellulose by applying 2,2,6,6-tetramethylpiperidinyl-1-oxyl (TEMPO) radicals). It has gained attraction over the last years due to the fast (~1-3 h) and easy fractionation of cellulose microfibrils when applied in combination with other mechanical treatments [59-61]. It is important to emphasize that the use of concentrated acids for obtaining nanocellulose requires further neutralization and post-treatment due to their corrosiveness and hazardousness, making the process less environmentally friendly. Alternatively, less aggressive processes have also been evaluated such as mechanical destructuration of cellulose microfibrils for the production of micro or nanofibrillated cellulose (MFC/NFC, by cryochrusing or high-pressure homogenization) [62, 63]. Nevertheless, the high energy usage required for these mechanical processes and the lower crystallinity degree of resulting nanocellulose considerably limits their applicability.

In addition, biological treatments and, in particular, enzymatic digestions (i.e. using cellulases or endoglycanases) have attracted major attention as more environmentally-friendly alternatives to the chemical treatments for obtaining CNCs. Their major drawbacks are their high associated costs (production of specific enzymes), and the limitations on the conversion rate by the enzymes due to lignocellulosic structural features. Thus, their application as an alternative to chemical conversions is not feasible. For example, the presence of lignin, even in minor contents, drastically diminishes the enzymatic efficiency, thus requiring a higher amount of purification steps for obtaining pure substrates that enable an optimum enzymatic activity [64, 65]. Consequently, chemical treatments represent the most effective current alternative due to their scalability, reaction time and process control. Their benefits in terms of time, cost-effectiveness and final performance overcome the associated aforementioned drawbacks, being currently the most widely used methodology for the production of nanocellulose [43, 63, 66].

2.2 Simplified protocols

In the previous section, one of the most reported conventional procedures to sequentially purify cellulose microfibrils from lignocellulosic biomass (followed by additional hydrolysis for obtaining nanocellulose) has been described. However, the application of each purification step might be evaluated, taking into account biomass composition. For example, aquatic plants usually have low lipid contents and lignin is absent in the case of macroalgae. As a result, simplified

versions of the previous protocol will be evaluated in this thesis (skipping one or several purification steps) when the starting biomass composition may allow doing so. This is also expected to improve the final yield while reducing the derived costs concerning pure cellulose fractions.

2.2.1 Cellulosic fractions

In the case of *P. oceanica* waste biomass (the main source studied in this work), only a minor amount of lipids is expected to be present (<3%) [67]. Consequently, cellulose-rich fractions (or cellulosic fractions) can be obtained omitting the steps involving lipids and hemicelluloses removal. It should be mentioned that most common lignocellulosic biomasses (from terrestrial to aquatic sources) usually have minor contents of lipidic compounds (often 1-10%) [68-70]. Therefore, skipping the Soxhlet extraction step would be valuable not only from an economical point of view but also environmentally, as the use of harmful organic solvents (such as toluene or chloroform) would be reduced or directly avoided.

2.2.2 Cellulosic nanocrystals

On the other hand, it is worth noting that hemicelluloses removal has been reported not to be essential to produce nanocellulose [71]. In addition, most hemicelluloses are also expected to be removed after sulphuric acid hydrolysis (due to their amorphous character). Despite so, the contribution of some of the most common types of hemicelluloses (i.e. xylans and mannans) to form the hierarchical lignocellulosic structure has been recently studied. Interestingly, a recalcitrant population of these sugars was observed which might, to a certain extent, limit the digestion of the amorphous domains of cellulose to obtain nanocellulose [72]. As a consequence, an additional analysis of the monosaccharide profile of each source might connect the hemicellulosic profile with the effectiveness of the sulphuric hydrolysis (in CNCs production) and will thus be studied along with this Ph. D. thesis by following standard methanolysis protocols [73]. In any case, the removal of this purification process (involving alkali treatment) should also be evaluated to study the potential benefits not only from an economical point of view but also in terms of total mass yield and performance of the resulting nanomaterials, with regards to the hemicellulosic content as well as their monosaccharide profile.

In conclusion, alternative protocols omitting lipids and/or hemicelluloses removal will result in what will be called "cellulosic fractions" (fractions where cellulose represents the main component but are not expected to be pure cellulose, as these minor components would still be present in them). These cellulosic fractions will as well act as the precursors for subsequent

sulphuric hydrolysis, which will yield what will be called "cellulosic nanocrystals". All these materials will be studied along with this Ph. D. thesis and compared with conventional pure cellulose, as the presence of these additional components is also expected to affect their performance. This information is essential to determine the most optimum materials in terms of performance and cost-effectiveness.

The application of simplified extraction protocols may also result in the production of cellulosic fractions and nanocrystals with additional functionalities, such as antioxidant capacity. Phenolic-rich biomass sources such as marine organisms and, in particular, *P. oceanica* waste biomass, might preserve part of its bioactive compounds [42] when applying simplified protocols where purification degree has been reduced. This would represent an added value for both waste biomass valorization and the applicability of simplified purification protocols, so the remaining bioactivity of the films made from the unpurified cellulosic materials will be characterized and compared with more conventional films made from pure cellulose.

3. Cellulose applications in food packaging

According to its outstanding properties (high strength, stiffness and high surface area [74]), cellulose and its derivatives have broad market opportunities in several industries, as they can be suitable for a wide range of applications.

The use of cellulose and its derivatives (MFC, NFC) in the pulp and paper industry is well-known and investigated according to their capability of improving the mechanical performance (stiffness) and gas barrier, as well as reducing the grammage of paper-based materials [18, 75]. However, cellulosic materials have gained importance over the past years in other relevant fields such as medical and pharma, acting as drug delivery and controlled release systems, wound healing, scaffolds in tissue engineering or implants, due to their low toxicity and high biocompatibility [76, 77]. In addition to the previously commented biomedical applications, nanocellulose has been suggested as a template for developing porous materials to be used in the diagnostics of highly relevant diseases such as Ebola, HIV or Hepatitis C due to their low cost and lightweight characteristics [78].

Another hot topic in the applicability of cellulosic materials is their potential of acting as a source of energy by their conversion into biofuels (i.e., ethanol, butanol…) after their enzymatic degradation into fermentable sugars. There is a large availability of microorganisms that can convert raw cellulose into these sugars, or even into ethanol. Nevertheless, their production costs are still very high and many metabolic routes poorly optimized [79, 80].

Cellulose microfibrils are also used as rheology modifiers in paints, cosmetics, 3D printing or even pharmaceutical products [81] as well as food stabilizers [82] due to their biocompatibility, high surface area and marked stiffness. These physicomechanical attributes, in addition to their low thermal conductivity and durability, have also proposed cellulose as a cheaper and more environmentally friendly alternative as construction and building materials [83].

Finally, the applicability of cellulose in the food industry, particularly for the development of food packaging materials, has always attracted a great deal of interest due to its non-toxic nature. Moreover, its biodegradability and renewability represent an advantage over other conventional polymers or plastics. This is particularly interesting with the current efforts which are focusing on the development of bio-based biodegradable packaging materials. It is well-known that plastics derived from fossil fuels are intended to be gradually replaced by more environmentally friendly biopolymers. As a result of the overuse of plastics, natural ecosystems have been damaged due to the pollution originated by human and industrial activities. Particularly, more than 90% of plastic residues cannot be recycled and they are accumulated in the environment. Moreover, up to 95% of the total amount of residues in the Mediterranean Sea are plastic debris [84]. On the other hand, synthetic plastics are obtained from fossil fuels, causing the steady depletion of these non-renewable resources [85]. Consequently, the applicability of cellulosic materials (derived from waste biomass) for developing novel and high-performance food packaging structures will be studied along with this Ph. D. thesis.

Above all the mentioned applications for cellulosic materials, their usability in packaging has drastically increased the research interest over the past years due to their stiffness, renewability and biodegradability, making cellulosic materials a promising alternative to conventional plastics or other petroleum-based materials, thus following the circular economy principles currently boosted worldwide [86]. As it will be seen, cellulose can be processed in many ways for the development of food packaging structures. During the following subsections, a description of the most relevant cellulose-based packaging structures and strategies is included.

3.1 Cellulose as filler in biopolymeric materials

The most conventional and reported use of cellulosic fractions and nanocrystals in packaging materials consists of their incorporation as fillers in other biopolymeric matrices to improve their performance. The addition of cellulose can enhance the mechanical stiffness and water vapour barrier performance of other biopolymers provided that a good dispersion is achieved. This is particularly relevant in the food packaging industry as the main drawbacks of many benchmark biopolymers (e.g., thermoplastic starch) are related to their lower mechanical and barrier performance, as well as higher moisture sensitivity (in comparison with conventional plastics).

Although many studies have reported on the incorporation of cellulose into biopolymeric structures prepared by casting [43, 87], the industrial applicability of this kind of processing method is quite limited. In turn, other industrial approaches such as melt-mixing or extrusion and injection molding, which are more relevant industrially should be explored. The melt-mixing approach, where biopolymers are homogeneously mixed and dispersed above the melting point of the matrix, can be easily implemented at lab scale and films or trays can be subsequently produced using a hot press or a thermoforming machine to produce specimens, which can be tested to evaluate their performance. As a result, melt-mixing will be preferentially selected for preparing cellulosic composites along with this Ph. D. thesis, when the composition of the films may allow to do so. The processing conditions, as well as the addition of plasticizers such as glycerol or sorbitol, play a key role in the development of the formulations and must be optimized for each specific biopolymer [88]. These methodologies can easily incorporate cellulosic filler contents generally from 1 to 10% (w/w for the biopolymer weight), reaching greater contents such as 20% (w/w) [89]. Cellulose and cellulose nanocrystals (whose dispersion and compatibility with other matrices are enhanced due to their nano-size) have been successfully incorporated into films from biopolymers such as PLA (polylactic acid) [90, 91] and PHB (polyhydroxybutyrate) [92] by melt-mixing and hot-pressing. Nevertheless, the most explored and reported biopolymer which has been combined with cellulosic fillers is undoubtedly starch. Starch can be derived from a broad range of land crops, such as corn [93], wheat [94], potato [95], pea [96], cassava [97] or rice [98] and it is one of the most studied and utilized biopolymers due to its capability of being thermo-processed. However, major drawbacks like the poor mechanical and barrier performance in comparison to petroleum-based plastics, as well as the low stability upon storage due to re-crystallization, have limited its practical application. Thus, cellulose and its nano-derivatives have been extensively proposed as a reinforcing agent in starch-based films to improve their performance and reduce their retrogradation upon prolonged storage times.

Consequently, cellulose and its different forms (CNCs, NFC…) have been shown to successfully improve the performance of many biopolymer-based materials and are especially relevant in the production of thermoplastic structures (via melt-mixing or extrusion and injection molding) when incorporated as fillers, according to their similar manufacturing with other conventional plastics such as PET or polyurethane. As a result, cellulosic fractions and derived nanocrystals produced in this thesis will be explored as reinforcing fillers in biopolymeric matrices, with special relevance in starch-based biocomposites due to their aforementioned high compatibility and optimum processability via melt-mixing.

3.2 Cellulose-based films

Although cellulose has been typically used as filler in other biopolymeric materials, it is also capable of forming self-standing films with interesting properties such as high barrier, transparency and stiffness [99]. Cellulosic films have been traditionally made by dispersing cellulose nanocrystals in water and vacuum filtration to rapidly remove water [100]. Alternative methodologies consisting of hot-pressing of de-aerated cellulosic suspensions have also been evaluated in the case of greater fibres such as MFC [101].

However, the inherent stiffness of these cellulose-based films might be also considered negative since the films may show excessive rigidity, thus hindering their applicability as food packaging structures. As a plausible approach, several cellulose-based composites have been developed by mixtures with other biopolymers to tune their performance (by significantly increasing their elongation). For instance, chitosan [102], lignin [103] or chitin [104] have been shown to successfully reduce the rigidity of raw cellulosic films by their addition (up to 50% w/w), always remaining cellulose as the main component of the formulations. Alternatively, these drawbacks might be overcome (or at least palliated) by the presence of other minor components such as hemicelluloses or lipids in less purified cellulosic fractions and nanocrystals, which might be able to increase the elongation of cellulose-based materials. Accordingly, their effect in cellulose-based films made from less purified fractions and nanocrystals will be later evaluated. This would represent an additional beneficial aspect of applying the more simplified protocols in cellulose purification (as described in section 2).

3.3 Aerogels

Another potential application of cellulosic fractions and nanocrystals consists on the development of biopolymer-based aerogels. Aerogels are extremely light and porous materials with high surface area whose research has drastically boosted over the past decades thanks to their outstanding characteristics and properties. As a result, they are suitable not only for food packaging purposes (as absorbent pads to be placed under meat or fish for absorbing the excess of liquids in packaging trays [105] but also for a wide range of applications: from pharmaceutical and biomedical (in tissue engineering or as drug carriers) to cosmetics (as oil absorbents or thickeners) or construction (as for thermal and acoustic insulators). Although aerogels have been traditionally made from inorganic materials such as silica or carbon, biopolymeric aerogels and, in particular, those obtained from cellulose, are gaining attention over the past few years [106]. In this context, the most conventional methodologies for developing cellulosic aerogels are (i) solvent-exchange processes, followed by drying via supercritical CO_2 and (ii) freeze-drying from aqueous suspensions. Several parameters such as cellulose source, cellulose concentration (i.e.,

0.5-5% w/v) or drying method are known to affect the final structure of the aerogels by modifying their porosity and density. Thus, the methodology and conditions followed should be carefully revised before the preparation of the aerogels [107].

Moreover, aerogels present outstanding sorption and desorption capacities due to their high porosity, which makes them optimum for food packaging applications as absorbent "pads" in meat or fish trays to collect the exudates of fresh food products. Additionally, these materials are excellent candidates for the incorporation and sustained release of antioxidant compounds [108] which could be used to increase the shelf-life of food products [105, 109]. This approach is in line with a current search for novel and more efficient active packaging structures which helps to reduce the annual food loss derived from longer transportation and increased demand which usually leads to food spoilage. Moreover, the biodegradable nature of cellulose-based aerogels prevents their accumulation as residues making these aerogels one of the most promising materials for future years. However, one of the main drawbacks of cellulose-based aerogels is their highly hydrophilic character, which can be detrimental to their application in food packaging. To overcome this issue, sophisticated strategies based on chemical modification, cross-linking and/or coating with hydrophobic non-food grade compounds are typically applied [110, 111], compromising the sustainability of the obtained materials. In this sense, alternative greener methodologies should be developed and thus, will comprise one of the main objectives of this Ph. D. thesis.

To sum up, it has been shown that cellulose represents one of the most abundant biopolymers on Earth, playing a key role in the structural arrangement of plant cell walls. Marine biomasses and, in particular, marine residues are currently gaining attention as cellulose-rich sources over more conventional terrestrial sources according to their composition (richer in bioactive molecules (in comparison with conventional cellulose plant sources), while lignin and hemicelluloses are present in lower amounts) and larger availability, as well as from an environmental point of view. However, specific purification methodologies are still required for purifying cellulose, although simpler protocols should be evaluated when the biomass composition might allow doing so. This would result in an improvement of their cost-efficiency by increasing their final yields. Finally, it has been recently shown that cellulose is considered an optimum biopolymer for a wide range of applications due to its outstanding properties. Accordingly, their application as reinforcing fillers, as well as their use as base materials for producing both cellulose-based films and aerogels, will be studied along with this Ph. D. thesis for developing novel and high-performance food packaging structures.

4. References

[1] S. Ventura-Cruz, A. Tecante, | Nanocellulose and microcrystalline cellulose from agricultural waste: Review on isolation and application as reinforcement in polymeric matrices, Food Hydrocolloids (2021) 106771.
[2] D.G. Coffey, D.A. Bell, A. Henderson, Cellulose and cellulose derivatives, Marcel Dekker Inc.: New York, NY, USA1995.
[3] B. Lindman, B. Medronho, L. Alves, C. Costa, H. Edlund, M. Norgren, The relevance of structural features of cellulose and its interactions to dissolution, regeneration, gelation and plasticization phenomena, Physical Chemistry Chemical Physics 19(35) (2017) 23704-23718.
[4] S. Wagner, M. Schlummer, Legacy additives in a circular economy of plastics: Current dilemma, policy analysis, and emerging countermeasures, Resources, Conservation and Recycling 158 (2020) 104800.
[5] E. Foschi, A. Bonoli, The commitment of packaging industry in the framework of the European strategy for plastics in a circular economy, Administrative Sciences 9(1) (2019) 18.
[6] MarketsandMarkets, Nanocellulose Market by Type (MFC & NFC, CNC/NCC, and Others), Application (Pulp&paper, composites, biomedical & pharmaceutical, electronics & sensors, and others), Region (Europe, North America, APAC, and Rest of World) - Global Forecast to 2025, marketsandmarkets.com (2020).
[7] H.-M. Ng, L.T. Sin, T.-T. Tee, S.-T. Bee, D. Hui, C.-Y. Low, A. Rahmat, Extraction of cellulose nanocrystals from plant sources for application as reinforcing agent in polymers, Composites Part B: Engineering 75 (2015) 176-200.
[8] M. Martínez-Sanz, D. Mikkelsen, B. Flanagan, M.J. Gidley, E.P. Gilbert, Multi-scale model for the hierarchical architecture of native cellulose hydrogels, Carbohydrate polymers 147 (2016) 542-555.
[9] S. Iwamoto, W. Kai, A. Isogai, T. Iwata, Elastic modulus of single cellulose microfibrils from tunicate measured by atomic force microscopy, Biomacromolecules 10(9) (2009) 2571-2576.
[10] M. Martínez-Sanz, P. Lopez-Sanchez, M. Gidley, E. Gilbert, Evidence for differential interaction mechanism of plant cell wall matrix polysaccharides in hierarchically-structured bacterial cellulose, Cellulose 22(3) (2015).
[11] Y.B. Park, D.J. Cosgrove, A revised architecture of primary cell walls based on biomechanical changes induced by substrate-specific endoglucanases, Plant Physiology 158(4) (2012) 1933-1943.
[12] M. Pauly, P. Albersheim, A. Darvill, W.S. York, Molecular domains of the cellulose/xyloglucan network in the cell walls of higher plants, The Plant Journal 20(6) (1999) 629-639.
[13] R. Palin, A. Geitmann, The role of pectin in plant morphogenesis, Biosystems 109(3) (2012) 397-402.
[14] H. Lee, S.B.A. Hamid, S. Zain, Conversion of lignocellulosic biomass to nanocellulose: structure and chemical process, The Scientific World Journal 2014 (2014).
[15] M. Frei, Lignin: characterization of a multifaceted crop component, The Scientific World Journal 2013 (2013).
[16] X. Liu, C. Le Bourvellec, C.M. Renard, Interactions between cell wall polysaccharides and polyphenols: Effect of molecular internal structure, Comprehensive Reviews in Food Science and Food Safety 19(6) (2020) 3574-3617.
[17] R.A. Burton, M.J. Gidley, G.B. Fincher, Heterogeneity in the chemistry, structure and function of plant cell walls, Nature chemical biology 6(10) (2010) 724-732.
[18] S.H. Osong, S. Norgren, P. Engstrand, Processing of wood-based microfibrillated cellulose and nanofibrillated cellulose, and applications relating to papermaking: a review, Cellulose 23(1) (2016) 93-123.
[19] D. Lavanya, P. Kulkarni, M. Dixit, P.K. Raavi, L.N.V. Krishna, Sources of cellulose and their applications—A review, International Journal of Drug Formulation and Research 2(6) (2011) 19-38.
[20] N.L.G. de Rodriguez, W. Thielemans, A. Dufresne, Sisal cellulose whiskers reinforced polyvinyl acetate nanocomposites, Cellulose 13(3) (2006) 261-270.
[21] L. Jiménez, V. Angulo, E. Ramos, M. De la Torre, J. Ferrer, Comparison of various pulping processes for producing pulp from vine shoots, Industrial Crops and Products 23(2) (2006) 122-130.
[22] R. Liu, H. Yu, Y. Huang, Structure and morphology of cellulose in wheat straw, Cellulose 12(1) (2005) 25-34.
[23] Y. Nakamura, Y. Ono, T. Saito, A. Isogai, Characterization of cellulose microfibrils, cellulose molecules, and hemicelluloses in buckwheat and rice husks, Cellulose 26(11) (2019) 6529-6541.
[24] H. Doh, M.H. Lee, W.S. Whiteside, Physicochemical characteristics of cellulose nanocrystals isolated from seaweed biomass, Food hydrocolloids 102 (2020) 105542.
[25] F. Bettaieb, R. Khiari, M.L. Hassan, M.N. Belgacem, J. Bras, A. Dufresne, M.F. Mhenni, Preparation and characterization of new cellulose nanocrystals from marine biomass Posidonia oceanica, Industrial Crops and Products 72 (2015) 175-182.

[26] C.-C. Fu, T.-C. Hung, J.-Y. Chen, C.-H. Su, W.-T. Wu, Hydrolysis of microalgae cell walls for production of reducing sugar and lipid extraction, Bioresource Technology 101(22) (2010) 8750-8754.
[27] M. Martínez-Sanz, A. Lopez-Rubio, J.M. Lagaron, Optimization of the nanofabrication by acid hydrolysis of bacterial cellulose nanowhiskers, Carbohydrate Polymers 85(1) (2011) 228-236.
[28] C. Olsson, G. Westman, Direct dissolution of cellulose: background, means and applications, Cellulose-fundamental aspects 10 (2013) 52144.
[29] N.A. Rosli, I. Ahmad, I. Abdullah, Isolation and characterization of cellulose nanocrystals from Agave angustifolia fibre, BioResources 8(2) (2013) 1893-1908.
[30] M. Yu, R. Yang, L. Huang, X. Cao, F. Yang, D. Liu, Preparation and characterization of bamboo nanocrystalline cellulose, BioResources 7(2) (2012) 1802-1812.
[31] P. Preethi, Physical and chemical properties of banana fibre extracted from commercial banana cultivars grown in Tamilnadu State, (2011).
[32] N.G. Jústiz-Smith, G.J. Virgo, V.E. Buchanan, Potential of Jamaican banana, coconut coir and bagasse fibres as composite materials, Materials characterization 59(9) (2008) 1273-1278.
[33] Y.W. Chen, H.V. Lee, J.C. Juan, S.-M. Phang, Production of new cellulose nanomaterial from red algae marine biomass Gelidium elegans, Carbohydrate polymers 151 (2016) 1210-1219.
[34] R.B.A. Kolsi, J. Fakhfakh, F. Krichen, I. Jribi, A. Chiarore, F.P. Patti, C. Blecker, N. Allouche, H. Belghith, K. Belghith, Structural characterization and functional properties of antihypertensive Cymodocea nodosa sulfated polysaccharide, Carbohydrate polymers 151 (2016) 511-522.
[35] R.B.A. Kolsi, H.B. Salah, S.A. Saidi, N. Allouche, H. Belghith, K. Belghith, Evaluation of nutritional value, characteristics, functional properties of Cymodocea nodosa and its benefits on health diseases, Lipids in health and disease 16(1) (2017) 1-13.
[36] P. Davies, C. Morvan, O. Sire, C. Baley, Structure and properties of fibres from sea-grass (Zostera marina), Journal of Materials Science 42(13) (2007) 4850-4857.
[37] Y. Zhao, J. Li, Excellent chemical and material cellulose from tunicates: diversity in cellulose production yield and chemical and morphological structures from different tunicate species, Cellulose 21(5) (2014) 3427-3441.
[38] A.M. Aguirre, A. Bassi, Investigation of biomass concentration, lipid production, and cellulose content in Chlorella vulgaris cultures using response surface methodology, Biotechnology and bioengineering 110(8) (2013) 2114-2122.
[39] M. Martínez-Sanz, A. Lopez-Rubio, J.M. Lagaron, High-barrier coated bacterial cellulose nanowhiskers films with reduced moisture sensitivity, Carbohydrate polymers 98(1) (2013) 1072-1082.
[40] G. Balata, A. Tola, Cost-opportunity analysis of the use of Posidonia oceanica as a source of bio-energy in tourism-oriented territories. The case of Alghero, Journal of Cleaner Production (2017).
[41] G. Castellano, J. Tena, F. Torrens, Classification of phenolic compounds by chemical structural indicators and its relation to antioxidant properties of Posidonia Oceanica (L.) Delile, environment 2 (2012) 6.
[42] M. Grignon-Dubois, B. Rezzonico, Phenolic fingerprint of the seagrass Posidonia oceanica from four locations in the Mediterranean Sea: First evidence for the large predominance of chicoric acid, Botanica Marina 58(5) (2015) 379-391.
[43] M. Martínez-Sanz, A.A. Vicente, N. Gontard, A. Lopez-Rubio, J.M. Lagaron, On the extraction of cellulose nanowhiskers from food by-products and their comparative reinforcing effect on a polyhydroxybutyrate-co-valerate polymer, Cellulose 22(1) (2015) 535-551.
[44] P. Lu, Y.-L. Hsieh, Preparation and characterization of cellulose nanocrystals from rice straw, Carbohydrate Polymers 87(1) (2012) 564-573.
[45] K. Abe, S. Iwamoto, H. Yano, Obtaining cellulose nanofibers with a uniform width of 15 nm from wood, Biomacromolecules 8(10) (2007) 3276-3278.
[46] J. Sun, X. Sun, H. Zhao, R. Sun, Isolation and characterization of cellulose from sugarcane bagasse, Polymer Degradation and Stability 84(2) (2004) 331-339.
[47] K. Abe, H. Yano, Comparison of the characteristics of cellulose microfibril aggregates isolated from fiber and parenchyma cells of Moso bamboo (Phyllostachys pubescens), Cellulose 17(2) (2010) 271-277.
[48] K. Ramluckan, K.G. Moodley, F. Bux, An evaluation of the efficacy of using selected solvents for the extraction of lipids from algal biomass by the soxhlet extraction method, Fuel 116 (2014) 103-108.
[49] G. Siqueira, A. Várnai, A. Ferraz, A.M. Milagres, Enhancement of cellulose hydrolysis in sugarcane bagasse by the selective removal of lignin with sodium chlorite, Applied Energy 102 (2013) 399-402.
[50] M. Taherdanak, H. Zilouei, Improving biogas production from wheat plant using alkaline pretreatment, Fuel 115 (2014) 714-719.
[51] M. Pedersen, A.S. Meyer, Lignocellulose pretreatment severity–relating pH to biomatrix opening, New biotechnology 27(6) (2010) 739-750.

[52] A. Limayem, S.C. Ricke, Lignocellulosic biomass for bioethanol production: current perspectives, potential issues and future prospects, Progress in energy and combustion science 38(4) (2012) 449-467.
[53] P. Kumar, D.M. Barrett, M.J. Delwiche, P. Stroeve, Methods for pretreatment of lignocellulosic biomass for efficient hydrolysis and biofuel production, Industrial & engineering chemistry research 48(8) (2009) 3713-3729.
[54] A. Hendriks, G. Zeeman, Pretreatments to enhance the digestibility of lignocellulosic biomass, Bioresource technology 100(1) (2009) 10-18.
[55] J.-W. Lee, T.W. Jeffries, Efficiencies of acid catalysts in the hydrolysis of lignocellulosic biomass over a range of combined severity factors, Bioresource technology 102(10) (2011) 5884-5890.
[56] S. Beck-Candanedo, M. Roman, D.G. Gray, Effect of reaction conditions on the properties and behavior of wood cellulose nanocrystal suspensions, Biomacromolecules 6(2) (2005) 1048-1054.
[57] M. Martínez-Sanz, R.T. Olsson, A. Lopez-Rubio, J.M. Lagaron, Development of electrospun EVOH fibres reinforced with bacterial cellulose nanowhiskers. Part I: Characterization and method optimization, Cellulose 18(2) (2011) 335-347.
[58] C.-M. Liu, K.-H. Lin, T.-C. Chang, F.-C. Chang, Preparation and Characterization of Moso Bamboo-based Cellulose Nanowhiskers under Various Acid Hydrolysis Conditions, BioResources 14(1) (2019) 1077-1090.
[59] C. Tahiri, M.R. Vignon, TEMPO-oxidation of cellulose: Synthesis and characterisation of polyglucuronans, Cellulose 7(2) (2000) 177-188.
[60] L. Zhai, H.C. Kim, J.W. Kim, E.S. Choi, J. Kim, Cellulose nanofibers isolated by TEMPO-oxidation and aqueous counter collision methods, Carbohydrate polymers 191 (2018) 65-70.
[61] C. Fraschini, G. Chauve, J. Bouchard, TEMPO-mediated surface oxidation of cellulose nanocrystals (CNCs), Cellulose 24(7) (2017) 2775-2790.
[62] J. Zhao, W. Zhang, X. Zhang, X. Zhang, C. Lu, Y. Deng, Extraction of cellulose nanofibrils from dry softwood pulp using high shear homogenization, Carbohydrate Polymers 97(2) (2013) 695-702.
[63] F. Jiang, Y.-L. Hsieh, Chemically and mechanically isolated nanocellulose and their self-assembled structures, Carbohydrate polymers 95(1) (2013) 32-40.
[64] K. Igarashi, T. Uchihashi, A. Koivula, M. Wada, S. Kimura, T. Okamoto, M. Penttilä, T. Ando, M. Samejima, Traffic jams reduce hydrolytic efficiency of cellulase on cellulose surface, Science 333(6047) (2011) 1279-1282.
[65] L. Zhu, J.P. O'Dwyer, V.S. Chang, C.B. Granda, M.T. Holtzapple, Structural features affecting biomass enzymatic digestibility, Bioresource technology 99(9) (2008) 3817-3828.
[66] M. Ioelovich, Study of cellulose interaction with concentrated solutions of sulfuric acid, International Scholarly Research Notices 2012 (2012).
[67] A.-C. Viso, D. Pesando, P. Bernard, J.-C. Marty, Lipid components of the Mediterranean seagrass Posidonia oceanica, Phytochemistry 34(2) (1993) 381-387.
[68] B. Maddi, S. Viamajala, S. Varanasi, Comparative study of pyrolysis of algal biomass from natural lake blooms with lignocellulosic biomass, Bioresource technology 102(23) (2011) 11018-11026.
[69] H.-j. Huang, X.-z. Yuan, H.-n. Zhu, H. Li, Y. Liu, X.-l. Wang, G.-m. Zeng, Comparative studies of thermochemical liquefaction characteristics of microalgae, lignocellulosic biomass and sewage sludge, Energy 56 (2013) 52-60.
[70] X. Chen, Y. Gu, X. Zhou, Y. Zhang, Asparagus stem as a new lignocellulosic biomass feedstock for anaerobic digestion: Increasing hydrolysis rate, methane production and biodegradability by alkaline pretreatment, Bioresource technology 164 (2014) 78-85.
[71] V.B. Agbor, N. Cicek, R. Sparling, A. Berlin, D.B. Levin, Biomass pretreatment: fundamentals toward application, Biotechnology advances 29(6) (2011) 675-685.
[72] A. Martínez-Abad, A. Jiménez-Quero, J. Wohlert, F. Vilaplana, Influence of the molecular motifs of mannan and xylan populations on their recalcitrance and organization in spruce softwoods, Green Chemistry 22(12) (2020) 3956-3970.
[73] A. Martínez-Abad, N. Giummarella, M. Lawoko, F. Vilaplana, Differences in extractability under subcritical water reveal interconnected hemicellulose and lignin recalcitrance in birch hardwoods, Green Chemistry 20(11) (2018) 2534-2546.
[74] P. Lu, Y.-L. Hsieh, Preparation and properties of cellulose nanocrystals: rods, spheres, and network, Carbohydrate polymers 82(2) (2010) 329-336.
[75] K. Mörseburg, G. Chinga-Carrasco, Assessing the combined benefits of clay and nanofibrillated cellulose in layered TMP-based sheets, Cellulose 16(5) (2009) 795-806.
[76] A. Gumrah Dumanli, Nanocellulose and its composites for biomedical applications, Current Medicinal Chemistry 24(5) (2017) 512-528.
[77] Y. Xue, Z. Mou, H. Xiao, Nanocellulose as a sustainable biomass material: structure, properties, present status and future prospects in biomedical applications, Nanoscale 9(39) (2017) 14758-14781.

[78] A.W. Martinez, S.T. Phillips, G.M. Whitesides, E. Carrilho, Diagnostics for the developing world: microfluidic paper-based analytical devices, ACS Publications, 2010.
[79] C.M. Gowen, S.S. Fong, Exploring biodiversity for cellulosic biofuel production, Chemistry & biodiversity 7(5) (2010) 1086-1097.
[80] L. Machineni, Lignocellulosic biofuel production: review of alternatives, Biomass Conversion and Biorefinery (2019) 1-13.
[81] Y. Shao, D. Chaussy, P. Grosseau, D. Beneventi, Use of microfibrillated cellulose/lignosulfonate blends as carbon precursors: impact of hydrogel rheology on 3D printing, Industrial & Engineering Chemistry Research 54(43) (2015) 10575-10582.
[82] T. Winuprasith, M. Suphantharika, Microfibrillated cellulose from mangosteen (Garcinia mangostana L.) rind: Preparation, characterization, and evaluation as an emulsion stabilizer, Food Hydrocolloids 32(2) (2013) 383-394.
[83] M.V. Madurwar, R.V. Ralegaonkar, S.A. Mandavgane, Application of agro-waste for sustainable construction materials: A review, construction and Building materials 38 (2013) 872-878.
[84] G.F. Schirinzi, M. Köck-Schulmeyer, M. Cabrera, D. González-Fernández, G. Hanke, M. Farré, D. Barceló, Riverine anthropogenic litter load to the Mediterranean Sea near the metropolitan area of Barcelona, Spain, Science of The Total Environment 714 (2020) 136807.
[85] J.N. Hahladakis, C.A. Velis, R. Weber, E. Iacovidou, P. Purnell, An overview of chemical additives present in plastics: Migration, release, fate and environmental impact during their use, disposal and recycling, Journal of hazardous materials 344 (2018) 179-199.
[86] M.A. Hubbe, A. Ferrer, P. Tyagi, Y. Yin, C. Salas, L. Pal, O.J. Rojas, Nanocellulose in thin films, coatings, and plies for packaging applications: A review, BioResources 12(1) (2017) 2143-2233.
[87] R. Ilyas, S. Sapuan, M. Sanyang, M. Ishak, Nanocrystalline cellulose reinforced starch-based nanocomposite: A review, 5th Postgraduate Seminar on Natural Fiber Composites, Universiti Putra Malaysia Serdang, Selangor, 2016, pp. 82-87.
[88] L. Avèrous, C. Fringant, L. Moro, Starch-based biodegradable materials suitable for thermoforming packaging, Starch-Stärke 53(8) (2001) 368-371.
[89] A.M. Salaberria, J. Labidi, S.C. Fernandes, Chitin nanocrystals and nanofibers as nano-sized fillers into thermoplastic starch-based biocomposites processed by melt-mixing, Chemical Engineering Journal 256 (2014) 356-364.
[90] A. Awal, M. Rana, M. Sain, Thermorheological and mechanical properties of cellulose reinforced PLA bio-composites, Mechanics of Materials 80 (2015) 87-95.
[91] E. Fortunati, F. Luzi, D. Puglia, R. Petrucci, J. Kenny, L. Torre, Processing of PLA nanocomposites with cellulose nanocrystals extracted from Posidonia oceanica waste: Innovative reuse of coastal plant, Industrial Crops and Products 67 (2015) 439-447.
[92] M.P. Arrieta, E. Fortunati, F. Dominici, E. Rayón, J. López, J.M. Kenny, PLA-PHB/cellulose based films: Mechanical, barrier and disintegration properties, Polymer Degradation and Stability 107 (2014) 139-149.
[93] M.J. Fabra, A. López-Rubio, J. Ambrosio-Martín, J.M. Lagaron, Improving the barrier properties of thermoplastic corn starch-based films containing bacterial cellulose nanowhiskers by means of PHA electrospun coatings of interest in food packaging, Food Hydrocolloids 61 (2016) 261-268.
[94] J. Xiong, Q. Li, Z. Shi, J. Ye, Interactions between wheat starch and cellulose derivatives in short-term retrogradation: Rheology and FTIR study, Food Research International 100 (2017) 858-863.
[95] P. Balakrishnan, S. Gopi, S. MS, S. Thomas, UV resistant transparent bionanocomposite films based on potato starch/cellulose for sustainable packaging, Starch-Stärke 70(1-2) (2018) 1700139.
[96] X. Li, C. Qiu, N. Ji, C. Sun, L. Xiong, Q. Sun, Mechanical, barrier and morphological properties of starch nanocrystals-reinforced pea starch films, Carbohydrate polymers 121 (2015) 155-162.
[97] E.d.M. Teixeira, D. Pasquini, A.A. Curvelo, E. Corradini, M.N. Belgacem, A. Dufresne, Cassava bagasse cellulose nanofibrils reinforced thermoplastic cassava starch, Carbohydrate polymers 78(3) (2009) 422-431.
[98] K. Piyada, S. Waranyou, W. Thawien, Mechanical, thermal and structural properties of rice starch films reinforced with rice starch nanocrystals, International Food Research Journal 20(1) (2013) 439.
[99] N.M. Stark, Opportunities for cellulose nanomaterials in packaging films: A review and future trends, Journal of Renewable Materials 4(5) (2016) 313-326.
[100] E. Kontturi, T. Tammelin, M. Österberg, Cellulose—model films and the fundamental approach, Chemical Society Reviews 35(12) (2006) 1287-1304.
[101] M. Henriksson, L.A. Berglund, Structure and properties of cellulose nanocomposite films containing melamine formaldehyde, Journal of Applied Polymer Science 106(4) (2007) 2817-2824.

[102] B. Wang, X. Yang, C. Qiao, Y. Li, T. Li, C. Xu, Effects of chitosan quaternary ammonium salt on the physicochemical properties of sodium carboxymethyl cellulose-based films, Carbohydrate polymers 184 (2018) 37-46.
[103] M. Michelin, A.M. Marques, L.M. Pastrana, J.A. Teixeira, M.A. Cerqueira, Carboxymethyl cellulose-based films: Effect of organosolv lignin incorporation on physicochemical and antioxidant properties, Journal of Food Engineering 285 (2020) 110107.
[104] A.A. Oun, J.-W. Rhim, Preparation of multifunctional carboxymethyl cellulose-based films incorporated with chitin nanocrystal and grapefruit seed extract, International journal of biological macromolecules 152 (2020) 1038-1046.
[105] C. Fontes-Candia, E. Erboz, A. Martínez-Abad, A. López-Rubio, M. Martínez-Sanz, Superabsorbent food packaging bioactive cellulose-based aerogels from Arundo donax waste biomass, Food Hydrocolloids 96 (2019) 151-160.
[106] T. Budtova, Cellulose II aerogels: A review, Cellulose 26(1) (2019) 81-121.
[107] F. Zou, T. Budtova, Tailoring the morphology and properties of starch aerogels and cryogels via starch source and process parameter, Carbohydrate Polymers 255 (2021) 117344.
[108] J.P. de Oliveira, G.P. Bruni, L.M. Fonseca, F.T. da Silva, J.C. da Rocha, E. da Rosa Zavareze, Characterization of aerogels as bioactive delivery vehicles produced through the valorization of yerba-mate (Illex paraguariensis), Food Hydrocolloids 107 (2020) 105931.
[109] L.M. Fonseca, F.T. da Silva, G.P. Bruni, C.D. Borges, E. da Rosa Zavareze, A.R.G. Dias, Aerogels based on corn starch as carriers for pinhão coat extract (Araucaria angustifolia) rich in phenolic compounds for active packaging, International Journal of Biological Macromolecules 169 (2021) 362-370.
[110] R. Baetens, B.P. Jelle, A. Gustavsen, Aerogel insulation for building applications: a state-of-the-art review, Energy and Buildings 43(4) (2011) 761-769.
[111] F. Schwertfeger, D. Frank, M. Schmidt, Hydrophobic waterglass based aerogels without solvent exchange or supercritical drying, Journal of Non-Crystalline Solids 225 (1998) 24-29.

II. Objectives

The main objective of this Ph. D. thesis consists on the development of more sustainable and cost-effective cellulose-based materials from waste biomass sources with application in food packaging, mainly focusing on the full valorization of *Posidonia oceanica* dead leaves. For this aim, several sub-objectives will be considered as follows:

1. Achieve an integral valorization of local aquatic waste biomass (*P. oceanica* dead leaves) for the development of cellulosic-based materials for food packaging applications. On one hand, the biomass will be valorized for the extraction of pure cellulose, as well as less purified cellulosic fractions and nanocrystals, for the development of food packaging structures. Additionally, the valorization of this biomass for the production of bioactive extracts will also be considered, as *P. oceanica* is known to be rich in phenolic compounds and other potentially bioactive molecules.

2. Evaluate the use of the extracted cellulosic fractions and nanocrystals as reinforcing fillers to develop starch-based biocomposites with enhanced performance. The main objective is to improve the mechanical properties and the water barrier performance of starch. Additionally, the effect of the fillers in the re-crystallization of starch upon storage will be evaluated. To assess the potential of the less purified/refined cellulosic fractions and nanocrystals, the effect of their incorporation will be evaluated and compared with more conventional purified cellulose materials.

3. Assess the applicability of the simplified purification protocols for the production of cellulosic fractions and nanocrystals using different sources of waste biomass. Biomass composition is suspected to play a crucial role in determining the properties of the extracted cellulosic materials since different types and amounts of additional components will remain in the materials following the simplified purification protocols. Thus, the properties of the cellulosic fractions and nanocrystals extracted from other biomass sources will be studied through their use as film-forming materials and as fillers in starch biocomposites.

4. Produce sustainable high-performance aerogels from cellulosic fractions and nanocrystals derived from *P. oceanica* waste biomass. Aerogels with sufficient mechanical integrity and good water resistance will be developed using cellulosic fractions and nanocrystals with different degrees of purification to evaluate the effect of additional components on the performance of the aerogels and determine the most optimum formulations for food packaging purposes. In addition, the most optimum aerogels will be used as templates for the incorporation of bioactive extracts from *P. oceanica* (previously developed, as stated in sub-objective 1) to develop bioactive aerogels capable of improving the shelf life of fresh food products.

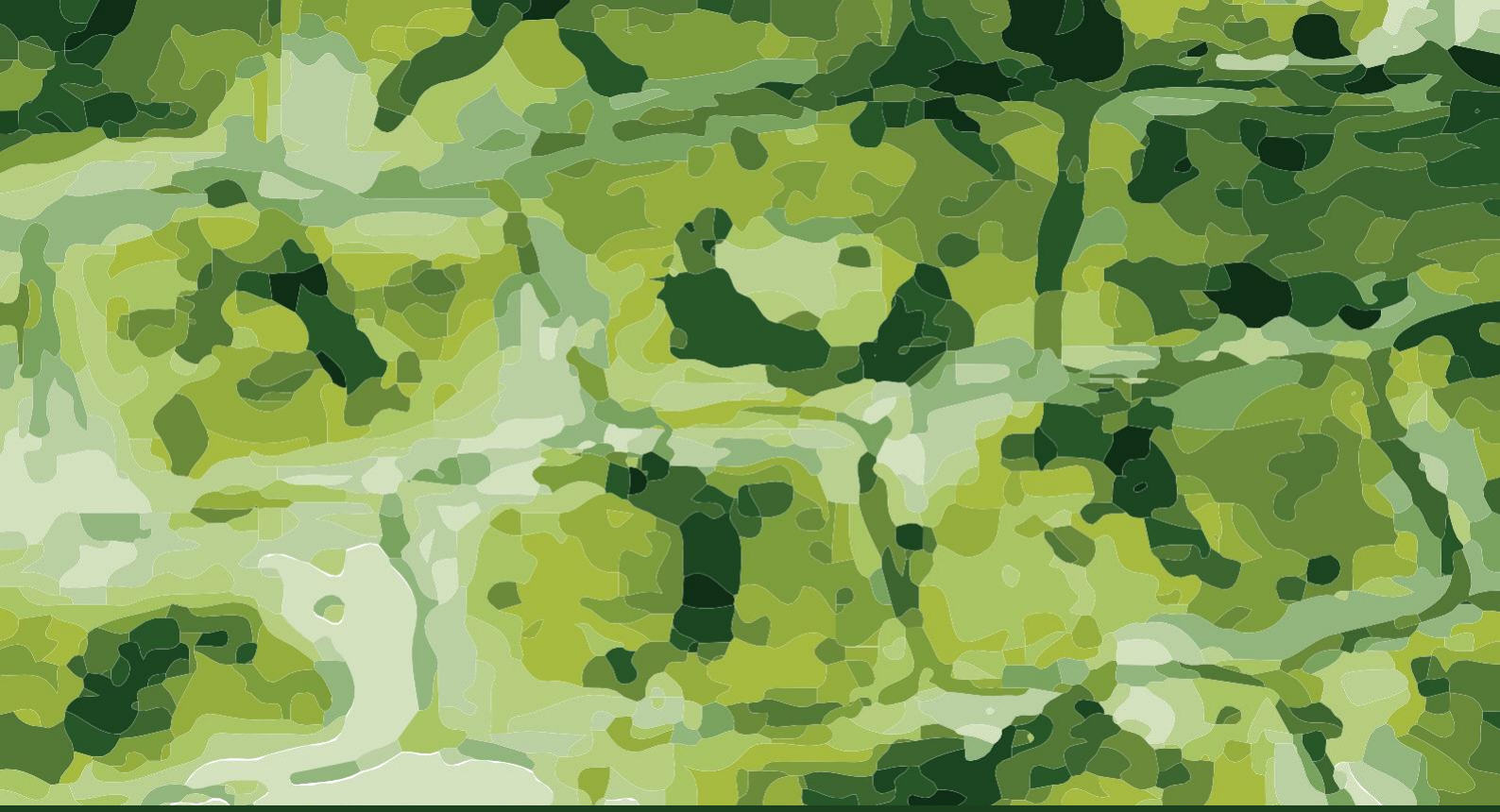

III. Results

Chapter 1

INTEGRAL VALORIZATION OF *P. OCEANICA* WASTE BIOMASS: PRODUCTION OF CELLULOSIC FRACTIONS AND NANOCRYSTALS AND BIOACTIVE EXTRACTS

1.1. Potential of lignocellulosic fractions from Posidonia oceanica to improve barrier and mechanical properties of bio-based packaging materials

1.2. Cellulose nanocrystal-based films produced by more sustainable extraction protocols from Posidonia oceanica waste biomass

1.3. In-depth characterization of bioactive extracts from Posidonia oceanica waste biomass

Introduction to chapter 1.

Posidonia oceanica is an aquatic plant endemic from the Mediterranean Sea. During its natural lifecycle, *Posidonia* leaves detach off their stems and are carried away by marine currents, accumulating on the shores in coastal areas. The accumulation of this waste biomass has a negative impact on the tourism and the quality of the beaches, since it generates bad odors due to decomposition. Consequently, local authorities must remove this residue, which implies a managing cost. Furthermore, no clear strategy has been developed in terms of waste valorization, being this biomass usually disposed for compost or directly burned, with all the environmental issues associated. As an alternative to this current situation, we propose valorizing this waste biomass to be utilized as a sustainable source for food packaging additives, according to its abundance on cellulose and bioactive compounds. To do so, we developed the following work plan:

Initially, in the first work of this chapter, the composition of *P. oceanica* leaves was characterized and the biomass was used for the extraction of pure cellulose by means of the standard protocol. Additionally, the possibility of producing less purified cellulosic fractions by omitting intermediate purification steps was investigated. The pure cellulose and the less purified cellulosic fractions were used to produce cellulose-based films by vacuum filtration and also as fillers in starch-based films produced by melt mixing and hot pressing. The properties of these materials were characterized to evaluate the performance of the different fractions and determine their potential as materials for food packaging applications.

In the second work of this chapter, the most promising cellulosic fractions from *P. oceanica* leaves were selected to produce cellulosic nanocrystals by applying an additional acid hydrolysis treatment. The structure and crystallinity of these nanocrystals were characterized (by TEM and XRD), and their performance as cellulose-based films was also evaluated.

Since marine biomass is also known to be rich phenolics and other interesting constituents, in the third work of this chapter *P. oceanica* leaves were proposed as a valuable source of bioactive compounds. Conventional organic solvent-based extractions were performed and, additionally, greener methods such as ultrasounds and hot water extraction were also tested. The resulting extracts were analyzed, and their antioxidant capacity and bioactivity were also evaluated.

1.1. Potential of lignocellulosic fractions from Posidonia oceanica to improve barrier and mechanical properties of bio-based packaging materials.

This section is an adapted version of the following published research article:
Benito-González, I., López-Rubio, A., & Martínez-Sanz, M. (2018). Potential of lignocellulosic fractions from *Posidonia oceanica* to improve barrier and mechanical properties of bio-based packaging materials. International Journal of Biological Macromolecules, 118, 542-551. DOI: https://doi.org/10.1016/j.ijbiomac.2018.06.052

1. Abstract

This work reports on the valorization of residues from *Posidonia oceanica* leaves for obtaining lignocellulosic fractions of interest for developing bio-based materials for food packaging. The lignocellulosic fractions were characterized, confirming the purification of cellulose and showing the increase in crystallinity and thermal stability after the consecutive extraction steps. Subsequently, pure lignocellulosic films were obtained and characterized, being the pure cellulose film the one that showed the best properties in terms of mechanical performance and water vapor permeability. Finally, composite starch films containing the lignocellulosic fractions were developed by melt compounding and characterized. Although the film containing the pure cellulose additive showed the optimum improvement in terms of mechanical properties (with an increase of 85% in the elastic modulus and 38% in the tensile strength), similar water vapor permeability reduction (~40%) was achieved with the less purified fractions, explained by their effect on the starch gelatinization as evidenced by SAXS/WAXS.

2. Introduction

Due to the steady depletion of fossil fuels and the growing concerns about the negative impact of plastic materials on the environment, great efforts are currently being focused on the development of bio-based polymers (also known as biopolymers or bioplastics). This implies a transition from the utilization of conventional petroleum-based resources to renewable resources and the application of circular economy principles.

Amongst the range of bioplastics currently available, thermoplastic starch, obtained from resources such as corn and rice, has attracted a great deal of interest due to its abundance, low cost and good processability. However, it presents several drawbacks such as low mechanical

performance and high hygroscopicity as compared to benchmark synthetic polymers, as well as retrogradation upon storage. In this sense, the incorporation of fillers has been proven to be an efficient strategy to enhance the properties of bio-based polymers and develop composite materials which are competitive for their intended applications [1, 2]. Lignocellulosic biomass, such as forestry and agro-industrial waste [3], provides a cheap feedstock for the extraction of different biopolymers (i.e. cellulose, lignin, hemicelluloses, etc.) which have a wide range of industrial applications, such as rheology modifiers, food additives, feedstock for bioenergy production and fillers for biocomposite materials [4].

An additional drawback of starch as packaging material is related to the consumption of food sources for its production. With the increasing rate of world population, the competition between forestry and farmlands and the current restriction laws against the use for feed purposes of transgenic organisms, food sources must be primarily used as food. An alternative to the use of land biomass is the utilization of marine resources such as algae and aquatic plants, which are available in large quantities. One of the most abundant aquatic plant species in the Mediterranean Sea is *Posidonia oceanica*. During its lifecycle, *Posidonia* leaves detach off the stems and are transported towards sea shores by marine currents, generating a residue that affects the quality of the beaches and, as a result, is detrimental for tourism [5]. This also implies a considerable disposal cost to local authorities, since these marine residues need to be collected and they are usually disposed to landfill. Several studies have been carried out for the valorization of *Posidonia* residues, with potential use as a low-cost adsorbent for the removal of dyes or phenol [6, 7], or for biofuel production [8, 9]. However, the presence of cell wall components limits the access of enzymes or chemicals towards the cellulosic fraction of *Posidonia* and as a result, the conversion rates are usually quite low. In a recent research work, *Posidonia* leaves have been used to produce cellulose nanocrystals by acid hydrolysis, which were then incorporated into poly-lactic acid (PLA) to produce nanocomposite films [10]. Although the cellulose nanocrystals presented high crystallinity and aspect ratio, they had to be modified with a commercial surfactant to overcome their low compatibility the PLA matrix, as it has been previously reported in 3D printing with microcrystalline cellulose (MCC) [11]. Furthermore, the solvent casting method used to produce the materials would make industrial scaling unfeasible.

In this work, we propose valorizing the residues from *Posidonia* leaves as a natural source of lignocellulosic materials. Using a sequential extraction method different lignocellulosic fractions were generated and characterized. Subsequently, their suitability as film forming components was evaluated. Moreover, their performance as fillers was investigated by incorporating the different fractions into starch films through the melt compounding method, partially replacing starch with marine biomass waste and obtaining materials with improved properties for their application in food packaging.

3. Materials and methods

3.1 Materials

3.1.1 Raw materials

Biomass waste material consisting of *Posidonia oceanica* leaves was collected directly from the shore in Calpe, Alicante (Spain) in February-March 2017. The material was washed vigorously with water to remove sand and salts. It was stored in the fridge until its use. Corn starch (27-28% amylose) was supplied by Roquette (Roquette Laisa España, Benifaio, Spain) and glycerol was purchased from Panreac Quimica, S.A. (Castellar Del Vallés, Barcelona, Spain).

3.1.2 Preparation of lignocellulosic fractions

A purification procedure previously applied to vegetal resources [12], was carried out to sequentially remove cell wall components and obtain different lignocellulosic fractions. Firstly, to remove wax, pigments and oils, 40 g of ground wet *Posidonia* leaves (approximately 4 g of dry material) were subjected to Soxhlet extraction with 800 ml of toluene/ethanol 2:1 (v/v) during 24 h. The resulting material was dried at room temperature overnight constituting the first fraction (referred to as F1). Subsequently, to dissolve lignin, the de-waxed material was ground into powder and treated for 5h at 70ºC with 700 ml of 1.4 % $NaClO_2$ solution, having the pH adjusted to 3 with acetic acid. After that, the reaction was stopped by quenching with ice, and the excess liquid was decanted. The yellow solid was collected and washed repeatedly with distilled water by vacuum filtration until the filtrate became approximately neutral, hence obtaining the second fraction (referred to as F2). The de-lignified material was then treated with 400 ml 5% KOH solution for 24 h at room temperature, followed by 2h at 90ºC, in order to remove the hemicelluloses, yielding pure cellulose (referred to as F3). A small amount of each fraction was subjected to freeze-drying for further analyses and the rest was stored in the fridge as a partially hydrated material.

3.1.3 Production of pure lignocellulosic films

Pure lignocellulosic films were producing by adding 0.25-0.5 g of lignocellulosic materials (F1, F2 and F3) to 50 mL of distilled water and dispersing them by mild sonication, followed by ultra-turrax homogenization until obtaining homogeneous suspensions. These were then vacuum filtered using PTFE filters with 0,2 µm pore size to remove water. The solid material remaining in the filter was then dried at room temperature overnight. The formed films were peeled off the filters and stored at 0%RH.

3.1.4 Production of starch films loaded with lignocellulosic additives

Pure corn starch and composite films with 10 wt.-% (with regards to the starch weight) of the three different lignocellulosic additives (F1, F2 and F3) were prepared. Corn starch and glycerol, as plasticizer, were dispersed in water using a polymer:glycerol:water ratio of 1:0.3:0.5 (w/w/w). For the composite films, the required amount material (which was partially hydrated) was also incorporated and mixed manually until a paste was made. This paste was then melt-mixed in a Brabender Plastograph internal mixer at 130 °C and 60 rpm for 4 min. Subsequently, 4 g of the obtained blends were spread evenly on Teflon and placed in a compression mold (Carver 4122, USA) at a pressure of 16 tons and 130 °C for 2 min to form one film. The samples were coded as follows: Starch (pure starch film), 10% F1 (starch + 10% F1), 10% F2 (starch + 10% F2) and 10% F3 (starch + 10% F3).

3.2 Chemical analysis

The standard methods TAPPI T211 om-07, T222 om-06 and ASTM D1104-56 were used to determine the ash, Klason lignin and holocellulose content, respectively, in the *Posidonia* biomass waste.

3.3 Scanning electron microscopy (SEM)

SEM was conducted on a Hitachi microscope (Hitachi S-4800) at an accelerating voltage of 10 kV and a working distance of 8-16 mm. The freeze-dried powder from the different fractions, the pure films plus its mixtures with corn starch were sputtered with a gold–palladium mixture under vacuum before their morphology was examined. In the case of the films, the samples were cryo-fractured after immersion in liquid nitrogen to observe the cross-sections.

3.4 Fourier Transform Infrared Spectroscopy (FT-IR)

To examine the different lignocellulosic fractions by FT-IR, samples of ca. 1.2 mg were ground and dispersed in 120 mg of spectroscopic grade KBr. A pellet was then formed by compressing the sample at ca. 10 tons. FT-IR experiments were recorded in transmission mode in a controlled chamber at 21ºC and dry air to avoid humidity and CO_2 using a Thermo Nicolet Nexus (GMI, USA) equipment. The spectra were taken at 4 cm^{-1} resolutions in a wavelength range between 400-4000 cm^{-1} and averaging a minimum of 32 scans.

3.5 Small and Wide-Angle X-ray scattering (SAXS/WAXS) and X-ray diffraction (XRD)

Combined small and wide angle X-ray scattering (SAXS and WAXS, respectively) experiments were carried out in the Non Crystalline Diffraction beamline, BL-11, at ALBA synchrotron light source (http://www.albasynchrotron.es) to characterize the starch films loaded with

lignocellulosic fractions. The experimental setup conditions, data reduction and WAXS data fitting procedures were the same as described in a previous work [13].

Additionally, XRD measurements of the freeze-dried lignocellulosic fractions were carried out on a D5005 Bruker diffractometer. The instrument was equipped with a Cu tube and a secondary monochromator. The configuration of the equipment was θ–2θ, and the samples were examined over the angular range of 3°–60° with a step size of 0.02° and a count time of 200 s per step. Peak fitting was carried out using the Igor software package (Wavemetrics, Lake Oswego, Oregon) as described in a previous work [14]. The crystallinity index was determined by the method reported by Wang et al. [15].

$$X_C(\%) = \frac{\sum A_{Crystal}}{A_{Total}} \times 100 \quad (1)$$

Where A_{Total} is the sum of the areas under all the diffraction peaks and $\Sigma A_{Crystal}$ is the sum of the areas corresponding to the three crystalline peaks from cellulose I. The crystallite sizes were estimated from the three different lattice planes of cellulose I_β using the well-known Scherrer equation:

$$D_{(hkl)} = \frac{k \cdot \lambda}{B_{(hkl)} \cdot \cos\theta} \quad (2)$$

3.6 Thermogravimetric analyses (TGA)

Thermogravimetric curves (TG) were recorded with a Setaram Setsys 16/18 (SETARAM Instrumentation, France). The samples (ca. 10 mg) were heated from 30 to 1000ºC with a heating rate of 10ºC/min under nitrogen atmosphere. Derivative TG curves (DTG) express the weight loss rate as a function of temperature.

3.7 Water vapor permeability (WVP)

Direct permeability to water was determined from the slope of the weight gain versus time curves at 24ºC. The films were sandwiched between the aluminum top (open O-ring) and bottom (deposit for the silica) parts of a specifically designed permeability cell with screws. A Viton rubber O-ring was placed between the film and bottom part of the cell to enhance sealability. These permeability cells containing silica were then placed in an equilibrated relative humidity cabinet at 75% RH and 25 °C. The weight gain through a film area of 0.001 m^2 was monitored and plotted as a function of time. Cells with aluminum films (with thickness of ca. 11 μm) were used as control samples to estimate weight gain through the sealing. The tests were done at least in triplicate.

3.8 Water uptake

The water uptake was estimated from sorption experiments at 25ºC and 75% RH by means of weight gain using a Precisa Gravimetrics AG SERIES 320XB analytical balance (Dietikon, Switzerland). The assays were carried out at least in triplicate.

3.9 Contact angle measurements

Contact angle measurements were carried out at 23 ± 2 °C and ambient relative humidity (ca. 60%RH) in a Video-Based Contact Angle Meter model OCA 20 (DataPhysics Instruments GmbH, Filderstadt, Germany). Contact angle values were obtained by analyzing the shape of a distilled water drop after it had been placed over the film for 15 s. Image analyses were carried out by SCA20 software.

3.10 Optical properties

The transparency of the films was determined through the surface reflectance spectra in a spectrocolorimeter CM-3600d (Minolta Co., Tokyo, Japan) with a 10 mm illuminated sample area. Measurements were taken in duplicate for each sample by using both a white and a black background.

Film transparency was evaluated through the internal transmittance (T_i) (0-1, theoretical range) by applying the Kubelka-Munk theory for multiple scattering to the reflection data. Internal transmittance (T_i) of the films was quantified using Eq. (3). In this equation, R_0 is the reflectance of the film on an ideal black background. Parameters a and b were calculated by Eqs. (4) and (5), where R is the reflectance of the sample layer backed by a known reflectance R_g. Additionally, total color differences (ΔE) were calculated by Eq. (6) being L*a*b* the color attributes obtained by a D65 illuminator and a 10º observer.

$$T_i = \sqrt{(a - R_0)^2 - b^2} \tag{3}$$

$$a = \frac{1}{2}\cdot\left(R + \frac{R_0 - R + R_g}{R_0 R_g} \right) \tag{4}$$

$$b = (a^2 - 1)^{\frac{1}{2}} \tag{5}$$

$$\Delta E^* = \sqrt{(\Delta a^{*2}) + (\Delta b^{*2}) + (\Delta L^{*2})} \tag{6}$$

3.11 Mechanical properties

Tensile tests were carried out at ambient conditions of typically 24ºC and 50% RH on a Mecmesin MultiTest 1-i (1 kN) machine (Virginia, USA) with the Emperor™ software. Pre-conditioned

rectangular-shaped specimens with initial gauge length of 8 cm and 1 cm in width were cut directly from the films. A fixed crosshead rate of 10 mm/min was utilized in all cases. Elastic Modulus (E), Tensile Strength (TS), and Elongation at Break (EAB) were determined from the stress-strain curves, estimated from force–distance data obtained for the different films. At least, three specimens of each film were tensile tested as to obtain statistically meaningful results.

3.12 Statistics

All data have been represented as the average ± standard deviation. Different letters show significant differences both in tables and graphs ($p \leq 0.05$). Analysis of variance (ANOVA) followed by a Tukey-test were used when comparing more than two data sets.

4. Results and discussion

4.1 Extraction and characterization of lignocellulosic fractions from *Posidonia oceanica* residues

The extraction of lignocellulosic fractions from residues of *Posidonia oceanica* leaves using the sequential process described in section 2.1.2 was investigated. The raw biomass material was determined to contain 13 ± 2% ash, 18 ± 2% lignin and 59 ± 1% holocellulose. These values are similar to those previously reported for *Posidonia* leaves [16, 17]. The extraction yields for the different lignocellulosic fractions were estimated, being 77 ± 5% for F1, 53 ± 5% for F2 and 24 ± 3% for F3. These yields are quite consistent with the raw material composition and evidence the efficiency of the applied processes to sequentially purify lignocellulose, holocellulose and cellulose fractions. The obtained cellulose extraction yield is higher than the values reported for different seaweed species [18, 19], highlighting the potential of this aquatic biomass source for the production of pure cellulose.

To investigate the structural changes undergone by the material after each purification step and assess the progressive removal of cell wall components, FT-IR analyses were carried out and the results are shown in Figure 1A. As observed, several characteristic bands which appear in the raw biomass are progressively removed after the applied extraction processes. The first clear observation is that the raw the *Posidonia* biomass showed two peaks located at 2918 and 2850 cm^{-1}, corresponding to the CH_2 asymmetrical and symmetrical stretching usually displayed in fatty acids [20], which were absent in the material after the Soxhlet treatment. This confirms the removal of lipidic compounds after this first purification step. It is also worth noting that the band centered at 1729 cm^{-1}, corresponding to the esters and acetyl groups from hemicelluloses and lignin [21], which is overlapped with the one corresponding to bound water (located at ca. 1630 cm^{-1}) in the spectrum from the raw material, becomes visible in the F1 fraction. The intensity of

this band was gradually reduced with the applied treatments and it was absent in the spectrum from the F3 fraction, confirming the fact that pure cellulose was obtained. The spectra from F3 was similar to those reported in the literature [12, 22, 23] for cellulose extracted from other resources, with characteristic bands such as those located at 1430, 1375 and 1318 cm^{-1} corresponding to CH_2 scissoring, C-H bending and CH_2 rocking, respectively [20], and the bands at 1165, 1061 and 1034 cm^{-1}, which as seen also in other carbohydrates arise from highly coupled modes corresponding to C-C, C-O, C-H stretching and C-OH bending modes [24-26].

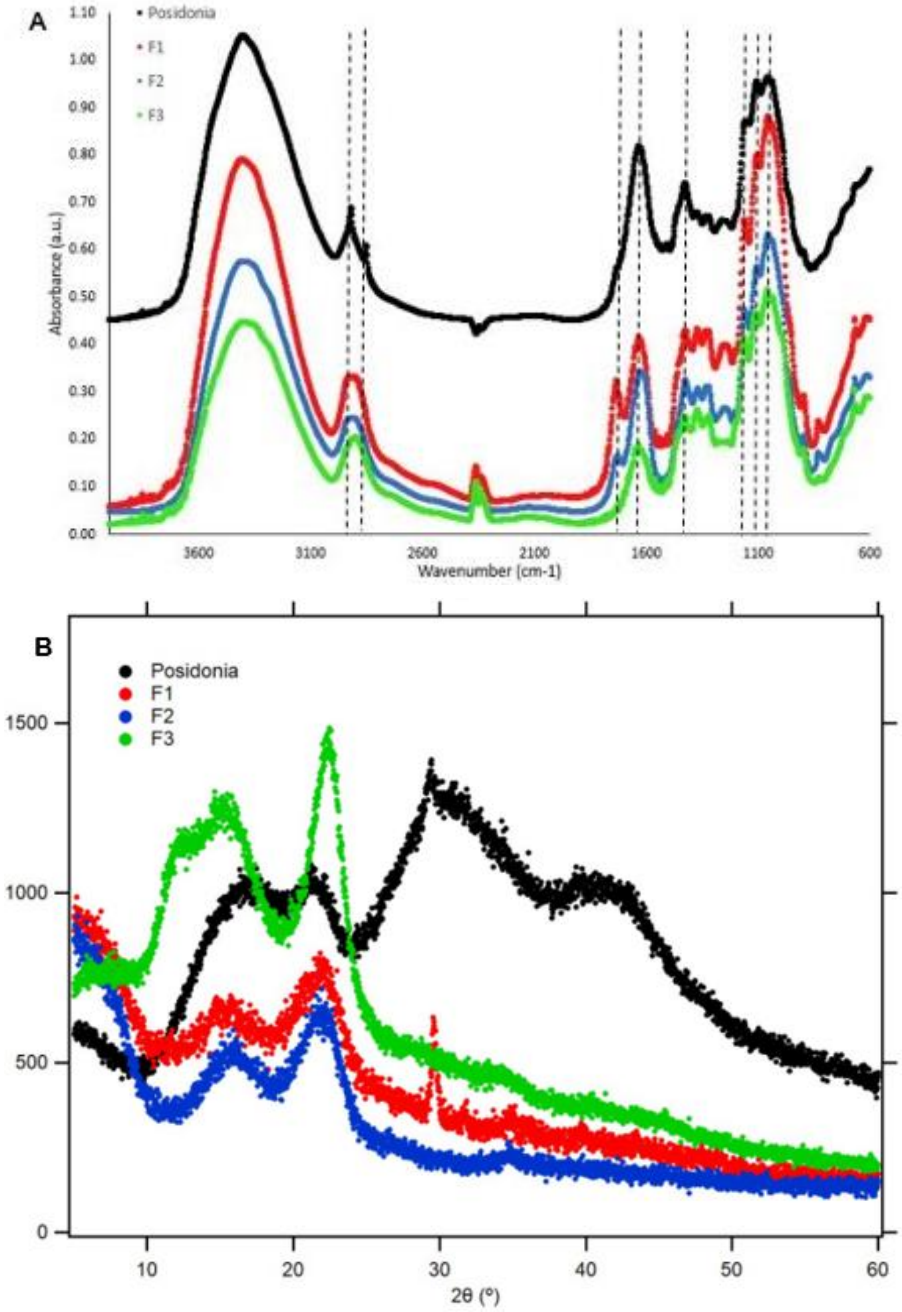

Figure 1. (A) FT-IR spectra of the residue from *Posidonia* leaves and the extracted lignocellulosic fractions. The most characteristic bands are marked by discontinuous lines. The spectrum from *Posidonia* has been offset for clarity. (B) XRD patterns of the freeze-dried samples.

Cellulose is the crystalline component providing integrity in plant cell walls, while components such as hemicelluloses and lignin provide an amorphous matrix to adapt the plant tissue properties to their specific requirements [27]. Thus, the progressive removal of lignin and hemicelluloses from the biomass is expected to yield a material with increased crystallinity. To corroborate this, the XRD patterns of the raw *Posidonia* biomass and the different lignocellulosic fractions were collected, and the results are displayed in Figure 1B. The first clear observation is that the shape of the diffraction patterns was strongly affected by the purification processes. All the samples presented the three diffraction peaks located at ca. $2\theta = 15.0°$, 16.6° and 22.7°, corresponding to the (1-10), (110) and (200) crystalline planes from the cellulose I_β crystalline allomorph [28-30]. However, the relative intensity of these peaks was very weak in the case of the native *Posidonia* biomass (where the first two peaks were completely overlapped) and the F2 and F3 fractions. Furthermore, the *Posidonia* and the F1 samples presented a peak located at $2\theta = 29.1°$, which disappears after the purification treatment with sodium chlorite. This peak has been detected in the XRD patterns from residual lignin and was seen to disappear upon thermal treatment at temperatures higher than 600ºC [31] , when lignin thermal degradation takes place (see TGA results, Figure 2).

The estimated crystallinity index and crystallite cross-sectional dimensions are summarized in Table 1. As observed, upon applying the purification steps and gradually removing the amorphous components, more crystalline materials were obtained, reaching a final value of 51.4% crystallinity for the F3 fraction (i.e. pure cellulose). This value is slightly higher than that previously reported for cellulose extracted from *Posidonia* leaves [16] and very similar to the value obtained from other marine sources such as the algae *Gelidium elegans* (X_C~51%) [19], while lower than that from plant vegetal resources such as cotton (X_C~68%) or flax (X_C~70%) [32]. The dimensions of the crystalline/paracrystalline regions, especially those in the direction perpendicular to the well-resolved (200) peak, also increased with the purification processes, which is a consequence of the removal of amorphous cell wall matrix components.

Table 1. Crystallinity index (X_C) and cross-sectional dimensions of crystallite sizes in the direction perpendicular to the (1-10), (110) and (200) planes ($D_{(1\text{–}10)}$, $D_{(110)}$ and $D_{(200)}$), determined from the XRD patterns.

	Posidonia	**F1**	**F2**	**F3**
X_C (%)	17.3	39.1	34.8	51.4
$D_{1\text{-}10}$ (nm)	---	2.7	2.2	3.0
D_{110} (nm)	---	2.3	2.6	1.9
D_{200} (nm)	2.6	3.1	3.1	4.1

Additionally, TGA characterization was carried out in order to determine the thermal stability of the raw *Posidonia* biomass and the extracted lignocellulosic fractions. The obtained derivative thermogravimetric profiles are displayed in Figure 2. The results evidence that the thermal stability of the different materials was related to their degree of purity and crystallinity, being the F3 the most thermally stable fraction, whereas the native *Posidonia* biomass was the most thermally unstable. While F3 presented a one-step degradation profile, the other materials exhibited multiple-step degradation processes. It should be noted that all the fractions presented a small peak at ca. 90-100ºC corresponding to the evaporation of the water held by the materials. The degradation process taking place at temperatures between 290 and 350ºC, which was detected in all the samples, has been ascribed to cellulose degradation processes such as depolymerization, dehydration and decomposition of glycosyl units [33-35]. The associated peak became sharper and shifted towards higher temperatures as the cell wall matrix components were removed and the cellulose was purified. F1 presented a second degradation step, occurring at temperatures between 400 and 460ºC, which has been previously attributed to the degradation of lignin [36-38]. Interestingly, after removing lignin from the material (obtaining F2), an additional peak appeared at around 260ºC. This peak might correspond to the degradation of hemicelluloses, which must have been released from the complex network provided by lignin after the sodium chlorite treatment. Finally, the F3 fraction mainly presented a narrow and defined peak corresponding to the degradation of cellulose at around 334ºC. Thus, the TGA results confirm, together with the FT-IR characterization (cf. Figure 1A) that the purification process yielded pure cellulose with a high thermal stability, partly due to its relatively high crystallinity index. Another important implication is that the native *Posidonia* biomass as well as all the extracted fractions are thermally resistant enough to undergo the temperatures typically applied during the processing of polymeric materials such as starch without suffering thermal degradation.

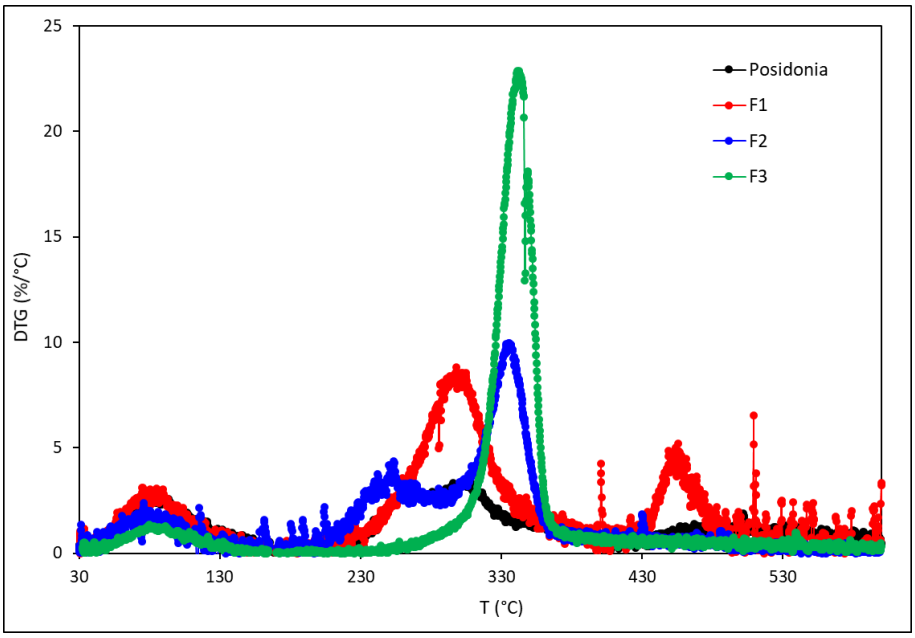

Figure 2. Derivative thermogravimetric (DTG) curves of residues from *Posidonia* leaves and the extracted lignocellulosic fractions.

4.2 Development of pure lignocellulosic films

As previously mentioned, one of the aims of this work was to evaluate the suitability of the obtained *Posidonia* lignocellulosic fractions to develop biopolymeric materials for packaging applications. For this purpose, the different fractions were initially used to generate pure films by means of vacuum filtration and the properties of the obtained materials were investigated.

Optical properties (including transparency and color) are important attributes in packaging, especially in the case of food packaging, which is the intended application of the materials developed in this work. As show in Figure S1A, the visual aspect of the obtained films was substantially different depending on the fraction utilized and it is evident that the transparency increased along the purification process. While the F1 film appeared completely opaque and showed a brownish coloration, the F2 and F3 films were translucent and presented no evident coloration. The transparency was also quantitatively assessed by means of internal transmittance (Ti) measurements. As show in Figure S1B, the internal transmittance markedly increased as the lignin and hemicelluloses were removed from the material, with the pure cellulose film (F3) being the most transparent of all. Additionally, color differences (ΔE) between the three different films were assessed. F1 presented the highest values according to its brown tonality (ΔE_{F1-F3} = 42.58 and ΔE_{F1-F2} = 31.91) although F2 and F3 were also significantly different between them (ΔE_{F2-F3} = 10.96).

The morphology of the cryo-fractured cross-sections of the films was analyzed by SEM. As evidenced in Figures S1C, S1D and S1E, the F3 film presented the most compact and uniform morphology. This is due to the presence of amorphous components in the F1 and F2 fractions which are interspaced with the cellulose microfibrils and prevent the formation of a densely packed structure upon drying.

The mechanical performance of the different films was assessed by tensile testing and the calculated values for the Young's modulus (E), tensile strength and elongation at break (ε_b) are summarized in Table 2. As observed from the results presented in Table 2, the three parameters were significantly improved when purifying the cellulose fraction. The F1 film presented very poor mechanical performance and it was not possible to determine its properties since it broke down very quickly. In contrast, the mechanical properties of the F3 film in terms of tensile strength and elongation at break outperformed those reported for other biomass-derived cellulosic materials such as microfibrillated cellulose (MFC) extracted from carrot [39]. The increased Young's modulus and tensile strength, indicative of greater stiffness, can be related to the higher crystallinity of F3 as compared with F2 (cf. Table 1). Interestingly, the F3 film also presented greater elongation at break than F2, indicating that the materials also became more ductile with the purification of cellulose. The poorer mechanical performance of the F1 and F2 films may also be explained by the greater difficulty in obtaining homogeneous aqueous dispersions from these fractions due to the presence of cell wall matrix components interacting with the cellulose hydroxyl groups which thus hindered their accessibility to water molecules [14]. It is worth highlighting the fact that the F3 film presented superior mechanical properties than a benchmark biopolymer such as corn starch (cf. Table 3).

Table 2. Mechanical properties (Young's modulus, tensile strength and elongation at break) from the lignocellulosic films.

	E (MPa)	**Tensile Strength (MPa)**	**ε_b (%)**
F1	---	---	---
F2	771.5 ± 46.4^{a}	4.6 ± 0.1^{a}	1.1 ± 0.3^{a}
F3	4260.2 ± 416.2^{b}	45.9 ± 6.9^{b}	2.1 ± 0.4^{b}

Values in the same column followed by different letters are significantly different ($p \leq 0.05$).

Water vapour permeability (WVP) of the films was also measured and the obtained results are shown in Figure 3A. The results evidence that the permeability of the films strongly decreased as the produced fractions were progressively purified, with a 74% and 91% WVP decrease for the F2 and F3 films, respectively with regards to the F1 film. This may be a consequence of the more densely packed structure attained with the F3 fraction (cf. Figure 3E) and its higher crystallinity index (cf. Table 1), hence blocking the transport of water vapour through the film more efficiently. The WPV value for the F3 film ($1.25 \cdot 10^{-13}$ Kg·m/s·m^2·Pa) is even lower than those reported for films from regenerated cellulose and nanocellulose (ca. $2.5 \cdot 10^{-13}$ Kg·m/s·m^2·Pa, measured at >25%RH) [40] and for corn starch ($2.59 \cdot 10^{-13}$ Kg·m/s·m^2·Pa, cf. Figure 4), highlighting the promising properties of the generated material in terms of water vapour barrier.

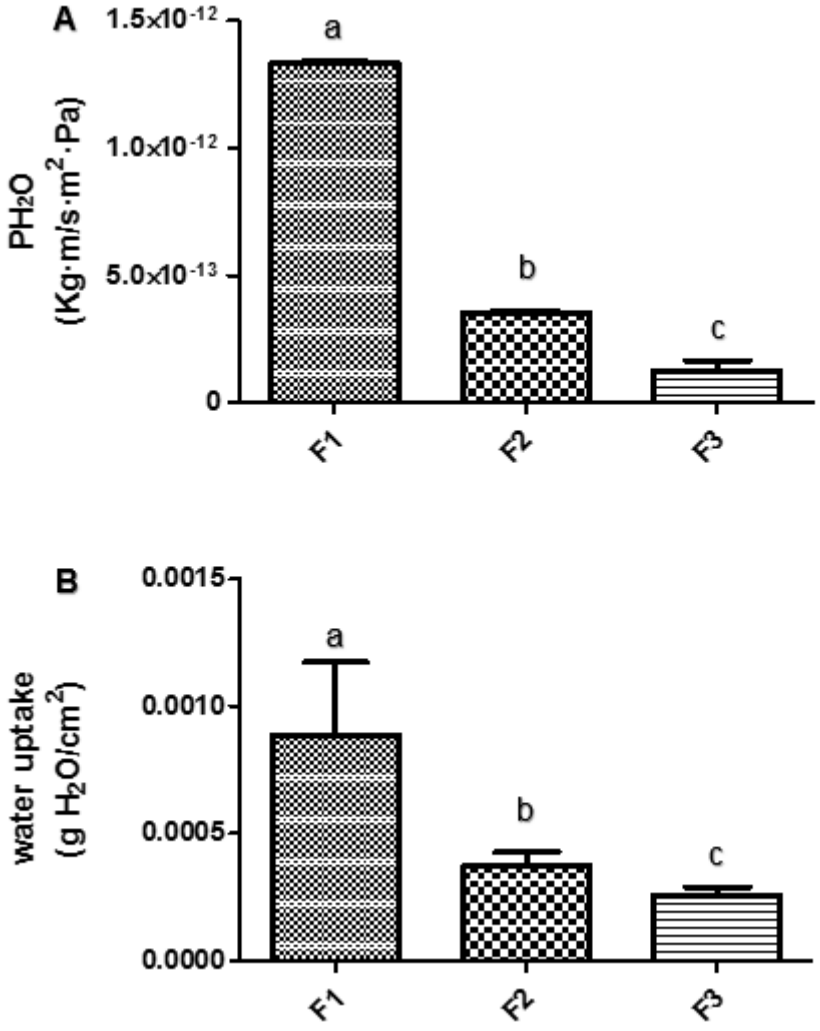

Figure 3. (A) Water vapor permeability and (B) water sorption for the pure lignocellulosic films. Values followed by different letters are significantly different ($p \leq 0.05$).

As water permeability is due to the combination of sorption and diffusion phenomena, the susceptibility of the different materials to sorb water was evaluated through gravimetrical tests and the results, expressed as weight gain per exposed film surface area, are displayed in Figure 3B. As observed in the graph, the F1 film presented the highest water sorption value, suggesting that this material presented the most hygroscopic behavior. On the contrary, F3 presented the lowest water uptake value. This is again related to the more crystalline structure of F3 (since crystalline regions are less accessible to moisture), but may also be explained by the strong self-association of cellulose microfibrils upon drying, thus limiting the amount of free hydroxyl groups available for water to interact with the cellulose composing the film [41].

4.3 Development of starch films loaded with lignocellulosic fractions

After characterizing the different extracted fractions and the pure films, the next step was to incorporate the lignocellulosic additives into starch matrices to produce composite films. The aim was to reduce the amount of starch while improving the properties of the obtained materials. Corn starch films containing 10 wt.-% of lignocellulosic additives were produced by means of the melt compounding method followed by compression molding and the properties of the obtained materials were evaluated. The additive concentration was selected based on previous tests performed on corn starch films with cellulosic additives, which presented optimum properties with loadings close to 10 wt.-% [42].

The effect of the incorporation of the lignocellulosic additives on the transparency of the starch films was evaluated through their transmittance values, (cf. Figure S2). It can be observed that while the addition of F1 caused a remarkable decrease in the transmittance (i.e. the transparency of the pure starch film was reduced), F2 and F3 fractions had a minor impact on film transparency. Additionally, the total color differences (ΔE) between the three different composite films and the control starch film, were measured. The results ($\Delta E_{F1\text{-}Starch} = 43.15$, $\Delta E_{F2\text{-}Starch} = 12.10$ and $\Delta E_{F3\text{-}Starch} = 16.25$), indicate that the film containing F1 presented the highest color difference due to its brown tonality.

The morphology of the pure starch and composite films as well as the degree of dispersion of the incorporated fractions were analyzed by observation of the films' cryo-fractured cross-sections by means of SEM. As observed in the representative micrographs shown in Figure S3, the presence of the lignocellulosic fractions was patent in all the composite materials, which showed large particles evenly distributed across the whole cross-sections, as opposed to the smooth surface observed in the control starch film. Although the size of the aggregates seemed to be smaller for the film containing F3 (i.e. pure cellulose), a proper filler dispersion was not attained

for any of the samples, which is a consequence of the strong self-aggregation phenomena typically undergone by lignocellulosic materials when present in the dry state [43].

Mechanical properties of the pure starch and the three composites were evaluated, and the results are summarized in Table 3. From the results it was observed that the incorporation of F1 and F2 fractions did not significantly improve the mechanical properties of starch and, moreover, the elongation at break was reduced. This indicates that the materials became less ductile with the addition of those two lignocellulosic additives, just as it had been previously described for PLA films loaded with cellulose nanocrystals extracted from *Posidonia* [44]. This effect might be a consequence of the presence of large and stiff particles of lignocellulosic additives, disrupting the starch matrix and impairing the plastic mechanical performance of the material. In contrast, the addition of F3 significantly increased the elastic modulus (85% increase with regards to the pure starch), while the elongation at break was not further reduced if compared to the composite containing F2. It is also evident from the results that, as the cellulose was sequentially purified, the additives conferred better mechanical properties (i.e. higher elastic modulus, tensile strength and elongation at break) when incorporated into starch. Therefore, F3 was the best additive in terms of mechanical performance. Although direct comparisons with other works are not straightforward given the variability in properties derived from starch source and processing conditions, our results are rather promising as significant relative improvements have been observed when compared with previous works. For instance, F3 films presented a lower decrease in elongation at break than composite starch films loaded with 3% (dry weight) cellulose nanocrystals from sugarcane bagasse (33% vs. 79% drop) [45] without a significant improvement of tensile strength values (Table 3).

Table 3. Mechanical properties (Young's modulus, tensile strength and elongation at break) from the pure starch and composite films.

	E (MPa)	**Tensile Strength (MPa)**	**ε_b (%)**
Starch	1039.8 ± 88.0^{b}	12.8 ± 1.2^{b}	2.1 ± 0.2^{a}
10% F1	1120.9 ± 132.0^{b}	6.0 ± 2.7^{c}	0.9 ± 0.2^{c}
10% F2	1233.7 ± 79.4^{b}	11.2 ± 2.8^{bc}	1.4 ± 0.2^{b}
10% F3	1919.9 ± 96.1^{a}	17.7 ± 1.1^{a}	1.4 ± 0.2^{b}

Values in the same column followed by different letters are significantly different ($p \leq 0.05$).

WVP was also measured and the results are shown in Figure 4A. Incorporation of the three types of lignocellulosic additives led to improved water vapor permeability when compared to the control starch film (ca. 39%, 38% and 43% WVP drop with the incorporation of F1, F2 and F3, respectively), with no significant differences between them. This marked decrease in the WVP might be due to a combination of factors: (i) the incorporation of fillers with a more hydrophobic behavior than the native starch and (ii) a decrease in the hydroxyl groups available for interacting with water as a consequence of strong intermolecular hydrogen bonds established between starch and the lignocellulosic materials [46]. Similar WVP reductions (ca. 52%, measured at 100%RH) have been reported for corn starch films loaded with 10% and 20% bacterial cellulose nanowhiskers [42]. Therefore, and from a cost perspective, F1 would be the best additive choice in terms of WVP properties, since it leads to optimum barrier enhancement with a minimal number of processing steps.

Water sorption and contact angle measurements were additionally carried out to evaluate the effect of the different lignocellulosic fractions on the water affinity of the films. From the water sorption results (cf. Figure 4B) it is clear that the addition of the lignocellulosic fractions led to a decrease in the water uptake, having a maximum drop of ca. 44% with the addition of pure cellulose. The more hydrophobic behavior of the 10% F3 film was also confirmed by the contact angle measurements (cf. Figure 4C). The calculated contact angle tended to increase (i.e. the materials became more hydrophobic) with the progressive purification of the added fractions (cf. Figure S3). However, only the 10% F3 film presented a significant increase of the contact angle (65º) as compared with the pure starch (47º). These results suggest that the pure cellulose presents a more hydrophobic behavior than the unpurified fractions, according to its greater crystallinity and strong self-association, as supported by the water permeability and water sorption results previously obtained for the pure films.

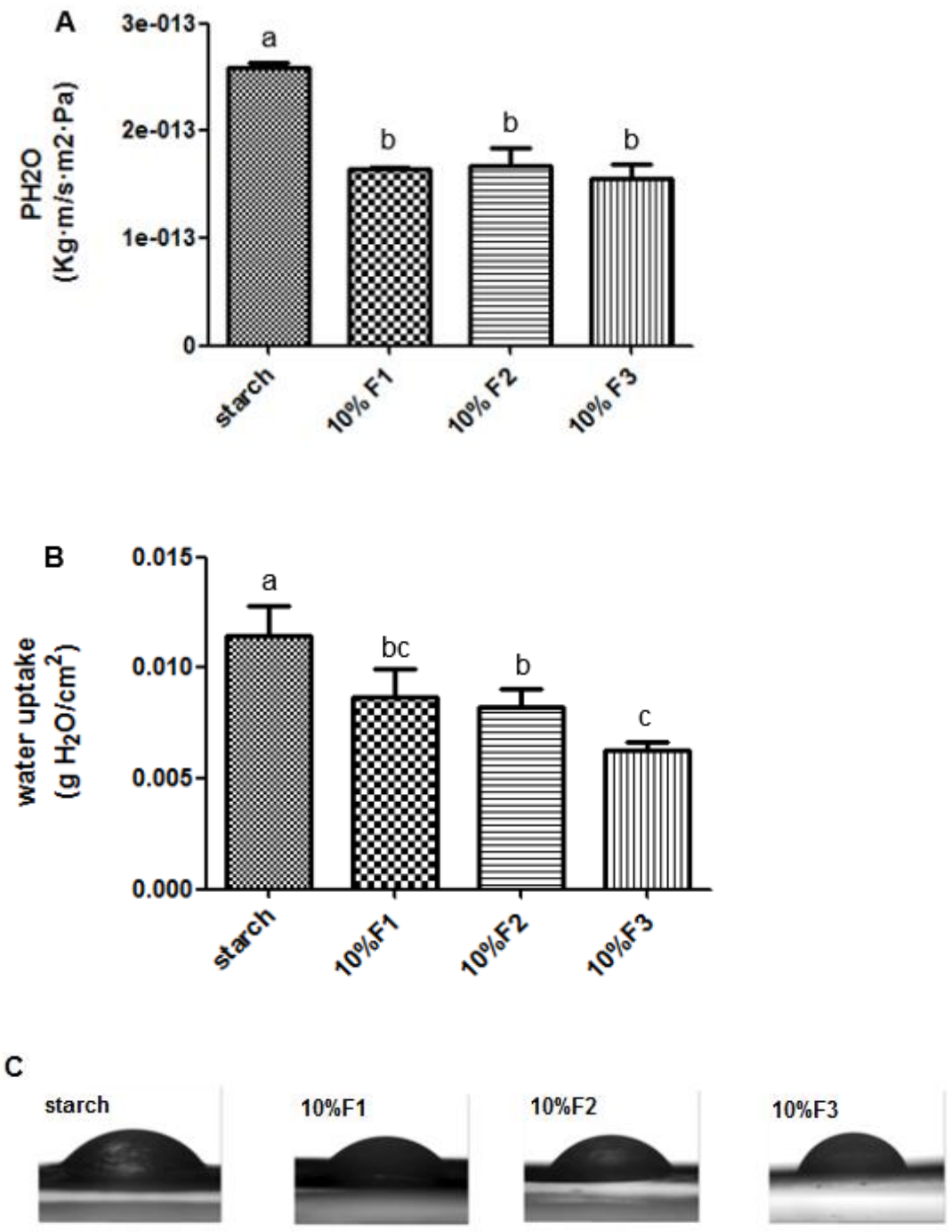

Figure 4. (A) Water vapor permeability and (B) water uptake of the pure starch and composite films. Values followed by different letters are significantly different ($p \leq 0.05$). (C) Images of water drops taken on the different film surfaces.

The fact that F3 was not able to reduce the water permeability of starch to a greater extent than the F1 and F2 fractions, despite its more hydrophobic behavior, might be related to a different effect of the lignin, the hemicelluloses and the cellulose on the gelatinization and retrogradation

processes undergone by starch during the melt mixing processing and subsequent storage of the films. To investigate the structure of the different materials, X-ray scattering experiments were carried out and the obtained WAXS and SAXS patterns are shown in Figures 5A and 5B, respectively. From the WAXS patterns (cf. Figure 5A) it can be observed that the corn starch presented a V-type crystalline structure, in particular, the V_H type. This transition from the original A-type structure in corn starch to the V-type structure has been previously reported to take place as a result of the melt mixing process at temperatures lower than 180ºC and relatively high-water contents [13] The calculated crystallinity values were 26.2 ± 0.1% for the pure starch, 33.0 ± 0.1% for the film loaded with 10% F1, 28.8 ± 0.1% for the 10% F2 composite and 31.1 ± 0.1% for the 10% F3 composite. Thus, the incorporation of the lignocellulosic fractions led to a slight increase on the crystallinity of the films, being this effect similar for the three fractions in spite of the higher crystallinity of the pure cellulose (i.e. F3). As observed in Figure 5B, the SAXS patterns from the pure starch and composite films display a broad shoulder which is centred at ca. 0.06 $Å^{-1}$, corresponding to a real distance of *ca*. 10.5 nm. This scattering feature has been previously reported for extruded starches and is characteristic of the heterogeneous semicrystalline structure into which starch re-organises after the extrusion process [13, 47, 48]. Within the low q region, the intensity presents a power-law behaviour, with an exponent of ca. -1.5 for pure starch. This value is much lower than those typically reported for native starches (ranging from ca. -4 to -3 [47, 48], reflecting the disruption of the starch lamellar structure during extrusion. Higher power-law exponents of -3.7, -2.8 and -2.7 are observed for the 10% F1, 10% F2 and 10% F3 films, respectively. The lower deviation of the composite films from the -4 slope (corresponding to Porod's ideal two-phase system) may be indicative of an effect of the lignocellulosic fractions, especially the less purified F1 fraction, in preventing to some extent the disruption of the starch lamellar structures. This hypothesis is supported by the greater crystallinity values estimated for the composite films and may explain the water permeability results. The impurities present in the F1 fraction seem to preserve the structure of starch during the melt mixing process to a higher extent than the pure cellulose. The more ordered structure in the 10% F1 sample is expected to result in a lower diffusion of water vapour molecules through the film, hence leading to permeability reductions greater than expected.

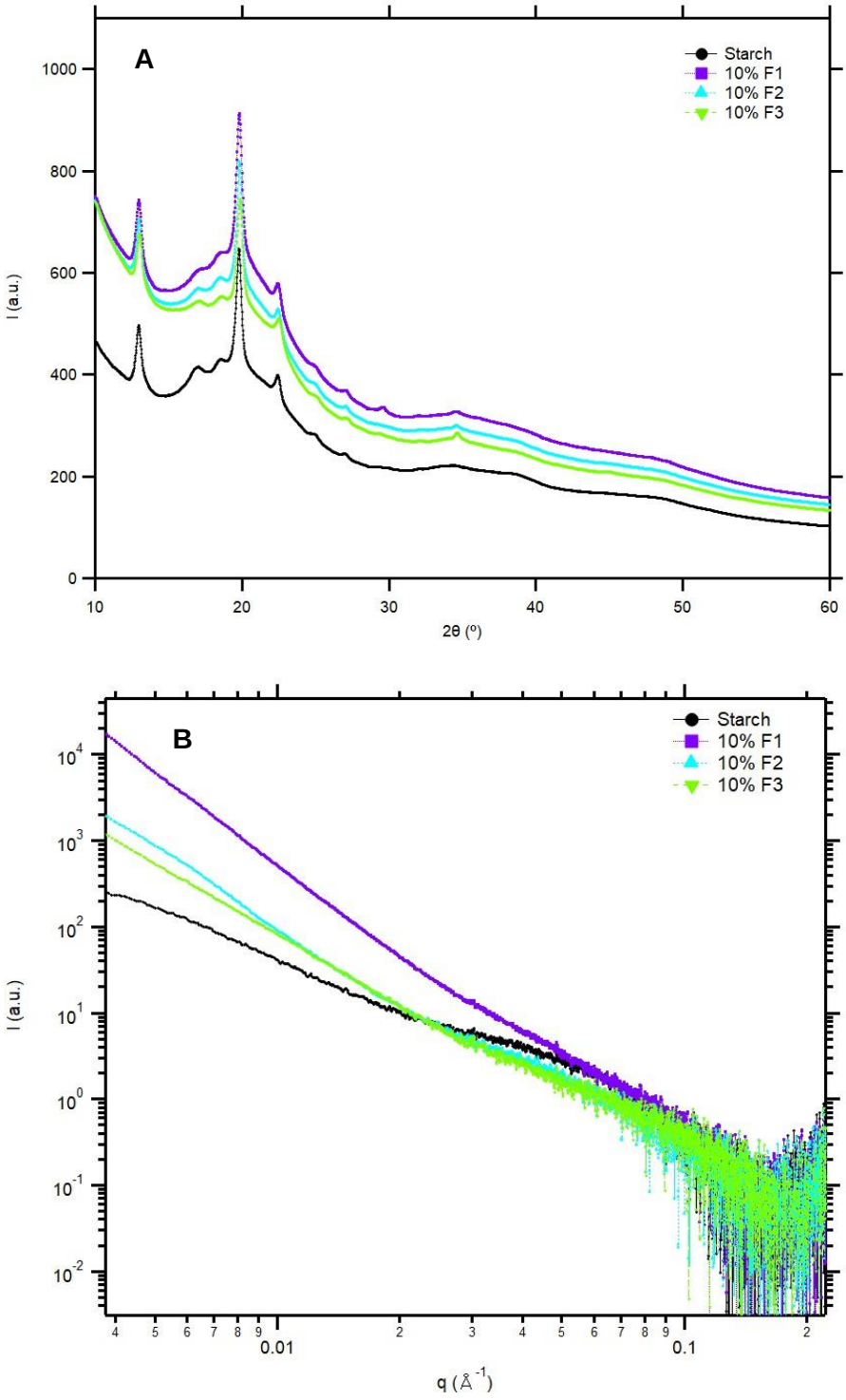

Figure 5. (A) WAXS and (B) SAXS patterns of the pure starch and its composite films.

5. Conclusions

Three different lignocellulosic fractions (F1, F2 and F3) were obtained from the residues of *Posidonia oceanica* leaves by sequentially removing cell wall components. The applied extraction treatments proved to be efficient in removing components such as lignin and hemicelluloses, obtaining a final fraction F3 with a yield of ca. 24%, which consisted of pure cellulose. The crystallinity and thermal stability of the lignocellulosic fractions increased progressively with the extraction processes, obtaining pure cellulose with a crystallinity index of ca. 51% and thermally stable at temperatures above 250ºC. The three lignocellulosic fractions were subsequently utilized either as base materials or as additives to generate films.

The removal of the lignin and hemicellulose components yielded a consistent improvement in the transparency, mechanical and water vapor barrier properties of the lignocellulosic films. The obtained pure cellulose film presented promising properties for its application in food packaging, showing better mechanical and water barrier performance than a commercial corn starch film.

Regarding the composite starch films prepared by melt mixing, incorporation of 10 wt.-% of the three lignocellulosic additives led to a 30-40% drop in the water vapor permeability with respect to the control starch. In terms of mechanical performance, the addition of pure cellulose was optimal since it was able to increase the stiffness of the material (with an increase of ca. 85% in the elastic modulus) while preventing an excessive reduction of its ductility.

These results demonstrate the potential of lignocellulosic fractions extracted from residues of *Posidonia* leaves for the development of sustainable bio-based materials for food packaging applications, while giving an added value to unutilized waste material, either by producing pure lignocellulosic films with superior mechanical and water barrier performance or by using them as additives to produce starch composite films with improved properties.

6. Supplementary Material

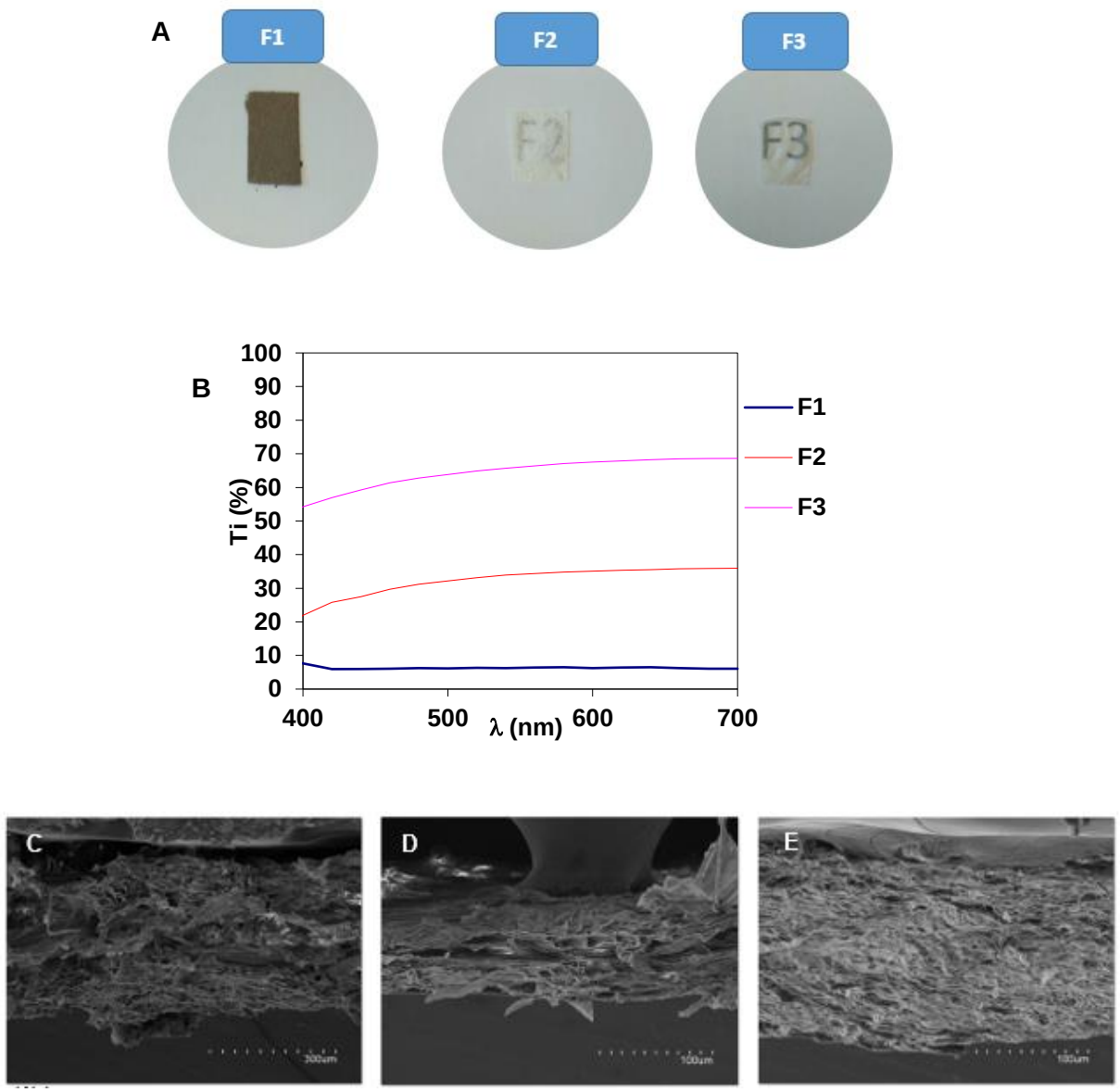

Figure S1. (A) Visual aspect and (B) spectral distribution of internal transmittance (Ti) of the lignocellulosic films. SEM images from the cryo-fractured cross-sections of the lignocellulosic films: (C) F1 film, (D) F2 film and (E) F3 film. Scale markers correspond to 300µm (C) and 100µm (D and E).

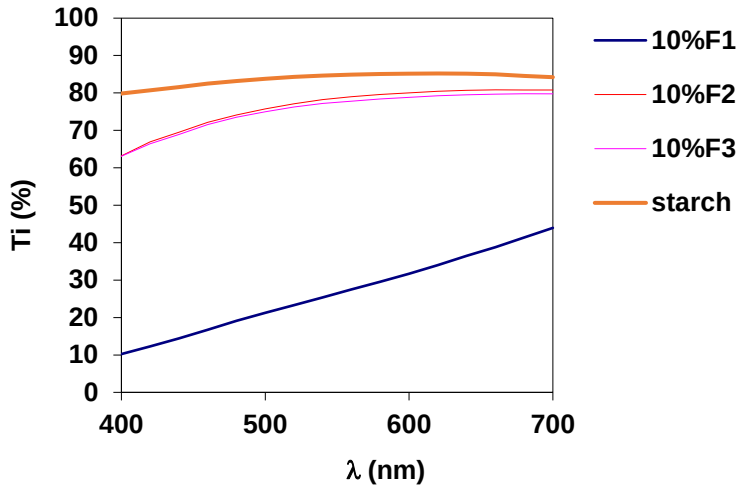

Figure S2. Spectral distribution of internal transmittance (Ti) of the pure corn starch and composite films.

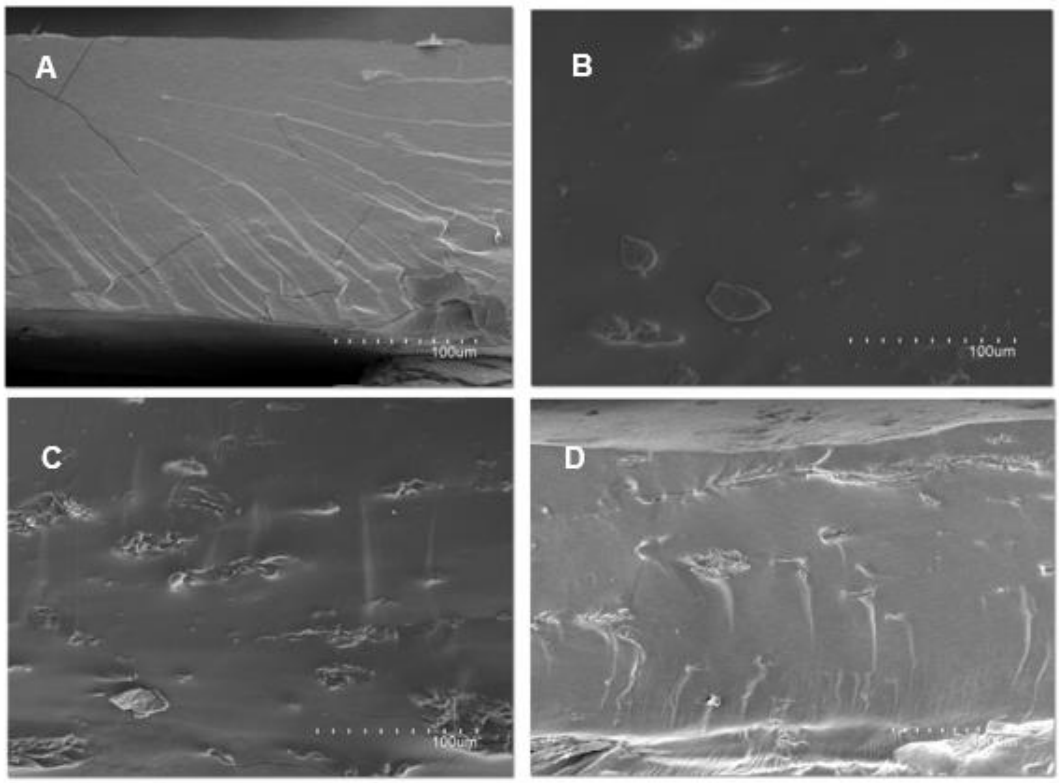

Figure S3. SEM images of the cryo-fractured sections from the corn starch film (A), 10% F1 (B), 10% F2 (C) and 10% F3 (D). Scale markers correspond to 100 µm.

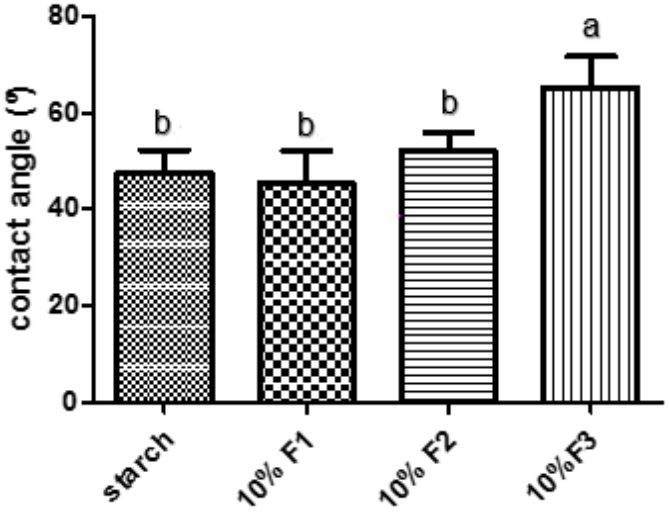

Figure S4. Contact angle values for the pure corn starch and composite films. Values in the same column followed by different letters are significantly different ($p \leq 0.05$).

1.2. Cellulose nanocrystal-based films produced by more sustainable extraction protocols from Posidonia oceanica waste biomass

This section is an adapted version of the following published research article:

Benito-González, I., López-Rubio, A., Gavara. R & Martínez-Sanz, M. (2019). Cellulose nanocrystal-based films produced by more sustainable extraction protocols from *Posidonia oceanica* waste biomass. Cellulose, 26, 8007-8024. DOI: https://doi.org/10.1007/s10570-019-02641-4

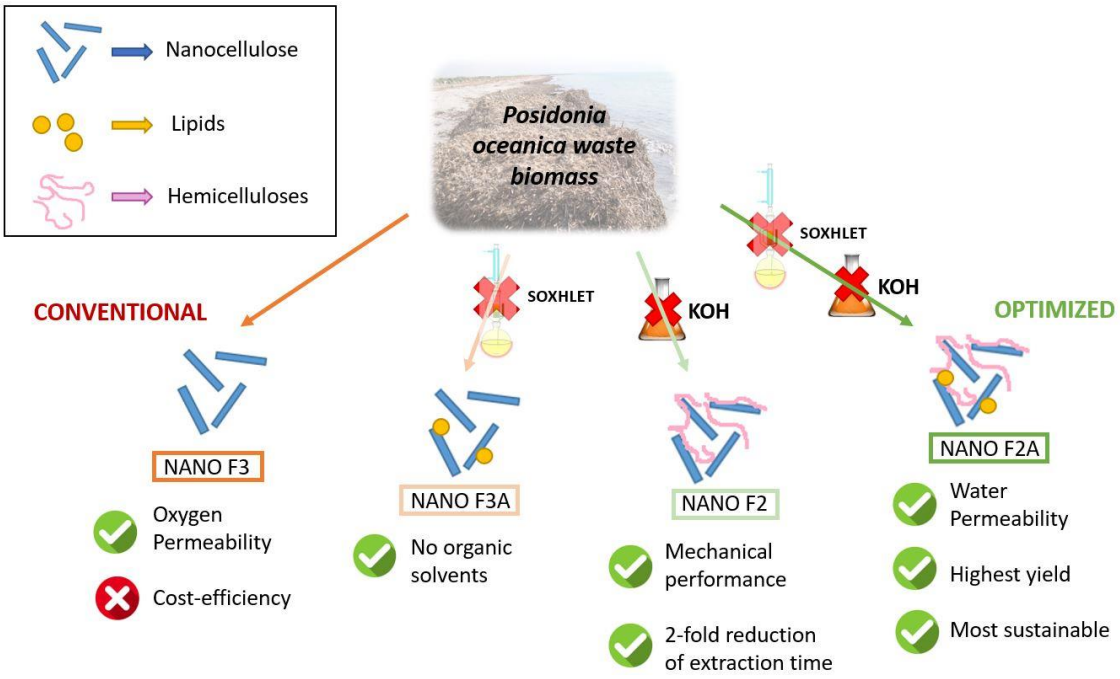

1. Abstract

Simplified extraction procedures (avoiding Soxhlet treatment and/or hemicellulose removal) were evaluated to valorize waste biomass from *Posidonia oceanica* leaves, obtaining cellulosic fractions and nanocrystals, which were subsequently used to produce films from their aqueous suspensions. Cellulose purification significantly improved mechanical and barrier properties of the films obtained from the fractions, while the extracted nanocrystals yielded films with remarkably improved properties, outperforming most benchmark biopolymers. The lipids initially present in the fractions without Soxhlet treatment were not completely digested by the hydrolysis treatment, having a positive impact on the water vapor permeability of the films (up to 63% drop), although negatively impacting oxygen permeability (increased by 20–30-fold). On the contrary, some hemicelluloses present in the less purified fractions, strongly interacting with cellulose, remained in the extracted nanocrystals leading to enhanced mechanical properties (45% higher tensile strength and 2-fold increase in the elongation at break), but lower water barrier (up to 70% higher permeability than the pure cellulose nanocrystals) due to their hydrophilic character. Films produced from the less purified nanocrystals showed the best compromise between mechanical and barrier performance, while offering a great advantage in terms of sustainability and reduced costs.

2. Introduction

Petroleum-based plastics have been extensively used during the last decades within the food packaging area because of their low-cost, good processability and tailored barrier and mechanical performance. However, besides the sustainability issues derived from the use of fossil fuels, the large amounts of waste generated as a result of their disposal derive in a severe environmental impact, since conventional plastics can take thousands of years to degrade, endangering terrestrial and aquatic ecosystems. Although recycling strategies contribute to palliate this problem, they are far from providing a long-term sustainable solution. As an alternative to petroleum-based plastics, biodegradable polymers derived from renewable resources, i.e. biopolymers, have been developed during the last years. Nevertheless, most biopolymers present significant drawbacks when compared to benchmark synthetic polymers, such as lower barrier and mechanical performance, as well as higher production costs. Furthermore, most of the starting raw materials are vegetable sources, whose utilization for the production of biopolymers competes with their primary use as food sources. In this context, the valorization of aquatic biomass, such as algae and aquatic plants, available in large quantities, represents an efficient alternative to the use of land biomass. These sources have been reported to contain large amounts of carbohydrates, which could be interesting for the development of bio-based plastics [18, 49-51].

In particular, *Posidonia oceanica*, one of the most abundant aquatic plant species in the Mediterranean Sea, has been demonstrated to be an optimum source for the extraction of cellulose and lignocellulosic fractions with promising properties for the development of cellulose-based packaging materials or to be used as fillers to enhance the properties of other biopolymers [10, 16, 50, 52]. During its lifecycle, *Posidonia* leaves detach off the stems and are transported towards the sea shores by marine currents, giving rise to a residue that affects the quality of the beaches [5] and generating costs to local authorities associated to its collection and disposal to landfills. Therefore, the utilization of this residue for the extraction of lignocellulosic materials would be particularly interesting and in line with circular economy policies.

Although cellulose itself has interesting properties for food packaging applications, its treatment by acid hydrolysis digests the amorphous domains, yielding highly crystalline nanocellulose or cellulose nanocrystals [16, 19]. These nanocrystals feature an attractive combination of properties such as biocompatibility, large specific surface area and aspect ratio, high elastic modulus, high thermal stability and excellent optical transparency [53], which have been exploited to improve the properties of other biopolymer matrices, such as poly(lactic acid) (PLA) [10, 54], polyhydroxyalkanoates (PHAs) [55, 56], polyisoprene [57] and pea starch [58]. Besides their utilization as nanofillers, cellulose nanocrystals themselves can be used to produce high-barrier films [59], although this approach has not been fully explored to date.

Despite most of the works available on the literature focus on achieving a complete purification of cellulose from its raw source, it has been recently reported that less purified lignocellulosic fractions may also possess interesting properties for their use in packaging materials [50, 51]. Using less purification steps to generate these fractions allows reducing the energy and time consumption, minimizing the economic gap between biopolymers and conventional fossil-fuel derived plastics.

In this work, the waste biomass from *Posidonia oceanica* leaves has been valorized as a natural source of cellulosic fractions and nanocrystals extracted by acid hydrolysis, while exploring the possibility of suppressing processing steps on the purification process. Aqueous suspensions from the different fractions and nanocrystals have been used to generate films and their structural and functional properties have been characterized to select the most promising materials for food packaging applications, while minimizing the processing steps to achieve more sustainable and economically viable materials. Our hypothesis is that reducing the purification steps may not only diminish the production costs and environmental impact, but also yield novel high-performance cellulose-based biopolymeric films able to replace petroleum-based polymers in food packaging.

3. Materials and methods

3.1 Raw materials

Posidonia oceanica leaf biomass was gathered from coastal areas in the Mediterranean sea, as reported in [50]. The composition of the raw biomass, obtained from previous analyses, is shown in Figure 1.

3.2 Preparation of cellulosic fractions

A purification procedure described in previous work [12, 50] was carried out to sequentially remove cell wall components and obtain pure cellulose. The general protocol, as well as the specific process parameters, are schematically shown in Figure 1. Briefly, this process consisted of an initial Soxhlet extraction to remove pigments and lipids, followed by a treatment with $NaClO_2$ to remove lignin (yielding F2 fraction) and a final alkaline treatment with KOH to remove the hemicelluloses (yielding F3 fraction). The possibility of suppressing the initial Soxhlet treatment was also evaluated, obtaining two additional fractions, one after treating the biomass with $NaClO_2$ (referred to as F2A) and another fraction after the treatment with KOH (designated as F3A). All the fractions (F2, F2A, F3 and F3A) were obtained as a partially hydrated gel-like material that was stored in the refrigerator until further use.

3.3 Preparation of cellulosic nanocrystals

The cellulosic fractions were used as starting materials for the production of nanocrystals by means of acid hydrolysis (cf. Figure 1). An optimized method, previously applied for the extraction of cellulose nanocrystals from bacterial cellulose [60], with some minor modifications, was applied. Briefly, the gel-like lignocellulosic fractions were immersed in a H_2SO_4 solution (30%w/w), with a ratio of 1.5 g dry fraction/100 mL H_2SO_4, at 50ºC and stirred for 1.5 hours. After that, the material was subjected to several centrifugation and washing cycles to remove the acid and the pH was adjusted to 7 with NaOH. The obtained nanocrystals (labelled as NANO F2, NANO F2A, NANO F3 and NANO F3A, depending on the fraction used as the starting material) were stored in the fridge as partially hydrated gel-like materials, until further use.

3.4 Production of cellulosic films

Cellulosic films were produced by dispersing 0.25-0.5 g of cellulosic fractions or cellulosic nanocrystals in 50 mL of distilled water. The aqueous suspensions were vacuum filtered using PTFE filters (0.2 µm pore) and the solid fraction remaining in the filter was dried at room temperature overnight (20ºC, 40% RH). The obtained films were stored in equilibrated relative humidity cabinets at 0% RH and 25ºC for three days prior to their characterization.

3.5 Attenuated total reflectance (ATR) FT-IR analysis

Freeze-dried fractions and nanocrystals were analysed by FT-IR in attenuated total reflectance (ATR) mode using a Thermo Nicolet Nexus (GMI, USA) equipment. The spectra were taken at 4 cm^{-1} resolution in a wavelength range between 400-4000 cm^{-1} and averaging a minimum of 32 scans.

3.6 ^{13}C CP/MAS Nuclear Magnetic Resonance (NMR) spectroscopy

The solid-state 13C CP/MAS NMR experiments were performed at a ^{13}C frequency of 100.63 MHz on a WB-AVIII Bruker spectrometer. The samples were packed in a 4-mm, PSZ (partially-stabilized zirconium oxide) rotor with a perfluorinated polymer (KelF) end cap. The rotor was spun at 10 kHz at the magic angle (54.7º). The 90º pulse width was 2.2 μs and a contact time of 2 ms was used for all samples with a recycle delay of 5 s. The spectral width was 30 kHz, acquisition time 34 ms, time domain points 2k, transform size 8k and line broadening 10 Hz. 20k scans were accumulated for each spectrum. Spectra were referenced to external glycine.

3.7 Scanning electron microscopy (SEM)

SEM characterization was carried out on a Hitachi microscope (Hitachi S-4800) at an accelerating voltage of 10 kV and a working distance of 8-16 mm. Small samples (~5 mm^2 area) of the cellulosic films were cut to observe their surface. The samples were then sputtered with a gold–palladium mixture under vacuum during 3 minutes.

3.8 Transmission electron microscopy (TEM)

One drop (8 μL) of a 0.001% aqueous suspension of the different nanocrystals was allowed to dry on a carbon coated grid (200 mesh). The nanocrystals were then stained with uranyl acetate. TEM was performed using a JEOL 1010 at an accelerating voltage of 80 kV.

3.9 Water vapour permeability (WVP) and water uptake

Water vapour permeability and water uptake values were estimated by registering the weight gain of film samples as a function of time when being exposed to 75% RH and 25 °C conditions. The detailed protocols are described in [50].

3.10 Oxygen permeability

O_2 permeability values in dry conditions were obtained by an isostatic method based on a permeation cell connected in series to a gas chromatograph (GC) equipped with a thermal conductivity detector (TCD) as described elsewhere [61]. In brief, the film under analysis

separates the two chambers of the permeation cell (Film area was 5 cm^2). In the low concentration chamber, a constant flow of nitrogen carries the permeated molecules out of the cell and to the injection valve of the GC. In the high concentration chamber, a constant flow of oxygen maintains the pressure of the gas constant at 1 atm. Gas pressures were adjusted by appropriate manometers and flows were controlled by needle valves and measured by mass flowmeters from Dakota Instruments (New York). Gas samples of the nitrogen flow stream were injected until peak area got constant, indicating the achievement of stationary state.

3.11 Contact angle measurements

Contact angle values were estimated from measurements performed in a Video-Based Contact Angle Meter model OCA 20 (DataPhysics Instruments GmbH, Filderstadt, Germany) at ambient conditions, as previously described in [50].

3.12 Optical properties

The transparency of the films was estimated from the internal transmittance values measured using a spectrocolorimeter CM-3600d (Minolta Co., Tokyo, Japan), using the same methodology described in [51].

3.13 Mechanical properties

Tensile tests were performed using a Mecmesin MultiTest 1-i (1 kN) machine (Virginia, USA) equipped with the EmperorTM software. The same parameters previously described in [50] were applied and the obtained stress-strain curves were used to calculate the elastic modulus, tensile strength and elongation at break of the tested films.

3.14 X-ray diffraction (XRD)

XRD characterization of the films was carried out using the same experimental conditions described in previous work (Benito-González et al. 2018). The crystallinity index was determined by integration of the peak areas and application of the following equation:

$$X_C(\%) = \frac{\sum A_{Crystal}}{A_{Total}} \times 100 \quad (1)$$

Where A_{Total} is the sum of the areas under all the diffraction peaks and $\Sigma A_{Crystal}$ is the sum of the areas corresponding to the three crystalline peaks from cellulose I. The crystallite sizes were estimated from the three different lattice planes of cellulose I_β using the well-known Scherrer equation:

$$D_{(hkl)} = \frac{k \cdot \lambda}{B_{(hkl)} \cdot \cos\theta} \quad (2)$$

3.15 Statistics

Analysis of variance (ANOVA) followed by a Tukey test were performed for the comparison of more than two data sets. Significant differences ($p \leq 0.05$) are denoted by showing the data provided in the tables with different letters.

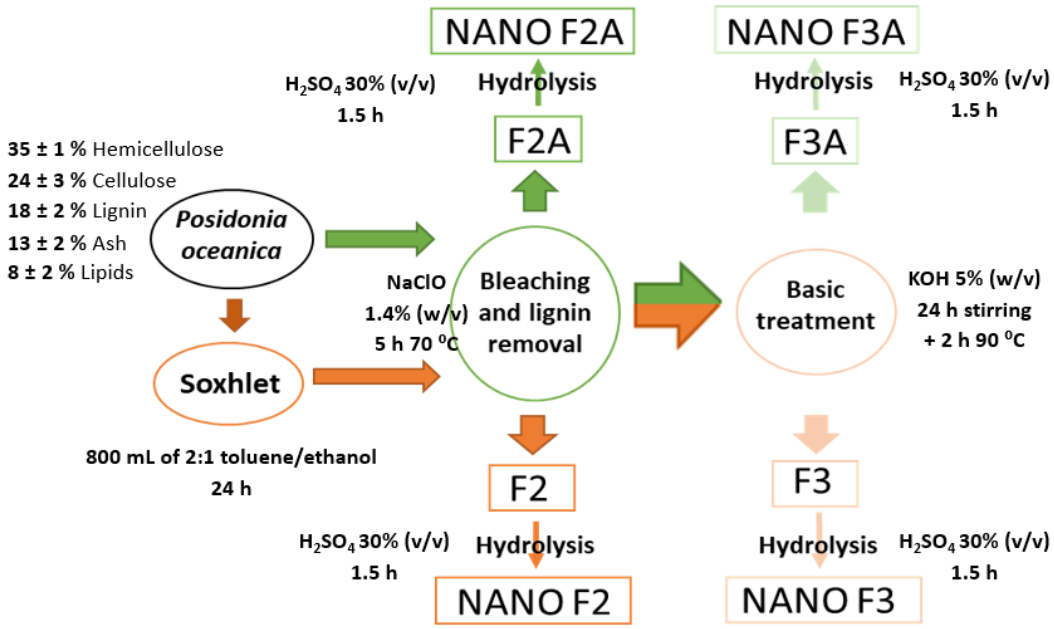

Figure 1. General protocol for the extraction of cellulosic fractions and nanocrystals from *Posidonia oceanica* waste biomass.

4. Results and discussion

4.1 Characterization of the cellulosic fractions and the extracted nanocrystals

Different cellulosic fractions were extracted from *Posidonia oceanica* biomass waste by applying a previously developed sequential extraction protocol [50]. According to previous results, F2 was expected to contain cellulose and hemicelluloses, while F3 was expected to consist of pure cellulose. Additionally, an alternative greener extraction protocol where the initial Soxhlet treatment was omitted (thus, avoiding the use of organic solvents), was also applied, yielding the fractions F2A and F3A. Apart from the cellulose and hemicelluloses, these two fractions were expected to contain some impurities such as lipids and pigments, which are typically removed by organic solvents during the Soxhlet treatment. The extraction yields were 50% for F2 and 25%

for F3, consistent with the raw *Posidonia* composition and in agreement with previous results [50]. As expected, the extraction yields increased slightly when omitting the Soxhlet treatment due to the presence of impurities in the material, leading to yields of 60% for F2A and 30% for F3A.

These four fractions were then subjected to an acid hydrolysis to digest the amorphous domains and isolate the crystalline fraction of the material. The yields (with respect to the raw *Posidonia* biomass) were estimated as 20%, 26%, 14% and 18% for the nanocrystals extracted from the F2, F2A, F3 and F3A fractions, respectively. Therefore, circa (ca.) 60% of the material was hydrolyzed for the F2 and F2A fractions, while only 40% of the material was hydrolyzed when using the F3 and F3A fractions. This is not surprising, since the F2 and F2A fractions contain amorphous hemicelluloses which can be easily digested by the acid. Even NANO F3 yield was consistent with others previously reported by the literature in *Posidonia oceanica* nanocrystals [10], and higher than others reported from different marine biomass like *Gelidium elegans* (8%) [19] or chardonnay grape-skins [62].

FT-IR analyses were carried out to assess the compositional differences between the extracted fractions and the nanocrystals and the results are shown in Figure 2. As observed, several differences were evidenced in the spectra from the different fractions (cf. Figure 2A). Firstly, the intensity of several bands characteristic of hemicelluloses, such as those located at 1735, 1621 and 1533 cm^{-1} (corresponding to esters and acetyl groups) [21], which were evident in the spectra from F2 and F2A, was seen to strongly decrease after the KOH treatment, being hardly visible in the spectra from the F3 and F3A fractions. Moreover, some cellulose characteristic peaks, such as those located at 1103, 1054 and 984 cm^{-1} (corresponding to C-C, C-O, C-H stretching and C-OH bending modes [24, 26], were more intense and defined in the spectra from F3 and F3A, supporting the effectiveness of the cellulose purification process.

With regards to the Soxhlet treatment, it was seen to have a clear effect on the peaks at 2912 and 2845 cm^{-1}, which appeared as very sharp peaks in the spectra from F2A and, to a lesser extent, F3A. These peaks correspond to the CH_2 asymmetrical and symmetrical stretching, usually associated with the fatty acids aliphatic chain [20, 63]. This suggests that, as already anticipated, some lipidic components remained in the fractions obtained without applying the Soxhlet treatment. The lower intensity of these bands in the case of F3A might be due to the application of an adittional purification step (i.e., KOH treatment) where some fatty acids might have been removed.

The spectra from the extracted nanocrystals were very similar, as shown in Figure 2B. The first clear observation is that after the acid hydrolysis, all the bands arising from the presence of hemicelluloses were strongly reduced, indicating that they were almost completely digested by

the sulphuric acid. This is reasonable, since the hemicelluloses are known to act as an amophous matrix interacting with the cellulose microfibrils in plant cell walls [64-66]. The most remarkable difference between the extracted nanocrystals was the presence of defined peaks located at 2912 and 2845 cm^{-1} in both NANO F3A and NANO F2A spectra. This indicates that some of the lipidic impurities remaining in the F2A and F3A fractions were not completely removed by the acid hydrolysis treatment. The same has been reported to happen during the hydrolysis of *Schizochytrium limacinum*, a high lipid content microalgae, for the production of biodiesel [67]. This may be due to either an inherent crystalline structure of the lipidic impurities or to strong interactions existing between these components and the cellulose microfibrils. In the latter case, the acid would have digested preferentially those components such as hemicelluloses which were more accessible. This seems to be the most plausible explanation, since no additional peaks arising from the presence of crystalline components, other than cellulose, were detected in the XRD espectra of neither NANO F2A nor NANO F3A (cf. Figure 3).

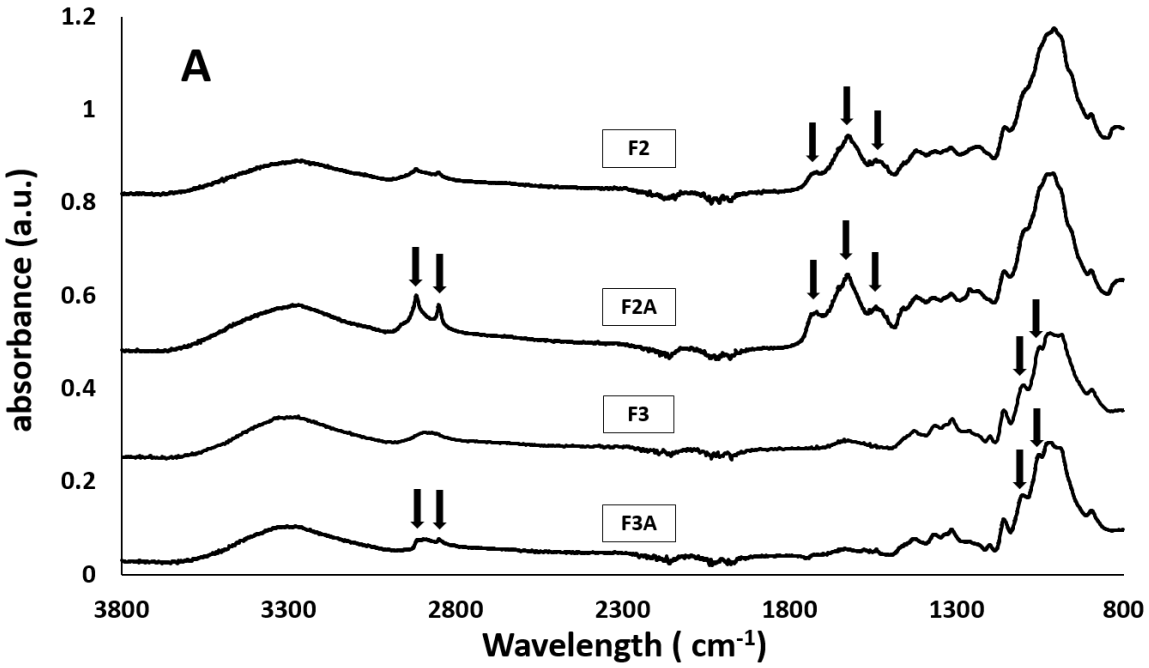

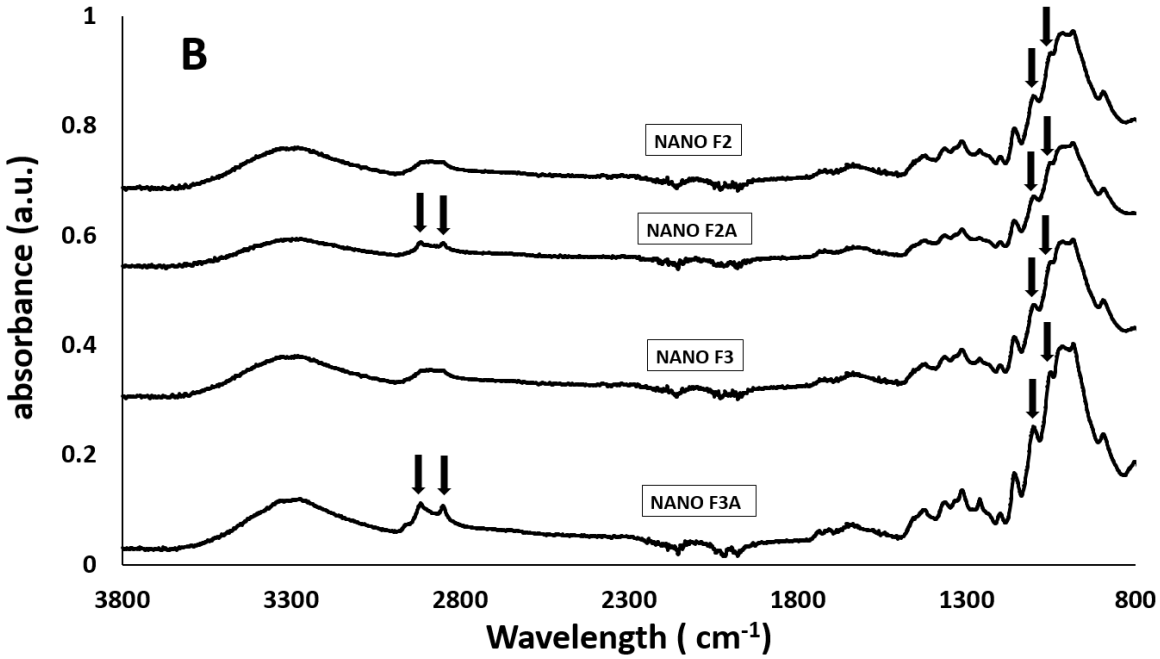

Figure 2. FT-IR spectra of (A) the cellulosic fractions and (B) the extracted nanocrystals. Spectra have been offset for clarity. Arrows point out to the spectral bands displaying the most significant changes amongst the different materials.

XRD analyses were carried out to corroborate the successful purification of the cellulosic fractions and assess the effect of hydrolysis on the crystallinity of the extracted nanocrystals. As observed in Figure 3, all the samples presented very similar spectra, composed of three peaks located at 15.0, 16.6 and 22.7º, which correspond to the (1-10), (110) and (200) crystalline planes from the cellulose Iβ crystalline allomorph [28-30]. Crystallinity indexes and crystallite sizes were calculated by fitting the experimental data and the results are summarized in Table 1. When comparing between the cellulosic fractions, F3 (i.e. pure cellulose) had the highest crystallinity index (66.9%), similar to that previously reported for the cellulose extracted from *Posidonia oceanica* [50]. The presence of amorphous hemicelluloses and other impurities in the rest of the fractions led to reduced crystallinity values in the obtained films. A significant increase in the crystallinity after the acid hydrolysis treatment was observed for all the fractions, although this effect was less pronounced for the F2A and F3A fractions. This suggests that the presence of lipidic impurities in these fractions hindered the accessibility of the acid to digest the amorphous hemicelluloses and the defective regions in the cellulose microfibrils. The heterogeneity in the effect observed in the crystallite sizes precludes from drawing any conclusions but, in general, it seems that the overall crystallite sizes remained unaffected, confirming that the acid digested preferentially amorphous matrix components such as hemicelluloses rather than cellulose amorphous/paracrystalline domains. The NANO F3 sample presented a relatively high crystallinity index of ca. 76.5%, which is greater than those previously reported for nanocrystals

extracted from *Gelidiella aceroso* [68] or garlic straw [69], and very similar to those obtained from *Gelidium elegans* [19], *Pennisetum sinese* [70] and bacterial cellulose nanocrystals obtained in similar reaction times [60].

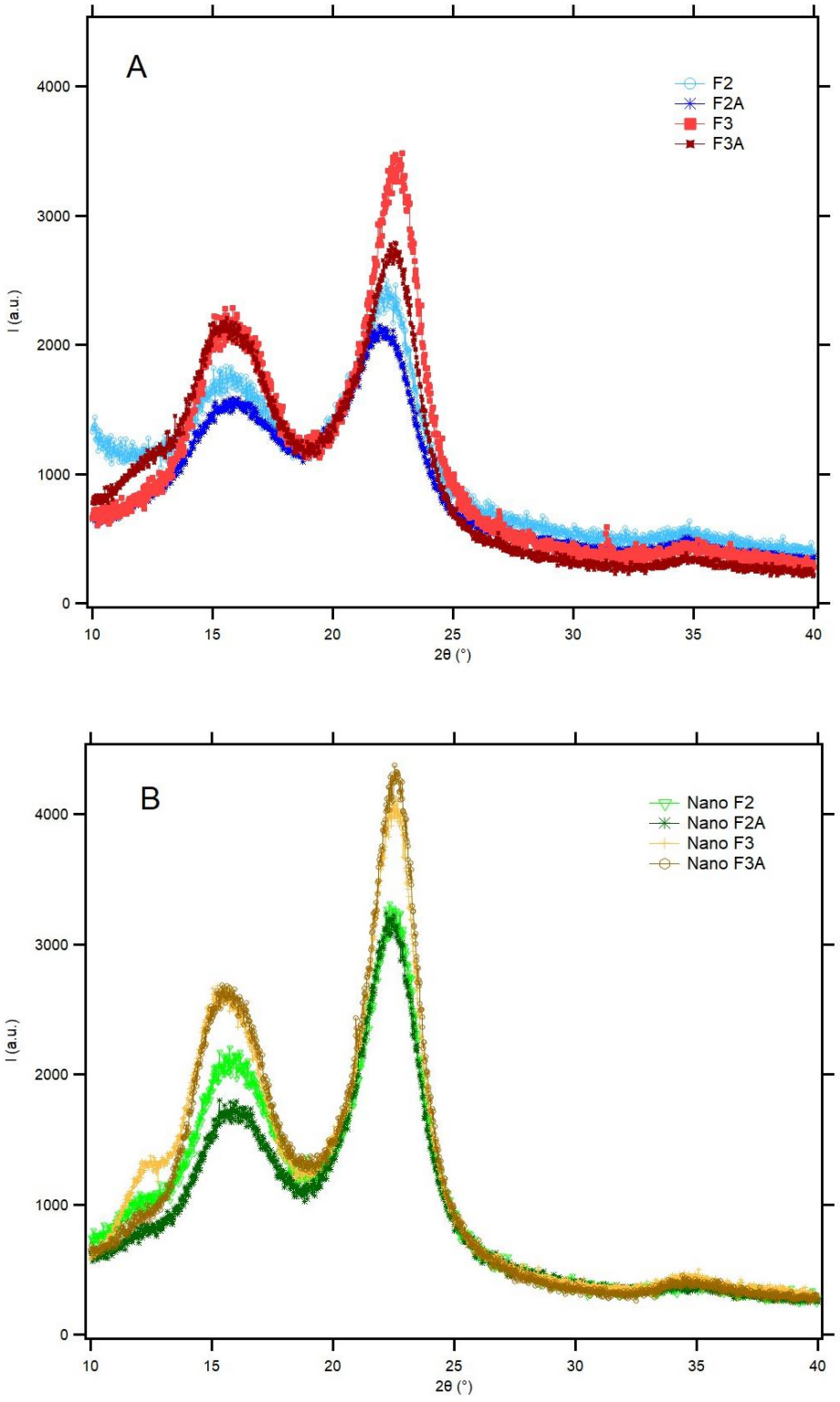

Figure 3. XRD patterns of (A) the cellulosic fractions and (B) the extracted nanocrystals.

Table 1. Crystallinity index (X_C) and cross-sectional dimensions of crystallite sizes in the direction perpendicular to the (1-10), (110) and (200) planes ($D_{(1-10)}$, $D_{(110)}$ and $D_{(200)}$), determined from the XRD patterns.

	X_C (%)	$D_{1\text{-}10}$ (nm)	D_{110} (nm)	D_{200} (nm)
F2	44.1	4.5	3.5	3.5
F2A	48.0	3.4	5.5	3.3
F3	66.9	2.9	6.5	3.7
F3A	54.8	4.1	4.2	3.8
NANO F2	55.8	3.2	5.5	3.5
NANO F2A	50.0	3.4	5.3	3.4
NANO F3	76.5	3.1	5.3	3.6
NANO F3A	62.2	3.3	5.5	3.8

The rigid cellulose components (i.e. those components with reduced mobility) in the extracted nanocrystals were examined using solid-state ^{13}C CP/MAS NMR and the spectra obtained are shown in Figure 4. The characteristic peaks of cellulose, which correspond to the different carbons in the cellulose structure as highlighted, were present in the four samples. As observed, the peak shape and position was different for the NANO F2-NANO F2A and the NANO F3-NANO F3A samples. The broader and less intense peaks detected in the NANO F2 and NANO F2A samples are indicative of the presence of hemicelluloses. The cellulose crystallinity index was estimated by integration of the signals at 85-92 ppm and at 80-85 ppm, corresponding to the C-4 carbons from the crystalline and non-crystalline cellulose regions, respectively (Foston, 2014). The calculated crystallinity values, ca. 42% for NANO F2, 36% for NANO F2A, 46% for NANO F3 and 39% for NANO F3A, were much lower than those estimated from the XRD results. A similar discrepancy between XRD and NMR has been reported for cellulose samples from diverse sources [71-74] and has been explained by the different ability of these techniques to distinguish between crystalline and paracrystalline domains. While the contribution from both the crystalline and paracrystalline fractions is accounted for in the XRD-calculated crystallinity, the NMR technique is able to differentiate the crystalline versus the paracrystalline domains since the carbons located within the interior crystalline regions have a chemical shift distinct from those carbons located on the crystallite surfaces or paracrystalline domains [75]. According to that, the NANO F2 and NANO F2A would be the samples with the highest amorphous cellulose content, while the NANO F3 and NANO F3A would present the greatest paracrystalline fractions. This provides further evidence for the presence of amorphous hemicelluloses tightly bound to the cellulose microfibrils, which remain in the less purified fractions even after the hydrolysis

process. Furthermore, it should also be noted that a small peak located at ca. 33.4 ppm was detected in the NANO F2A and NANO F3A fractions. This peak has been previously assigned to the presence of lipids in cellulose-derived samples [76-78] and therefore, it supports the presence of a certain lipidic fraction in the nanocrystals obtained from the fractions which were not subjected to the Soxhlet treatment.

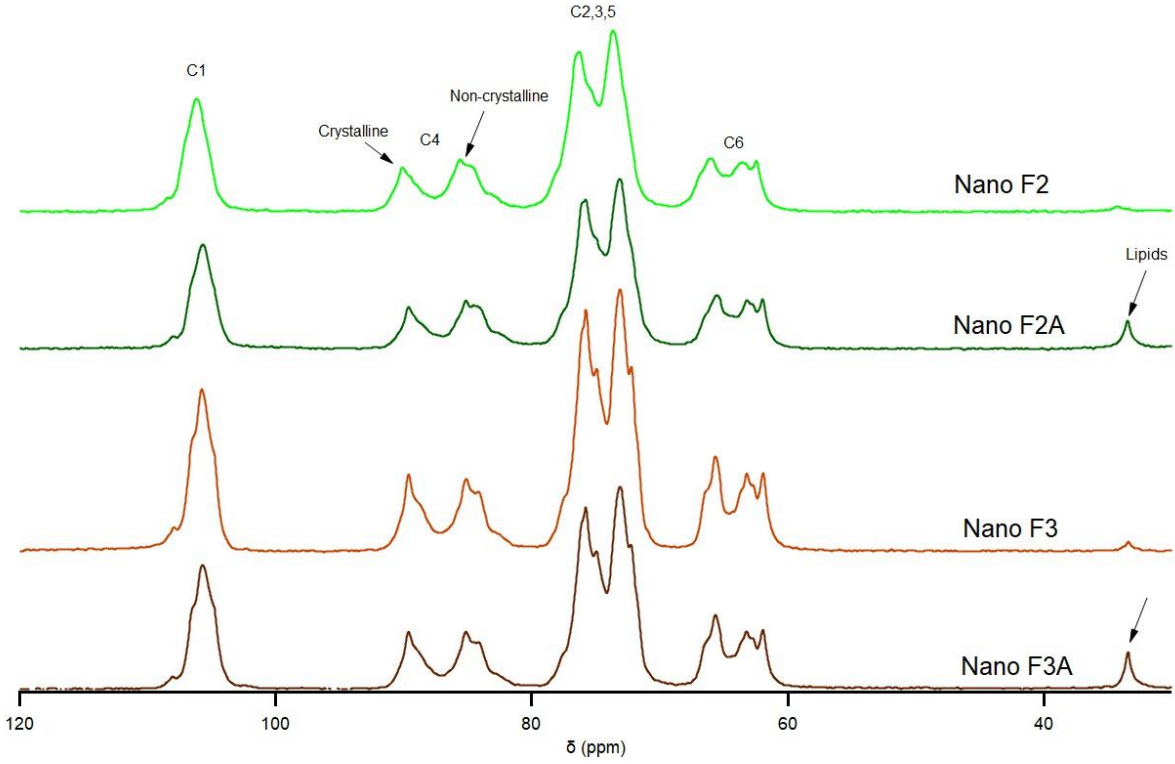

Figure 4. NMR patterns of the different nanocrystals obtained. Carbons 1-6, crystalline and non-crystalline regions and lipid peaks are pointed by an arrow.

The morphology of the extracted nanocrystals was evaluated by TEM and representative images are shown in Figure 5. The material extracted from F3 (pure cellulose) presented a very similar morphology to that of cellulose nanocrystals previously extracted by the sulphuric acid hydrolysis protocol used in this work [12, 60]. This type of nanostructures are often designated as cellulose nanowhiskers due to their needle-like morphology. On the other hand, the nanocrystals obtained from the non-purified fractions clearly contained some impurities. Interestingly, a greater degree of agglomeration was observed for the NANO F2 and NANO F2A samples. This might be due to the presence of very limited amounts of hemicelluloses, which were resistant to the acid hydrolsysis. In fact, it has been previously reported that minor fractions of hemicelluloses are intimately interacting with the cellulose microfibrils in plant cell walls [64] and can only be removed by using specific enzymes [79]. In the case of NANO F3A and NANO F2A, some

impurities, which were stained providing higher contrast than the cellulose nanocrystals, were identified. This is indicative of the presence of compounds attached to the surface of the nanocrystals, which had higher affinity for the uranile acetate dye, such as fatty acids and pigments. Despite the presence of impurities in some of the samples, all the extracted nanocrystals had very similar dimensions (cf. Table 2), with lenghts ranging from ca. 488 nm to 586 nm and widths between ca. 10 nm to 15 nm, which were comparable to those reported for cellulose nanocrystals obtained from bacterial cellulose [60] and slightly larger than cotton cellulose nanocrystals [80]. The large aspect ratios of the extracted nanocrystals, greater than 30, highlight the potential of those materials for being used as reinforcing materials in polymeric composites.

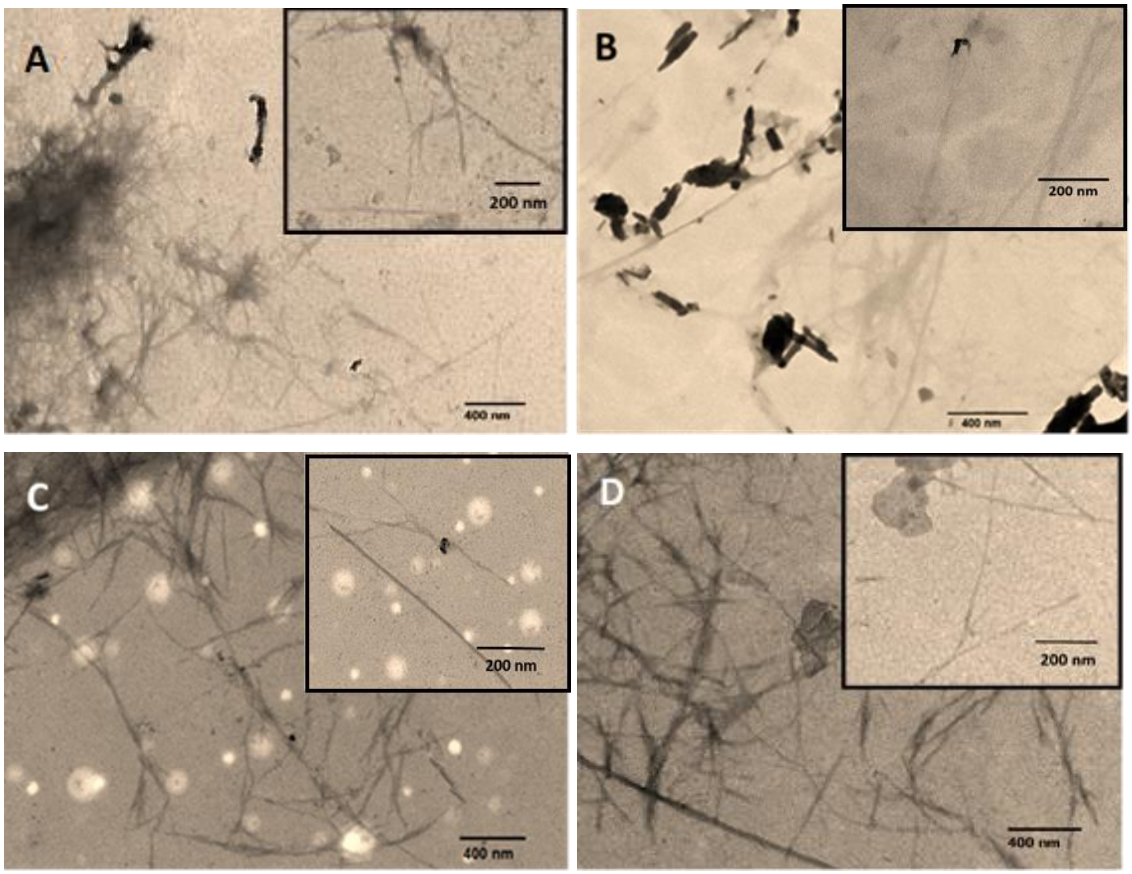

Figure 5. Representative TEM images of the extracted nanocrystals: (A) NANO F2, (B) NANO F2A, (C) NANO F3 and (D) NANO F3A. Inserts correspond to higher magnification images.

Table 2. Size (width and length) and aspect ratio of the extracted nanocrystals.

	Width (nm)	**Length (nm)**	**Aspect ratio**
NANO F2	10.7 ± 2.8[a]	487.5 ± 86.3[a]	45.6
NANO F2A	14.9 ± 4.7[a]	499.0 ± 96.1[a]	33.5
NANO F3	10.8 ± 2.2[a]	514.0 ± 82.5[a]	47.6
NANO F3A	10.1 ± 3.3[a]	586.4 ± 103.4[a]	58.1

4.2 Characterization of the cellulosic films

The different cellulosic fractions and the extracted nanocrystals were used to generate cellulosic films by means of a simple vacuum filtration method using aqueous dispersions. The surface morphology of the obtained films was evaluated by SEM and representative images are displayed in Figure 6. On the one hand, a lower magnification was used to observe the general structure of the cellulosic films (scale bars corresponding to 1 mm), evidencing a clearly higher porosity in both the F2 and F2A films (where even different layers of fibres could be easily appreciated) in comparison with the F3 and F3A films. The latter ones presented much smoother surfaces, with the cellulose fibres being clearly identified in the F3 film. The F3A film presented a much more compact structure, most likely caused by the presence of lipidic compounds which formed a coating layer on the surface of the film. On the other hand, the structure of the films produced from the nanocrystals were compared at a higher magnification (scale bars corresponding to 100 µm) since all the samples appeared identical, with very smooth surfaces, at the lower magnification used for the cellulosic films. As observed, all the films showed a very compact structure with no significant differences between them.

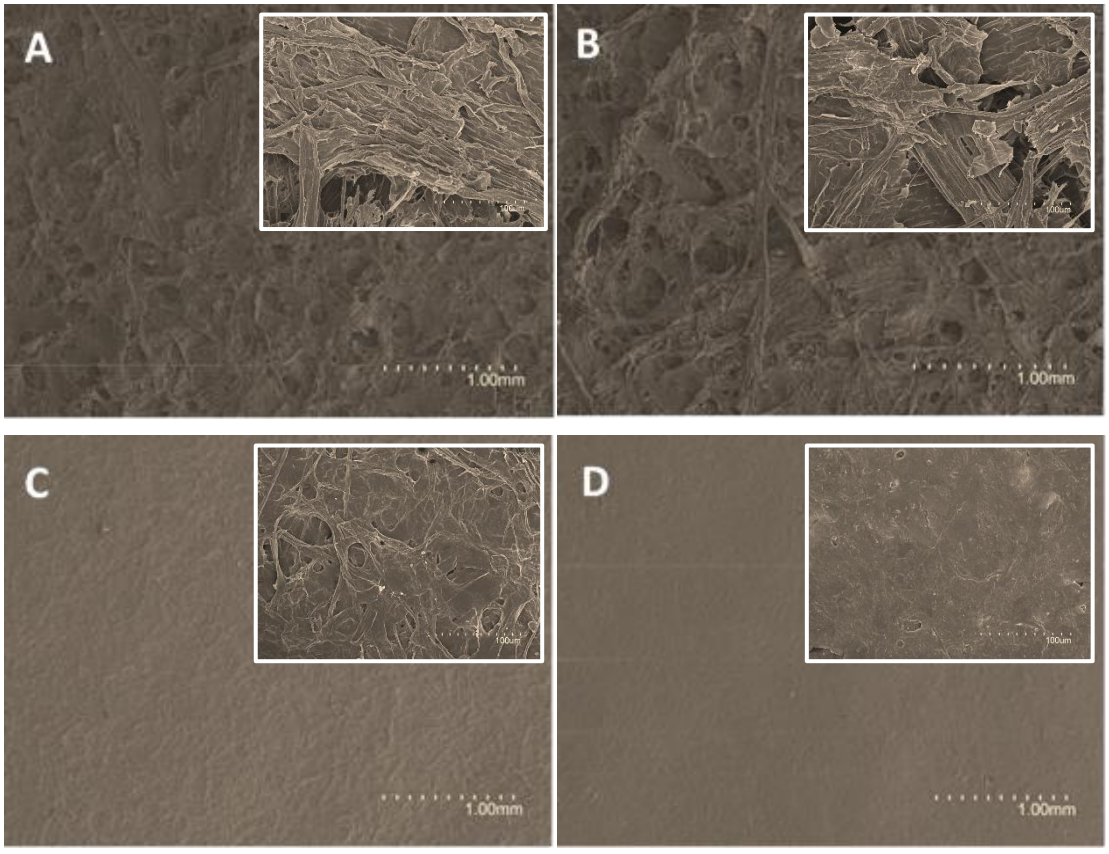

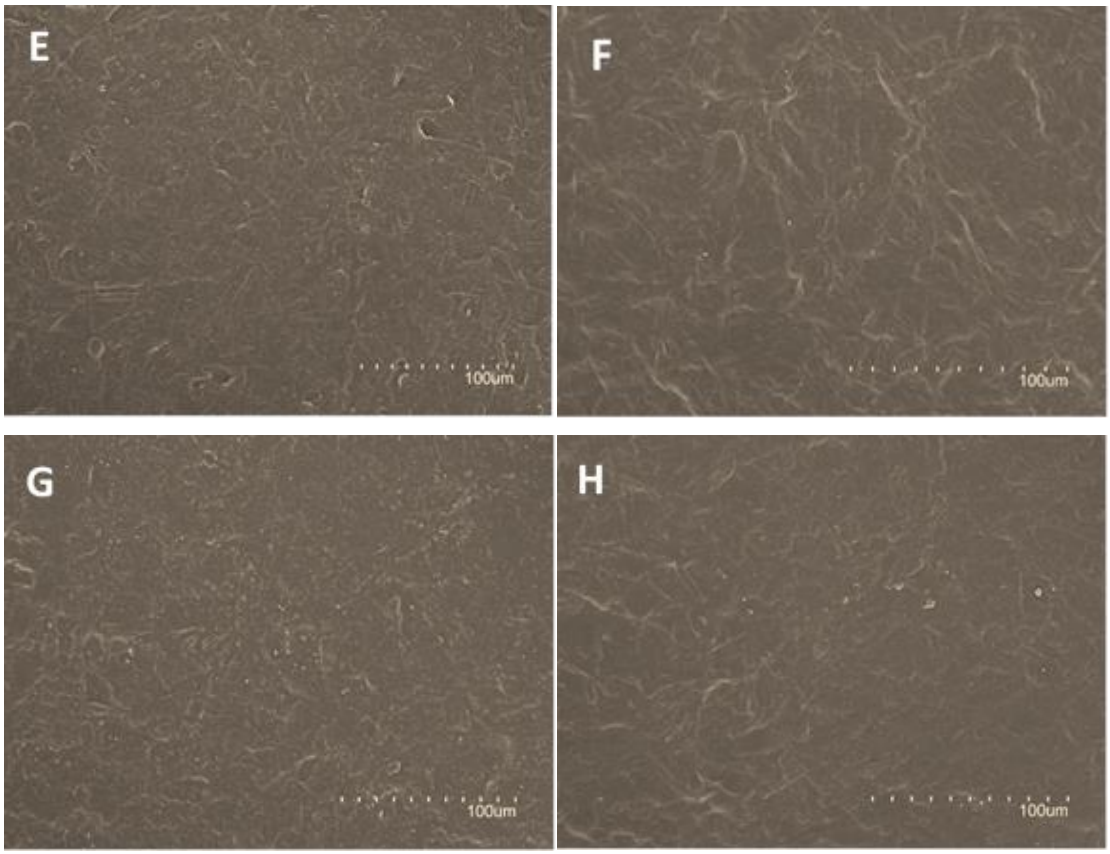

Figure 6. SEM images of the surface from the cellulosic films: (A) F2, (B) F2A, (C) F3 and (D) F3A, (E) NANO F2, (F) NANO F2A, (G) NANO F3 and (H) NANO F3A. Inserts in A-D correspond to higher magnification images.

Since these films were intended to be used in food packaging applications, transparency was an important attribute to be evaluated. Figure 7A shows the visual appearance of the different films. It can be clearly observed that while the films obtained from the fractions were completely opaque (F2, F2A and F3A) with a white tonality, or translucent (F3), all the films produced from the nanocrystals were transparent. Therefore, while in the case of the fractions, the most purified ones were more transparent, the acid hydrolysis tended to equalize transparency with a substantial increase of it in all cases. The transparency of the films was quantitatively assessed by measuring their internal transmittance, as shown in Figure 7B. As observed, all the films obtained from the cellulosic fractions, except the F3 film, displayed low transmittance values (i.e. low transparency) since they had a translucid appearance with a strong white tonality. The greater transparency of the F3 film may be due to the better dispersion of the cellulose fibers in this particular sample, giving rise to films with more homogenous surfaces, as suggested by SEM (cf. Figure 5C). As expected, the films prepared from the nanocrystals showed much higher transparency due to the decreased particle size produced after the acid hydrolysis treatment. No significant differences were found between the four nanocrystal films, which displayed similar results to those of corn starch films [50].

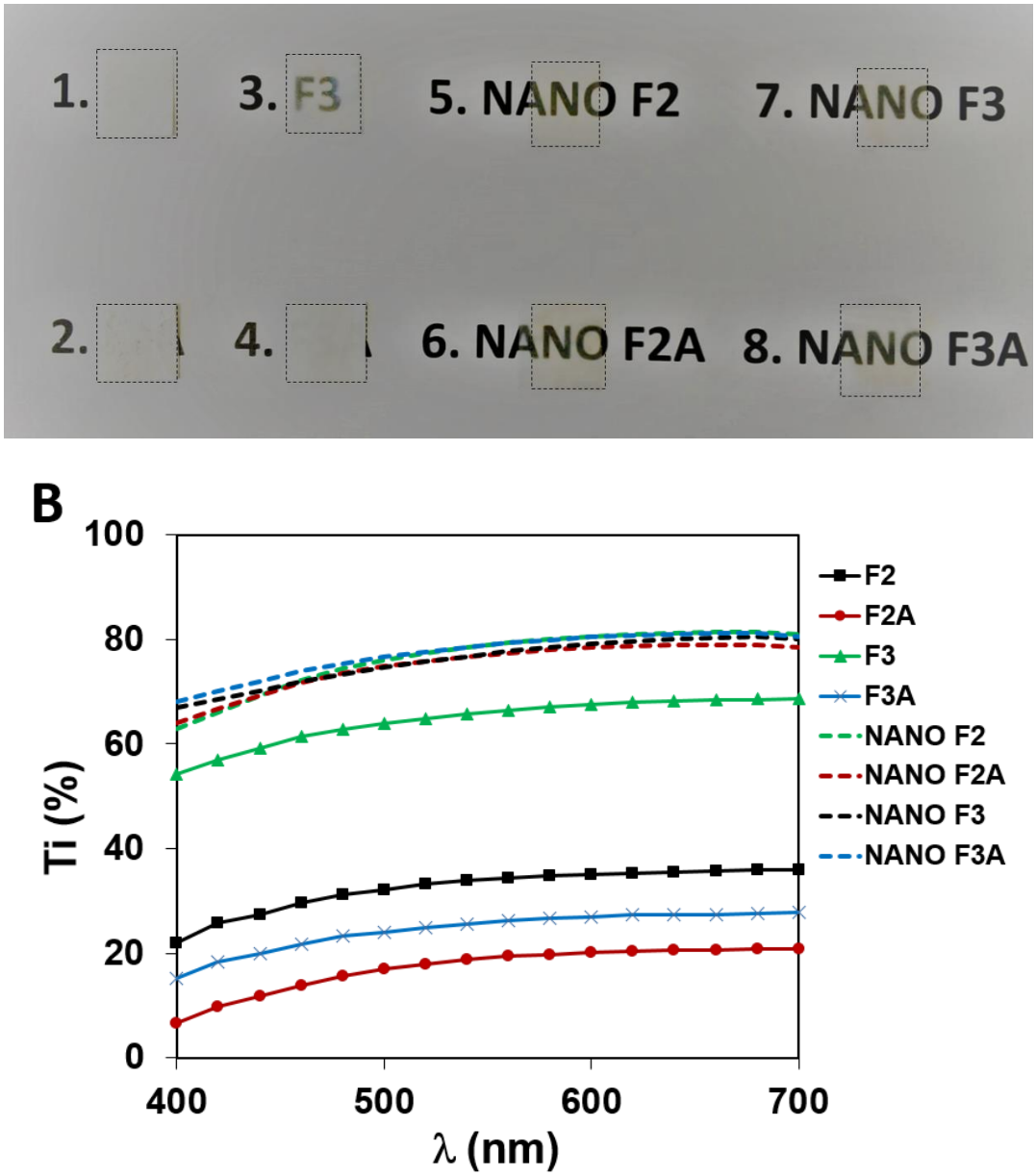

Figure 7. (A) Visual appearance and (B) spectral distribution of internal transmittance (Ti) of the different cellulosic fractions and nanocrystals obtained.

The mechanical properties of the films from the cellulosic fractions and the extracted nanocrystals were evaluated, and the results are summarized in Table 3. When comparing the films from the cellulosic fractions, the first clear observation was that the removal of hemicelluloses had a great impact in the mechanical performance of the films, as the F3 and F3A films presented significantly greater elastic modulus, tensile strength and elongation at break than the F2 and F2A films. The improved mechanical performance of pure cellulose films has been previously reported [50] and ascribed to an easier dispersion of cellulose in water when hemicelluloses are removed, hence producing more homogeneous aqueous dispersions for the production of films.

Additionally, the presence of lipidic impurities when omitting the initial Soxhlet treatment had a negative impact in the mechanical properties, reducing the stiffness of the material (F3 presented higher elastic modulus and tensile strength than F3A). Thus, the pure cellulose film would be the optimum in terms of mechanical performance.

The acid hydrolysis of the different fractions had a strong positive effect on the mechanical properties of the produced films. This was much more evident for the F2 and F2A fractions, with ca. 30-fold increase in the tensile strength and more than 10-fold increase in the elastic modulus. While the elongation at break increased after hydrolyzing the F2 and F2A fractions, it slightly decreased in the case of the F3 and F3A fractions. These results suggest that the acid hydrolysis was able to digest some of the amorphous hemicelluloses present in the F2 and F2A fractions, leading to a favorable effect in the mechanical properties of the NANO F2 and NANO F2A films. On the other hand, in the case of the F3 and F3A fractions, the hydrolysis process resulted in the digestion of the cellulose amorphous/paracrystalline domains, yielding more rigid crystalline structures. Surprisingly, although there were no significant differences in the elastic modulus of the films prepared from the nanocrystals, the tensile strength and elongation at break were substantially higher in NANO F2 and NANO F2A as compared with NANO F3 and NANO F3A. It has been demonstrated that in plant cell walls, a certain fraction of hemicelluloses intimately interacts with cellulose microfibrils [64], having a very limited accessibility and only being removed by the action of specific enzymes [79]. Therefore, it is reasonable to hypothesize that a certain fraction of hemicelluloses, strongly interacting with the cellulose microfibrils, remained in the material even after the acid hydrolysis. The presence of these hemicelluloses improved the strength and ductility of the films, which is in agreement with previous studies that demonstrated the crucial role of some hemicelluloses, such as xyloglucan and mannans, in the micromechanics of plant cell walls and cellulose hydrogels [81, 82]. The films obtained from the nanocrystals extracted from F2A and F3A (i.e. avoiding the Soxhlet extraction) presented similar properties to those obtained from the F2 and F3 nanocrystals, with only a slight reduction in the tensile strength. This implies that it is possible to obtain materials with very similar mechanical properties with less purification steps (i.e. reducing the processing time and the associated costs and avoiding the use of organic solvents).

It is worth noting that all the films prepared from the extracted nanocrystals displayed excellent mechanical performance, showing higher elastic modulus, tensile strength and elongation at break than films from bacterial cellulose nanocrystals (BCNW) [59] and microfibrillated cellulose (MFC) [83]. The greater elastic modulus and tensile strength of the NANO F3 film as compared with BCNW is surprising considering the significantly higher crystallinity index previously reported for BCNW (Xc~95%) [59]. One possible explanation for the improved mechanical performance of the *Posidonia oceanica* nanocrystals is related to their greater aspect ratio (ca. 48

for NANO F3 versus 30 for BCNW [59]). Furthermore, the film density and relative humidity at which the films are conditioned prior to the mechanical testing have been reported to have an impact in the mechanical performance of the films [84]. It is possible that the low relative humidity used for the pre-conditioning of the *Posidonia* nanocrystals films (0% RH) may be also responsible for their stiffer behavior. When comparing with benchmark biopolymers such as thermoplastic corn starch (TPCS) [42] and PLA [85], all the nanocrystal films showed an obvious improvement in terms of Young's modulus and tensile strength, making these films a promising alternative for food packaging. The results were even comparable to those from petroleum-based polymers widely used in food packaging applications, such as polyethylene terephthalate (PET) and oriented polystyrene (OPS) [86] and in particular, the nanocrystal films were superior to these materials in terms of stiffness.

Table 3. Mechanical properties (Young's modulus, tensile strength and elongation at break) from the films obtained from cellulosic fractions and nanocrystals.

	E (GPa)	**Tensile Strength (MPa)**	**ε_b (%)**
F2	0.8 ± 0.1^{a}	4.6 ± 0.1^{a}	1.1 ± 0.3^{ab}
F2A	1.0 ± 0.1^{a}	4.8 ± 0.6^{a}	0.7 ± 0.1^{a}
F3	4.2 ± 0.4^{c}	45.9 ± 6.9^{c}	2.1 ± 0.4^{c}
F3A	2.6 ± 0.4^{b}	22.1 ± 1.8^{b}	1.6 ± 0.3^{bc}
NANO F2	11.5 ± 0.8^{d}	142.0 ± 4.3^{g}	2.8 ± 0.2^{d}
NANO F2A	10.5 ± 1.4^{d}	124.7 ± 7.2^{f}	2.4 ± 0.4^{cd}
NANO F3	11.5 ± 1.1^{d}	98.0 ± 6.8^{e}	1.1 ± 0.3^{ab}
NANO F3A	12.2 ± 0.5^{d}	72.1 ± 3.7^{d}	1.2 ± 0.1^{b}
BCNW [59]	7.9 ± 0.1	74.6 ± 11.5	1.0 ± 0.1
MCF [83]	2.1 ± 0.1	39.0 ± 8.0	2.8 ± 0.9
PLA [85, 87]	3.6 ± 0.2	53.8 ± 1.2	4.9 ± 0.5
TPCS [42]	0.1 ± 0.0	11.2 ± 0.8	7.3 ± 1.9
PET [86]	~ 1.6	~ 55.1	~ 4.2
OPS [86]	~ 1.6	~ 58.6	~ 4.3

The water vapour permeability (WVP) of the different films was also measured and the results are shown in Table 4. When comparing the films from the cellulosic fractions, the F3 film was clearly the optimum. Similarly to the mechanical properties, the water vapour barrier effect was improved by removing most of the hemicelluloses. Furthermore, the presence of lipids when eliminating the Soxhlet step did not have a positive impact in the water permeability of the films. As deduced from the results, the films obtained from the nanocrystals displayed remarkably lower water permeability (an order of magnitude lower than those of the films from their respective fractions). This is most likely due to the increased crystallinity of the materials after the hydrolysis and the more compacted film structure, as evidenced by SEM. Amongst them, NANO F2 was clearly the least impermeable film, while NANO F2A presented the highest barrier possibly due to the lipidic presence as reported by other authors [88, 89]. From the results, it seems that the removal of hydrophilic compounds such as the hemicelluloses gave rise to a reduced permeability, while the presence of hydrophobic impurities such as those removed by the Soxhlet treatment had a positive effect.

The water permeability values from all the nanocrystal films were similar or even slightly better than those previously reported for films from BCNW [59] and from MFC [90]. All the cellulosic fractions and nanocrystals outperformed TPCS in terms of water vapour barrier [42], while only the NANO F2A film was comparable to more hydrophobic biopolymers such as PLA [87]. However, all the developed films were still far from reaching comparable water vapour barrier values to those from highly hydrophobic petroleum-based polymers such as PET and OPS [86]. The improvement in the water barrier performance originated by the presence of the impurities remaining in the NANO F2A and NANO F3A, mostly lipids as suggested by the FTIR results, is an interesting result since it implies the possibility of obtaining materials with excellent barrier performance using a greener and simpler extraction protocol.

Water uptake measurements are also compiled in Table 4. From all the cellulosic fractions, the pure cellulose (i.e. F3) presented the lowest water sorption capacity. This is related to the lower water accessibility towards the more crystalline structure of F3. The presence of fatty acids remaining in the F2A fraction seemed to promote a more hydrophobic behavior as compared with F2, thus reducing the water uptake. This effect was not observed for F3A most likely due to its lower crystallinity when compared with F3. On the other hand, water uptake results for the nanocrystals were consistent with results displayed in Table 1. As the crystallinity index increased, a more hydrophobic behavior was shown by the surface, being F3 the material with lower water sorption values. The fact that there were no significant differences between the cellulosic fractions and the nanocrystals might be explained by means of thickness, as the ratio surface exposure/total weight was much higher in the case of nanocrystals. Furthermore, contact

angle measurements were carried out to confirm the water affinity of the surface from the different films. Due to their highly hydrophilic behavior, the F2, F2A and F3A films could not be tested since they absorbed the water drop as soon as it was deposited on top of the film surface. Interestingly, the F3 film presented a much more hydrophobic behavior, which may be explained by the greater crystallinity of the pure cellulose as opposed to the less purified fractions. Furthermore, although cellulose is known to contain a large amount of hydroxyl groups, the cellulose microfibrils tend to self-associate through the formation of strong hydrogen bonds and as a result, most of these hydrophilic groups are not available to interact with water. The sulphuric acid treatment clearly promoted a more hydrophobic behavior of the films' surface by removing hydrophilic hemicelluloses and amorphous cellulose. The most hydrophobic surface was that from the NANO F3 film, which was not surprising due to the higher crystallinity of this material and the strong self-association of pure cellulose when impurities were absent. The presence of hemicelluloses, even at very limited amounts, yielded more hydrophilic surfaces due to the presence of free hydroxyl groups. Surprisingly, the lipidic impurities remaining in the NANO F2A and NANO F3A films led to more hydrophilic surfaces. This might be due to the disruption of the cellulose hydrogen bonding network caused by the presence of impurities, hence increasing the amount of free hydroxyl groups available to interact with water. This indicates that the reduced water vapour permeability induced by the presence of lipidic impurities was mostly caused by a reduction in the water diffusion through the films.

Oxygen permeability of the films was also determined and results are shown in Table 4. Lipids seemed to have a clear disrupting effect as the films produced from the nanocrystals obtained without Soxhlet treatment presented higher values when compared with those obtained from the more purified fractions (up to 30 times). Similar results have been previously obtained for films loaded with essential oils [89, 91]. On the other hand, both NANO F2 and NANO F3 displayed outstanding values similar to PLA [87] demonstrating the potential of the fraction containing hemicelluloses for developing biodegradable packaging materials reducing associated costs.

Table 4. Water vapour permeability, water uptake, contact angle and oxigen permeability of the films obtained from the cellulosic fractions and nanocrystals.

	WVP·10^{13} (kg·m/s·m^2·Pa)	**Water uptake (%)**	**Contact angle (º)**	**OP·10^{18} (m^3·m/Pa·s·m^2)**
F2	35.2 ± 0.6^{a}	18.0 ± 3.1^{a}	n.m.	n.m.
F2A	34.4 ± 2.2^{a}	20.8 ± 1.7^{a}	n.m.	n.m.
F3	12.5 ± 3.3^{c}	6.8 ± 2.3^{c}	80.0 ± 2.8^{b}	311.4 ± 10.2^{e}
F3A	22.2 ± 2.7^{b}	13.1 ± 0.7^{b}	n.m.	n.m.
NANO F2	4.8 ± 0.4^{d}	17.7 ± 3.1^{a}	77.4 ± 7.1^{ab}	2.0 ± 0.4^{b}
NANO F2A	1.8 ± 0.1^{f}	20.2 ± 0.9^{a}	68.3 ± 2.9^{a}	60.7 ± 6.9^{d}
NANO F3	2.7 ± 0.4^{e}	10.5 ± 1.8^{bc}	102.1 ± 3.9^{c}	1.1 ± 0.1^{a}
NANO F3A	2.2 ± 0.2^{ef}	13.8 ± 0.9^{b}	76.4 ± 8.0^{ab}	22.9 ± 0.4^{c}
BCNW [59]	3.6 ± 1.1	5.0 ± 0.7	43.8 ± 1.0	6.0
MFC [83]	3.8	---	---	22
PLA [87]	1.3 ± 0.1	1.0 ± 0.1	---	1.8
TPCS [42]	15.5 ± 0.1	---	10.5 ± 2.1	41.0 ± 2.3
PET [86, 92]	0.03 ± 0.0002	---	---	0.3 ± 0.02
OPS [86]	0.04 ± 0.0002	---	---	---

n.m.: Not measurable.

5. Conclusions

The waste biomass from *Posidonia oceanica* leaves has been valorized to extract cellulosic fractions with distinct composition by exploring different extraction protocols. The presence of hemicelluloses in the F2 and F2A fractions was confirmed and it was seen to reduce the overall crystallinity of the fractions. On the other hand, omitting the Soxhlet treatment led to the presence of lipidic impurities in the F2A and F3A fractions, which were also detrimental in terms of crystallinity. Additionally, these fractions were subjected to an acid hydrolysis treatment to digest the amorphous domains of the material, yielding cellulosic nanocrystals with aspect ratios higher than 30. Although the amorphous hemicelluloses were preferentially digested by the acid, a small fraction seemed to remain in NANO F2 and NANO F2A. Lipids were also somehow resistant to the hydrolysis and hindered to some extent the access of sulphuric acid towards the cellulose amorphous domains. The pure cellulose nanocrystals showed the most optimal properties, with an aspect ratio of ca. 48 and crystallinity of ca. 77%.

Aqueous suspensions from all these fractions and nanocrystals were used to generate films by a simple vacuum filtration method. For the films produced from the fractions, cellulose purification

led to a major improvement in the visual appearance, mechanical performance and barrier properties. Moreover, the acid hydrolysis of the amorphous components in the fractions had a strong positive impact in the properties of the films, especially in the case of the less purified fractions, yielding films with superior mechanical properties to that of benchmark biopolymers and barrier properties comparable even to that of more hydrophobic biopolymers such as PLA. The presence of lipids in the nanocrystals had a limited effect in the mechanical properties but was seen to induce a decrease in the water vapor permeability by hindering the diffusion of water molecules through the films, while oxygen permeability was negatively affected. On the other hand, the presence of a minor fraction of hemicelluloses, strongly interacting with the cellulose nanocrystals, showed a high positive impact on the mechanical performance but led to decreased water barrier due to the more hydrophilic character of the material. Overall, the less purified hemicellulose-containing NANO F2 and NANO F2A films were the optimum materials, offering a good compromise in terms of mechanical and barrier performance, while reducing the amount of purification steps and, in the case of F2A, avoiding the use of organic solvents.

These results show the enormous potential of *Posidonia oceanica* waste biomass to produce less purified cellulose-based nanocrystals by applying simpler and greener extraction protocols and develop high-performance films, which outperform many benchmark biopolymers, valuable for food packaging applications.

1.3. In-depth characterization of bioactive extracts from Posidonia oceanica waste biomass

This section is an adapted version of the following published research article:
Benito-González, I., López-Rubio, A., Martínez-Abad, A., Ballester, A. R., Falcó, I., González-Candelas, L., Sánchez, G., Lozano-Sánchez, J., Borrás-Linares, I., Segura-Carretero, A. & Martínez-Sanz, M.
(2019). In-depth characterization of bioactive extracts from *Posidonia oceanica* waste biomass Marine Drugs, 17 (7), 49. DOI: https://doi.org/10.3390/md17070409

1. Abstract

Posidonia oceanica waste biomass has been valorised to produce extracts by means of different methodologies and their bioactive properties have been evaluated. Water-based extracts were produced using ultrasound-assisted and hot water methods and classified according to their ethanol-affinity (E1: ethanol soluble; E2: non-soluble). Moreover, a conventional protocol with organic solvents was applied, yielding E3 extracts. Compositional and structural characterization confirmed that while E1 and E3 extracts were mainly composed of minerals and lipids, respectively, E2 extracts were a mixture of minerals, proteins and carbohydrates. All the extracts showed remarkably high antioxidant capacity, which was not only related to phenolic compounds but also to the presence of proteins and polysaccharides. All E2 and E3 extracts inhibited the growth of several foodborne fungi, while only E3 extracts decreased substantially the infectivity of feline calicivirus and murine norovirus. These results show the potential of *P. oceanica* waste biomass for the production of bioactive extracts.

2. Introduction

Bioactive compounds with antioxidant and antimicrobial activity have found applications in a broad range of areas, like biomedicine or food science and, thus, prospection of new biomass resources to obtain extracts with these functional properties is a topic of great interest [93, 94]. Specifically in the food science area, certain microorganisms can negatively affect the quality, safety and shelf-life of food products. Furthermore, oxidative processes can have an impact on food quality promoting, for instance, rancidity. These oxidative processes are also known to affect human health due to free radical formation leading to changes in protective enzymes, membrane lipids or even DNA, fact which has been correlated to the development of several diseases.

With regards to the raw materials used for the production of bioactive-rich extracts, although medicinal plants have been typically used up to date [95], the circular economy policies currently being promoted in Europe, aiming to reduce and re-use the different types of residues, are fostering the exploration of alternative biomass resources [50, 51, 96]. In particular, aquatic biomass, such as seaweeds and aquatic plants, represent an interesting alternative for the production of bioactive extracts, given their great availability and abundance and their high content in bioactive components, such as sulphated polysaccharides, polyphenols and fatty acids [97]. *Posidonia oceanica (P. oceanica)* is a marine plant endemic to the Mediterranean Sea which forms extensive meadows, preventing erosion and hosting many marine species. However, during its lifecycle the leaves detach off their stems and accumulate on the coasts, generating a residue which is detrimental to the quality of the beaches and whose elimination generates significant expenses to the local authorities. Bioactive extracts from *P.oceanica* with antioxidant and/or antidiabetic potential have been reported [98, 99], but these were produced using organic solvents, with associated environmental issues and not desirable for food applications, and made use of the native plant, extracted from its natural habitat, instead of the residue.

In contrast, the use of innocuous solvents, such as water, has been very limited and very few works have reported on the production of water-extracted bioactive materials [100]. On the other hand, greener methodologies, which avoid the use of organic and/or toxic solvents, reduce the emission of contaminants to the environment and minimize the amount of processing steps and processing time, are currently being explored. The potential of greener methodologies such as enzyme-assisted, microwave-assisted and pressurized-liquid extractions for the production of bioactive molecules from marine sources has been reported in several works [101-103]. In particular, the potential of ultrasound (US)-based treatments has been evaluated as they can reduce both time and the energy input required (lower temperatures are needed) while maintaining the yield [102, 104]. Moreover, US capability of disrupting cell walls benefits mass transfer and

thus, promotes the extraction of bioactive components with lower solvent ratio [104]. On the other hand, hot-water treatments have been reported to efficiently extract different carbohydrates such as rhamnose, xylose or glucose, as well as proteins from different marine seaweed species [104]. Despite both the extraction medium and methodology used are expected to affect the composition and functional properties of plant-based extracts, complete characterizations of the extracts are barely carried out [98, 105]. This combined compositional and functional characterization is required in order to optimize the extraction protocols and make a proper correlation between composition and functional properties. In fact, most of the existing literature only relates the antioxidant and/or antimicrobial activity capacity of extracts with their total phenolic content [95, 105-108] although it is known that other compounds, such as polysaccharides and peptides, can also show a high bioactive potential [109, 110].

In this work, the main objective was to exploit *P. oceanica* waste biomass as a potential source of bioactive extracts. In addition to the conventional organic solvent extraction protocol, alternative greener water-based extraction protocols based on heat and ultrasound-assisted methods were explored for the production of extracts. An exhaustive analysis of the composition and bioactive properties (antioxidant, antifungal and antiviral capacity) of the generated extracts was carried out with the aim of evaluating their potential as bioactive food or pharma ingredients, as well as extending the knowledge on the direct impact of the extraction method on the properties of the extracts.

3. Materials and Methods

3.1 Materials and reagents

Biomass waste material consisting of *Posidonia oceanica* (*P. oceanica*) leaves was collected from the shore in Calpe, Alicante (Spain) (38°38′09″N 0°04′16″E) in February-March 2017 (two different batches were collected). The collected leaves had a dark brown coloration. The material was washed vigorously with water to remove sand and salts and stored at 4º C until its use.
2.,2´-Azino-bis (3-ethylbenzothiazoline-6-sulfonic acid) diammonium salt (ABTS), (±)-6-Hydroxy-2,5,7,8-tetramethylchromane-2-carboxylic acid (Trolox) 97%, ethanol (>99.8%), toluene, acetic acid, formic acid and sodium persulfate were purchased from Sigma–Aldrich. The Folin-Ciocalteau reagent, modified Lowry reagent and bovine serum albumin were obtained from the "modified Lowry protein assay kit" purchased from Thermo Fisher scientific (Spain). All the salts, reagents and monosaccharides used for the carbohydrate composition analysis were purchased from Merck (Sigma).

3.2 Production of P. oceanica extracts

Different extracts were generated by treating the *P. oceanica* waste biomass to diverse extraction protocols, which are described in the following sub-sections. A brief description of the different extracts generated is compiled in Table 3.

3.2.1 Water-based extractions

Water-soluble extracts were obtained by adding 100 g of wet *P. oceanica* leaves (~10 g of dry material) into 250 mL of distilled water and mixing in an electric blender until obtaining a homogeneous paste. This paste was then subjected to two different treatments:

(i) Heating treatment: The paste was heated up to 90ºC with stirring for 2 hours. After that, the material was centrifuged at 24,000 RCF and 15ºC for 20 minutes. The solid precipitate was separated, dried and stored at 0% relative humidity (RH) for the production of the organic-soluble extracts (see section 2.2.2). The liquid supernatant was placed in an ice bath and the required volume of ethanol (75% with regards to the supernatant volume) was added dropwise. The material was kept stirring overnight and subsequently, it was centrifuged at 24,000 RCF and 15ºC for 20 minutes. The supernatant was placed in an oven at 60ºC to evaporate the ethanol and it was then freeze-dried to obtain a whitish powder extract coded as E1 H_2O. On the other hand, the precipitate was re-suspended in distilled water and freeze-dried, yielding a darker powder coded as E2 H_2O.

(ii) Ultrasound treatment: The paste was subjected to an ultrasound treatment by immersing an ultrasound probe UP-400S (Hielscher GmbH, Germany) operating at a maximum power of 400W and a constant frequency of 24 kHz for 30 minutes. After that, the same protocol described for the E1 H_2O and E2 H_2O extracts was followed, obtaining the materials coded as E1 US and E2 US. The extracts were stored at 0% RH until their use.

3.2.2. Organic solvent-based extractions

The solid residues obtained after the first centrifugation in the heating and ultrasound treatments were subjected to a Soxhlet extraction with 800 mL of toluene:ethanol (2:1) for 24 h. The liquid phase was then collected and the solvents were evaporated by distillation on a rotary evaporator (G3 Heidolph, Germany) operating at 60ºC and vacuum conditions. The dry material was re-suspended in 50 mL of pure ethanol, which was subsequently evaporated at room temperature to obtain the extracts coded as E3 H_2O (obtained from the solid residue of the heating treatment) and E3 US (obtained from the solid residue of the ultrasound treatment). The extracts were stored at 0% RH until their use.

Table 3. Sample codes for the different P. oceanica extracts.

Sample code	Pre-treatment	Extraction method	Solvent	Fraction (Ethanol precipitation)
E1 US	---	Ultrasound	Water	Supernatant
E1 H_2O	---	Heating	Water	Supernatant
E2 US	---	Ultrasound	Water	Precipitate
E2 H_2O	---	Heating	Water	Precipitate
E3 US	Ultrasound	Soxhlet	Toluene:ethanol	---
E3 H_2O	Heating	Soxhlet	Toluene:ethanol	---

3.3 Chemical composition analysis

3.3.1 Total phenolic content

The total phenolic content of the extracts was estimated by the Folin-Ciocalteau colorimetric assay [111]. Briefly, Folin-Ciocalteau reagent was diluted 1:10 (v/v) with distilled water and 1 mL of the final dilution was mixed with 0.2 mL of the extract sample (diluted in water, in the case of the water-soluble extracts or in ethanol, in the case of the organic-soluble extracts) at room temperature. Finally, 0.8 mL of sodium carbonate (75 mg/mL) were added and the samples were heated up to 50ºC during 30 minutes. Absorbance values were read at 750 nm. A calibration curve was built by using gallic acid as the standard and the total phenolic content was expressed as mg of gallic acid (GA)/g extract. All determinations were carried out in triplicate.

3.3.2 Protein content

Total protein content was measured following the Lowry method with some minor modifications [112]. Briefly, 1 mL of the modified Lowry reagent was mixed with 0.2 mL of the extracts and incubated for 10 minutes at room temperature. Then, 0.1 mL of Folin-Ciocalteau reagent (previously diluted 1:1 with distilled water) were added and vortexed, incubating the resulting solution for 30 minutes at room temperature. A blank was prepared with 0.2 mL of distilled water and the reagents and absorbance were read at 750 nm. A calibration curve was prepared with serial dilutions of bovine serum albumin (BSA) and the total protein content was expressed as mg BSA/g extract. All determinations were carried out in triplicate.

3.3.3 Lipid content

Total lipid content was measured following the sulpho-phosphovanillin method with some minor modifications [113]. In brief, phosphovanillin reagent was prepared by dissolving vanillin in

water (6g/L) and then mixing 350 mL with 50 mL of H_2O and 600 mL of phosphoric acid. For sample analysis, 20 µL of sample were mixed with 0.2 mL of concentrated sulphuric acid, stirred and incubated in boiling water for 10 minutes. Then, samples were conditioned with cold water during 5 minutes and 10 mL of phosphovanillin were added, and incubated at 37ºC during 15 min. A blank was prepared with 20 µL of ethanol and the reagents and the absorbance was finally read at 540 nm. A calibration curve was made using known concentrations of sunflower oil, and the total lipid content was expressed as mg lipids/g extract. All determinations were carried out in triplicate.

3.3.4 Ash content

Ash content was determined by the standard method TAPPI T211 om-07. Briefly, dry samples were placed in a muffle for at least 4 hours at 525 ºC ± 25 ºC. Ash content was measured by the ratio of the resulting material divided by the initial weight. Determinations were carried out in duplicate.

3.4 Carbohydrate composition

The carbohydrate content and sugar composition of the extracts was determined after acidic methanolysis, as previously described [114]. The monosaccharides were analysed using high performance anion exchange chromatography with pulsed amperometric detection (HPAEC-PAD) with a 940 IC system (Metrohm) equipped with a Metrosep Carb 2 column (4 × 250 mm, Metrohm). Control samples of known concentrations of mixtures of glucose, fucose, galactose, arabinose, xylose, mannose, galacturonic acid and glucuronic acid were used for calibration. All experiments were carried out in triplicate.

3.5 Fourier Transform Infrared Spectroscopy (FT-IR)

Freeze-dried extract samples of ca. 1.2 mg were ground and dispersed in 120 mg of spectroscopic grade KBr. A pellet was then formed by compressing the sample at ca. 10 tons. FT-IR experiments were recorded in transmission mode in a controlled chamber at 21ºC and dry air using a Thermo Nicolet Nexus (GMI, USA) equipment. The spectra were taken at 4 cm^{-1} resolution in a wavelength range between 400-4000 cm^{-1} and averaging a minimum of 32 scans.

3.6 X-ray diffraction (XRD)

XRD measurements of the freeze-dried extracts were carried out on a D5005 Bruker diffractometer. The instrument was equipped with a Cu tube and a secondary monochromator. The configuration of the equipment was θ–2θ, and the samples were examined over the angular range of 3°–60° with a step size of 0.02° and a count time of 200 s per step.

3.7 Thermogravimetric analyses (TGA)

Thermogravimetric curves (TG) were recorded with a Setaram Setsys 16/18 (SETARAM Instrumentation, France). The samples (ca. 10 mg) were heated from 30 to 1000ºC with a heating rate of 10ºC/min under nitrogen atmosphere. Derivative TG curves (DTG) express the weight loss rate as a function of temperature.

3.8 ABTS$^{\cdot+}$ radical cation scavenging activity

The ABTS$^{\cdot+}$ radical cation scavenging activity was used to determine the antioxidant capacity of the extracts [115]. Briefly, 0.192 g of ABTS were dissolved in 50 mL of PBS at pH = 7.4 (for water-soluble extracts) or ethanol (organic-soluble extracts) and mixed with 33 mg of potassium persulfate overnight in the dark to yield the ABTS$^{\cdot+}$ radical cation. Prior to use in the assay, the ABTS$^{\cdot+}$ was diluted with either PBS or ethanol for an initial absorbance of ~0.70 ± 0.02 (1:50 ratio) at 734 nm, at room temperature. Free radical scavenging activity was assessed by mixing 1.0 mL diluted ABTS$^{\cdot+}$ with 10 µL of test antioxidant and monitoring the change in absorbance at 0, 1, 5, 10, 15 and 120 min (until a steady state was achieved). A calibration curve was built by using 6-Hydroxy-2,5,7,8-tetramethylchromane-2-carboxylic acid (Trolox). The antioxidant capacity of the extracts was expressed as µmol Trolox equivalents (TE)/g extract. All determinations were carried out in triplicate.

3.9 β-Carotene-linoleic acid assay

The antioxidant capacity of the extracts was also evaluated by the β-carotene-linoleic acid assay [116]. In brief, 4 mg of β-carotene were dissolved in 20 mL of chloroform. 2 mL of this solution were placed on a rotary evaporator and the chloroform was evaporated. Then, 50 µL of linoleic acid and 400 mg of Tween 40 were added and the content of the flask was mixed with stirring. After that, 100 mL of aerated distilled water was transferred to the flask and stirred vigorously. 5 mL of the prepared β-carotene emulsion were transferred to a series of tubes containing 0.5 mL of each extract (0.5-5 mg/mL), BHT (0.1-1 mg/mL) as a positive control and ethanol as the negative control. The samples were incubated in a water bath at 50 °C for 120 min. The absorbance of each sample at 470 nm was measured every 15 minutes using a spectrophotometer. The E1 and E3 extracts were tested at 0.5-5 mg/mL, while lower concentrations of 0.5-3 mg/mL had to be used for the E2 extracts, due to their higher antioxidant capacity. All the determinations were carried out in triplicate.

3.10 Antifungal activity assays

Penicillium digitatum (Pers.:Fri.) Sacc. Pd1 (denoted as PDIP and deposited in the Spanish Type Culture Collection with accession code CECT20795) was isolated from an infected grapefruit in Valencia. *Penicillium italicum* isolate PHI1 (denoted as PITC, CECT20909) was isolated from a

mandarin stored at 4º C in Valencia, Spain. *Penicillium expansum* Link isolate CMP-1 from Spain (denoted as PEX1, CECT20906) was isolated from a decayed 'Golden' apple after several months in storage in Lleida, Spain. *Geotrichum candidum* (isolate IATA 144) was isolated from an orange. *Botryitinia fuckeliana* (de Bary) Whetzel 1945 (*Botrytis cinerea* as anoamorph) and *Aspergillus niger* van Tieghem 1867 were obtained from the Spanish Type Culture Collection (CECT2100 and CECT2088, respectively).

Conidial suspensions were prepared in sterile distilled water from a 7-day-old culture grown on potato dextrose agar (PDA) at 24 ºC. The spore concentration was adjusted as required with the aid of a hemacytometer.

Growth inhibition assays were performed in 24-well microtiter plates (Nunc, Roskilde, Denmark) in a total volume of 800 µL of PDA containing serial dilutions of the extracts. Growth of strains was evaluated by depositing 5 µL of a conidial suspension (10^5 conidia/mL) on each well. All samples were prepared in triplicate. Plates were incubated up to 7 days at 24 ºC. Growth was determined by measuring the diameter of the colony using the software ImageJ.

3.11 Antiviral activity assays

Feline calicivirus (FCV) F9 strain (ATCC VR-782) and murine norovirus (MNV) (kindly provided by Prof. H.W. Virgin, Washington University School of Medicine, USA) were assayed and propagated in CRFK (ATCC CCL-94) and RAW 264.7 cell lines (also provided by Prof. H.W. Virgin), respectively. Viruses were harvested and titrated as described by [117]. Briefly, infectious viruses were enumerated by determining the 50% tissue culture infectious dose ($TCID_{50}$) with eight wells per dilution and 20 µl of inoculum per well using the Spearman-Karber method.

To elucidate the antiviral activity of *P. oceanica* extracts, 0.05 and 0.5 % of E1 US, E1 H_2O, E2 US, E2 H_2O, E3 US and E3 H_2O extracts were incubated overnight with an equal volume of FCV or MNV suspensions (about ca. 7 log $TCID_{50}$/mL) at 25 (FCV) or 37ºC (MNV). The samples were then diluted with 1.8 mL of Dulbecco's Modified Eagle's Medium (DMEM) supplemented with 10% fetal calf serum (FCS) and residual infectivity was determined by $TCID_{50}$. Ten-fold dilutions of treated and untreated virus suspensions were inoculated into confluent in CRFK and RAW monolayers in 96-well plates. Then, infectious viruses were enumerated by cell culture assays as described above.

Each treatment was done in triplicate. Positive controls were virus suspensions added with PBS only under the same experimental conditions. The decay of FCV and MNV titers was calculated

as $\log_{10}$ (N_x/N_0), where N_0 is the infectious virus titer for untreated samples and Nx is the infectious virus titer for *P. oceanica*-treated samples.

3.12 Statistical analysis

Data analysis was carried out using Statgraphics Stratus by Statgraphics Technologies, Inc. One-way analysis of variance (ANOVA) was done to determine the significant differences between sample means, at a significance level of $P < 0.05$. Mean comparisons were performed by the Tukey Test.

4. Results and Discussion

4.1 Composition and structural characterization of the *P. oceanica* extracts

P. oceanica biomass extracts were produced by using water-based and organic solvent-based extraction protocols. Both the nature of the solvent and the extraction method used were expected to result in extracts with different composition and properties [101, 102]. The yields for the water-based extractions, calculated with respect to the initial dry weight of *P. oceanica* biomass, were 6.0 ± 0.8% for E1 US, 9.3 ± 2.8% for E1 H_2O, 2.1 ± 0.1% for E2 US and 3.0 ± 0.3% for E2 H_2O. These results were very similar to those obtained by applying ultrasound and hot water extraction techniques to raw biomass from *Lentinus edodes* [104]. Interestingly, the ultrasound treatment allowed to decrease 4-fold the extraction time with respect to the heating treatment, but the extraction yields were not significantly ($p>0.05$) reduced, hence highlighting its potential as an alternative cost-effective and energy-saving method. The organic solvent-based extractions gave rise to yields of 10.8 ± 2.2% for E3 US and 9.4 ± 2.8% for E3 H_2O, which were higher than the values previously reported for *P. oceanica* extracts obtained with organic solvents using ultrasound and NaOH pre-treatments (ca. 1.0-7.5%) [118]. The differences in the yields from the E1, E2 and E3 extracts are expected to arise from their distinct composition and the relative abundance of their components in the raw *P. oceanica* biomass.

The composition of the extracts was quantitatively evaluated and the results are compiled in Table 1. As deduced from the results, the E1, E2 and E3 extracts presented very different compositions. While the E1 extracts were mainly constituted of ashes (72-75%), the E2 extracts contained relatively high fractions of ashes (34-41%), proteins (27-37%) and carbohydrates (12-29%). On the other hand, and as already anticipated, the E3 extracts, obtained using organic solvents, were mainly composed of lipids (56-79%). It is worth noting that for the water-based extractions, the ultrasound treatment led to higher amount of extracted ashes, whereas greater amounts of carbohydrates, proteins and polyphenols were extracted by the heating treatment. Although ultrasound techniques have been previously reported to effectively disrupt the cell wall structure

in aquatic biomass materials, aiding the extraction of less accessible components [119], the reduced extraction time applied in this case was most likely responsible for the lower quantities of extracted components. On the other hand, despite the reduced extraction time, the cell wall disruption produced by the ultrasound treatment seemed to promote a greater extraction of lipids in E3 US as compared to E3 H_2O.

Table 1. Total carbohydrate, protein, lipid and phenolic content and antioxidant capacity of the extracts, evaluated by the ABTS and β-carotene bleaching methods. Different letters within the same column denote significant differences between extracts ($p \leq 0.05$).

	Carbohydrate content (mg/ g extract)	**Protein content (mg BSA/ g extract)**	**Lipid content (mg/ g extract)**	**Total phenolics (mg GAE/ g extract)**	**Ash content (mg/ g extract)**	**TEAC (µmol TE/ g extract) (*)**	**% β-carotene bleaching inhibition (†)**
E1 US	12.2 ± 2.9^{c}	58.4 ± 3.2^{d}	n.d.	7.6 ± 2.2^{c}	751.5 ± 1.4^{a}	275.9 ± 10.2^{cd}	57.0 ± 2.3^{c}
E1 H_2O	12.9 ± 2.4^{c}	70.9 ± 1.4^{c}	n.d.	37.9 ± 8.0^{b}	723.1 ± 6.6^{b}	236.5 ± 16.5^{e}	45.0 ± 1.8^{d}
E2 US	117.7 ± 18.5^{b}	269.3 ± 5.5^{b}	n.d.	48.7 ± 5.5^{b}	413.3 ± 8.8^{c}	346.7 ± 5.6^{b}	68.7 ± 4.2^{b}
E2 H_2O	287.1 ± 2.5^{a}	363.0 ± 1.9^{a}	n.d.	90.2 ± 17.6^{a}	339.1 ± 9.5^{d}	730.0 ± 12.2^{a}	65.5 ± 5.3^{b}
E3 US	-	-	785.3 ± 73.5^{a}	79.6 ± 23.1^{a}	180.7 ± 3.6^{e}	211.2 ± 51.2^{de}	70.8 ± 2.6^{b}
E3 H_2O	-	-	560.3 ± 85.3^{b}	76.2 ± 3.3^{a}	347.5 ± 22.9^{d}	443.8 ± 150.2^{bc}	82.8 ± 3.5^{a}

(*) TEAC values were calculated after 30 minutes. (†) Calculated for the extracts at a concentration of 0.5 mg/mL.

Phenolic compounds are one of the most relevant components targeted in plant extracts, since their abundance is usually correlated with high antioxidant capacity values [105]. Although organic solvents are commonly preferred to produce polyphenol-rich extracts, glycosylated polyphenols are expected to be more easily extracted with water [120]. This may explain the fact that the E2 H_2O extract presented the highest total phenolic content (ca. 9%) from all the samples, followed by the E3 extracts (ca. 8%). The total phenolic contents in these extracts were lower when compared with those from extracts from *P. oceanica* leaves where free and bound phenolic compounds were concentrated by standard but more complex methodologies. For instance, a procedure consisting of an ultrasound treatment (90 minutes) using a mixture of methanol-water (80:20 v/v), followed by hydrolysis with NaOH and extraction with ethyl acetate, was reported for the extraction of free and bound phenolic compounds (328-407 mg GAE/g extract respectively) [118]. Thus, it seems that longer or more disruptive methods are required for the release of phenolic compounds which may be bound to proteins and/or polysaccharides in the cell walls of *P. oceanica* biomass. Different phenolic compounds have been identified in P. oceanica leaves by HPLC, being chicoric acid the most abundant one and also having significant amounts

of gentisic acid and ferulic acid [121]. These phenolic compounds might play a significant role in the bioactivity of the obtained extracts.

Apart from the phenolic compounds, the bioactive properties of extracts from aquatic biomass have also been attributed to the presence of polysaccharides [97]. Given their potential interest, a compositional carbohydrate analysis was carried out in E1 and E2 extracts (as E3 did not contain significant amounts of carbohydrates (cf. Table 1). As observed in Figure 1A, the low carbohydrate content in the E1 extracts (ca. 1 wt%) can only be attributed to low molecular weight oligosaccharides or monosaccharides, since these extracts corresponded to the fraction that did not precipitate upon ethanol addition. The composition was rather similar for E1 H_2O and E1 US, glucose being the main sugar component (ca. 0.8 wt%), followed by very minor quantities of xylose and galactose. These minor oligo- or monosaccharides might be present as part of metabolic (in the case of glucose) or cell wall synthesis processes, or even arise from a minor polymer degradation during the extraction process. The E2 extracts contained the ethanol precipitated polysaccharides. In this case the E2 US and E2 H_2O extracts differed in their quantitative and qualitative composition. As shown in Figure 1B, the E2 H_2O extract showed higher contents in most sugar units, especially galactose, as well as glucose, whereas the E2 US extract was comparatively enriched in galacturonic acid and xylose. Similar results have been obtained by applying microwave extractions to *P. oceanica* leaves in terms of galactose and glucose contents [103]. Given the mild extraction conditions (neutral pH and temperature <100°C), cellulose or tightly bonded hemicelluloses were not likely to be extracted [122, 123]. Therefore, we speculate that the differences might be associated to pectin extraction (galacturonans in the case of E2 US and galactans in E2 H_2O extracts), while loosely or more soluble hemicelluloses (mainly glucans and xylans), might also be extracted to some extent. The more efficient extraction under heat treatment (E2 H_2O) would therefore yield higher pectin content, in form of galactans and arabinogalactans, as the probable major pectin component in *Posidonia* species [124]. The preferential extraction of galacturonans with the ultrasonic treatment, at the expense of lower extraction yields, is in line with previously published results [119]. Glucuronoarabinoxylans are the main hemicellulose component in herbaceous plants and seem to be equally extracted with both techniques, while glucan extraction would be favoured with the heating treatment [125]. To the best of our knowledge, there is no previous literature related to the polysaccharide composition of *P. oceanica*. A more detailed compositional analysis of the raw material is out of the scope of this article and may constitute the subject of future research.

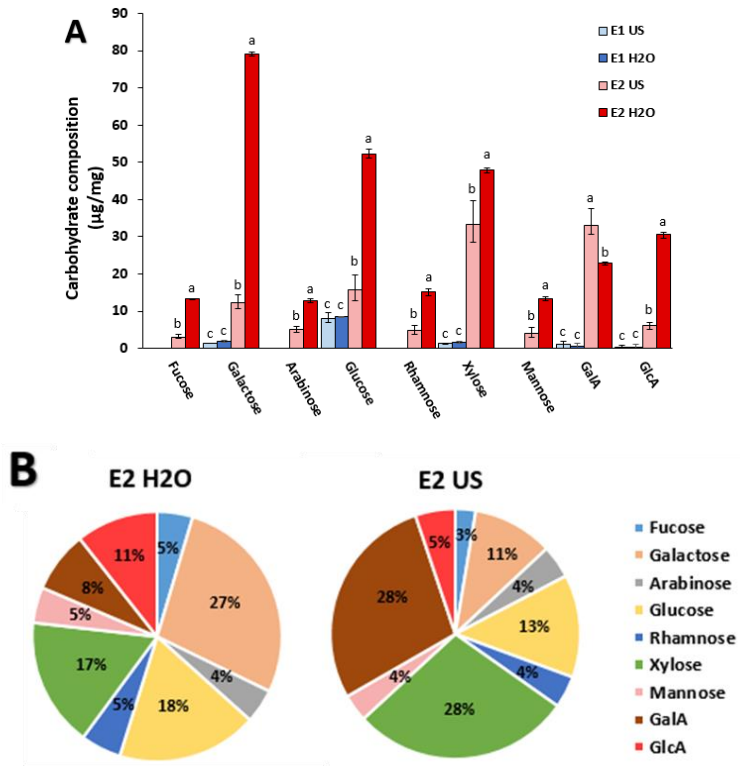

Figure 1. Carbohydrate composition of the aqueous *P. oceanica* extracts. (A) Absolute concentration values for E1 and E2 extracts and (B) their relative abundance in the E2 extracts. Different letters denote significant monosaccharide content differences between extracts ($p \leq 0.05$).

FT-IR analyses were carried out to confirm the compositional differences in the *P. oceanica* extracts. The obtained spectra, shown in Figure 2, evidence the marked compositional differences between the E1 and E2 extracts (water-based extractions) and the E3 extracts (organic solvent-based extractions), with the former ones showing several characteristic bands corresponding to proteins, polyphenols and polysaccharides, while characteristic bands from lipidic components were detected in the spectra from the latter ones. The FT-IR spectra of E1 and E2 extracts contained signals at around 3392, 2912, 2848, 1616, 1430 and 1124 cm^{-1}. The broad band observed around 3392 cm^{-1} is assigned to the stretching vibrations of the O−H groups present in phenolic compounds and polysaccharides as well as N-H stretching vibrations from proteins. The small bands located at 2912 and 2848 cm^{-1} are attributed to symmetric and asymmetric C−H, CH_2 and CH_3 stretching and bending vibrations. The peak observed at ca. 1618 cm^{-1} is characteristic of protein amides, whereas the region located at 1200–600 cm^{-1} can be associated to polysaccharide characteristic peaks, ascribed to C−C and C−O stretching modes. The aforementioned bands could not be unequivocally attributed to the presence of proteins, polysaccharides and polyphenols in the extracts, as they have also been reported to arise from the presence of mineral compounds [126].

According to the compositional analysis (cf. Table 1), the E1 extracts were mainly composed of ashes, i.e. mineral compounds. The FT-IR spectra from these samples were very similar to those from a low combusted ash sample of eastern Spain Mediterranean biomass (containing *Pinus halepensis*, *Quercus coccifera* and *Rosmarinus officinalis*) [127]. Furthermore, the band located between 1080-1180 cm^{-1} has been previously attributed to the stretching vibration of Si—O groups from the inorganic components in native soil samples (ash content > 80%) [128] and was present in both E1 extracts, in agreement with the high ash content detected for these extracts (cf. Table 1). Furthermore, the appearance of a sharp and intense peak at 621 cm^{-1}, which has been previously ascribed to different compounds such as sulphur, phosphorous or silica [129] confirmed the high inorganic matter content in the E1 extracts.

Although the spectra from the E2 extracts showed some similarities with the E1 extracts (due to their high mineral content), the shape of the most intense peaks differed significantly, most probably due to the overlapping of mineral characteristic peaks with bands arising from the presence of polysaccharides and proteins in the E2 extracts. This is the case of the 1700-1400 cm^{-1} region, where two intense peaks at around 1616 and 1430 cm^{-1} (typically associated to the primary amide and CH_2 and CH_3 asymmetric deformation of proteins, respectively) had a sharper appearance in the case of the E2 extracts. Several peaks were detected for the E2 extracts within the polysaccharide "fingerprint" region (i.e. 1200-800 cm^{-1}). For instance, the intense and sharp peak detected at around 877 cm^{-1} in both E2 extracts is known to correspond to the pyranose rings from mannose and galactose [130], whose content was remarkably high, especially in the case of E2 H_2O. Additionally, the peaks located at ca. 673 and 601 cm^{-1}, which appeared sharper in the E2 US extract, have been previously assigned to the presence of xylan-type polysaccharides [[131], supporting the greater xylose content in E2 US as evidenced by the carbohydrate compositional analysis (Fig. 1B).

Finally, in agreement with the high lipidic content of the E3 extracts, two sharp and intense peaks were detected at 2918 and 2850 cm^{-1}, corresponding to the CH_2 asymmetrical and symmetrical stretching from fatty acids. Additional peaks arising from the presence of lipids were also detected at ca. 1730 cm^{-1} (C==O of ester groups), 1616 cm^{-1} (carboxylic group) and 1136 cm^{-1} (C—O). It should be noted that *P. oceanica* has been characterized by the presence of long-chain fatty acids (C_{22}-C_{34}), such as palmitic, palmitoleic, oleic, and linoleic acids [132].

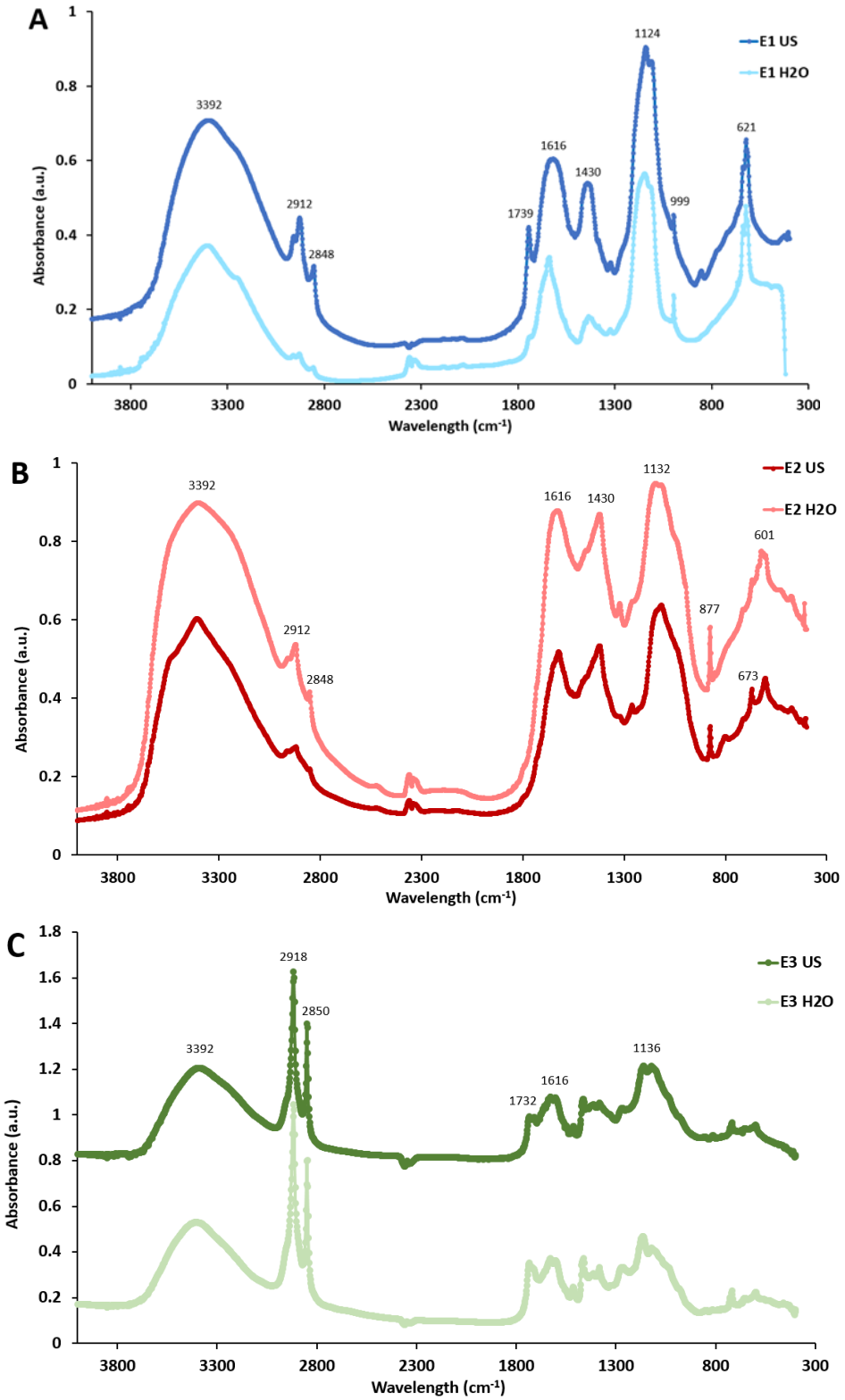

Figure 2. FT-IR spectra of the different P. oceanica extracts obtained by means of water-based extractions (A and B) and organic solvent-based extractions (C). E1 US, E2 US and E3 US spectra have been offset for clarity.

The X-ray diffraction patterns of the different extracts are shown in Figure 3. As observed, both E1 extracts showed three intense peaks at 20º, 27º and 32º. These diffraction peaks have been previously related to the presence of mineral compounds. The peak at 20º has been assigned to the presence of silicates [133], the peak at 27º has been attributed to calcite in ash samples from lignocellulosic biomass [134, 135] and the peak at 32º has been attributed to serendibite in seaweed ash biomass [133]. Moreover, three additional peaks located at 16º, 17º and 22º were present in the case of E1 US, which have been associated to sulphate-containing minerals [135]. Most of these mineral components, particularly silicates, are responsible for maintaining the rigidity of plant tissues and are supposed to be introduced into the feedstock through endocytosis during the growth stage [134]. The E2 extracts displayed their most remarkable diffraction peaks located at 12º, 21º and 29º, being these much more intense and defined in E2 US. The peak at 12º has previously been related to crystalline structures containing galacturonic acid [136], while the peak at 21º has been reported to be present in xylanes [137]. These results are consistent with the carbohydrate composition analyses (Fig. 1B), which showed greater ratios of galacturonic acid and xylose in E2 US. On the other hand, the peak at 29º has been attributed to the presence of KCl in an extract obtained from *Enteromorpha clathrata* with a protein, carbohydrate and ash composition similar to that from the E2 extracts [133].

In the case of E3 extracts, the detected diffraction peaks were expected to arise from the presence of lipids and minerals, according to their composition. While the most intense peaks in the E3 H_2O extract were those located at 21º and 24º, the most intense peak for the E3 US extract was that located at 32º. The peak at 21º has been detected in different linoleic acid polymorphs [138]. Although it was not possible to unequivocally assign these peaks to specific fatty acids, the results seem to indicate that a different lipidic profile was attained in the extracts depending on the treatment applied prior to the organic solvent extraction.

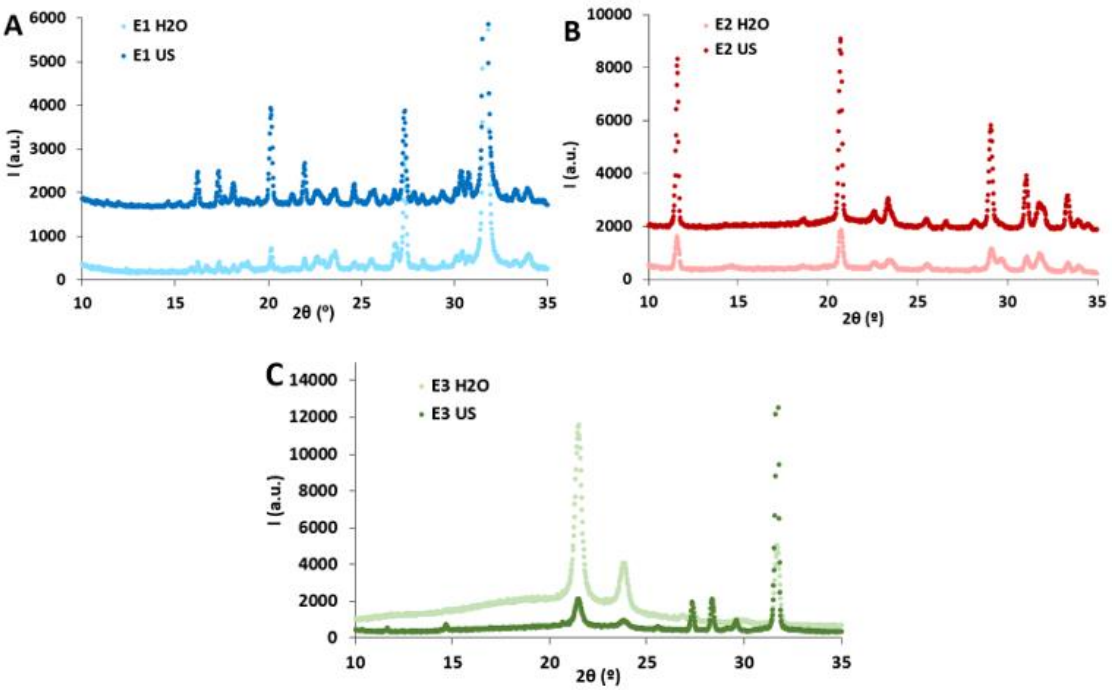

Figure 3. XRD patterns of the freeze-dried extracts. (A and B) water-soluble extracts and (C) organic-soluble extracts. The spectra from E1 US and E2 US have been offset for clarity.

The thermal stability of the different extracts was evaluated by means of TGA and the results are shown in Figure S1 (Supplementary Material). As observed, once again, the water-extracted E1 and E2 extracts presented a very different behaviour to that from the organic solvent-extracted E3 extracts. While the total weight loss at 600 ºC was of ca. 20-30% and 30-50% for the E1 and E2 extracts, respectively, it was >60% for the E3 extracts. This again confirms the presence of significant amounts of thermally-resistant minerals in the E1 and E2 extracts. The peaks detected within the range of 50-150 ºC correspond to dehydration processes and were more evident in the E1 and E2 extracts, given their more hydrophilic character. The E1 extracts did not show any evident degradation peaks within the range of 150-550 ºC, which was most likely due to the higher thermal stability of the inorganic materials mainly composing these extracts (which typically undergo thermal degradation at 600-800º C [127]. On the other hand, the E2 extracts presented a broad peak with the maximum located at ca. 260 ºC, which may arise from the degradation of carbohydrates [126]. In fact, a previous study reported that the hemicelluloses and the cellulose contained in *P. oceanica* biomass show degradation processes with their maximum located at 260º C and 334º C, respectively [50]. A second peak, centred at ca. 480 ºC, was also detected in E2 H_2O. This could arise from the presence of arabinoxylan [139], arabinogalactan and galactomannan [140], which were more abundant in E2 H_2O.

The E3 extracts were characterized by a multiple degradation step profile, starting at temperatures higher than 220 ºC. The maximum degradation rate occurred at 240 ºC for E3 US, while for E3 H_2O the maximum degradation rate corresponded to the higher temperature peak at 430 ºC. This

might be due to the thermal degradation of major lipidic compounds present in *P. oceanica*, such as oleic and linoleic acid, whose degradation temperatures range between 350 ºC and 450 ºC [141]. Moreover, the association of these lipids with more thermally stable minerals in the E3 H_2O extract may be responsible for the greater thermal stability of this extract.

4.2 Evaluation of the bioactive properties from the P. oceanica extracts

4.1.1 Antioxidant capacity

The antioxidant capacity of the extracts was evaluated by the ABTS and β-carotene bleaching assays and the results are gathered in Table 1. As observed, the E2 H_2O extract presented the highest antioxidant capacity according to the ABTS method (ca. 730 µmol TE/g extract), followed by E3 H_2O and E2 US. Considering the results from the compositional analysis (cf. Table 1), there was not a direct correlation between the antioxidant capacity and the polyphenol content in the extracts. Although the E2 H_2O and E3 H_2O were within the extracts having the highest polyphenol contents, that was not the case for E2 US. It seems that, as previously noted for other water-based extracts from aquatic biomass [142], apart from polyphenols some other compounds such as proteins and polysaccharides may also contribute to the antioxidant potential of the extracts. All the extracts presented values higher than 200 µmol TE/g extract, which are comparatively greater than the extracts from other plants such as a range of medicinal Indian plants [105] (which presented an average value of 270 µmol TE/g extract) and fifteen different species of medicinal Mediterranean plants (with their water and methanolic extracts ranging from ~100 to ~1000 µmol TE/g extract) [143]. This highlights the great potential of the *P. oceanica* extracts as antioxidant agents. In particular, given its environmentally friendly character and ease of production, the E2 H_2O extract represents an interesting material.

In order to confirm the antioxidant capacity using a method more directly related to their application in food systems, the β-carotene bleaching inhibitory assay was carried out with the extracts tested at different concentrations (results shown in Figure S2, Supplementary Material). From this figure it can be observed that all the extracts completely inhibited the *β*-carotene bleaching when tested at their highest concentration (5 mg/mL). However, when tested at the lowest concentration (0.5 mg/mL), E3 H_2O showed the highest bleaching inhibition, followed by E3 US, E2 US and E2 H_2O (cf. Table 1). The inhibition capacity values of the E3 extracts were very similar to those reported for the methanolic extracts from *Rhodomyrtus tomentosa* (~80% inhibitory activity tested at a concentration of 0.5 mg/mL) [144], which contained a remarkable amount of polyphenols (190 mg GAE/g extract) and flavonoids (111 mg/g extract), once again confirming that other components present in the extracts also contributed to their antioxidant capacity. On the other hand, water-soluble extracts from potato peels with high polysaccharide

content (similar to the E2 extracts) showed quite lower bleaching inhibitory capacity (between 30-40% when tested at a concentration of 10-50 mg/mL) [145]. Lower inhibition values were also reported for aqueous extracts from almond-gum (30-80% when tested at a concentration of 5 mg/mL) [146] and *Arundo donax* (61-93% when tested at a concentration of 5 mg/mL) [51], again confirming the excellent antioxidant potential of *P. oceanica* extracts.

4.2.2 Antifungal activity assays

Antifungal activity assays were carried out in order to assess the potential of the extracts to inhibit or reduce the growth of several fungi with significant incidence in the food industry. Antifungal activity was tested *in vitro* against a collection of isolates from the postharvest fungal pathogens *P. digitatum*, *P. italicum*, *P. expansum*, *B. cinerea*, *G. candidum* and *A. niger* after 3 and 6-7 days post inoculation (dpi) (Table 2 and Fig. S3). No differences in fungal growth were observed by using different concentrations of the E1 extracts neither at 3 dpi nor at 7 dpi (data not shown). However, the application of both E2 US and E2 H_2O extracts reduced the growth of *P. digitatum* and *B. cinerea* at 3 dpi, being effective against *P. digitatum* even after 7 days. The antifungal activity of E2 US was higher than that of the E2 H_2O extract, with a 37% and 12% of reduction in the diameter of *P. digitatum* at 3 dpi, respectively. These differences might correspond to the distinct composition between E2 extracts (carbohydrates, proteins and ashes).

Among the three extraction methods, the E3 extracts were the most effective ones reducing the growth of all six postharvest pathogens assayed, being particularly effective with a reduction of 100% in the diameter of *B. cinerea* at day 3 of both E3 US and E3 H_2O extracts. It is also important to highlight their effectiveness in reducing the sporulation of some strains, especially *A. niger* (Fig. S3). The higher effectiveness of E3 US extract compared to E3 H_2O extract may be due to their different bioactive profiles, with a higher lipidic content in E3 US (cf. Table 1).

In comparison with other extracts obtained from marine and terrestrial plants, including medicinal plants such as rosemary, peppermint or oregano, these extracts showed significant inhibitions in the growth of *B. cinerea* at concentrations between 6 and 25%. Plants from genus *Allium* and *Capsicum* showed highest inhibitory activities after 24 and 48 h [147]. Moreover, root extracts from the medicinal plant *Arctotis arctotoides* displayed significant reductions (from 5 to 95% at the highest concentration tested corresponding to 5 mg/Ml) of the growth of *P. digitatum* and *P. italicum* [148]. However, it is important to highlight that these activities correspond to organic extractions of medicinal plants, while *P.oceanica* E2 extracts have been obtained from a residue using water-based green extraction methodologies. The antifungal activity assays of the *P. oceanica* extracts suggest the capability of these extracts to prevent food contamination by fungi,

augmenting the shelf-life of the products whether being incorporated in the packaging matrixes or encapsulated in safe coatings in order to be controllably released into the food environment.

Table 2. Summary of the antifungal activity showed by all the different extracts tested in the following microorganisms at 3 and 7 dpi at their highest concentration (5 mg/mL). Antifungal activity was shown as the reduction in the diameter ± SD (%).

Microorganism	**E1 US**	**E1 H_2O**	**E2 US**	**E2 H_2O**	**E3 US**	**E3 H_2O**
3. dpi.						
Penicillium digitatum	-	-	37 ± 9	12 ± 3	46 ± 2	14 ± 4
Penicillium italicum	-	-	-	-	40 ± 2	24 ± 2
Penicillium expansum	-	-	-	-	-(42 ± 3)[a]	-(27 ± 3)[a]
Botrytis cinerea	-	-	41 ± 12	19 ± 8	100	100
Geotrichum candidum	-	-	-	-	-	-
Aspergillus niger	-	-	-	-	-(100)[a]	-(90 ± 4)[a]
6-7 dpi						
Penicillium digitatum	-	-	24 ± 8	12 ± 4	-	-
Penicillium italicum	-	-	-	-	15 ± 3[b]	-[b]
Penicillium expansum	-	-	-	-	-(22 ± 3)[a]	-(19 ± 2)[a]
Botrytis cinerea	-	-	-	-	61 ± 4	69 ± 5
Geotrichum candidum	-	-	-	-	-	-
Aspergillus niger	-	-	-	-	-(100)[a]	-(70 ± 11)[a]

[a] Numbers between brackets show the % reduction in the sporulation.; [b] With remarkable reduction in the hypha's development (Fig. 5C).

4.2.3 Antiviral activity assays

Human noroviruses (NoVs) significantly contribute to foodborne diseases being the causative agent of one-fifth of acute gastroenteritis worldwide [149]. As propagation of NoVs is not routinely available, the infectivity of NoVs has mainly been inferred through culturable surrogates, such as feline calicivirus (FCV) and murine norovirus (MNV). Thus, in the present study the antiviral activity of the different extracts was evaluated against these two surrogates. Incubation of FCV and MNV with E1 and E2 extracts did not decrease FCV and MNV infectivity when compared to the control (Fig. 4). However, results clearly show that E3 US and E3 H_2O extracts were effective in reducing the titers of FCV and MNV in a dose-dependent manner, where increasing concentrations of E3 extracts showed increased reduction in viral titers. The antiviral activity of the E3 extracts must be therefore related to the presence of hydrophobic compounds

such as non-glycosilated polyphenols and lipids. Incubation of FCV with E3 US and E3 H_2O extracts at concentrations of 0.5 % after overnight incubation at 25°C (Fig. 4A) significantly decreased FCV titers by 3.4 and 3.1 log $TCID_{50}$/ml, respectively, while at 0.05% FCV titers were reduced by 2.7 and 2.1 log $TCID_{50}$/ml. These results are similar to those previously reported for a range of green tea extracts obtained using different organic solvents such as ethyl-acetate, methanol and hexane, when tested within the same range of concentrations than the *P.oceanica* extracts [150]. Additionally, the infectivity of a more resistant surrogate virus, MNV, was reduced by 2.6 log and 2.1 log and 0.7 and 0.5 $TCID_{50}$/mL after treatment with E3 US and E3 H_2O extracts at 0.5% and 0.05 respectively (Fig. 4B). Similar reductions of FCV and MNV titers have been previously reported for a commercial aqueous grape seed extract tested at concentrations between 0.25-1 mg/mL [151]. As the food industry is driven to seek natural alternative strategies to control foodborne pathogens E3 extracts have the potential to be used in food applications to control virus contamination. Currently, several natural compounds such as grape seed extract, green tea extract, essentials oils or their main compounds have been tested against NoV surrogates, demonstrating their potential in food applications as natural sanitizers or incorporated into biopolymers for their used as antiviral packaging or coatings (reviewed by [149]).

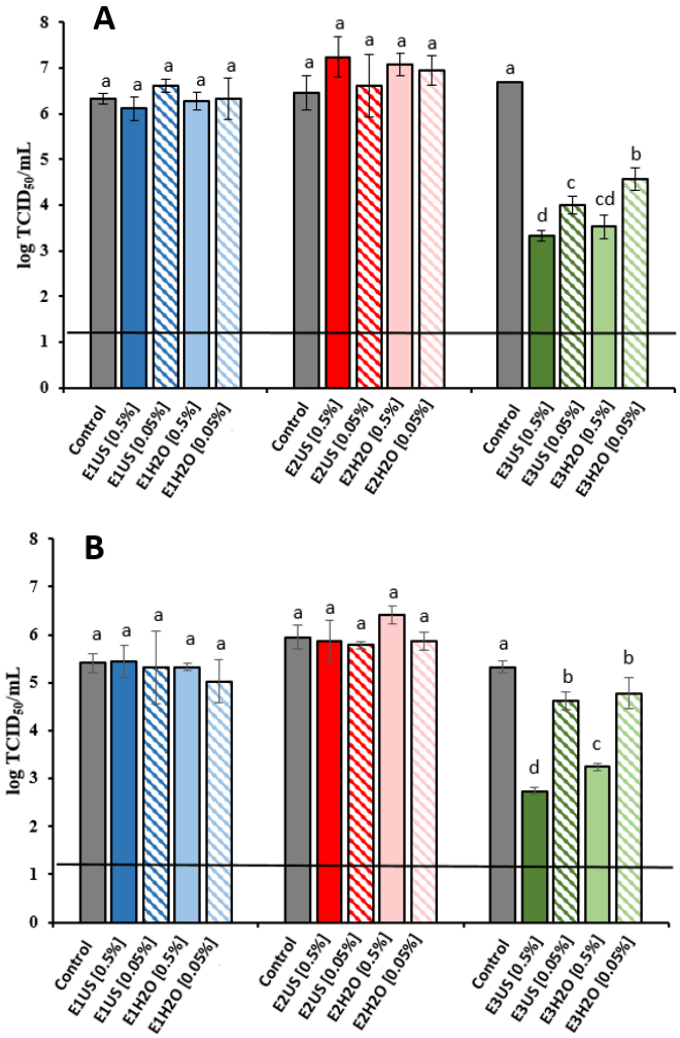

Figure 4. Reduction of (A) feline calicivirus (FCV) titers (log $TCID_{50}$/mL) and (B) murine norovirus (MNV) titers (log $TCID_{50}$/mL) treated with *P. oceanica* extracts at different concentrations (0.5 or 0.05%) after 25 ºC and 37 ºC ON incubations respectively.

*Each bar represents the average of triplicates. Within each column, different letters denote significant differences between treatments. ** Horizontal line depicts the detection limit.

5. Conclusions

Water-soluble extracts from *Posidonia oceanica* waste biomass have been produced by means of the conventional organic solvent-based extraction method, as well as alternative greener methods based on heating and ultrasound-assisted methodologies from aqueous suspensions. An in-depth characterization of the generated extracts has been carried out to assess the differences in the composition and bioactivity of the extracts depending on the extraction method. The ethanol-soluble extracts (E1 H_2O and E1 US) were mainly composed of minerals (72-75%), while the non-soluble extracts (E2 H_2O and E2 US) contained minerals (34-41%), proteins (27-37%) and carbohydrates (12-29%). On the other hand, the organic solvent-extracted fractions (E3 extracts) were mainly composed of lipids (56-79%). Specifically, the ultrasound treatment promoted the extraction of ashes and lipids, while greater amounts of carbohydrates, proteins and polyphenols were obtained with the heating extraction. The carbohydrate fraction in the E2 H_2O extract was richer in galactose and glucose, while greater relative amounts of galacturonic acid and xylose were present in E2 US.

Interestingly, all the extracts displayed remarkable antioxidant capacity values (higher than 200 µmol TE/g extract), as evidenced by the ABTS and β-carotene bleaching assays, which were not directly correlated to the phenolic contents, but rather seemed to be originated by the presence of some other compounds such as proteins and polysaccharides. Although the E3 extracts were the most effective ones reducing the growth of food-pathogen fungi such as *P.digitatum, B.cinerea* and *P.italicum,* the E2 extracts were capable of inhibiting the growth of *P.digitatum* and *B.cinerea,* being the E2 US more effective. In terms of antiviral activity, only the E3 extracts were able to reduce the infectivity of FCV and MNV in more than 2 log $TCID_{50}$/mL.

These results show the potential of *Posidonia oceanica* waste biomass for the production of bioactive extracts with interest in food-related applications. Although bioactive compounds such as non-glycosylated polyphenols are more easily extracted by organic solvents, some other compounds such as polysaccharides, proteins and glycosylated polyphenols can be extracted by means of greener methodologies avoiding the use of toxic organic solvents. In particular, given

their antioxidant and antifungal capacities, as well as their environmentally friendly character and ease of production, E2 H2O and E2 US extracts seem to be those with the most promising results, being both the hot-water and ultrasound-assisted extractions promising alternatives to the conventional organic-solvent extraction methodology. Therefore, the potential of the alternative greener extraction methodologies has been demonstrated and a complete optimization of the processes to maximize extraction yields and bioactivity of the extracts will be carried out in the future.

6. Supplementary Materials

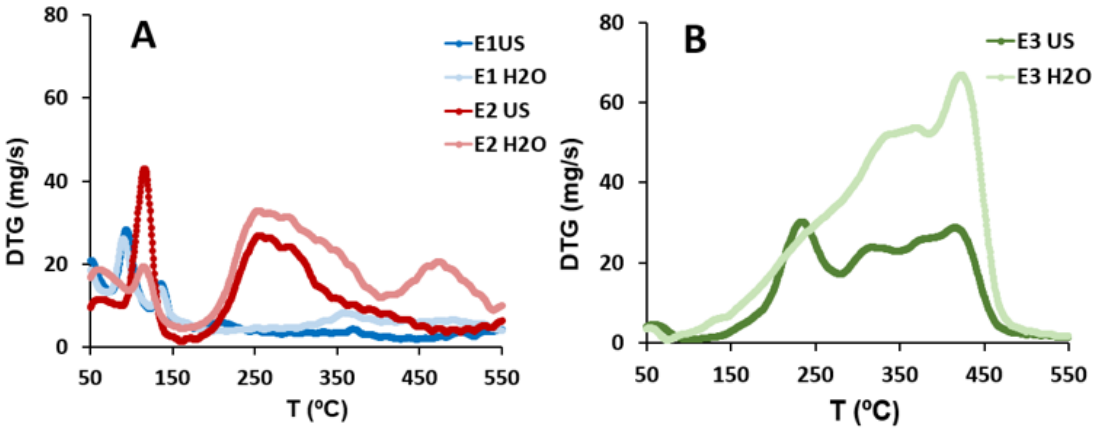

Figure S1. Derivative thermogravimetric (DTG) curves of *P. oceanica* extracts obtained by water-based extractions (A) and organic solvent-based extractions (B).

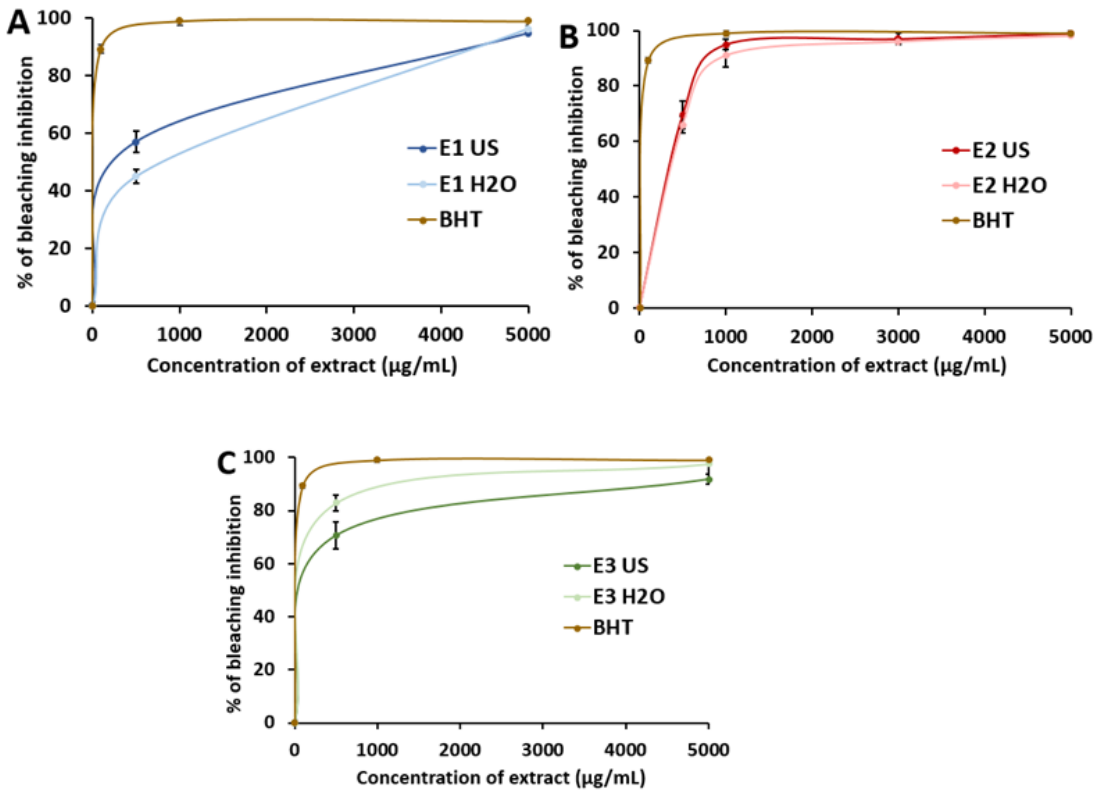

Figure S2. β-carotene bleaching inhibitory activity of the *P. oceanica* extracts tested at different concentrations. (A) E1, (B) E2 and (C) E3.

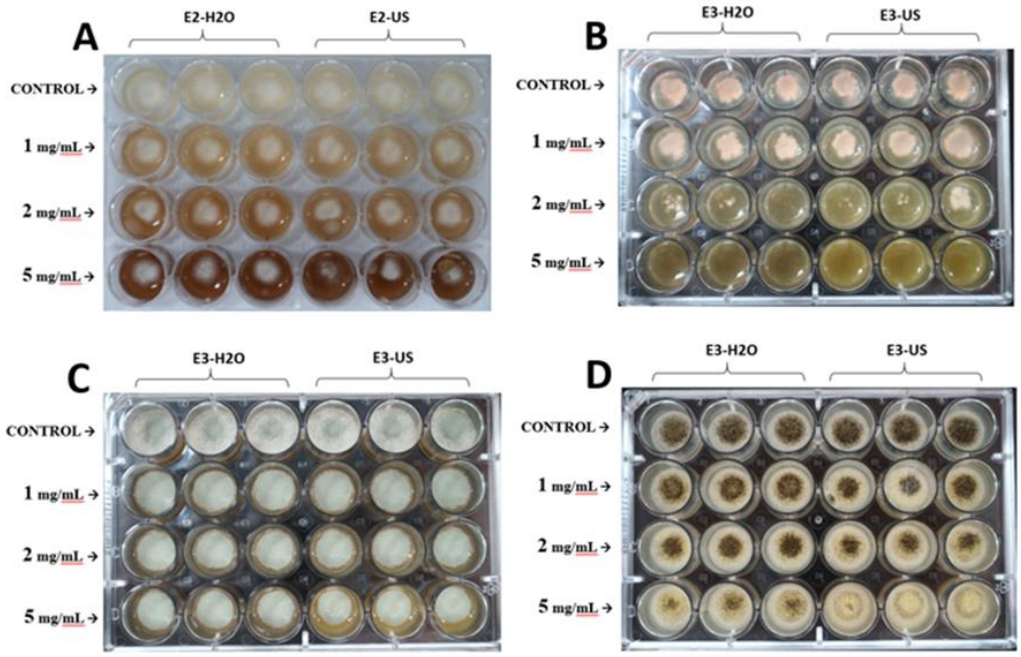

Figure S3. Antifungal activity of E2 extracts vs. *P. digitatum* (A) and E3 vs. *B. cinerea* (B) at 3 days post inoculation, and E3 vs. *P. italicum* (C) and *A. niger* (D) at 7 days post inoculation.

List of references of Chapter 1

[1] M. Darder, P. Aranda, E. Ruiz-Hitzky, Bionanocomposites: A New Concept of Ecological, Bioinspired, and Functional Hybrid Materials, Advanced Materials 19(10) (2007) 1309-1319.
[2] N. Peelman, P. Ragaert, B. De Meulenaer, D. Adons, R. Peeters, L. Cardon, F. Van Impe, F. Devlieghere, Application of bioplastics for food packaging, Trends in Food Science & Technology 32(2) (2013) 128-141.
[3] K.A. Rosentrater, A.W. Otieno, Considerations for manufacturing bio-based plastic products, Journal of Polymers and the Environment 14(4) (2006) 335-346.
[4] M. Brodin, M. Vallejos, M.T. Opedal, M.C. Area, G. Chinga-Carrasco, Lignocellulosics as sustainable resources for production of bioplastics–a review, Journal of Cleaner Production (2017).
[5] G. Balata, A. Tola, Cost-opportunity analysis of the use of Posidonia oceanica as a source of bio-energy in tourism-oriented territories. The case of Alghero, Journal of Cleaner Production (2017).
[6] M.C. Ncibi, B. Mahjoub, M. Seffen, Kinetic and equilibrium studies of methylene blue biosorption by Posidonia oceanica (L.) fibres, Journal of Hazardous Materials 139(2) (2007) 280-285.
[7] A. Chadlia, Removal of basic blue 41 from aqueous solution by carboxymethylated Posidonia oceanica, Journal of applied polymer science 103(2) (2007) 1215-1225.
[8] M. Pilavtepe, M.S. Celiktas, S. Sargin, O. Yesil-Celiktas, Transformation of Posidonia oceanica residues to bioethanol, Industrial Crops and Products 51 (2013) 348-354.
[9] K. Zaafouri, A.B.H. Trabelsi, S. Krichah, A. Ouerghi, A. Aydi, C.A. Claumann, Z.A. Wüst, S. Naoui, L. Bergaoui, M. Hamdi, Enhancement of biofuels production by means of co-pyrolysis of Posidonia oceanica (L.) and frying oil wastes: Experimental study and process modeling, Bioresource technology 207 (2016) 387-398.
[10] E. Fortunati, F. Luzi, D. Puglia, R. Petrucci, J. Kenny, L. Torre, Processing of PLA nanocomposites with cellulose nanocrystals extracted from Posidonia oceanica waste: Innovative reuse of coastal plant, Industrial Crops and Products 67 (2015) 439-447.
[11] C.A. Murphy, M.N. Collins, Microcrystalline cellulose reinforced polylactic acid biocomposite filaments for 3D printing, Polymer Composites (2016).
[12] M. Martínez-Sanz, A.A. Vicente, N. Gontard, A. Lopez-Rubio, J.M. Lagaron, On the extraction of cellulose nanowhiskers from food by-products and their comparative reinforcing effect on a polyhydroxybutyrate-co-valerate polymer, Cellulose 22(1) (2015) 535-551.
[13] M.J. Fabra, M. Martínez-Sanz, L.G. Gómez-Mascaraque, R. Gavara, A. López-Rubio, Structural and physicochemical characterization of novel thermoplastic corn starch films containing microalgae, Carbohydrate Polymers Under review (2017).
[14] M. Martínez-Sanz, P. Lopez-Sanchez, M. Gidley, E. Gilbert, Evidence for differential interaction mechanism of plant cell wall matrix polysaccharides in hierarchically-structured bacterial cellulose, Cellulose 22(3) (2015).
[15] N. Wang, E. Ding, R. Cheng, Thermal degradation behaviors of spherical cellulose nanocrystals with sulfate groups, Polymer 48(12) (2007) 3486-3493.
[16] F. Bettaieb, R. Khiari, M.L. Hassan, M.N. Belgacem, J. Bras, A. Dufresne, M.F. Mhenni, Preparation and characterization of new cellulose nanocrystals from marine biomass Posidonia oceanica, Industrial Crops and Products 72 (2015) 175-182.
[17] J. Kaal, O. Serrano, K.G. Nierop, J. Schellekens, A.M. Cortizas, M.-Á. Mateo, Molecular composition of plant parts and sediment organic matter in a Mediterranean seagrass (Posidonia oceanica) mat, Aquatic Botany 133 (2016) 50-61.
[18] A. Siddhanta, K. Prasad, R. Meena, G. Prasad, G.K. Mehta, M.U. Chhatbar, M.D. Oza, S. Kumar, N.D. Sanandiya, Profiling of cellulose content in Indian seaweed species, Bioresource technology 100(24) (2009) 6669-6673.
[19] Y.W. Chen, H.V. Lee, J.C. Juan, S.-M. Phang, Production of new cellulose nanomaterial from red algae marine biomass Gelidium elegans, Carbohydrate polymers 151 (2016) 1210-1219.
[20] N. Abidi, L. Cabrales, C.H. Haigler, Changes in the cell wall and cellulose content of developing cotton fibers investigated by FTIR spectroscopy, Carbohydrate Polymers 100 (2014) 9-16.

[21] X. Sun, F. Xu, R. Sun, P. Fowler, M. Baird, Characteristics of degraded cellulose obtained from steam-exploded wheat straw, Carbohydrate research 340(1) (2005) 97-106.
[22] P. Satyamurthy, P. Jain, R.H. Balasubramanya, N. Vigneshwaran, Preparation and characterization of cellulose nanowhiskers from cotton fibres by controlled microbial hydrolysis, Carbohydrate Polymers 83(1) (2011) 122-129.
[23] L.K. Kian, M. Jawaid, H. Ariffin, O.Y. Alothman, Isolation and Characterization of Microcrystalline Cellulose from Roselle Fibers, International Journal of Biological Macromolecules (2017).
[24] S.Y. Oh, D.I. Yoo, Y. Shin, G. Seo, FTIR analysis of cellulose treated with sodium hydroxide and carbon dioxide, Carbohydrate Research 340(3) (2005) 417-428.
[25] A. Lopez-Rubio, B.M. Flanagan, A.K. Shrestha, M.J. Gidley, E.P. Gilbert, Molecular rearrangement of starch during in vitro digestion: toward a better understanding of enzyme resistant starch formation in processed starches, Biomacromolecules 9(7) (2008) 1951-1958.
[26] R. Khiari, Z. Marrakchi, M.N. Belgacem, E. Mauret, F. Mhenni, New lignocellulosic fibres-reinforced composite materials: A stepforward in the valorisation of the Posidonia oceanica balls, Composites Science and Technology 71(16) (2011) 1867-1872.
[27] M. Martínez-Sanz, M.J. Gidley, E.P. Gilbert, Application of X-ray and neutron small angle scattering techniques to study the hierarchical structure of plant cell walls: a review, Carbohydrate Polymers 125 (2015) 120-134.
[28] M. Wada, J. Sugiyama, T. Okano, Native celluloses on the basis of two crystalline phase (Iα/Iβ) system, Journal of Applied Polymer Science 49(8) (1993) 1491-1496.
[29] L.H. Thomas, V.T. Forsyth, A. Šturcová, C.J. Kennedy, R.P. May, C.M. Altaner, D.C. Apperley, T.J. Wess, M.C. Jarvis, Structure of cellulose microfibrils in primary cell walls from collenchyma, Plant physiology 161(1) (2013) 465-476.
[30] V. Gupta, P. Carrott, R. Singh, M. Chaudhary, S. Kushwaha, Cellulose: a review as natural, modified and activated carbon adsorbent, Bioresource technology 216 (2016) 1066-1076.
[31] R. Khanna, M. Ikram-Ul-Haq, R. Rajarao, R. Cayumil, A. Rawal, V. Sahajwalla, P.S. Mukherjee, Novel multidimensional carbons from structural transformations of waste lignin: A low temperature pyrolysis investigation, Fuel Processing Technology 166 (2017) 312-321.
[32] A. Balaji, K. Nagarajan, Characterization of alkali treated and untreated new cellulosic fiber from Saharan aloe vera cactus leaves, Carbohydrate Polymers 174 (2017) 200-208.
[33] J. Araki, M. Wada, S. Kuga, T. Okano, Flow properties of microcrystalline cellulose suspension prepared by acid treatment of native cellulose, Colloids and Surfaces A: Physicochemical and Engineering Aspects 142(1) (1998) 75-82.
[34] M. Miranda, C. Bica, S. Nachtigall, N. Rehman, S. Rosa, Kinetical thermal degradation study of maize straw and soybean hull celluloses by simultaneous DSC–TGA and MDSC techniques, Thermochimica acta 565 (2013) 65-71.
[35] L. Manzato, L. Rabelo, S. de Souza, C. da Silva, E. Sanches, D. Rabelo, L. Mariuba, J. Simonsen, New approach for extraction of cellulose from tucumã's endocarp and its structural characterization, Journal of Molecular Structure 1143 (2017) 229-234.
[36] B. Montaño-Leyva, G.G.D. da Silva, E. Gastaldi, P. Torres-Chávez, N. Gontard, H. Angellier-Coussy, Biocomposites from wheat proteins and fibers: Structure/mechanical properties relationships, Industrial crops and products 43 (2013) 545-555.
[37] Z. Ma, Q. Sun, J. Ye, Q. Yao, C. Zhao, Study on the thermal degradation behaviors and kinetics of alkali lignin for production of phenolic-rich bio-oil using TGA–FTIR and Py–GC/MS, Journal of Analytical and Applied Pyrolysis 117 (2016) 116-124.
[38] D. Ahuja, A. Kaushik, G.S. Chauhan, Fractionation and physicochemical characterization of lignin from waste jute bags: Effect of process parameters on yield and thermal degradation, International journal of biological macromolecules 97 (2017) 403-410.
[39] I.C. Guimarães, K.C. dos Reis, E.G.T. Menezes, A.C. Rodrigues, T.F. da Silva, I.R.N. de Oliveira, E.V.d.B.V. Boas, Cellulose microfibrillated suspension of carrots obtained by mechanical defibrillation and their application in edible starch films, Industrial Crops and Products 89 (2016) 285-294.
[40] A.H. Bedane, M. Eić, M. Farmahini-Farahani, H. Xiao, Water vapor transport properties of regenerated cellulose and nanofibrillated cellulose films, Journal of Membrane Science 493 (2015) 46-57.

[41] J. Lv, G. Zhang, H. Zhang, F. Yang, Exploration of permeability and antifouling performance on modified cellulose acetate ultrafiltration membrane with cellulose nanocrystals, Carbohydrate Polymers 174 (2017) 190-199.
[42] M.J. Fabra, A. López-Rubio, J. Ambrosio-Martín, J.M. Lagaron, Improving the barrier properties of thermoplastic corn starch-based films containing bacterial cellulose nanowhiskers by means of PHA electrospun coatings of interest in food packaging, Food Hydrocolloids 61 (2016) 261-268.
[43] L. Hassaini, M. Kaci, N. Touati, I. Pillin, A. Kervoelen, S. Bruzaud, Valorization of olive husk flour as a filler for biocomposites based on poly (3-hydroxybutyrate-co-3-hydroxyvalerate): Effects of silane treatment, Polymer Testing 59 (2017) 430-440.
[44] E. Fortunati, W. Yang, F. Luzi, J. Kenny, L. Torre, D. Puglia, Lignocellulosic nanostructures as reinforcement in extruded and solvent casted polymeric nanocomposites: an overview, European Polymer Journal 80 (2016) 295-316.
[45] A.M. Slavutsky, M.A. Bertuzzi, Water barrier properties of starch films reinforced with cellulose nanocrystals obtained from sugarcane bagasse, Carbohydrate polymers 110 (2014) 53-61.
[46] L. Ren, X. Yan, J. Zhou, J. Tong, X. Su, Influence of chitosan concentration on mechanical and barrier properties of corn starch/chitosan films, International Journal of Biological Macromolecules (2017).
[47] H. Chanvrier, S. Uthayakumaran, I.A. Appelqvist, M.J. Gidley, E.P. Gilbert, A. López-Rubio, Influence of storage conditions on the structure, thermal behavior, and formation of enzyme-resistant starch in extruded starches, Journal of Agricultural and Food Chemistry 55(24) (2007) 9883-9890.
[48] A. Lopez-Rubio, A. Htoon, E.P. Gilbert, Influence of extrusion and digestion on the nanostructure of high-amylose maize starch, Biomacromolecules 8(5) (2007) 1564-1572.
[49] B. Ray, M. Lahaye, Cell-wall polysaccharides from the marine green alga Ulva "rigida"(Ulvales, Chlorophyta). Extraction and chemical composition, Carbohydrate Research 274 (1995) 251-261.
[50] I. Benito-González, A. López-Rubio, M. Martínez-Sanz, Potential of lignocellulosic fractions from Posidonia oceanica to improve barrier and mechanical properties of bio-based packaging materials, International journal of biological macromolecules 118 (2018) 542-551.
[51] M. Martínez-Sanz, E. Erboz, C. Fontes, A. López-Rubio, Valorization of Arundo donax for the production of high performance lignocellulosic films, Carbohydrate polymers 199 (2018) 276-285.
[52] I. Benito-González, A. López-Rubio, M. Martínez-Sanz, HIGH-PERFORMANCE STARCH BIOCOMPOSITES WITH CELULLOSE FROM WASTE BIOMASS: FILM PROPERTIES AND RETROGRADATION BEHAVIOUR, Carbohydrate Polymers (2019).
[53] A. Dufresne, Comparing the mechanical properties of high performances polymer nanocomposites from biological sources, Journal of nanoscience and nanotechnology 6(2) (2006) 322-330.
[54] E. Lizundia, E. Fortunati, F. Dominici, J.L. Vilas, L.M. León, I. Armentano, L. Torre, J.M. Kenny, PLLA-grafted cellulose nanocrystals: Role of the CNC content and grafting on the PLA bionanocomposite film properties, Carbohydrate polymers 142 (2016) 105-113.
[55] I.T. Seoane, E. Fortunati, D. Puglia, V.P. Cyras, L.B. Manfredi, Development and characterization of bionanocomposites based on poly (3-hydroxybutyrate) and cellulose nanocrystals for packaging applications, Polymer International 65(9) (2016) 1046-1053.
[56] M.P. Arrieta, E. Fortunati, F. Dominici, E. Rayón, J. López, J.M. Kenny, PLA-PHB/cellulose based films: Mechanical, barrier and disintegration properties, Polymer Degradation and Stability 107 (2014) 139-149.
[57] G. Siqueira, H. Abdillahi, J. Bras, A. Dufresne, High reinforcing capability cellulose nanocrystals extracted from Syngonanthus nitens (Capim Dourado), Cellulose 17(2) (2010) 289-298.
[58] X. Cao, Y. Chen, P.R. Chang, M. Stumborg, M.A. Huneault, Green composites reinforced with hemp nanocrystals in plasticized starch, Journal of Applied Polymer Science 109(6) (2008) 3804-3810.
[59] M. Martínez-Sanz, A. Lopez-Rubio, J.M. Lagaron, High-barrier coated bacterial cellulose nanowhiskers films with reduced moisture sensitivity, Carbohydrate polymers 98(1) (2013) 1072-1082.
[60] M. Martínez-Sanz, A. Lopez-Rubio, J.M. Lagaron, Optimization of the nanofabrication by acid hydrolysis of bacterial cellulose nanowhiskers, Carbohydrate Polymers 85(1) (2011) 228-236.
[61] J.P. Cerisuelo, J. Alonso, S. Aucejo, R. Gavara, P. Hernández-Muñoz, Modifications induced by the addition of a nanoclay in the functional and active properties of an EVOH film containing carvacrol for food packaging, Journal of membrane science 423 (2012) 247-256.

[62] P. Lu, Y.-L. Hsieh, Cellulose isolation and core–shell nanostructures of cellulose nanocrystals from chardonnay grape skins, Carbohydrate polymers 87(4) (2012) 2546-2553.
[63] C. Freire, A. Silvestre, C.P. Neto, M.N. Belgacem, A. Gandini, Controlled heterogeneous modification of cellulose fibers with fatty acids: effect of reaction conditions on the extent of esterification and fiber properties, Journal of Applied Polymer Science 100(2) (2006) 1093-1102.
[64] M. Martínez-Sanz, P. Lopez-Sanchez, M.J. Gidley, E.P. Gilbert, Evidence for differential interaction mechanism of plant cell wall matrix polysaccharides in hierarchically-structured bacterial cellulose, Cellulose 22(3) (2015) 1541-1563.
[65] D.C. Cosgrove, Comparative structure and biomechanics of plant primary and secondary cell walls, Frontiers in plant science 3 (2012) 204.
[66] M. Dick-Pérez, Y. Zhang, J. Hayes, A. Salazar, O.A. Zabotina, M. Hong, Structure and interactions of plant cell-wall polysaccharides by two-and three-dimensional magic-angle-spinning solid-state NMR, Biochemistry 50(6) (2011) 989-1000.
[67] M.B. Johnson, Z. Wen, Production of biodiesel fuel from the microalga Schizochytrium limacinum by direct transesterification of algal biomass, Energy & Fuels 23(10) (2009) 5179-5183.
[68] S. Singh, K.K. Gaikwad, S.-I. Park, Y.S. Lee, Microwave-assisted step reduced extraction of seaweed (Gelidiella aceroso) cellulose nanocrystals, International journal of biological macromolecules 99 (2017) 506-510.
[69] F. Kallel, F. Bettaieb, R. Khiari, A. García, J. Bras, S.E. Chaabouni, Isolation and structural characterization of cellulose nanocrystals extracted from garlic straw residues, Industrial crops and products 87 (2016) 287-296.
[70] Q.-l. Lu, L.-r. Tang, S. Wang, B. Huang, Y.-d. Chen, X.-r. Chen, An investigation on the characteristics of cellulose nanocrystals from Pennisetum sinese, biomass and bioenergy 70 (2014) 267-272.
[71] S.-Q. Chen, D. Mikkelsen, P. Lopez-Sanchez, D. Wang, M. Martinez-Sanz, E.P. Gilbert, B.M. Flanagan, M.J. Gidley, Characterisation of bacterial cellulose from diverse Komagataeibacter strains and their application to construct plant cell wall analogues, Cellulose 24(3) (2017) 1211-1226.
[72] M. Martínez-Sanz, D. Mikkelsen, B. Flanagan, M.J. Gidley, E.P. Gilbert, Multi-scale model for the hierarchical architecture of native cellulose hydrogels, Carbohydrate Polymers 147 (2016) 542-555.
[73] S. Park, D. Johnson, C. Ishizawa, P. Parilla, M. Davis, Measuring the crystallinity index of cellulose by solid state 13C nuclear magnetic resonance, Cellulose 16(4) (2009) 641-647.
[74] M. Martínez-Sanz, F. Pettolino, B. Flanagan, M.J. Gidley, E.P. Gilbert, Structure of cellulose microfibrils in mature cotton fibres, Carbohydrate polymers 175 (2017) 450-463.
[75] D.P. Oehme, M.T. Downton, M.S. Doblin, J. Wagner, M.J. Gidley, A. Bacic, Unique Aspects of the Structure and Dynamics of Elementary Iβ Cellulose Microfibrils Revealed by Computational Simulations, Plant physiology 168(1) (2015) 3-17.
[76] T. Wang, Y.B. Park, D.J. Cosgrove, M. Hong, Cellulose-Pectin Spatial Contacts Are Inherent to Never-Dried Arabidopsis Primary Cell Walls: Evidence from Solid-State Nuclear Magnetic Resonance, Plant Physiology 168(3) (2015) 871-884.
[77] A. Yamazawa, T. Iikura, A. Shino, Y. Date, J. Kikuchi, Solid-, Solution-, and Gas-state NMR Monitoring of 13C-Cellulose Degradation in an Anaerobic Microbial Ecosystem, Molecules 18(8) (2013) 9021.
[78] J. Kikuchi, M.P. Williamson, K. Shimada, T. Asakura, Structure and dynamics of photosynthetic membrane-bound proteins in Rhodobacter sphaeroides, studied with solid-state NMR spectroscopy, Photosynthesis research 63(3) (2000) 259-267.
[79] M. Pauly, P. Albersheim, A. Darvill, W.S. York, Molecular domains of the cellulose/xyloglucan network in the cell walls of higher plants, The Plant Journal 20(6) (1999) 629-639.
[80] J.P. Lagerwall, C. Schütz, M. Salajkova, J. Noh, J.H. Park, G. Scalia, L. Bergström, Cellulose nanocrystal-based materials: from liquid crystal self-assembly and glass formation to multifunctional thin films, NPG Asia Materials 6(1) (2014) e80.
[81] S.E. Whitney, J.E. Brigham, A.H. Darke, J.G. Reid, M.J. Gidley, Structural aspects of the interaction of mannan-based polysaccharides with bacterial cellulose, Carbohydrate Research 307(3-4) (1998) 299-309.

[82] P. Lopez-Sanchez, J. Cersosimo, D. Wang, B. Flanagan, J.R. Stokes, M.J. Gidley, Poroelastic mechanical effects of hemicelluloses on cellulosic hydrogels under compression, PLoS One 10(3) (2015) e0122132.
[83] D. Plackett, H. Anturi, M. Hedenqvist, M. Ankerfors, M. Gällstedt, T. Lindström, I. Siró, Physical properties and morphology of films prepared from microfibrillated cellulose and microfibrillated cellulose in combination with amylopectin, Journal of applied polymer science 117(6) (2010) 3601-3609.
[84] A.B. Reising, R.J. Moon, J.P. Youngblood, Effect of particle alignment on mechanical properties of neat cellulose nanocrystal films, J Sci Technol For Prod Process 2(6) (2012) 32-41.
[85] A.P. Mathew, K. Oksman, M. Sain, Mechanical properties of biodegradable composites from poly lactic acid (PLA) and microcrystalline cellulose (MCC), Journal of applied polymer science 97(5) (2005) 2014-2025.
[86] R.A. Auras, S.P. Singh, J.J. Singh, Evaluation of oriented poly (lactide) polymers vs. existing PET and oriented PS for fresh food service containers, Packaging Technology and Science: An International Journal 18(4) (2005) 207-216.
[87] M. Martínez-Sanz, A. Lopez-Rubio, J.M. Lagaron, Optimization of the dispersion of unmodified bacterial cellulose nanowhiskers into polylactide via melt compounding to significantly enhance barrier and mechanical properties, Biomacromolecules 13(11) (2012) 3887-3899.
[88] L. Sánchez-González, M. Vargas, C. González-Martínez, A. Chiralt, M. Cháfer, Characterization of edible films based on hydroxypropylmethylcellulose and tea tree essential oil, Food Hydrocolloids 23(8) (2009) 2102-2109.
[89] S. Galus, J. Kadzińska, Whey protein edible films modified with almond and walnut oils, Food Hydrocolloids 52 (2016) 78-86.
[90] G. Rodionova, M. Lenes, Ø. Eriksen, Ø. Gregersen, Surface chemical modification of microfibrillated cellulose: improvement of barrier properties for packaging applications, Cellulose 18(1) (2011) 127-134.
[91] M. Ghasemlou, N. Aliheidari, R. Fahmi, S. Shojaee-Aliabadi, B. Keshavarz, M.J. Cran, R. Khaksar, Physical, mechanical and barrier properties of corn starch films incorporated with plant essential oils, Carbohydrate polymers 98(1) (2013) 1117-1126.
[92] A. Polyakova, R. Liu, D. Schiraldi, A. Hiltner, E. Baer, Oxygen-barrier properties of copolymers based on ethylene terephthalate, Journal of Polymer Science Part B: Polymer Physics 39(16) (2001) 1889-1899.
[93] J. Lorenzo, R. Agregán, P. Munekata, D. Franco, J. Carballo, S. Şahin, R. Lacomba, F. Barba, Proximate composition and nutritional value of three macroalgae: Ascophyllum nodosum, Fucus vesiculosus and Bifurcaria bifurcata, Marine drugs 15(11) (2017) 360.
[94] J.M. Lorenzo, P.E. Munekata, B. Gomez, F.J. Barba, L. Mora, C. Perez-Santaescolastica, F. Toldra, Bioactive peptides as natural antioxidants in food products–A review, Trends in food science & technology (2018).
[95] A. Djeridane, M. Yousfi, B. Nadjemi, D. Boutassouna, P. Stocker, N. Vidal, Antioxidant activity of some Algerian medicinal plants extracts containing phenolic compounds, Food chemistry 97(4) (2006) 654-660.
[96] I. Benito-González, A. López-Rubio, M. Martínez-Sanz, High-performance starch biocomposites with celullose from waste biomass: Film properties and retrogradation behaviour, Carbohydrate polymers 216 (2019) 180-188.
[97] J.A. Aguilar-Briseño, L.E. Cruz-Suarez, J.-F. Sassi, D. Ricque-Marie, P. Zapata-Benavides, E. Mendoza-Gamboa, C. Rodríguez-Padilla, L.M. Trejo-Avila, Sulphated polysaccharides from Ulva clathrata and Cladosiphon okamuranus seaweeds both inhibit viral attachment/entry and cell-cell fusion, in NDV infection, Marine drugs 13(2) (2015) 697-712.
[98] G. Piva, D. Fracassetti, A. Tirelli, E. Mascheroni, A. Musatti, P. Inglese, L. Piergiovanni, M. Rollini, Evaluation of the antioxidant/antimicrobial performance of Posidonia oceanica in comparison with three commercial natural extracts and as a treatment on fresh-cut peaches (Prunus persica Batsch), Postharvest Biology and Technology 124 (2017) 54-61.
[99] G. Gokce, M.Z. Haznedaroglu, Evaluation of antidiabetic, antioxidant and vasoprotective effects of Posidonia oceanica extract, Journal of ethnopharmacology 115(1) (2008) 122-130.
[100] I.-S. Kim, M. Yang, O.-H. Lee, S.-N. Kang, The antioxidant activity and the bioactive compound content of Stevia rebaudiana water extracts, LWT-Food Science and Technology 44(5) (2011) 1328-1332.

[101] J. Sosa-Hernández, Z. Escobedo-Avellaneda, H. Iqbal, J. Welti-Chanes, State-of-the-art extraction methodologies for bioactive compounds from algal biome to meet bio-economy challenges and opportunities, Molecules 23(11) (2018) 2953.
[102] A.-M. Cikoš, S. Jokić, D. Šubarić, I. Jerković, Overview on the application of modern methods for the extraction of bioactive compounds from marine macroalgae, Marine drugs 16(10) (2018) 348.
[103] Y. Ben Salem, A. Abdelhamid, K. Mkadmini Hammi, D. Le Cerf, A. Bouraoui, H. Majdoub, Microwave-assisted extraction and pharmacological evaluation of polysaccharides from Posidonia oceanica, Bioscience, biotechnology, and biochemistry 81(10) (2017) 1917-1925.
[104] C. Yin, X. Fan, Z. Fan, D. Shi, H. Gao, Optimization of enzymes-microwave-ultrasound assisted extraction of Lentinus edodes polysaccharides and determination of its antioxidant activity, International journal of biological macromolecules (2018).
[105] S. Surveswaran, Y.-Z. Cai, H. Corke, M. Sun, Systematic evaluation of natural phenolic antioxidants from 133 Indian medicinal plants, Food Chemistry 102(3) (2007) 938-953.
[106] S.A. Baba, S.A. Malik, Determination of total phenolic and flavonoid content, antimicrobial and antioxidant activity of a root extract of Arisaema jacquemontii Blume, Journal of Taibah University for Science 9(4) (2015) 449-454.
[107] L. Machu, L. Misurcova, J. Vavra Ambrozova, J. Orsavova, J. Mlcek, J. Sochor, T. Jurikova, Phenolic content and antioxidant capacity in algal food products, Molecules 20(1) (2015) 1118-1133.
[108] P. Van Hung, Phenolic compounds of cereals and their antioxidant capacity, Critical reviews in food science and nutrition 56(1) (2016) 25-35.
[109] A. Jiménez-Escrig, E. Gómez-Ordóñez, P. Rupérez, Infrared characterisation, monosaccharide profile and antioxidant activity of chemical fractionated polysaccharides from the edible seaweed sugar Kombu (Saccharina latissima), International Journal of Food Science & Technology 50(2) (2015) 340-346.
[110] A. Sila, A. Bougatef, Antioxidant peptides from marine by-products: Isolation, identification and application in food systems. A review, Journal of functional foods 21 (2016) 10-26.
[111] V.L. Singleton, R. Orthofer, R.M. Lamuela-Raventós, [14] Analysis of total phenols and other oxidation substrates and antioxidants by means of folin-ciocalteu reagent, Methods in enzymology, Elsevier1999, pp. 152-178.
[112] O.H. Lowry, N.J. Rosebrough, A.L. Farr, R.J. Randall, Protein measurement with the Folin phenol reagent, Journal of biological chemistry 193 (1951) 265-275.
[113] C.S. Frings, R.T. Dunn, A colorimetric method for determination of total serum lipids based on the sulfo-phospho-vanillin reaction, American Journal of Clinical Pathology 53(1) (1970) 89-91.
[114] A. Martínez-Abad, N. Giummarella, M. Lawoko, F. Vilaplana, Differences in extractability under subcritical water reveal interconnected hemicellulose and lignin recalcitrance in birch hardwoods, Green Chemistry (2018).
[115] R. Re, N. Pellegrini, A. Proteggente, A. Pannala, M. Yang, C. Rice-Evans, Antioxidant activity applying an improved ABTS radical cation decolorization assay, Free radical biology and medicine 26(9-10) (1999) 1231-1237.
[116] H. Miller, A simplified method for the evaluation of antioxidants, Journal of the American Oil Chemists' Society 48(2) (1971) 91-91.
[117] I. Falcó, W. Randazzo, L.G. Gómez-Mascaraque, R. Aznar, A. López-Rubio, G. Sánchez, Fostering the antiviral activity of green tea extract for sanitizing purposes through controlled storage conditions, Food Control 84 (2018) 485-492.
[118] O. Kesraoui, M.N. Marzouki, T. Maugard, F. Limam, In vitro evaluation of antioxidant activities of free and bound phenolic compounds from Posidonia oceanica (l.) Delile leaves, African Journal of Biotechnology 10(16) (2011) 3176.
[119] M. Martínez-Sanz, L.G. Gómez-Mascaraque, A.R. Ballester, A. Martínez-Abad, A. Brodkorb, A. López-Rubio, Production of unpurified agar-based extracts from red seaweed Gelidium sesquipedale by means of simplified extraction protocols, Algal Research 38 (2019) 101420.
[120] Y.-F. Chu, J. Sun, X. Wu, R.H. Liu, Antioxidant and antiproliferative activities of common vegetables, Journal of agricultural and food chemistry 50(23) (2002) 6910-6916.

[121] M. Grignon-Dubois, B. Rezzonico, Phenolic fingerprint of the seagrass Posidonia oceanica from four locations in the Mediterranean Sea: First evidence for the large predominance of chicoric acid, Botanica Marina 58(5) (2015) 379-391.
[122] A.C. Ruthes, A. Martínez-Abad, H.-T. Tan, V. Bulone, F. Vilaplana, Sequential fractionation of feruloylated hemicelluloses and oligosaccharides from wheat bran using subcritical water and xylanolytic enzymes, Green Chemistry 19(8) (2017) 1919-1931.
[123] A. Martínez-Abad, N. Giummarella, M. Lawoko, F. Vilaplana, Differences in extractability under subcritical water reveal interconnected hemicellulose and lignin recalcitrance in birch hardwoods, Green Chemistry 20(11) (2018) 2534-2546.
[124] J. Kaal, O. Serrano, C. José, J. Rencoret, Radically different lignin composition in Posidonia species may link to differences in organic carbon sequestration capacity, Organic Geochemistry 124 (2018) 247-256.
[125] M.J. Pena, A.R. Kulkarni, J. Backe, M. Boyd, M.A. O'Neill, W.S. York, Structural diversity of xylans in the cell walls of monocots, Planta 244(3) (2016) 589-606.
[126] M. Izquierdo, P. Marzal, C. Gabaldón, M. Silvetti, P. Castaldi, Study of the Interaction Mechanism in the Biosorption of Copper (II) Ions onto Posidonia oceanica and Peat, CLEAN–Soil, Air, Water 40(4) (2012) 428-437.
[127] P. Dlapa, M.B. Bodí, J. Mataix-Solera, A. Cerdà, S.H. Doerr, FT-IR spectroscopy reveals that ash water repellency is highly dependent on ash chemical composition, Catena 108 (2013) 35-43.
[128] D.P. Dick, H. Knicker, L.G. Ávila, A.V. Inda Jr, E. Giasson, C.A. Bissani, Organic matter in constructed soils from a coal mining area in southern Brazil, Organic Geochemistry 37(11) (2006) 1537-1545.
[129] A.A. Shaltout, M.A. Allam, M.A. Moharram, FTIR spectroscopic, thermal and XRD characterization of hydroxyapatite from new natural sources, Spectrochimica Acta Part A: Molecular and Biomolecular Spectroscopy 83(1) (2011) 56-60.
[130] X. Yang, M. Huang, C. Qin, B. Lv, Q. Mao, Z. Liu, Structural characterization and evaluation of the antioxidant activities of polysaccharides extracted from Qingzhuan brick tea, International Journal of Biological Macromolecules 101 (2017) 768-775.
[131] H. Schulz, M. Baranska, Identification and quantification of valuable plant substances by IR and Raman spectroscopy, Vibrational Spectroscopy 43(1) (2007) 13-25.
[132] L. Cornara, G. Pastorino, B. Borghesi, A. Salis, M. Clericuzio, C. Marchetti, G. Damonte, B. Burlando, Posidonia oceanica (L.) Delile Ethanolic Extract Modulates Cell Activities with Skin Health Applications, Marine drugs 16(1) (2018) 21.
[133] S. Wang, X. Jiang, X. Han, H. Wang, Fusion characteristic study on seaweed biomass ash, Energy & Fuels 22(4) (2008) 2229-2235.
[134] S. Nanda, P. Mohanty, K.K. Pant, S. Naik, J.A. Kozinski, A.K. Dalai, Characterization of North American lignocellulosic biomass and biochars in terms of their candidacy for alternate renewable fuels, Bioenergy Research 6(2) (2013) 663-677.
[135] S.V. Vassilev, C. Braekman-Danheux, P. Laurent, Characterization of refuse-derived char from municipal solid waste: 1. Phase-mineral and chemical composition, Fuel processing technology 59(2-3) (1999) 95-134.
[136] R. Lutz, A. Aserin, L. Wicker, N. Garti, Structure and physical properties of pectins with block-wise distribution of carboxylic acid groups, Food Hydrocolloids 23(3) (2009) 786-794.
[137] P.D. Carà, M. Pagliaro, A. Elmekawy, D.R. Brown, P. Verschuren, N.R. Shiju, G. Rothenberg, Hemicellulose hydrolysis catalysed by solid acids, Catalysis Science & Technology 3(8) (2013) 2057-2061.
[138] S. Ueno, A. Miyazaki, J. Yano, Y. Furukawa, M. Suzuki, K. Sato, Polymorphism of linoleic acid (cis-9, cis-12-Octadecadienoic acid) and α-linolenic acid (cis-9, cis-12, cis-15-Octadecatrienoic acid), Chemistry and physics of lipids 107(2) (2000) 169-178.
[139] M.S. Iqbal, J. Akbar, M.A. Hussain, S. Saghir, M. Sher, Evaluation of hot-water extracted arabinoxylans from ispaghula seeds as drug carriers, Carbohydrate polymers 83(3) (2011) 1218-1225.
[140] G. Aleksandrova, M. Lesnichaya, Y.A. Myachin, B. Sukhov, B. Trofimov, Effect of silver nanoparticles on the thermal characteristics of nanocomposites of galactose-containing polysaccharides, Doklady Chemistry, Springer, 2011, pp. 187-189.

[141] N. Jayadas, K.P. Nair, Coconut oil as base oil for industrial lubricants—evaluation and modification of thermal, oxidative and low temperature properties, Tribology international 39(9) (2006) 873-878.
[142] J.P. de Oliveira, G.P. Bruni, M.J. Fabra, E. da Rosa Zavareze, A. López-Rubio, M. Martínez-Sanz, Development of food packaging bioactive aerogels through the valorization of Gelidium sesquipedale seaweed, Food Hydrocolloids 89 (2019) 337-350.
[143] M. Tupec, V. Hýsková, K. Bělonožníková, J. Hraníček, V. Červený, H. Ryšlavá, Characterization of some potential medicinal plants from Central Europe by their antioxidant capacity and the presence of metal elements, Food Bioscience 20 (2017) 43-50.
[144] H.A. Hamid, R. Mutazah, M.M. Yusoff, N.A.A. Karim, A.F.A. Razis, Comparative analysis of antioxidant and antiproliferative activities of Rhodomyrtus tomentosa extracts prepared with various solvents, Food and Chemical Toxicology (2016).
[145] K.B. Jeddou, F. Chaari, S. Maktouf, O. Nouri-Ellouz, C.B. Helbert, R.E. Ghorbel, Structural, functional, and antioxidant properties of water-soluble polysaccharides from potatoes peels, Food chemistry 205 (2016) 97-105.
[146] F. Bouaziz, M. Koubaa, R.E. Ghorbel, S.E. Chaabouni, Biological properties of water-soluble polysaccharides and hemicelluloses from almond gum, International journal of biological macromolecules 95 (2017) 667-674.
[147] C. Wilson, J. Solar, A. El Ghaouth, M. Wisniewski, Rapid evaluation of plant extracts and essential oils for antifungal activity against Botrytis cinerea, Plant disease 81(2) (1997) 204-210.
[148] A. Afolayan, Extracts from the shoots of Arctotis arctotoides inhibit the growth of bacteria and fungi, Pharmaceutical Biology 41(1) (2003) 22-25.
[149] W. Randazzo, M.J. Fabra, I. Falcó, A. López-Rubio, G. Sánchez, Polymers and Biopolymers with Antiviral Activity: Potential Applications for Improving Food Safety, Comprehensive Reviews in Food Science and Food Safety 17(3) (2018) 754-768.
[150] E.-G. Oh, K.-L. Kim, S.B. Shin, K.-T. Son, H.-J. Lee, T.H. Kim, Y.-M. Kim, E.-J. Cho, D.-K. Kim, E.-W. Lee, Antiviral activity of green tea catechins against feline calicivirus as a surrogate for norovirus, Food Science and Biotechnology 22(2) (2013) 593-598.
[151] X. Su, D.H. D'Souza, Grape seed extract for the control of human enteric viruses, Applied and environmental microbiology (2011) AEM. 00193-11.

Chapter 2

DEVELOPMENT OF HIGH-PERFORMANCE STARCH-BASED BIOCOMPOSITES USING CELLULOSIC FRACTIONS AND NANOCRYSTALS FROM *P. OCEANICA* AS FILLERS

2.1. High-performance starch biocomposites with cellulose from waste biomass: Film properties and retrogradation behaviour

2.2. Pilot plant scale-up of the production of optimized starch-based biocomposites loaded with cellulosic Nanocrystals from Posidonia oceanica waste biomass

Introduction to chapter 2.

In this second chapter, the utilization of the previously optimized cellulosic fractions and nanocrystals as fillers in biopolymers to develop high-performance bio-based packaging materials was evaluated. To do so, commercial thermoplastic starch was chosen as the matrix, since it presents a good compatibility with cellulose.

In the first work, pure cellulose was incorporated into starch at different loadings (5, 10, 20 and 40% w/w with regards to starch) to evaluate its effect in terms of mechanical performance, water vapor barrier and processability and determine the optimum loading. Additionally, the effect of cellulose incorporation on the retrogradation of starch was evaluated upon prolonged storage of the films by studying the evolution of the crystallinity and mechanical properties.

In the second work, the upscaling for the production of cellulosic nanocrystals (using both simplified and conventional protocols) was also evaluated at a pilot-plant level. Subsequently, the addition of cellulosic nanocrystals as reinforcing fillers in starch was tested. In a first stage, the composite films were obtained at lab-scale by melt-mixing and the most promising formulations were used for the production of films and trays by extrusion and thermoforming at pilot-plant scale.

2.1. High-performance starch biocomposites with celullose from waste biomass: Film properties and retrogradation behaviour.

This section is an adapted version of the following published research article:
Benito-González, I., López-Rubio, A., & Martínez-Sanz, M. (2019). High-performance starch biocomposites with celullose from waste biomass: Film properties and retrogradation behaviour. Carbohydrate Polymers, 216, 180-188. DOI: https://doi.org/10.1016/j.carbpol.2019.04.030

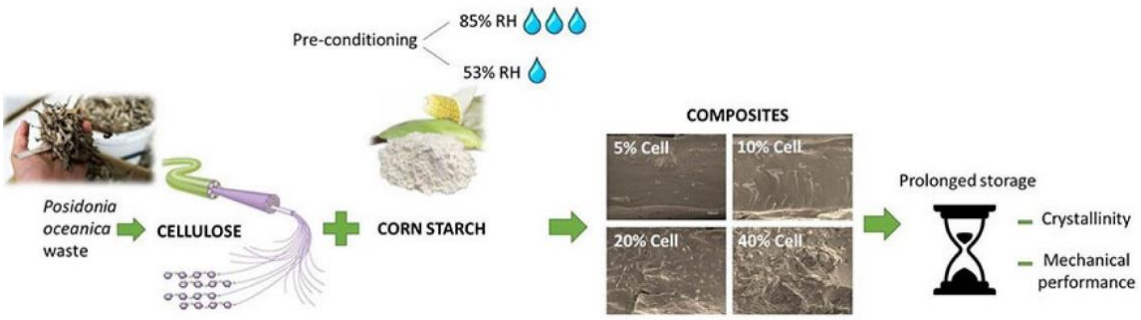

1. Abstract

In this work, the effects of relative humidity (RH) pre-conditioning (53% vs. 85% RH) and incorporation of cellulose fillers (from *Posidonia* waste biomass) on the properties and retrogradation of melt compounded starch biocomposites were investigated. Pre-conditioning at 85% RH promoted starch gelatinization during processing, leading to more amorphous materials with reduced stiffness but better barrier properties. Furthermore, these films were less stable upon storage due to greater starch retrogradation. Cellulose incorporation improved significantly the mechanical and water barrier performance, especially in the films pre-conditioned at 85% RH due to enhanced filler dispersion. Although incomplete gelatinization of the starch pre-conditioned at 53% RH led to films with bigger cellulose aggregates, their mechanical and water barrier properties were better, outperforming starch-cellulose biocomposites typically reported in the literature. Moreover, the presence of cellulose limited the degree of starch retrogradation upon storage, highlighting the potential of *Posidonia* biomass as a cheap source of high-performance fillers.

2. Introduction

Synthetic plastics, conventionally obtained from fossil fuel-derived resources, constitute the most widely used material in the food packaging sector due to their low cost, good processability and possibility to adapt their properties to comply with specific food product requirements. However, the widespread use of these materials entails severe environmental issues, associated with the steady depletion of fossil-fuels and the enormous stream of non-degradable waste generated. As a consequence, current trends in the food packaging sector are fostering the development of more sustainable biopolymeric materials, i.e. derived from renewable resources. Amongst them, starch, a natural polysaccharide typically extracted from corn, wheat, rice, potatoes and peas [1], has attracted a great deal of interest and has been widely used to produce biopolymeric films, especially by casting methodologies [2-5]. Nevertheless, films cast from aqueous solutions of gelatinized starch have no industrial applicability and processing methods based on melt compounding strategies have a greater potential for industrial implementation.

In this context, thermoplastic starch, produced by the addition of plasticizers with the combined effect of temperature and shear [6], could be a good candidate for the commercialization of bio-based packaging, since it can be converted into rigid and flexible packaging using conventional plastics processing equipment [7]. However, this material presents several drawbacks, such as high hygroscopicity and poor mechanical performance, which are still limiting its commercial applicability. In this sense, the incorporation of fillers has proved to be an efficient strategy to enhance the properties of bio-based polymers, generally improving their mechanical and barrier properties to produce biocomposite materials which are competitive for their intended applications [1, 8-10]. In the particular case of starch biocomposites, cellulose is one of the most widely used fillers due to its relatively high abundance, outstanding mechanical and barrier properties, as well as its hydrophilic character, making it compatible with starch [1, 11-14]. An additional drawback associated to starch is related to its low stability upon storage due to re-crystallization processes (commonly known as retrogradation). This retrogradation phenomenon affects the properties of starch films over storage time. For instance, their opacity and brittleness have been seen to increase [15, 16], representing a major issue in food packaging applications, since the performance of starch films may be deteriorated with time, affecting the quality and shelf-life of the food (Smits et al., 1998, Yu et al., 2013). The retrogradation rate is known to be influenced by the amylose content, starch source and storage conditions [17]. However, to the best of our knowledge, the effect of cellulosic fillers on the retrogradation process in biocomposite starch films has not been previously studied.

Although cellulose is typically extracted from terrestrial resources, it can also be obtained from marine organisms which do not compete with food applications, as it occurs with terrestrial ones. Preliminary results presented in a previous study showed the potential of cellulosic fillers extracted from *Posidonia oceanica* waste biomass to improve the properties of starch films [18]. In light of those results, the aim of the present work was to achieve a maximum enhancement in the properties of starch biocomposites by incorporating cellulose obtained from *Posidonia oceanica* waste biomass. Specifically, the effect of starch pre-conditioning at different relative humidity conditions and cellulose loading on the properties of the obtained films by means of melt compounding have been investigated. Moreover, the impact of cellulose on the retrogradation process upon storage was evaluated in order to assess the suitability of these materials for food packaging applications. Our hypothesis is that relative humidity pre-conditioning must be key to control the starch gelatinization process taking place during the melt compounding step and this, at the same time, will have an impact on the starch-cellulose interactions established. The presence of cellulose and its interaction with starch are expected to affect the functional properties of the biocomposite films, as well as their retrogradation behavior.

3. Materials and methods

3.1 Raw materials

Biomass waste material consisting of *Posidonia oceanica* leaves was collected directly from the shore in Calpe, Alicante (Spain) in February-March 2017. The material was washed vigorously with water in order to remove sand and salts and stored in the fridge until its use. Corn starch (27-28% amylose) was supplied by Roquette (Roquette Laisa España, Benifaio, Spain) and glycerol (technical grade) was purchased from Panreac Quimica, S.A. (Castellar Del Vallés, Barcelona, Spain).

3.2 Cellulose extraction from *Posidonia oceanica* biomass

A purification procedure, described in a previous work [18], was carried out to sequentially remove cell wall components and obtain pure cellulose (25% final yield). Briefly, this process consisted of an initial Soxhlet extraction with a toluene:ethanol mixture (2:1) overnight to remove pigments and lipids. This was followed by a treatment with 1.4% $NaClO_2$ (70 ºC, 5 h) to remove lignin. Finally, an alkaline treatment with 5% KOH was carried out (room temperature for 24 h, followed by 2 h at 90 ºC) to remove the hemicelluloses. Cellulose was obtained as a partially hydrated gel-like material that was stored in the fridge until further use. The percentage of dry weight was calculated by drying a known amount of hydrated cellulose at 60 ºC overnight.

3.3 Production of neat and biocomposite starch films loaded with cellulose

Prior to processing, granular corn starch (initially stored at 0% RH) was pre-conditioned for a minimum of two weeks by placing the material in cabinets equilibrated at two different relative humidity conditions (using the required saturated salt solutions): (i) 53% RH and 25ºC and (ii) 85% RH and 25ºC. The water content in the starch samples after the pre-conditioning stage was evaluated gravimetrically by drying at least 1 g of corn starch in an oven at 60º C overnight. The determinations were done at least in triplicate.

Pure corn starch and biocomposite films with loadings of 5, 10, 20 and 40 wt.-% of *Posidonia oceanica* cellulose (with regards to the starch weight) were prepared by melt compounding, followed by compression molding. Corn starch and glycerol, as plasticizer, were dispersed in water using a polymer:glycerol:water ratio of 1:0.3:0.5 (w/w/w). For the biocomposite films, the required amount of cellulose (in its partially hydrated form) was incorporated to the mixture of starch, glycerol and water and mixed manually with a spatula until a homogeneous paste was made. This paste was then melt-mixed in a Brabender Plastograph (Germany) internal mixer at 130 °C and 60 rpm for 4 min. Subsequently, 4 g of the obtained blends were spread evenly on Teflon films and placed in a compression mold (Carver 4122, USA) at a pressure of 16 tons and 130 °C for 2 min to form one film [18, 19]. The samples were coded as follows: S53 and S85 (pure starch films obtained from starch pre-conditioned at 53% RH or 85% RH, respectively), S53+5%Cell, S53+10%Cell, S53+20%Cell and S53+40%Cell (biocomposite films from starch pre-conditioned at 53% RH, loaded with 5, 10, 20 and 40% cellulose) and S85+5%Cell, S85+10%Cell, S85+20%Cell (biocomposite films from starch pre-conditioned at 85% RH, loaded with 5, 10 and 20% cellulose). The thickness of the films varied between 170 and 300 µm. Since the addition of 40% cellulose markedly reduced the processability of the material, only the blend with starch pre-conditioned at 53% RH (close to ambient conditions and therefore, better simulating the conditions typically found in industrial processes) was produced.

3.4 Conditioning and storage of pure and biocomposite starch films

All the obtained films were stored in equilibrated relative humidity cabinets at 53% RH and 25ºC for three days prior to their characterization. Additionally, selected samples (S53, S85, S53+10%Cell and S85+10%Cell) were stored at the same conditions for a prolonged period of two months to investigate the effect of cellulose on the starch re-crystallization process by means of XRD and tensile testing.

3.5 Scanning electron microscopy (SEM)

SEM was conducted on a Hitachi microscope (Hitachi S-4800, Japan) at an accelerating voltage of 10 kV and a working distance of 8-16 mm. The pure and biocomposite starch films were cryo-

fractured after immersion in liquid nitrogen to observe the cross-sections. The samples were then sputtered with a gold–palladium mixture under vacuum during 3 minutes before their morphology was examined.

3.6 Water vapor permeability (WVP)

Direct permeability to water was determined from the slope of the weight gain versus time curves at 25ºC, according to the ASTM E96/E96M-10 gravimetric method. The films were sandwiched between the aluminum top (open O-ring) and bottom (deposit for the silica) parts of a specifically designed permeability cell with screws. A Viton rubber O-ring was placed between the film and bottom part of the cell to enhance sealability. These permeability cells containing silica were then placed in an equilibrated relative humidity cabinet at 75% RH and 25 °C. The weight gain through a film area of 0.001 m^2 was monitored and plotted as a function of time. Cells with aluminum films (with thickness of ca. 11 µm) were used as control samples to estimate the weight gain through the sealing. The tests were done at least in triplicate.

3.7 Contact angle measurements

Contact angle measurements were carried out at ambient conditions in a Video-Based Contact Angle Meter model OCA 20 (DataPhysics Instruments GmbH, Filderstadt, Germany). Contact angle values were obtained by analyzing the shape of a distilled water drop after it had been placed over the film for 15 s. Image analyses were carried out by SCA20 software.

3.8 Optical properties

The transparency of the films was determined through the surface reflectance spectra in a spectrocolorimeter CM-3600d (Minolta Co., Tokyo, Japan) with a 10 mm illuminated sample area. Measurements were taken in duplicate for each sample by using both a white and a black background.

Film transparency was evaluated through the internal transmittance (T_i) (0-1, theoretical range) by applying the Kubelka-Munk theory for multiple scattering to the reflection data. As each light flux passes through the layer, it is affected by the absorption coefficient (K) and the scattering coefficient (S) (Eq. (1)). In this equation, R_∞ is the reflectance of an infinitely thick layer of the material, determined through Eqs. (2), (3) and (4), where R is the reflectance of the sample layer backed by a known reflectance R_g and R_0 is the reflectance of the sample layer on an ideal black background. Internal transmittance (T_i) of the films was quantified using Eq. (5).

$$\frac{K}{S} = \frac{(1 - R_\infty)^2}{2R_\infty} \quad (1)$$

$$R_\infty = a - b \quad (2)$$

$$a = \frac{1}{2}\cdot\left(R + \frac{R_0 - R + R_g}{R_0 R_g} \right) \quad (3)$$

$$b = (a^2 - 1)^{\frac{1}{2}} \quad (4)$$

$$T_i = \sqrt{(a - R_0)^2 - b^2} \quad (5)$$

3.9 Mechanical properties

Tensile tests were carried out at ambient conditions on a Mecmesin MultiTest 1-i (1 kN) machine (Virginia, USA) with the Emperor™ software, according to ASTM standard method D882-09 18 [20]. Pre-conditioned rectangular-shaped specimens with initial gauge length of 8 cm and 1 cm in width were cut directly from the films. A fixed crosshead rate of 10 mm/min was utilized in all cases. Elastic modulus (E), tensile strength and elongation at break (ε_b) were determined from the stress-strain curves, estimated from force–distance data obtained for the different films. At least, five specimens of each film were tensile tested to obtain statistically meaningful results.

3.10 X-ray diffraction (XRD)

XRD measurements of pure and biocomposite films were carried out on a D5005 Bruker diffractometer. The instrument was equipped with a Cu tube and a secondary monochromator. The configuration of the equipment was θ–2θ, and the samples were examined over the angular range between 3°–60° with a step size of 0.02° and a count time of 200 s per step. Peak fitting was carried out by using the Igor software package (Wavemetrics, Lake Oswego, Oregon) as described in a previous work [21]. The obtained values from the fitting coefficients are those that minimize the value of Chi-squared, which is defined as:

$$\chi^2 = \sum \left(\frac{y - y_i}{\sigma_i} \right)^2 \quad (4)$$

where y is a fitted value for a given point, y_i is the measured data value for the point and σ_i is an estimate of the standard deviation for y_i. The curve fitting operation is carried out iteratively and for each iteration, the fitting coefficients are refined to minimize χ^2. The crystallinity index X_C was determined from the obtained fitting results by applying the following equation:

$$X_C(\%) = \frac{\sum A_{Crystal}}{A_{Total}} \times 100 \quad (5)$$

where A_{Total} is the sum of the areas under all the diffraction peaks and $\Sigma A_{Crystal}$ is the sum of the areas corresponding to the crystalline peaks.

3.11 Statistical analysis

All data have been represented as the average ± standard deviation. Different letters show significant differences both in tables and graphs ($p \leq 0.05$). Analysis of variance (ANOVA) followed by a Tukey-b test were used when comparing more than two data sets.

4. Results and Discussion

4.1 Effects of pre-conditioning RH and *Posidonia oceanica* cellulose incorporation on the initial properties of melt compounded starch films

Preliminary results reported on a previous study highlighted the potential of the pure cellulose extracted from *Posidonia oceanica* waste biomass to enhance the properties of starch films [18]. In this work, the potential of *Posidonia* cellulose to partially replace starch and improve the properties of melt compounded packaging films was further explored by incorporating different loadings of cellulose, up to 40 wt.-%, into starch and evaluating the effect of the filler in the properties of the biocomposite films. A complete structural characterization of *Posidonia oceanica* cellulose can be found in a previous work [18]. It was not possible to incorporate loadings greater than 40% cellulose, since the material did not melt homogeneously (as cellulose does not melt during processing) and could not be adequately processed.

Since starch crystallinity and properties are known to be strongly affected by the presence of moisture [22, 23], the effect of starch pre-conditioning at two different relative humidity conditions (53% RH and 85% RH) was also evaluated. Water content in starch was 8.9 ± 0.1 and 11.4 ± 0.4% (w/w) for corn starch pre-conditioned at 53% and 85% RH, respectively. This implies that the total amount of water introduced into the internal mixer was slightly higher in the case of the starch pre-conditioned at 85% RH. Apart from having an effect on the structural properties of the granular starch fed into the mixer, the different water contents of the samples are expected to affect the gelatinization process undergone by starch during the melt blending step, as deduced from several previous works [24-27]. In fact, XRD analyses proved that, although the water content differences were relatively small, they had a significant impact on the gelatinization of the samples. Figure 1 shows the XRD patterns of the raw granular starch (before being processed), *Posidonia oceanica* cellulose and the pure starch and biocomposite films with 20% cellulose obtained after being processed and stored for 3 days. From the shape of the diffraction patterns and the appearance of sharp peaks located at ca. 13º and 20º, it is observed that while the native corn starch presented an A-type crystalline structure, it re-crystallized into a V-type structure, after being processed in the internal mixer, which is in agreement with previous works [18, 19, 28]. It should be noted that the position and relative intensity of the peaks did not correspond to any of the pure crystalline allomorphs described in the literature. This suggests that the low

crystalline fraction detected in starch shortly after being processed consists of a mixture of different allomorphs. Interestingly, the presence of cellulose induced the re-crystallization of starch into a different structure, as suggested by the distinct position and relative intensities of the diffraction peaks. As a reference, the XRD pattern of the native *Posidonia oceanica* cellulose is also plotted in Figure 1, confirming that the strongest diffraction peaks in the starch biocomposites did not arise from the crystalline cellulose component. Thus, a different crystalline structure built by strongly interacting starch-cellulose molecular chains may have been formed after processing the materials in the internal mixer. The crystallinity values estimated from the diffraction patterns were 32.0% for the raw corn starch, 19.2% for S53, 5.6% for S85, 14.6% for S53+20%Cell and 11.7% for S85+20%Cell. These results confirm that the raw granular starch underwent a gelatinization process during the melt mixing step, hence leading to materials with very low crystallinity values shortly after being processed. The presence of higher moisture contents in the S85 samples promoted the gelatinization process and, therefore, more amorphous materials were obtained after processing.

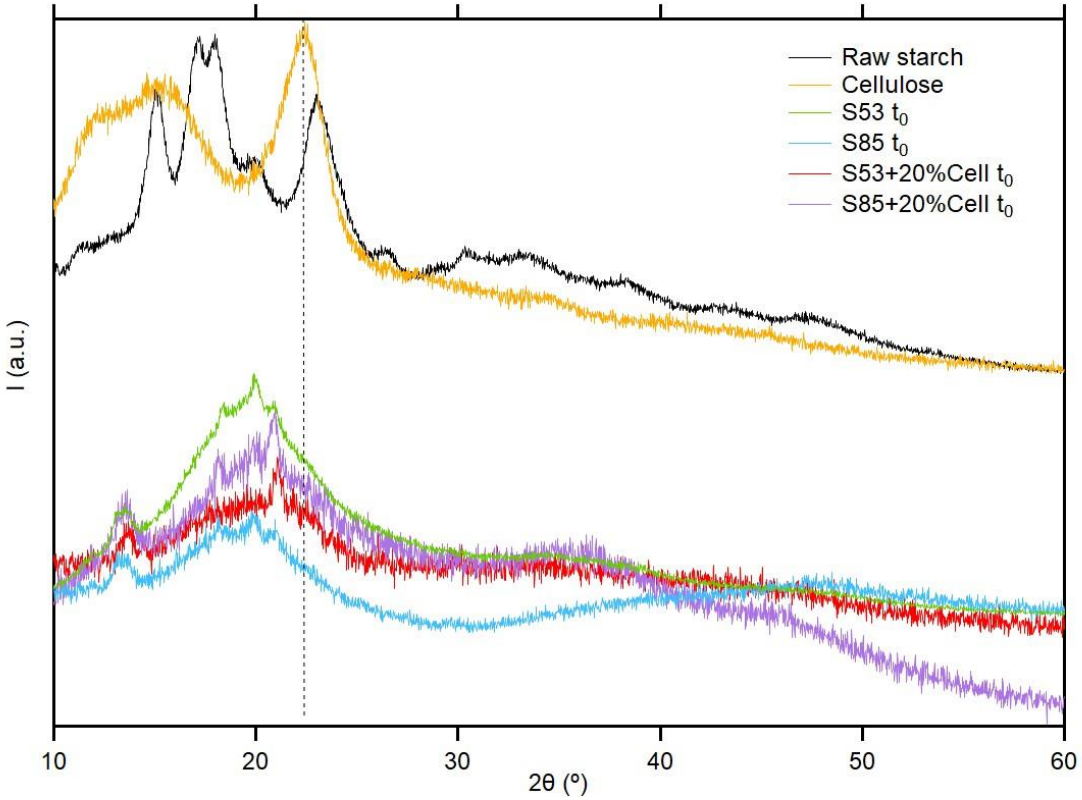

Figure 1. XRD patterns of the corn starch control films and the biocomposites with 20% cellulose after storage for three days (t_0). The raw starch and native *Posidonia oceanica* cellulose patterns have been offset for clarity.

The morphology of the produced films was investigated by SEM analyses of their cryo-fractured cross-sections (cf. Figure 2 for starch pre-conditioned at 53% RH and Figure 3 for starch pre-conditioned at 85% RH). As observed, no significant differences were detected in the morphology of the pure starch films pre-conditioned at different relative humidities and both S53 and S85 presented smooth and homogeneous fractured surfaces. Cellulose aggregates were clearly visible in all the biocomposite films, although a higher level of dispersion was observed in comparison with previous works dealing with extruded starch loaded with cellulose nanofibers extracted from softwood wood flour [29]. Interestingly, there was a clear positive effect of moisture in the dispersion of cellulose. While large cellulose aggregates were detected in the S53 films, that was not the case for the S85 biocomposites, where cellulose was evenly distributed forming much smaller particles. This can be explained by two factors: (i) the hydrophilic nature of both starch and cellulose and (ii) the greater extent of corn starch gelatinization promoted by the presence of higher water contents, (as confirmed by XRD, cf. Figure 1) [30]. Pre-conditioning at higher relative humidity conditions favors the incorporation of water into the starch matrix [31, 32]. This facilitates the integration of cellulose into the paste generated before the melt blending process (due to the high amount of free hydroxyl groups present in cellulose and its water affinity), thus, promoting a better dispersion of the filler. Furthermore, the plasticization effect of water and the increased gelatinization extent attained with higher moisture contents are known to promote a lower viscosity of starch during melt processing [33] which, at the same time, may also favor the dispersion of cellulose within the starch matrix.

It should be noted that the cellulose agglomeration in the S53 samples became especially relevant in the film with 40% cellulose (S53+40%Cell), where the filler was poorly dispersed and forming large aggregates. This was due to the very difficult processability of this blend in the mixer. This was not unexpected since cellulose melting temperature is ca. 330ºC [18], being a substantially higher temperature than that applied during the melt mixing process and, hence, hindering a proper homogenization of the material when added in excessive amounts.

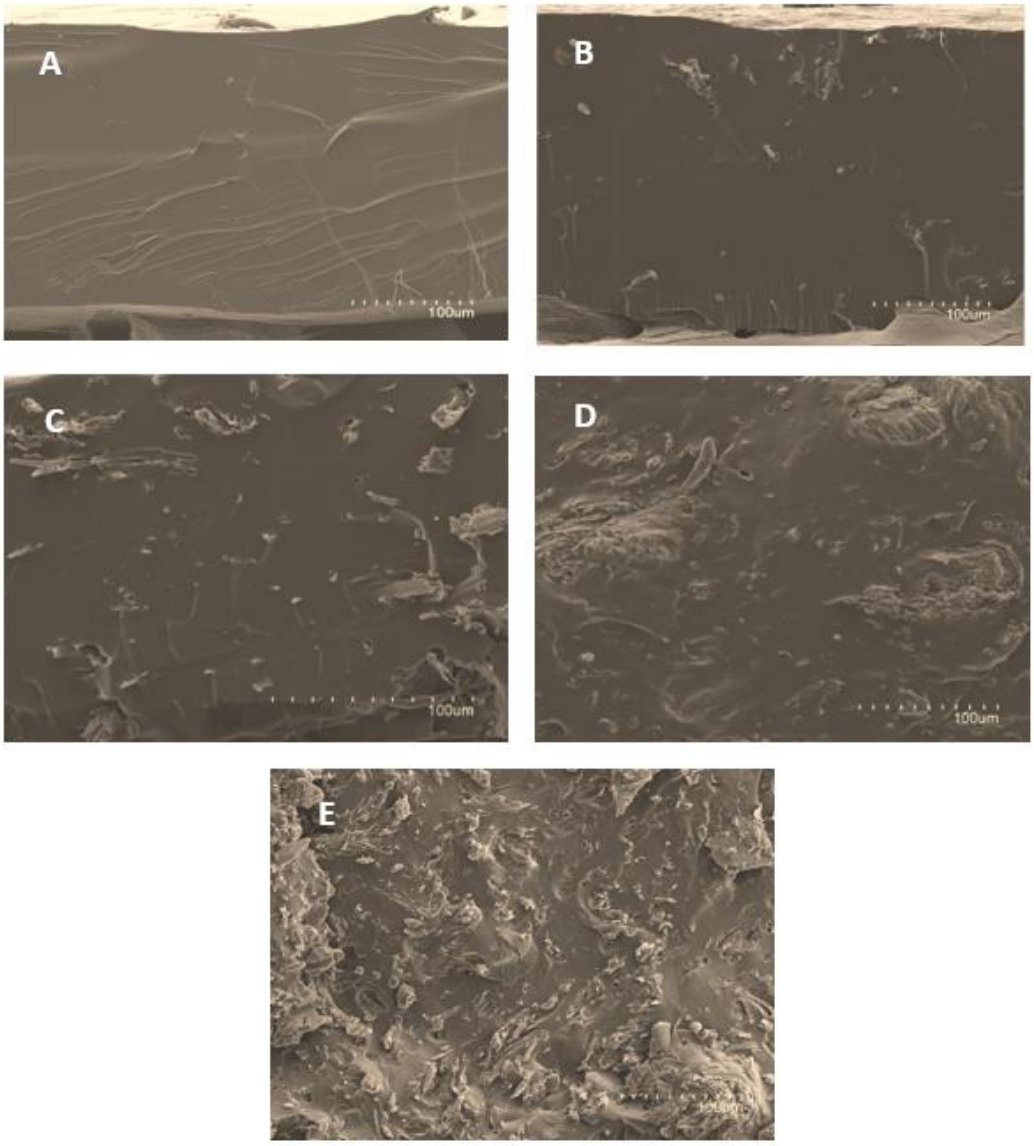

Figure 2. SEM images of the cryo-fractured sections from the different corn starch films pre-conditioned at 53% RH: (A) S53, (B) S53+5%Cell, (C) S53+10%Cell, (D) S53+20%Cell and (E) S53+40%Cell.

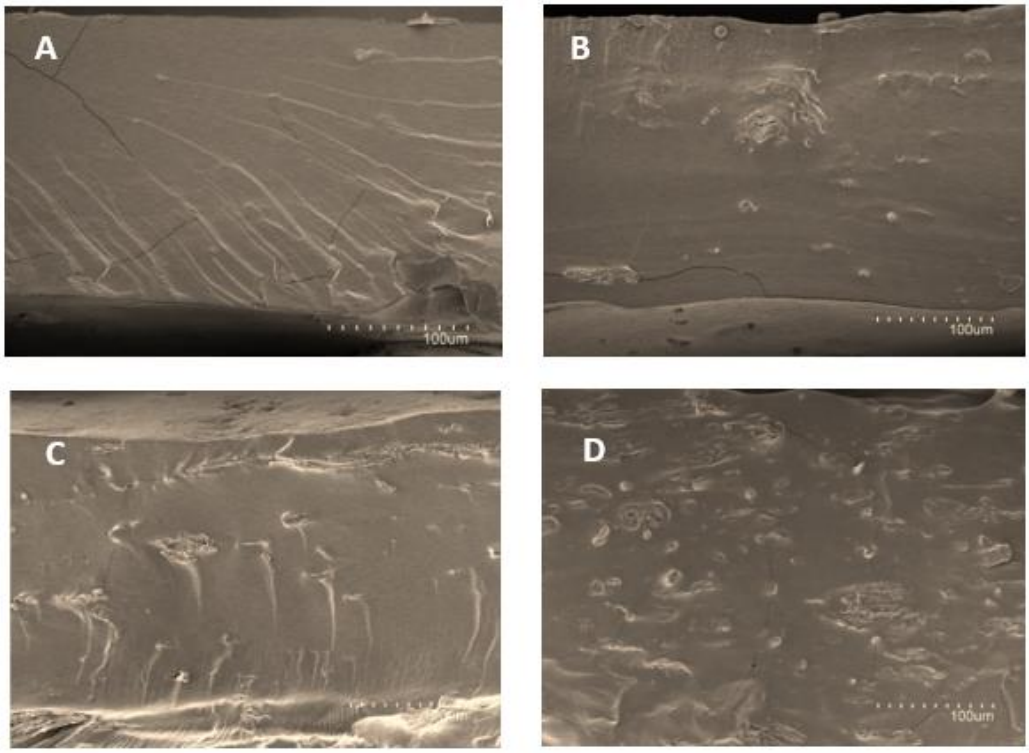

Figure 3. SEM images of the cryo-fractured sections from the different corn starch films pre-conditioned at 85% RH: (A) S85, (B) S85+5%Cell, (C) S85+10%Cell and (D) S85+20%Cell.

Since these films are intended to be used in food packaging applications, transparency is a vital attribute to be evaluated. This was done by measuring their internal transmittance, as shown in Figure 4. As deduced from the results, the S85 films showed slightly higher transmittance values (i.e. greater transparency) than the S53 films. This is indicative of the lower crystallinity in the former ones due to the greater starch gelatinization extent induced by moisture (cf. Figure 1). The general trend with the incorporation of cellulose loadings up to 20% was a slight gradual decrease in the transparency of the films, originated by the presence of small cellulose aggregates, as evidenced by SEM. A marked decrease in the transparency of the S53+40%Cell film was observed, which is in agreement with the poor filler dispersion attained in this sample.

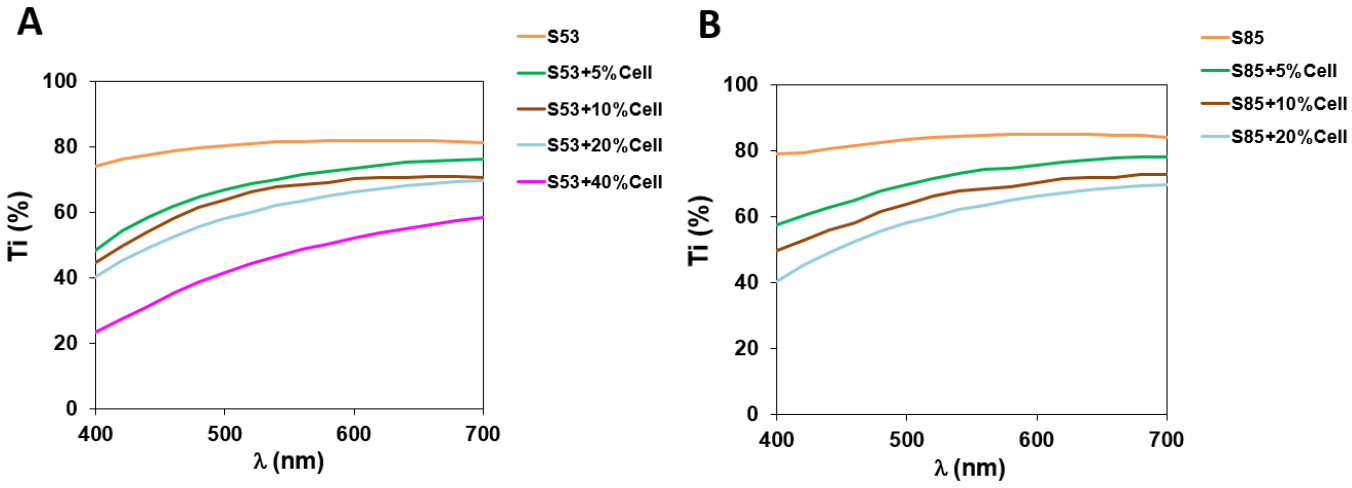

Figure 4. Spectral distribution of internal transmittance (Ti) of the pure corn starch and biocomposite films with cellulose. Starch pre-conditioned at (A) 53% RH and (B) 85% RH.

The mechanical properties of the pure starch and the biocomposite films were evaluated, and the results are summarized in Table 1. The first clear observation is that, when comparing the pure starch films, the one pre-conditioned at a lower relative humidity, i.e. S53, showed ca. 2-fold greater values for the elastic modulus and the tensile strength and more than 3-fold lower elongation at break than the S85 film. This again, can be correlated with the fact that starch pre-conditioning at lower relative humidity conditions limited the gelatinization extent during the mixing step, thus leading to the formation of more crystalline films (as confirmed by XRD analyses, cf. Figure 1 and Table 2) which were stiffer and less ductile. Regardless of the starch pre-conditioning conditions, the general trend with the incorporation of cellulose was an increase in the elastic modulus and tensile strength, while the elongation at break was reduced, i.e. stiffer materials were obtained with the cellulose addition. The same effect has been previously reported for starch films reinforced with cellulosic fillers due to the inherent greater mechanical performance of cellulose as compared with starch [13, 29, 34].

A relevant aspect to be highlighted is that, although the general trend was the same, the extent to which the incorporation of cellulose affected the mechanical performance of the starch films was different depending on the starch pre-conditioning. In particular, while the addition of 20% cellulose led to an increase of ca. 4-fold in the elastic modulus and tensile strength and a reduction of ca. 5-fold in the elongation at break of the S53 film, an increase of ca. 19-fold and 5-fold in the elastic modulus and tensile strength, respectively and a reduction of ca. 21-fold in the elongation at break was observed in the case of the S85 film. From these results, it is evident that the incorporation of cellulose had a much stronger impact on the mechanical performance of the starch pre-conditioned at higher relative humidity. Although this might be related to the better dispersion of cellulose in the S85 blends, it should also be taken into account that due to the more amorphous character of the pure S85 starch, there was a greater improvement margin with the addition of cellulose. Overall, the best material in terms of mechanical properties was the S53+20%Cell, since it presented a stiffer behavior, while minimizing the reduction in the elongation.

Several difficulties have been found when comparing these results with those previously reported in the literature: (i) most of the works make use of the casting methodology (which is easier to develop at lab scale, but has a very limited industrial applicability), (ii) there is a huge variation in the processing conditions (starch pre-conditioning, moisture content during processing, melt mixing or extrusion parameters, amount and type of plasticizer added) and (iii) the properties of

the cellulose filler may be strongly dependent on the raw source and on the mechanical and/or chemical treatments to which it may have been subjected. As a reference, the cellulose extracted from *Posidonia oceanica* biomass presented a greater reinforcing effect than that reported for softwood cellulose fibers incorporated into corn starch pre-conditioned at 58% RH by casting [12], cotton cellulose microfibers incorporated into corn starch by extrusion at different RHs [35], or even kaolin fillers added at higher contents (up to 60%) in corn starch by melt compounding at 43% RH [36]. These results demonstrate the potential of the cellulose extracted from *Posidonia oceanica* biomass to improve the mechanical properties of starch.

Table 1. Mechanical properties (Young's modulus (E), tensile strength and elongation at break(ε_b) from the pure starch and biocomposite films loaded with *Posidonia oceanica* cellulose.

	E (MPa)	**Tensile Strength (MPa)**	**ε_b (%)**
S53	546.3 ± 181.1^{a}	6.1 ± 0.7^{a}	8.5 ± 3.1^{a}
S53+5%Cell	1259.0 ± 168.9^{b}	14.7 ± 2.3^{b}	2.6 ± 0.7^{b}
S53+10%Cell	1771.3 ± 164.5^{c}	18.1 ± 1.6^{c}	2.0 ± 0.3^{b}
S53+20%Cell	2347.9 ± 161.0^{d}	24.1 ± 0.4^{d}	1.8 ± 0.1^{b}
S53+40%Cell	3214.1 ± 164.9^{e}	24.6 ± 3.1^{d}	1.4 ± 0.1^{b}
S85	93.1 ± 14.7^{a}*	3.5 ± 0.5^{a}*	29.7 ± 2.9^{a}*
S85+5%Cell	419.9 ± 91.4^{a}*	4.8 ± 0.3^{a}*	13.3 ± 2.1^{b}*
S85+10%Cell	1036.2 ± 222.4^{b}*	12.2 ± 2.7^{b}*	2.6 ± 0.4^{c}
S85+20%Cell	1782.4 ± 124.2^{c}*	18.0 ± 2.8^{c}*	1.4 ± 0.2^{d}

Values in the same column with different letters are significantly different ($p \leq 0.05$). * indicates significant differences ($p \leq 0.05$) between the S53 and S85 samples with the same cellulose content.

Water vapor permeability (WVP) was also measured and the results are shown in Figure 5. As observed, the pure starch film pre-conditioned at higher relative humidity (S85) showed higher barrier in comparison with that pre-conditioned at lower relative humidity (S53). This was unexpected since the lower crystallinity of the S85 film, due to its greater gelatinization extent during processing, should, in principle, lead to the formation of more permeable materials. The more amorphous character of the S85 film may have promoted water sorption in the material, producing greater swelling of the starch matrix and, hence, yielding a more compact structure which impedes water diffusion to a greater extent. To corroborate this hypothesis, water contact angle measurements were carried out to evaluate the water affinity of the films. As shown in Figure 6, the S85 film presented significantly lower contact angle values than S53, showing its

much more hydrophilic nature, in agreement with its decreased crystallinity (see XRD results, cf. Figure 1 and Table 2). This supports the hypothesis of an increased water sorption in the S85 film due to its more hydrophilic character.

The incorporation of cellulose led to a significant decrease in the WVP of starch, with a maximum reduction of 54% (with respect to the pure starch) for the S53+40%Cell film. The barrier effect of cellulose has been widely reported in several studies [14, 18, 37, 38] and has been attributed to its relatively high crystallinity. In the particular case of starch, cellulose nanofibers have been reported to reduce the moisture diffusion coefficient and the water sorption in extruded biocomposites [13, 29]. However, loadings greater than 10% were seen to be detrimental for the barrier and mechanical performance, which was attributed to nanofiller agglomeration. Interestingly, the incorporation of cellulose had a stronger effect in the S85 films than in the S53 films, leading to a larger WVP drop for the same cellulose loading (i.e. 43% vs 23% for a cellulose loading of 20%). As shown in Figure 6, the addition of cellulose affected in a different way the water affinity of the S53 and S85 films. While the relatively hydrophobic behaviour of the S53 film was unaffected (since the crystallinity was not affected by the presence of cellulose), the more hydrophilic character of the S85 film was significantly modified towards a more hydrophobic behaviour when the cellulose content was increased. This effect may be originated by the higher crystallinity induced by the presence of cellulose in the S85 samples (cf. Table 2). Moreover, the water permeability and mechanical properties of the films showed a greater impact of cellulose in the films pre-conditioned at higher relative humidity conditions, pointing out that, apart from the better dispersion of cellulose, the greater gelatinization extent produced in the S85 samples may have also promoted the formation of stronger starch-cellulose interactions. Thus, the formation of more hydrophobic film surfaces may also be explained by a decrease in the amount of free hydroxyl groups due to the establishment of starch-cellulose interactions.

It is worth noting that the WVP values of the materials presented in this work were lower than those previously reported for starch biocomposites reinforced with nanocrystals from corn or rice, at similar or even higher loadings [39], once again showing the interesting properties of *Posidonia oceanica* cellulose as filler for the production of high performance biocomposites.

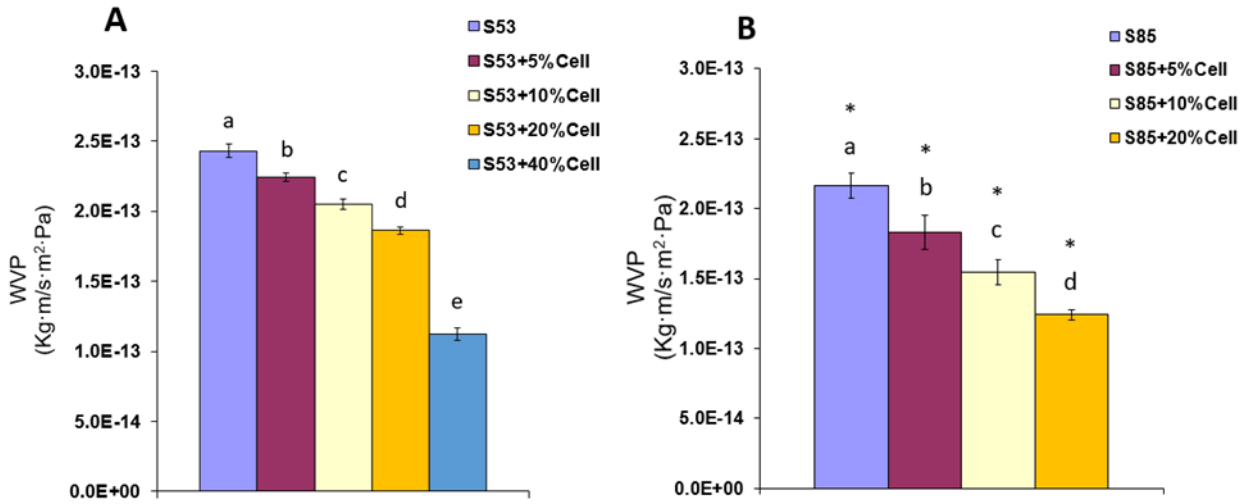

Figure 5. Water vapor permeability of the pure starch and biocomposite films with cellulose. Starch pre-conditioned at (A) 53 % RH and (B) 85% RH. Values followed by different letters are significantly different ($p \leq 0.05$). * indicates significant differences ($p \leq 0.05$) between the S53 and S85 samples with the same cellulose content.

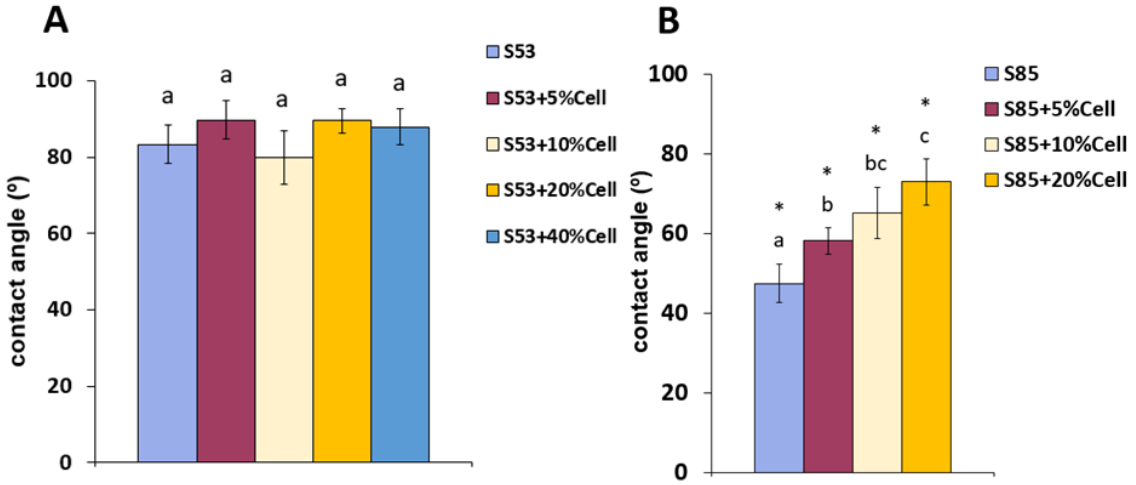

Figure 6. Calculated contact angle values for pure starch and biocomposite films with cellulose. Starch pre-conditioned at (A) 53 % RH and (B) 85% RH. Values followed by different letters are significantly different ($p \leq 0.05$). * indicates significant differences ($p \leq 0.05$) between the S53 and S85 samples with the same cellulose content.

4.2 Effect of pre-conditioning RH and *Posidonia oceanica* cellulose incorporation on the retrogradation of neat and biocomposite starch films

After being gelatinized, starch undergoes a re-crystallization process upon cooling and storage, known as retrogradation, in which mainly the amylose chains are able to re-associate and re-organize gradually to form a different ordered structure [40]. To evaluate the impact of cellulose on this retrogradation process, the pure starch films and the biocomposites loaded with 20%

cellulose were stored over an extended time of two months (t_f) and the crystallinity and mechanical properties of the films were studied and compared to those attained after storage for 3 days following the melt mixing process (t_0). Figure 7 displays the XRD patterns of the films at t_f and Table 2 compiles the estimated crystallinity index values for the films at t_0 and t_f. As observed, upon storage the crystalline structure of the films changed from the non-stable V-type mixture observed at t_0 towards a V_A type structure [28]. Interestingly, two peaks located at ca. 17º and 22º, which are characteristic from the B-type allomorph, were also detected. Corn starch has been reported to re-crystallize into a B-type structure when stored at low temperature [41] or high relative humidity conditions [42].

After storage for two months, all the samples showed increased crystallinity values as a result of the retrogradation process. This effect was much more evident in the case of the S85 and S85+20%Cell films. In particular, the S85 film showed the highest crystallinity increase (ca. 22.7%), as opposed to the low crystallinity increase detected in the S53 film (ca. 4%). The more amorphous character of the S85 film may have promoted water sorption upon storage. It is known that greater moisture contents favour starch re-crystallization [26, 40], hence explaining the greater crystallinity increase in the S85 and S85+20%Cell films as compared with S53 and S53+20%Cell. The presence of cellulose also restricted the re-crystallization process (crystallinity increased ca. 7.8% in S85+20%Cell and 1.2% in S53+20%Cell, corresponding to crystallinity increases 66% and 72% lower than those observed in their respective starch controls). This could be due to a limited water sorption upon storage induced by the presence of the more crystalline cellulose component. Previous works have also pointed out that the retrogradation of starch may be hindered by the addition of fillers which interact with the hydroxyl groups from starch by the formation of hydrogen bonds [43, 44].

The retrogradation process was also assessed through the analysis of the mechanical properties, which are compiled in Table 2. As expected, as a consequence of the re-crystallization produced upon storage, all the materials became stiffer (higher Young's modulus and tensile strength) and the elongation at break remained almost constant for most of the samples, while it decreased for S85. Since a greater re-crystallization occurred in the S85 and S85+20%Cell samples, the effect on their mechanical properties was more pronounced than in the S53 corresponding samples.

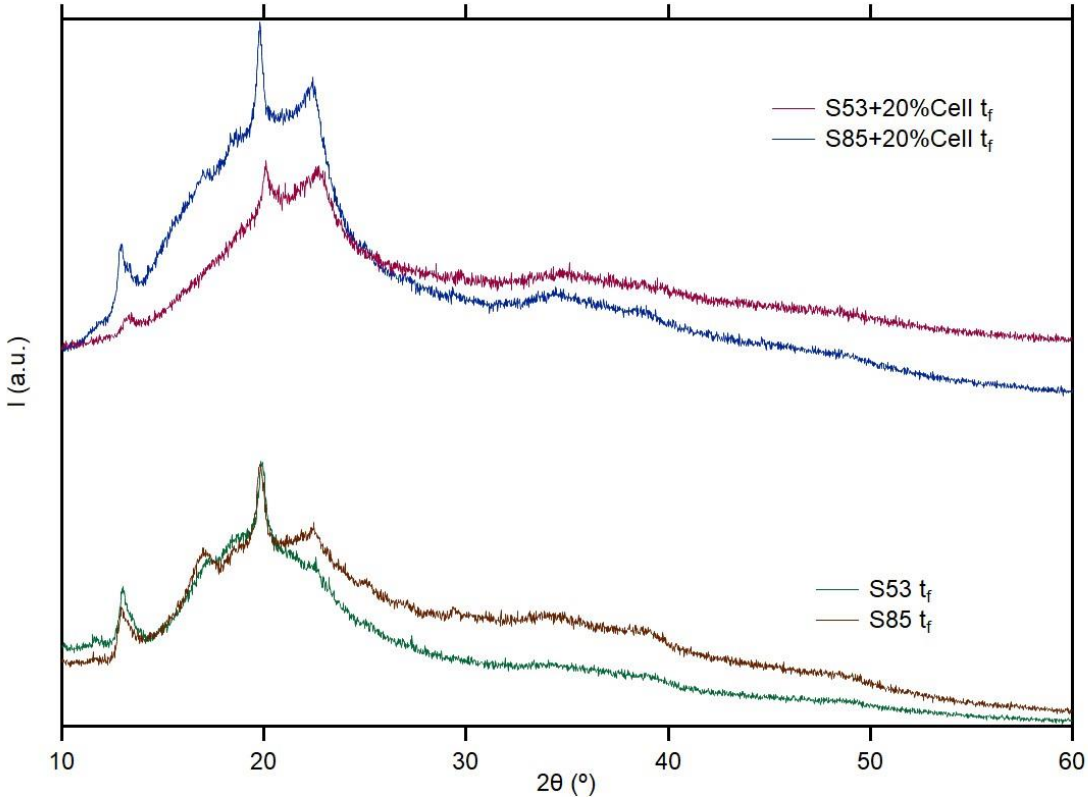

Figure 7. XRD patterns of the corn starch control films and the biocomposites with 20% cellulose after storage for two months (t_f). The patterns have been offset for clarity.

Furthermore, the incorporation of 20% cellulose also limited the impact on the mechanical properties of the films after prolonged storage. Interestingly, since the increase in the Young's modulus and tensile strength were much more remarkable in S85+20%Cell (47% and 25%, respectively) than in the case of S53+20%Cell, (25% and 15%, respectively), the mechanical properties of both films were very similar after storage. These results show that comparable improvements in the mechanical performance of starch films may be attained with the addition of *Posidonia* cellulose irrespective of the pre-conditioning of starch prior to the melt mixing process. However, S53+20%Cell would be the optimum choice in terms of material stability upon storage.

Table 2. Crystallinity index determined from the XRD patterns and mechanical properties of the different corn starch and biocomposite films with 20% cellulose immediately after being processed by melt mixing (t_0) and after storage for two months (t_f).

	Xc (%)	E (MPa)	Tensile Strength (MPa)	ε_b (%)
S53 t_0	19.2	546.3 ± 181.1	6.1 ± 0.7	8.5 ± 3.1
S53 t_f	23.5	1034.2 ± 127.3*	11.9 ± 1.0*	8.6 ± 2.1
S53+20%Cell t_0	14.6	2347.9 ± 161.0	24.1 ± 0.4	1.8 ± 0.1
S53+20%Cell t_f	15.8	3000.8 ± 286.7*	27.8 ± 0.9*	1.9 ± 0.1
S85 t_0	5.6	93.1 ± 14.7	3.5 ± 0.5	29.7 ± 2.9
S85 t_f	28.3	285.5 ± 29.7*	5.1 ± 0.6*	15.7 ± 1.4*
S85+20%Cell t_0	11.7	1782.4 ± 124.2	18.0 ± 2.8	1.4 ± 0.2
S85+20%Cell t_f	19.5	2634.5 ± 211.3*	22.6 ± 2.3*	1.6 ± 0.1

* indicates the existence of significant differences between the values corresponding to t_0 and t_f ($p \leq 0.05$).

5. Conclusions

Biocomposite materials based on corn starch and cellulose extracted from *Posidonia oceanica* waste biomass have been developed by the industrially meaningful melt compounding technique and their properties and retrogradation behaviour upon storage have been investigated. Cellulose loadings up to 40% were incorporated into starch, although the poor processability at the highest cellulose loading would restrict its industrial applicability.

Pre-conditioning of corn starch at different relative humidity conditions (53 and 85% RH) has been shown to substantially modify the properties of the films. The greater amount of moisture held by starch pre-conditioned at 85% RH (S85) promoted the gelatinization process during the melt mixing step, hence producing more amorphous materials. As a result, more hydrophilic, transparent and ductile starch films were obtained. These films presented a greater barrier to water vapor, which can be explained by a reduction in the diffusion as a result of water sorption and starch swelling.

The incorporation of cellulose seemed to prevent to some extent the disruption of the crystalline starch structure during melt mixing also improving mechanical and water barrier performance. The greater amount of moisture in the S85 samples facilitated the dispersion of cellulose and the establishment of stronger starch-cellulose interactions.

The retrogradation of starch was significantly affected by the amount of moisture during the melt mixing processing and the presence of cellulose. The more amorphous starch in the S85 films was seen to re-crystallize to a greater extent than the S53 samples. The presence of cellulose limited

the degree of re-crystallization, most likely due to a reduced water uptake of the materials upon storage. Thus, the S53+20%Cell film would be the optimum material presenting a good compromise between processability, mechanical and barrier properties, as well as material stability upon storage.

These results show the potential of *Posidonia oceanica* cellulose as a filler to partially replace corn starch and produce biocomposites with improved mechanical and barrier performance, as well as increased stability upon storage, outperforming the properties previously reported for starch biocomposites loaded with cellulose or cellulose nanocrystals obtained from other natural sources.

2.2. Pilot plant scale-up of the production of optimized starch-based biocomposites loaded with cellulosic Nanocrystals from Posidonia oceanica waste biomass

This section is an adapted version of the following published research article:

Benito-González, I., Göksen, G., Pérez-Bassart, Z., López-Rubio, A., Sánchez, R., Alonso, J.M., Gavara, R., Gallur, M. & Martínez-Sanz, M. (2021). Pilot plant scale-up of the production of optimized starch-based biocomposites loaded with cellulosic nanocrystals from *Posidonia oceanica* waste biomass Food Packaging and Shelf life. 30, 100730. DOI: https://doi.org/10.1016/j.fpsl.2021.100730

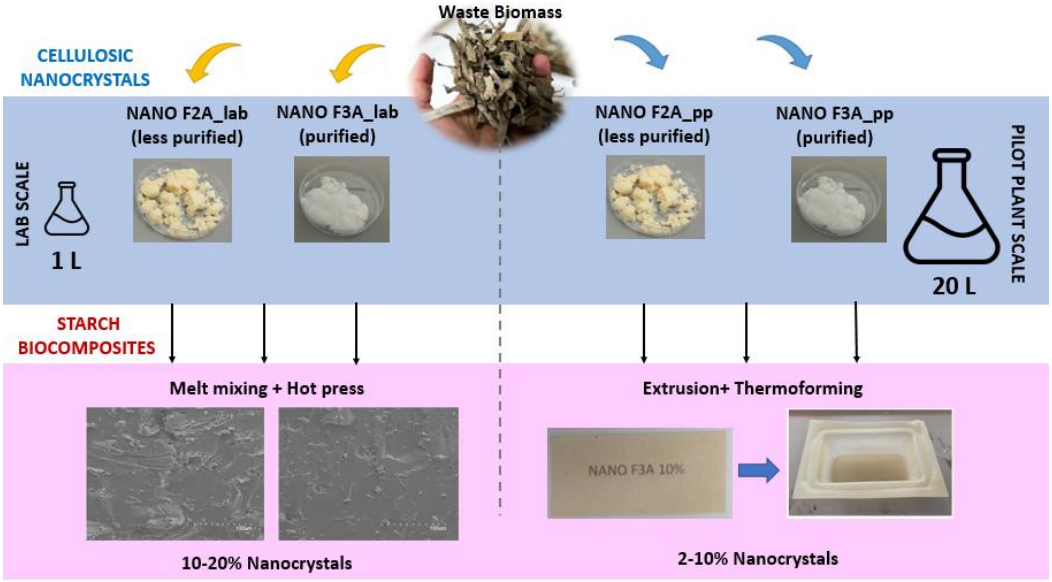

1. Abstract

Posidonia oceanica waste biomass has been valorized to produce cellulosic nanocrystals with different purification degrees at lab- and pilot plant-scale. The slightly greater yields obtained from the extraction treatments at pilot plant-scale resulted in slightly less purified nanocrystals.

Subsequently, the cellulosic nanocrystals (loadings of 10% and 20% (w/w)) were incorporated into corn starch to produce biocomposite films by melt mixing and hot-pressing at lab-scale. Biocomposite films showed remarkable improvements on the mechanical and water barrier performance (up to 10-fold increase in the elastic modulus and 2-fold decrease in the water permeability). Biocomposite packaging structures were also produced at pilot plant-scale by extrusion and thermoforming. Adjusting the plasticizer formulation and increasing the nanocrystals' loading up to the maximum content which allowed a good processability (10% (w/w)) allowed the production of trays with enhanced water barrier and mechanical performance, which, unlike the pure starch, were able to better keep their shape upon storage. These results highlight the potential of *P. oceanica* nanocrystals to improve the performance of starch-based

packaging structures and demonstrates the potential of the production process to be industrially applied.

2. Introduction

Petroleum-based plastics have been extensively used during the last decades within the food packaging area because of their low-cost, good processability and outstanding barrier and mechanical performance. However, the large amounts of waste generated as a result of their disposal derive in a severe environmental impact, endangering the environment and ecosystems. Consequently, biopolymers (i.e. biodegradable polymers derived from renewable resources) have been developed during the last years and proposed as a feasible alternative to conventional plastics. Nevertheless, their lower barrier and mechanical performance, as well as higher production costs, represent their most important limitations and have strongly restricted their field of application. Consequently, the incorporation of bio-based additives with good mechanical and barrier properties has been explored to improve the performance of biopolymers. In particular, cellulose is one of the most widely used bio-based additives in biocomposite materials and it has been reported to significantly increase the mechanical performance and water vapor permeability of commercial biopolymers such as starch [18, 45]. Furthermore, the addition of cellulose into starch matrices has been seen to improve the ageing and mechanical performance of thermoformed trays [46]. However, more studies need to be carried out to achieve a final product whose performance and/or cost-efficiency may compete with the conventional thermoformed structures [47].

Although cellulose itself has interesting properties for food packaging applications, its treatment by acid hydrolysis digests the amorphous domains, yielding highly crystalline nanocellulose or cellulose nanocrystals [48, 49], which feature an attractive combination of properties such as biocompatibility, large specific surface area and aspect ratio, high elastic modulus, high thermal stability and excellent optical transparency [50]. These have also been exploited to improve the properties of other biopolymer matrices, such as poly(lactic acid) (PLA) [51, 52], polyhydroxyalkanoates (PHAs) [53-55], polyisoprene [56] and pea starch [57], but their production at industrial level should be also tested [58]. Furthermore, despite most of the works available on the literature are focused on achieving a complete purification of cellulose from its raw source, a greener simplified method giving rise to less purified cellulosic nanocrystals (containing other components such as hemicelluloses and lipids) has been recently reported, that apart from providing advantages in terms of production costs and environmental impact, also led to improved performance of the derived packaging materials as compared to pure cellulose nanocrystals [59-61]. The reduction on the required purification steps, decreasing the energy and

time consumption, can also minimize the economic gap between biopolymers and conventional fossil-fuel derived plastics currently produced at industrial level.

An additional drawback of the most widespread biopolymers (such as PLA or starch) is that they are typically obtained from plant crops, competing with their primary use as food sources. In this context, the valorization of aquatic biomass, such as algae and aquatic plants, represents an efficient alternative to the use of land biomass. Indeed, aquatic biomass has been reported to contain large amounts of carbohydrates, which could be interesting for the development of bio-based plastics [18, 62-64]. In particular, *Posidonia oceanica*, an aquatic plant endemic to the Mediterranean Sea, whose dead leaves accumulate on the coasts generating a residue [65], has already been demonstrated to be an optimum source for the extraction of cellulose and lignocellulosic fractions with promising properties for the development of bio-based packaging materials [18, 48, 51]. Therefore, the utilization of this residue would be particularly interesting and in line with circular economy policies.

Thus, the overall aim of this work consisted in scaling-up the production of cellulosic nanocrystals with different degrees of purification from *P. oceanica* waste biomass from the lab-scale to pilot plant-scale in order to diminish the economic gap between conventional plastics and biopolymers. Furthermore, their subsequent utilization for the production of starch-based biocomposites with improved performance was also scaled-up using industrial methods such as extrusion and thermoforming processing and the properties of the produced materials were evaluated.

3. Materials and Methods

3.1 Raw materials

Waste biomass consisting on *Posidonia oceanica* leaves was collected from the sea shore of Denia (Alicante, Spain) in February 2019. The material was washed with water to remove sand and salts and then stored at refrigeration conditions (4 ºC) until its use. The initial composition of the P. oceanica biomass has been previously reported to be composed of 59% holocellulose, 18% lignin, 13% ashes, 7% proteins and 4% lipids [18].

3.2 Preparation of cellulosic nanocrystals

3.2.1 Lab-scale production

A purification procedure described in previous work [59] was carried out to sequentially remove cell wall components and obtain pure cellulose. Briefly, this process consisted of a treatment with

$NaClO_2$ to remove lignin (obtaining a fraction labelled as F2A) and a final alkaline treatment with KOH to remove the hemicelluloses, yielding purer cellulose (labelled as F3A fraction). Selected cellulosic fractions were then used as the starting materials to produce nanocrystals by means of a previously optimized acid hydrolysis method [59]. Briefly, the gel-like cellulosic fractions were immersed in a H_2SO_4 solution (30% w/w), with a ratio of 1.5 g dry fraction/100 mL H_2SO_4, at 50 ºC and kept under stirring for 1.5 hours. After that, the materials were subjected to several centrifugation and washing cycles to remove the acid and the pH was adjusted to 7 with NaOH. The obtained nanocrystals (labelled as NANO F2A_lab and NANO F3A_lab) were stored in the fridge as partially hydrated gel-like materials, until further use.

3.2.2 Pilot plant-scale production

The previously described protocols were adapted to generate NANO F2A and NANO F3A nanocrystals at larger pilot plant-scale, using 20 L digestor for chlorine-free bleaching treatment ($NaClO_2$), followed by basic treatment (KOH) in the case of purified nanocrystals (as described in section 2.2.1). Both were carried out in a 20 L digestor DBLP digestor (IDM, Spain) with internal stirring. After that, the bleached material was treated by hydrolysis acid following the same process outlined in section 2.2.1, using a 20L acid digestor (Radleys).

The obtained nanocrystals were labelled as NANO F2A_pp (less purified nanocrystals) and NANO F3A_pp (purified nanocrystals) and stored in the fridge as partially hydrated gel-like materials, until further use.

3.3 Production of starch-based biocomposites loaded with cellulosic nanocrystals

Prior to processing, granular corn starch was pre-conditioned for a minimum of two weeks in equilibrated relative humidity cabinets at 85% RH and 25ºC.

3.3.1 Lab-scale production of films by melt mixing

Pure corn starch and biocomposite films with loadings of 10 and 20 wt% (with regards to the starch weight) of *Posidonia oceanica* cellulosic nanocrystals (NANO F2A_lab and NANO F3_lab), were prepared by melt compounding followed by compression molding. Corn starch and glycerol (added as plasticizer) were dispersed in water using a polymer:glycerol:water ratio of 1:0.3:0.5 (w/w/w). For the biocomposite films, the required amount of nanocrystals (partially hydrated) was also incorporated and manually mixed until a paste was made. This paste was then melt-mixed in a Brabender Plastograph internal mixer at 130 °C and 60 rpm for 4 min. Subsequently, 4 g of the obtained blends were spread evenly on Teflon films and placed in a

compression mold (Carver 4122, USA) at a pressure of 16 tons and 130 °C for 2 min to form one film. The samples were coded as follows: CS (pure starch film), 10% NANO F2A_lab, 20% NANO F2A_lab, 10% NANO F3A_lab and 20% NANO F3A_lab (biocomposite films from corn starch loaded with 10 and 20% of nanocrystals). All the obtained films were stored in equilibrated relative humidity cabinets at 53% RH and 25ºC for three days prior to their characterization.

3.3.2 Pilot plant-scale production of films by extrusion

Starch-based biocomposite films were prepared at pilot plant-scale using an extruder model Brabender DSE 20/40. In this case, the cellulosic nanocrystals obtained at pilot plant-scale (NANO F2A_pp and NANO F3A_pp) were used as additives. The parameters were: 40D configuration, ramp temperature from 150 to 170 ºC with a melting temperature of 172 ºC, pressure of 38 bar and 19.9 N·m torque, yielding a production ratio of 1 kg/h. The same processing conditions previously optimized for melt blending were not applicable for extrusion and different plasticizer proportions were required. In particular, two different formulations were tested: 70% corn starch (CS), 25% glycerol and 5% sorbitol (named as CS 25-5) and 70% CS, 15% glycerol and 15 % sorbitol (named as CS 15-15). Due to processing issues, loadings of cellulosic nanocrystals lower than those previously used for melt mixing could be added to the formulations. Based on preliminary trials, a loading of 2 wt% nanocrystals was selected as the starting point. Keeping the nanocrystals' loading constant, the two combinations of plasticizers previously used for pure starch were tested, hence developing two different formulations named as 2% NANO F3A_pp (25-5) and 2% NANO F3A_pp (15-15). After optimization, the content of nanocrystals could be increased up to 10 wt% and two additional formulations were prepared, labelled as 10% NANO F2A_pp (15-15) and 10% NANO F3A_pp (15-15). All the extruded films' thicknesses ranged between 400-700 µm. The films were placed under controlled storage conditions (25 ºC and 53% RH) during 3 days prior to their characterization.

3.3.3 Pilot plant-scale production of trays by thermoforming

The extruded films with the most optimum performance, i.e. those with a 10 wt% loading of cellulosic nanocrystals, were thermoformed in a manual thermoformer model Formech Former 450 using a mold self-developed by ITENE of 11cm length x6 width x2 cm deep. The conditions followed were: 15 seconds, a heating temperature of 180-190 ºC and a vacuum pressure of -0.8 bar. The resulting trays were labelled as T-CS (15-15), T-10% NANO F2A (15-15) and T-10% NANO F3A (15-15). The trays were characterized after 2-3 days of storage at 25 ºC and 53% RH.

3.4 Attenuated total reflectance (ATR) FT-IR analysis

The lab-scale and pilot plant-scale produced nanocrystals were analysed by FT-IR in attenuated total reflectance (ATR) mode using a Thermo Nicolet Nexus (GMI, USA) equipment. Aqueous suspensions of the cellulosic nanocrystals were vacuum dried to obtain films, according to the method described previously [59], and the samples were then analysed. The spectra were taken at 4 cm^{-1} resolution in a wavenumber range between 400-4000 cm^{-1} and averaging a minimum of 32 scans.

3.5 Thermogravimetric analyses (TGA)

Thermogravimetric curves (TG) were recorded with a Setaram Setsys 16/18 (SETARAM Instrumentation, France). The samples (ca. 10 mg of the vacuum-dried cellulosic nanocrystals) were heated from 30 to 1000ºC with a heating rate of 10ºC/min under nitrogen atmosphere. Derivative TG curves (DTG) express the weight loss rate as a function of temperature.

3.6 X-ray diffraction (XRD)

XRD measurements of the cellulosic nanocrystals (in the form of films) were carried out on a D5005 Bruker diffractometer (Bruker Biosciences, Spain). The instrument was equipped with a Cu tube and a secondary monochromator. The configuration of the equipment was θ–2θ, and the samples were examined over the angular range between 3°–60° with a step size of 0.02° and a count time of 200 s per step. Peak fitting was carried out by using the Igor software package (Wavemetrics, Lake Oswego, Oregon) as described in a previous work [21]. The crystallinity index X_C was determined from the obtained fitting results by applying the following equation:

$$X_C(\%) = \frac{\sum A_{Crystal}}{A_{Total}} \times 100 \quad (1)$$

where A_{Total} is the sum of the areas under all the diffraction peaks and $\Sigma A_{Crystal}$ is the sum of the areas corresponding to the three crystalline peaks from cellulose I.

3.7 Transmission electron microscopy (TEM)

One drop (8 µL) of 0.001% aqueous suspensions of the produced cellulosic nanocrystals was allowed to dry on a carbon coated grid (200 mesh). The nanocrystals were stained with uranyl acetate. TEM was performed using a JEOL 1010 (JEOL, Massachusetts, USA) at an accelerating voltage of 80 kV. Morphology of the observed nanocrystals was characterized using ImageJ-win64 software by means of at least 5 different images.

3.8 Scanning electron microscopy (SEM)

SEM was conducted on a Hitachi microscope (Hitachi S-4800, Hitachi High-Tech, Germany) at an accelerating voltage of 10 kV and a working distance of 8-16 mm. Small samples (~5 mm^2 area) of the starch-based films were cut to observe their surface. The samples were then sputtered with a gold–palladium mixture under vacuum during 3 minutes before their morphology was examined.

3.9 Mechanical properties

Tensile tests were carried out at ambient conditions on a Mecmesin MultiTest 1-i (1 kN) machine (Virginia, USA) with the Emperor™ software, according to ASTM standard method D882-09 18 [20]. Pre-conditioned rectangular-shaped specimens with initial gauge length of 8 cm and 1 cm in width were cut directly from the films. A fixed crosshead rate of 10 mm/min was utilized in all cases. Elastic modulus (E), tensile strength (TS), and elongation at break (εb) were determined from the stress-strain curves, estimated from force–distance data obtained for the different films. At least, five specimens of each film were tensile tested to obtain statistically meaningful results.

3.10 Water vapor permeability (WVP)

Direct permeability to water was determined from the slope of the weight gain versus time curves at 25 ºC. The films were sandwiched between the aluminum top (open O-ring) and bottom (deposit for the silica) parts of a specifically designed permeability cell with screws. A Viton rubber O-ring was placed between the film and bottom part of the cell to enhance tightness. These permeability cells containing silica were then placed in an equilibrated relative humidity cabinet at 75% RH and 25 °C. The weight gain through a film area of 0.001 m^2 was monitored and plotted as a function of time. Cells with aluminum films (with thickness of ca. 11 μm) were used as control samples to estimate the weight gain through the sealing. The tests were done at least in triplicate.

3.11 Optical properties

The transparency of the films was determined through the surface reflectance spectra in a spectrocolorimeter CM-3600d (Minolta Co., Tokyo, Japan) with a 10 mm illuminated sample area. Measurements were taken in duplicate for each sample by using both a white and a black background.

Film transparency was evaluated through the internal transmittance (T_i) (0-1, theoretical range) by applying the Kubelka-Munk theory for multiple scattering to the reflection data. Internal

transmittance (T_i) of the films was quantified using Eq. (2). In this equation, R_0 is the reflectance of the film on an ideal black background. Parameters a and b were calculated by Eqs. (3) and (4), where R is the reflectance of the sample layer backed by a known reflectance R_g.

$$T_i = \sqrt{(a - R_0)^2 - b^2} \quad (2)$$

$$a = \frac{1}{2}\cdot\left(R + \frac{R_0 - R + R_g}{R_0 R_g}\right) \quad (3)$$

$$b = (a^2 - 1)^{\frac{1}{2}} \quad (4)$$

3.12 Statistical analysis

All data have been represented as the average ± standard deviation. Different letters show significant differences both in tables and graphs ($p \leq 0.05$). Analysis of variance (ANOVA) followed by a Tukey-b test were used when comparing more than two data sets.

4. Results and Discussion

4.1 Comparison between lab-scale and pilot plant-scale cellulosic nanocrystals

As a first step in the scaling-up process for the production of biocomposites loaded with cellulosic nanocrystals, the extraction process of the nanocrystals from *Posidonia oceanica* waste biomass was adapted to the pilot plant scale (20 L). To confirm that the obtained cellulosic nanocrystals were similar to those obtained at the laboratory, an initial characterization and comparison was carried out. Firstly, the yield of the different fractions and nanocrystals was calculated. As expected, the yields were progressively reduced with the application of the different purification steps. While the cellulosic fractions presented yields of 62 ± 3% for F2A_pp and 35 ± 3% for F3A_pp, their corresponding nanocrystals were obtained with lower yields of 34 ± 3% for NANO F2A_pp and 26 ± 2% for NANO F3A_pp. These yields were slightly higher than those corresponding to the fractions and nanocrystals previously obtained at lab scale (60 ± 5 % for F2A_lab, 30 ± 3% for F3A_lab, 26 ± 4% for NANO F2A_lab and 18 ± 1% for NANO F3A_lab [59]); however, the values followed the same trend, i.e. the less purified F2A fraction provided greater yields and the yields decreased more than 50% after the acid hydrolysis. Using bigger tanks for the pilot plant production may diminish the effectiveness of the extraction treatments

due to a less efficient stirring and/or to greater heat dissipation, thus producing slightly less purified materials with greater yields.

FT-IR analyses were carried out to characterize the obtained nanocrystals and the results are shown in Figures 1A and 1B. As observed, the resulting spectra were very similar regardless of the extraction protocol followed. As expected, the bands characteristic of cellulose (1000-1200 cm^{-1} region) [18] appeared sharper and more intense in the spectra from the purified nanocrystals (NANO F3A) as compared to the less purified ones (NANO F2A), demonstrating the greater cellulose content in the former ones. Interestingly, the band located at 1734 cm^{-1}, which can be attributed to the presence of hemicelluloses [18], was slightly more intense in the less purified nanocrystals obtained at pilot plant-scale in comparison with those obtained at lab-scale. This minor difference could be related, as mentioned before, to the presumably lower effectiveness of the alkaline treatment in the pilot plant-scale process, which led to the production of less purified nanocrystals with a higher yield.

Additionally, TGA characterization was carried out to determine the thermal stability of the obtained nanocrystals and the results are shown in Figures 1C and 1D. As expected, the degradation profile of the more purified nanocrystals (NANO F3A) was dominated by a narrow and intense peak with its maximum at ca. 335 ºC, which has been typically reported to cellulose degradation [18]. In the case of the less purified nanocrystals (NANO F2A), an additional degradation step took place, as indicated by the appearance of a small shoulder at lower temperatures (250-280 ºC), which has typically been assigned to the presence of hemicelluloses [61]. On the other hand, the degradation step occurring at high temperatures (400-550 ºC) can be attributed to the degradation of lipidic components naturally present in *P. oceanica* leaves [66] and still remaining in the produced nanocrystals (since the Soxhlet treatment was not applied). It should be noted that this degradation step took place at lower temperatures in the case of the pilot plant-scale nanocrystals and the intensity of the degradation peaks was also greater. This again suggests a slightly lower effectiveness of the purification steps when scaling-up the process.

To determine the crystallinity of the cellulosic nanocrystals, XRD analyses were also performed and Figure 1E shows the obtained diffraction patterns. As observed, all the produced nanocrystals displayed patterns characteristic of crystalline cellulose I, with one broad shoulder at ca. 16º (which is composed of two overlapped peaks located at 15.0-15.5° and 16.6-16.8°) and one sharp and intense peak at 22.6º. These peaks correspond to the (1-10), (110) and (200) crystalline planes from the cellulose I_β crystalline allomorph [67, 68]. In general, all the samples presented very similar patterns, although the pilot plant-scale nanocrystals showed some minor differences. In particular, NANO F2A_pp showed an additional sharp peak at around 27º, which can be attributed to mineral compounds [61] remaining in the material. This peak was not visible in NANO

F3A_pp; however, a small shoulder at ca. 12º, which was faintly visible in the less purified NANO F2A_pp nanocrystals and arises from the presence of hemicelluloses [69, 70], became more visible. This may indicate that some of the hemicelluloses initially present in F2A were not completely removed by the pilot plant-scale alkaline treatment applied to produce F3A and these remaining hemicelluloses were resistant to the acid hydrolysis. These results provide further evidence for the lower efficiency of the pilot plant-scale process as compared to the lab-scale protocol in purifying the cellulosic fractions. The crystallinity indexes of the nanocrystals were calculated from the XRD patterns, obtaining values of ca. 50% for NANO F2A_lab, 62% for NANO F3A_lab, 55% for NANO F2A_pp and 51% for NANO F3A_pp. The slightly lower crystallinity of NANO F3A_pp as compared with NANO F2A_pp is contrary to what would be expected, since the former correspond to the nanocrystals obtained from a more purified cellulosic fraction. One possible explanation is related to the lower efficiency of the acid hydrolysis treatment when components such as xylans and lipidic compounds are still remaining in the fraction to be hydrolysed [59, 61]. In fact, a recent study has shown that some xylans can hinder the accessibility of the acid towards the amorphous domains of cellulose [61]. These non-accessible regions remain non-digested even when increasing the hydrolysis time and instead, accessible crystalline regions start to be digested, decreasing the overall crystallinity of the material. As previously mentioned, the shoulder detected in NANO F3A_pp indicates the presence of non-hydrolysed hemicelluloses. Thus, it seems reasonable to assume that the hemicelluloses remaining after the pilot plant-scale alkaline treatment hindered the acid hydrolysis of amorphous cellulose.

Finally, the morphology of the extracted nanocrystals was studied by TEM and representative images are displayed in Figure 2. The morphology of cellulose fibrils could be identified more clearly in the most purified nanocrystals, i.e. NANO F3A_lab, while the fibrils were more agglomerated in the rest of the samples, especially in the NANO F2A nanocrystals. As expected, a higher degree of agglomeration was observed in NANO F2A_pp due to the presence of hemicelluloses, which, as previously reported [59, 71], act as cross-linking agents between cellulose fibrils. In the case of NANO F3A_pp, some areas with higher agglomeration degree were also observed in comparison with NANO F3A_lab, although not big differences were appreciated between them. The average measured fibril dimensions of NANO F2A_pp (Fig. 2C) were a length of 515 ± 51 nm and a width of 11 ± 3 nm, while NANO F3A_pp (Fig. 2D) showed a length of 563 ± 58 nm and a width of 9 ± 2 nm. In terms of dimensions, there were no significant differences between the pilot plant-scale nanocrystals and their lab-scale counterparts, which showed a length of 499 ± 96 nm and a width of 15 ± 5 nm in the case of NANO F2A_lab (Fig. 2A) and a length of 586 ± 103 nm and a width of 10 ± 3 nm in the case of NANO F3A_lab (Fig. 2B) [59].

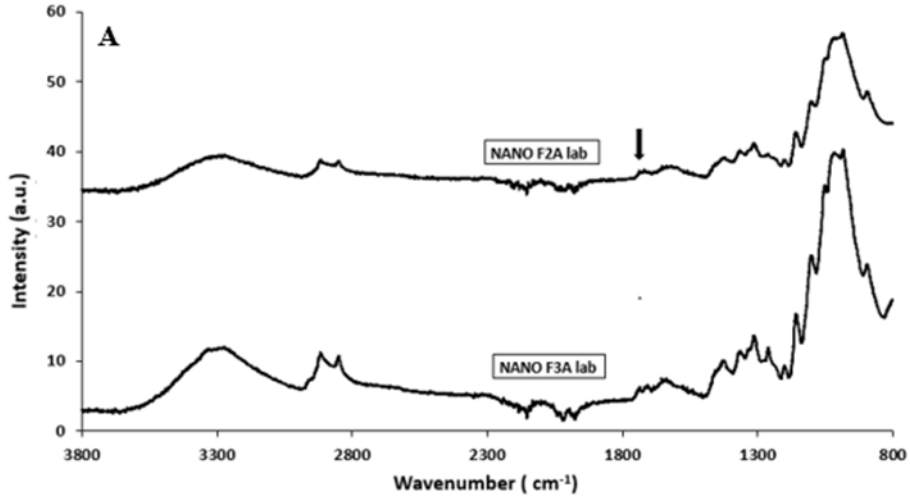
A
NANO F2A lab
NANO F3A lab
Intensity (a.u.)
Wavenumber (cm-1)

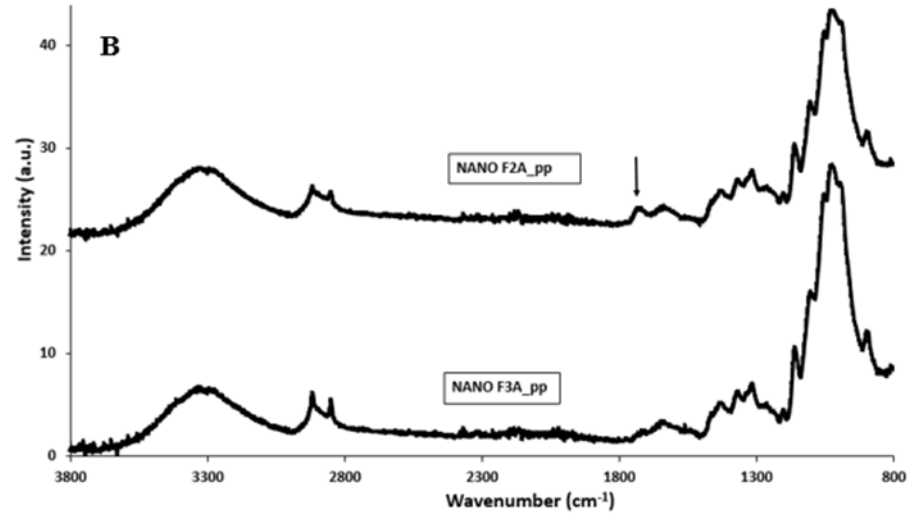
B
NANO F2A_pp
NANO F3A_pp
Intensity (a.u.)
Wavenumber (cm-1)

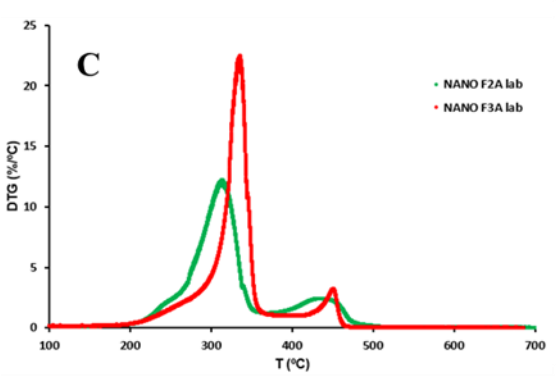
C
NANO F2A lab
NANO F3A lab
DTG (%/ºC)
T (ºC)

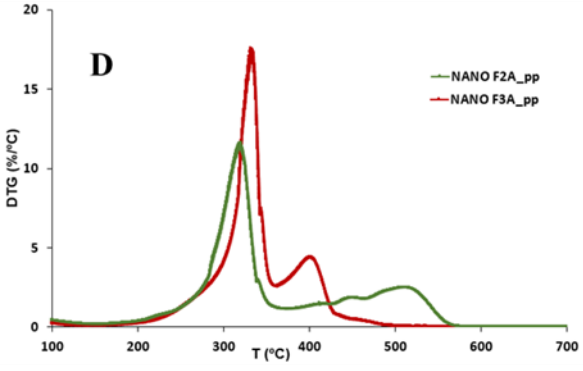
D
NANO F2A_pp
NANO F3A_pp
DTG (%/ºC)
T (ºC)

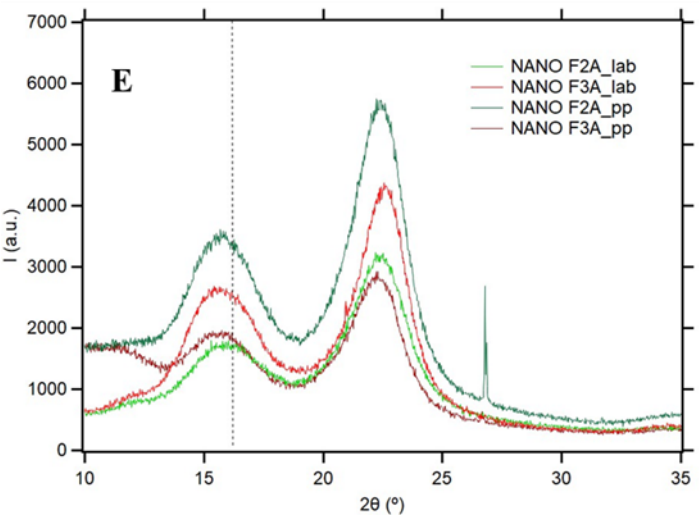
E
NANO F2A_lab
NANO F3A_lab
NANO F2A_pp
NANO F3A_pp
I (a.u.)
2θ (º)

Figure 1. FT-IR spectra of the (A) lab-scale and (B) pilot plant-scale cellulosic nanocrystals with different degrees of purification. Spectra have been offset for clarity. Arrows point out to the spectral band located at ~1730 cm^{-1}. Derivative thermogravimetric (DTG) curves of (C) lab-scale and (D) pilot plant-scale produced cellulosic nanocrystals. (E) XRD patterns of the cellulosic nanocrystals obtained at lab-scale and pilot plant-scale.

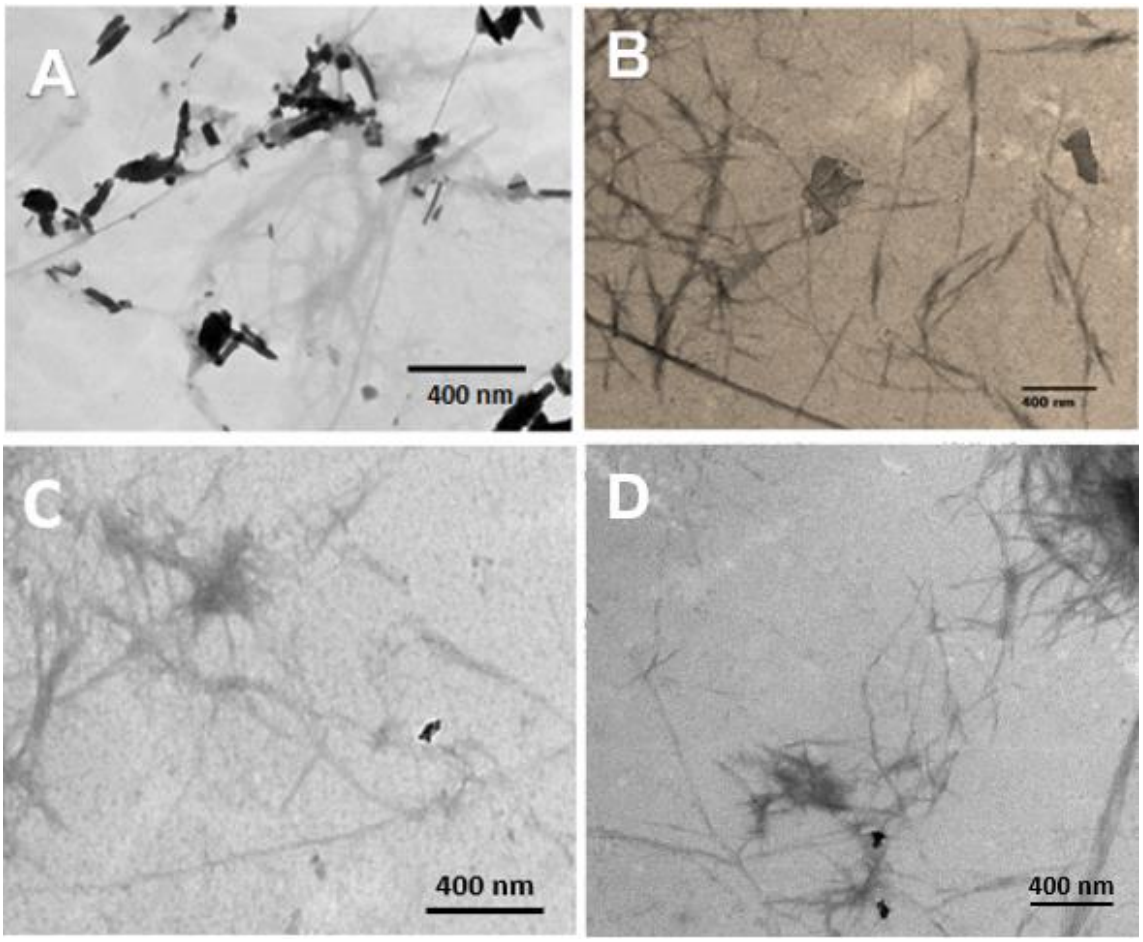

Figure 2. Representative TEM images of the lab-scale and pilot plant-scale produced cellulosic nanocrystals: (A) NANO F2A_lab, (B) NANO F3A_lab, (C) NANO F2A_pp and (D) NANO F3A_pp.

4.2 Lab-scale production of starch-based biocomposites loaded with cellulosic nanocrystals

The aim of this work was to develop starch-based biocomposites loaded with cellulosic nanocrystals from *Posidonia oceanica* biomass, maximizing the nanocrystals' loading while allowing a good processability and yielding materials with optimum performance properties. As an initial step, the nanocrystals produced at lab-scale were incorporated into corn starch to produce films by means of a lab-scale internal mixer and a hot press to determine the optimal

formulations for packaging structures in terms of mechanical and barrier performance. Based on previous studies in which *P. oceanica* cellulosic fractions were incorporated into corn starch [45], loadings of 10% and 20% (w/w) (for both NANO F2A and NANO F3) were selected and the obtained films were characterized.

To evaluate the compatibility of both biopolymers and the degree of dispersion of the cellulosic nanocrystals, the cross-sectional area of the films was examined through SEM and Figure 3 displays representative images. As clearly observed, a more homogeneous dispersion of the nanocrystals was achieved in the formulations containing NANO F3A_lab (Fig. 3D and 3E). As opposed, the less purified NANO F2A_lab (Fig. 3B and 3C) were more agglomerated and bundles of cellulose fibrils could be visualized in the cross-section of the corresponding biocomposites, especially with higher loadings (see arrows in Fig. 3C). This is not unexpected, since the hemicelluloses remaining in NANO F2A may act as cross-linking agents and impede a proper dispersion of the cellulose fibrils.

The mechanical and water barrier performance of the pure starch and the biocomposite films were evaluated, and the results are summarized in Table 1. As expected, the incorporation of the cellulosic nanocrystals significantly increased the rigidity of the films, even with the lowest loading of 10%. Interestingly, this rigidizing effect was more evident in the formulations using the less purified nanocrystals (NANO F2A), suggesting that the presence of hemicelluloses had a positive impact on the mechanical performance of the films. For the highest loading of 20% the elastic modulus of starch was increased more than 10-fold and the tensile strength increased 6-10-fold; on the other hand, the elongation at break was also significantly reduced, i.e. the materials were less ductile. While 20% NANO F2A_lab was the formulation providing the most rigid films, the greater ductility of 10% NANO F2A_lab might be more desirable for packaging applications.

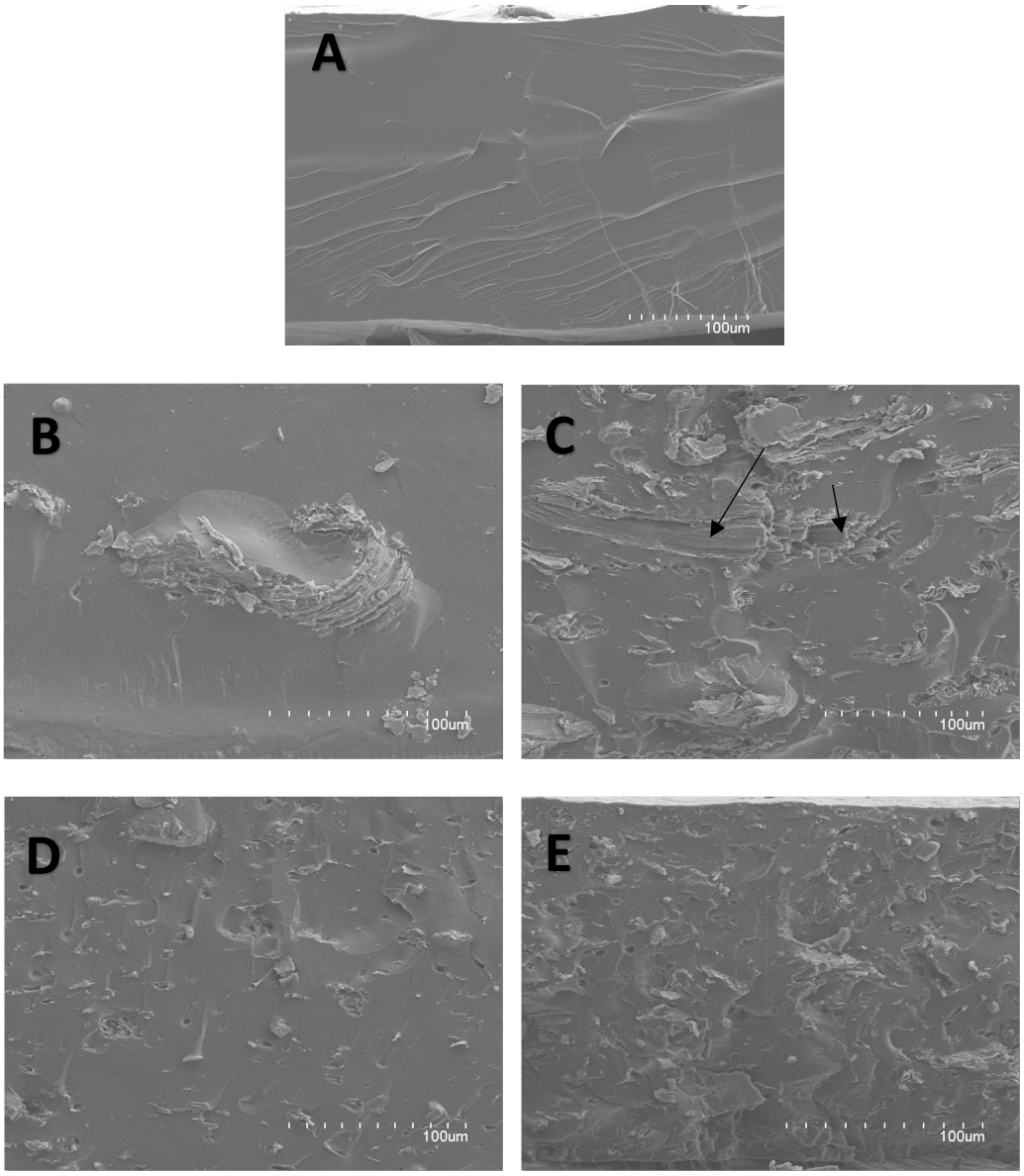

Figure 3. Cross section SEM images of (A) CS, (B) 10% NANO F2A_lab, (C) 20% NANO F2A_lab, (D) 10% NANO F3A_lab and (E) 20% NANO F3A_lab.

With regards to the WVP, the results evidenced a higher barrier effect for the purified cellulose nanocrystals, which can be explained by (i) their better dispersion along the corn starch matrix, thus hindering the diffusion of water vapor through the film and (ii) their greater crystallinity index, limiting water sorption. 20% NANO F3A_lab was the most optimum formulation in terms of water vapor barrier, with a 2-fold increase. Nevertheless, it should be noted that all the formulations tested could significantly diminish the WVP of the pure starch film. Similar relative improvements in terms of mechanical and WVP performance were achieved when incorporating 40% (w/w) of pure cellulose from *P. oceanica* into a corn starch matrix [45].

Table 1. Mechanical properties and water vapor permeability of lab-scale produced films from corn starch and biocomposites with NANO F2A and NANO F3. E: elastic modulus; εb: elongation at break; WVP: water vapor permeability. Values in the same column followed by different letters are significantly different ($p \leq 0.05$).

	E (MPa)	**Tensile Strength (MPa)**	**ε_b (%)**	**WVP ($kg \cdot m/s \cdot m^2 \cdot Pa) \cdot 10^{-13}$**
CS	76.4 ± 17.8^{a}	1.6 ± 0.2^{a}	33.5 ± 3.4^{a}	2.27 ± 0.01^{a}
10% NANO F2A_lab	254.5 ± 24.5^{b}	4.0 ± 0.4^{b}	11.4 ± 0.2^{b}	1.74 ± 0.01^{b}
20% NANO F2A_lab	1270.9 ± 83.6^{d}	15.8 ± 1.4^{d}	2.8 ± 0.4^{c}	1.67 ± 0.03^{bc}
10% NANO F3A_lab	228.3 ± 15.8^{b}	2.8 ± 0.3^{b}	15.8 ± 4.5^{b}	1.58 ± 0.02^{c}
20% NANO F3A_lab	856.0 ± 33.8^{c}	10.6 ± 0.3^{c}	4.3 ± 1.5^{c}	1.11 ± 0.03^{d}

As an additional attribute relevant for their application as packaging materials, the transparency of the films was measured, and the results are represented in Figure S1. Briefly, all the films displayed high transparency values (Ti~60-80%). Minor reductions were observed with the addition of cellulosic nanocrystals, being more evident at the highest loading of 20%. Furthermore, the biocomposite films showed a light yellowish coloration. This slight transparency loss and coloration of the biocomposite films might not necessarily be considered as a negative aspect, since it could increase the self-life of the product by limiting UV-induced deterioration, without preventing the consumers from identifying the packaged foodstuff (all samples presented transparency values above ~70% Ti).

Overall, all the formulations tested could significantly improve the mechanical and barrier performance of the CS. Although greater degree of improvement was achieved with the higher loading of nanocrystals (i.e. 20% (w/w)), the formulations with 10% (w/w) nanocrystals were easier to process and, thus, might be more optimum for the scale-up process using extrusion and thermoforming. In particular, 10% NANO F3A_lab presented slightly better barrier performance than 10% NANO F2A_lab, but it implied an additional purification step. Thus, 10% NANO F2A_lab showed the best compromise between performance (remarkable improvement in WVP and stiffness without an excessive drop in the elongation) and sustainability (most cost-efficient purification procedure).

4.3 Pilot plant-scale production of starch-based biocomposite films and trays

After upscaling the extraction of the cellulosic nanocrystals, hence ensuring the availability of large quantities of material, the production of starch-based biocomposites was also upscaled using an extrusion machine for the production of films and followed by thermoforming for the production of trays. Initially, several formulations were tested for the production of films and their mechanical properties and WVP were characterized to identify the most optimum materials (avoiding excessive elongation and plasticization) for the subsequent thermoforming step. Due to the difficulties encountered when processing formulations with higher nanocrystals' loadings in the extruder, a low loading of 2% (w/w) was selected as the starting point to optimize the formulations. Based on preliminary trials, the utilization of glycerol as the only plasticizer was seen to be unfavourable. Instead, a mixture of glycerol and sorbitol was used, varying the proportion of both to evaluate their effect on the properties of the obtained films. The mechanical properties of the starch films, collected in Table 2, show that increasing the proportion of sorbitol in the plasticizer mixture had a clear positive rigidizing effect, increasing more than 80-fold the elastic modulus while reducing less than 3-fold the elongation at break. This rigidizing effect of sorbitol vs. glycerol in starch matrices has been already reported in the existing literature [72]. As expected, the incorporation of cellulosic nanocrystals, even at a low loading of 2%, rigidized all the films regardless of the plasticizer formulation. It should be noted that the formulations with 25% glycerol and 5% sorbitol presented an excessive ductility (with elongation values ranging from ca. 33 to 58%) and, therefore, they may not be suitable for the thermoforming step. On the other hand, the WVP was not significantly affected by the plasticizer formulation, but it was reduced with the incorporation of NANO F3A_pp. All these films were subjected to the thermoforming process and trays were successfully produced; however, none of those trays was stiff enough to maintain their shape upon storage and, thus, they would not be adequate for packaging structures (see Figure S2). In particular, and as already anticipated on the basis of their mechanical properties, the trays with 25% glycerol and 5% sorbitol were the least stable and lost their shape after a couple of hours.

After these first trials, given the improved performance of the CS trays with 15% glycerol and 15% sorbitol, new film formulations were developed by keeping the same plasticizer ratio and increasing the loading of cellulosic nanocrystals as much as to possible to confer higher rigidity to the films. 10% (w/w) was the maximum loading of cellulosic nanocrystals which allowed a proper processing of the blends by extrusion. The cellulosic nanocrystals were added to the formulations as partially hydrated gels (to avoid drying and ensure an optimum dispersion), but the amount of water contained in these gels resulted in the formation of air bubbles in the extruder. This was especially relevant in the case of NANO F2A_pp, which were more hydrophilic due to the presence of hemicelluloses. As a result, the obtained films and trays presented some bubbles

in their surface (cf. Figures 4A and 4B). This was not an issue in the formulations containing NANO F3A_pp, most likely due to the lower amount of water held by the more purified cellulose nanocrystals, thus yielding more homogeneous films and trays (cf. Figures 4A and 4C). These bubbles significantly affected the transparency of the packaging structures, with a ~20% decrease in the transparency of the trays containing 10% NANO F2A with respect to the trays from CS and 10% NANO F3A_pp, as determined by means of internal transmittance (cf. Figure S3).

Regarding the mechanical performance of the films, it could be inferred that increasing the loading of the cellulosic nanocrystals up to 10% had a positive effect, enhancing the elastic modulus up to 600-700 MPa, while still keeping the elongation at break within a reasonable interval of 8-11%. This effect was more notable when adding the more purified nanocrystals (i.e. NANO F3A_pp). Furthermore, a decrease in the WVP was also noted with the incorporation of NANO F3A_pp. The mechanical performance and WVP of the trays obtained after thermoforming are also gathered in Table 2. Surprisingly, the thermoforming process seemed to have a plasticizing effect on the materials, with a significant reduction on the stiffness (15-19-fold reduction on the elastic modulus and 5-4-fold reduction on the tensile strength) and a substantial increase in the elongation at break (up to 3-fold) of the trays as compared to the initial films. This suggests that a greater degree of starch gelatinization was achieved after the thermoforming process (i.e. starch presented a more amorphous structure in the trays as compared to the original films) [45]. This would also explain why formulations which were apparently suitable for films, were not suitable for trays since they were not sufficiently rigid and were not able to keep their shape after being thermoformed. This was especially remarkable in the pure CS trays (T-CS (15-15)), with elongation values higher than 30% and very poor mechanical resistance, clearly limiting their application for food packaging. The loss in mechanical performance after thermoforming was slightly mitigated by the presence of cellulosic nanocrystals. This is in line with previous studies showing that cellulosic fillers may limit the extent of starch gelatinization upon processing at high temperature and moisture conditions [45]. Thus, the addition of cellulosic nanocrystals led to a substantial increase in the rigidity of the trays as compared to the pure starch (between 2- and 3-fold increase in the stiffness) while avoiding an excessive reduction in the elongation (ranging between 17-25%). Following the same trend observed in the films, the mechanical properties of the trays were not strongly affected by the purification degree of the cellulosic nanocrystals. Interestingly, the water vapour barrier was seen to increase after the thermoforming process, especially in the biocomposite trays (16% decrease in the WVP for the trays with 10% NANO F2A_pp and 36% for the trays with NANO F3A_pp, with respect to the original films). Thus, the incorporation of cellulosic nanocrystals into starch not only yielded trays with better mechanical performance but also improved the barrier capacity.

Due to the great effect of the processing and storage conditions on the structure of starch, the properties reported in the literature for starch-based materials are highly variable. For instance, a previous study reporting on the thermoforming of plasticized wheat starch (PWS) loaded with commercial cellulosic fibres (15-30% w/w) showed stiffness values for the films similar to the ones determined in this work (elastic modulus~600 MPa and tensile strength~10-15 MPa) but greater elongation values (10-30%); however, the obtained trays were not characterized [46]. In contrast, other work in which PWS was loaded with barley straw and grape cellulosic fibres (2-15% w/w), reported poorer mechanical performance of the films (with elastic modulus <100 MPa and tensile strength<5 MPa) [73].

Table 2. Mechanical properties and water vapor permeability of pilot plant-scale produced films and thermoformed trays from corn starch and biocomposites with NANO F2A and NANO F3A. E: elastic modulus; ε_b: elongation at break; WVP: water vapor permeability. Values within the same column followed by different letters are significantly different ($p \leq 0.05$). The statistical analysis was carried out separately for the films with each plasticizer formulation and for the trays.

	E (MPa)	**TS (MPa)**	**ε_b (%)**	**WVP (kg·m/s·m^2·Pa) ·10^{-13}**
Extruded Films				
CS (25-5)	2.3 ± 0.5^a	1.5 ± 0.1^a	57.5 ± 3.8^a	4.5 ± 0.2^a
2% NANO F2A (25-5)	6.0 ± 0.6^b	2.2 ± 0.2^b	33.1 ± 5.8^b	4.1 ± 0.2^a
2% NANO F3A (25-5)	3.7 ± 0.4^a	1.6 ± 0.1^a	40.5 ± 6.6^b	2.9 ± 0.2^b
CS (15-15)	192.2 ± 52.2^a	4.6 ± 0.6^a	20.1 ± 2.5^a	3.4 ± 0.1^a
2% NANO F2A (15-15)	---	---	---	---
2% NANO F3A (15-15)	311.1 ± 74.5^a	6.0 ± 0.4^{ab}	17.2 ± 5.2^{ab}	2.6 ± 0.0^b
10% NANO F2A (15-15)	610.8 ± 38.1^b	6.8 ± 0.6^b	7.9 ± 1.3^c	3.0 ± 0.2^{ab}
10% NANO F3A (15-15)	660.9 ± 40.1^b	9.6 ± 0.3^c	11.2 ± 2.1^{bc}	2.5 ± 0.2^b
Thermoformed trays				
T-CS (15-15)	9.9 ± 2.2^a	0.9 ± 0.2^a	35.8 ± 5.2^a	3.2 ± 0.1^a
T-10% NANO F2A (15-15)	34.4 ± 7.2^b	1.6 ± 0.2^{ab}	24.8 ± 2.2^{ab}	2.5 ± 0.1^b
T-10% NANO F3A (15-15)	43.9 ± 8.1^b	2.6 ± 0.2^b	17.2 ± 1.4^b	1.6 ± 0.0^c

Despite the substantial improvement in the mechanical and barrier performance of starch-based trays achieved with the incorporation of the cellulosic nanocrystals, their mechanical properties

are still far from those of other biopolymers typically commercialized in the packaging market, such as PLA (with values of 3000 MPa for the elastic modulus and 50 MPa for the tensile strength in the case of films produced by melt blending) or PET (3000 MPa, 80 MPa) [59, 73]. In this sense, a possible strategy to improve further the mechanical properties of the starch-based trays, which will be explored in the future, consists on the incorporation of minor loadings of PLA [74] and/or PVOH [75], and optimizing the formulations and the extrusion process to increase as much as possible the loading of the cellulosic nanocrystals extracted from *P. oceanica* waste biomass.

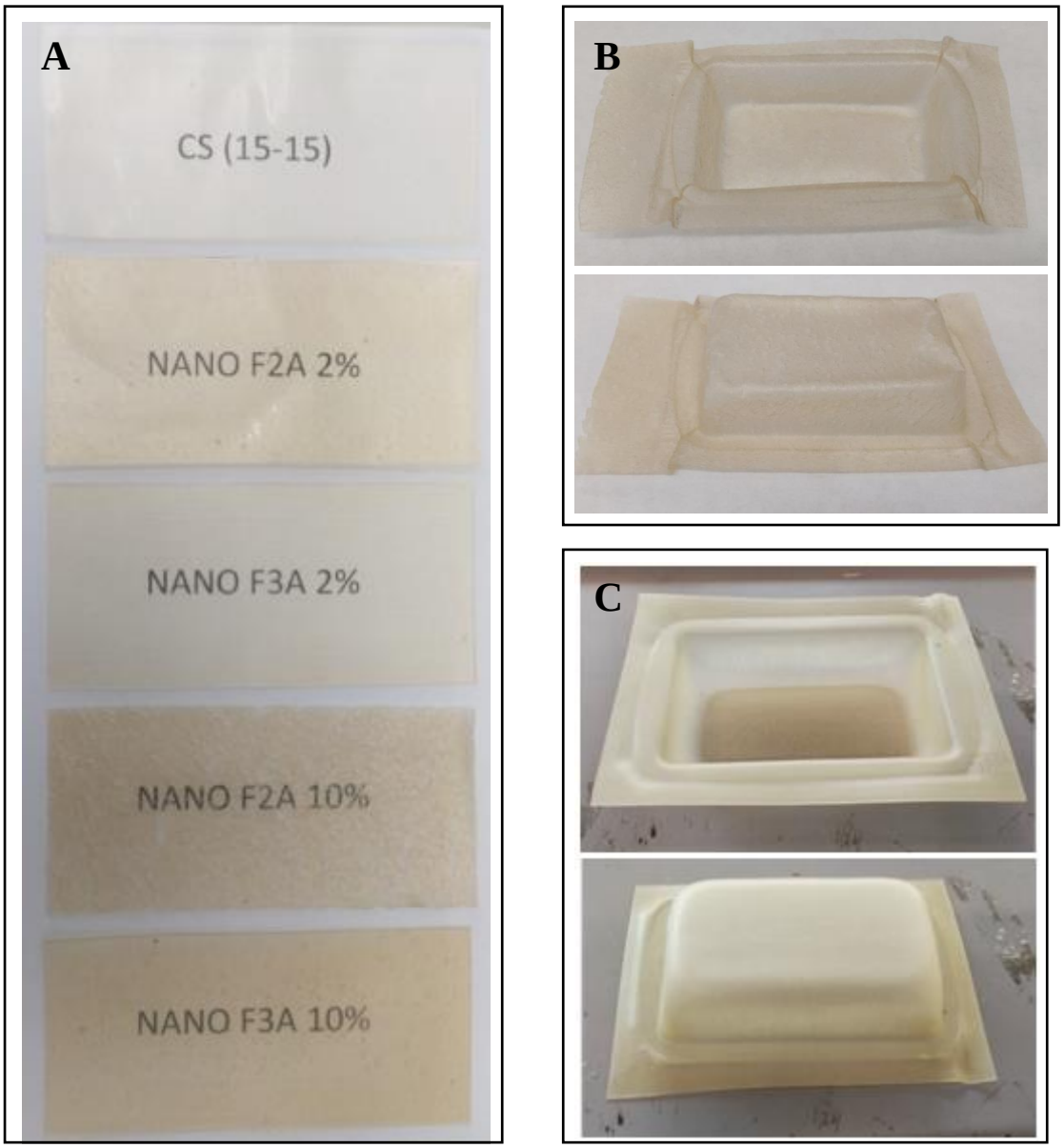

Figure 4. Visual appearance of: (A) pilot plant-scale produced films from corn starch and biocomposites with NANO F2A_pp and NANO F3A_pp, containing 15% glycerol and 15% sorbitol as plasticizers; (B) thermoformed tray T-10% NANO F2A (15-15) and (C) thermoformed tray T-10% NANO F3A (15-15).

5. Conclusions

Posidonia oceanica waste biomass has been valorized to produce cellulosic nanocrystals with different purification degrees and the lab-scale process has been scaled-up to pilot plant-scale, obtaining yields of ca. 34% for the less purified nanocrystals (NANO F2A_pp) and ca. 26% for the most purified ones (NANO F3A_pp). Characterization of the obtained nanocrystals showed that the efficiency of the extraction treatments was reduced when scaling-up, thus producing less purified cellulosic nanocrystals.

Subsequently, the produced nanocrystals were incorporated into corn starch to generate biocomposite materials with enhanced performance properties. At lab-scale, the incorporation of NANO F2A_lab and NANO F3A_lab into corn starch (loadings of 10% and 20% (w/w)) significantly improved the mechanical stiffness and water barrier of films produced by melt mixing and hot pressing. In particular, 10% NANO F2A_lab showed the best compromise between improvement in the stiffness and water permeability and sustainability of the production process. The production of starch-based biocomposites was also scaled-up and NANO F2A_pp and NANO F3A_pp were incorporated into starch by extrusion, followed by thermoforming to produce trays. The plasticizer formulation was seen to be key to produce materials more suitable for thermoforming, being the combination of 15% glycerol plus 15% sorbitol the most optimum. Increasing the nanocrystals' loading improved the barrier performance and the mechanical properties of the extruded films and trays. Notably, unlike the pure starch trays, the biocomposite trays were able to preserve their shape upon storage. However, 10% (w/w) was the maximum loading which could be incorporated by extrusion since the presence of moisture in the nanocrystals led to processing issues. This was more notable in NANO F2A_pp, producing bubbles in the obtained packaging structures and reducing their transparency.

It should be noted that the approval of cellulose nanocrystals to be used as food contact materials (FCMs) is still under evaluation in Europe, although recent studies are being taken into account by the EFSA for their positive assessment [76, 77]. However, other countries like Canada have recently unrestricted the commercialization and use of cellulose nanocrystals, according to their lack of toxicity as observed by several regulatory protocols. Thus, it only seems a matter of relatively short time for cellulosic nanocrystals to be completely regarded as safe in Europe.

These results highlight the potential of cellulosic nanocrystals extracted from *P. oceanica* waste biomass to produce starch-based packaging structures with improved performance and demonstrate the feasibility of the production process to be industrially applied.

List of references of Chapter 2:

[1] A. Dufresne, M.R. Vignon, Improvement of starch film performances using cellulose microfibrils, Macromolecules 31(8) (1998) 2693-2696.
[2] C.M. Müller, F. Yamashita, J.B. Laurindo, Evaluation of the effects of glycerol and sorbitol concentration and water activity on the water barrier properties of cassava starch films through a solubility approach, Carbohydrate Polymers 72(1) (2008) 82-87.
[3] V.P. Cyras, L.B. Manfredi, M.-T. Ton-That, A. Vázquez, Physical and mechanical properties of thermoplastic starch/montmorillonite nanocomposite films, Carbohydrate Polymers 73(1) (2008) 55-63.
[4] E. Csiszár, S. Nagy, A comparative study on cellulose nanocrystals extracted from bleached cotton and flax and used for casting films with glycerol and sorbitol plasticisers, Carbohydrate polymers 174 (2017) 740-749.
[5] D. Liu, Y. Dong, D. Bhattacharyya, G. Sui, Novel sandwiched structures in starch/cellulose nanowhiskers (CNWs) composite films, Composites Communications 4 (2017) 5-9.
[6] J. Yu, J. Gao, T. Lin, Biodegradable thermoplastic starch, Journal of applied polymer science 62(9) (1996) 1491-1494.
[7] B. Khan, M. Bilal Khan Niazi, G. Samin, Z. Jahan, Thermoplastic starch: a possible biodegradable food packaging material—a review, Journal of Food Process Engineering 40(3) (2017) e12447.
[8] L. Avérous, C. Fringant, L. Moro, Plasticized starch–cellulose interactions in polysaccharide composites, Polymer 42(15) (2001) 6565-6572.
[9] M. Gaspar, Z. Benkő, G. Dogossy, K. Reczey, T. Czigany, Reducing water absorption in compostable starch-based plastics, Polymer Degradation and Stability 90(3) (2005) 563-569.
[10] N. Savadekar, S. Mhaske, Synthesis of nano cellulose fibers and effect on thermoplastics starch based films, Carbohydrate polymers 89(1) (2012) 146-151.
[11] I.C. Guimarães, K.C. dos Reis, E.G.T. Menezes, A.C. Rodrigues, T.F. da Silva, I.R.N. de Oliveira, E.V.d.B.V. Boas, Cellulose microfibrillated suspension of carrots obtained by mechanical defibrillation and their application in edible starch films, Industrial Crops and Products 89 (2016) 285-294.
[12] C.M. Müller, J.B. Laurindo, F. Yamashita, Effect of cellulose fibers addition on the mechanical properties and water vapor barrier of starch-based films, Food Hydrocolloids 23(5) (2009) 1328-1333.
[13] A. Kaushik, M. Singh, G. Verma, Green nanocomposites based on thermoplastic starch and steam exploded cellulose nanofibrils from wheat straw, Carbohydrate Polymers 82(2) (2010) 337-345.
[14] S. Aila-Suárez, H.M. Palma-Rodríguez, A.I. Rodríguez-Hernández, J.P. Hernández-Uribe, L.A. Bello-Pérez, A. Vargas-Torres, Characterization of films made with chayote tuber and potato starches blending with cellulose nanoparticles, Carbohydrate polymers 98(1) (2013) 102-107.
[15] A.L. Smits, F.C. Ruhnau, J.F. Vliegenthart, J.J. van Soest, Ageing of starch based systems as observed with FT-IR and solid state NMR spectroscopy, Starch-Stärke 50(11-12) (1998) 478-483.
[16] F. Yu, K. Prashantha, J. Soulestin, M.-F. Lacrampe, P. Krawczak, Plasticized-starch/poly (ethylene oxide) blends prepared by extrusion, Carbohydrate polymers 91(1) (2013) 253-261.
[17] J.J. Van Soest, J.F. Vliegenthart, Crystallinity in starch plastics: consequences for material properties, Trends in biotechnology 15(6) (1997) 208-213.
[18] I. Benito-González, A. López-Rubio, M. Martínez-Sanz, Potential of lignocellulosic fractions from Posidonia oceanica to improve barrier and mechanical properties of bio-based packaging materials, International journal of biological macromolecules 118 (2018) 542-551.
[19] M.J. Fabra, M. Martínez-Sanz, L.G. Gómez-Mascaraque, R. Gavara, A. López-Rubio, Structural and physicochemical characterization of thermoplastic corn starch films containing microalgae, Carbohydrate polymers 186 (2018) 184-191.
[20] ASTM, Standard test method for tensile properties of plastics, ASTM International2010.
[21] A. Lopez-Rubio, B.M. Flanagan, E.P. Gilbert, M.J. Gidley, A novel approach for calculating starch crystallinity and its correlation with double helix content: A combined XRD and NMR study, Biopolymers 89(9) (2008) 761-768.
[22] T.A. Waigh, M.J. Gidley, B.U. Komanshek, A.M. Donald, The phase transformations in starch during gelatinisation: a liquid crystalline approach, Carbohydrate Research 328(2) (2000) 165-176.

[23] Å. Rindlava, S.H. Hulleman, P. Gatenholma, Formation of starch films with varying crystallinity, Carbohydrate Polymers 34(1-2) (1997) 25-30.
[24] R. Chinnaswamy, M. Hanna, Optimum extrusion-cooking conditions for maximum expansion of corn starch, Journal of Food Science 53(3) (1988) 834-836.
[25] A.A. El-Dash, R. Gonzales, M. Ciol, Response surface methodology in the control of thermoplastic extrusion of starch, Journal of Food Engineering 2(2) (1983) 129-152.
[26] J. Van Soest, N. Knooren, Influence of glycerol and water content on the structure and properties of extruded starch plastic sheets during aging, Journal of Applied Polymer Science 64(7) (1997) 1411-1422.
[27] T. Ke, X. Sun, Effects of moisture content and heat treatment on the physical properties of starch and poly (lactic acid) blends, Journal of Applied Polymer Science 81(12) (2001) 3069-3082.
[28] J.J. Van Soest, S. Hulleman, D. De Wit, J. Vliegenthart, Crystallinity in starch bioplastics, Industrial Crops and Products 5(1) (1996) 11-22.
[29] M. Hietala, A.P. Mathew, K. Oksman, Bionanocomposites of thermoplastic starch and cellulose nanofibers manufactured using twin-screw extrusion, European Polymer Journal 49(4) (2013) 950-956.
[30] H. Liu, L. Yu, F. Xie, L. Chen, Gelatinization of cornstarch with different amylose/amylopectin content, Carbohydrate Polymers 65(3) (2006) 357-363.
[31] E. George, T. Sullivan, E. Park, Thermoplastic starch blends with a poly (ethylene-co-vinyl alcohol): processability and physical properties, Polymer Engineering & Science 34(1) (1994) 17-23.
[32] U. Trommsdorff, I. Tomka, Structure of amorphous starch. 2. Molecular interactions with water, Macromolecules 28(18) (1995) 6138-6150.
[33] L. Lai, J. Kokini, Physicochemical changes and rheological properties of starch during extrusion.(a review), Biotechnology progress 7(3) (1991) 251-266.
[34] L. Avérous, C. Fringant, L. Moro, Starch-based biodegradable materials suitable for thermoforming packaging, Starch-Stärke 53(8) (2001) 368-371.
[35] X. Ma, J. Yu, J.F. Kennedy, Studies on the properties of natural fibers-reinforced thermoplastic starch composites, Carbohydrate Polymers 62(1) (2005) 19-24.
[36] A. De Carvalho, A. Curvelo, J. Agnelli, A first insight on composites of thermoplastic starch and kaolin, Carbohydrate Polymers 45(2) (2001) 189-194.
[37] X. Ma, P.R. Chang, J. Yu, Properties of biodegradable thermoplastic pea starch/carboxymethyl cellulose and pea starch/microcrystalline cellulose composites, Carbohydrate Polymers 72(3) (2008) 369-375.
[38] T. Wittaya, Microcomposites of rice starch film reinforced with microcrystalline cellulose from palm pressed fiber, International Food Research Journal 16(4) (2009) 493-500.
[39] D. Le Corre, J. Bras, A. Dufresne, Starch nanoparticles: a review, Biomacromolecules 11(5) (2010) 1139-1153.
[40] S. Wang, C. Li, L. Copeland, Q. Niu, S. Wang, Starch retrogradation: A comprehensive review, Comprehensive Reviews in Food Science and Food Safety 14(5) (2015) 568-585.
[41] K. Shamai, H. Bianco-Peled, E. Shimoni, Polymorphism of resistant starch type III, Carbohydrate Polymers 54(3) (2003) 363-369.
[42] Z.-q. Fu, L.-j. Wang, D. Li, Y.-g. Zhou, B. Adhikari, The effect of partial gelatinization of corn starch on its retrogradation, Carbohydrate polymers 97(2) (2013) 512-517.
[43] B. Ghanbarzadeh, H. Almasi, A.A. Entezami, Improving the barrier and mechanical properties of corn starch-based edible films: Effect of citric acid and carboxymethyl cellulose, Industrial Crops and products 33(1) (2011) 229-235.
[44] C. Ferrero, M. Martino, N. Zaritzky, Corn starch-xanthan gum interaction and its effect on the stability during storage of frozen gelatinized suspension, Starch-Stärke 46(8) (1994) 300-308.
[45] I. Benito-González, A. López-Rubio, M. Martínez-Sanz, High-performance starch biocomposites with celullose from waste biomass: Film properties and retrogradation behaviour, Carbohydrate polymers 216 (2019) 180-188.
[46] L. Avèrous, C. Fringant, L. Moro, Starch-based biodegradable materials suitable for thermoforming packaging, Starch-Stärke 53(8) (2001) 368-371.

[47] U. Suwanmanee, V. Varabuntoonvit, P. Chaiwutthinan, M. Tajan, T. Mungcharoen, T. Leejarkpai, Life cycle assessment of single use thermoform boxes made from polystyrene (PS), polylactic acid,(PLA), and PLA/starch: cradle to consumer gate, The International Journal of Life Cycle Assessment 18(2) (2013) 401-417.
[48] F. Bettaieb, R. Khiari, M.L. Hassan, M.N. Belgacem, J. Bras, A. Dufresne, M.F. Mhenni, Preparation and characterization of new cellulose nanocrystals from marine biomass Posidonia oceanica, Industrial Crops and Products 72 (2015) 175-182.
[49] Y.W. Chen, H.V. Lee, J.C. Juan, S.-M. Phang, Production of new cellulose nanomaterial from red algae marine biomass Gelidium elegans, Carbohydrate polymers 151 (2016) 1210-1219.
[50] A. Dufresne, Comparing the mechanical properties of high performances polymer nanocomposites from biological sources, Journal of nanoscience and nanotechnology 6(2) (2006) 322-330.
[51] E. Fortunati, F. Luzi, D. Puglia, R. Petrucci, J. Kenny, L. Torre, Processing of PLA nanocomposites with cellulose nanocrystals extracted from Posidonia oceanica waste: Innovative reuse of coastal plant, Industrial Crops and Products 67 (2015) 439-447.
[52] M. Martínez-Sanz, A. Lopez-Rubio, J.M. Lagaron, Optimization of the dispersion of unmodified bacterial cellulose nanowhiskers into polylactide via melt compounding to significantly enhance barrier and mechanical properties, Biomacromolecules 13(11) (2012) 3887-3899.
[53] M. Martínez-Sanz, A.A. Vicente, N. Gontard, A. Lopez-Rubio, J.M. Lagaron, On the extraction of cellulose nanowhiskers from food by-products and their comparative reinforcing effect on a polyhydroxybutyrate-co-valerate polymer, Cellulose 22(1) (2015) 535-551.
[54] M. Martínez-Sanz, M. Villano, C. Oliveira, M.G. Albuquerque, M. Majone, M. Reis, A. Lopez-Rubio, J.M. Lagaron, Characterization of polyhydroxyalkanoates synthesized from microbial mixed cultures and of their nanobiocomposites with bacterial cellulose nanowhiskers, New biotechnology 31(4) (2014) 364-376.
[55] M. Martínez-Sanz, A. Lopez-Rubio, M. Villano, C.S. Oliveira, M. Majone, M. Reis, J.M. Lagarón, Production of bacterial nanobiocomposites of polyhydroxyalkanoates derived from waste and bacterial nanocellulose by the electrospinning enabling melt compounding method, Journal of Applied Polymer Science 133(2) (2016).
[56] G. Siqueira, H. Abdillahi, J. Bras, A. Dufresne, High reinforcing capability cellulose nanocrystals extracted from Syngonanthus nitens (Capim Dourado), Cellulose 17(2) (2010) 289-298.
[57] X. Cao, Y. Chen, P.R. Chang, M. Stumborg, M.A. Huneault, Green composites reinforced with hemp nanocrystals in plasticized starch, Journal of Applied Polymer Science 109(6) (2008) 3804-3810.
[58] M.S. Reid, M. Villalobos, E.D. Cranston, Benchmarking cellulose nanocrystals: from the laboratory to industrial production, Langmuir 33(7) (2017) 1583-1598.
[59] I. Benito-González, A. López-Rubio, R. Gavara, M. Martínez-Sanz, Cellulose nanocrystal-based films produced by more sustainable extraction protocols from Posidonia oceanica waste biomass, Cellulose 26(13-14) (2019) 8007-8024.
[60] I. Benito-González, A. López-Rubio, L.G. Gómez-Mascaraque, M. Martínez-Sanz, PLA coating improves the performance of renewable adsorbent pads based on cellulosic aerogels from aquatic waste biomass, Chemical Engineering Journal (2020) 124607.
[61] I. Benito-González, C.M. Jaén-Cano, A. López-Rubio, A. Martínez-Abad, M. Martínez-Sanz, Valorisation of vine shoots for the development of cellulose-based biocomposite films with improved performance and bioactivity, International Journal of Biological Macromolecules (2020).
[62] A. Siddhanta, K. Prasad, R. Meena, G. Prasad, G.K. Mehta, M.U. Chhatbar, M.D. Oza, S. Kumar, N.D. Sanandiya, Profiling of cellulose content in Indian seaweed species, Bioresource technology 100(24) (2009) 6669-6673.
[63] B. Ray, M. Lahaye, Cell-wall polysaccharides from the marine green alga Ulva "rigida"(Ulvales, Chlorophyta). Extraction and chemical composition, Carbohydrate Research 274 (1995) 251-261.
[64] M. Martínez-Sanz, E. Erboz, C. Fontes, A. López-Rubio, Valorization of Arundo donax for the production of high performance lignocellulosic films, Carbohydrate polymers 199 (2018) 276-285.
[65] G. Balata, A. Tola, Cost-opportunity analysis of the use of Posidonia oceanica as a source of bio-energy in tourism-oriented territories. The case of Alghero, Journal of Cleaner Production (2017).

[66] I. Benito-González, A. López-Rubio, A. Martínez-Abad, A.-R. Ballester, I. Falcó, L. González-Candelas, G. Sánchez, J. Lozano-Sánchez, I. Borrás-Linares, A. Segura-Carretero, In-Depth Characterization of Bioactive Extracts from Posidonia oceanica Waste Biomass, Marine drugs 17(7) (2019) 409.
[67] L.H. Thomas, V.T. Forsyth, A. Šturcová, C.J. Kennedy, R.P. May, C.M. Altaner, D.C. Apperley, T.J. Wess, M.C. Jarvis, Structure of cellulose microfibrils in primary cell walls from collenchyma, Plant physiology 161(1) (2013) 465-476.
[68] M. Wada, J. Sugiyama, T. Okano, Native celluloses on the basis of two crystalline phase (Iα/Iβ) system, Journal of Applied Polymer Science 49(8) (1993) 1491-1496.
[69] P. Lopez-Sanchez, M. Martinez-Sanz, M.R. Bonilla, D. Wang, E.P. Gilbert, J.R. Stokes, M.J. Gidley, Cellulose-pectin composite hydrogels: Intermolecular interactions and material properties depend on order of assembly, Carbohydrate polymers 162 (2017) 71-81.
[70] K.S. Mikkonen, S. Heikkinen, A. Soovre, M. Peura, R. Serimaa, R.A. Talja, H. Helén, L. Hyvönen, M. Tenkanen, Films from oat spelt arabinoxylan plasticized with glycerol and sorbitol, Journal of Applied Polymer Science 114(1) (2009) 457-466.
[71] M. Martínez-Sanz, P. Lopez-Sanchez, M.J. Gidley, E.P. Gilbert, Evidence for differential interaction mechanism of plant cell wall matrix polysaccharides in hierarchically-structured bacterial cellulose, Cellulose 22(3) (2015) 1541-1563.
[72] H. Li, M.A. Huneault, Comparison of sorbitol and glycerol as plasticizers for thermoplastic starch in TPS/PLA blends, Journal of Applied Polymer Science 119(4) (2011) 2439-2448.
[73] A. Lopez-Gil, M. Rodriguez-Perez, J.A. De Saja, Strategies to improve the mechanical properties of starch-based materials: plasticization and natural fibers reinforcement, Polímeros 24(SPE) (2014) 36-42.
[74] N. Wang, J. Yu, X. Ma, Preparation and characterization of thermoplastic starch/PLA blends by one-step reactive extrusion, Polymer International 56(11) (2007) 1440-1447.
[75] T. Ke, X.S. Sun, Starch, poly (lactic acid), and poly (vinyl alcohol) blends, Journal of Polymers and the Environment 11(1) (2003) 7-14.
[76] G. Fotie, S. Limbo, L. Piergiovanni, Manufacturing of Food Packaging Based on Nanocellulose: Current Advances and Challenges, Nanomaterials 10(9) (2020) 1726.
[77] L. Piergiovanni, G. Fotie, L. Amoroso, B. Akgun, S. Limbo, Are cellulose nanocrystals “alien particles” to human experience?, Packaging Technology and Science 32(12) (2019) 637-640.

Chapter 3

APPLICATION OF THE SIMPLER METHODOLOGIES FOR THE EXTRACTION OF CELLULOSIC FRACTIONS AND NANOCRYSTALS TO OTHER BIOMASS SOURCES

3.1. Valorisation of vine shoots for the development of cellulose-based biocomposite films with improved performance and bioactivity

3.2. Sustainable biocomposite films fully based on white rice (Oryza sativa) agro-industrial by-products

Introduction to chapter 3.

After assessing the properties and performance of less purified cellulosic fractions and nanocrystals from *P. oceanica* leaves, the same simplified extraction protocol was applied to other abundant waste biomass sources to evaluate the suitability of this method to be applied within a broad range of materials.

In the first work from this chapter, vine shoots, a terrestrial and nationally abundant underutilized residue, were characterized and proposed as a promising source of cellulosic fractions and nanocrystals. The obtained cellulose-based materials were then used to generate films by vacuum filtration and composites were also prepared by blending with agar at different contents (20, 40 and 80% w/w) to overcome the excessive stiffness inherent to cellulosic materials.

In the second work, rice by-products (such as rice husks, rice straw and broken rice), which are one of the most abundant waste biomass sources both locally (in the Valencian community) and internationally (China, Japan, etc.), were evaluated as a source for the development of bioactive food packaging films. Rice husks and rice straw were used for the extraction of cellulosic nanocrystals by the developed simplified extraction protocol. On the other hand, broken rice was used, either itself or after the extraction of starch, as the matrix component, which was then blended with the cellulosic nanocrystals by melt mixing.

3.1. Valorisation of vine shoots for the development of cellulose-based biocomposite films with improved performance and bioactivity

This section is an adapted version of the following published research article:

Benito-González, I., Jaén-Cano, C.M., López-Rubio, A., Martínez-Abad, A. & Martínez-Sanz, M.
(2020). Valorisation of vine shoots for the development of cellulose-based biocomposite films with improved performance and bioactivity

International Journal of Biological Macromolecules, 165, 1540-1551. DOI:

https://doi.org/10.1016/j.ijbiomac.2020.09.240

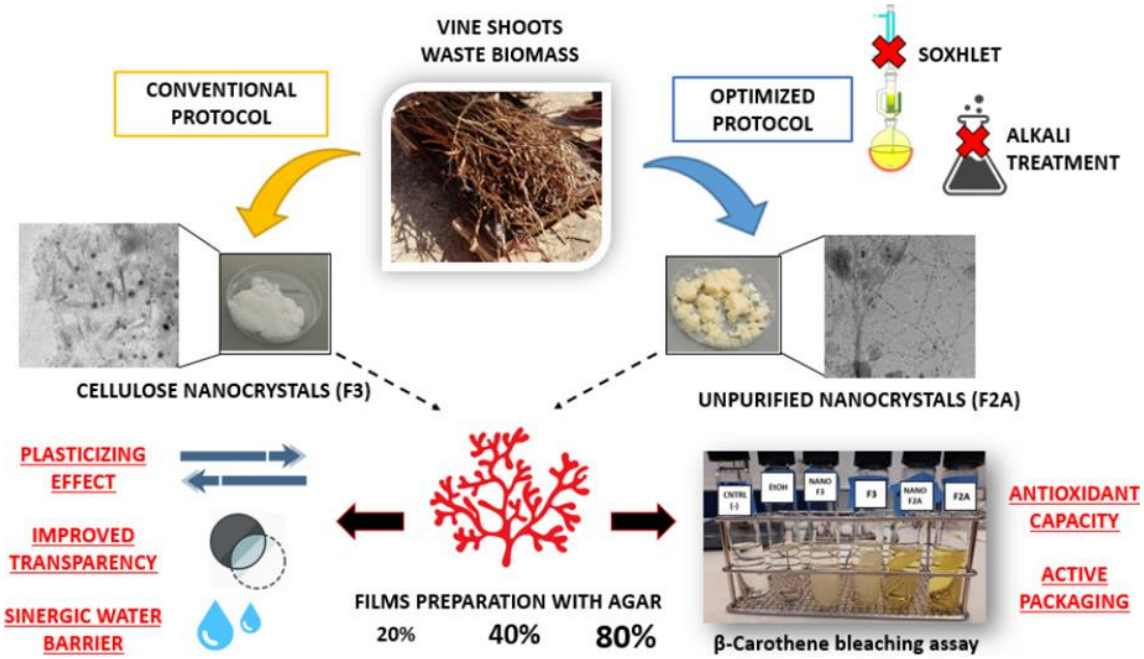

1. Abstract

This work reports on the valorization of *Tempranillo* vine shoots for the development of bio-based packaging materials. Cellulose (F3) and nanocellulose (NANO F3) were produced by the conventional method, while less purified cellulosic fractions (F2A) and nanocrystals (NANO F2A) were extracted by simplified protocols (omitting Soxhlet and alkaline treatments) to reduce production costs and environmental impact and evaluate the potential added functionalities of these less purified materials. Although most of the hemicelluloses in F2A were digested upon acid hydrolysis, a small fraction remained in NANO F2A. On the other hand, the presence of a minor xylan fraction in F3 limited the access of sulphuric acid towards the cellulose microfibrils, hindering hydrolysis and producing heterogeneous fibrillar structures in NANO F3. The obtained materials were used to produce cellulosic films, as well as blends with agar, and their performance properties were evaluated. Overall, NANO F2A films showed the best compromise between performance and sustainability and presented additional antioxidant capacity. The properties of the films could be adjusted by the incorporation of agar, improving their ductility and water permeability.

2. Introduction

During the last decades, both human and scientific developments have brought the overexploitation of natural resources and led to a massive consumption of fossil fuels, triggering the severe environmental issues that we are currently facing. On the one hand, natural ecosystems have been damaged due to the pollution originated by human and industrial activities. Plastic residues are a particularly hot topic: More than 90% of plastic residues cannot be recycled and they are accumulated in the environment. For instance, up to 95% of the total amount of residues in the Mediterranean Sea are plastic debris [1]. On the other hand, synthetic plastics are obtained from fossil fuels, causing the steady depletion of these non-renewable resources.

In this context, biopolymers (biodegradable polymers and/or obtained from renewable resources) have been explored over the past few years as a sustainable alternative for the replacement of synthetic plastics. Although some biopolymers such as starch and poly(lactic) acid (PLA) are already used in the packaging industry, their commercial grades are often blends with synthetic polymers and the biodegradability of these products is certainly questionable. To make them competitive against conventional plastics, the properties of biopolymers are yet to be improved (especially in terms of mechanical and barrier performance) and their production costs need to be reduced. Furthermore, biopolymers are frequently obtained from food sources such as rice, corn or potato, which is against the circular economy principles. This has motivated the search of

alternative and more sustainable sources for the extraction of biopolymers, such as agroindustrial waste and marine biomass. While terrestrial biomass is typically richer in cellulose, marine biomass contains other biopolymers such as agar or alginate [2].

Cellulose is one of the most widely studied biopolymers for the development of bio-based food packaging. Due to its semicrystalline structure, it presents excellent mechanical and barrier properties but limited processability; thus, it is typically used as a reinforcing filler in blends with other biopolymers such as starch [3]. Additionally, when subjected to acid hydrolysis, the amorphous domains of cellulose microfibrils are digested, yielding a highly crystalline material with increased thermal resistance, water and oxygen barrier and stiffness, known as cellulose nanocrystals or nanocellulose. Nanocellulose has been extensively reported in the literature not only as a reinforcing agent in other biopolymers such as starch or PLA [4, 5], but also as film-forming material for food packaging applications [6]. However, as expected, the more the crystalline cellulose is isolated, the lower are the extraction yields. To increase the sustainability of the process, reduce the processing times and increase the yields, alternative protocols which omit several of the cellulose purification steps have been recently reported in the literature for marine waste biomass from *Posidonia oceanica* leaves [6]. The hydrolysis of less purified cellulosic fractions has been shown to produce cellulosic nanocrystals containing hemicelluloses and lipidic compounds, which presented improved mechanical and barrier performance as compared to pure nanocellulose [6]. Due to the very distinct composition of cellulosic biomass depending on its origin, the potential of these alternative protocols is still to be explored when applied to terrestrial sources.

Vine shoots represent an abundant agricultural residue derived from the wine industry [7]. Due to the large costs associated to the management of such an abundant and low-density residue, vine shoots have been traditionally either left in the vineyard to be used as fertilizers or burned. However, burning practices pose severe environmental issues and strict restrictions are applicable in most wine-producing countries [8]. In this context, strategies for the valorisation of vine shoots, mostly related to biofuel production [7], are currently being sought. Due to the high lignocellulosic content of vine shoots [9], they can also be considered as an exploitable source of cellulose. In fact, some works have reported on the production of pulp and paper [9, 10] and on the extraction of cellulose nanocrystals [11] by the conventional method, although no details on the extraction yields were provided. Moreover, vine shoots have a great potential for the development of bioactive materials, since they are rich in proteins and polyphenols [12] and have been shown to present prebiotic activity [13].

In this work, we investigated the suitability of vine shoots for the extraction of cellulosic fractions and nanocrystals through conventional and simplified protocols. Initially, the composition of vine shoots from two different varieties (*Verdejo* and *Tempranillo*) was characterized to determine the most optimum material for cellulose extraction. The extracted fractions and nanocrystals were subsequently used to produce (nano)cellulosic films and the properties of the obtained materials were evaluated to assess their suitability for food packaging applications. Furthermore, hybrid materials were produced by adding agar into the nanocellulosic films with the aim of reducing their excessively rigid behaviour. Our hypothesis is that simplified purification protocols can yield less purified (nano)cellulosic films from vine shoots waste biomass with similar or even better performance than those obtained using conventional protocols, thus representing a more sustainable way to develop bio-based packaging materials. Moreover, we believe that addition of agar will improve the processability and mechanical properties (in terms of elongation at break) of the typically rigid (nano)cellulosic films.

3. Materials and methods

3.1 Raw materials

Biomass waste material consisting of vine shoots from *Tempranillo* (referred to as TM) and *Verdejo* (referred to as VJ) varieties was kindly provided by Matarromera, Valladolid (Spain) in February 2019. Vine shoots were initially converted into smaller pieces in order to facilitate their further processing by an industrial crusher. The resulting material was milled and sieved manually until obtaining a homogeneous powder (0.5 mm). Commercial agar PRONAGAR (batch reference H-3544/19) was supplied by Hispanagar (Burgos, Spain).

3.2 Compositional analysis of vine shoots

3.2.1 Lignin content

The Klason lignin content was determined according to the TAPPI T222 om-06 method. Briefly, 3 mL of 72% H_2SO_4 (v/v) were vigorously mixed with 300 mg of dry biomass (from both TM and VJ varieties) in glass tubes. The tubes were then placed in a water bath at 30 ºC for 1 hour and vortexed every 10 minutes. After that, 84 mL of distilled water were added to each tube and mixed. The resulting material was autoclaved for 1 hour at 121 ºC and then cooled down with ice until reaching room temperature. The content of the tubes was subsequently filtered, and the solid material was dried in an oven at 105 ºC overnight. The lignin content was calculated gravimetrically. The determinations were carried out in triplicate.

3.2.2 Holocellulose content

The holocellulose content was determined according to the ASTM D1104-56 method. Briefly, 1 g of dry biomass was added to 150 mL of distilled water, pre-heated at 70 ºC. While stirring, 1 g

of $NaClO_2$ and 0.2 mL of acetic acid were added every 1 hour. This process was repeated three times, accounting for a total time of 4 hours. The obtained material was then placed in an ice-bath to stop the reaction. After several washing cycles with distilled water (until obtaining a clear filtrate), the material was dried in an oven at 105 ºC overnight. The holocellulose content was calculated gravimetrically. The determinations were carried out in triplicate.

3.2.3 Ash content

The ash content was determined by dry biomass calcination, according to the standard TAPPI T211 om-07 method [14]. Briefly, dry biomass samples were placed in a muffle at 525 ºC for at least 4 hours. The ash content was gravimetrically determined after combustion. The determinations were carried out in duplicate.

3.2.4 Lipid content

The lipid content was estimated by the Soxhlet extraction method. Approximately 9 g of dry biomass were placed in a Dumas filter and treated with 800 mL of a 2:1 toluene:ethanol mixture overnight. The lipid content was calculated gravimetrically after drying the extracted solid fraction. The determinations were carried out at least in triplicate.

3.2.5 Protein content

Samples were analyzed for total nitrogen content using an Elemental Analyser Rapid N Exceed (Paralab S.L., Spain). Approximately 100 mg of dry biomass were pressed into pellets and then analyzed using the Dumas method, which is based on the combustion of the sample and subsequent detection of the released N_2 [15]. The protein content was calculated from the nitrogen content multiplied by a factor of 6.25. The determinations were carried out in triplicate.

3.2.6 Total phenolic content

The total phenolic content of the vine shoots was estimated by the Folin-Ciocalteau colorimetric assay [16]. Briefly, the Folin-Ciocalteau reagent was diluted 1:10 (v/v) with distilled water and 1 mL of the final dilution was mixed with 0.2 mL of the sample (aqueous dispersions of the biomass at 20 mg/mL) at room temperature. Finally, 0.8 mL of sodium carbonate (75 mg/mL) were added and the samples were heated up to 50 ºC for 30 minutes. Absorbance values were read at 750 nm wavelength. The determinations were carried out in triplicate.

3.3 Preparation of cellulosic fractions and nanocrystals

Two purification procedures described in a previous work [6] were carried out to sequentially remove cell wall components from the raw vine shoots and obtain pure or partially pure cellulose. The conventional process consisted of an initial Soxhlet extraction to remove pigments and lipids,

followed by a treatment with $NaClO_2$ to remove lignin and a final alkaline treatment with KOH to remove the hemicelluloses, yielding more purified cellulose (labelled as F3). The alternative protocol omitting the Soxhlet and KOH treatments was also applied, obtaining a less purified cellulosic fraction (referred to as F2A). Both fractions (F3 and F2A) were obtained as partially hydrated gel-like materials, which were stored in the fridge until further use.

Both cellulosic fractions were used as the starting materials to produce cellulosic nanocrystals by means of acid hydrolysis. An optimized method, previously applied for the extraction of cellulose nanocrystals from *Posidonia oceanica* waste biomass [6], with some minor modifications, was applied. Briefly, the gel-like cellulosic fractions were immersed in a hot (50 ºC) H_2SO_4 solution (30% w/w), with a ratio of 1.5 g fraction (in dry basis)/100 mL H_2SO_4 and kept under stirring for 1 hour. Additionally, the F3 fraction was subjected to a longer hydrolysis of 5 hours to evaluate the effect of hydrolysis time on the properties of the nanocrystals. After the hydrolysis, the acid slurries were subjected to several centrifugation and washing cycles to remove the acid and the pH was adjusted to 7 with diluted NaOH. The obtained nanocrystals (labelled as NANO F2A, NANO F3 and NANO F3 5h) were stored in the fridge as partially hydrated gel-like materials, until further use.

3.4 Production of pure (nano)cellulosic films and hybrid films with agar

Pure cellulosic films were produced by adding 0.25 g of cellulosic materials to 50 mL of distilled water and dispersing them by ultra-turrax homogenization followed by mild sonication until obtaining homogeneous suspensions. These suspensions were then vacuum filtered using PTFE filters with 0.2 µm pore size to remove water. The solid material remaining in the filter was subsequently dried at room temperature overnight (ca. 20 ºC, 40% RH). The obtained films were named as F2A, F3, NANO F2A, NANO F3 and NANO F3 5h.

Additionally, composite films were prepared using commercial agar in proportions of 20%, 40% and 80% with respect to the total amount of solids (fixed at 0.25 g). For this aim, the proportional weight of agar was dissolved in the corresponding water volume (10 mL, 20 mL and 40 mL) at 50 ºC while the nanocellulosic materials (NANO F2A and NANO F3) were dissolved in the remaining water volume until reaching 50 mL. The obtained suspensions followed the same protocol as the one followed for pure cellulosic films. The resulting films were named as NANO F2A 20% AGAR, NANO F2A 40% AGAR, NANO F2A 80% AGAR, NANO F3 20% AGAR, NANO F3 40% AGAR, NANO F3 80% AGAR.

All obtained films were stored in equilibrated relative humidity cabinets at 53% RH and 25 ºC for three days prior to their characterization.

3.5 Carbohydrate composition of the cellulosic fractions and nanocrystals

The carbohydrate content and sugar composition of the cellulosic fractions and nanocrystals was determined after sulphuric hydrolysis, as previously described [17]. The monosaccharides were analysed using high performance anion exchange chromatography with pulsed amperometric detection (HPAEC-PAD) with a ICS-3000 (Dionex) equipped with a Carbopac PA 1 column (4 × 250 mm, 10 µm, Dionex). Control samples of known concentrations of mixtures of glucose, fucose, galactose, arabinose, xylose, mannose, galacturonic acid and glucuronic acid were used for calibration. All experiments were carried out in triplicate.

3.6 Attenuated total reflectance (ATR) FT-IR analysis

Freeze-dried fractions and nanocrystals were analysed by FT-IR in attenuated total reflectance (ATR) mode using a Thermo Nicolet Nexus (GMI, USA) equipment. The spectra were taken at 4 cm^{-1} resolution in a wavelength range between 400-4000 cm^{-1} and averaging a minimum of 32 scans.

3.7 Thermogravimetric analyses (TGA)

Thermogravimetric curves (TG) were recorded with a Setaram Setsys 16/18 (SETARAM Instrumentation, France). The samples (ca. 10 mg of the cellulosic fractions and nanocrystals) were heated from 30 to 1000ºC with a heating rate of 10ºC/min under nitrogen atmosphere. Derivative TG curves (DTG) express the weight loss rate as a function of temperature.

3.8 Transmission electron microscopy (TEM)

One drop (8 µL) of a 0.001% aqueous suspension of the different cellulosic nanocrystals obtained was allowed to dry on a carbon coated grid (200 mesh). The nanocrystals were stained with uranyl acetate. TEM was performed using a JEOL 1010 at an accelerating voltage of 80 kV. Morphology of the observed nanocrystals was characterized using ImageJ-win64 software by means of at least 5 different images. Results were expressed as mean ± standard deviation.

3.9 Scanning electron microscopy (SEM)

SEM was conducted on a Hitachi microscope (Hitachi S-4800) at an accelerating voltage of 10 kV and a working distance of 8-16 mm. Small samples (~5 mm^2 area) of the (nano)cellulosic films and their blends with agar were cut to observe their surface. The samples were then sputtered with a gold–palladium mixture under vacuum during 3 minutes before their morphology was examined.

3.10 X-ray diffraction (XRD)

XRD measurements of the pure (nano)cellulosic films and their blends with agar were carried out on a D5005 Bruker diffractometer. The instrument was equipped with a Cu tube and a secondary monochromator. The configuration of the equipment was θ–2θ, and the samples were examined over the angular range between 3°–60° with a step size of 0.02° and a count time of 200 s per step. Peak fitting was carried out by using the Igor software package (Wavemetrics, Lake Oswego, Oregon) as described in a previous work [18]. The crystallinity index X_C was determined from the obtained fitting results by applying the following equation:

$$X_C(\%) = \frac{\sum A_{Crystal}}{A_{Total}} \times 100 \quad (1)$$

where A_{Total} is the sum of the areas under all the diffraction peaks and $\Sigma A_{Crystal}$ is the sum of the areas corresponding to the three crystalline peaks from cellulose I.

3.11 Mechanical properties

Tensile tests were carried out at ambient conditions on a Mecmesin MultiTest 1-i (1 kN) machine (Virginia, USA) with the Emperor™ software, according to ASTM standard method D882-09 18 [19]. Pre-conditioned rectangular-shaped specimens with initial gauge length of 8 cm and 1 cm in width were cut directly from the films. A fixed crosshead rate of 10 mm/min was utilized in all cases. The elastic modulus (E), tensile strength (TS), and elongation at break (EAB) were determined from the stress-strain curves, estimated from force–distance data obtained for the different films. At least, five specimens of each film were tensile tested to obtain statistically meaningful results.

3.12 Water vapor permeability (WVP)

Direct permeability to water was determined from the slope of the weight gain versus time curves at 25 ºC. The films were sandwiched between the aluminum top (open O-ring) and bottom (deposit for the silica) parts of a specifically designed permeability cell with screws. A Viton rubber O-ring was placed between the film and bottom part of the cell to enhance sealability. These permeability cells containing silica were then placed in an equilibrated relative humidity cabinet at 75% RH and 25 °C. The weight gain through a film area of 0.001 m^2 was monitored and plotted as a function of time. Cells with aluminum films (with thickness of ca. 11 μm) were used as control samples to estimate the weight gain through the sealing. The tests were done at least in triplicate.

3.13 Contact angle measurements

Contact angle measurements were carried out at ambient conditions in a Video-Based Contact Angle Meter model OCA 20 (DataPhysics Instruments GmbH, Filderstadt, Germany). Contact angle values were obtained by analyzing the shape of a distilled water drop after it had been placed over the film for 15 s. Image analyses were carried out by SCA20 software.

3.14 Optical properties

The transparency of the films was determined through the surface reflectance spectra in a spectrocolorimeter CM-3600d (Minolta Co., Tokyo, Japan) with a 10 mm^2 illuminated sample area. Measurements were taken in duplicate for each sample using both a white and a black background.

Film transparency was evaluated through the internal transmittance (T_i) (0-1, theoretical range) by applying the Kubelka-Munk theory for multiple scattering to the reflection data. Internal transmittance (T_i) of the films was quantified using Eq. (2). In this equation, R_0 is the reflectance of the film on an ideal black background. Parameters a and b were calculated by Eqs. (3) and (4), where R is the reflectance of the sample layer backed by a known reflectance R_g.

$$T_i = \sqrt{(a - R_0)^2 - b^2} \tag{2}$$

$$a = \frac{1}{2}\cdot\left(R + \frac{R_0 - R + R_g}{R_0 R_g} \right) \tag{3}$$

$$b = (a^2 - 1)^{\frac{1}{2}} \tag{4}$$

3.15 β-Carotene-linoleic acid assay

The antioxidant capacity of the (nano)cellulosic fractions was also evaluated by the β-carotene-linoleic acid assay [20]. In brief, 4 mg of β-carotene were dissolved in 20 mL of chloroform. 2 mL of this solution were placed on a rotary evaporator and the chloroform was evaporated. Then, 50 µL of linoleic acid and 400 mg of Tween 40 were added and the content of the flask was mixed with stirring. After that, 100 mL of aerated distilled water was transferred to the flask and stirred vigorously. 5 mL of the prepared β-carotene emulsion were transferred to a series of tubes containing a fixed weight of 10 mg of each (nano)cellulosic fraction in film-form, or 0.5 mL of BHT (0.1-1 mg/mL) (as a positive control) and 0.5 mL of distilled water (as the negative control). The samples were incubated in a water bath at 50 °C for 120 min. The absorbance of each fraction at 470 nm was measured every 30 minutes using a spectrophotometer. All the determinations were carried out in triplicate.

3.16 Statistical analysis

Analysis of variance (ANOVA) followed by a Tukey-b test were used when comparing more than two data sets, after confirming the homogeneity of variances by the Levene test using IBM SPSS Statistics software v.26. All data have been represented as the average ± standard deviation. Significant differences ($p \leq 0.05$) are denoted by showing the data provided in tables with different letters.

4. Results and Discussion

4.1 Compositional characterization of vine shoots

In the first stage of this work, the composition of vine shoots from two different varieties (TM and VJ) was characterized to determine the most optimum raw material for the extraction of cellulose. The results, shown in Table 1, evidenced no significant differences between varieties, except for the higher lipid content in VJ. This is in agreement with a previous work in which very similar composition was reported for four different vine shoot varieties [10]. Holocellulose represented the major component in both varieties, with contents of ca. 71% for VJ and 72% for TM. As expected, lignin was the second major component, representing ca. 22-23% of the biomass, in line with previous studies [10]. Only minor amounts of lipids (ca. 2-7%), proteins (ca. 4-5%) and ashes (ca. 2-4%) were detected in both varieties. Additionally, no phenolic compounds could be quantified using the Folin-Ciocalteau method. This does not necessarily imply a low phenolic content in the raw biomass, since, in fact, vine shoots have been proposed as a good source for the extraction of polyphenols [12, 21]. Instead, this suggests that the existing phenolic compounds are bound to the lignocellulosic structure in the intact cell walls composing the vine shoot tissues. Overall, our results, together with the compositional data previously reported in the literature for other varieties [10, 22, 23], demonstrate that the composition of vine shoots is quite reproducible along different varieties.

Table 1. Composition of the raw biomass from *Tempranillo*-TM and *Verdejo*-VJ vine shoots. Values in the same column followed by different letters are significantly different ($p \leq 0.05$).

	Lignin (%)	**Holocellulose (%)**	**Ash (%)**	**Lipids (%)**	**Proteins (%)**
TM	22.4 ± 2.4[a]	72.0 ± 4.4[a]	2.3 ± 0.3[a]	6.7 ± 2.1[a]	5.3 ± 0.3[a]
VJ	23.1 ± 2.4[a]	70.7 ± 2.4[a]	3.6 ± 0.4[a]	2.4 ± 1.3[b]	4.0 ± 0.4[a]

FT-IR characterization was also carried out to further investigate any possible minor compositional differences. As shown in Figure 1A, both vine shoot varieties showed very similar spectra. The broad bands at 3600-3200 cm^{-1} and 3000-2900 cm^{-1}, characteristic from O—H and C—H stretching, respectively [24], presented very similar shapes. Moreover, the band located at 1730 cm^{-1}, corresponding to the C=O stretching vibration of ester groups from lignin and hemicelluloses [25], was also present in both varieties. Interestingly, the band at 1040 cm^{-1}, which is usually related to xylans [24, 26], was also visible. Finally, the presence of cellulose in both varieties was confirmed by the appearance of several characteristic bands, such as those located at 1420, 1300 and 1100 cm^{-1} [24, 27].

The thermal stability of both vine shoot varieties was also assessed by TGA analyses and the results are shown in Figure 1B. As observed, both varieties showed a very similar behavior, typical from multicomponent materials, displaying a three-step degradation profile. The most intense peak was the one with its maximum at ~330 ºC, which corresponds to the thermal degradation of cellulose [25]. This peak was slightly overlapped with a less intense peak with its maximum around 260 ºC, which is typically attributed to the degradation of hemicelluloses [25]. Overall, both vine shoot varieties presented almost identical thermal stability, which is not surprising given their compositional similarity (cf. Table 1).

Given the compositional similarity between both vine shoot varieties and, in particular, their comparable holocellulosic content, TM was chosen as the raw material to extract cellulosic fractions and nanocrystals. The choice was done on the basis of the greater availability of TM vine shoots as compared with VJ, since the former is much more cultivated around the world (and at a local/regional level) and thus represents a more profitable market opportunity [28].

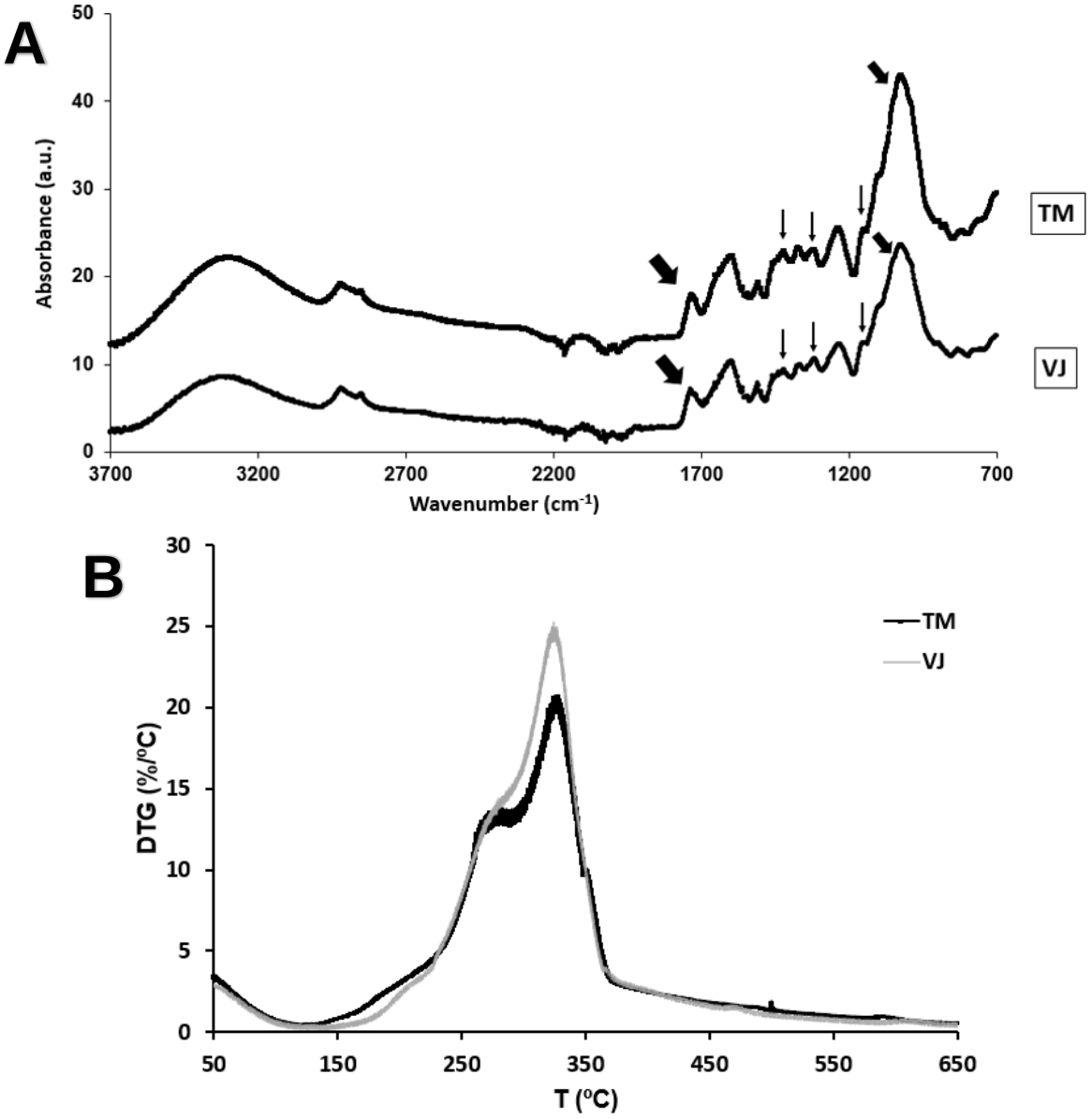

Figure 1. (A) FT-IR spectra of both vine shoots varieties (*Tempranillo*-TM and *Verdejo*-VJ). TM spectrum has been offset for clarity. Arrows are pointing towards the bands characteristic from lignin and hemicelluloses such as xylans (thick arrows), and cellulosic crystalline peaks (thin arrows). (B) Derivative thermogravimetric (DTG) curves of TM and VJ vine shoots.

4.2 Production and characterization of cellulosic fractions and nanocrystals

TM vine shoots were subjected to the purification protocols described in section 2.3 to produce cellulosic fractions and nanocrystals with different degrees of purity. As expected, the simplified protocol produced less purified fractions and nanocrystals with higher yields (ca. 63±3% for F2A and 27±3% for NANO F2A) than the standard cellulose purification method (ca. 22±2% for F3 and 14±1% for NANO F3). On the other hand, the application of the acid hydrolysis reduced the extraction yields, being this decrease more evident in the case of the F2A fraction. This is reasonable taking into account that amorphous hemicelluloses were expected to remain in F2A,

while F3 was expected to be almost pure cellulose. The obtained extraction yields are consistent with those previously reported for the fractions (60% for F2A and 25% for F3) and nanocrystals (26% for NANO F2A and 14% for NANO F3) extracted from *Posidonia oceanica* waste biomass by applying the same protocols [6]. The overall initial composition of *Posidonia* was not substantially different to that from vine shoots (13% ash, 18% lignin and 59% holocellulose) [6] and, therefore, similar extraction yields were expected for both biomass sources.

XRD analyses were also carried out to study the crystalline structure of cellulose in the fractions and nanocrystals and the obtained patterns are shown in Figure 2. As observed, all the samples were characterized by the appearance of a broad diffraction band at 12–18° (which is actually composed of two overlapped peaks located at 15.0°, 16.6°), followed by a sharper peak located at ca. 22.6°, indicating the presence of crystalline cellulose I [29]. Additionally, a small peak, located at 27 º, most likely arising from the presence of mineral compounds [30] was visible in F2A. Figure 2 clearly shows that the intensity of the cellulose crystalline peaks significantly increased when subjecting the less purified F2A fraction to the acid hydrolysis, while minor differences were seen between the purified cellulose fraction F3 and the extracted nanocrystals. In fact, cellulose crystallinity, which was calculated by estimating the area of the three crystalline peaks, markedly increased for F2A after the hydrolysis treatment (from ca. 43% for F2A to 85% for NANO F2A), while it remained almost constant for F3 (ca. 85% for F3 to 89% for NANO F3). The increased crystallinity of F3 as compared to F2A can be explained by the removal of a significant amount of amorphous material, such as hemicelluloses, by the conventional purification protocol applied. Similarly, when subjecting F2A to the acid hydrolysis, the remaining hemicelluloses and other components such as lipids are expected to be easily digested. However, the very minor effect of the acid hydrolysis on the cellulose crystallinity was surprising and it was against the crystallinity increase previously reported for the fractions and nanocrystals extracted from *Posidonia oceanica* biomass using the same purification protocol (from ca. 67% for F3 to 77% for NANO F3) [6]. However, it should be noted that the cellulosic fraction F3 extracted from *Posidonia oceanica* presented a less crystalline structure than that of the cellulose from vine shoots, hence making the former more susceptible to acid digestion. To evaluate whether the hydrolysis time had been insufficient to digest the cellulose amorphous domains in F3, a longer hydrolysis time of 5h was also tested. The yield for the extracted nanocrystals (13.8% ± 1.1%) was similar to the conventional shorter hydrolysis, while the crystallinity index (ca. 87%) was seen to slightly decrease. This is consistent with previous studies, as longer hydrolysis times might decrease crystallinity values after the optimum time is reached [31]. As a result, the hydrolysis parameters need to be adjusted to each biomass source as applying excessive acid concentrations or too long hydrolysis times can also lead to partial degradation of the cellulose crystalline structure [31]. In the case of the TM vine shoots, it seems that the purified cellulose

presented a quite crystalline structure, with a minor fraction of amorphous cellulose which was not accessible to the sulphuric acid and thus, remained non-digested even when extending the hydrolysis time.

Table 2. Extraction yield and crystallinity index (Xc) of the different cellulosic fractions and nanocrystals extracted from TM vine shoots.

	Yield (%)	**Xc (%)**
F2A	62.5 ± 1.8	43.3
F3	21.7 ± 2.5	85.4
NANO F2A	27.2 ± 0.4	84.9
NANO F3	14.2 ± 2.7	89.3

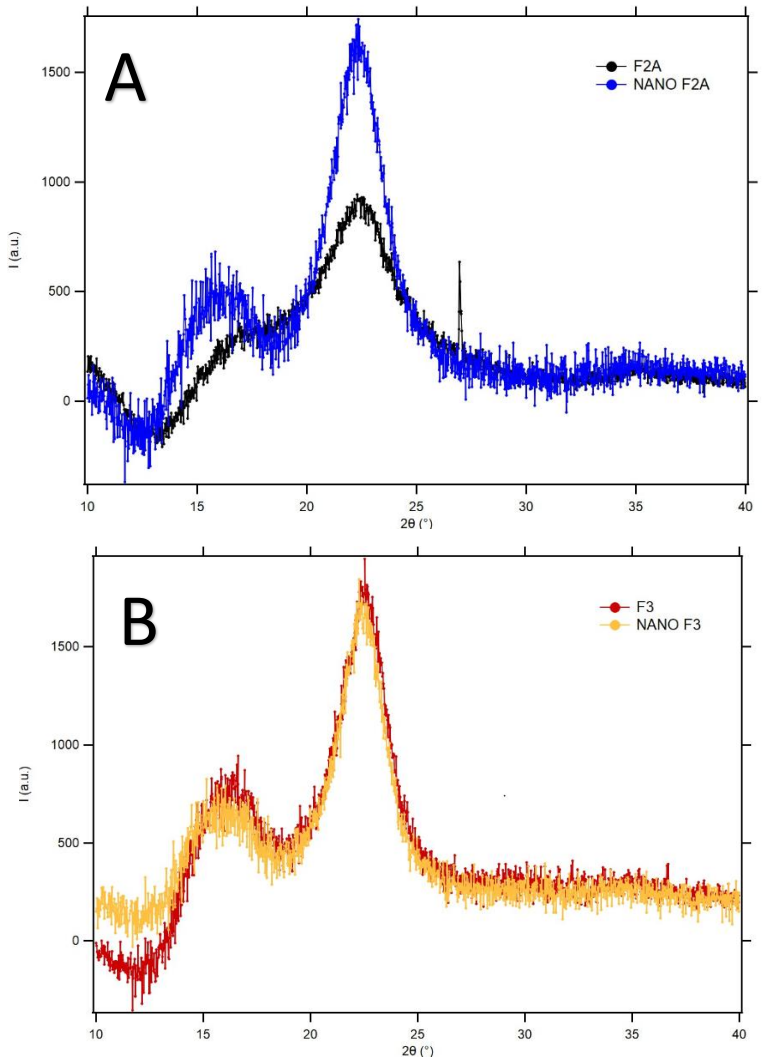

Figure 2. XRD patterns from the unpurified cellulosic fractions and nanocrystals (F2A and NANO F2A) (A) and pure cellulose and nanocrystals (F3 and NANO F3) (B) extracted from TM vine shoots.

The FT-IR spectra from the cellulosic fractions and nanocrystals extracted from TM vine shoots are shown in Figure 3A. The peak located at 1730 cm^{-1}, characteristic from the acetyl groups from hemicelluloses and/or lignin [24], was visible in F2A (as expected, since the simplified extraction was not aimed to remove all the hemicelluloses present in the raw biomass). Interestingly, the peak remained visible, although with lower intensity, in NANO F2A, suggesting that a certain fraction of the hemicelluloses present in F2A was resistant to the hydrolysis. This peak was not visible in F3, suggesting that, if hemicelluloses remained in the material, they represented only a very minor fraction. Moreover, the region where most of the cellulose characteristic bands are located (~1200-800 cm^{-1} [24, 27]) was affected depending on the applied treatment. As expected, the peaks within this region became sharper and more intense after hydrolysis of the less purified fraction (F2A). However, in the case of the purified cellulose (F3), the intensities of these bands did not increase (or were even slightly decreased) after the hydrolysis. This suggests, in line with the XRD results, that while the sulphuric acid was able to digest most of the amorphous hemicelluloses initially present in F2A, it was not able to penetrate the structure of cellulose microfibrils in F3 to digest the remaining amorphous domains. It should also be noted that the band located at 768 cm^{-1} (pointed out with arrows in Figure 3A) was detected in NANO F2A and NANO F3, suggesting the presence of sulphate groups as a result of the sulphuric acid hydrolysis [27].

TGA analyses of the cellulosic fractions and nanocrystals were also performed to assess their thermal stability and the results are shown in Figure 3B. As expected, F3 and NANO F3 only showed one sharp and defined peak with its maximum at around 334 ºC, characteristic from the thermal degradation of cellulose [25]. On the other hand, F2A showed the same additional peak detected in the raw vine shoots at around 260 ºC (cf. Figure 1B), ascribed to the degradation of hemicelluloses. This peak became less intense after acid hydrolysis, but it could still be detected in NANO F2A, confirming that although most of the amorphous hemicelluloses were digested by the sulphuric acid, a small fraction of more resistant hemicelluloses was not hydrolyzed. It should be noted that in the case of NANO F2A, the cellulosic degradation peak was slightly shifted towards lower temperatures. This could be ascribed to the presence of residual sulphate groups in the surface of the extracted nanocrystals, which are known to decrease the thermal resistance of cellulose [32].

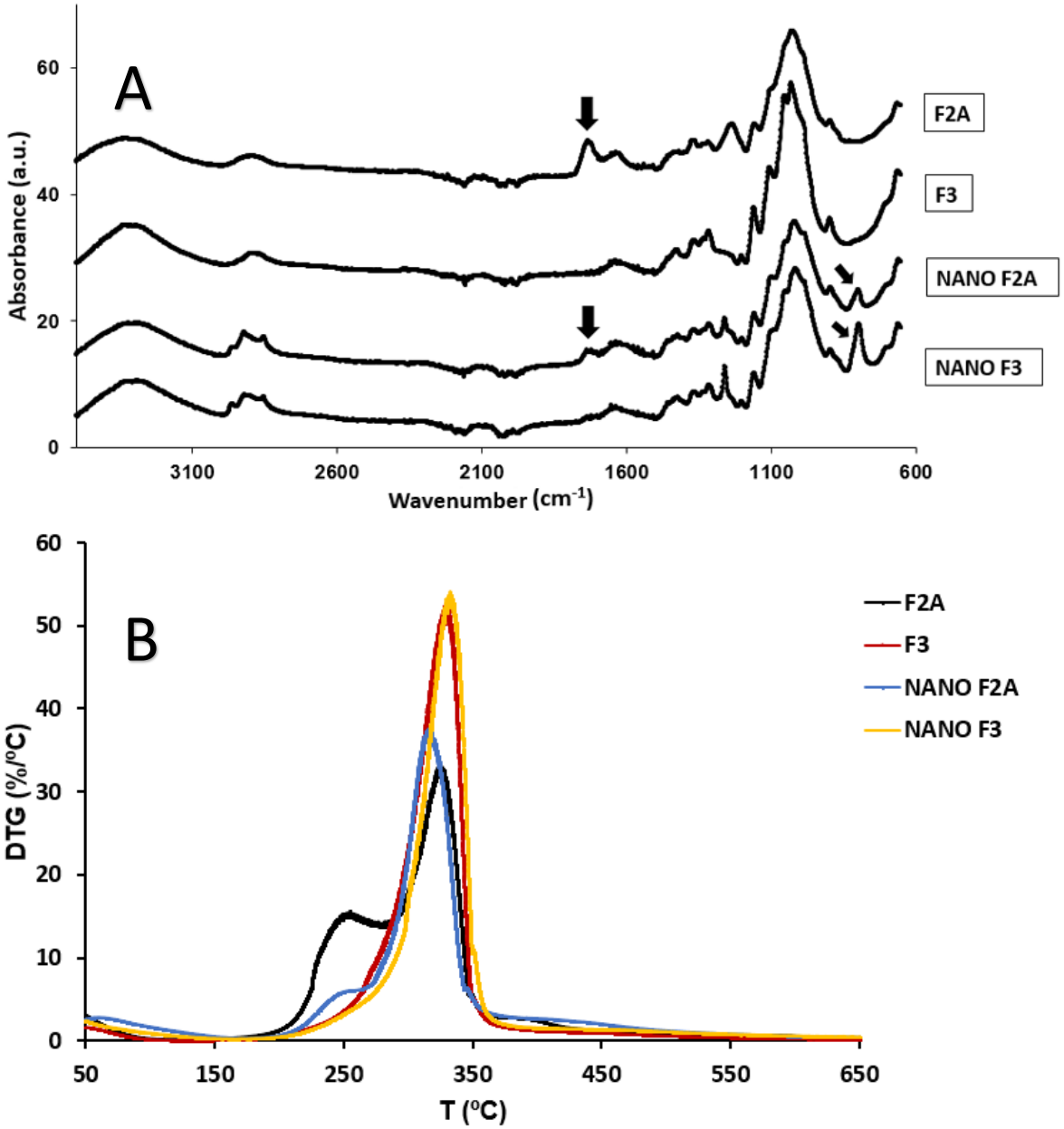

Figure 3. (A) FT-IR spectra of the cellulosic fractions and nanocrystals extracted from *Tempranillo*-TM vine shoots. Arrows are pointing towards characteristic bands in the spectra. (B) derivative thermogravimetric (DTG) curves of the cellulosic fractions and nanocrystals extracted from *Tempranillo*-TM vine shoots.

Sulphuric acid treatment of cellulosic materials has been shown to proceed with a preferential digestion of amorphous domains in the longitudinal axis of cellulose microfibrils. Thus, longer or more aggressive hydrolysis conditions have a strong impact on the aspect ratio (length/width) of the extracted nanocrystals [32]. To evaluate the morphology of the cellulosic nanocrystals extracted from vine shoots, they were characterized by TEM and representative images are shown in Figure 4. It could be seen that NANO F2A (Fig. 4A) was composed of long fibrillar structures (847 ± 51 µm, with an aspect ratio of 43.4) with a significant degree of agglomeration. This is

reasonable considering that, as suggested by FT-IR and TGA analyses, a significant amount of hemicelluloses remained in NANO F2A, since hemicelluloses are known to act as a cross-linking agents in plant cell walls [6]. In the case of NANO F3, more heterogeneous structures could be visualized. Most of the material corresponded to isolated long fibrils (604 ± 48 µm, with an aspect ratio of 31.9) (Fig. 4B). However, additional structures with much shorter lengths (208 ± 12 µm, with an aspect ratio of 13.5), which may correspond to hydrolyzed cellulose fragments, could be also detected (Fig. 4C). These results suggest that the sulphuric acid hydrolysis proceeded heterogeneously, with most of the cellulose microfibrils remaining intact, while the hydrolysis of more exposed cellulose regions produced a minor fraction of shorter needle-like structures.

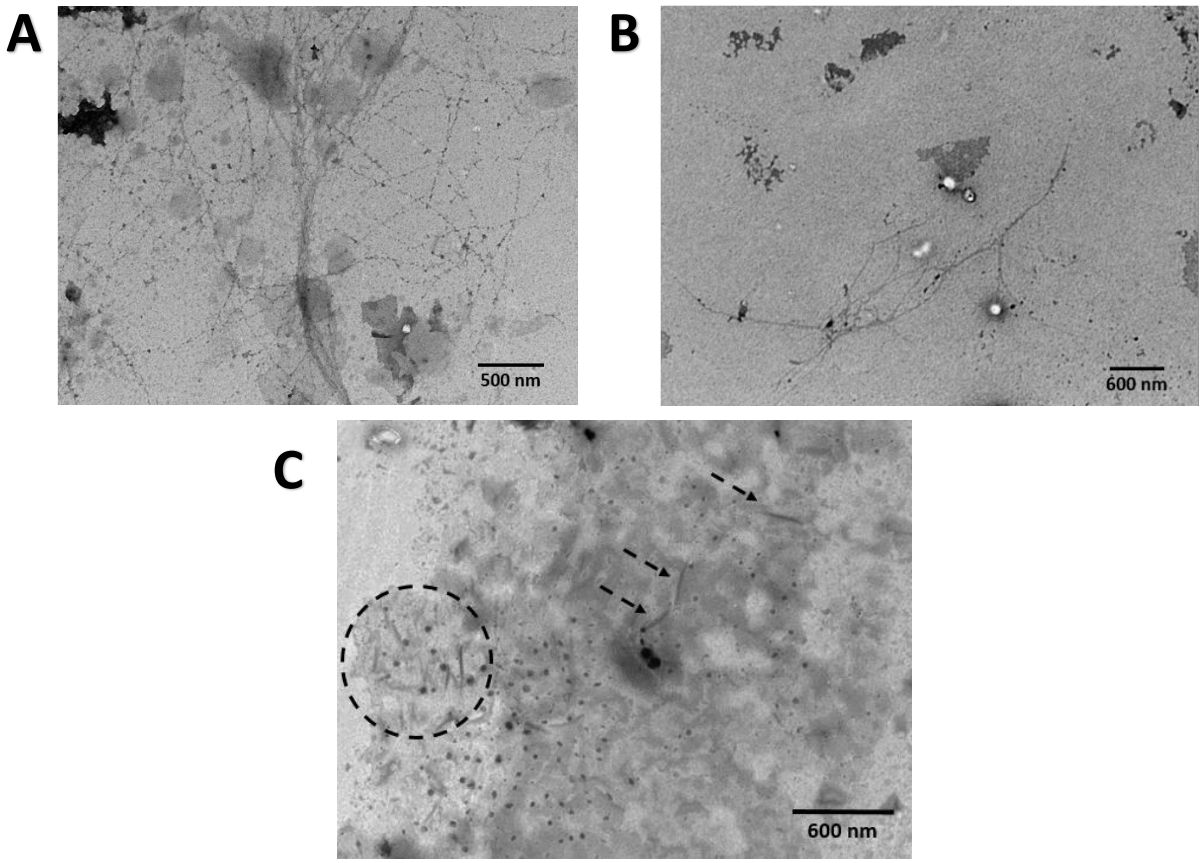

Figure 4. TEM images of the cellulosic nanocrystals extracted from vine shoots. (A) NANO F2A (unpurified nanocrystals) and (B and C) NANO F3 (pure cellulose nanocrystals).

The obtained results seemed to point towards two interesting hypotheses: (i) a certain fraction of hemicelluloses was resistant to the sulphuric acid hydrolysis and remained in the less purified NANO F2A nanocrystals and (ii) the access of sulphuric acid towards the cellulose microfibrils in F3 was somehow obstructed; as a result, the hydrolysis was not efficient and proceeded heterogeneously. To investigate the impact of the different extraction protocols on the carbohydrate composition of the fractions and nanocrystals extracted from TM vine shoots, monosaccharide analyses were carried out and the results are displayed in Table 3. As expected,

glucose was the major component in all fractions and could be fully ascribed to cellulose, as small quantities of mixed linkage β-glucan (previously reported as <5% of the polysaccharide fraction in the raw material) [33], may have been probably removed in the treated fractions. As in hardwoods, xylan in *Vitis vinifera* has been reported to consist of an acetylated glucuronoxylan with a backbone of β-(1→4)-linked xylopyranosyl units with α-(1→2)-linked 4-O-methyl-α-glucupyranosyl residues (MeGlcA). It is well known that xylan is the main hemicellulose in most flowering plants, including vine shoots, playing a crucial role in their cell wall architecture by its direct interaction with cellulose and lignin [34]. Previous works have demonstrated that even minor amounts of xylans in the secondary cell walls from higher plants have a strong impact on the structure of cellulose microfibrils [35].

Recent studies have elucidated that an even pattern of substitution of MeGlcA or acetyl moieties in xylan allows for the xylan chains to be docked onto the hydrophobic or hydrohillic surfaces, respectively, of cellulose microfibrils, adopting a preferential two-fold screw conformation [36-38]. This tight interaction of xylan with cellulose is partly responsible for the inherent recalcitrance of lignocellulosic biomass and might explain a xylan fraction remaining in all samples [39, 40]. This is mostly patent in the less aggressively treated F2A, and slightly decreasing xylan contents are noted with increasing aggressiveness of the applied treatments. Interestingly, a remarkable xylose fraction was present in NANO F2A, seemingly resistant to the sulphuric hydrolysis (~12 %). This xylan may have prevented the sulphuric acid to reach the amorphous cellulosic domains and thus reduced its effectiveness. Previous reports have also noted an abnormal resistance of vine stalks to kraft pulping, compared to hardwood, which was attributed to a different lignin structure [41].

Table 3. Monosaccharide relative content (%) of the cellulosic fractions (F2A and F3) and nanocrystals (NANO F2A and NANO F3) extracted from TM vine shoots. Values in the same line followed by different letters are significantly different ($p \leq 0.05$).

%*	F2A	F3	NANO F2A	NANO F3
Arabinose	1.48 ± 0.25^{a}	0.06 ± 0.03^{b}	0.06 ± 0.01^{b}	0.01 ± 0.01^{b}
Galactose	1.89 ± 0.97^{a}	0.46 ± 0.03^{b}	0.19 ± 0.05^{c}	0.05 ± 0.02^{c}
Glucose	71.18 ± 1.24^{a}	85.99 ± 0.48^{b}	90.75 ± 0.32^{c}	93.54 ± 0.23^{d}
Xylose	20.24 ± 0.30^{a}	10.64 ± 0.55^{b}	7.98 ± 0.52^{c}	5.66 ± 0.45^{d}
GalA	3.27 ± 0.06^{a}	2.20 ± 0.09^{b}	0.50 ± 0.15^{c}	0.29 ± 0.04^{c}

*The contents of fucose, rhamnose, mannose and 4-O-methyl-glucuronic acid was below 1% in all fractions.

4.3 Characterization of pure (nano)cellulosic films and their blends with agar

The extracted cellulosic fractions and nanocrystals were subsequently used to produce biopolymeric films and their performance properties were characterized to evaluate their potential to be used as food packaging materials. Since one of the main issues of cellulosic films is their excessive rigidity [6, 42], agar was incorporated into the nanocellulosic films at different concentrations to evaluate its compatibility with cellulose and the effect on the performance of the hybrid films. Agar was chosen as the additive for these films since previous works have reported on the more ductile behavior of this biopolymer as compared with cellulose [43, 44].

The morphology of the produced films was evaluated by SEM and representative images are shown in Figure 5. As expected, rougher surfaces with larger fibrillar structures could be observed in the less purified materials (F2A and NANO F2A), while smoother surfaces were seen in F3 and NANO F3. There was also a clear tendency of more homogeneous and smoother film surfaces after the acid hydrolysis in the more purified F3 materials. However, F2A fraction showed a more homogeneous surface in comparison with NANO F2A that hindered the presence of larger hemicellulosic structures (inset in Fig. 5A). Interestingly, the addition of agar, even at the lowest content (20% w/w), had a strong impact on the surface morphology of the films. In general, more continuous surfaces, where the cellulosic fibrillar structures seemed to be embedded in an amorphous agar coating layer, could be observed. A similar effect has been previously reported for the residual agar remaining in less purified cellulosic films from red seaweed residues [30].
The visual aspect and transparency of the films were also evaluated. As observed in Figure S1A, the larger size of the fibrillar structures composing the films from the cellulosic fractions produced more opaque materials, while the transparency was dramatically improved with the application of the acid hydrolysis, especially in NANO F2A due to the removal of amorphous hemicelluloses and the production of more homogeneous materials with smaller fibrils. Moreover, the presence of non-cellulosic components produced a yellowish tonality in the F2A and NANO F2A films. The hybrid films containing agar were found to be more transparent than the pure (nano)cellulosic films, which may be explained by the amorphous structure of agar [45]. The internal transmittance values of the films, shown in Figures S1B and S1C, confirmed that the acid hydrolysis treatment produced a marked increase in the transparency of the films. Furthermore, while the blends with agar displayed higher transparency values than the pure (nano)cellulosic films, the amount of added agar did not show any significant effect.

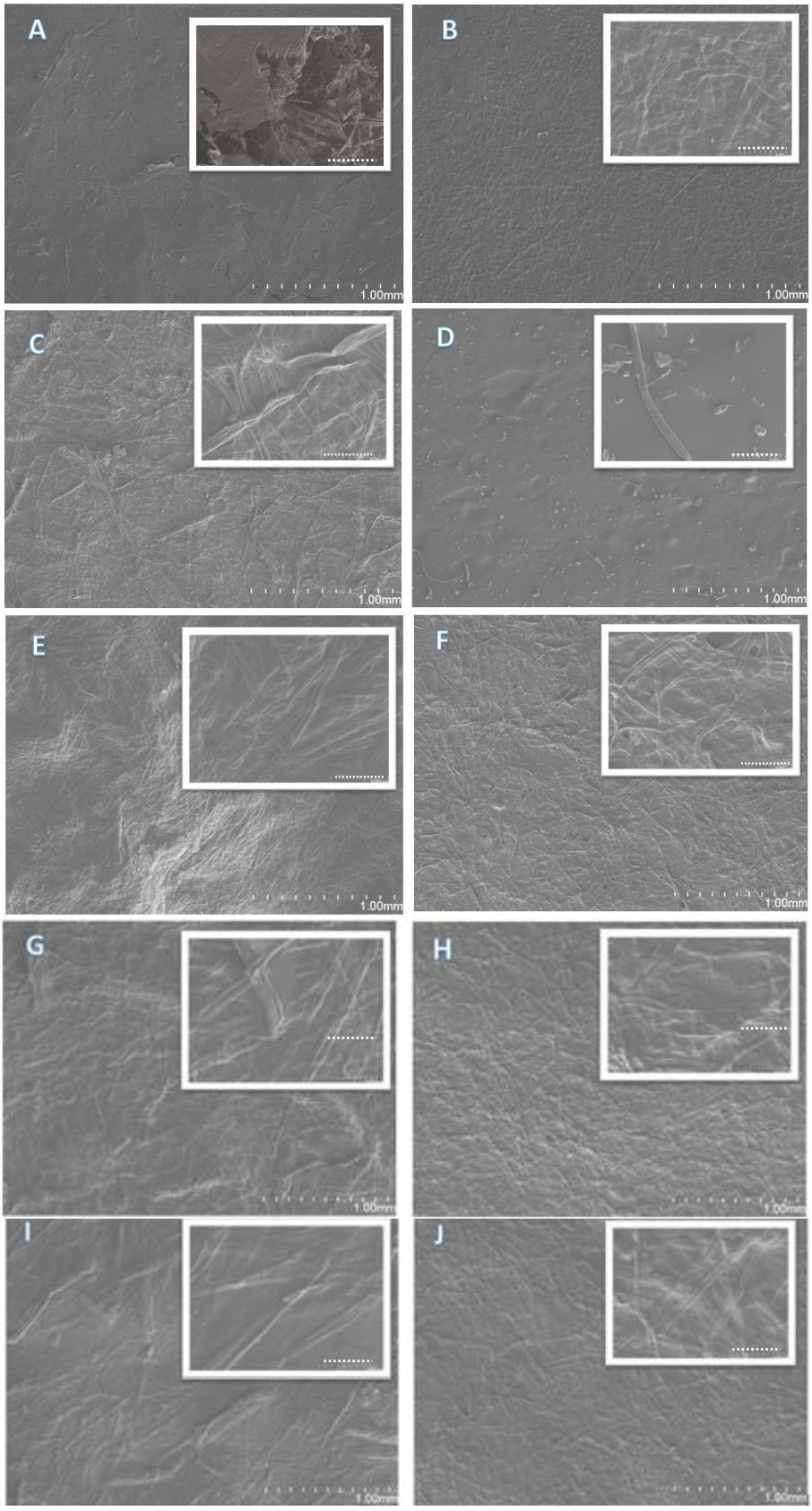

Figure 5. SEM images of the surface from the pure (nano)cellulosic films obtained from vine shoots (A) F2A (unpurified fraction), (B) F3 (pure cellulose), (C) NANO F2A (unpurified nanocrystals), (D) NANO F3 (cellulose nanocrystals) and of their blends with agar (E) NANO

F2A+20%AGAR, (F) NANO F3+20%AGAR, (G) NANO F2A+40%AGAR, (H) NANO F3+40%AGAR, (I) NANO F2A+80%AGAR and (J) NANO F3+80%AGAR. Insets represent regions of the films at higher magnification (scale bars represent 100 μm).

The performance of the films was evaluated in terms of mechanical and water barrier properties and the obtained results are summarized in Table 4. With regards to the mechanical properties, the films from the different (nano)cellulosic fractions showed a clearly distinct behavior. The less purified fraction (F2A) presented very poor mechanical performance; however, after the short hydrolysis treatment the properties of the material (NANO F2A) were significantly improved, especially in terms of rigidity and strength (as suggested by the elastic modulus and tensile strength values). Such a dramatic improvement can be attributed to the digestion of most of the amorphous hemicelluloses initially present in F2A, giving rise to more crystalline materials, with a much homogeneous structure. Indeed, the purification of cellulose by applying the conventional protocol had a more marked positive effect and F3 presented the best compromise between strength and ductility. Surprisingly, the acid hydrolysis of F3 was detrimental for the mechanical performance of the films, reducing the elastic modulus, tensile strength and elongation at break of NANO F3. This supports the hypothesis that most of the cellulose microfibrils in F3 were not accessible to the sulphuric acid and only a small fraction of more accessible cellulose was digested. As a result, heterogeneous nanofibrillar structures with very different sizes, as shown by TEM (cf. Figure 4), were produced. The presence of shorter needle-like structures, with lower aspect ratios, may have been detrimental for the mechanical properties of NANO F3. In fact, the films from the cellulosic nanocrystals extracted by applying a longer hydrolysis of 5h showed even worse mechanical performance than NANO F3, presenting similar elastic modulus (6.5 ± 0.5 GPa) but remarkably lower tensile strength (27.8 ± 1.7 MPa) and elongation (0.8 ± 0.1 %). This is in line with the reduced extraction yield and crystallinity determined for these nanocrystals and confirms that achieving a complete hydrolysis of the amorphous cellulose was not a matter of time. It seems that the small fraction of tightly bound xylan remaining in F3 hindered the access of the sulphuric acid towards certain regions of the cellulose microfibrils.

As already anticipated, the (nano)cellulosic films presented a very rigid behavior, with high elastic moduli but low elongation values. As deduced from the results shown in Table 4, the addition of agar into the nanocellulosic films had a plasticizing effect (reducing the elastic modulus, while increasing the elongation). This effect was more evident with increasing agar contents, reaching a ~3-fold increase in the elongation at break with 80% agar. However, higher EAB values can be typically reported for packaging structures in the literature. In this sense, lower cellulosic contents could be tested (10% or 5%). Nevertheless, obtained structures might be suitable for transportation where more rigid values are needed. On the other hand, tensile strength was

significantly improved at higher agar contents (40% and 80%). It should be noted that the higher the agar content in the hybrid films, the more their mechanical properties resembled those of pure agar films [43]. Previous works have reported on the opposite effect of adding moderate loadings (1-20% w/w) of cellulosic additives (such as commercial microcrystalline cellulose and nanocrystals) to agar-based films produced by casting, i.e. cellulose acted as a plasticizing agent with slight significant increase on the stiffness of the composites [46, 47]. Thus, the mechanical properties of the hybrid films can be adjusted depending on their intended application by selecting the optimum content of (nano)cellulosic fractions and agar. It is to be highlighted that, in general, the (nano)cellulosic films and their blends with agar presented similar or even superior mechanical performance than commercial biopolymers such as thermoplastic starch (TPCS) or PLA (cf. Table 4). In parallel, similar materials obtained from *Posidonia oceanica* waste biomass showed increased rigidity (E and TS) with similar or lower EAB, demonstrating the effectiveness of applying these kinds of protocols to both terrestrial and marine resources [6].

As deduced from Table 4, the water vapor permeability (WVP) of the films was also greatly affected by the purification degree of the cellulosic fractions and nanocrystals, as well as by the addition of agar. The less purified fraction (F2A) displayed the lowest barrier performance, which was drastically improved (10-fold reduction in the water permeability) for the nanocrystals produced after the short acid hydrolysis (NANO F2A). This is again related to the removal of amorphous hemicelluloses by the sulphuric acid treatment. Accordingly, the purified cellulose fraction (F3) also showed greater barrier than F2A. In this case, the hydrolysis of F3 had a positive impact on the barrier properties. This could be a combined effect of the slightly greater crystalline character of the nanocrystals as well as the more compacted microstructure of the films (cf. Figure 5). Even though the formation of smaller nanocrystals was detrimental for the mechanical properties of the films, their presence enabled the formation of less porous films, hence inhibiting water diffusion. The WVP of the films from the cellulosic fraction subjected to the longer hydrolysis was also evaluated. As expected, given the reduced crystallinity of the extracted nanocrystals, they produced films with higher WVP ($(8.6 \pm 0.4)\cdot 10^{-14}$ Kg·m/s·m^{2}·Pa) than NANO F3, again demonstrating that extending the hydrolysis time did not produce further digestion of the amorphous cellulose domains.

Table 4. Mechanical properties, water vapor permeability and contact angle of the pure (nano)cellulosic films obtained from vine shoots and of their blends with agar.

E: elastic modulus; TS: tensile strength; EAB: elongation at break; WVP: water vapor permeability. Values in the same column followed by different letters are significantly different ($p \leq 0.05$).

n.m.: not measured.

	E (GPa)	TS (MPa)	EAB (%)	WVP (Kg·m/s·m^2·Pa) ·10^{-14}	Contact Angle (º)
F2A	0.2 ± 0.0^{e}	0.8 ± 0.1^{e}	0.5 ± 0.1^{d}	58 ± 0.2^{c}	n.m.
NANO F2A	5.5 ± 0.2^{b}	42.1 ± 2.0^{c}	1.1 ± 0.1^{c}	5.9 ± 0.2^{a}	48.5 ± 5.1^{c}
NANO F2A+20% AGAR	4.5 ± 0.4^{c}	44.6 ± 2.4^{c}	1.6 ± 0.1^{c}	5.6 ± 0.3^{a}	105.9 ± 10.2^{a}
NANO F2A+40% AGAR	4.2 ± 0.4^{c}	50.8 ± 2.7^{b}	2.2 ± 0.2^{b}	6.2 ± 0.1^{a}	99.3 ± 5.8^{a}
NANO F2A+80% AGAR	3.3 ± 0.3^{d}	56.8 ± 5.1^{ab}	3.1 ± 0.3^{a}	8.1 ± 0.2^{b}	95.3 ± 8.0^{a}
F3	7.8 ± 0.7^{a}	67.1 ± 4.9^{a}	2.1 ± 0.2^{b}	8.5 ± 0.2^{b}	n.m.
NANO F3	5.9 ± 0.8^{b}	47.2 ± 4.2^{bc}	1.2 ± 0.1^{c}	4.9 ± 0.2^{a}	67.9 ± 10.2^{b}
NANO F3+20% AGAR	4.9 ± 0.3^{bc}	44.8 ± 3.5^{c}	1.2 ± 0.1^{c}	6.2 ± 0.6^{a}	71.4 ± 9.0^{b}
NANO F3+40% AGAR	4.0 ± 0.2^{c}	53.3 ± 3.6^{b}	1.6 ± 0.1^{c}	5.2 ± 0.2^{a}	98.0 ± 6.7^{a}
NANO F3+80% AGAR	2.9 ± 0.4^{d}	55.7 ± 1.8^{b}	2.8 ± 0.3^{ab}	4.7 ± 0.4^{a}	85.4 ± 10.0^{ab}
AGAR [43]	3.3 ± 0.3	68.3 ± 10.2	7.9 ± 1.2	8.0 ± 0.5	78 ± 10
PLA [42, 48, 49]	5.1 ± 0.1	44.7 ± 3.8	9.0 ± 1.1	1.3 ± 0.1	77
TPCS [3]	0.5 ± 0.2	6.1 ± 0.7	8.5 ± 3.1	25.2 ± 0.5	47

Since agar presented higher WVP than the pure nanocellulosic films, its incorporation was expected to reduce the water barrier performance of the hybrid materials. This was indeed the case for the NANO F2A hybrid films, with the blend containing 80% agar showing a very similar WVP value to that of pure agar [43]. In contrast, the presence of agar in the NANO F3 blends did not have a significant effect on the permeability. This could be explained by a synergistic effect between both biopolymers, i.e. even though the incorporation of an amorphous component such

as agar would be detrimental for the barrier performance, the establishment of interactions between agar and cellulose via strong hydrogen bonds would lead to the formation of a stronger and more hydrophobic network, counteracting the negative effect of agar. With regards to similar agar composites previously reported in the literature where nanocellulosic reinforcement ranged from 1% to 10%, WVP results were between 1-2 orders of magnitud higher (~$1.2 \cdot 10^{-12}$ $Kg \cdot m/s \cdot m^{2} \cdot Pa$) in comparison with those reported in Table 4, probably due to higher nanocellulosic content (20%-80%) and thus showing the optimum barrier performance of TM vine shoots residues when incorporated into agar [46, 47]. Regarding other conventional biopolymers, these composites presented an intermediate barrier between PLA and TPCS [25, 42]. On the other hand, similar materials obtained from *Posidonia oceanica* showed lower barrier when compared with the more purified F3 fraction, but better barrier properties at nanocrystal purification level (both NANO F2A and NANO F3) [6].

To better understand the effect of the incorporation of agar on the water affinity of the hybrid films, contact angle measurements were also performed and the estimated contact angle values are listed in Table 4. While F3 and F2A presented a highly hydrophilic behaviour, which impeded a correct measurement of their water contact angle values, the acid hydrolysis substantially increased the hydrophobic character of the films. As expected, the removal of amorphous components after the acid hydrolysis yielded materials with more hydrophobic surfaces, especially in the more purified NANO F3 film. In keeping with our previous results, a longer hydrolysis treatment led to a slight decrease in the contact angle (64.7 ± 7.0º) of the films, which is reasonable due to the reduced crystallinity of the extracted nanocrystals. On the other hand, the addition of agar produced more hydrophobic surfaces in the hybrid films, which was not unexpected due to the more hydrophobic behavior of pure agar films [43]. Surprisingly, the hybrid films presented similar or even higher contact angle values than pure agar, again suggesting a synergistic effect between cellulose and agar. Other biopolymers such as PLA and TPCS showed similar or even lower values (77º and 47º respectively) to those obtained from TM films and composites demonstrating the high hydrophobicity of these materials and their applicability for food packaging [25, 49].

Although no polyphenols could not be quantified by means of the Folin-Ciocalteau method in the cellulosic fractions and nanocrystals, vine shoots have been previously reported as a phenolic-rich source [12]. Our hypothesis was that the phenolic compounds were actually bound to other components such as hemicelluloses and, therefore, they could not be detected by this colorimetric approach. To assess the bioactivity of the (nano)cellulosic films, a more practical method such as the β-carotene bleaching assay was used and the results are shown in Figure 6. As observed, both of the cellulosic fractions showed remarkable bleaching inhibition, especially the less purified

fraction (F2A), which showed outstanding values of ~50% inhibition after 120 min. However, the antioxidant potential of both fractions was significantly reduced after being subjected to the acid hydrolysis. While NANO F3 did not show a significant antioxidant capacity, NANO F2A still showed a bleaching inhibition of ~30%. These results are much higher than those previously reported for the films from the cellulosic fractions extracted from *Arundo donax* waste biomass (ca. 6% inhibition [50]), thus highlighting the potential of the less purified (nano)cellulosic fractions extracted from vine shoots to develop bioactive materials for food packaging applications.

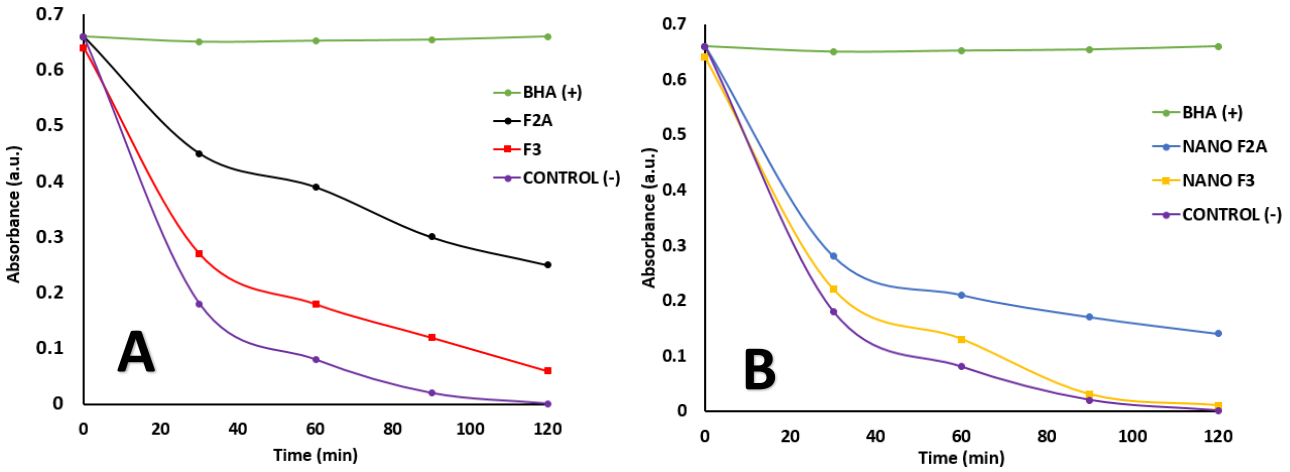

Figure 6. β-carotene bleaching inhibition kinetics for the films produced from the cellulosic fractions (A) and nanocrystals (B) extracted from *Tempranillo*-TM vine shoots.

5. Conclusions

In this work, vine shoots have been proposed as alternative sources for the development of sustainable biopolymeric materials for food packaging applications. The composition of two different varieties (*Tempranillo* (TM) and *Verdejo* (VJ)) was firstly characterized. Given their great similarity, TM was selected as the raw material due to its greater worldwide abundance. TM vine shoots were then used to extract cellulosic fractions and nanocrystals with different degrees of purity. The simplified extraction protocol led to less purified materials (F2A and NANO F2A) with much higher yields and lower crystallinities than those produced by the standard cellulose purification method (F3 and NANO F3). The hydrolysis of F2A produced the digestion of most amorphous hemicelluloses. On the contrary, most of the cellulose microfibril regions in F3 were not accessible to sulphuric acid and the hydrolysis process did not occur uniformly. As a result, NANO F3 was composed of heterogeneous fibrillar structures with different sizes and similar crystallinity to that of F3. Finally, films were made from the cellulosic fractions and nanocrystals

in order to evaluate their performance. The digestion of most of the amorphous hemicelluloses in F2A produced a dramatic improvement in the mechanical and water barrier performance of NANO F2A. On the other hand, the more purified F3 fraction produced films with superb mechanical and barrier performance, which were not remarkably improved in NANO F3 after the acid hydrolysis. Interestingly, F2A and NANO F2A films showed a remarkable antioxidant potential, as determined by the β-carotene bleaching assay. Agar was also incorporated at different concentrations (20%, 40% and 80%) into the nanocellulosic films, producing more ductile materials, with greater transparency and smoother surfaces, where the cellulose nanofibrils were embedded in a continuous agar layer. Thus, properties of the hybrid films can be adjusted depending on their intended application by selecting the optimum content of (nano)cellulosic fractions and agar.

These results highlight the importance of evaluating alternative purification protocols which yield less purified materials, since they are not only beneficial from an economical and environmental perspective, but they can generate materials with improved performance and additional functionalities, such as antioxidant capacity, with interest for food packaging applications.

6. Supplementary material

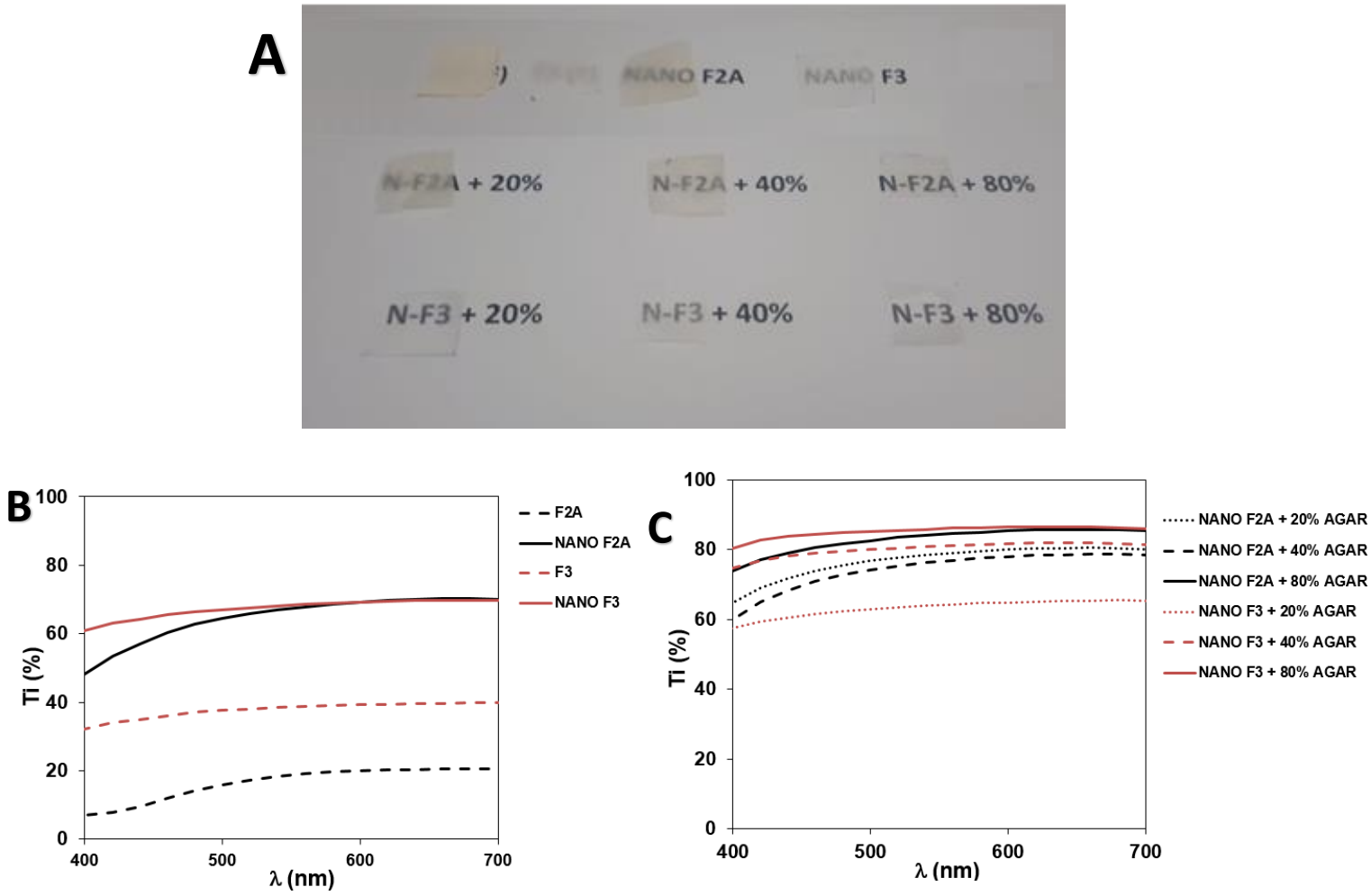

Figure S1. (A) Visual aspect of the pure (nano)cellulosic films obtained from vine shoots and of their blends with agar. Contact transparency of the pure (nano)cellulosic films (B) and of their blends with agar (C).

3.2. Sustainable biocomposite films fully-based on white rice (Oryza sativa) agroindustrial by-products.

This section is an adapted version of the following submitted research article:

Benito-González, I., Ortiz-Gimeno, M.M., López-Rubio, A., Martínez-Abad, A., Garrido-Fernández, A. & Martínez-Sanz, M.

(2021). Bioactive composite films from white rice (*Oryza sativa*) by-products. Rice flour vs rice starch.

Carbohydrate Polymers. *Under review*

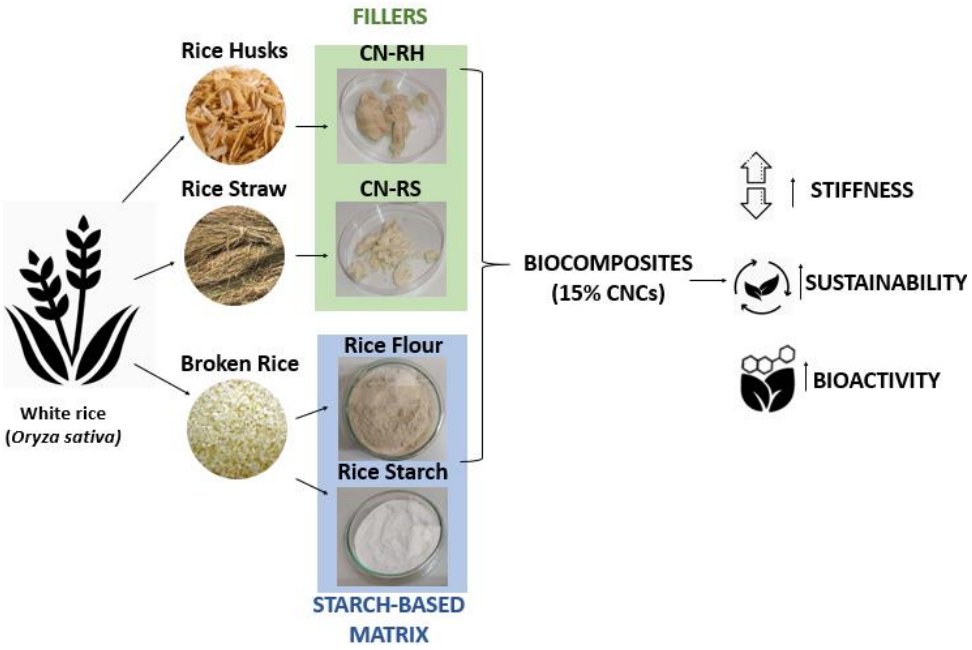

1. Abstract

In this work, biocomposites fully-based on the valorization of white rice agroindustrial by-products have been produced by melt mixing. The film matrix consisted on rice flour (RF) or rice starch (RS) obtained from broken rice, which was reinforced with cellulose-rich nanocrystals obtained through simplified extraction processes from rice husks (CN-RH) and rice straw (CN-RS). The presence of impurities in RF induced the re-crystallization of starch, producing more crystalline films with better mechanical performance, but greater water vapor permeability than RS. This was overcome by the addition of 15% (w/w) cellulosic nanocrystals. Moreover, the cellulosic nanocrystals increased the stiffness of the films, with the CN-RS yielding better mechanical performance due to their more homogeneous morphology and distribution within the RF matrix. Interestingly, all the RF films showed remarkable antioxidant capacity (>20% inhibition of β-carotene bleaching), highlighting the potential of less purified materials to develop sustainable food packaging with additional functionalities.

2. Introduction

The steady depletion of fossil fuels, the negative environmental impact of conventional plastics and the insufficient results of recycling strategies to palliate this issue, have led to the investigation of novel alternative and more sustainable materials over the past years. In particular, biodegradable polymers have attracted a great deal of attention, mainly due to their sustainability and/or renewable character [51-54]. Nevertheless, most commercial biopolymers such as polyhydroxyalkanoates (PHAs) [55] or poly-lactic acid (PLA) [56] have been shown to present lower cost-efficiency than petroleum-based plastics and low degradation rates under certain environmental conditions, thus limiting their current market applications. One of the most promising biopolymers for food packaging applications is starch, which is typically extracted from land crops such as corn, rice, wheat and potatoes [57]. This biopolymer is already commercially available in the form of thermoplastic starch, which is produced by the addition of plasticizers and presents a relatively good processability [58, 59]. Furthermore, no ecotoxicity of starch-based biocomposites (containing 5-25% w/w plant-based fibers) has been observed in biodegradability assays [60], making them a promising alternative for the development of sustainable packaging. However, starch-based materials usually have relatively poor mechanical performance and present high hygroscopicity. In this context, the addition of cellulose and nanocellulose has been extensively reported to be a useful approach to improve the mechanical and barrier performance of starch, ascribed to the highly crystalline character of cellulose and the optimum compatibility between both carbohydrate polymers [5, 61, 62]. Another important

consideration is the fact that the land crops typically used for the extraction of starch compete with their primary use as food, thus limiting the application of this biopolymer for packaging. In this sense, the valorization of waste biomass is gaining interest in the past few years, as it represents a cheap and valuable source of biopolymers, such as cellulose [63-65] and starch [66, 67]. In fact, cellulosic fractions have been extracted from several waste biomass sources and subsequently incorporated into different biopolymers such as starch [3], agar [68], PLA [4] or latex [69], improving their performance.

Traditionally, rice cultivation has generated several environmental issues due inefficient waste management strategies. Although the use of rice waste biomass as compost, energy source or animal feed has been explored, there are in fact more optimum resources for these particular applications, thus limiting the interest in collecting and treating this biomass waste [70]. For instance, more than 100 million kg of rice straws generated in the Albufera National Park (ANP, Valencia, Spain) are traditionally burned in situ every autumn, causing severe environmental problems. This phenomenon is not exclusive for this region; it occurs in other national areas (such as Ebro Delta in Catalonia) and at international level in rice-producing countries such as China and Japan [71]. In this context, rice by-products, such as broken rice, rice straw and rice husks, may also be evaluated as a valuable source of both starch and cellulosic nanocrystals for developing biodegradable food packaging structures due to their carbohydrate-rich composition. While rice endosperm and broken rice have been used to extract starch [72, 73] , rice straw and husks are mainly considered as a cellulose sources [74, 75] . Rice flour has also been used to develop edible films [76] and biocomposites reinforced with commercial eucalyptus cellulosic fibers [77] by casting. It should also be considered that these biomass sources are also rich in polyphenols [78] and phytochemicals [79] and, thus, it may be interesting to apply simplified protocols for the extraction of less purified starch and cellulose while preserving some of these bioactive compounds. Accordingly, in this work we propose the valorization of rice waste biomass for the development of bio-based packaging materials. Rice flour was used as the matrix, due to its high starch content. In order to improve the mechanical and barrier performance, cellulosic nanocrystals with lower purification degree were extracted from rice straw and rice husks by previously developed simpler protocols [6] and incorporated into rice flour via melt-mixing and hot-pressing. Our hypothesis claims that the utilization and combination of less purified starch-based and cellulose-based materials obtained from rice waste can yield biocomposite materials which outperform pure starch in terms of mechanical and barrier performance and are more efficient from an economic and environmental perspective. Furthermore, the presence of antioxidant compounds in these less purified materials may confer them additional antioxidant capacity, increasing their potential as bioactive packaging structures.

3. Materials & Methods

3.1 Materials

White broken rice, rice husks (RH) and rice straw (RS) were kindly provided by the Valencian Institute of Agrarian Investigations (IVIA, Valencia, Spain) in April 2020.

Sulphuric acid (≥97.5%), ethanol (>98%), toluene (>99%), β-carotene (≥97%), linoleic acid (≥99%), Tween® 40, were obtained from Sigma-Aldrich (Spain). Sodium chlorite 80% was obtained from Acros Organics (Spain). Commercial corn starch (27–28% amylose) was kindly supplied by Roquette (Roquette Laisa España, Benifaio, Spain). Glycerol was purchased from Panreac Quimica, S.A. (Castellar Del Vallés, Barcelona, Spain).

3.2 Production of starch-based fractions

To produce the rice flour (RF), white broken rice was directly milled (IKA A11 basic analytic mill, Merck, Germany) until a homogeneous powder (particle size <0.5 mm) was achieved. This flour was then used as the source to obtain rice starch by means of a simplified methodology previously described in the literature [73]. Briefly, a mild alkali extraction (30 min, 0.18% NaOH in two steps) was carried out and the obtained material was subjected to several centrifugation cycles to remove the proteins. The whole starchy residue labelled as rice starch (RS) was collected and neutralized with HCl 0.1 M. Both RF and RS were oven-dried at 60 ºC for at least 48 h, to remove the excess of water prior to their use.

3.3 Production of cellulosic nanocrystals from rice husks and rice straw

Cellulosic nanocrystals were extracted from both RH and RS following a simplified protocol, in which the Soxhlet and alkali treatments typically applied to purify cellulose from land biomass, were skipped to increase yields, reduce costs and consequently improve the sustainability of the obtained materials [6]. Briefly, an initial treatment with 1.4% $NaClO_2$ (w/v) (pH=3) during 5 hours at 70 ºC was applied to remove lignin. This was followed by an acid hydrolysis treatment for 1.5 hours at 50 ºC with 30% H_2SO_4 (v/v) to digest the cellulosic amorphous domains. As a result, less purified cellulosic nanocrystals, containing hemicelluloses and minor amounts of lipids [6], were obtained from both biomass sources. The cellulosic nanocrystals (labelled as CN-RH and CN-RS) were stored as partially hydrated materials under refrigeration conditions (4 ºC).

3.4 Compositional characterization

3.4.1. Starch content

The total starch in the starch-based fractions was estimated using a total starch HK kit (Megazyme, Ireland) (K-TSHK method containing resistant starch) as a modification of ICC Standard Method nº 168. Briefly, ~100 mg of milled samples (RF and RS) were incubated in aqueous ethanol (80% v/v) at 80-85 ºC for 5 minutes and then centrifuged, keeping the precipitate fraction. Then, 0.1 mL of 2 M KOH and 1.2 M sodium acetate buffer were added to the thermostable α-amylase and amyloglucosidase, respectively. After 30 minutes, contents were transferred to a flask for a final centrifugation (3000 rpm, 10 min). The samples, which were expected to have more than 10% starch, were then diluted in water (1:10) and the absorbance at 340 nm was measured in a spectrophotometer. The determinations were carried out at least in triplicate.

3.4.2 Lignin, holocellulose and ash content

The lignin and holocellulose content in rice husks and rice straw were determined using the TAPPI T222 om-06, ASTM D1104-56 standard methods, respectively, while the ash content in the rice husks, rice straw, their derived nanocrystals and starch-based fractions was determined by the TAPPI T211 om-07 method. The determinations were carried out in triplicate.

3.4.3 Lipid content

The lipid content was estimated by the Soxhlet extraction method. Approximately 9 g of dry biomass were placed in a Dumas filter and treated with 800 mL of a 2:1 toluene:ethanol mixture overnight. The lipid content was calculated gravimetrically after drying the extracted solid fraction. The determinations were carried out, at least, in triplicate.

3.4.4 Protein content

Samples were analysed for total Nitrogen content using an Elemental Analyser Rapid N Exceed (Paralab S.L., Spain). Approximately 100 mg of dry biomass were pressed into pellets and then analysed using the Dumas method, which is based on the combustion of the sample and subsequent detection of the released N_2 [15]. The protein content was calculated from the nitrogen content multiplied by a factor of 6.25. The determinations were carried out in triplicate.

3.4.5 Carbohydrate composition

The carbohydrate content and sugar composition of the raw rice husks and rice straw, as well as of the extracted cellulosic nanocrystals, was determined after acidic methanolysis, as previously described [34]. The monosaccharides were analysed using high performance anion exchange

chromatography with pulsed amperometric detection (HPAEC-PAD) with a 940 IC system (Metrohm) equipped with a Metrosep Carb 2 column (4 × 250 mm, Metrohm). Control samples of known concentrations of mixtures of glucose, fucose, galactose, arabinose, xylose, mannose, galacturonic acid and glucuronic acid were used for calibration. This procedure is less aggressive than other hydrolysis methods, being able to determine uronic acids more accurately without degradation [80]. Although this procedure is not able to hydrolyse crystalline parts of the lignocellulosic substrate, the mild extraction conditions make it very unlikely that any crystalline cellulose might be present in the samples. All experiments were carried out in triplicate.

3.5 Production of starch-based biocomposite films

Starch-based films were produced by means of melt-mixing and hot-pressing in order to simulate industrial conditions. Briefly, ~8 g of starch-based fractions (RF or RS) and glycerol, as plasticizer, were dispersed in water using a polymer:glycerol:water ratio of 1:0.3:0.5 (w/w/w). The obtained paste was then melt-mixed (Brabender Plastograph, Germany) at 130 °C and 60 rpm for 4 min. Subsequently, 4 g of the obtained blends were spread on Teflon and placed in a compression mold (Carver 4122, USA) at a pressure of 5 tons and 130 °C for 5 min to form one film. The obtained films were coded as RF and RS. Additionally, composite films were prepared by incorporating 15% of the cellulosic nanocrystals (w/w with regards to the flour weight) extracted from rice husks and rice straw into the rice flour matrix. In that case, the required amount of nanocrystals (which were partially hydrated) was incorporated into the rice flour paste, together with water and glycerol. The materials were then processed as described above. The obtained films were coded as RF + 15% CN-RH and RF + 15% CN-RS. All films were stored at 53% RH for at least 3 days prior to their characterization.

3.6 Fourier Transform Infrared Spectroscopy (FT-IR)

FT-IR analyses were performed in attenuated total reflectance (ATR) mode using a Thermo Nicolet Nexus (GMI, USA) equipment. The spectra were taken at 4 cm^{-1} resolution in a wavelength range between 400-4000 cm^{-1} and averaging a minimum of 32 scans.

3.7 Thermogravimetric analyses (TGA)

Thermogravimetric curves (TG) were recorded with a Setaram Setsys 16/18 (SETARAM Instrumentation, France). The samples (ca. 10 mg) were heated from 30 to 1000ºC with a heating rate of 10ºC/min under nitrogen atmosphere. Derivative TG curves (DTG) express the weight loss rate as a function of temperature.

3.8 XRD diffraction

XRD measurements of the raw biomass materials, the extracted cellulosic nanocrystals and the starch-based films were carried out on a D5005 Bruker diffractometer. The instrument was equipped with a Cu tube and a secondary monochromator. The configuration of the equipment was θ–2θ, and the samples were examined over the angular range of 3°–60° with a step size of 0.02° and a count time of 200 s per step. Peak fitting was carried out using the Igor software package (Wavemetrics, Lake Oswego, Oregon). For the cellulose-based materials (i.e. rice husks, rice straw and their corresponding cellulosic nanocrystals) the diffraction patterns were fitted as described in [81], while in the case of the starch-based materials (i.e. rice flour, rice starch and starch-based films) the protocol described in [82] was followed. The obtained values from the fitting coefficients are those that minimize the value of Chi-squared, which is defined as:

$$\chi^2 = \sum \left(\frac{y - y_i}{\sigma_i}\right)^2 \quad (1)$$

where y is a fitted value for a given point, y_i is the measured data value for the point and σ_i is an estimate of the standard deviation for y_i. The curve fitting operation is carried out iteratively and for each iteration, the fitting coefficients are refined to minimize χ^2. The crystallinity index X_C was determined from the obtained fitting results by applying the following equation:

$$X_C(\%) = \frac{\sum A_{Crystal}}{A_{Total}} \times 100 \quad (2)$$

where A_{Total} is the sum of the areas under all the diffraction peaks and $\Sigma A_{Crystal}$ is the sum of the areas corresponding to the crystalline peaks.

3.9 Scanning electron microscopy (SEM)

SEM was conducted on a Hitachi microscope (Hitachi S-4800) at an accelerating voltage of 10 kV and a working distance of 8-16 mm. Small samples (~5 mm^2 area) of the films were cut to observe their cross-section. The samples were then sputtered with a gold–palladium mixture under vacuum during 3 minutes before their morphology was examined.

3.10 Water vapor permeability (WVP)

Direct permeability to water was determined from the slope of the weight gain versus time curves at 25 ºC. The films were sandwiched between the aluminium top (open O-ring) and bottom (deposit for the silica) parts of a specifically designed permeability cell with screws. A Viton rubber O-ring was placed between the film and bottom part of the cell to enhance sealability. These permeability cells containing silica were then placed in an equilibrated relative humidity

cabinet at 75% RH and 25 °C. The weight gain through a film area of 0.001 m^2 was monitored and plotted as a function of time. Cells with aluminium films (with thickness of ca. 11 μm) were used as control samples to estimate weight gain through the sealing. The tests were done at least in triplicate.

3.11 Mechanical properties

Tensile tests were carried out at ambient conditions of typically 24ºC and 50% RH on a Mecmesin MultiTest 1-i (1 kN) machine (Virginia, USA) with the Emperor™ software. Pre-conditioned rectangular-shaped specimens with initial gauge length of 8 cm and 1 cm in width were cut directly from the films. A fixed crosshead rate of 10 mm/min was utilized in all cases. Elastic Modulus (E), Tensile Strength (TS), and Elongation at Break (EAB) were determined from the stress-strain curves, estimated from force–distance data obtained for the different films. At least, five specimens of each film were tensile tested to obtain statistically meaningful results.

3.12 Optical properties

The transparency of the films was determined through the surface reflectance spectra in a spectrocolorimeter CM-3600d (Minolta Co., Tokyo, Japan) with a 10 mm illuminated sample area. Measurements were taken in duplicate for each sample by using both a white and a black background. Film transparency was evaluated through the internal transmittance (T_i) (0-1, theoretical range) by applying the Kubelka-Munk theory for multiple scattering to the reflection data. Internal transmittance (T_i) of the films was quantified using Eq. (3). In this equation, R_0 is the reflectance of the film on an ideal black background. Parameters a and b were calculated by Eqs. (4) and (5), where R is the reflectance of the sample layer backed by a known reflectance R_g.

$$T_i = \sqrt{(a - R_0)^2 - b^2} \tag{3}$$

$$a = \frac{1}{2}\cdot\left(R + \frac{R_0 - R + R_g}{R_0 R_g} \right) \tag{4}$$

$$b = (a^2 - 1)^{\frac{1}{2}} \tag{5}$$

3.13 β-Carotene-linoleic acid assay

The antioxidant capacity of the starch-based films was evaluated by the β-carotene-linoleic acid assay [20]. In brief, 4 mg of β-carotene were dissolved in 20 mL of chloroform. 2 mL of this solution were placed on a rotary evaporator and the chloroform was evaporated. Then, 50 μL of linoleic acid and 400 mg of Tween 40 were added and the content of the flask was mixed with

stirring. After that, 100 mL of aerated distilled water was transferred to the flask and stirred vigorously. 5 mL of the prepared β-carotene emulsion were transferred to a series of tubes containing a fixed weight of ~10 mg of each film, or 0.5 mL of BHT (0.1-1 mg/mL) (as the positive control) and 0.5 mL of distilled water (as the negative control). The samples were incubated in a water bath at 50 °C for 120 min. The absorbance of each fraction at 470 nm was measured every 30 minutes using a spectrophotometer. All the determinations were carried out in triplicate.

3.14 Statistical analysis

Analysis of variance (ANOVA) followed by a Tukey-b test were used when comparing more than two data sets, after confirming the homogeneity of variances by the Levene test using IBM SPSS Statistics software v.26. All data have been represented as the average ± standard deviation. Significant differences ($p \leq 0.05$) are denoted by showing the data provided in tables with different letters.

4. Results and Discussion

4.1 Characterization of rice by-products and the extracted cellulosic nanocrystals

The composition of the raw biomass sources (i.e. rice husks and rice straw) and starch-based fractions was firstly determined, and the results are summarized in Table 1. As expected, starch was the main component in the rice-derived fractions (89-96%), while proteins, lipids and ashes were detected in minor amounts. The starch content is within reasonable agreement with the value of 90% previously reported for white broken rice residues [73]. Notably, the applied method for the purification of starch was able to mainly reduce the amount of proteins present in the native rice flour, producing a relatively pure starch. It should be noted that the amount of starch in rice flour was already quite high and, thus, a high starch extraction yield of 96.5 ± 0.1% was attained. Apart from the starch-based fractions, two rice agroindustrial waste biomass sources, such as husks and straw, were valorised for the extraction of cellulosic nanocrystals. The composition of both biomass sources was initially characterized to evaluate their potential for the extraction of cellulosic nanocrystals (cf. Table 1). As observed, both materials were mainly composed of holocellulose (i.e. cellulose and hemicelluloses), which ranged from 71% to 78%. These values are within the range of those previously reported for other waste biomass sources such as *P. oceanica* dead leaves (~60% [25]) and vine shoots (~71% [68]), which have been successfully utilized to extract cellulosic nanocrystals. Therefore, this confirms the suitability of rice husks and rice straw for the extraction of cellulose-based fractions. Interestingly, rice husks also contained significant amounts of lignin and ashes, while that was not the case of rice straw, which

contained slightly greater amounts of protein. These results are in agreement with literature, where higher amounts of ashes, especially silica, are typically reported in rice husks [83, 84]. It should be noted that some ashes are reported to remain in the holocellulosic fraction obtained after the $NaClO_2$ treatment, accounting for up to 20% [83]. This may have led to an overestimation of the holocellulose content in rice husks, hence explaining the mass balance for this sample being higher than 100%. The extraction yields were determined after the first extraction step (i.e. treatment with $NaClO_2$) and after the subsequent acid hydrolysis, being 63.8% ± 4.7% and 52.9% ± 3.6%, respectively for rice husks, while rice straw provided yields of 59.8% ± 2.9% and 39.2 ± 4.0% after the chlorite and acid treatments, respectively. Since the apparent holocellulose content in both biomass sources was not very different, the yields for the first extraction step were comparable. However, the yield for the cellulosic nanocrystals obtained after acid hydrolysis was significantly higher in the case of rice husks. This may be indicative of a more crystalline cellulose being present in rice husks, as less amount of amorphous material was digested in this step. Moreover, the previously reported presence of a resistant ash fraction in rice husks [83] suggested that a significant content of them might be still present in the cellulosic nanocrystals. Indeed, significant amounts of ashes were determined in CN-RH (26.2 ± 0.0%) and CN-RS (16.4 ± 0.0%). This is reasonable given the fact that the nanocrystals were produced by applying a simplified purification protocol where Soxhlet and alkali treatments, typically applied to purify cellulose, were omitted. Additionally, the significant amount of ashes remaining in the nanocrystals explains why their extraction yields were significantly higher than those previously reported for the cellulosic nanocrystals obtained from other biomass sources such as vine shoots (~27%) using similar simplified purification protocols [68], where the presence of minerals in the raw biomass was significantly lower. Moreover, the greater ash content remaining in CN-RH, may explain their higher extraction yield as compared with CN-RS.

Table 1. Compositional analysis of rice by-products. Different letters in each column show significantly different values ($p \leq 0.05$).

	Starch (%)	**Proteins (%)**	**Lipids (%)**	**Ashes (%)**	**Holocellulose (%)**	**Lignin (%)**
Rice flour	89.4 ± 2.3^b	7.4 ± 0.3^a	2.4 ± 0.1^a	1.2 ± 0.1^a	---	---
Rice starch	96.5 ± 0.1^a	2.0 ± 0.2^b	1.7 ± 0.0^a	1.8 ± 0.2^a	---	---
Rice husks	---	2.5 ± 0.1^b	5.6 ± 0.8^a	19.0 ± 0.6^a	78.0 ± 3.4^a	14.4 ± 0.6^a
Rice straw	---	7.6 ± 0.3^a	4.1 ± 0.5^a	4.0 ± 0.3^b	70.7 ± 1.7^a	8.5 ± 0.3^b

As expected, a detailed sugar composition analysis on both the raw biomass and the resulting nanocrystals revealed cellulose and xylan as the main carbohydrate constituents. The glucose content arises from both cellulose and very minor contents in soluble mixed-linkage beta-glucan, which was most probably removed upon acidic treatments towards the nanocrystal formulation. Arabinoxylan, on the contrary, is a much more recalcitrant hemicellulose component composed of (1→4)-linked β-D-xylopyranosyl units, which in cereals is mainly substituted with (1→2)- and/or (1→3)-linked α-L-arabinofuranosyl residues. The total xylan content in both rice straw and rice husks raw materials was found to be around 18% of the total dry weight, with an arabinose to xylose ratio about 1:5, in accordance with previous reports on this biomass [85-88]. Upon acidic treatment, a major part of the xylan is removed and the more labile glycosidic linkages of arabinofuranosyl units are cleaved, which explains the lack of arabinose in the nanocrystal fractions [89]. Interestingly, the reduction of the xylan fraction in CN-RS was much lower compared to CN-RH treated samples, evidencing higher recalcitrance of the straw arabinoxylan.

Table 2. Monosaccharide relative content (%) of rice husks, rice straw and the corresponding extracted cellulosic nanocrystals. Different letters in each line show significantly different values ($p \leq 0.05$).

(%)	Rice Husks	Rice Straw	CN-RH	CN-RS
Arabinose	4.4 ± 0.8^{c}	6.3 ± 0.7^{c}	tr*	tr*
Galactose	1.4 ± 0.2^{d}	1.2 ± 0.2^{d}	tr*	tr*
Glucose	68.6 ± 11.9^{a}	67.3 ± 3.4^{a}	89.9 ± 14.5^{a}	83.3 ± 4.4^{a}
Xylose	25.6 ± 4.4^{b}	25.2 ± 1.5^{b}	10.1 ± 1.7^{b}	16.7 ± 1.2^{b}

*Fucose, Rhamnose, Mannose, Galacturonic acid and glucuronic acid were not detected or only detected in trace amounts (tr) in all samples (<0.1%). The bacterial cellulose positive control yielded only glucose in 100.7±1.1 %.

The rice husks and rice straw, as well as the extracted cellulosic nanocrystals, were also characterized by means of FT-IR and the obtained spectra are shown in Figure 1A. As already anticipated, given their similar composition (cf. Table 1), rice husks and rice straw showed very similar spectra. The most prominent peaks located at around 1100-900 cm^{-1}, corresponding to the presence of cellulose [24, 27], were broad and poorly defined. The band located at 1730 cm^{-1}

(marked with arrows in Figure 1A), corresponding to the C=O stretching vibration of ester groups from lignin and hemicelluloses [25], was also present in both samples. After applying the hydrolysis treatment, the obtained nanocrystals presented more defined bands within the region of 3600-3200 cm^{-1} and 3000-2900 cm^{-1}, which are characteristic from O—H and C—H stretching, respectively [24]. Furthermore, the cellulose-characteristic bands, such as those located at 1420, 1300 and 1100 cm^{-1} [24, 27], were much more defined and intense in the case of the nanocrystals, confirming their greater purification degree. The C=O stretching characteristic band at 1730 cm^{-1} was not visible in the nanocrystals, suggesting that the amount of acetylated hemicelluloses/lignin remaining in the samples was low. This result contrasts with a previous work where this band was visible in the FTIR spectrum from cellulosic nanocrystals obtained from vine shoots, due to the presence of recalcitrant xylan [68]. This suggests that the structure of the xylan remaining in the CN-RH and CN-RS was different to that of the xylan remaining in the cellulosic nanocrystals from vine shoots, probably presenting a lower degree of acetylation.

The thermal stability of the biomass sources and the extracted cellulosic nanocrystals was also assessed by TGA and the results are shown in Figure 1B. As observed, all the samples presented a main degradation peak with its maximum at ~330 ºC, which corresponds to the thermal degradation of cellulose [25]. This peak was overlapped with a less intense peak with its maximum around 280 ºC, which is typically attributed to the degradation of hemicelluloses [25]. Interestingly, a broad band around 400-550 ºC, which has been previously attributed to lignin degradation [25, 90] was shown with higher intensity in rice husks, both in the raw biomass and the extracted nanocrystals, which is in agreement with the greater lignin content of rice husks as compared with rice straw. These results suggest the presence of a minor fraction of resistant lignin in CN-RH, which most likely may have remained linked to the residual ash (i.e. silica) fraction [91, 92].

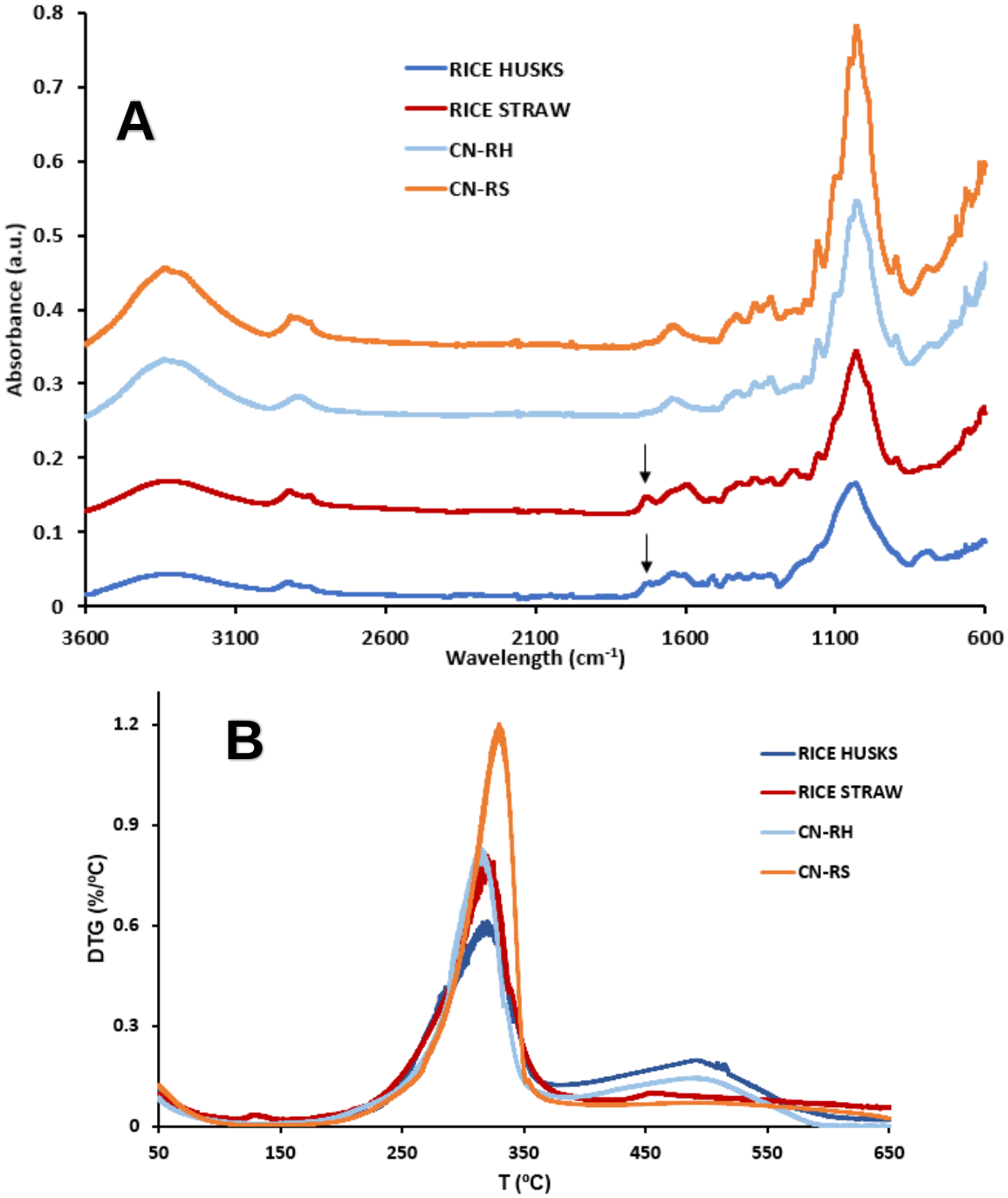

Figure 1. (A) FT-IR spectra and (B) DTG curves of rice husks and rice straw and the corresponding extracted cellulosic nanocrystals. Spectra in (A) have been offset for clarity.

To evaluate the morphology of the extracted cellulosic nanocrystals, they were characterized by TEM and representative images are shown in Figure 2. It could be seen that CN-RH (Figure 2A) had a more heterogeneous appearance, with larger fibrillar structures (some of them greater than 1 µm in length) and a significant degree of agglomeration. On the contrary, CN-RS (Figure 2B) displayed isolated fibrillar structures with much smaller lengths (being the average length 402 ±

12 nm). As suggested by the extraction yields, acid hydrolysis seemed to act more effectively in the case of RS; this might explain the smaller size of the CN-RS, where the amorphous components were digested to a greater extent isolating the cellulose crystallites. Oppositely to what was shown in a previous work [68], the greater amount of resistant xylan fraction remaining in CN-RS did not seem to have a strong impact in preventing the hydrolysis of amorphous cellulose, which again may be pointing towards a different structure of the xylan fraction remaining in each type of biomass. Instead, the more aggregated appearance of CN-RH might be explained by the presence of ashes (i.e. silica) and lignin which would impede a proper penetration of the acid towards the cellulose microfibrils.

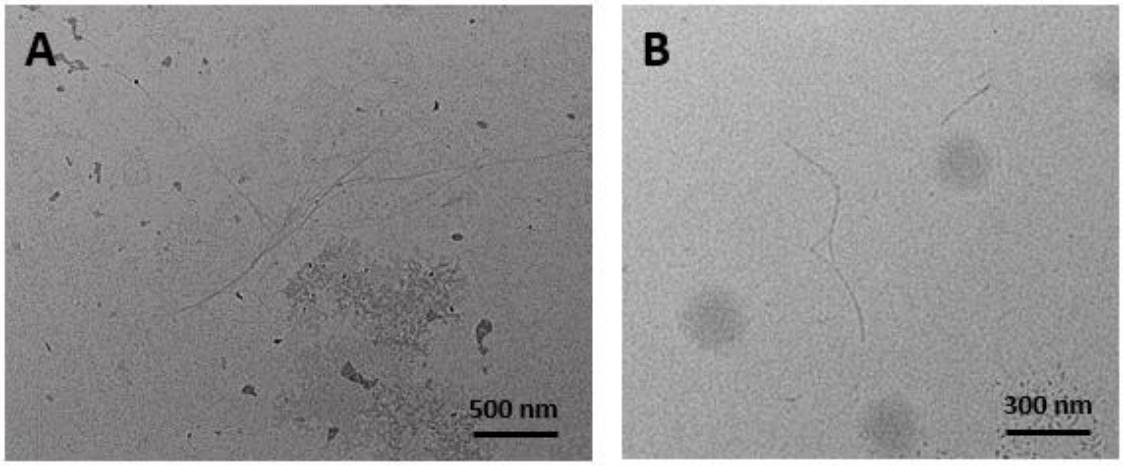

Figure 2. TEM images of the cellulosic nanocrystals extracted from (A) rice husks and (B) rice straw.

XRD analyses were also carried out to investigate the crystalline structure of cellulose in the rice biomass sources and the extracted nanocrystals, and the obtained diffraction patterns are shown in Figure 3. As observed, most of the samples presented similar patterns, which were characterized by the appearance of a broad diffraction band at 13–18° (composed of two overlapped peaks located at 15.0°, 16.6°), followed by a sharper peak located at ca. 22.2°, indicating the presence of crystalline cellulose I [29]. Rice straw presented a slightly different diffraction pattern, where the shoulder at 13–18° was very faint and instead, several small peaks were detected at approximately 14.1°, 14.7°, 24.2°, 29.9° and 32.1°. As expected, the crystallinity values, calculated by mathematically fitting the diffraction patterns, were higher for the cellulosic nanocrystals as compared to the raw biomass sources. The obtained values were 50% for rice husks, 43% for rice straw, 74% for CN-RH and 67% for CN-RS. As observed, cellulose seemed to present a more crystalline structure in rice husks, which is in agreement with the

monosaccharide analyses and would also contribute to the greater extraction yield for the cellulosic nanocrystals from this source. Other similar cellulosic nanocrystals obtained from *P. oceanica* [6] and vine shoots [68] waste biomasses using the same protocols showed crystallinity values of 50% and 85% respectively. This evidences that not only cellulose may present a different crystalline structure depending on the source, but also the composition of the raw biomass is determinant on the effectiveness of the acid hydrolysis treatment.

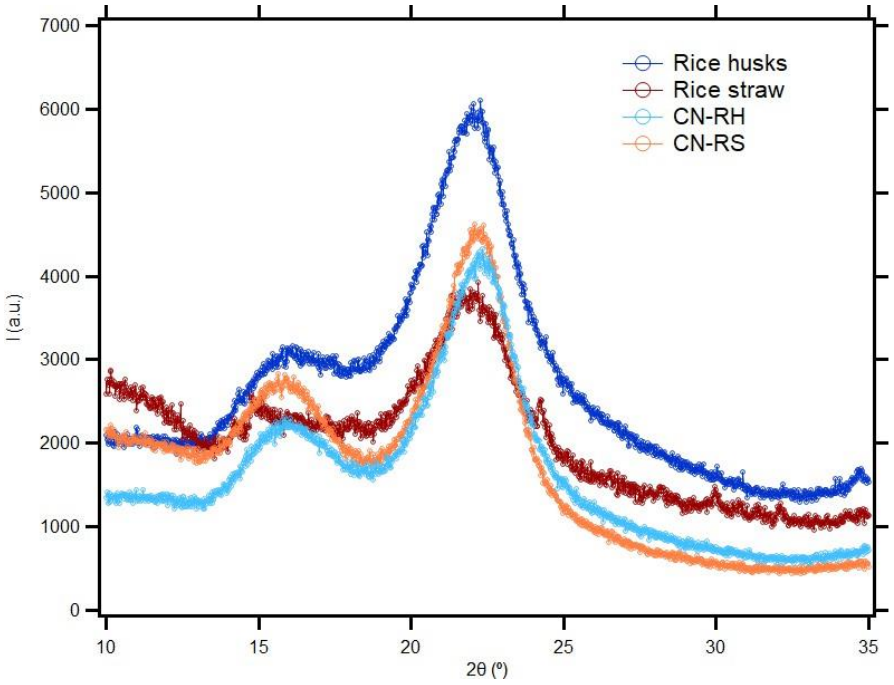

Figure 3. XRD patterns of rice husks and rice straw and the corresponding extracted cellulosic nanocrystals.

4.2 Production and characterization of starch-based biocomposite films

The cellulosic nanocrystals extracted from rice husks and rice straw were used as fillers to improve the properties of starch-based films in which broken rice flour was used as the base material. The morphology of the obtained films was evaluated through examination of their cross-sections by SEM, and representative images are displayed in Figure 4A. As expected, both RS and RF films showed a homogeneous and smooth surface in their cross-sections, derived from the good compatibility between both materials. With regards to the RF biocomposites containing cellulosic nanocrystals, it was clearly observed that those obtained from rice straw (CN-RS) were interspersed into the starchy matrix more homogeneously than those from rice husks (CN-RH), which formed much larger clusters. This can be explained by the inherent difficulty of dispersing the more crystalline CN-RH, which were also seen to form larger fibrillar structures and

aggregated into clusters in their native state due to the greater presence of impurities (cf. Figure 2).

The transparency of the films was evaluated by means of their internal transmittance and results are shown in Figure 4B. As expected, RS showed the highest transparency (~82%), while RF showed a slightly lower transparency (~77%), which can be attributed to the higher purification degree of the former (cf. Table 1). Although the addition of CN-RH decreased the transparency of the RF film (~68%), that was not the case for CN-RS, whose incorporation did not affect the transparency of RF. These results were correlated with the better dispersion of CN-RS within the RF matrix, as suggested by SEM (Figure 4A). With regards to the visual aspect of the films, displayed in Figure 4C, it can be clearly seen how the biocomposite films presented darker yellowish tonalities due to the presence of less purified cellulosic nanocrystals, especially in the case of CN-RH. Furthermore, as a consequence of the poor dispersion of CN-RH within the RF matrix, aggregates could be visually detected in the corresponding film. While transparency is usually a good attribute for food packaging applications, more opaque materials may be useful to prevent the excessive exposure of the food to sunlight or other external oxidative agents.

A

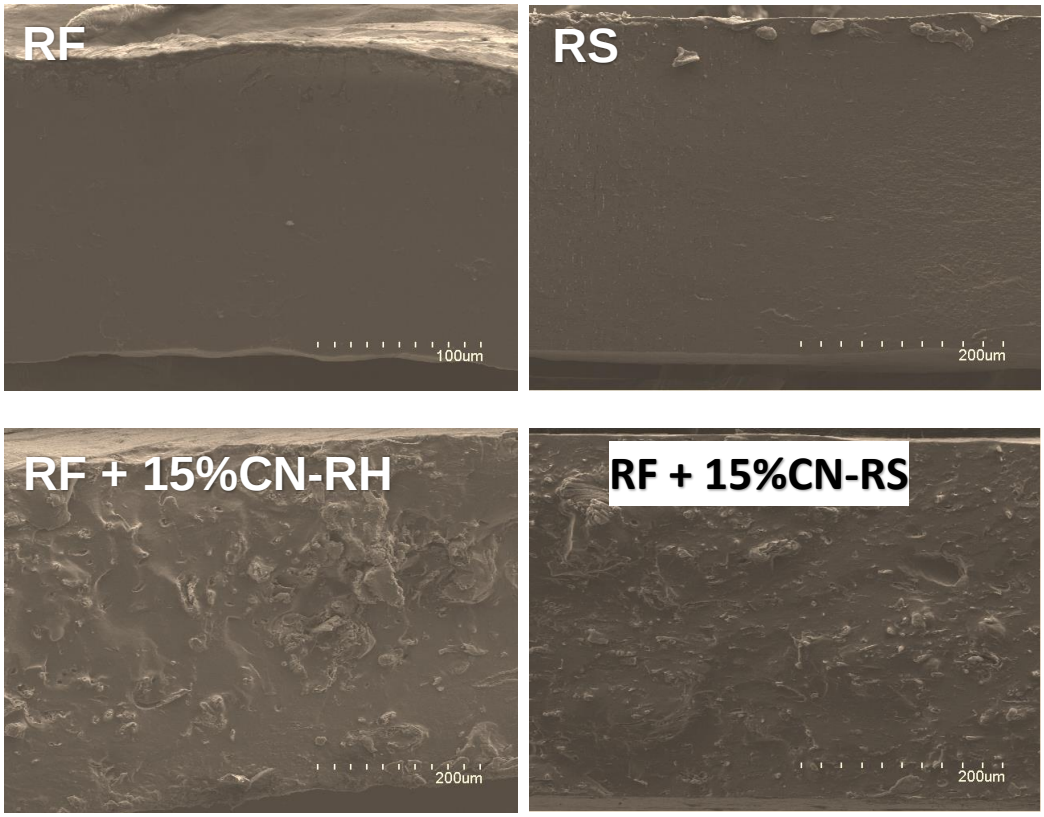

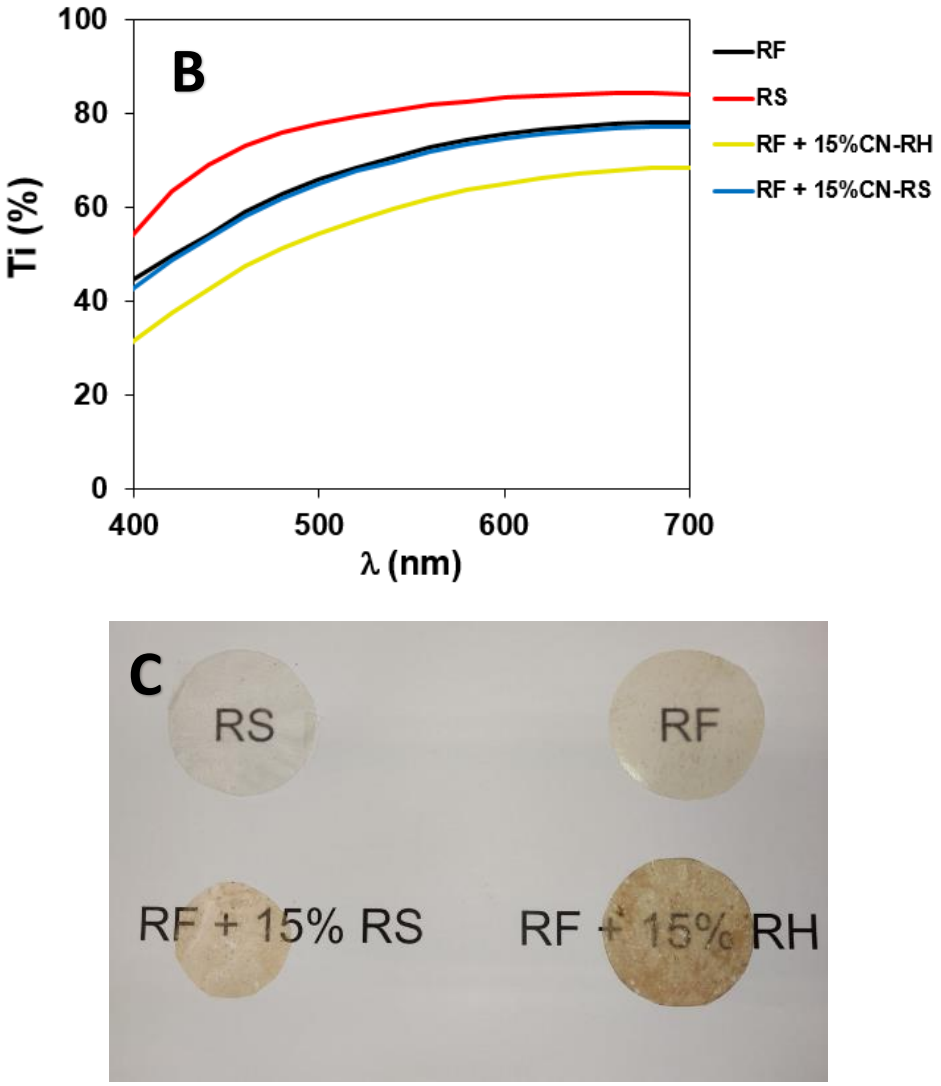

Figure 4. (A) SEM images of the cross-section, (B) contact transparency and (C) visual aspect of the starch-based biocomposite films.

Previous studies have demonstrated that the incorporation of cellulosic fillers has an effect on the gelatinization of starch upon processing in an internal mixer, as well as on the subsequent re-crystallization upon storage of the films [3, 25]. To evaluate the effect of the cellulosic nanocrystals on the crystalline structure of the starch-based films, the rice flour and rice starch before and after being processed into films, as well as the biocomposite films with cellulosic nanocrystals were characterized by XRD and the obtained patterns are shown in Figure 5, while the estimated crystallinity values are summarized in Table S1. As expected, the unprocessed rice flour and rice starch presented diffraction patterns characteristic of the A-type crystalline structure [82, 93], with similar calculated crystallinity indexes for both samples (38-41%), which is reasonable given the small difference in the starch content from both materials. The films obtained after processing the samples in the internal mixer and hot press showed completely different

patterns to those from the unprocessed materials, with diffraction peaks characteristic from the presence of V-type allomorphs. Although starch is expected to undergo gelatinization upon processing in the internal mixer, thus disrupting its crystalline structure, it is able to re-crystallize upon storage under certain relative humidity conditions [94]. However, as it has been previously reported, starch re-crystallizes forming a different crystalline structure to that of the original material [95]. In particular, A-type starch from cereal sources has been seen to re-crystallize into a V-type [3, 25] or B-type structure [96, 97]. Interestingly, while rice flour re-crystallized into a V_A allomorph, rice starch re-crystallized into a V_H structure, which is characterized by the appearance of sharp peaks at 7º, 13º, 20º and 22º [98]. Rice starch samples have been reported to re-crystallize into the V_A allomorph after extrusion in lower moisture conditions [99]. Furthermore, the crystallinity index of the rice flour film (ca. 43%) was greater than that from the rice starch film (ca. 35%). Thus, the presence of minor impurities in the rice flour (mainly proteins and lipids) seemed to have a strong impact on the re-crystallization behavior of starch, as it has been previously observed and ascribed to the presence of rice proteins [100]. According to the estimated crystallinity values (cf. Table S1), starch was able to re-crystallize to a similar extent in all the films, reaching very similar crystallinity values (35-44%).

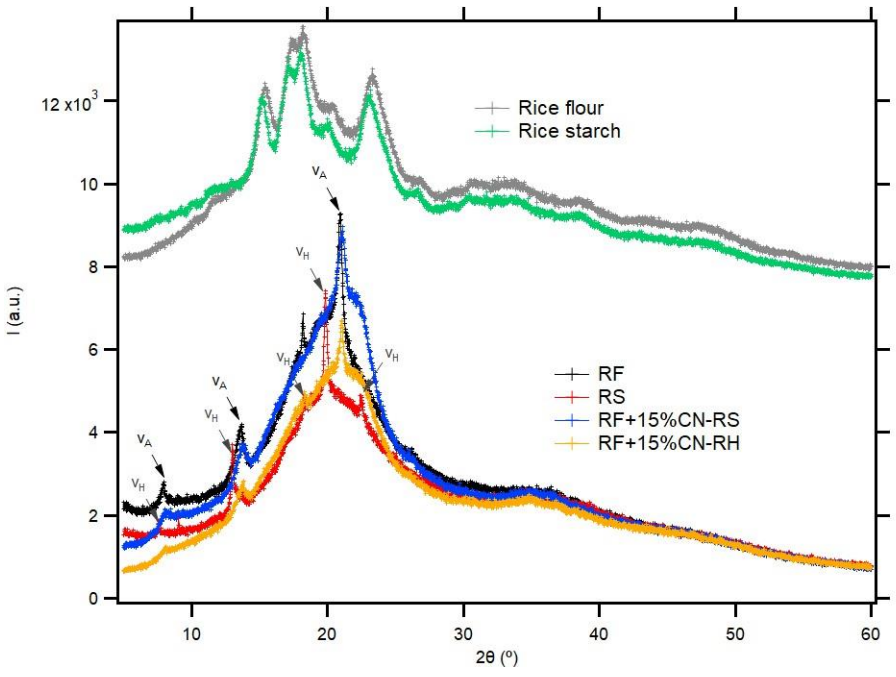

Figure 5. XRD diffraction patterns of (A) both cellulosic biomasses and their respective nanocrystals and (B) rice sources and their film composites with both nanocrystals. Rice flour and rice starch spectra have been offset for clarity.

Mechanical performance and water vapour permeability (WVP) of the starch-based films were characterized and the results are summarized in Table 3. Interestingly, the presence of impurities in rice flour (RF) seemed to have a positive effect on the stiffness of the films, showing a 7-fold and 5-fold increase in the Young's modulus and tensile strength values, respectively, with regards to the films from purified rice starch (RS). On the other hand, the films became less ductile (i.e. the elongation at break was significantly diminished). The more rigid behaviour of the RF films was not unexpected given its greater crystallinity index, as determined by XRD (cf. Table S1). The addition of cellulosic nanocrystals drastically improved the stiffness of the RF films (with more than 200-fold increase in the Young's modulus and up to 10-fold increase in the tensile strength), while the ductility was significantly reduced (lowering the elongation to less than 2%). As expected, the improved dispersion of CN-RS within the RF matrix led to biocomposite films with better mechanical performance than the films containing CN-RH. To the best of our knowledge, there are no previous studies reporting on the characterization of rice flour and rice starch films prepared by melt mixing. However, rice flour and rice starch films prepared by casting and plasticized with 30% glycerol have been previously characterized, showing the rice starch films better performance than those from rice flour [76]. This evidences that the method and the conditions used for the production of starch-based films have a strong impact on their final properties and results from films produced by casting cannot be extrapolated to those prepared by melt mixing. Other rice starch composite films prepared by melt mixing showed a 3-fold improvement for both the Young's modulus and tensile strength values when adding 5-15% (w/w) cellulosic cotton fibres of high aspect ratio (500:1), attaining an optimum improvement at a loading of 10% w/w [101]. Additionally, a previous work also reported on the positive effect of the addition of cellulosic nanocrystals extracted from *P. oceanica* leaves by applying the same protocol used in this work (at loadings of 10-20% w/w) into commercial corn starch [102]. In that case, the stiffness of the films was increased up to 17-fold with respect to the neat starch [102].

Regarding WVP, as deduced from Table 3, the presence of other compounds apart from starch in RF had a negative impact, having the RS film ~30% lower permeability than the RF film. In fact, the greater amounts of proteins and lipids in RF have been previously reported to result in higher diffusion coefficients for RF films as compared with RS [103]. On the other hand, the addition of cellulosic nanocrystals reduced ca. 30-40% the WVP of the RF films, demonstrating again the potential of the less purified nanocrystals as fillers to improve the properties of starch-based films. In this case, despite their uneven dispersion in the RF matrix, CN-RH were able to improve the water barrier to a similar extent that CN-RS. This might be explained by the higher crystallinity of CN-RH, thus acting as barrier elements and limiting water vapour diffusion through the films. Furthermore, the presence of a greater amount of lignin and ashes in CN-RH might have also contributed to a greater barrier capacity due to the more hydrophobic character of lignin and the

water sorption capacity of some minerals [104]. Several previous works have already reported that the addition of cellulosic nanocrystals [102, 105, 106] or less purified cellulose-based fractions [25] can significantly enhance the mechanical properties and the water vapour barrier of starch-based materials. In line with that, in this work we have gone a step further and demonstrated that it is possible to produce biocomposite materials fully based on less purified starch-based and cellulose-based fractions obtained by valorising the agroindustrial residues from rice crops. Interestingly, these biocomposites presented greater rigidity and water vapour barrier than the films from purified rice starch, hence showing the potential of these materials from an environmental and functional perspective.

Table 3. Mechanical properties (Young's modulus (E), tensile strength (TS) and elongation at break (ε) and water vapor permeability (WVP) starch-based films. Different letters in each column show significantly different values ($p \leq 0.05$).

	E (MPa)	**TS (MPa)**	**ε (%)**	**WVP (Kg·m/s·m^2·Pa) ·10^{-13}**
RS	0.8 ± 0.1^a	0.3 ± 0.0^a	48.9 ± 5.7^a	2.5 ± 0.1^b
RF	5.4 ± 1.6^b	1.5 ± 0.1^b	22.5 ± 4.1^b	3.5 ± 0.2^a
RF + 15% CN-RH	1232.2 ± 122.9^c	8.3 ± 1.4^c	1.1 ± 0.2^c	2.1 ± 0.3^b
RF + 15% CN- RS	1579.1 ± 58.8^d	15.7 ± 2.0^d	1.5 ± 0.3^c	2.3 ± 0.1^b

According to the literature, rice husks and rice straw, as well as white rice (although to a lesser extent), contain a remarkable amount of phenolic compounds such as *p*-coumaric, caffeic and ferulic acids [78, 79, 107]. Since the biocomposites developed in this work were composed of less purified materials, such as rice flour and cellulose-based nanocrystals containing hemicelluloses and other minor impurities, it was hypothesized that some of the bioactive compounds present in the raw biomass sources might remain in the produced materials. To test

the potential bioactivity of the developed films, their antioxidant capacity was determined by means of the β-carotene bleaching inhibition assay. An additional sample consisting of a commercial corn starch film was also tested as a control. The results, gathered in Table 4, evidenced that all the films had a significant inhibitory effect as compared to the commercial corn starch film. While the commercial corn starch film showed inhibition of ~5%, the RS films presented inhibition of ca. 12%, which may be explained by the simplified purification process applied for the extraction of rice starch (described in section 2.2) leading to the presence of minor impurities in the material. Notably, the RF films displayed a significantly higher inhibition value of ca. 21%, according to their lower purification degree. The incorporation of cellulosic nanocrystals did not produce a significant increase in the antioxidant potential of the films, providing inhibition values of 25 and 24% for CN-RH and CN-RS, respectively. Previous studies have demonstrated the antioxidant capacity of similar less purified cellulosic fractions; however, the inhibition values were lower or very similar to those from the non-purified rice flour. For instance, cellulosic films from *Arundo donax* leaves and stems showed 6% inhibition [50], while cellulosic films from *Tempranillo* vine shoots showed up to 30% inhibition [68]. Thus, it seems that the antioxidant potential of the films was mainly provided by the bioactive compounds present in the rice flour matrix. These results demonstrate again the potential of using materials with lower purification degree, which can not only be competitive from an economical point of view, but also in terms of providing additional functionalities.

Table 4. β-carotene bleaching inhibition of starch-based films and control samples. Different letters show significantly different values ($p \leq 0.05$).

	β-carotene bleaching inhibition (%)
RS	12.1 ± 2.2^{b}
RF	21.1 ± 0.9^{c}
RF + CN-RH	24.8 ± 2.4^{c}
RF + CN-RS	24.4 ± 2.3^{c}
Commercial Corn Starch	5.2 ± 0.8^{a}
Control (+)	97.7 ± 0.9
Control (-)	3.1 ± 0.7

5. Conclusions

Sustainable biocomposite films with improved properties for food packaging applications have been prepared by valorising three agroindustrial by-products from white rice (*Oryza sativa*). Rice flour (with ca. 90% of starch) was used, unprocessed and after being subjected to a simplified starch purification method, to produce the film matrix materials. On the other hand, rice husks and straw (with apparent holocellulose contents of ca. 71-78%) were used to produce less purified cellulosic nanocrystals by means of a simplified protocol, attaining yields of 39-53%. The cellulosic nanocrystals from rice husks (CN-RH) presented higher crystallinity (74%) and a more heterogeneous morphology, with large and agglomerated fibrillar structures due to the greater presence of structural impurities, such as ashes and lignin, than the nanocrystals from rice straw (CN-RS). The latter showed a crystallinity index of 67% and homogeneous fibrils with ca. 400 nm length.

Starch-based films were then produced by melt mixing using the unprocessed rice flour (RF) and the purified rice starch (RS), and the extracted cellulosic nanocrystals were used as fillers at a loading of 15% w/w in the RF films. The presence of minor impurities, mainly proteins and lipids, in RF had a significant effect on the re-crystallization of starch after the melt mixing step, producing more crystalline films with lower transparency and more rigid behaviour than RS. On the other hand, these impurities reduced the water vapour barrier of the RF films, but conferred them much greater antioxidant capacity than that of RS and commercial starch films. The incorporation of cellulosic nanocrystals drastically improved the stiffness of the RF films, being this effect more evident with CN-RS. This was explained by the better dispersion of these nanocrystals as compared to CN-RH, which also led to more transparent and homogeneous films. Furthermore, both CN-RS and CN-RH were able to improve the barrier of RF films and provide similar antioxidant capacities. These results highlight the potential of valorising agroindustrial waste biomass to extract less purified biopolymers with interest for the development of food packaging materials with a more sustainable character and improved functional properties.

6. Supplementary Material

Table S1. Crystallinity index (%) and starch crystalline allomorph of the starch-based fractions and films.

	Xc (%)	Allomorph
Rice Flour	38	A
Rice Starch	41	A
Rice Flour + 30%Gly	43	V_A
Rice Starch + 30%Gly	35	V_H
Rice Flour + 15% NANO F2A RH	44	V_A
Rice Flour + 15% NANO F2A RS	44	V_A

List of references of Chapter 3:

[1] G.F. Schirinzi, M. Köck-Schulmeyer, M. Cabrera, D. González-Fernández, G. Hanke, M. Farré, D. Barceló, Riverine anthropogenic litter load to the Mediterranean Sea near the metropolitan area of Barcelona, Spain, Science of The Total Environment 714 (2020) 136807.
[2] A. Ahmadi, S. Zorofchian Moghadamtousi, S. Abubakar, K. Zandi, Antiviral potential of algae polysaccharides isolated from marine sources: a review, BioMed research international 2015 (2015).
[3] I. Benito-González, A. López-Rubio, M. Martínez-Sanz, High-performance starch biocomposites with celullose from waste biomass: Film properties and retrogradation behaviour, Carbohydrate polymers 216 (2019) 180-188.
[4] E. Fortunati, F. Luzi, D. Puglia, R. Petrucci, J. Kenny, L. Torre, Processing of PLA nanocomposites with cellulose nanocrystals extracted from Posidonia oceanica waste: Innovative reuse of coastal plant, Industrial Crops and Products 67 (2015) 439-447.
[5] R. Ilyas, S. Sapuan, M. Ishak, E. Zainudin, M. Atikah, Nanocellulose reinforced starch polymer composites: A review of preparation, properties and application, Proceeding: 5th International Conference on Applied Sciences and Engineering (ICASEA, 2018), Global Academic Excellence (M) SDN BHD Capthorne Hotel, Cameron Highlands …, 2018, pp. 325-341.
[6] I. Benito-González, A. López-Rubio, R. Gavara, M. Martínez-Sanz, Cellulose nanocrystal-based films produced by more sustainable extraction protocols from Posidonia oceanica waste biomass, Cellulose 26(13-14) (2019) 8007-8024.
[7] I. Mediavilla, M. Fernández, L. Esteban, Optimization of pelletisation and combustion in a boiler of 17.5 kWth for vine shoots and industrial cork residue, Fuel Processing Technology 90(4) (2009) 621-628.
[8] B.M. Jenkins, A.D. Jones, S.Q. Turn, R.B. Williams, Emission factors for polycyclic aromatic hydrocarbons from biomass burning, Environmental Science & Technology 30(8) (1996) 2462-2469.
[9] L. Jiménez, V. Angulo, A. Rodríguez, R. Sánchez, A. Ferrer, Pulp and paper from vine shoots: Neural fuzzy modeling of ethylene glycol pulping, Bioresource technology 100(2) (2009) 756-762.
[10] L. Jiménez, V. Angulo, E. Ramos, M. De la Torre, J. Ferrer, Comparison of various pulping processes for producing pulp from vine shoots, Industrial Crops and Products 23(2) (2006) 122-130.
[11] M. El Achaby, N. El Miri, H. Hannache, S. Gmouh, A. Aboulkas, Production of cellulose nanocrystals from vine shoots and their use for the development of nanocomposite materials, International journal of biological macromolecules 117 (2018) 592-600.
[12] H.N. Rajha, N. Boussetta, N. Louka, R.G. Maroun, E. Vorobiev, A comparative study of physical pretreatments for the extraction of polyphenols and proteins from vine shoots, Food Research International 65 (2014) 462-468.
[13] G. Bustos, A.B. Moldes, J.M. Cruz, J.M. Domínguez, Influence of the metabolism pathway on lactic acid production from hemicellulosic trimming vine shoots hydrolyzates using Lactobacillus pentosus, Biotechnology progress 21(3) (2005) 793-798.
[14] T. Tappi, Ash in wood, pulp, paper and paperboard: combustion at 525 C, TAPPI test methods T 211 (1993).
[15] P.G. Wiles, I.K. Gray, R.C. Kissling, Routine analysis of proteins by Kjeldahl and Dumas methods: review and interlaboratory study using dairy products, Journal of AOAC International 81(3) (1998) 620-632.
[16] V.L. Singleton, R. Orthofer, R.M. Lamuela-Raventós, [14] Analysis of total phenols and other oxidation substrates and antioxidants by means of folin-ciocalteu reagent, Methods in enzymology 299 (1999) 152-178.
[17] J.F. Saeman, Kinetics of Wood Saccharification - Hydrolysis of Cellulose and Decomposition of Sugars in Dilute Acid at High Temperature, Industrial & Engineering Chemistry 37(1) (1945) 43-52.
[18] A. Lopez-Rubio, B.M. Flanagan, E.P. Gilbert, M.J. Gidley, A novel approach for calculating starch crystallinity and its correlation with double helix content: A combined XRD and NMR study, Biopolymers 89(9) (2008) 761-768.
[19] ASTM, Standard test method for tensile properties of plastics, ASTM International2010.
[20] H. Miller, A simplified method for the evaluation of antioxidants, Journal of the American Oil Chemists Society 48(2) (1971) 91-91.

[21] J.M. Luque-Rodríguez, P. Pérez-Juan, M.D. Luque De Castro, Extraction of polyphenols from vine shoots of Vitis vinifera by superheated ethanol− water mixtures, Journal of agricultural and food chemistry 54(23) (2006) 8775-8781.
[22] I. Dávila, O. Gordobil, J. Labidi, P. Gullón, Assessment of suitability of vine shoots for hemicellulosic oligosaccharides production through aqueous processing, Bioresource technology 211 (2016) 636-644.
[23] L. Jiménez, A. Pérez, M.J. de la Torre, A. Moral, L. Serrano, Characterization of vine shoots, cotton stalks, Leucaena leucocephala and Chamaecytisus proliferus, and of their ethyleneglycol pulps, Bioresource technology 98(18) (2007) 3487-3490.
[24] X. Sun, F. Xu, R. Sun, P. Fowler, M. Baird, Characteristics of degraded cellulose obtained from steam-exploded wheat straw, Carbohydrate research 340(1) (2005) 97-106.
[25] I. Benito-González, A. López-Rubio, M. Martínez-Sanz, Potential of lignocellulosic fractions from Posidonia oceanica to improve barrier and mechanical properties of bio-based packaging materials, International journal of biological macromolecules 118 (2018) 542-551.
[26] I. Egüés, A. Eceiza, J. Labidi, Effect of different hemicelluloses characteristics on film forming properties, Industrial Crops and Products 47 (2013) 331-338.
[27] P. Satyamurthy, P. Jain, R.H. Balasubramanya, N. Vigneshwaran, Preparation and characterization of cellulose nanowhiskers from cotton fibres by controlled microbial hydrolysis, Carbohydrate Polymers 83(1) (2011) 122-129.
[28] J. Gariñena, M. Amparo, Análisis de la evolución de las exportaciones del sector vitivinícola en la Comunidad Valenciana, 2016.
[29] L.H. Thomas, V.T. Forsyth, A. Šturcová, C.J. Kennedy, R.P. May, C.M. Altaner, D.C. Apperley, T.J. Wess, M.C. Jarvis, Structure of cellulose microfibrils in primary cell walls from collenchyma, Plant physiology 161(1) (2013) 465-476.
[30] M. Martínez-Sanz, V. Cebrián-Lloret, J. Mazarro-Ruiz, A. López-Rubio, Improved performance of less purified cellulosic films obtained from agar waste biomass, Carbohydrate Polymers (2020) 115887.
[31] H. Kargarzadeh, I. Ahmad, I. Abdullah, A. Dufresne, S.Y. Zainudin, R.M. Sheltami, Effects of hydrolysis conditions on the morphology, crystallinity, and thermal stability of cellulose nanocrystals extracted from kenaf bast fibers, Cellulose 19(3) (2012) 855-866.
[32] M. Martínez-Sanz, A. Lopez-Rubio, J.M. Lagaron, Optimization of the nanofabrication by acid hydrolysis of bacterial cellulose nanowhiskers, Carbohydrate Polymers 85(1) (2011) 228-236.
[33] S.O. Prozil, E.V. Costa, D.V. Evtuguin, L.P. Cruz Lopes, M.R.M. Domingues, Structural characterization of polysaccharides isolated from grape stalks of Vitis vinifera L, Carbohydr. Res. 356 (2012) 252-259.
[34] A. Martínez-Abad, N. Giummarella, M. Lawoko, F. Vilaplana, Differences in extractability under subcritical water reveal interconnected hemicellulose and lignin recalcitrance in birch hardwoods, Green Chemistry (2018).
[35] M. Martínez-Sanz, F. Pettolino, B. Flanagan, M.J. Gidley, E.P. Gilbert, Structure of cellulose microfibrils in mature cotton fibres, Carbohydrate polymers 175 (2017) 450-463.
[36] N.J. Grantham, J. Wurman-Rodrich, O.M. Terrett, J.J. Lyczakowski, K. Stott, D. Iuga, T.J. Simmons, M. Durand-Tardif, S.P. Brown, R. Dupree, M. Busse-Wicher, P. Dupree, An even pattern of xylan substitution is critical for interaction with cellulose in plant cell walls, Nature Plants 3(11) (2017) 859-865.
[37] Z. Jaafar, K. Mazeau, A. Boissière, S. Le Gall, A. Villares, J. Vigouroux, N. Beury, C. Moreau, M. Lahaye, B. Cathala, Meaning of xylan acetylation on xylan-cellulose interactions: A quartz crystal microbalance with dissipation (QCM-D) and molecular dynamic study, Carbohydr Polym 226 (2019).
[38] A. Martínez-Abad, J. Berglund, G. Toriz, P. Gatenholm, G. Henriksson, M. Lindström, J. Wohlert, F. Vilaplana, Regular motifs in xylan modulate molecular flexibility and interactions with cellulose surfaces, Plant Physiol. 175(4) (2017) 1579-1592.
[39] M. Martínez-Sanz, D. Mikkelsen, B.M. Flanagan, M.J. Gidley, E.P. Gilbert, Multi-scale characterisation of deuterated cellulose composite hydrogels reveals evidence for different interaction mechanisms with arabinoxylan, mixed-linkage glucan and xyloglucan, Polymer 124 (2017) 1-11.
[40] M. Martínez-Sanz, P. Lopez-Sanchez, M.J. Gidley, E.P. Gilbert, Evidence for differential interaction mechanism of plant cell wall matrix polysaccharides in hierarchically-structured bacterial cellulose, Cellulose 22(3) (2015) 1541-1563.

[41] S.O. Prozil, D.V. Evtuguin, L.P.C. Lopes, Chemical composition of grape stalks of Vitis vinifera L. from red grape pomaces, Industrial Crops and Products 35(1) (2012) 178-184.
[42] M. Martínez-Sanz, A. Lopez-Rubio, J.M. Lagaron, High-barrier coated bacterial cellulose nanowhiskers films with reduced moisture sensitivity, Carbohydrate polymers 98(1) (2013) 1072-1082.
[43] M. Martínez-Sanz, A. Martínez-Abad, A. López-Rubio, Cost-efficient bio-based food packaging films from unpurified agar-based extracts, Food Packaging and Shelf Life 21 (2019) 100367.
[44] J.W. Rhim, Physical-mechanical properties of agar/κ-carrageenan blend film and derived clay nanocomposite film, Journal of Food Science 77(12) (2012) N66-N73.
[45] P. Guerrero, A. Etxabide, I. Leceta, M. Peñalba, K. De la Caba, Extraction of agar from Gelidium sesquipedale (Rodhopyta) and surface characterization of agar based films, Carbohydrate polymers 99 (2014) 491-498.
[46] S. Shankar, J.-W. Rhim, Preparation of nanocellulose from micro-crystalline cellulose: The effect on the performance and properties of agar-based composite films, Carbohydrate polymers 135 (2016) 18-26.
[47] J.-W. Rhim, J.P. Reddy, X. Luo, Isolation of cellulose nanocrystals from onion skin and their utilization for the preparation of agar-based bio-nanocomposites films, Cellulose 22(1) (2015) 407-420.
[48] S.M. Bhasney, P. Bhagabati, A. Kumar, V. Katiyar, Morphology and crystalline characteristics of polylactic acid [PLA]/linear low density polyethylene [LLDPE]/microcrystalline cellulose [MCC] fiber composite, Composites Science and Technology 171 (2019) 54-61.
[49] D. Edith, J.-L. Six, Surface characteristics of PLA and PLGA films, Applied Surface Science 253(5) (2006) 2758-2764.
[50] C. Fontes-Candia, E. Erboz, A. Martínez-Abad, A. López-Rubio, M. Martínez-Sanz, Superabsorbent food packaging bioactive cellulose-based aerogels from Arundo donax waste biomass, Food Hydrocolloids 96 (2019) 151-160.
[51] J.N. Hahladakis, C.A. Velis, R. Weber, E. Iacovidou, P. Purnell, An overview of chemical additives present in plastics: Migration, release, fate and environmental impact during their use, disposal and recycling, Journal of hazardous materials 344 (2018) 179-199.
[52] N.A. Welden, The environmental impacts of plastic pollution, Plastic Waste and Recycling, Elsevier2020, pp. 195-222.
[53] H.H. Khoo, LCA of plastic waste recovery into recycled materials, energy and fuels in Singapore, Resources, Conservation and Recycling 145 (2019) 67-77.
[54] M.G. Rao, P. Bharathi, R. Akila, A comprehensive review on biopolymers, Sci. Revs. Chem. Commun 4(2) (2014) 61-68.
[55] H.H. Khoo, R.B. Tan, K.W. Chng, Environmental impacts of conventional plastic and bio-based carrier bags, The international journal of life cycle assessment 15(3) (2010) 284-293.
[56] T.P. Haider, C. Völker, J. Kramm, K. Landfester, F.R. Wurm, Plastics of the future? The impact of biodegradable polymers on the environment and on society, Angewandte Chemie International Edition 58(1) (2019) 50-62.
[57] E. Fuentes-Zaragoza, M. Riquelme-Navarrete, E. Sánchez-Zapata, J. Pérez-Álvarez, Resistant starch as functional ingredient: A review, Food Research International 43(4) (2010) 931-942.
[58] H. Li, M.A. Huneault, Comparison of sorbitol and glycerol as plasticizers for thermoplastic starch in TPS/PLA blends, Journal of Applied Polymer Science 119(4) (2011) 2439-2448.
[59] M.J. Fabra, M. Martínez-Sanz, L.G. Gómez-Mascaraque, R. Gavara, A. López-Rubio, Structural and physicochemical characterization of novel thermoplastic corn starch films containing microalgae, Carbohydrate Polymers Under review (2017).
[60] E. Rudnik, N. Milanov, G. Matuschek, A. Kettrup, Ecotoxicity of biocomposites based on renewable feedstock–Preliminary studies, Chemosphere 70(2) (2007) 337-340.
[61] S. Ventura-Cruz, A. Tecante, | Nanocellulose and microcrystalline cellulose from agricultural waste: Review on isolation and application as reinforcement in polymeric matrices, Food Hydrocolloids (2021) 106771.
[62] H.A. Khalil, A. Bhat, A.I. Yusra, Green composites from sustainable cellulose nanofibrils: A review, Carbohydrate polymers 87(2) (2012) 963-979.

[63] F. Bettaieb, R. Khiari, M.L. Hassan, M.N. Belgacem, J. Bras, A. Dufresne, M.F. Mhenni, Preparation and characterization of new cellulose nanocrystals from marine biomass Posidonia oceanica, Industrial Crops and Products 72 (2015) 175-182.
[64] P. Preethi, Physical and chemical properties of banana fibre extracted from commercial banana cultivars grown in Tamilnadu State, (2011).
[65] R. Liu, H. Yu, Y. Huang, Structure and morphology of cellulose in wheat straw, Cellulose 12(1) (2005) 25-34.
[66] I. Gonçalves, J. Lopes, A. Barra, D. Hernández, C. Nunes, K. Kapusniak, J. Kapusniak, D.V. Evtyugin, J.A.L. da Silva, P. Ferreira, Tailoring the surface properties and flexibility of starch-based films using oil and waxes recovered from potato chips byproducts, International Journal of Biological Macromolecules 163 (2020) 251-259.
[67] J. Lopes, I. Gonçalves, C. Nunes, B. Teixeira, R. Mendes, P. Ferreira, M.A. Coimbra, Potato peel phenolics as additives for developing active starch-based films with potential to pack smoked fish fillets, Food Packaging and Shelf Life 28 (2021) 100644.
[68] I. Benito-González, C.M. Jaén-Cano, A. López-Rubio, A. Martínez-Abad, M. Martínez-Sanz, Valorisation of vine shoots for the development of cellulose-based biocomposite films with improved performance and bioactivity, International Journal of Biological Macromolecules (2020).
[69] R. Khiari, Valorization of agricultural residues for cellulose nanofibrils production and their use in nanocomposite manufacturing, International Journal of Polymer Science 2017 (2017).
[70] C. Sarnklong, J. Cone, W. Pellikaan, W. Hendriks, Utilization of rice straw and different treatments to improve its feed value for ruminants: a review, Asian-Australasian Journal of Animal Sciences 23(5) (2010) 680-692.
[71] M. Iranzo, J.V. Cañizares, L. Roca-Perez, I. Sainz-Pardo, S. Mormeneo, R. Boluda, Characteristics of rice straw and sewage sludge as composting materials in Valencia (Spain), Bioresource Technology 95(1) (2004) 107-112.
[72] G. Totaro, L. Sisti, M. Vannini, P. Marchese, A. Tassoni, M.S. Lenucci, M. Lamborghini, S. Kalia, A. Celli, A new route of valorization of rice endosperm by-product: production of polymeric biocomposites, Composites Part B: Engineering 139 (2018) 195-202.
[73] D. de Souza, A.F. Sbardelotto, D.R. Ziegler, L.D.F. Marczak, I.C. Tessaro, Characterization of rice starch and protein obtained by a fast alkaline extraction method, Food Chemistry 191 (2016) 36-44.
[74] P. Lu, Y.-L. Hsieh, Preparation and characterization of cellulose nanocrystals from rice straw, Carbohydrate Polymers 87(1) (2012) 564-573.
[75] S.Y. Ooi, I. Ahmad, M.C.I.M. Amin, Cellulose nanocrystals extracted from rice husks as a reinforcing material in gelatin hydrogels for use in controlled drug delivery systems, Industrial Crops and Products 93 (2016) 227-234.
[76] A.B. Dias, C.M. Müller, F.D. Larotonda, J.B. Laurindo, Biodegradable films based on rice starch and rice flour, Journal of cereal science 51(2) (2010) 213-219.
[77] A.B. Dias, C.M. Müller, F.D. Larotonda, J.B. Laurindo, Mechanical and barrier properties of composite films based on rice flour and cellulose fibers, LWT-Food Science and Technology 44(2) (2011) 535-542.
[78] P.A. Freitas, C. González-Martínez, A. Chiralt, Application of Ultrasound Pre-Treatment for Enhancing Extraction of Bioactive Compounds from Rice Straw, Foods 9(11) (2020) 1657.
[79] Y. Gao, X. Guo, Y. Liu, Z. Fang, M. Zhang, R. Zhang, L. You, T. Li, R.H. Liu, A full utilization of rice husk to evaluate phytochemical bioactivities and prepare cellulose nanocrystals, Scientific reports 8(1) (2018) 1-8.
[80] G.A. De Ruiter, H.A. Schols, A.G. Voragen, F.M. Rombouts, Carbohydrate analysis of water-soluble uronic acid-containing polysaccharides with high-performance anion-exchange chromatography using methanolysis combined with TFA hydrolysis is superior to four other methods, Analytical biochemistry 207(1) (1992) 176-185.
[81] M. Martínez-Sanz, P. Lopez-Sanchez, M. Gidley, E. Gilbert, Evidence for differential interaction mechanism of plant cell wall matrix polysaccharides in hierarchically-structured bacterial cellulose, Cellulose 22(3) (2015).

[82] A. Lopez-Rubio, B.M. Flanagan, E.P. Gilbert, M.J. Gidley, A novel approach for calculating starch crystallinity and its correlation with double helix content: A combined XRD and NMR study, Biopolymers: Original Research on Biomolecules 89(9) (2008) 761-768.
[83] Y. Nakamura, Y. Ono, T. Saito, A. Isogai, Characterization of cellulose microfibrils, cellulose molecules, and hemicelluloses in buckwheat and rice husks, Cellulose 26(11) (2019) 6529-6541.
[84] M.S. Ismail, A. Waliuddin, Effect of rice husk ash on high strength concrete, Construction and building materials 10(7) (1996) 521-526.
[85] H. Pastell, L. Virkki, E. Harju, P. Tuomainen, M. Tenkanen, Presence of 1→ 3-linked 2-O-β-d-xylopyranosyl-α-l-arabinofuranosyl side chains in cereal arabinoxylans, Carbohydrate research 344(18) (2009) 2480-2488.
[86] R. Requena, A. Jiménez-Quero, M.a. Vargas, R. Moriana, A. Chiralt, F. Vilaplana, Integral fractionation of rice husks into bioactive arabinoxylans, cellulose nanocrystals, and silica particles, ACS Sustainable Chemistry & Engineering 7(6) (2019) 6275-6286.
[87] F. Gu, W. Wang, L. Jing, Y. Jin, Effects of green liquor pretreatment on the chemical composition and enzymatic digestibility of rice straw, Bioresource technology 149 (2013) 375-382.
[88] S. Rivas, E. Conde, A. Moure, H. Domínguez, J.C. Parajó, Characterization, refining and antioxidant activity of saccharides derived from hemicelluloses of wood and rice husks, Food chemistry 141(1) (2013) 495-502.
[89] A. Martínez-Abad, A. Jiménez-Quero, J. Wohlert, F. Vilaplana, Influence of the molecular motifs of mannan and xylan populations on their recalcitrance and organization in spruce softwoods, Green Chemistry 22(12) (2020) 3956-3970.
[90] Z. Ma, Q. Sun, J. Ye, Q. Yao, C. Zhao, Study on the thermal degradation behaviors and kinetics of alkali lignin for production of phenolic-rich bio-oil using TGA–FTIR and Py–GC/MS, Journal of Analytical and Applied Pyrolysis 117 (2016) 116-124.
[91] A. Ma'ruf, B. Pramudono, N. Aryanti, Lignin isolation process from rice husk by alkaline hydrogen peroxide: Lignin and silica extracted, AIP Conference Proceedings, AIP Publishing LLC, 2017, p. 020013.
[92] Y. Qu, Y. Tian, B. Zou, J. Zhang, Y. Zheng, L. Wang, Y. Li, C. Rong, Z. Wang, A novel mesoporous lignin/silica hybrid from rice husk produced by a sol–gel method, Bioresource technology 101(21) (2010) 8402-8405.
[93] F. Shih, J. King, K. Daigle, H.J. An, R. Ali, Physicochemical properties of rice starch modified by hydrothermal treatments, Cereal Chemistry 84(5) (2007) 527-531.
[94] S. Wang, C. Li, L. Copeland, Q. Niu, S. Wang, Starch retrogradation: A comprehensive review, Comprehensive Reviews in Food Science and Food Safety 14(5) (2015) 568-585.
[95] M.J. Fabra, M. Martínez-Sanz, L.G. Gómez-Mascaraque, R. Gavara, A. López-Rubio, Structural and physicochemical characterization of thermoplastic corn starch films containing microalgae, Carbohydrate polymers 186 (2018) 184-191.
[96] Z.-q. Fu, L.-j. Wang, D. Li, Y.-g. Zhou, B. Adhikari, The effect of partial gelatinization of corn starch on its retrogradation, Carbohydrate polymers 97(2) (2013) 512-517.
[97] K. Shamai, H. Bianco-Peled, E. Shimoni, Polymorphism of resistant starch type III, Carbohydrate Polymers 54(3) (2003) 363-369.
[98] A. Buleon, P. Le Bail, P. Colonna, H. Bizot, Phase and polymorphic transitions of starches at low and intermediate water contents, The Properties of Water in Foods ISOPOW 6, Springer1998, pp. 160-178.
[99] J.J. Van Soest, S. Hulleman, D. De Wit, J. Vliegenthart, Crystallinity in starch bioplastics, Industrial Crops and Products 5(1) (1996) 11-22.
[100] Y. Wu, Z. Chen, X. Li, Z. Wang, Retrogradation properties of high amylose rice flour and rice starch by physical modification, LWT-Food Science and Technology 43(3) (2010) 492-497.
[101] J. Prachayawarakorn, P. Sangnitidej, P. Boonpasith, Properties of thermoplastic rice starch composites reinforced by cotton fiber or low-density polyethylene, Carbohydrate Polymers 81(2) (2010) 425-433.
[102] I. Benito-González, G. Göksen, Z. Pérez-Bassart, A. López-Rubio, R. Sánchez, J.M. Alonso, R. Gavara, M. Gallur, M. Martínez-Sanz, Pilot plant scale-up of the production of optimized starch-biocomposites loaded with cellulose nanocrystals from *Posidonia oceanica* waste biomass, Food Packaging and Shelf Life *Accepted* (2021).

[103] M. Majzoobi, Y. Pesaran, G. Mesbahi, M.T. Golmakani, A. Farahnaky, Physical properties of biodegradable films from heat-moisture-treated rice flour and rice starch, Starch-Stärke 67(11-12) (2015) 1053-1060.
[104] L. Fusade, H. Viles, C. Wood, C. Burns, The effect of wood ash on the properties and durability of lime mortar for repointing damp historic buildings, Construction and Building Materials 212 (2019) 500-513.
[105] A.P.M. Silva, A.V. Oliveira, S.M. Pontes, A.L. Pereira, M.F. Rosa, H.M. Azeredo, Mango kernel starch films as affected by starch nanocrystals and cellulose nanocrystals, Carbohydrate polymers 211 (2019) 209-216.
[106] J. Alves, K. Dos Reis, E. Menezes, F. Pereira, J. Pereira, Effect of cellulose nanocrystals and gelatin in corn starch plasticized films, Carbohydrate polymers 115 (2015) 215-222.
[107] C. Arribas, B. Cabellos, C. Cuadrado, E. Guillamón, M. M Pedrosa, Bioactive compounds, antioxidant activity, and sensory analysis of rice-based extruded snacks-like fortified with bean and carob fruit flours, Foods 8(9) (2019) 381.

Chapter 4

PRODUCTION AND CHARACTERIZATION OF HIGH-PERFORMANCE CELLULOSE-BASED AEROGELS

4.1. PLA coating improves the performance of renewable adsorbent pads based on cellulosic aerogels from aquatic waste biomass

4.2. Confocal Raman imaging as a useful tool to understand the internal microstructure of multicomponent aerogels

4.3. Multifunctional cellulosic aerogels from Posidonia oceanica waste biomass with antioxidant properties for meat preservation

Introduction to chapter 4.

As already commented in the introduction, cellulosic fractions and nanocrystals can be also used for the development of bio-based aerogels. These light and porous materials have a great potential to be used in food packaging as superabsorbent materials due to their biocompatibility and lack of toxicity. However, cellulosic aerogels usually lack an optimum mechanical performance (since they are too fragile) and lose their integrity when soaked in water or exposed to high humidity conditions, which are typically found in food products.

In the first work from this chapter, cellulosic fractions and nanocrystals with different degrees of purification, obtained using the protocols described in previous chapters, were used for the development of aerogels by freeze-drying. These aerogels were characterized in terms of density, sorption capacity and porosity. Subsequently, the most promising aerogels were subjected to a novel hydrophobization methodology (patent PCT/ES2019/070448), consisting of a PLA dipping step, to improve their mechanical performance and water resistance without compromising their biodegradable and biocompatible character.

In the second work from this chapter, an in-depth characterization of the structure of the optimized aerogels was conducted using a novel approach based on confocal Raman microscopy, in combination with more conventional techniques such as confocal laser scanning microscopy.

Finally, in the last work from this chapter the high-performance cellulosic aerogels were used as templates for the incorporation of bioactive extracts from *P. oceanica* waste biomass (obtained according to the methods developed in chapter 1). These hybrid aerogels were proposed as absorbent pads in active food packaging structures and were tested for increasing the shelf-life of conventional food products such as red meat.

4.1. PLA coating improves the performance of renewable adsorbent pads based on cellulosic aerogels from aquatic waste biomass

This section is an adapted version of the following published research article:

Benito-González, I., López-Rubio, A., Gómez-Mascaraque, L. G. & Martínez-Sanz, M. (2020). PLA coating improves the performance of renewable adsorbent pads based on cellulosic aerogels from aquatic waste biomass

Chemical Engineering Journal, 390, 124607. DOI:

https://doi.org/10.1016/j.cej.2020.124607

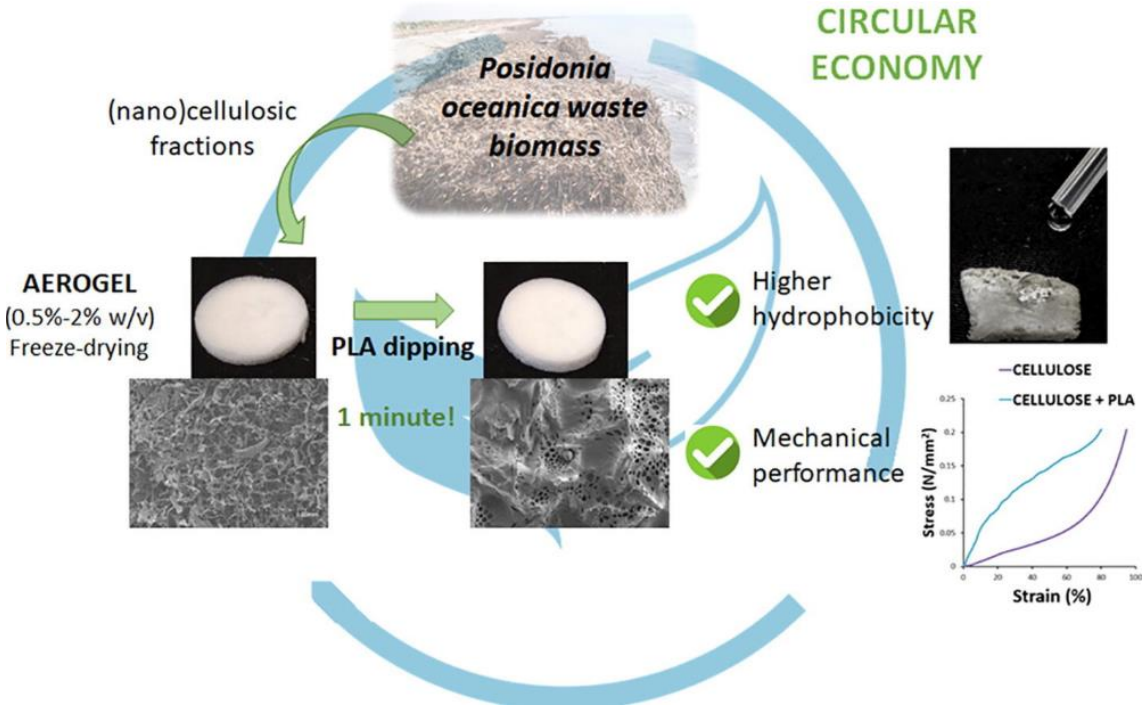

1. Abstract

Lightweight, hydrophobic, adsorbent pads based on aerogels from different cellulosic and nanocellulosic fractions extracted from *Posidonia oceanica* waste biomass were developed by a simple freeze-drying and PLA dipping method. The pure (nano)cellulosic aerogels presented highly porous structures, capable of adsorbing large amounts of oil (up to ~34 g oil/g aerogel); however, they lost their integrity when soaked in water. The incorporation of PLA hydrophobized the aerogels and improved significantly their mechanical performance (up to 10-fold increase in the compression stress). The most porous aerogel structures, obtained with the lowest (nano)cellulosic concentrations and with the less purified fractions, incorporated greater amounts of PLA upon dipping, which was mostly distributed filling in the pores. All the PLA-coated (nano)cellulosic aerogels presented a hydrophobic behavior, with contact angles of 95–130° and selectively adsorbing greater amounts of oil (5.9–9.2 g oil/g aerogel) than water (2.8–6.7 g H_2O/g aerogel). These materials present a great potential as adsorbent pads for oil spill cleaning and food packaging applications.

2. Introduction

The large increase in population over the last century, together with the globalization of the markets and the consumerist society have generated a significant increase on the demand of goods and services. As a result, large amounts of residues are generated worldwide, being plastic materials one of the most abundant residues. Synthetic plastics are widely used nowadays due to their excellent mechanical performance, cost-efficiency and high chemical stability. Although the latter attribute can benefit the use of synthetic plastics in certain applications, such as food packaging (to protect the products from the external environment and extend their shelf life), it also gives rise to severe environmental issues. These materials require extremely long times to disintegrate after their disposal into landfills. Moreover, they can reach marine ecosystems, where they are transformed into the so-called micro-plastics, which are not only a great hazard to aquatic organisms [1], but can also be incorporated into the food chain, posing a threat to human health [2, 3]. In this context, circular economy policies, aiming to reduce waste through the whole production chain by the utilization of alternative natural bio-based raw materials and the application of re-valorization strategies, are currently being boosted by European governments. Not only alternative renewable resources are being studied to replace less environmentally friendly materials, but also greener processes, reducing the use of chemicals and energy, are being explored to minimize the environmental impact of the manufacturing chain.

In the particular case of the food packaging sector, biopolymers, i.e. bio-based and biodegradable polymers, are being extensively explored for the replacement of synthetic plastics in several types of packaging structures such as trays, lids and sorbent pads [4, 5]. Each type of packaging

structure needs to meet certain specific requirements and, thus, the properties of biopolymers have to be adapted accordingly. For instance, sorbent pads are commonly used in packages to minimize the amount of excess liquids released by fresh products upon storage, although they can also be utilized as templates for the incorporation and sustained release of bioactive compounds towards the food products [6, 7]. Aerogels are extremely light and porous materials with high surface area and low density, which are useful for environmental, construction, pharmaceutical, bio-medical, food and cosmetic applications due to their high absorption and adsorption capacities [8-10]. Although aerogels have been traditionally made from inorganic materials such as silica or alumina [11, 12], their application as pads in the food packaging area requires the search of sustainable materials with properties that resemble those from the commercially used synthetic polymeric pads. In this sense, aerogels made from biopolymers such as cellulose, pectin or chitin have been recently proposed as promising materials [13]. In particular, many recent works reporting on the production of cellulose-based aerogels can be found in the literature [14-16]. Despite their great potential, the application of these materials within food packaging is still a largely unexplored area, which is mostly due to the complexity of their manufacturing processes, often involving the use of chemical agents and/or organic solvents unsuitable for food applications, and their poor performance under high relative humidity conditions [6, 17]. Cellulose-based aerogels are typically produced by complex methodologies involving an initial disruption of the crystalline structure to dissolve cellulose (through the use of ionic liquids or mercerization treatments) [16, 18], gelation, cellulose regeneration, solvent exchange and a final drying step by means of supercritical CO_2 or freeze-drying [19, 20]. Due to the highly hydrophilic nature of cellulose, the obtained aerogels are susceptible to disintegrate upon moisture contact, thus requiring the application of hydrophobization treatments. These treatments normally consist of chemical modification of cellulose, cross-linking and/or coating with hydrophobic agents such as silanes [14, 21, 22], which are not acceptable for food-related applications and confront the sustainability and circular economy principles.

In this work, the valorization of *Posidonia oceanica* waste biomass for the production of bio-based cellulosic and nanocellulosic aerogels is proposed. Previous work has demonstrated that less purified (nano)cellulosic fractions may present superior performance than pure cellulose, while increasing the sustainability of the obtained materials [23]. Based on this, the properties of aerogels produced from different (nano)cellulosic fractions by freeze-drying of their aqueous suspensions have been evaluated. Furthermore, a simple PLA (poly(lactic acid)) dipping method has been tested for the hydrophobization and improvement of the mechanical performance of selected aerogels. The developed materials are therefore fully bio-based, adsorbent systems suitable for food packaging applications and produced by means of a cost-effective and sustainable method.

3. Materials and methods

3.1 Raw materials

Biomass waste material consisting of *Posidonia oceanica* leaves was directly collected in the sea shore of Calpe (Alicante, Spain) in January 2018. The material was washed vigorously with water in order to remove sand and stored under refrigeration (4º C) until its use.

3.2 Preparation of cellulosic fractions and nanocrystals from *Posidonia oceanica* biomass

A purification procedure described in previous works [24, 25] and consisting of a Soxhlet extraction (4 g of dry material were extracted with 800 mL of 2:1 toluene:ethanol for 24 h), followed by bleaching (the material obtained from the first step was treated for 5 h at 70 °C with 700 mL of 1.4% w/v $NaClO_2$) and an alkaline treatment (the material was treated with 400 mL 5% w/v KOH for 24 h at room temperature, followed by 2 h at 90 °C), was applied to sequentially remove cell wall components and obtain holocellulose (F2) and pure cellulose (F3). Less purified fractions were also obtained by omitting the Soxhlet step (F2A and F3A). These fractions were then subjected to an optimized hydrolysis treatment with sulphuric acid, as described in [23], to produce nanocellulosic materials (labelled as NANO F2, NANO F2A, NANO F3 and NANO F3A). Briefly, the fractions were immersed in a H_2SO_4 solution (30% v/v), with a ratio of 1.5 g (dry fraction) / 100 mL of H_2SO_4 and were heated to 50 ºC during 2 h under stirring conditions. The obtained fractions and nanocrystals were stored in the fridge as partially hydrated gel-like materials, until further use.

3.3 Production of cellulosic aerogels

Aerogels were produced by dispersing the required amount of cellulosic or nanocellulosic materials in 15 mL of distilled water by ultra-turrax homogenization to obtain concentrations of 0.5, 1, 1.5 and 2 wt.-%. These suspensions were transferred to plastic Petri dishes (5 cm diameter), frozen at −80 °C for 4 h and then freeze-dried using a Genesis 35-EL freeze-dryer (Virtis). The obtained cellulosic and nanocellulosic aerogels were labeled according to the fraction used as starting material (F2, F2A, F3, F3A, NANO F2, NANO F2A, NANO F3 and NANO F3A).

Additionally, selected aerogels (F3, NANO F3, NANO F2A and NANO F2) were used to produce hybrid cellulosic-PLA aerogels using a proprietary technology [26]. Briefly, PLA was dissolved in chloroform at a fixed concentration of 5% (w/v) by stirring at 50ºC during 30 minutes. The (nano)cellulosic aerogels were dipped in the PLA solution for 1 minute and the samples were then dried at room temperature in a fume hood until the chloroform was completely evaporated (at least 24 h). The obtained aerogels were stored in equilibrated relative humidity cabinets at 0% RH and 25ºC for at least three days prior to their characterization. The amount of PLA sorbed by the aerogels was calculated as follows:

$$\% PLA = \frac{Wf - W0}{W0} x\ 100 \quad (1)$$

where $W0$ refers to the (nano)cellulosic aerogel initial weight and Wf corresponds to the final sample weight (aerogel + PLA). Al least four samples were prepared for each (nano)cellulosic aerogel type.

3.4 Scanning electron microscopy (SEM)

SEM was conducted on a Hitachi microscope (Hitachi S-4800) at an accelerating voltage of 10 kV and a working distance of 8-16 mm. Small samples (~5 mm^2 area) of the pure (nano)cellulosic and PLA-coated (nano)cellulosic aerogels were cut to observe their surface. The samples were then sputtered with a gold–palladium mixture under vacuum during 3 minutes before their morphology was examined.

3.5 Density of aerogels

Aerogel densities were determined from the weight and volume of each individual aerogel. The weight was determined by an analytical balance (Precisa Gravimetrics AG SERIES320XB, Dietikon, Switzerland) and the dimensions were measured by a digital calliper at three different positions.

3.6 Water and oil sorption

Squared aerogel specimens with a total surface area of 1 cm^2 were cut, weighed and immersed in sealed containers containing 15 mL of distilled water or sunflower oil. The samples were periodically taken out of the liquid and weighed after removing the liquid excess. Measurements were taken until the samples were equilibrated and the total weight gain was calculated. After equilibration, the samples were removed from the liquid, placed on top of aluminum foil (in the case of water) and filter paper (in the case of oil) and left drying at ambient conditions. The weight was registered periodically, until it was constant (~1 week). The water and oil retention capacity was calculated from the difference between the weight after drying and the initial weight of the samples, before soaking them in the liquids. All the measurements were carried out at least in triplicate.

The experimental curves obtained for the water and oil sorption processes were fitted using pseudo-first order and pseudo-second order models.

The pseudo-first order model is described by the following expression:

$$q\ (t) = q_e\ [1 - e^{k_1 t}] \quad (2)$$

where $q\ (t)$ is the amount of adsorbed solute, q_e its value at equilibrium and k_1 is the pseudo-first order kinetic rate constant.

On the other hand, the pseudo-second order model is described by the following expression:

$$q\ (t) = q_e\ \frac{k_2^* t}{1+k_2^* t} \quad (3)$$

where $k_2^* = k_2 \cdot q_e$ and k_2 is the pseudo-second order kinetic rate constant.

3.7 Immersion of PLA-coated (nano)cellulosic aerogels in water/oil media

To investigate the selectivity of the PLA-coated (nano)cellulosic aerogels to adsorb water and oil, a mixture of 50/50 water/sunflower oil (v/v) was prepared. Distilled water was stained with methylene blue and sunflower oil was stained with Congo red to differentiate the two media. The PLA-coated (nano)cellulosic aerogels were firstly immersed in the water phase and subsequently in the interphase between water and oil.

3.8 Contact angle measurements

Contact angle measurements were carried out at 23 ± 2 °C and ambient relative humidity (ca. 60%RH) in a Video-Based Contact Angle Meter model OCA 20 (DataPhysics Instruments GmbH, Filderstadt, Germany). Contact angle values were obtained by analyzing the shape of a distilled water drop after it had been placed over the film for 15 s. Image analyses were carried out by SCA20 software. Results were obtained from an average of at least 5 measurements.

3.9 Confocal laser scanning microscopy (CLSM)

Sunflower oil was stained by adding 0.1% (v/v) of Nile Red in ethanol (1:10 Nile Red:Oil) and vortexing vigorously until a homogeneous solution was achieved. Aerogels were then immersed in the stained oil for at least 10 minutes in order to maximize oil sorption. Immersed aerogels were then visualized using a Leica TCS SP5 confocal laser scanning microscope (Leica Microsystems CMS GmbH, Wetzlar, Germany) with 5x and 10x dry objectives (numerical apertures of 0.12, 0.30 and 0.70, respectively) and the pinhole set at 1 Airy Unit. Nile red was excited at 488 nm using an Argon laser, and the emission filter was set at 560-600 nm. A second filter set at 488 nm was also used to observe the light reflected by the cellulosic materials. Leica LAS AV software (v 2.7.3.9723) was used to acquire digital images of 1024 x 1024 pixels in size

at day 1 and 50 after immersion. Samples were placed in darkness conditions between imaging to avoid fluorescence loss.

3.10 Compression tests

Uniaxial compression tests were carried out at 20 ºC on a texture analyser (Stable Micro Systems model TA-XTplus, Surrey, UK). The sample size for the compression test ranged between 8-10 mm (diameter) × 8-10 mm (thickness) with a cylindrical shape. A cylindrical aluminium probe with a diameter of 25 mm was used to compress the specimen at a compression rate of 0.1 mm s^{-1} using a 5 kg load. Samples were analyzed at least in duplicate.

3.11 Statistics

Analysis of variance (ANOVA) followed by a Tukey-b test were used when comparing more than two data sets. All data have been represented as the average ± standard deviation. Significant differences ($p \leq 0.05$) are denoted by showing the data provided in tables and figures with different letters.

4. Results and discussion

4.1 Characterization of pure (nano)cellulosic aerogels

Initially, pure (nano)cellulosic aerogels were produced by using aqueous dispersions (0.5 wt.-%) of the cellulosic and nanocellulosic fractions extracted from *P. oceanica*. All the produced aerogels presented a sponge-like appearance (cf. Figure 1A and Figure 1B). As observed, the degree of purification tremendously affected the integrity and structure of the aerogels, especially in the ones produced from the cellulosic fractions. While F2 and F2A (containing hemicelluloses [23]) formed agglomerated and heterogeneous structures with very poor mechanical integrity, F3 and F3A (consisting of almost pure cellulose [23]) formed more uniform aerogels. The morphology of the aerogels at the micron scale, evaluated by SEM, consisted of fibrillar porous structures, which were indeed much more homogeneous in F3 and F3A. Conversely, larger structures, originated from the native *P. oceanica* cell walls, were detected in F2 and F2A. A higher extent of agglomeration was evident in F2A, giving rise to aerogels with a weaker powder-like consistency. The observed differences were expected due to the higher degree of purification of the F3 and F3A fractions, where cell wall components such as lignin and hemicelluloses had been eliminated. The absence of additional components may facilitate the formation of a strong hydrogen-bonded network of cellulose [23, 25], thus giving rise to aerogels with improved mechanical integrity. Interestingly, the hydrolysis of the cellulosic fractions had a large impact on the morphology and consistency of the obtained nanocellulosic aerogels. In particular, the NANO F3 aerogel (containing pure nanocellulose [23]) presented the most uniform morphology.

As shown in the SEM images (cf. Figure 1B), the NANO F2 and NANO F2A aerogels showed the most porous structure, while NANO F3A presented a more compacted structure, where a layer of material coating the surface and reducing the porosity was observed.

As expected, the morphological differences had a significant effect on the density of the aerogels (cf. Table 1). The greater degree of agglomeration and heterogeneity of the F2 and F2A aerogels were also evidenced by their greater density values. On the other hand, in general, the greater porosity and uniformity of the nanocellulosic aerogels resulted in a marked decrease in their densities with respect to the corresponding cellulosic aerogels. This effect was more obvious in the case of the least purified fractions (with a 6-fold and 9-fold decrease in the case of NANO F2 and NANO F2A, respectively, with respect to the F2 and F2A aerogels). Thus, NANO F2 and NANO F2A yielded the most porous and lightweight aerogels. Surprisingly, the structure of NANO F3A became denser than F3A, as further supported by the corresponding SEM images. As demonstrated by a previous work, a small amount of the lipidic impurities remaining in the F2A and F3A fractions are resistant to the hydrolysis treatment and therefore, they are still present in NANO F2A and NANO F3A. These lipidic compounds were most likely interacting with the hemicelluloses present in NANO F2A; however, the removal of hemicelluloses by the application of a basic treatment in the case of NANO F3A, seemed to promote the release of these lipids, which were then phase-separated from the pure cellulose and formed a layer coating the surface of the aerogel. The same effect has been previously reported for films prepared from aqueous suspensions of NANO F3A [23]. Thus, these lipidic impurities seem to be responsible for the more compacted structure of the aerogel.

The density values of the NANO F2 and NANO F2A aerogels were significantly lower in comparison with those previously reported for aerogels from cotton cellulose nanowhiskers (78 mg/cm^3) prepared at the same concentration (0.5 wt.-%) by solvent exchange and supercritical CO_2 drying [8]. Similar densities were obtained in hybrid nanocellulose aerogels with added carbon nanotubes, achieving values ranging between 10-56 mg/cm^3 [27]. Lower densities have only been reported for modified cellulose aerogels. For instance, densities of 1.7-8 mg/cm^3 have been reported for aerogels from rice straw nanofibrils modified by vapour deposition of triethoxyl(octyl) silane [28].

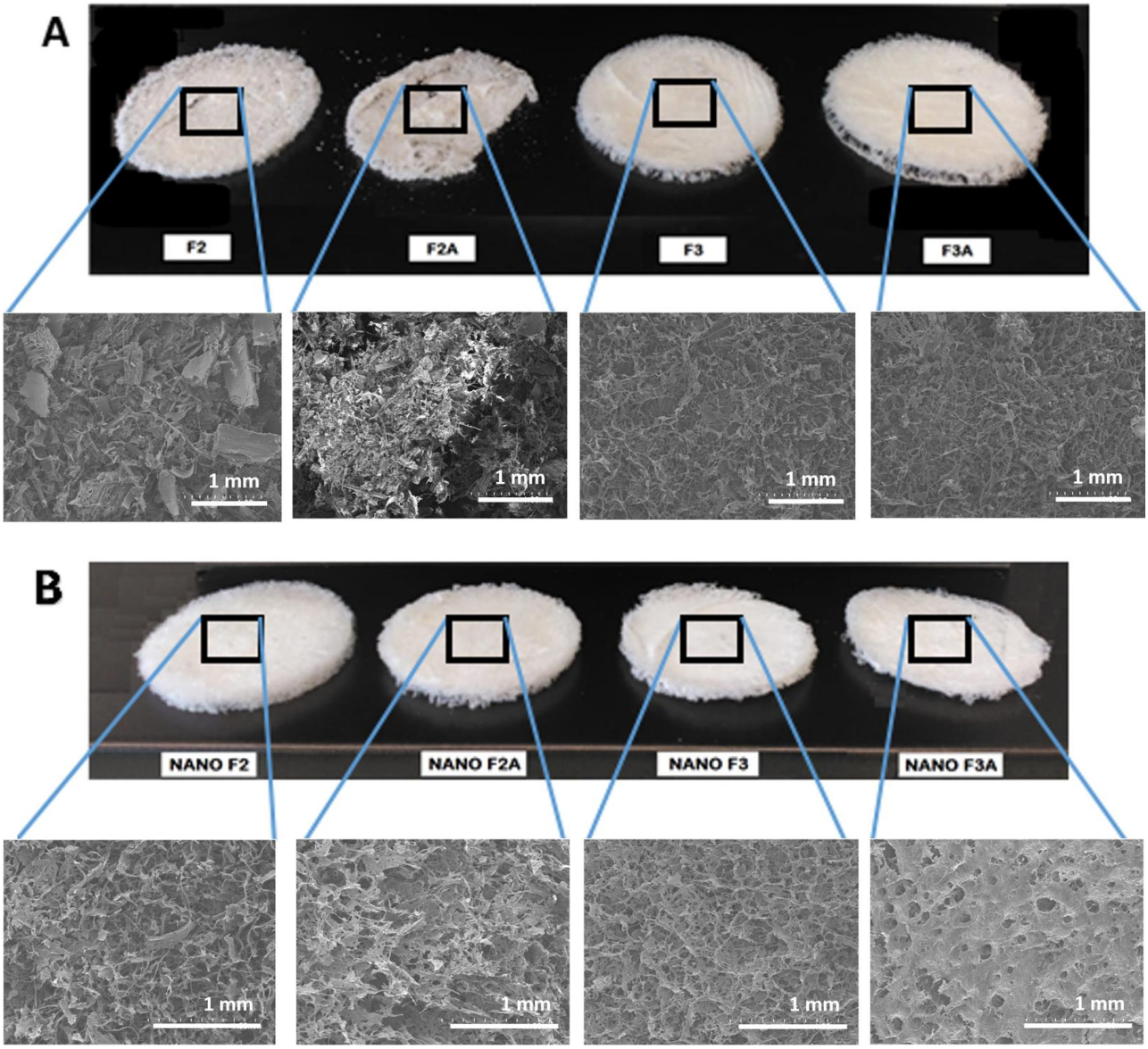

Figure 1. Visual aspect and SEM micrographs from the surface of the *P. oceanica* cellulosic (A) and nanocellulosic (B) aerogels. Scale bars in the SEM micrographs correspond to 1 mm.

To evaluate the effect of the distinct composition and morphology of the aerogels on their sorption capacity, water and oil sorption tests were carried out. Unfortunately, due to the highly hydrophilic character of the (nano)cellulosic aerogels, they disintegrated when immersed in water and therefore, water sorption could not be assessed. The results from the oil sorption tests showed a clear correlation between the porosity and sorption capacity of the aerogels (cf. Table 1). It should be noted that the poor mechanical integrity of the F2 and F2A aerogels impeded reliable results to be obtained from the oil sorption tests and thus, these values have not been reported.

Table 1. Density and oil sorption capacity of the *P. oceanica* cellulosic and nanocellulosic aerogels. Different letters show significant differences between samples ($p \leq 0.05$).

	Density (mg/cm^3)	Oil sorption capacity (g oil/g aerogel)
F2	79.4 ± 2.8^{d}	n.m.
F2A	114.3 ± 7.9^{e}	n.m.
F3	42.3 ± 1.3^{b}	20.0 ± 0.1^{b}
F3A	46.8 ± 0.8^{bc}	17.4 ± 0.2^{c}
NANO F2	13.2 ± 0.2^{a}	34.3 ± 0.4^{a}
NANO F2A	12.8 ± 0.1^{a}	33.8 ± 0.5^{a}
NANO F3	38.4 ± 0.3^{b}	20.1 ± 0.2^{b}
NANO F3A	58.1 ± 0.2^{c}	12.2 ± 0.2^{d}

The most porous NANO F2 and NANO F2A aerogels presented the highest oil sorption capacity, while the more compacted structures found in NANO F3A limited their performance. Similar sorption values were observed in *A. donax* cellulosic aerogels (10-60 g oil/g aerogel) [6], while lower capacities (18-20 g oil/g aerogel) have been reported for methyltrimethoxysilane-coated cellulose aerogels [29]. As shown in the sorption curves (cf. Figure S1), the oil was absorbed into the aerogels relatively quickly, reaching equilibrium values approximately after 4h. With regards to the oil release, it was noticeable that all the aerogels released almost completely the oil after 3 days. It should be noted that the most compacted aerogels, especially F2A, displayed the slower oil release kinetics, showing the importance of the aerogel microstructure on the sorption and desorption processes.

Overall, the NANO F2 and NANO F2A aerogels seem to be the most promising materials, given their reduced production costs and environmental impact (as compared to the more purified nanocellulosic fractions), their optimal microstructure in terms of porosity and homogeneity and their lightweight characteristics.

4.2. Production of hydrophobic PLA-coated (nano)cellulosic aerogels

The poor resistance of the (nano)cellulosic aerogels to high humidity conditions would strongly limit their range of applications. A straightforward methodology based on dipping the (nano)cellulosic aerogels in PLA solutions was evaluated for their hydrophobization and the obtained aerogels were characterized to determine the effect of PLA incorporation on their mechanical performance and sorption capacity. To this end, four aerogels were selected: NANO F2 and NANO F2A (the most optimum in terms of microstructure and sorption capacity) and F3 and NANO F3 (the most purified cellulosic and nanocellulosic fractions). The latter ones were selected to assess the effect of the degree of purification and of the cellulose hydrolysis. Furthermore, four different solid concentrations (0.5, 1, 1.5 and 2 wt.-%) were tested to determine the effect of (nano)cellulose concentration on the morphology, sorption capacity and mechanical integrity of the produced aerogels. The visual aspect and representative SEM images from the obtained aerogels, shown in Figure 2, evidenced that, for a given concentration, the NANO F2 and NANO F2A aerogels presented more porous structures. As expected, increasing concentrations of the (nano)cellulosic fractions led to denser aerogel structures. The density of the aerogels (cf. Table 2) was directly related to their microstructure, being the most porous materials the ones presenting the lowest density values (i.e. NANO F2 and NANO F2A at their lowest concentration).

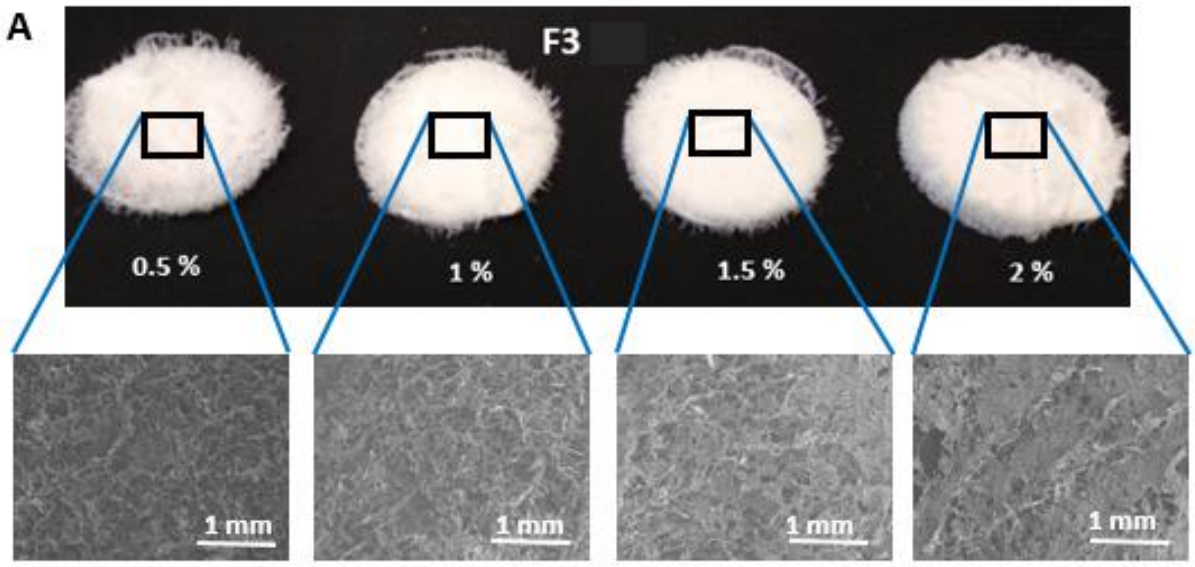

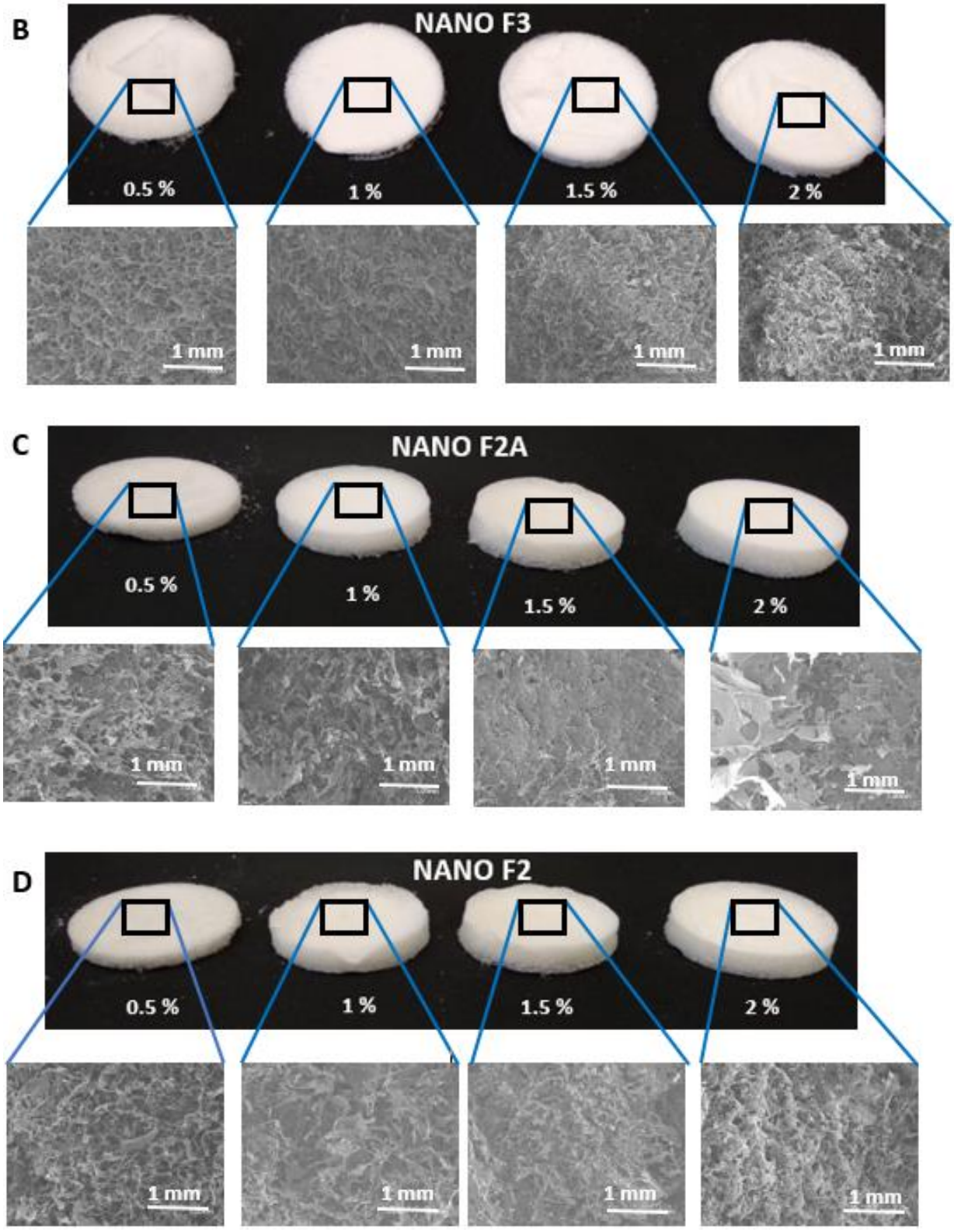

Figure 2. Visual aspect and SEM micrographs of the selected *P. oceanica* (nano)cellulosic aerogels at four different concentrations. (A) F3, (B) NANO F3, (C) NANO F2A and (D) NANO F2. Scale bars in the SEM micrographs correspond to 1 mm.

Table 2. Density of the selected *P. oceanica* (nano)cellulosic aerogels at the different tested concentrations and of the corresponding PLA-coated (nano)cellulosic aerogels. Different letters show significant differences between the same concentration (column) while * show significant differences between concentrations for the same material ($p \leq 0.05$).

Density (mg/cm^3)	**0.5%**	**1%**	**1.5%**	**2%**
F3	42.3 ± 1.3^{b}	$76.1 \pm 2.3^{b*}$	$98.8 \pm 2.8^{b**}$	$125.9 \pm 5.5^{b***}$
F3 + PLA	118.4 ± 5.8^{c}	$180.6 \pm 5.3^{c*}$	$197.6 \pm 10.0^{c*}$	$232.9 \pm 15.3^{c**}$
NANO F3	38.4 ± 0.3^{b}	$73.8 \pm 0.8^{b*}$	$97.5 \pm 1.2^{b**}$	$113.9 \pm 3.7^{b***}$
NANO F3 + PLA	109.6 ± 4.3^{c}	$177.0 \pm 7.3^{c*}$	$188.3 \pm 1.9^{c*}$	$216.1 \pm 12.5^{c**}$
NANO F2A	12.8 ± 0.1^{a}	$23.3 \pm 0.5^{a*}$	$35.1 \pm 1.4^{a**}$	$46.8 \pm 1.8^{a***}$
NANO F2A + PLA	41.6 ± 2.9^{b}	$73.4 \pm 4.5^{b*}$	$91.3 \pm 5.4^{b**}$	$112.3 \pm 6.6^{b***}$
NANO F2	13.2 ± 0.2^{a}	$25.7 \pm 0.3^{a*}$	$38.3 \pm 0.8^{a**}$	$51.6 \pm 1.7^{a***}$
NANO F2 + PLA	45.5 ± 4.4^{b}	$77.1 \pm 4.3^{b*}$	$103.3 \pm 6.3^{b**}$	$116.1 \pm 7.3^{b**}$

After dipping the materials into the PLA solutions, the amount of polymer retained by the aerogels was estimated. As deduced from Figure 3, there was a clear tendency of decreasing the PLA incorporation when increasing the (nano)cellulose concentration. Moreover, the less purified aerogels (NANO F2A and NANO F2) were able to retain greater amounts of PLA than the pure cellulose aerogels. Remarkably, NANO F2A and NANO F2 were able to incorporate more than 200% PLA (with regards to their initial weight) when the nanocellulose concentration in the starting aerogels was 0.5-1 wt.-%. These results were consistent with the higher porosity observed in these particular samples (cf. Figure 2). The density values of the obtained PLA-coated (nano)cellulosic aerogels were also estimated and the obtained values are gathered in Table 2. As expected, the incorporation of PLA significantly increased the density of the aerogels, being this effect more remarkable at the lowest (nano)cellulosic concentration (0.5 wt.-%) since the PLA weight gain was greater in that case. The highest absolute density values (110-230 mg/cm^3) corresponded to the 2 wt.-% aerogels, which were within the range of those previously reported for bacterial cellulose aerogels reinforced with PLA produced by ethanol precipitation and supercritical CO_2 drying (162 mg/cm^3) [30].

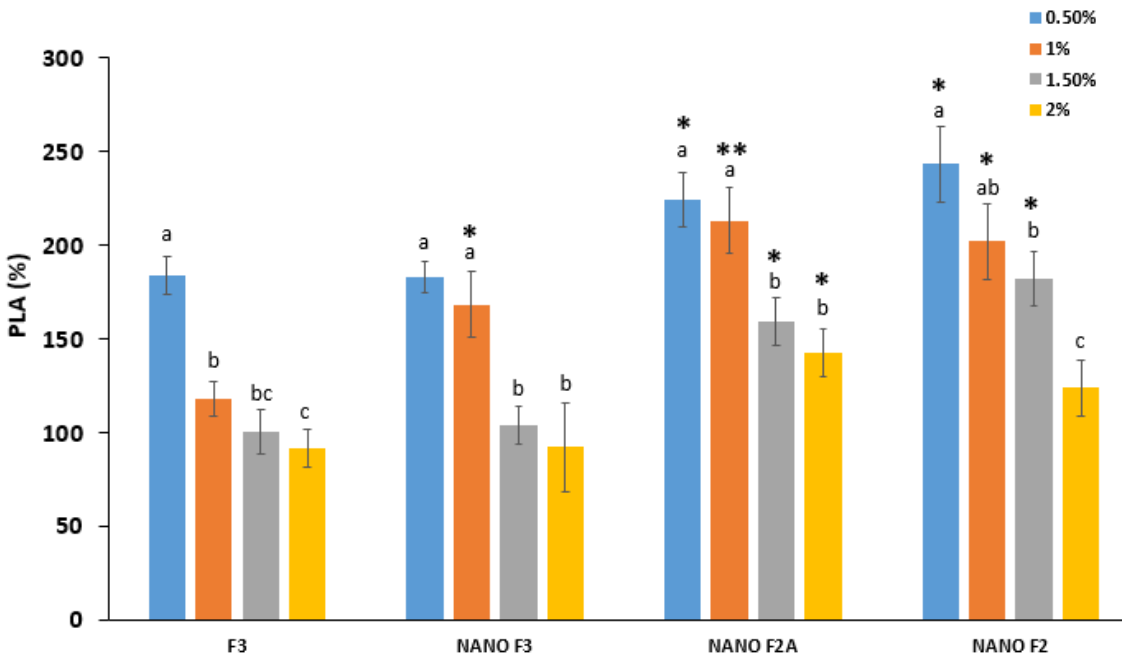

Figure 3. Amount of PLA incorporated into the *P. oceanica* (nano)cellulosic aerogels (% with respect to the initial aerogel weight). Different letters denote significant differences between concentrations for the same aerogel type while * show significant differences between different aerogels at the same concentration ($p \leq 0.05$).

SEM characterization was also carried out to assess the distribution of the PLA phase in the coated (nano)cellulosic aerogels and representative micrographs are shown in Figure 4. As observed, the PLA-coated aerogels presented much more compact and continuous structures than the pristine (nano)cellulosic aerogels. The PLA seemed to be mostly located filling in the pores and also covering the surface of the aerogels in a particular way: PLA created a continuous layer showing a very singular network of micro-holes (diameter ~3 μm) which were particularly visible in the 1.5% and 2% aerogels (see insets in Figure 4). These micro-holes were most likely originated by the evaporation of chloroform after the PLA dipping process, and therefore they are expected to appear within the PLA-rich regions.

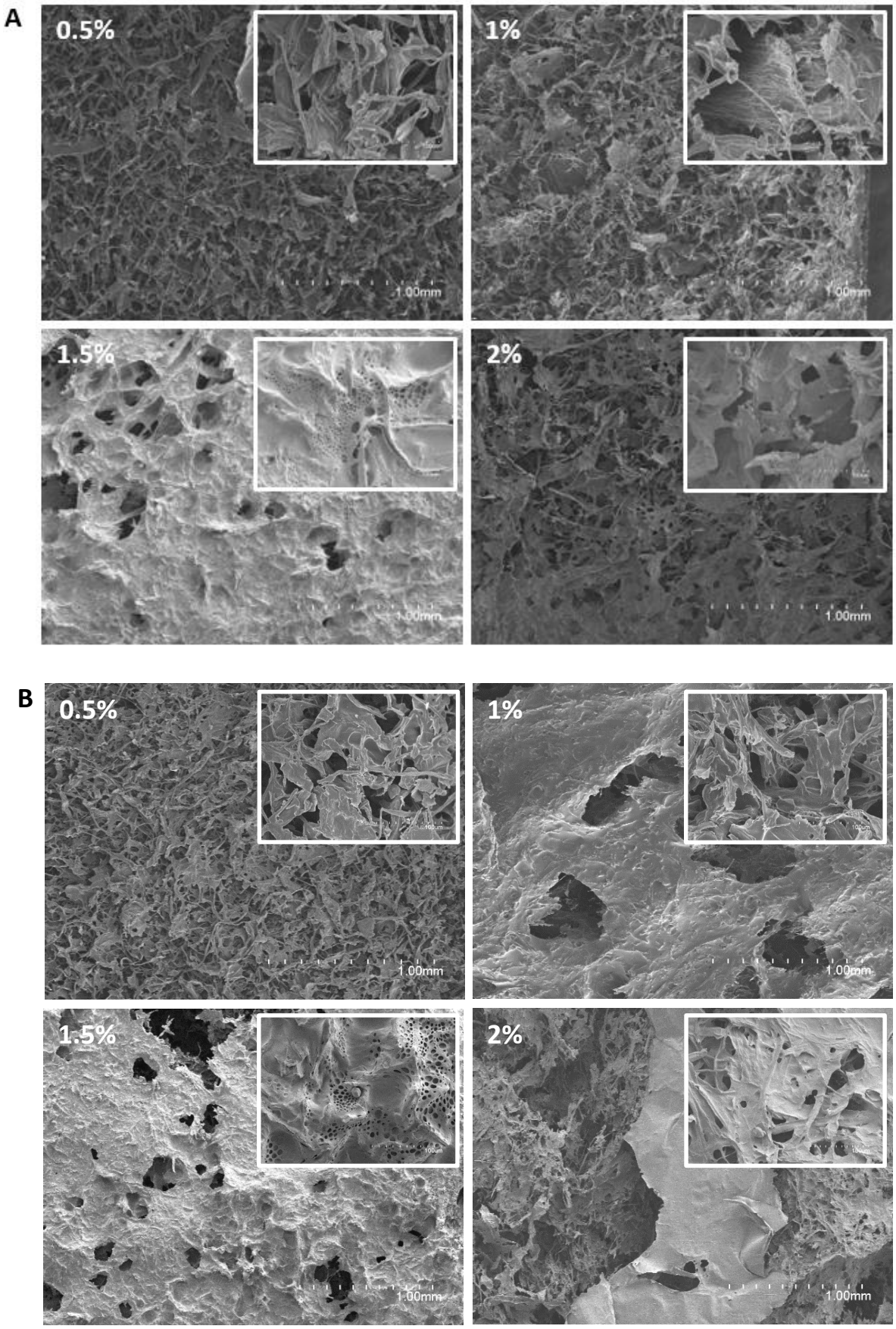
A
0.5%
1%
1.5%
2%
1.00mm
B
0.5%
1%
1.5%
2%
1.00mm

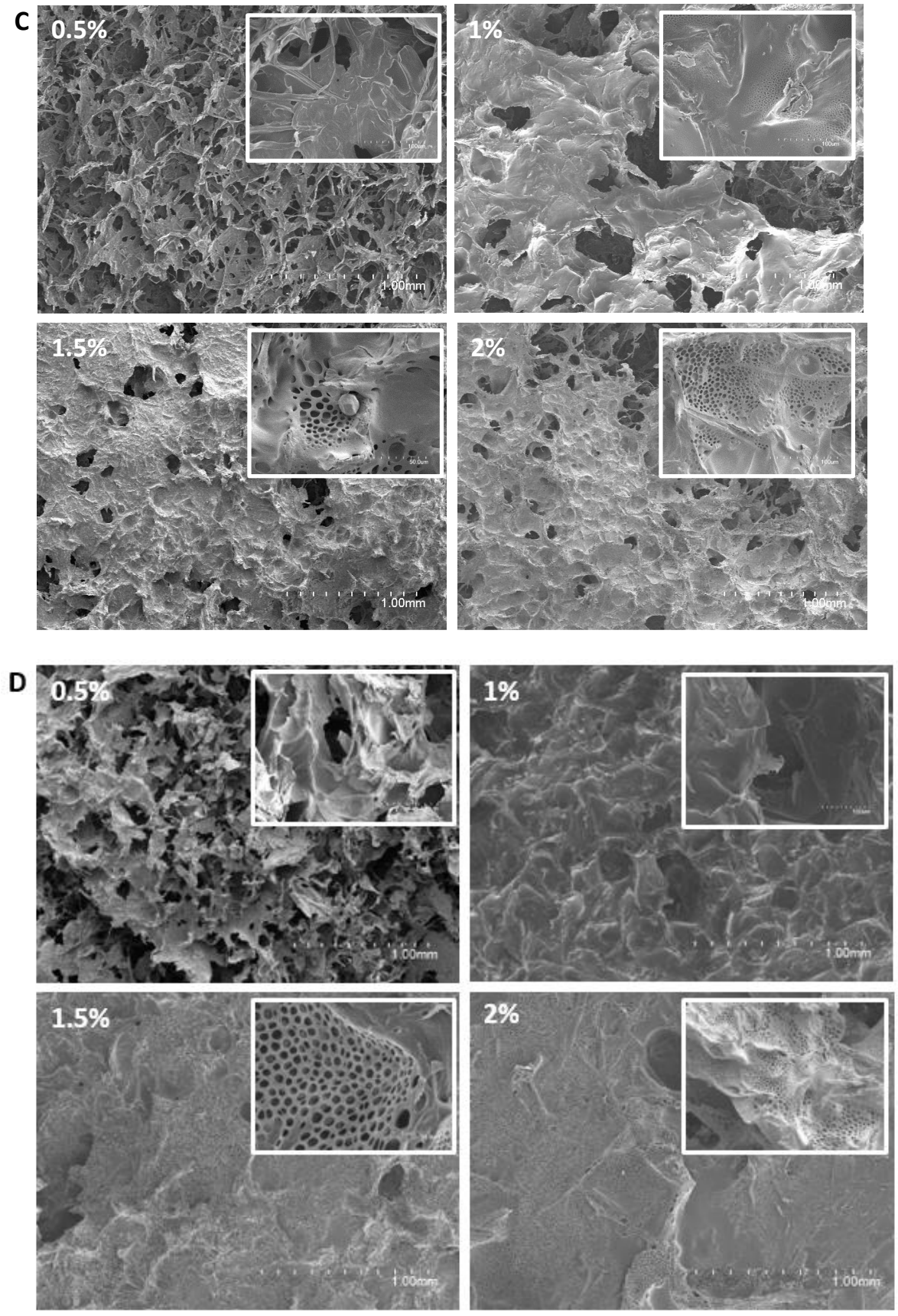

Figure 4. SEM images of the PLA-coated (nano)cellulosic aerogels. (A) F3, (B) NANO F3, (C) NANO F2A and (D) NANO F2. Insets represent regions of the aerogels at higher magnification.

Since PLA is known to possess a more hydrophobic behaviour than cellulose [31, 32], contact angle measurements were performed on selected aerogels to identify the effect of PLA incorporation on the water affinity of the aerogels' surface. The coating of the aerogels with PLA had a dramatic effect; while the original (nano)cellulosic aerogels were not even measurable due to the highly hydrophilic nature of these materials [23], the PLA-coated (nano)cellulosic aerogels presented contact angle values between 100º and 125º. Such values are similar to those reported for PLA films [31] and demonstrate the marked hydrophobization effect of the PLA dipping method. Interestingly, the most purified fractions (F3 and NANO F3) showed a more hydrophobic behaviour at the lowest (nano)cellulose concentration (0.5 wt.-%), which was most likely due to the greater amount of PLA incorporated, while this was not the case for the less purified fractions (NANO F2A and NANO F2). These results suggest that in the case of the more porous aerogels PLA was preferentially incorporated into the inner region, filling in the pores. On the other hand, there seemed to be an optimum density range (40-50 mg/cm^3, cf. Table 2) for which the PLA was capable of filling the internal pores and the excess polymer was distributed coating the surface of the aerogels, therefore maximizing the hydrophobization effect. Indeed, the most purified aerogels (i.e. F3 and NANO F3) at their lowest concentration (0.5%) and the least purified aerogels (i.e. NANO F2A and NANO F2) at their highest concentration (2%), which presented densities within the "optimum range", showed the maximum contact angle values, ranging from 110 to 130º.

Table 3. Calculated contact angle, water sorption, oil sorption and oil retention capacities for PLA-coated (nano)cellulosic aerogels at their lowest (0.5%) and highest (2%) concentrations. Values followed by different letters are significantly different ($p \leq 0.05$).

	Contact angle (º)	Water sorption capacity (g H_2O/g aerogel)	Oil sorption capacity (g oil/g aerogel)	Oil retention capacity (g oil/g aerogel)
F3 0.5% + PLA	124.5 ± 9.9^{a}	3.3 ± 0.1^{de}	6.9 ± 0.1^{f}	0.4 ± 0.1^{d}
F3 2% + PLA	100.9 ± 4.6^{b}	2.8 ± 0.1^{e}	5.9 ± 0.1^{g}	3.9 ± 0.5^{a}
NANO F3 0.5% + PLA	127.1 ± 5.6^{a}	3.7 ± 0.2^{cd}	8.4 ± 0.1^{d}	1.2 ± 0.2^{c}
NANO F3 2% + PLA	95.2 ± 8.6^{b}	2.9 ± 0.1^{e}	6.1 ± 0.1^{g}	2.4 ± 0.3^{b}
NANO F2A 0.5% + PLA	101.4 ± 5.7^{b}	6.7 ± 0.1^{a}	9.2 ± 0.2^{c}	0.7 ± 0.1^{d}
NANO F2A 2% + PLA	120.0 ± 3.1^{a}	4.2 ± 0.1^{c}	7.6 ± 0.2^{e}	3.0 ± 0.2^{ab}
NANO F2 0.5% + PLA	107.1 ± 6.5^{ab}	5.3 ± 0.1^{b}	8.4 ± 0.1^{d}	0.8 ± 0.2^{cd}
NANO F2 2%+ PLA	112.3 ± 7.0^{ab}	3.8 ± 0.1^{c}	7.3 ± 0.1^{ef}	2.6 ± 0.3^{b}

The dramatic changes in the microstructure and water affinity of the aerogels induced by the incorporation of PLA were expected to affect their sorption capacity. Thus, water and oil sorption experiments were carried out on the PLA-coated (nano)cellulosic aerogels. Water sorption curves for all the aerogels could be fitted by a pseudo-first order equation, while a pseudo-second order model worked better for the kinetics of oil sorption (cf. Figure S2). All the kinetic parameters obtained from the fitting are compiled in the supplementary material (cf. Table S1). Although the surface of the PLA-coated (nano)cellulosic aerogels showed a hydrophobic behaviour, as suggested by the contact angle measurements, the aerogels were able to adsorb water while also keeping their integrity (unlike the pure (nano)cellulose aerogels). The results from the water sorption/desorption experiments (cf. Figure S3) show that the sorption and desorption processes were relatively fast (with all the samples reaching equilibrium values in ca. 4 h for the sorption and 4-8 h for the desorption), suggesting weak interactions between water and the structure of the aerogels. The aerogels containing the less purified fractions (NANO F2 and NANO F2A) presented the highest water sorption capacities, reaching values up to ca. 500-700% (cf. Table 3). It should also be noted that, for all the aerogel types, lower (nano)cellulosic concentrations produced higher adsorption capacities. These results can be directly related to the microstructure of the aerogels, i.e. a lower degree of purification and lower (nano)cellulosic concentrations gave rise to more porous structures, which were able to adsorb more water. The PLA-coated (nano)cellulosic aerogels were clearly more hydrophobic than other biopolymeric aerogels reported in the literature, such as PVA aerogels loaded with cellulose/nanocellulose, which were able to adsorb up to 800% water [7].

Additionally, oil sorption/desorption tests were carried out to determine the sorption capacity of the aerogels in hydrophobic media. The oil sorption process (reaching equilibrium after ca. 1 h) was much faster than the desorption process (with a steep weight decrease after ca. 3 days and reaching equilibrium after 30 days) (cf. Figure S4). The oil release process took place more slowly in comparison with water, which was expected due to its higher viscosity (ca. 0.049 Pa s at 20 °C [33] versus 0.001 Pa s for water) and evaporation temperature. As for the water sorption capacity, the microstructure of the aerogels played a crucial role in their oil sorption capacity. The oil sorption capacity of the PLA-coated aerogels was clearly diminished in comparison with the highly porous pure (nano)cellulosic aerogels, which can be ascribed to the much more compacted structure attained after the PLA dipping process. Amongst all the PLA-coated (nano)cellulosic aerogels, the more porous structures found in the aerogels from less purified fractions and with lower (nano)cellulosic concentrations led to greater oil sorption values. In particular, the porous NANO F2A aerogels were able to adsorb up to ~920% oil, while the more compacted F3 aerogels adsorbed up to ~690% oil. Higher sorption values of 60 g oil/g aerogel have been reported for recycled cellulose aerogels coated with vapour deposition of methyltrimethoxysilane [14]. These

materials presented lower densities than the PLA-coated (nano)cellulosic aerogels presented in this work, again supporting the fact that the porous microstructure plays a crucial role in the adsorption capacity of the aerogels. Interestingly, after drying for an extended time (~50 days), a large amount of oil was released from the most porous aerogels, which could be favourable for their re-utilization if used as adsorbent materials. The denser structures present in the more concentrated aerogels (i.e. 2 wt.-% (nano)cellulose) were capable of retaining larger amounts of oil, with a maximum oil retention capacity of 66% (with respect to the initial amount of sorbed oil) for the F3 aerogel. The morphology of the aerogels at the end of the oil desorption experiments (~50 days) was characterized by SEM, showing that their microstructure significantly changed with respect to their native state (cf. Figure S5). A more solid-like structure of the aerogels was displayed after the incorporation of oil. Both the larger pores and the micro-holes formed within the PLA-rich phase were completely filled by the sunflower oil. Additionally, confocal laser scanning microscopy was used to investigate the oil distribution within the PLA-coated aerogels' structure and a sequential imaging of the oil immersion process is shown in Figure 5 for NANO F2A (0.5%) as a representative example. The micrographs of the pristine aerogels showed the reflexion of the monochromatic light at 488 nm on the materials, exhibiting their porous structure. After soaking the samples in stained sunflower oil, a considerable amount of the latter was adsorbed, being homogeneously distributed all along the aerogel matrix. In contrast, after drying the aerogel, most of the oil was released from the structure and the remaining oil droplets were seen to be mainly located at the surface of the PLA phase.

The results indicate that the PLA-coated (nano)cellulosic aerogels were able to adsorb greater amounts of oil than water, which can be explained by the hydrophobic character provided by the PLA phase. The selectivity of the aerogels to preferentially adsorb oil when soaked in water/oil mixtures was visually examined (cf. Figure 5D). It was observed that after immersed in the liquid mixture, the PLA-coated (nano)cellulosic aerogels barely adsorbed water, while they were able to selectively adsorb sunflower oil when immersed in the water/oil interphase. Moreover, the aerogel integrity was not damaged at all along the process, proving the higher mechanical resistance acquired after the PLA dipping.

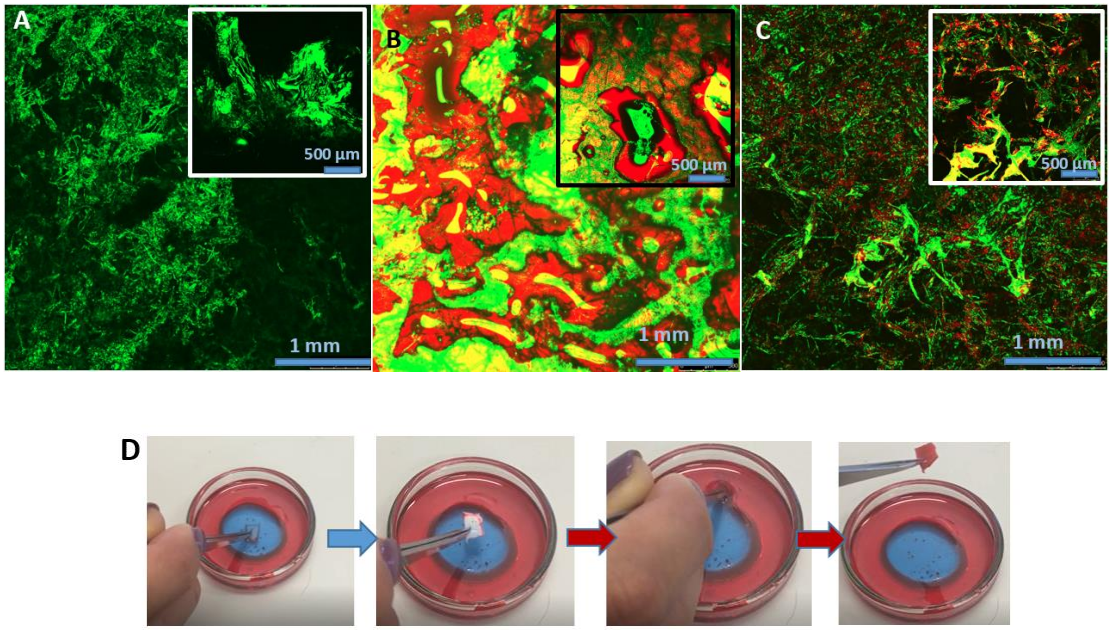

Figure 5. (A-C) Confocal microscopy images of the NANO F2A (0.5%) + PLA aerogel during the oil sorption process. (A) pristine PLA-coated (nano)cellulosic aerogel, (B) after oil immersion and (C) after drying for 50 days. Insets represent higher magnification images from selected aerogel regions. (D) Sequence of the aerogel immersion in a water (blue-stained) and oil (red-stained) mixture.

Compression tests were also carried out to evaluate the effect of the distinct microstructure of the aerogels on their mechanical performance, before and after the incorporation of the PLA, and representative compression stress curves are shown in Figure 6, while the stress values corresponding to 60% deformation are listed in Table 4. It should be mentioned that specimens with the exact dimensions required for the compression tests could not be obtained for the NANO F3 0.5% aerogels due to cellulose agglomeration upon freeze-drying in the sample moulds. As observed in Figure 6, none of the tested samples broke when subjected to a maximum stress of 0.2 N/mm^2. The pure (nano)cellulosic aerogels showed an initial linear stress-strain region, followed by a region where the stress increased more markedly. In general, increasing the (nano)cellulose concentration improved the mechanical performance of the aerogels. Thus, a greater porosity seemed to be directly linked to a poorer mechanical performance of the aerogels. As expected, the incorporation of PLA substantially increased the compression resistance of all the aerogels, with up to 10-fold improved performance. These results were in agreement with those obtained for nanocellulosic aerogels chemically cross-linked with nanoparticles obtained by freeze-drying (0.01 and 0.05 N/mm^2) [34] or those from recycled cellulose aerogels (~0.06 N/mm^2 for a concentration of 2 wt.-% cellulose) [15].

Noticeably, some of the PLA-coated aerogels displayed a biphasic behaviour. Interestingly, this biphasic behaviour was especially prominent for those aerogels whose density (before PLA

coating) ranged between 40-50 mg/cm^3. As previously commented, it seems that the porous structures formed within this particular density range allowed the incorporation of PLA within the inner aerogel pores and the excess material was also located coating the surface of the aerogels. Thus, the more marked initial slope detected in the aerogels with biphasic behaviour was originated by the PLA surface domains. This is in agreement with the SEM characterization, which showed the preferential distribution of the PLA phase filling in the pores of the aerogels and coating the external layers, i.e. no intimate interactions between the cellulose and PLA phase seemed to take place.

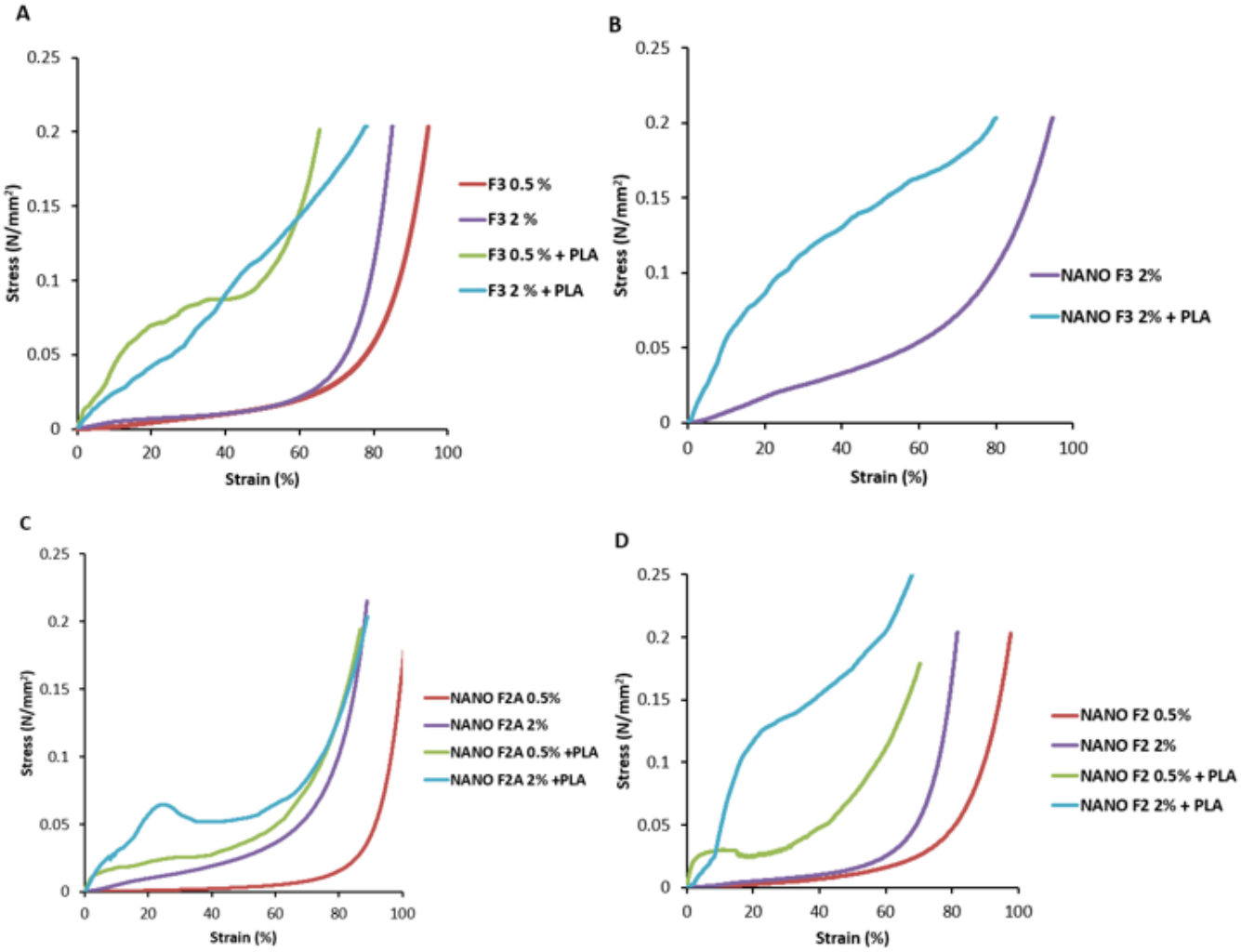

Figure 6. Compression stress curves of selected pure (nano)cellulosic aerogels and their respective PLA-coated counterparts.

Table 4. Compressive stress of the selected aerogels with and without PLA-coating at 60% strain. Different letters show significant differences between samples within the same column. * shows significant differences between the pure (nano)cellulosic aerogels and their respective PLA-coated counterparts. ($p \leq 0.05$).

Compressive Stress (N/mm^2)	Pure (nano)cellulosic aerogel	PLA-coated aerogel
F3 0.5%	1.9 ± 0.1^{b}	$15.1 \pm 0.3^{d*}$
F3 2%	2.0 ± 0.1^{b}	$16.5 \pm 0.2^{d*}$
NANO F3 0.5%	---	---
NANO F3 2%	5.8 ± 0.5^{c}	$15.5 \pm 1.4^{cd*}$
NANO F2A 0.5%	0.5 ± 0.1^{a}	$4.8 \pm 0.2^{a*}$
NANO F2A 2%	3.1 ± 0.3^{b}	$6.6 \pm 0.1^{b*}$
NANO F2 0.5%	1.9 ± 0.4^{b}	$12.5 \pm 0.5^{c*}$
NANO F2 2%	2.5 ± 0.6^{b}	$18.8 \pm 3.1^{d*}$

5. Conclusions

Posidonia oceanica waste biomass has been valorised for the development of lightweight, hydrophobic cellulose-based adsorbent aerogels. Initially, several (nano)cellulosic fractions with different degrees of purification were extracted and used to produce aerogels by freeze-drying. The least purified nanocellulosic fractions (NANO F2 and NANO F2A) gave rise to more porous and lightweight aerogels, capable of adsorbing greater amounts of oil (~34 g oil/g aerogel). However, all the produced aerogels showed very poor performance in high humidity conditions.

The most promising aerogels (NANO F2 and NANO F2A), together with the pure cellulose-based aerogels (F3 and NANO F3), were subsequently subjected to a simple PLA dipping method to hydrophobize their surface, producing PLA-coated (nano)cellulosic aerogels. The concentration of (nano)cellulose in the starting aerogels had a strong impact on their microstructure: more porous aerogels, capable of incorporating greater amounts of PLA into their structures, were obtained with lower (nano)cellulose concentrations. PLA incorporation led to surface hydrophobization, with all the coated aerogels presenting contact angles of 95-130º and being able to keep their integrity when soaked in water. These PLA-coated (nano)cellulosic aerogels were capable of selectively adsorbing greater amounts of oil (5.9-9.2 g oil/g aerogel) than water (2.8-6.7 g H_2O/g aerogel). The sorption capacity of the aerogels was correlated with their microstructure, with the most porous materials being more susceptible to the sorption/desorption

of liquid media. The incorporation of PLA led to a substantial increase on the compression stress (up to 10-fold) of the coated aerogels. Moreover, the mechanical performance was also strongly related to the microstructure, being a greater porosity linked to poorer mechanical performance. Overall, the aerogels' microstructure plays a crucial role on their properties, before and after PLA coating.

These results show that the least purified fractions from *Posidonia oceanica* waste biomass have a great potential to develop fully bio-based, extremely lightweight, hydrophobic and highly adsorbent aerogels with good mechanical properties by using a simple PLA dipping method. These materials represent a greener and more sustainable alternative for the development of adsorbent structures useful in diverse applications, such as oil spill cleaning and food packaging.

6. Supplementary Material

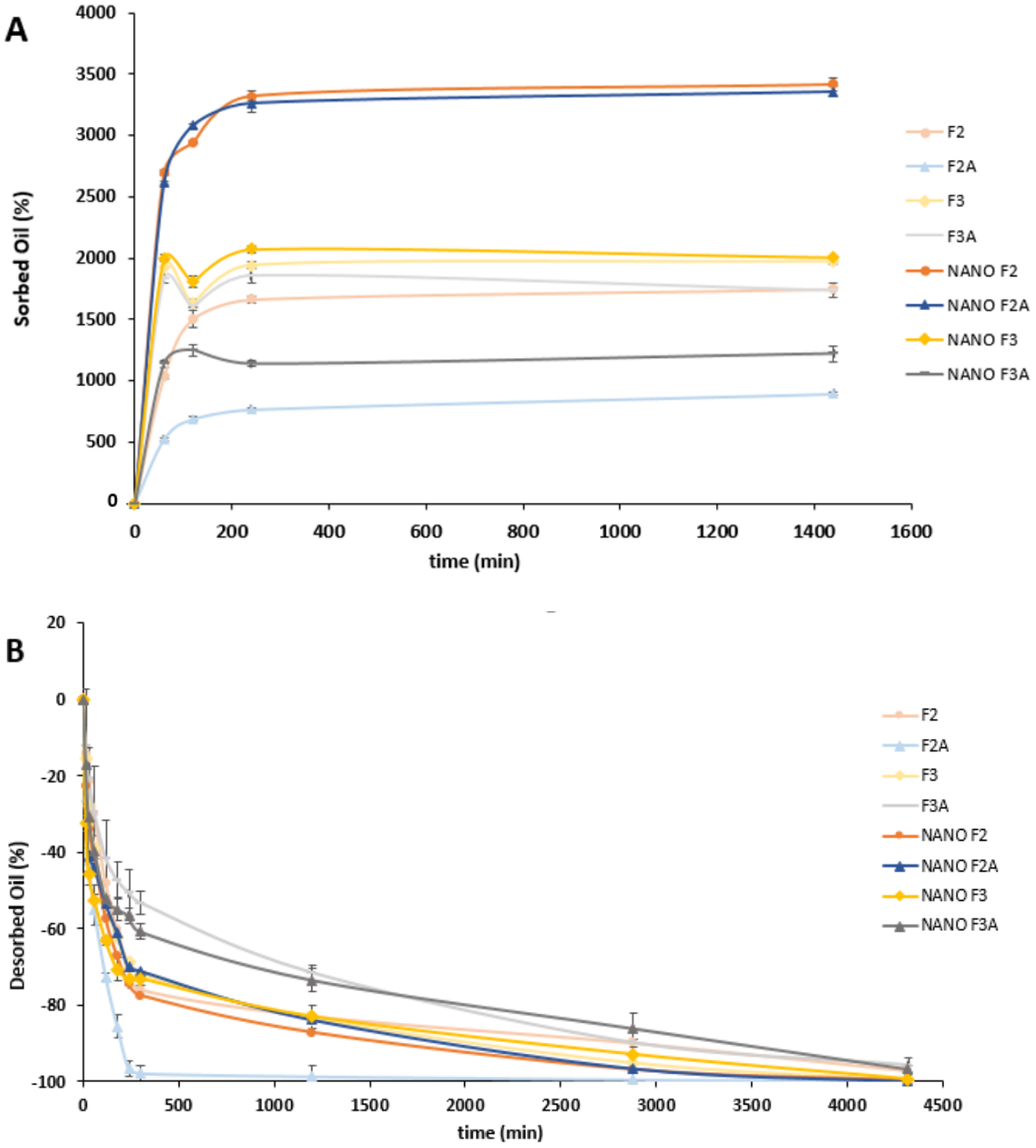

Figure S1. Oil sorption (A) and desorption (B) kinetics for the *P. oceanica* (nano)cellulosic aerogels (0.5 wt.-%).

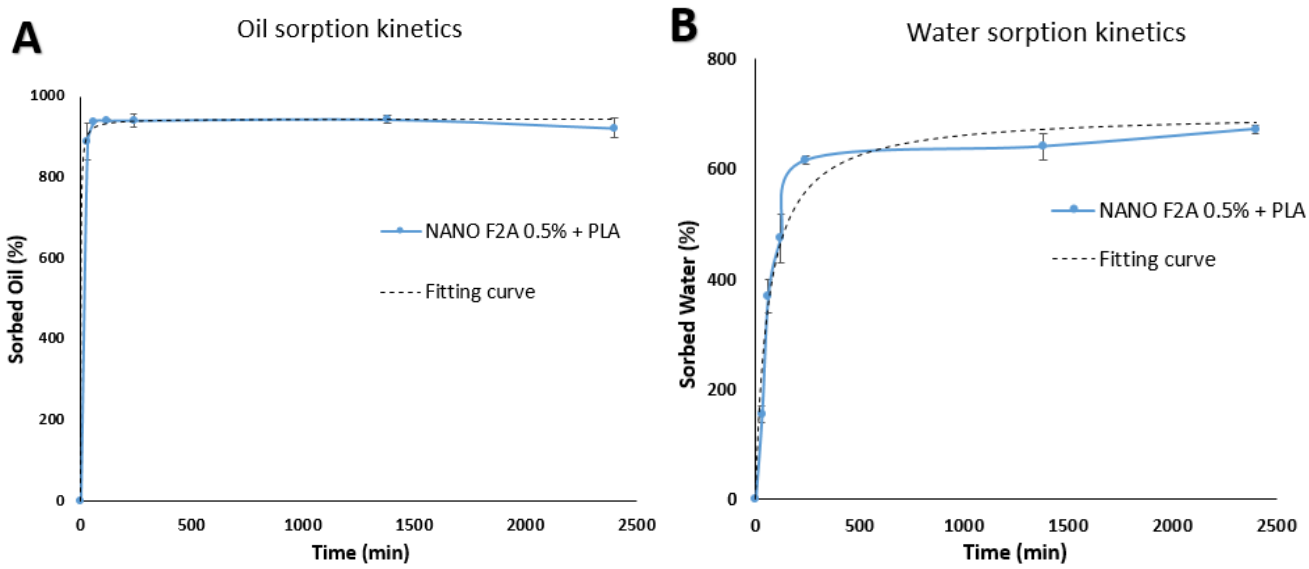

Figure S2. Oil (A) and water (B) sorption kinetics for the NANO F2A 0.5% + PLA aerogel. The dotted lines correspond to the fitting curves obtained using pseudo-first order and pseudo-second order models.

Table S1. Kinetic parameters obtained by fitting the oil and water sorption curves to pseudo-first order and pseudo-second order models.

	OIL			WATER		
	q_e (%)	k_2	R^2	q_e (%)	k_1	R^2
F3 0.5% + PLA	686.7	$3.4 \cdot 10^{-4}$	0.9980	305.8	$4.3 \cdot 10^{-4}$	0.9837
F3 1% + PLA	627.1	$1.7 \cdot 10^{-4}$	0.9994	288.2	$7.0 \cdot 10^{-5}$	0.9207
F3 1.5% + PLA	639.5	$3.8 \cdot 10^{-4}$	0.9969	291.5	$7.7 \cdot 10^{-5}$	0.9597
F3 2% + PLA	583.8	$1.1 \cdot 10^{-3}$	0.9996	260.4	$1.7 \cdot 10^{-4}$	0.9735
NANO F3 0.5% + PLA	835.5	$6.7 \cdot 10^{-4}$	0.9997	355.9	$7.3 \cdot 10^{-5}$	0.9942
NANO F3 1% + PLA	804.8	$3.7 \cdot 10^{-3}$	0.9985	321.5	$6.5 \cdot 10^{-5}$	0.9916
NANO F3 1.5% + PLA	641.3	$9.7 \cdot 10^{-4}$	0.9937	294.1	$9.4 \cdot 10^{-5}$	0.9856
NANO F3 2% + PLA	594.8	$8.2 \cdot 10^{-4}$	0.9986	274.0	$1.9 \cdot 10^{-4}$	0.9843
NANO F2A 0.5% + PLA	942.6	$7.4 \cdot 10^{-4}$	0.9987	699.3	$2.3 \cdot 10^{-5}$	0.9733
NANO F2A 1% + PLA	788.7	$4.1 \cdot 10^{-4}$	0.9962	584.8	$2.7 \cdot 10^{-5}$	0.9746
NANO F2A 1.5% + PLA	730.6	$5.4 \cdot 10^{-3}$	0.9994	456.6	$5.9 \cdot 10^{-5}$	0.9863
NANO F2A 2% + PLA	745.8	$1.7 \cdot 10^{-3}$	0.9992	458.7	$3.3 \cdot 10^{-5}$	0.9575
NANO F2 0.5% + PLA	836.7	$2.0 \cdot 10^{-4}$	0.9987	531.9	$4.1 \cdot 10^{-5}$	0.9936
NANO F2 1% + PLA	771.7	$3.7 \cdot 10^{-4}$	0.9975	401.6	$3.2 \cdot 10^{-5}$	0.9673
NANO F2 1.5% + PLA	748.7	$3.1 \cdot 10^{-3}$	0.9991	369.0	$5.7 \cdot 10^{-5}$	0.9226
NANO F2 2%+ PLA	722.9	$4.0 \cdot 10^{-3}$	0.9996	371.7	$3.9 \cdot 10^{-5}$	0.9642

A

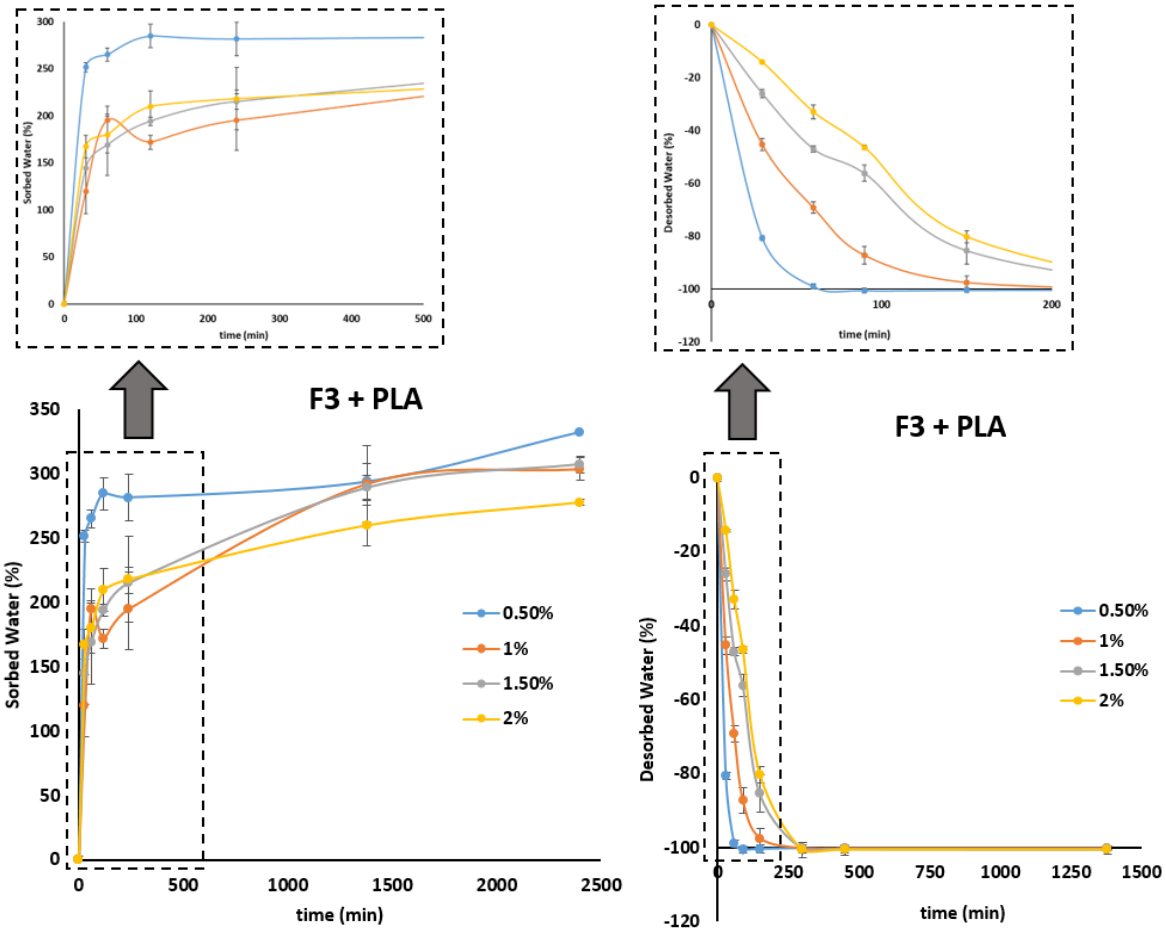
F3 + PLA
Sorbed Water (%)
time (min)
0.50%
1%
1.50%
2%
F3 + PLA
Desorbed Water (%)
time (min)
0.50%
1%
1.50%
2%

B

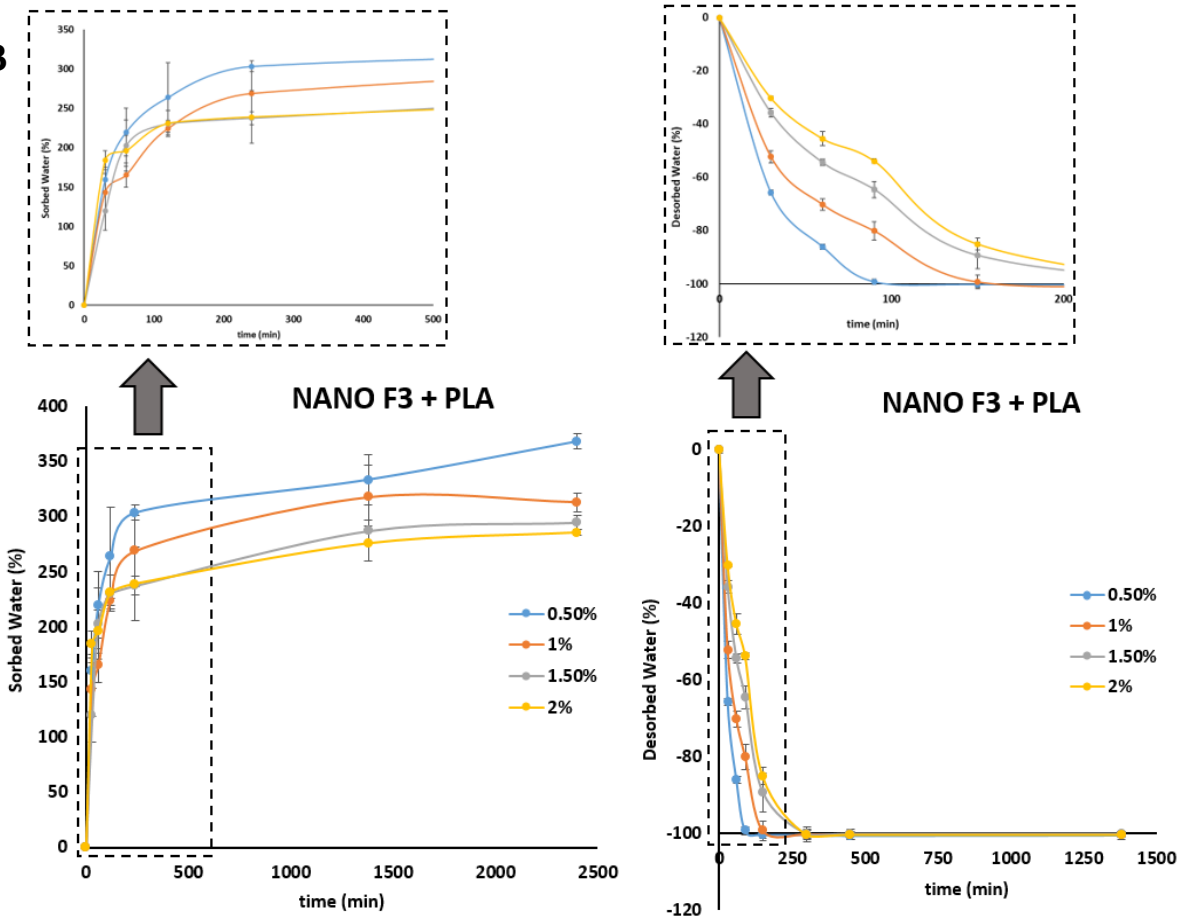
NANO F3 + PLA
Sorbed Water (%)
time (min)
0.50%
1%
1.50%
2%
NANO F3 + PLA
Desorbed Water (%)
time (min)
0.50%
1%
1.50%
2%

C

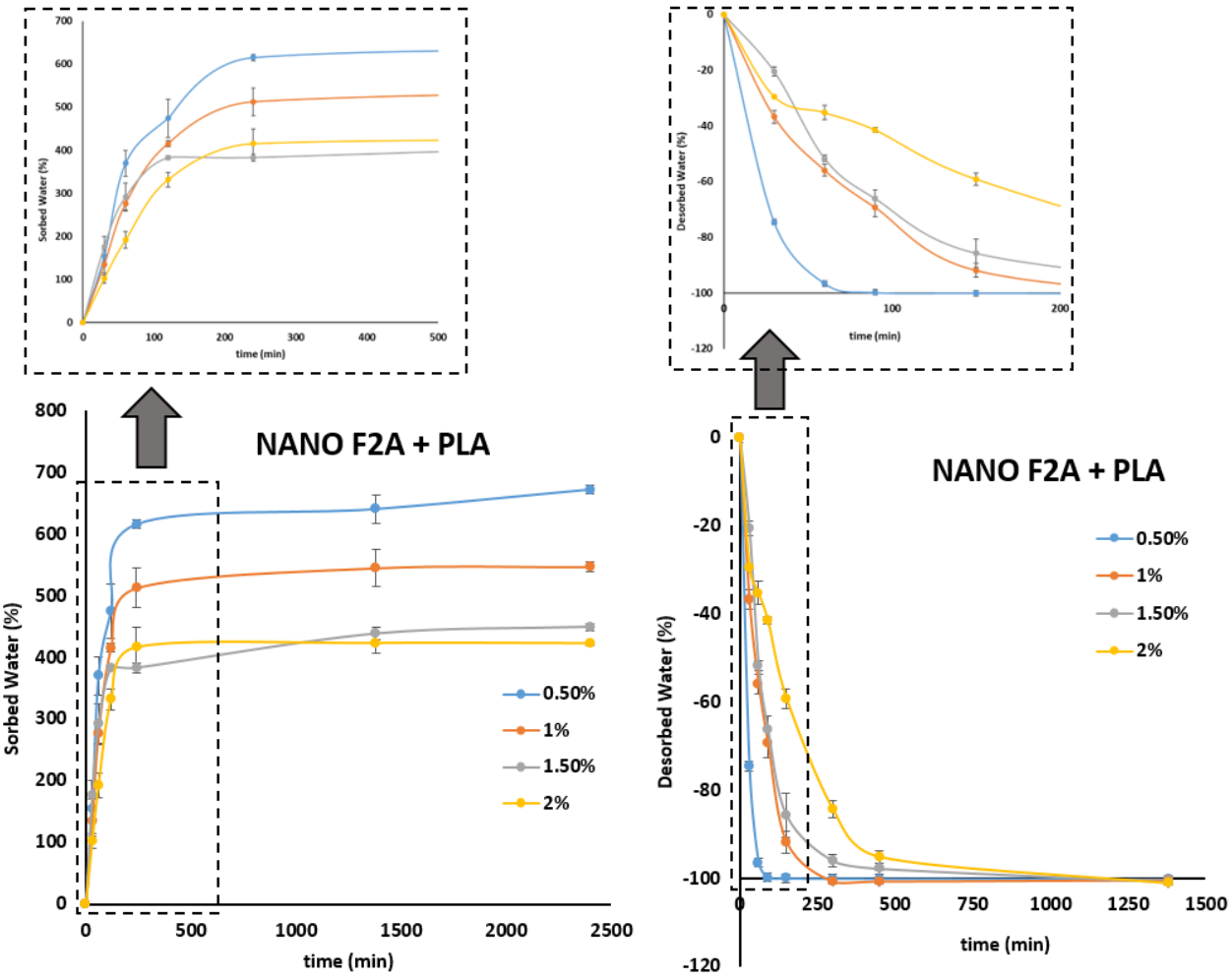
NANO F2A + PLA
Sorbed Water (%)
time (min)
0.50%
1%
1.50%
2%
NANO F2A + PLA
Desorbed Water (%)
time (min)
0.50%
1%
1.50%
2%

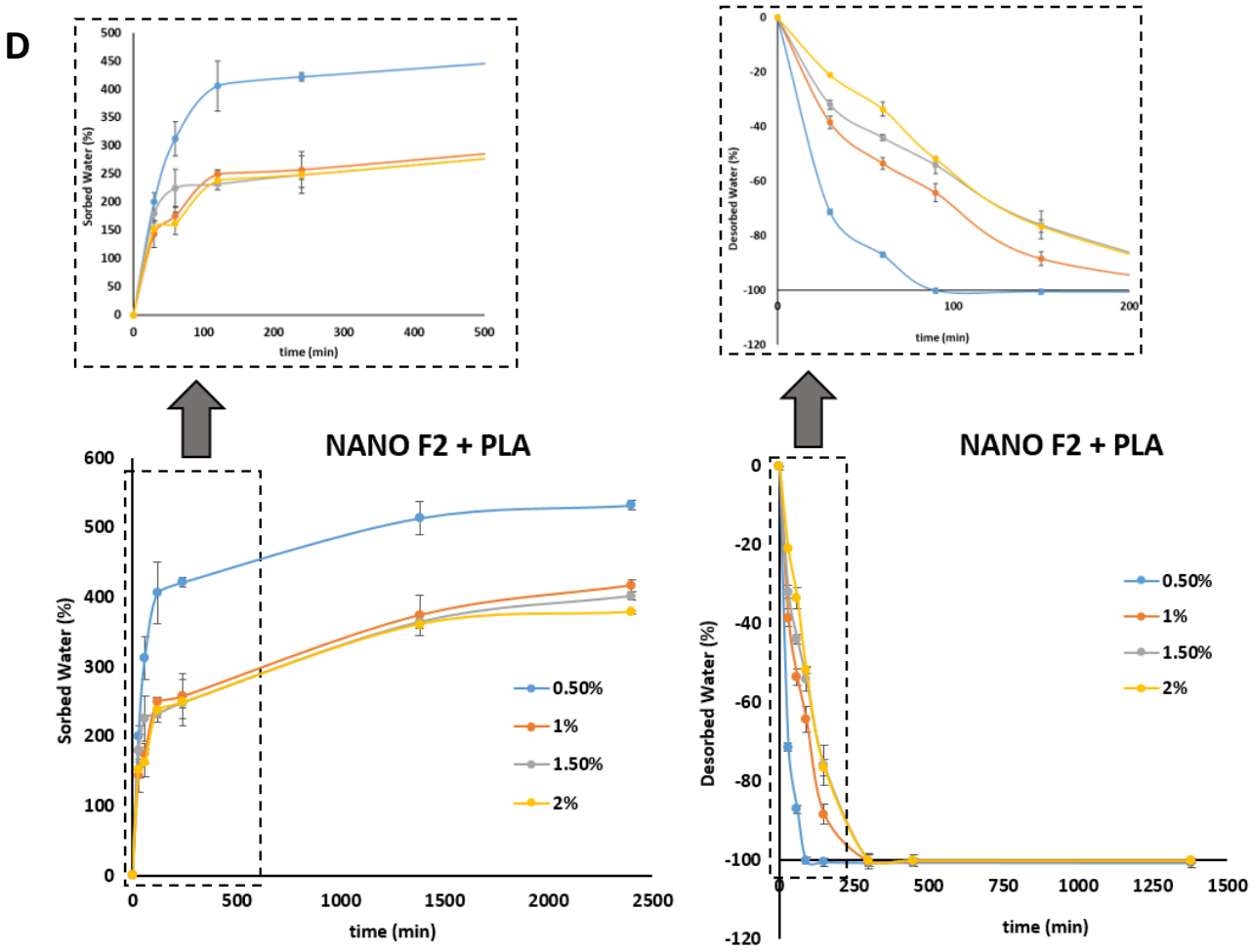

Figure S3. Water sorption/desorption kinetics of the different aerogels at their different concentrations (0.5-2%) being (A) F3, (B) NANO F3, (C) NANO F2A and (D) NANO F2.

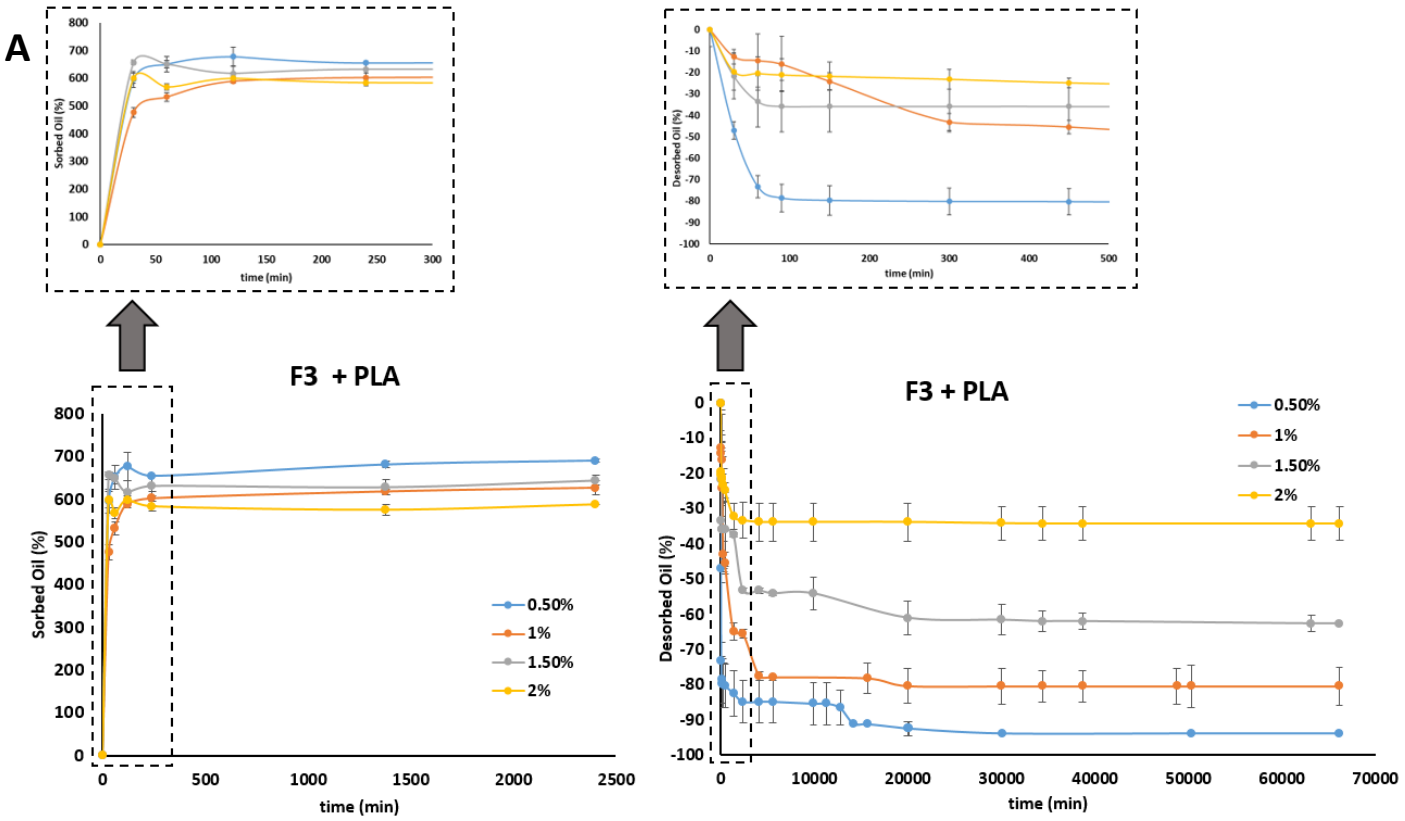
A
Sorbed Oil (%)
time (min)
F3 + PLA
0.50%
1%
1.50%
2%
Desorbed Oil (%)
time (min)
F3 + PLA
0.50%
1%
1.50%
2%

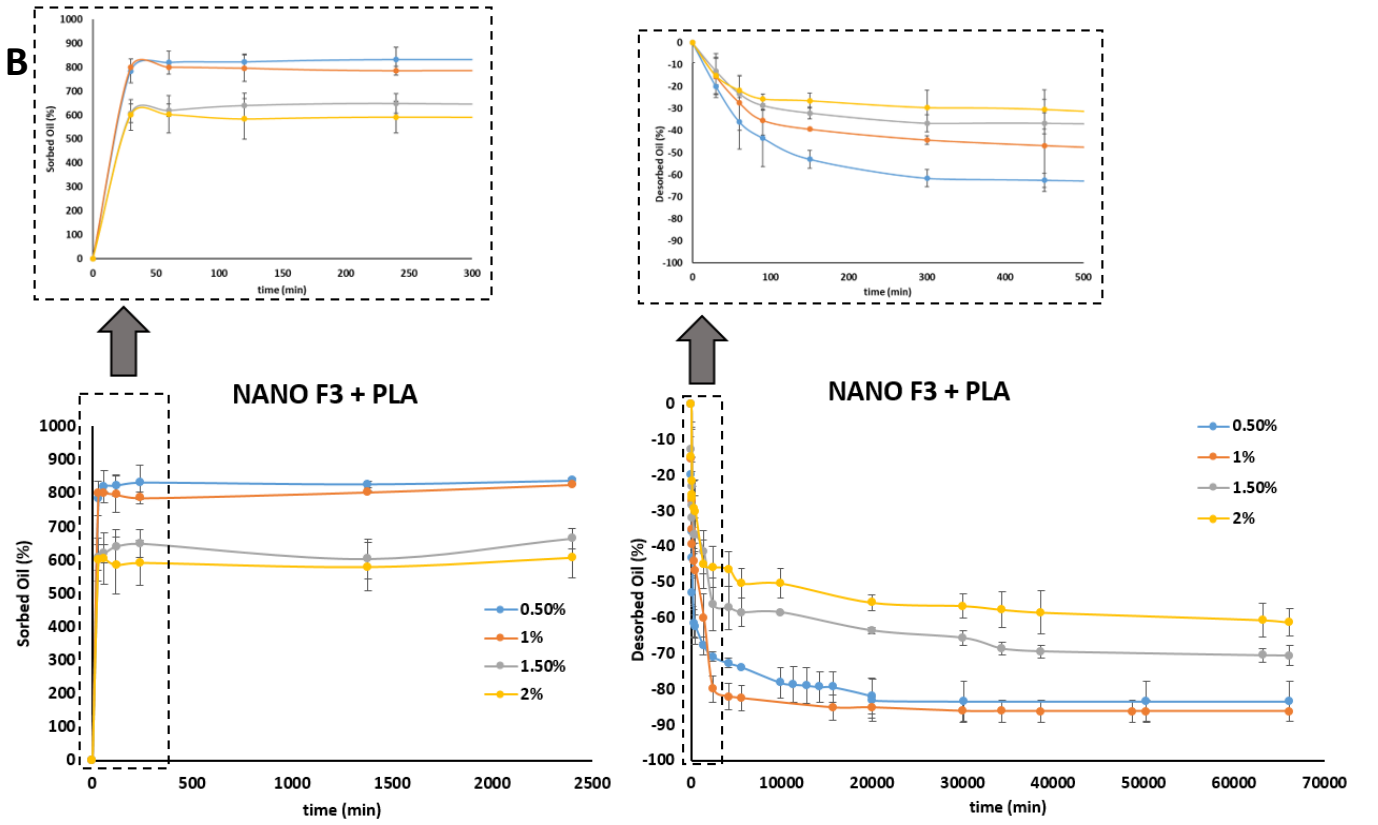
B
Sorbed Oil (%)
time (min)
NANO F3 + PLA
0.50%
1%
1.50%
2%
Desorbed Oil (%)
time (min)
NANO F3 + PLA
0.50%
1%
1.50%
2%

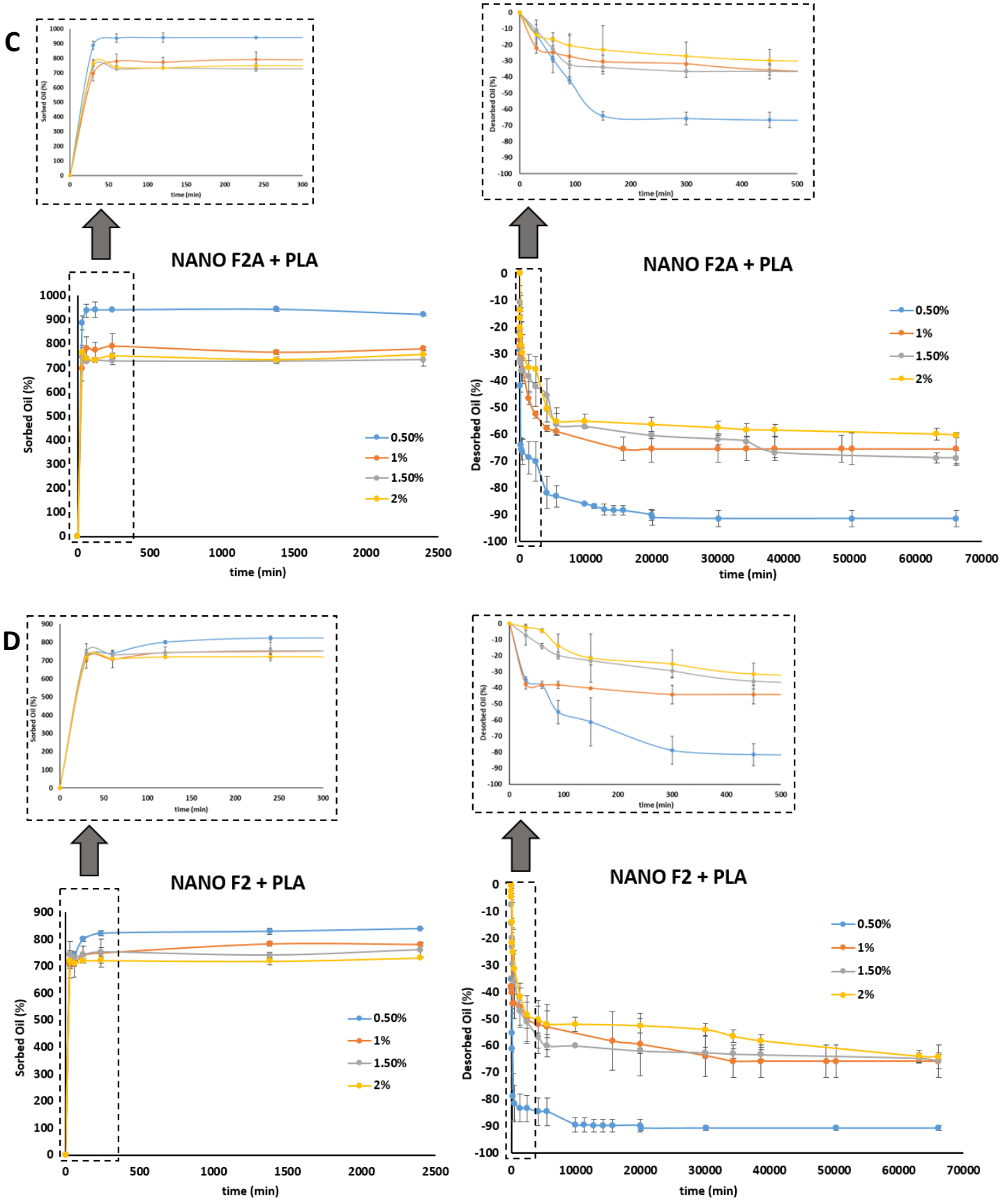

Figure S4. Oil sorption/desorption kinetics of the different aerogels at their different concentrations (0.5-2%) being (A) F3 (F), (B) NANO F3, (C) NANO F2A and (D) NANO F2.

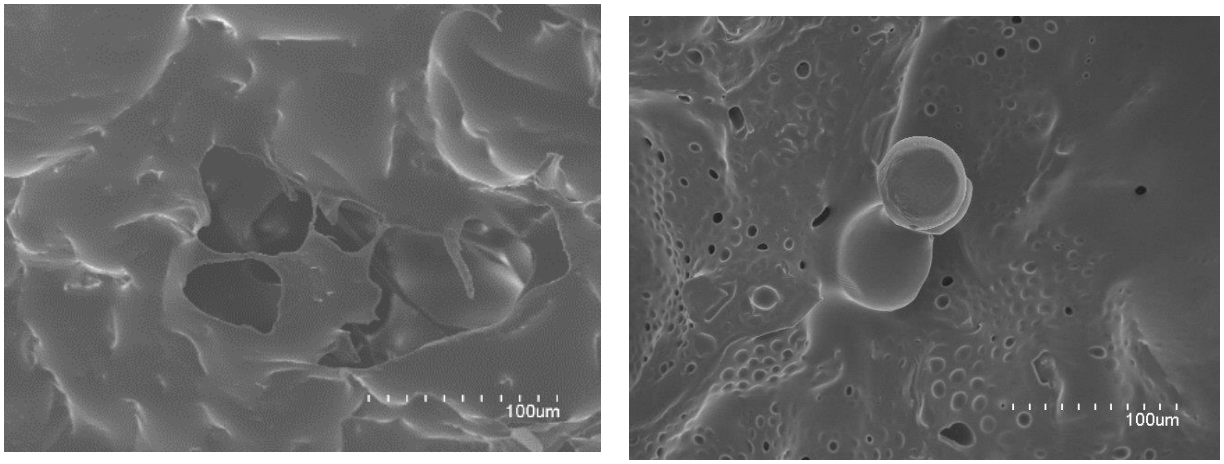

Figure S5. SEM images of the selected PLA-coated (nano)cellulosic aerogels after the oil desorption experiments. (A) corresponds to NANO F2 0.5% and (B) to NANO F2 2%.

4.2. Confocal Raman imaging as a useful tool to understand the internal microstructure of multicomponent aerogels

---

This section is an adapted version of the following published research article:

Benito-González, I., López-Rubio, A., Martínez-Sanz, M. & Gómez-Mascaraque, L. G. (2020). Confocal Raman imaging as a useful tool to understand the internal microstructure of multicomponent aerogels

Journal of Raman Spectroscopy, 51, 2022-2035. DOI:

https://doi.org/10.1002/jrs.5936

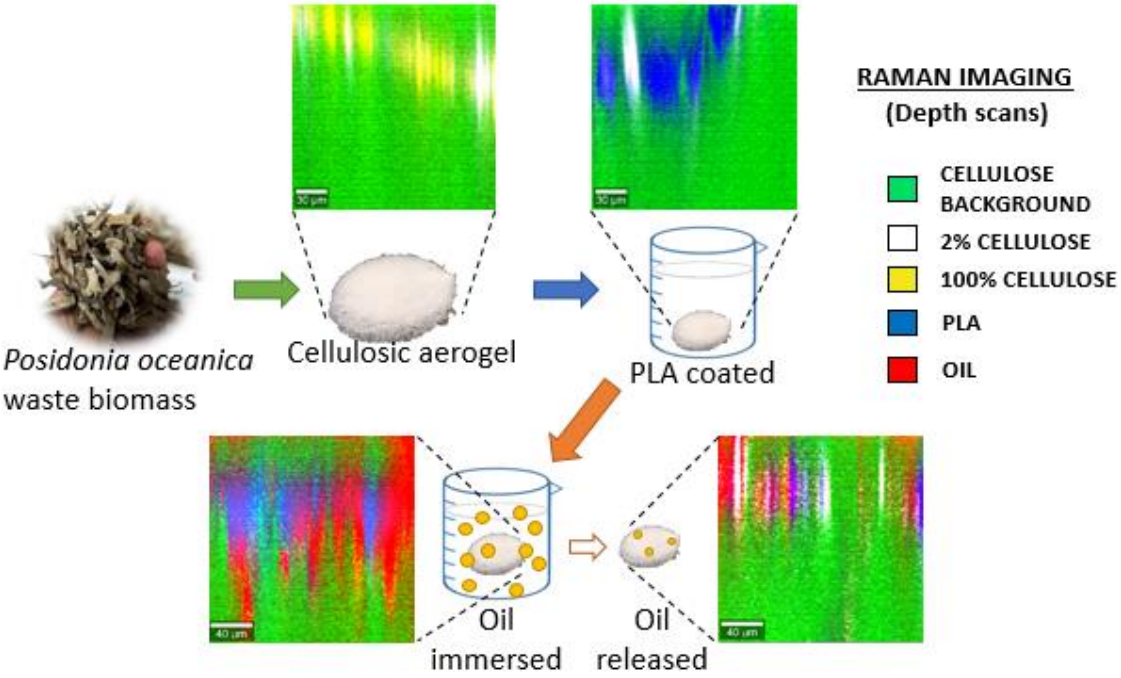

1. Abstract

This work shows the characterization of (nano)cellulosic aerogels prepared from *Posidonia oceanica* waste biomass by means of confocal Raman microscopy (CRM). For this aim, aerogels were prepared by simple freeze-drying of aqueous dispersions of four (nano)cellulosic fractions with different purification degrees, tested at two different concentrations (0.5% and 2%). These were then coated with polylactic acid (PLA) in order to improve their hydrophobicity and subjected to oil sorption–desorption experiments. Both univariate and multivariate analyses, including an approach based on comparing the spectra with those of reference materials and another one based on automatic detection of components, were compared in terms of the quality and the accuracy of the information provided. Univariate analysis only provided accurate information in the simplest systems (native (nano)cellulosic aerogels), while multivariate analyses facilitated the detection of the different components even for the most complex structures. Automatic identification of components was selected as the optimal methodology, although it also underestimated the abundance of the components with the least intense Raman spectra (cellulosic clusters) in the presence of PLA and oil. Comparison with the reference materials resulted in unrealistic images for the most complex systems. Micron-sized regions of concentrated cellulose were detected using CRM, being more abundant in the denser aerogels. Results also confirmed that PLA was preferentially located close to the surface, while oil could penetrate deeper along the matrix. Overall, the results showed the potential of Raman imaging as a novel approach for the characterization of complex biopolymeric aerogels.

2. Introduction

Aerogels are extremely light and porous materials with high surface area and low density, which are useful for a wide range of applications due to their high absorption and adsorption capacities [8-10]. Although aerogels have been traditionally made from inorganic materials [11, 12], their application as adsorbent/absorbent structures (pads) in food packaging requires the search of alternative and more sustainable materials with properties that resemble those from the commercially used synthetic polymeric pads. In this sense, cellulose is being explored as one of the most promising biopolymers for the development of high performance aerogels [14-16, 35]. Cellulose can be extracted from several resources such as cotton, spruce or wood [36-38]. However, these resources usually compete with their agricultural purpose and so become unsustainable. As a result, alternative sources such as aquatic biomass and, in particular, waste biomass, have been recently proposed as sustainable sources for the extraction of cellulosic fractions [6, 25, 39].

Posidonia oceanica (*P. oceanica*) is a marine seagrass endemic to the Mediterranean Sea whose native form can be beneficial for other marine organisms and seashores. However, during its lifecycle, *P. oceanica* leaves detach off their stems and, after being dragged by marine currents, accumulate on the coasts, generating a residue which is detrimental for the quality of the beaches, tourism and local economy [40]. In an effort to valorise this residue, its utilization as a renewable source of cellulose and nanocellulose has been recently proposed [41]. The common processes for the extraction and purification of cellulose from plant-derived biomass generally involve aggressive Soxhlet, alkali and acid treatments [24]. Interestingly, less purified cellulosic and nanocellulosic fractions have been obtained by simpler extraction protocols, in which both the Soxhlet and alkali treatments were omitted. These fractions were reported to contain lipidic and hemicellulosic components [41], whose presence was beneficial for the preparation of aerogels, significantly affecting their microstructure. These (nano)cellulosic aerogels exhibited lower density and higher surface area than the pure (nano)cellulose aerogels, being capable of adsorbing large amounts of oil; however, they presented very poor performance in contact with water. In this context, a simple PLA dipping strategy was developed in order to increase their hydrophobicity and mechanical performance, yielding PLA-coated aerogels with remarkable oil-sorption capacity (more than 900% w/w) making them suitable for food-packaging applications as adsorbent pads or for oil spill cleaning applications [42].

Unarguably, the microstructure of these materials has a critical impact on their functional and mechanical properties. Although a preliminary analysis of the microstructure of the (nano)cellulosic aerogels and the effect of PLA coating was carried out in our previous work [42], the study was only performed on the surface of the materials. Confocal microscopy techniques allow visualisation of different thin optical sections of samples and, thus, can provide three-dimensional information without physically sectioning the samples or disturbing their internal structure [43]. As opposed to the more commonly used Confocal Scanning Laser Microscopy (CSLM) technique, which often requires the use of fluorescent dyes that can potentially alter the microstructure of the specimens [44], Confocal Raman Microscopy (CRM) is based on the principles of Raman spectroscopy, where each pixel of the resulting images comprises the chemical information obtained from the Raman spectra collected from each spot in the sample. Therefore, it can simultaneously provide visual and compositional information of the mapped sample area. The usefulness of CRM to study the microstructure of different systems such as plant cell membranes [45] or even specific food components present in bread or cheese has been already demonstrated [46, 47]. However, to the best of our knowledge, the study of aerogels by CRM represents an innovative approach.

When mapping the distribution of different components in a material through CRM, there are different data processing approaches to transform the information of the Raman spectra into an

image, and the selected method can have a critical impact on the quality and accuracy of the information obtained. These methods can be divided in univariate and multivariate. On one hand, univariate methods consist of analysing the sample by taking into account a small concrete region of the spectrum and is the methodology most commonly followed and reported in the literature [45, 48, 49]. On the other hand, multivariate analyses are more complex approaches which allow taking into account the whole spectra of the analysed area and, thus, consider all the chemical information available [46, 47].

This work explores the potential of CRM to study the microstructure of PLA-coated (nano)cellulosic aerogels produced from *P. oceanica* waste biomass by optimized protocols. The aerogels were studied before and after the PLA dipping process, as well as the internal distribution of oil within the PLA-coated aerogels after oil immersion. Different data processing approaches (univariate and multivariate) were applied and compared in order to establish the optimal methodology for the analysis of this type of materials through CRM. CLSM was used as a complementary technique to compare the results obtained from CRM.

3. Materials and methods

3.1 Raw material

Biomass waste material consisting of *Posidonia oceanica* leaves was collected in the sea shore of Calpe (Alicante, Spain) in January 2018, washed with water to remove sand and salts, and stored under refrigeration conditions (4º C) until further use.

3.2 Preparation of cellulosic fractions and nanocrystals

A purification procedure described in previous works [24, 25, 50], consisting of a Soxhlet extraction, followed by acid bleaching and an alkaline treatment, was carried out to sequentially remove cell wall components from *P. oceanica* waste biomass and obtain pure cellulose (F3). Additionally, less purified holocellulosic fractions were produced by omitting the alkaline treatment (F2) or both the Soxhlet and alkaline treatments (F2A). Subsequently, these three fractions were subjected to an acid hydrolysis [41], yielding nanocellulosic fractions (NANO F3, NANO F2 and NANO F2A).

3.3 Production of the aerogels

Cellulosic and nanocellulosic aerogels were produced from aqueous dispersions of the (nano)cellulosic materials at concentrations of 0.5% and 2% (w/v). The dispersions were freeze-dried to remove water and obtain the (nano)cellulosic primary scaffolds. These aerogels, which were selected due to their high sorption capacity and good processability [42], were coded

according to the (nano)cellulosic fraction used (F3, NANO F3, NANO F2A and NANO F2). The aerogels were then coated with PLA using a proprietary technology [42, 51] to form the final hybrid structures (F3 + PLA, NANO F3 + PLA, NANO F2A + PLA and NANO F2 + PLA). All the aerogels were stored in equilibrated relative humidity cabinets at 0% RH and 25ºC for at least three days prior to their characterization.

3.4 Oil immersion

Small pieces (~1cm^2) of the PLA-coated (nano)cellulosic aerogels were immersed in sunflower oil for at least 1 minute. Oil excess was carefully withdrawn until the material stopped dripping. Oil-immersed aerogels were coded as F3 + OIL, NANO F3 + OIL, NANO F2A + OIL and NANO F2 + OIL. These aerogels were then stored at ambient conditions and placed on top of filter paper to accelerate oil release. After 7 days, equilibrium was considered to be reached for the oil desorption process, according to previous studies [42], and the equilibrated aerogels were also characterized and named as F3 + OIL (f), NANO F3 + OIL (f), NANO F2A + OIL (f) and NANO F2 + OIL (f).

3.5 Confocal laser scanning microscopy (CLSM)

Sunflower oil was stained by adding 0.1% (v/v) of Nile Red in ethanol (1:10 Nile Red:Oil) and vortexed vigorously until a homogeneous solution was achieved. Aerogels were then immersed in the stained oil for at least 10 minutes in order to maximize oil sorption. Immersed aerogels were then visualized using a Leica TCS SP5 confocal laser scanning microscope (Leica Microsystems CMS GmbH, Wetzlar, Germany) with 5x dry objective (numerical aperture of 0.12) and the pinhole set at 1 Airy Unit. Nile red was excited at 488 nm using an Argon laser, and the emission filter was set at 560-600 nm. A second filter set at 488 nm was also used to observe the light reflected by the cellulosic materials. Leica LAS AV software (v 2.7.3.9723) was used to acquire digital images of 1024 x 1024 pixels in size at day 1 and 7 after immersion. Samples were placed in darkness conditions between imaging to avoid fluorescence loss.

3.6 Confocal Raman microscopy (CRM)

3.6.1 Equipment and software

An Alpha300 R confocal Raman microscope (WITec, Germany) equipped with a 532 nm laser and an ultra-fast Raman imaging CCD camera was used for all the CRM analysis. The Raman shift was calibrated using silicon. Project Five software v5.0 (WITec, Germany) was used for image processing and analysis.

3.6.2. Acquisition of single Raman spectra of reference materials

Single Raman spectra of the reference materials were initially obtained. Pieces of the (nano)cellulosic aerogels (0.5% and 2%), raw PLA pellets and an oil droplet were placed on microscopy slides. Additionally, the original (nano)cellulosic fractions were oven-dried at 60 ºC for at least 2 h in order to obtain denser materials. This was expected to result in more intense Raman spectra, given that the aerogels were mainly composed by air (> 98% v/v [42]). These samples were named "dry (100%)" and also mounted on microscopy slides. A 50x microscope objective (0.55 numerical aperture) was then used to collect the Raman spectra of the samples at 5 different points, with 20 accumulations of 1 s of integration time each and laser power of 30 mW. The raw spectra were processed using the cosmic ray removal correction function of the software (filter size 3, dynamic factor 8) and a shape function for the background subtraction (shape size 250, noise factor 1). Finally, the 5 spectra of each sample were averaged and added to a library to be used as reference spectra.

3.6.3 Confocal Raman imaging of the aerogels

2D micrographs (depth scans, i.e. cross section images) of the four different (nano)cellulosic aerogels and their respective PLA-coated aerogels were obtained using a 10x objective (0.25 numerical aperture). Areas of 200 μm × 200 μm (X, Z) were scanned at 150 points per line and 150 lines per image, and spectra were collected with a laser power of 25 mW and an integration time of 0.25 s, which resulted in a measurement time of approx. 40 minutes. Three different cross sections were scanned for each aerogel. Hybrid PLA-coated aerogels were also imaged in triplicate after oil immersion and oil release (after 7 days).

Image z-stacks were also obtained for the aerogel which previously showed the most optimum performance (NANO F2A 2%) [42], in order to study the three-dimensional distribution of components in the original aerogel. In addition, images were acquired for the PLA-coated aerogel before (NANO F2A 2% + PLA) and after oil immersion (NANO F2A 2% + OIL). In this case, volumes of 200 μm x 50 μm x 200 μm (X, Y, Z) were scanned at 100 points per line, 25 lines per image and 100 layers per stack with an integration time of 0.35 s per point, resulting in a measurement time of approx. 8 hours. The laser power was fixed at 30 mW while 10x was the selected objective.

3.6.4 Bright field imaging

Optical 2D micrographs of the aerogels were also obtained using the bright field mode of the confocal Raman microscope, with the 50x objective on the aerogels' raw surface, after PLA coating and after oil immersion and release. Surface areas of 1000 μm × 1000 μm (X, Y) were imaged at 1000 points per line x 1000 lines per image.

3.7 Image processing and analysis

After cosmic ray removal and background subtraction, performed as described in Section 2.6.2, the spectra from the depth scans were processed following three different procedures to map the spatial distribution of the different components (i.e. cellulose, PLA and oil), the first two based on those previously explored by Huen, Weikusat, Bayer-Giraldi, Weikusat, Ringer and Lösche [46]. These three methods were then compared to evaluate differences in the information provided.

3.7.1 Integration of single Raman bands (univariate analysis)

In the first method, single Raman bands characteristic for each component were integrated. Monochromatic images were generated, where the intensity of the pixels was proportional to the area of those individual bands in each measurement point. The specific spectral ranges selected for each component are marked in blue in Fig. 1, and are identified by their central value in the text and figures. Every filter used had a width of 60 cm^{-1} except the one centred at 2955 cm^{-1} whose width was 30 cm^{-1} in order to avoid overlapping with nearby bands. Additionally, a combined image was created overlapping the resulting images of single filters derived from each component at every aerogel.

3.7.2 Multivariate analysis based on reference materials

The second method considered the full Raman spectra rather than single bands using the True Component Analysis tool of the software. This function is based on the basis analysis algorithm, and describes each measured spectrum of a hyperspectral dataset by a linear combination of reference spectra, as depicted in equation 1, where $\overrightarrow{S_i}$ is spectrum *i* from the hyperspectral dataset, $\overrightarrow{H_i}$ is the mixing values for spectrum i, $\overrightarrow{E_i}$ is the error spectrum and $\hat{B}$ is the matrix of basis (reference) spectra. The mixing values are fitted by the method of least squares minimizing the expression shown in equation 2.

$$\overrightarrow{S_i} = \hat{B}\overrightarrow{H_i} + \overrightarrow{E_i} \qquad \text{Eq. 1}$$

$$(\overrightarrow{S_i} - \hat{B}\overrightarrow{H_i})^2 = Minimum \qquad \text{Eq. 2}$$

In practice, the spectra of the reference materials are the inputs, and the outputs are one image for each component spectra showing the intensity distribution for this spectrum. For this analysis, every single spectrum expected to be present in each sample was added as inputs (i.e. all cellulosic spectra in raw aerogels, cellulosic spectra + PLA in PLA-coated aerogels and cellulosic spectra + PLA + oil in immersed PLA-coated aerogels both before and after oil release). ImageJ-win64 software was utilised for calculating the relative abundance (%) of each component in every

image by analysing their coloured histogram. Briefly, the distribution and area (in pixels) of each colour was obtained and compared to the total area of the image.

3.7.3 Multivariate analysis based on automatic component identification

A third method based on the automatic component identification was carried out. This method also used the True Component Analysis function of the software but without providing any reference spectra. Instead, the software was asked to select a first spectrum from the whole dataset (the most intense) as a base spectrum and calculate the residual image. If the residual image is structured, subsequent cycles of adding components automatically and calculating the corresponding residual images are performed until it was considered that the residual image showed only noise. Figure S1 (Supporting Information) shows an example of a final residual image. The components automatically detected where then demixed, compared with a library built with the reference spectra, and assigned to the one with the highest similarity index (≥ 90%) using the True Match software. Again, ImageJ software was used for calculating the relative abundance (%) of each component in every image by analysing their coloured histogram. In both the second and third methodologies, each sample point was assumed to proceed from a linear combination of the single components of the systems analysed.

3.7.4 3D image analysis

The individual 100 layers of the z-stack were processed using the third method (Section 3.7.3) and exported as a stack. The different components were later combined using ImageJ-win64 software.

3.8 Statistics

Analysis of variance (ANOVA) followed by a Tukey-b test were used when comparing more than two data sets, after confirming the homogeneity of variances by the Levene test using IBM SPSS Statistics software v.26. All data have been represented as the average ± standard deviation. Significant differences ($p \leq 0.05$) are denoted by showing the data provided in tables with different letters.

4. Results and discussion

4.1 Raman spectra of single components

Spectra of every single component were obtained and are shown in Fig. 1, and the most representative peaks are referenced in Table 1. Due to the high similarity between the different (nano)cellulosic fractions, as shown in Fig. S2 (Supporting Information), pure cellulose (F3) was selected as the most representative one in Fig. 1. As expected, there was a substantial difference between (nano)cellulose spectra depending on the concentration used to prepare the samples (0.5% or 2% in the case of the aerogels, and 100% assumed for the dry fraction). While only two peaks at 480 cm^{-1} and 2430 cm^{-1} could be observed at the lowest concentration (0.5%), the characteristic peaks of cellulose at 1100 cm^{-1} and 2900 cm^{-1} (Table 1) became more intense in the aerogels prepared from 2% (nano)cellulose dispersions, and were even more evident in the dried cellulose (Figure 1). The spectra of the 0.5% aerogels, thus, seemed to arise from light scattering phenomena as a result of the crystalline nature of the cellulosic materials, rather than corresponding to the Raman spectrum of cellulose itself. Given that air comprised >99% of the volume of these structures [42], these aerogels can be considered very diluted systems with very weak Raman signals. This suggested that the selected instrumental conditions were not able to identify the components present in the lightest hydrogels, so these spectra will be referred as "cellulose background" throughout the manuscript. On the other hand, in the case of the (nano)cellulose dried in the oven, additional peaks in the 100-500 cm^{-1} and 1400 cm^{-1} regions were present in accordance with those extensively reported for cellulose in the literature (Table 1) [52]. However, there were no major differences found between the spectra of the different (nano)cellulosic fractions. As observed in Fig. S2 (Supporting Information), NANO F2A showed slightly broader peaks than the rest in the 1200-1500 cm^{-1} region (dry spectrum), while the 2970-2840 cm^{-1} region became sharper in the spectrum of its 2% aerogels, suggesting more abundance of the C—H stretching vibrations instead of C—C—H bending, CH_2 wagging and C—O—H bending in comparison with the other (nano)cellulosic fractions. This can be attributed to the presence of a minor fraction of lipids in this material [41]. It is worth highlighting that the relative intensities of the Raman spectral bands from the (nano)cellulosic aerogels were more sensitive to the density of the material than to the differences in composition, despite the presence of a significant fraction of hemicelluloses (in both NANO F2A and NANO F2) and lipids (NANO F2A) that were resistant to the sulphuric acid hydrolysis [41].

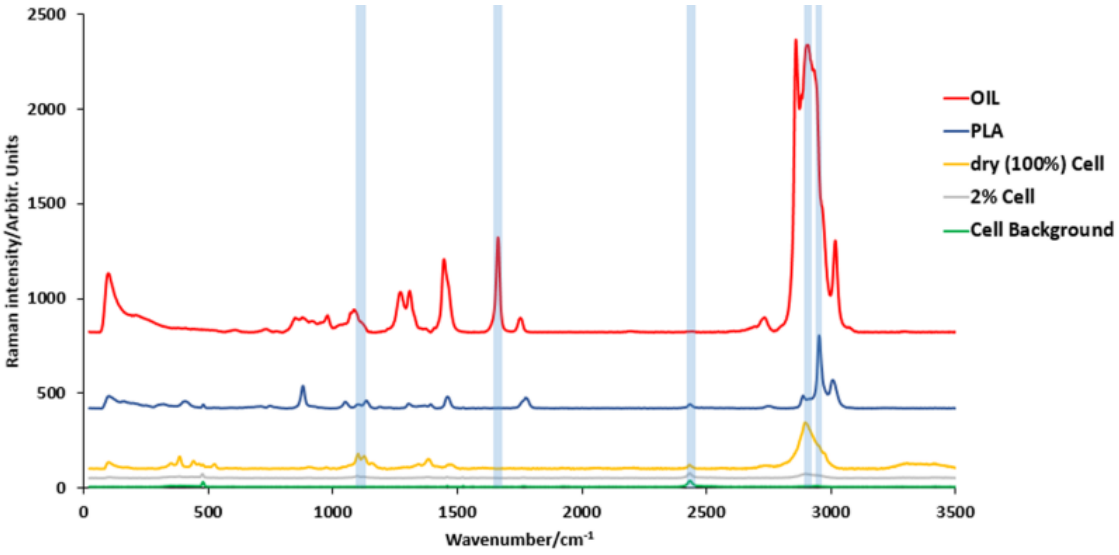

Figure 1. Average Raman spectra of the reference components: cellulose background, 2% aerogels, dry cellulose (100%), PLA and oil. Blue bands indicate the spectral ranges used for the image analysis based on the integration of single bands.

Table 1. Characteristic spectral ranges of cellulose, PLA and oil identified in the samples

Component	Spectral range (cm^{-1})	Band assignment	Reference
Cellulose	2970-2840	C—H stretching vibrations	[52]
	1450-1200	C—C—H bending, CH_2 wagging and C—O—H bending	[52]
	1150-950	C—O Stretching vibrations	[52]
	600-300	Ring torsion and bending vibrations	[52]
PLA	3000-2900	CH_3 asymmetric stretching	[53]
Oil	3020-2980	=C–H symmetric stretching	[54]
	2980-2850	C–H stretching of methyl and methylene groups	[54]
	1680-1640	*cis* C=C stretching	[54]

4.2 2D Raman micrographs (depth scans) of the (nano)cellulosic aerogels

4.2.1 Impact of the analysis method on the extent of structural information obtained

In order to evaluate the suitability of the different methodologies described in sections 3.7.1, 3.7.2. and 3.7.3 to carry out a compositional analysis using Raman imaging, the same aerogel was analysed using the three different methodologies.

For the univariate analysis, different spectral ranges were selected depending on the complexity of the samples ((nano)cellulosic aerogel, (nano)cellulosic aerogel + PLA and (nano)cellulosic aerogel + PLA + oil). The band at 2430 cm^{-1} was selected to identify the cellulose background, while both 2900 cm^{-1} and 1100 cm^{-1} bands were selected for identifying denser cellulosic regions (tagged 2% and 100% respectively, to emphasize the significant differences in density). Although the 2900 cm^{-1} vibrational band was clearly much more intense than that at 1100 cm^{-1}, the latter was preferentially selected as it did not overlap with the oil spectra (cf. Figure 1). In any case, both bands were finally tested in order to show the possible differences and evaluate how band selection can affect the final analysis.

With respect to the oil and PLA spectra, PLA presented similar intensity than dry cellulose while the oil spectrum was much more intense. The Raman spectra of fats are generally intense due to the abundance of C-C single and double bonds in these compounds, derived from the presence of long non-polar acyl chains in their structures [55]. Again, in order to avoid overlapping, the vibrational band positioned at 1660 cm^{-1} was selected in the case of the oil. For PLA, its most intense band at 2955 cm^{-1} was selected.

Figure 2A shows a representative depth scan of one of the aerogels prepared from 2% NANO F2A dispersions, analysed by the three different methods. With the univariate analysis the image obtained using the band at 2430 cm^{-1} did not provide any structural information, as cellulose background was present throughout the aerogel (Fig. 1). However, the images obtained using the characteristic bands of cellulose (i.e. 1100 and 2900 cm^{-1}) showed different regions where the polysaccharide was clearly concentrated (especially with the 1100 cm^{-1} filter) (Fig. 1). Similarly, the combined images obtained from the multivariate analyses showed a major contribution of the cellulose background (green), while the spectra identified as cellulose (2% in white and 100% in yellow) were jointly located forming clusters closer to the aerogels' surface. For the simplest systems, such as these uncoated aerogels, there was no visual difference between the images obtained using both multivariate analysis methodologies. Indeed, the combined image obtained from the overlapping of the single filters showed a high similarity with respect to the multivariate analyses, suggesting this methodology as a valid alternative for the (nano)cellulosic aerogels. Overall, cellulose distribution was easily observed in every coloured combined image with minor differences that did not impede determining its approximate distribution according to its

concentration, although the quality and precision of the final image seemed to be somewhat improved using the multivariate analysis.

Figure 2B shows a representative depth scan of a PLA-coated NANO F2A aerogel prepared from a 2% dispersion of the nanocellulosic fraction, again analysed by the three different methods. With regards to the univariate analysis and after incorporating the PLA, neither the spectral range centred at 2430 cm^{-1} nor the one at 1100 cm^{-1} (cellulose background and cellulose) were affected by the addition of the new component. However, the image obtained using the 2900 cm^{-1} filter was affected by the presence of PLA, whose spectrum presented its most intense peak at 2955 cm^{-1} (Fig. 1). Consequently, the information about the presence of denser cellulose clusters close to the aerogel surface was lost in this image (see circled areas in Fig. 2B), which is the inverse of the one obtained using the 2955 cm^{-1} peak. In this context, the univariate analysis was more sensitive to the overlapping of bands in the spectra of different components. Thus, the 1100 cm^{-1} filter was selected as the most appropriate one in terms of observing cellulose in PLA-coated aerogels. However, the combined image of the filters did not show an optimum contrast for determining the distribution of the components in this particular case, with a clear overestimation of the concentrated cellulose clusters (yellow and white). On the other hand, both the second and third methodologies showed a similar distribution of PLA and cellulose, with PLA forming clusters covering more concentrated cellulosic regions (Fig. 2B). Nevertheless, manual insertion showed less defined structures in the case of more concentrated celluloses (especially in the 2% one, which was interspersed throughout PLA and dry cellulose clusters), while automatic detection clearly displayed defined structures in accordance with those previously observed in the native nanocellulosic aerogels (Fig. 2A).

In the oil-immersed aerogels, the 2430 cm^{-1} filter from the cellulosic background remained continuous along the analysed areas according to its low intensity. However, both the 1100 cm^{-1} and 2900 cm^{-1} filters were affected by the overlapping of the spectrum of the oil with that of the cellulose, having the former a much higher intensity (Fig. 1). This hindered the proper identification of cellulose-rich regions by the univariate analysis. As a consequence, the images obtained using these filters showed a very similar distribution to that from the oil filter (1660 cm^{-1}), revealing an interference of the components (Fig. 2C). In contrast, PLA could still be clearly identified by the 2955 cm^{-1} filter in spite of a minor overlapping with the oil spectrum as seen in Fig 2C. By overlapping the distribution of the different filters in the combined image, it could be observed that both oil (red) and PLA (blue) were completely overlapped with concentrated cellulose,hindering a proper identification of every component. However, with the multivariate methodologies, the oil was seen to be distributed over a continuous layer that, in some regions, could penetrate to the inner parts of the aerogel. Moreover, the oil seemed to be preferentially located in regions of the aerogel covered with PLA, which is reasonable due to its higher

hydrophobicity in comparison with cellulose. As it has been already mentioned, the combined image might differ in the manual method as concentrated cellulose (2%) represents a minority component in comparison with the total area. In this context, when this spectrum is manually included in the analysis, it can be mistakenly assigned to areas which are actually covered by PLA or oil due to the similarities between their spectra (Fig. 2B and 2C). Furthermore, more intense and defined spectra (like 100% cellulose, in yellow) might be overestimated in systems like this one, where the peaks from different components are overlapped (becoming the oil the most relevant component); hence displaying poorly defined regions in areas covered by PLA or oil, which can lead to confusion (Fig. 2C).

Overall, the methodology based on univariate analysis could provide information on the microstructure of the native (nano)cellulosic aerogels (i.e. the simplest systems). However, as the number of components in the materials increased, there was rather extensive band overlapping, which resulted in uncertainties about the distribution of individual components in the samples and even masked the presence of components with less intense Raman spectra. This represents a limitation of this methodology of analysis in more complex systems with many components and, thus, it should not be considered as the unique methodology followed for image analysis as it has been typically reported in the literature [45, 48, 49].

On the other hand, multivariate analysis by comparison with reference materials seemed to provide less precise or, in the best case, similar information than the method based on automatic component detection, as the former needs preliminary knowledge of the sample components and forcing the software to detect certain components may lead to their overestimation. This became especially relevant in the case of components with similar spectra such as cellulose and oil (strongest peak at 2800-3000 cm^{-1}), which led to misinterpretation of the signals. This is shown in Figures 2B and 2C, where a minority component such as cellulose (2% and/or even 100%) were detected in areas that belonged to PLA and/or oil due to the relative similarities in their spectra. As observed in the existing literature, multivariate analysis is starting to be the method of preference for more complex systems in order to allow a more accurate mapping of component distribution, although integration of single filters is still being used as the main analysis methodology in many works [46, 47]. In this context, automatic detection of the components was selected as the most optimum methodology for analysing this kind of aerogels.

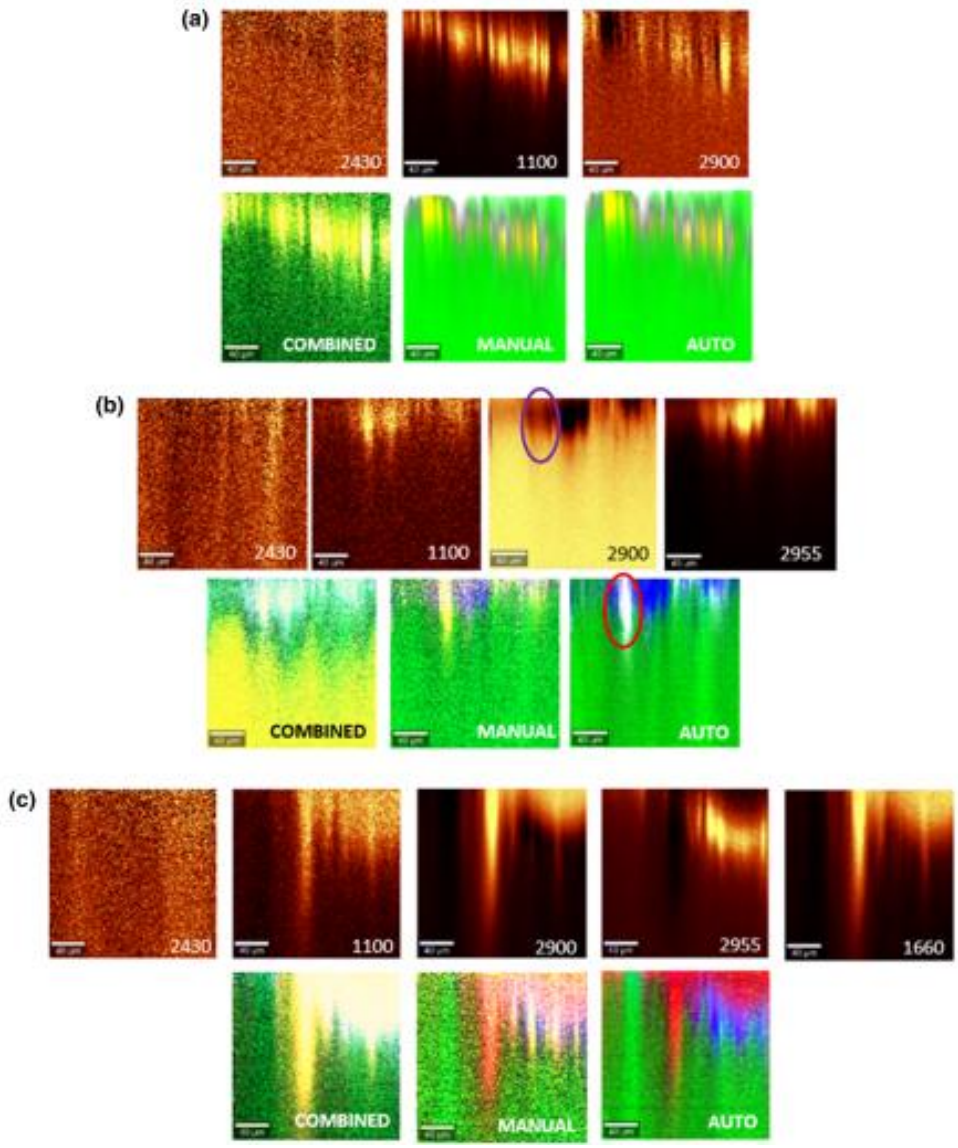

Figure 2. Monochromatic images of (A) pure nanocellulosic aerogel (2% NANO F2A), (B) PLA-coated aerogel and (C) PLA-coated oil-immersed aerogel. The central wavelengh of each filter is annotated in the legend. Combined images are represented by cellulose background (green), 2% cellulose (white), 100% cellulose (yellow), PLA (blue) and oil (red).

4.2.2 Impact of aerogel density/composition on component distribution

Each aerogel was observed by 2D depth scans in triplicate using the most optimum methodology tested (automatic detection of the components). Representative images of two aerogels with significantly different densities (i.e. NANO F2A 0.5% with 13 mg/cm^3, and NANO F3 2% with 114 mg/cm^3 [42]) are shown in Figure 3 at each stage (native nanocellulosic aerogels, PLA-coated aerogels and PLA-coated aerogels after oil immersion and subsequent release). The denser and more compact aerogels from pure nanocellulose displayed regions with greater cellulose

concentration, which were not detected in the lighter and more porous aerogels obtained from less purified (nano)cellulosic fractions [41]. This was even more evident in Fig. 3, due to the greater concentration of the dispersion used to prepare the NANO F3 aerogel as compared with NANO F2A (2% vs 0.5%).

The three cross-sections of each type of aerogel were analysed using the histogram of the single components of the image. A complete compilation of the components' relative abundance is shown in Tables 2-5. As expected, more porous and expanded structures, such as NANO F2 and NANO F2A, displayed the greatest cellulose background values (due to their higher air volume), while F3 and NANO F3 showed denser cellulosic areas (both of lower and higher cellulose concentration spectra, coloured in white and yellow respectively). These results demonstrate significant differences on how cellulose forms the internal aerogels' skeleton. While the hemicelluloses present in the least purified fractions resulted in a decrease in the density of the aerogels (from 42 mg/cm^3 for F3 0.5% to 13 mg/cm^3 for NANO F2A 0.5%), stronger hydrogen-bonded networks were formed in the more purified cellulose and nanocellulose fractions [42], leading to the formation of denser cellulose regions (referred to as 2% (white) and 100% (yellow) regions). Indeed, denser aerogels (such as F3 2%, with 125 mg/cm^3 [42]) displayed higher percentages of white and yellow areas (Table 2).

Table 2. Cellulose distribution in the different native (nano)cellulosic aerogels. Different letters show significant differences between samples in the same column. All values were displayed as mean ± standard deviation.

	CELLULOSE		
Sample	Background (green, %)	Cellulose aerogel (2%) (white, %)	Dense cellulose (100%, dry) (yellow, %)
F3 0.5%	86.1 ± 3.3^b	13.9 ± 3.3^a	0
F3 2%	81.9 ± 3.1^b	3.4 ± 1.6^b	14.7 ± 2.3^a
NANO F3 0.5%	89.6 ± 3.3^b	6.7 ± 3.7^{ab}	3.7 ± 2.9^b
NANO F3 2%	80.5 ± 2.4^b	3.6 ± 0.6^b	15.9 ± 1.8^a
NANO F2A 0.5%	96.1 ± 2.2^a	3.9 ± 2.2^b	0
NANO F2A 2%	92.6 ± 4.2^{ab}	6.0 ± 4.2^{ab}	1.4 ± 1.1^b
NANO F2 0.5%	100^a	0	0
NANO F2 2%	96.4 ± 1.2^a	3.6 ± 1.2^b	0

2D images of PLA-coated aerogels were also analysed and the results are shown in Table 3. It was previously demonstrated that more porous aerogels were able to incorporate greater amounts of PLA into their structures [42]. Thus, the PLA relative abundance was expected to become much higher in lighter aerogels, such as NANO F2A and NANO F2, since these presented the highest background values (related to the greater porosity) (cf. Table 2). The results from our previous work suggested that aerogel densities below 20 mg/cm^3 could promote the incorporation of PLA into the inner pores of the aerogel, as opposed to the denser aerogels where PLA was preferentially present on the surface [42]. Since it was not feasible to obtain micrographs of the whole cross-sectional areas of the aerogels and imaging was only performed close to the surface, standard deviations were higher in those particular cases where PLA could penetrate deeper; as a result, the differences observed amongst the most expanded aerogels (NANO F2 and NANO F2A) at different concentrations were not statistically significant. Nevertheless, for the same concentration, the incorporation of PLA into the denser aerogels, such as F3 and NANO F3, remained significantly lower in comparison with their NANO F2 and NANO F2A counterparts.

Table 3. Cellulose and PLA distribution of the different PLA-coated (nano)cellulosic aerogels. Different letters show significant differences between samples in the same column. All values were displayed as mean ± standard deviation.

	CELLULOSE			PLA
Sample	Background (green, %)	2% aerogel (white, %)	100% (dry) (yellow, %)	Blue (%)
F3 0.5%	83.9 ± 1.9^{a}	5.6 ± 0.8^{a}	0	10.5 ± 2.2^{b}
F3 2%	88.2 ± 3.5^{a}	5.2 ± 2.2^{ab}	1.8 ± 1.6^{b}	4.8 ± 1.9^{c}
NANO F3 0.5%	86.3 ± 2.1^{a}	5.1 ± 1.3^{a}	0	8.6 ± 1.1^{bc}
NANO F3 2%	86.7 ± 2.7^{a}	1.6 ± 1.4^{b}	7.4 ± 3.7^{a}	4.3 ± 1.6^{c}
NANO F2A 0.5%	76.5 ± 1.9^{b}	6.3 ± 1.5^{a}	0	17.2 ± 7.7^{ab}
NANO F2A 2%	72.0 ± 4.6^{a}	6.9 ± 3.3^{ab}	0	21.1 ± 1.4^{a}
NANO F2 0.5%	81.7 ± 3.5^{b}	0	0	18.3 ± 9.9^{ab}
NANO F2 2%	67.2 ± 3.6^{a}	7.4 ± 2.9^{a}	0	25.4 ± 3.3^{a}

Interestingly, these denser aerogels (2% F3 and NANO F3, with 126 and 114 mg/cm^3, respectively) became the only ones where more compacted cellulose areas (yellow) were still seen, even in the presence of PLA. These results are in accordance with the higher amounts of PLA incorporation reported for the less purified aerogels (NANO F2 and NANO F2A), according

to their lower density [42]. Regarding spatial distribution, PLA was preferentially distributed near the surface in all cases (Fig. 3B). Interestingly, in the denser aerogels (NANO F3 2% in Fig. 3B) PLA seemed to be preferentially located around cellulose–rich regions (in white), suggesting that these clots hindered a proper PLA diffusion along the porous (nano)cellulosic network.

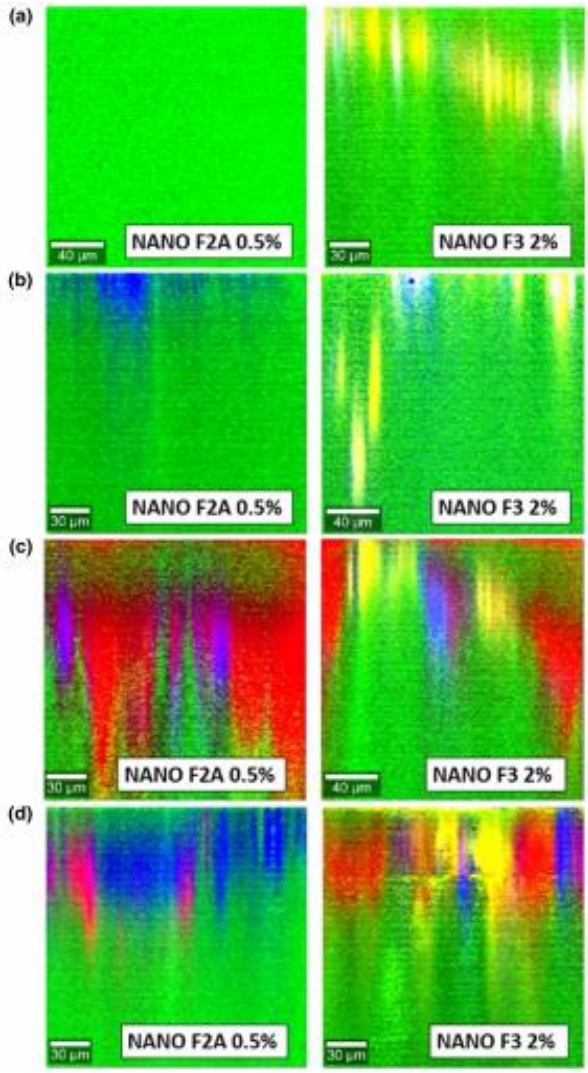

Figure 3. 2D Raman images of the cross-section (X, Z) of (A) native nanocellulosic aerogels, (B) PLA-coated aerogels, (C) PLA-coated aerogels just after oil immersion and (D) PLA-coated aerogels after oil release (7 days).

Oil distribution along the aerogels was also analysed and the results are shown in Table 4. Again, the density and porosity played a crucial role in the incorporation and visualization of new components. Although remarkable standard deviations prevented from extracting clear conclusions, there seemed to be a tendency correlating less dense aerogels with higher amounts of oil incorporated. This hypothesis is consistent with the gravimetric results from the oil sorption experiments carried out in our previous work [42]. As expected, all the aerogels showed a higher cellulose background value at their lowest (nano)cellulosic concentration (0.5%) with respect to their 2% counterpart. Moreover, the most compacted aerogels (i.e. F3 and NANO F3) showed lower percentages of both PLA and oil. In the particular case of NANO F2A 0.5% and NANO F2 0.5%, PLA values might be expected to be higher according to their low density (~13 mg/cm^3). However, this lower density may also imply a greater incorporation of both oil and PLA into the internal pores; thus, these components might not be only present in the external 200 µm layers examined for the analyses and deeper screenings should be carried out in forthcoming research to enrich the analyses. After the oil sorption process for the PLA-coated aerogels, the white areas (2%) significantly decreased their abundance, being only present in NANO F2A 2%, while the most intense spectra corresponding to dry cellulose (yellow) were still present in the more compacted aerogels. A masking or overlapping of minor components whose spectra cannot be easily differentiated (such as 2% cellulose) was suggested in the presence of more intense spectra with similar or overlapped representative peaks (such as oil), and could be considered as a possible limitation of this method for a complete detection of the components in complex systems.

In this context, Raman analysis may omit some information due to the mentioned overlapping; thus, the relative intensity of the spectra of the different components analysed is a crucial factor to be considered. Regarding the spatial distribution of oil, this component seemed to penetrate across the (nano)cellulosic matrix with a progressive decrease of its presence towards the inner parts of the cross-sections. Interestingly, the oil seemed to be preferentially located in close contact with PLA, since the PLA-rich regions were overlapped with the oil, leading to a purple colouration. On the other hand, the excess oil also covered an extensive region of the (nano)cellulosic matrix (Fig. 3C).

Table 4. Cellulose, PLA and oil distribution of the different (nano)cellulosic PLA-coated aerogels after oil immersion. Different letters show significant differences between samples in the same column. All values were displayed as mean ± standard deviation.

		CELLULOSE		PLA	OIL (day 1)
Sample	Background (green, %)	2% aerogel (white, %)	100% (dry) (yellow, %)	Blue (%)	Red (%)
F3 0.5%	38.2 ± 6.8^{b}	0	2.6 ± 1.4^{b}	18.5 ± 0.2^{b}	40.7 ± 7.6^{ab}
F3 2%	38.0 ± 9.9^{ab}	0	6.2 ± 2.4^{ab}	13.3 ± 1.6^{c}	35.5 ± 2.4^{b}
NANO F3 0.5%	36.1 ± 5.2^{b}	0	2.9 ± 0.6^{b}	16.3 ± 5.1^{bc}	44.7 ± 5.1^{a}
NANO F3 2%	47.8 ± 2.7^{a}	0	8.6 ± 1.3^{a}	12.1 ± 1.2^{c}	31.5 ± 0.4^{b}
NANO F2A 0.5%	35.4 ± 10.6^{b}	0	0	23.9 ± 1.8^{a}	40.7 ± 1.7^{a}
NANO F2A 2%	39.3 ± 4.9^{b}	1.6 ± 1.9^{a}	0	19.3 ± 5.5^{ab}	39.8 ± 3.7^{ab}
NANO F2 0.5%	39.6 ± 3.5^{b}	0	0	13.2 ± 1.1^{c}	47.2 ± 6.4^{a}
NANO F2 2%	44.4 ± 8.7^{ab}	0	0	18.5 ± 1.0^{b}	37.1 ± 5.8^{ab}

One of the advantages of confocal Raman microscopy is the possibility of mapping several sections within the materials. Z-stacks were also carried out in order to obtain a three-dimensional visualization of all the components in the aerogel. Accordingly, the distribution of the different components in the hybrid aerogels was confirmed using a larger sample area. Figure S4 (supporting information) shows a representative example where, in accordance with the 2D images, a gradual decrease of sorbed oil when penetrating deeper along the (nano)cellulosic matrix was observed. Moreover, the preferential location of PLA on the surface of the aerogels was clearly demonstrated. A video showing the 3D image from different angles is also available as part of the Supplementary Material.

The micrographs obtained after oil release were also analysed and the results are shown in Table 5. Firstly, all the values for the relative abundance of oil were significantly lower in comparison with those obtained right after the oil sorption process (cf. Table 4). Unfortunately, a clear correlation between the density of the aerogels and the amount of oil retained could not be extracted from Table 5. According to previous results, the oil was shown to be more easily retained in the more compacted structures of F3 and NANO F3 [42]. However, since the analysed area was 200 μm, only the most superficial layers of the aerogels were studied and a bigger scan of the aerogels might have been more representative for this particular case (similarly to the case of PLA incorporation, as already mentioned when discussing the results from Table 3). Nevertheless, the study of larger areas may cause a significant decrease on the image's quality, as laser intensity must be lowered when increasing the exposition time in order to avoid the

overexposure and burning of the aerogels. This could also be considered as one of the possible limitations of Raman imaging when analysing low density materials such as these (nano)cellulosic aerogels. With regards to the (nano)cellulosic clusters, the less dense clusters (white ones) that were not detected in the presence of a higher amount of oil, were detected again as the oil was released, being present in three different aerogels. The yellow clusters were again more representative for denser aerogels with a relative abundance higher than 12% in the case of NANO F3 2% aerogel. This confirms that the automatic detection of components, although selected as the optimal approach, was not completely accurate in the most complex systems. Regarding spatial distribution, the oil remaining after the release process seemed to be preferentially located in close contact with PLA, as suggested by the purple tonality. Moreover, most of the initially sorbed oil was released after 7 days, as also demonstrated by the BF images in Figure S3 (Supporting Information), being these results consistent with previous gravimetric analyses for the oil sorption-desorption processes [42].

Table 5. Cellulose, PLA and oil distribution of the different (nano)cellulosic PLA-coated aerogels after oil release (7 days). Different letters show significant differences between samples at the same column. All values were displayed as mean ± standard deviation.

	CELLULOSE			PLA	OIL (day 7)
Sample	Background (green, %)	2% aerogel (white, %)	100% (dry) (yellow, %)	Blue (%)	Red (%)
F3 0.5%	64.5 ± 4.9^{bc}	0	0	5.9 ± 4.4^{a}	27.6 ± 5.3^{a}
F3 2%	72.3 ± 4.0^{b}	4.8 ± 3.9^{a}	0	7.2 ± 2.8^{a}	15.7 ± 6.5^{ab}
NANO F3 0.5%	69.5 ± 5.1^{bc}	3.3 ± 2.8^{a}	4.6 ± 2.4^{b}	9.4 ± 1.9^{a}	13.2 ± 2.7^{b}
NANO F3 2%	58.6 ± 2.1^{c}	0	16.6 ± 3.6^{a}	8.9 ± 0.3^{a}	15.9 ± 3.7^{ab}
NANO F2A 0.5%	81.5 ± 1.4^{a}	0	0	12.0 ± 2.9^{a}	6.5 ± 1.0^{c}
NANO F2A 2%	81.9 ± 5.5^{ab}	2.6 ± 2.0^{a}	0	9.4 ± 1.5^{a}	6.1 ± 1.5^{c}
NANO F2 0.5%	86.4 ± 5.2^{a}	0	0	8.3 ± 2.2^{a}	5.3 ± 4.6^{c}
NANO F2 2%	77.6 ± 2.9^{b}	0	0	12.5 ± 4.4^{a}	9.9 ± 5.6^{ab}

4.3 Confocal laser scanning microscopy (CLSM)

One of the limitations of confocal Raman microscopy is that scattering of the Raman photons and interaction with interfaces in the sample can reduce the resolution with respect to the theoretical optical resolution. As a complementary technique for evaluating the different aerogel morphology and compound distribution, CLSM images of the materials surface, able to provide a better resolution, are shown in Figure 4. Greater porosity could be evidenced in the native (nano)cellulosic aerogels, especially in the most expanded structure of NANO F2A 0.5% (Fig. 3A). After PLA coating and, as this process led to a ~2:1 ratio of PLA:cellulose it can be inferred that PLA was not only covering the (nano)cellulose fibres, but also filling in some of the pores, thus substantially reducing the porosity of the materials.

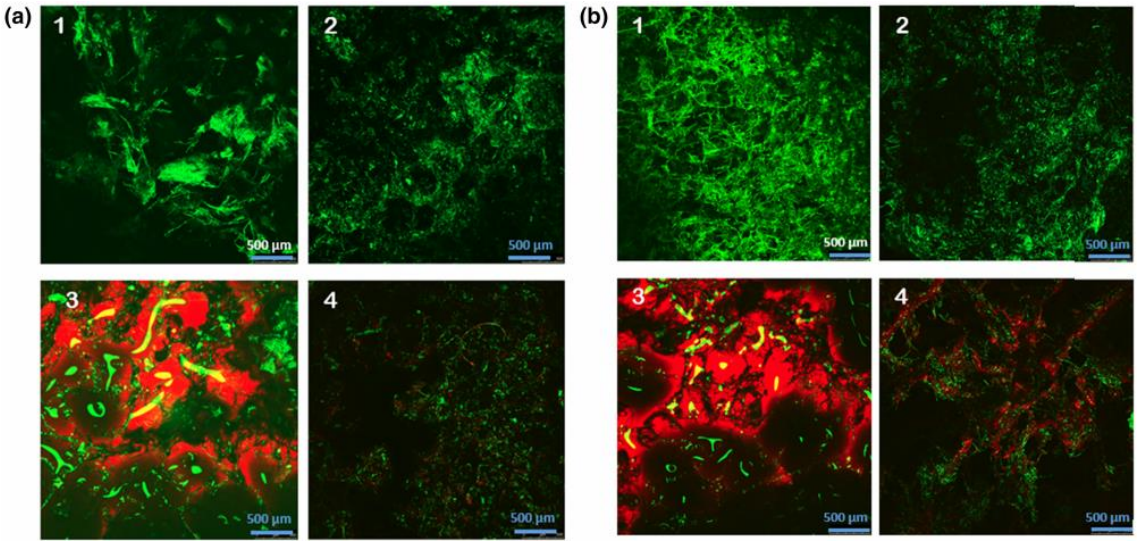

Figure 4. CLSM images of (A) NANO F2A 0.5% and (B) NANO F3 2% aerogels at the four analysed stages ((1) native (nano)cellulosic aerogel, (2) PLA-coated aerogel, (3) PLA-coated aerogel + OIL and (4) PLA-coated aerogel + OIL (f)). (Nano)cellulosic fractions and PLA are shown in green, while oil is shown in red.

After immersion, the oil was distributed across the material surface, not only being adsorbed to the cellulose-rich regions but also filling the pores. After the oil release process, the remaining oil stayed attached to the PLA-coated (nano)cellulosic skeleton. Interestingly, a greater amount of oil seemed to remain in the denser aerogel (Fig. 5B vs Fig. 5A), which was expected according to its greater oil retention capacity (2.4 g oil/g aerogel for NANO F3 2% vs 0.7 g oil/g aerogel for NANO F2A 0.5%) [42] and was in agreement with the tendency previously seen in Tables 4 and 5.

5. Conclusions

(Nano)cellulosic aerogels have been prepared from several (nano)cellulosic fractions obtained from *Posidonia oceanica* waste biomass with different purification degrees (NANO F3 > F3 > NANO F2 > NANO F2A) and at two different concentrations (0.5% and 2%). These aerogels were subsequently coated with PLA to improve their hydrophobicity and oil-affinity. Confocal Raman Imaging has been used to characterize the internal microstructure of these biopolymeric aerogels with different degrees of complexity. Both univariate and multivariate analyses were used and compared in order to determine the most optimum methodology for analysing the structure of multicomponent aerogels.

Univariate analysis only provided accurate information in the simplest systems (native (nano)cellulosic aerogels). However, in the case of the more complex hybrid aerogels, the more intense spectra from PLA and, especially, oil, masked the characteristic bands of cellulose and precluded its identification. In contrast, multivariate analyses provided images showing the distribution of every component simultaneously. The data processing approach based on the automatic identification of components was selected as the optimal methodology, since the method based on comparison with reference materials resulted in unrealistic images for the most complex systems. However, this method may also underestimate the presence of less intense components in the most complex systems due to peak overlapping.

On the other hand, micron-sized regions with more concentrated cellulose were more abundant in denser aerogels, while the spectrum of the cellulose background was significantly more abundant in the most porous aerogels. The results also confirmed that PLA was preferentially located close to the surface, while the oil could penetrate deeper along the matrix. Regarding the amount of oil being retained after the release process, although the results from Confocal Raman Imaging were not conclusive due to the relatively short depths analysed, CLSM images confirmed a higher oil retention in the denser aerogels.

Overall, this manuscript shows the potential of Raman imaging for the characterization of the microstructure of complex biopolymeric aerogels, and highlights some of its limitations.

6. Supplementary material

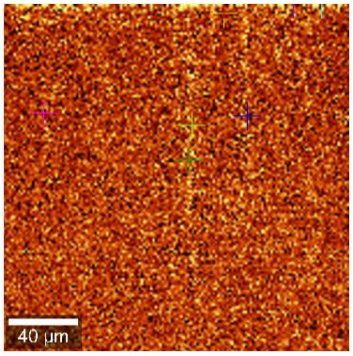

Figure S1. Representative image of the final background after a complete Auto analysis of the single components of NANO F3 2% + PLA.

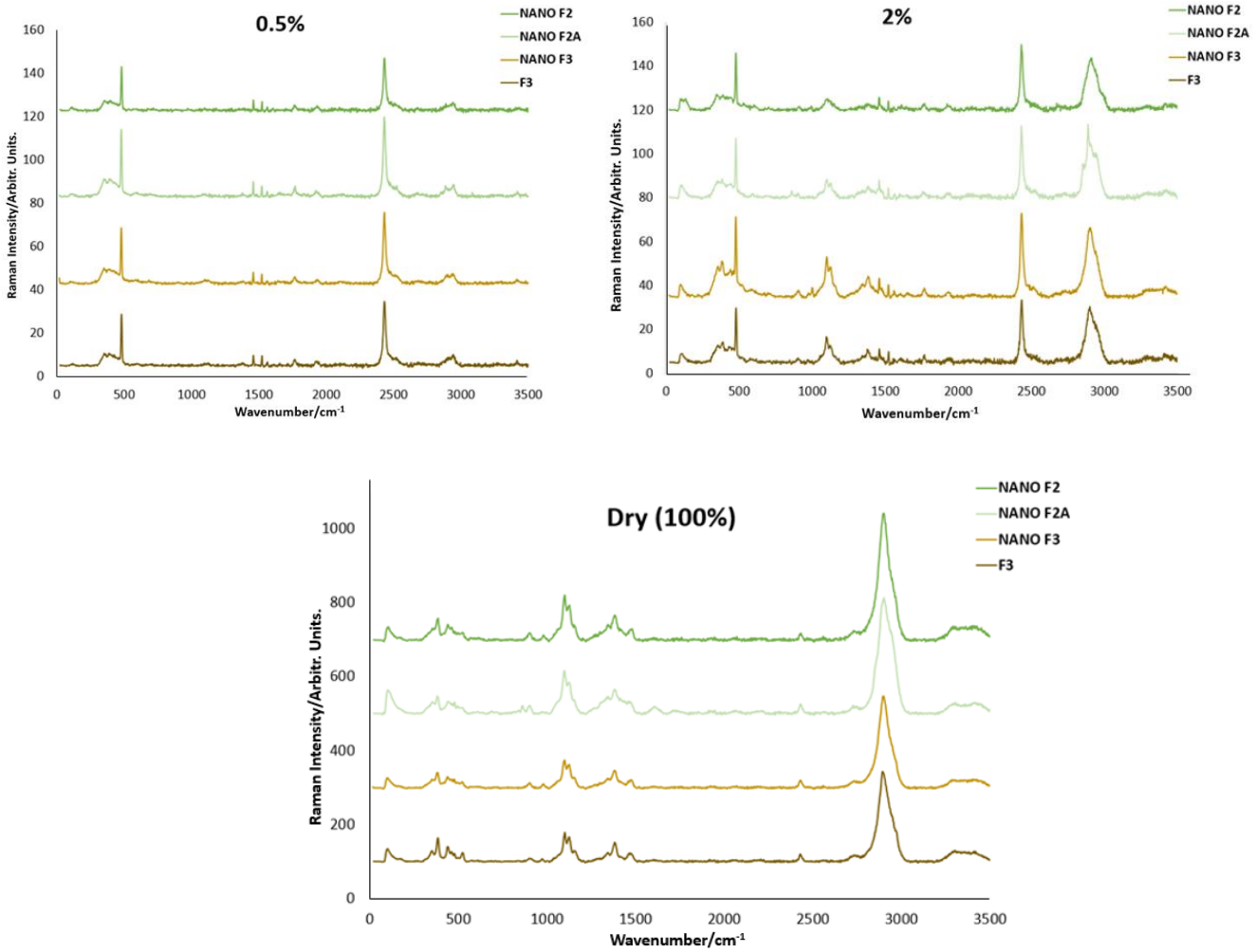

Figure S2. Spectra of the different (nano)cellulosic aerogels at both concentrations tested (0.5% and 2%) and the corresponding (nano)cellulosic fractions dried in the oven (100%).

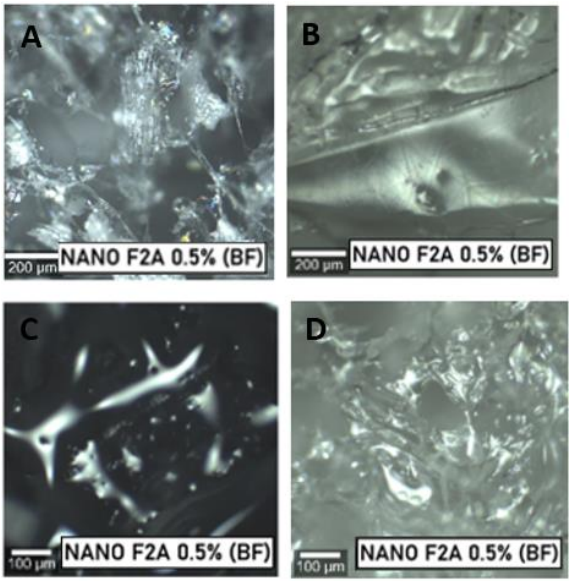

Figure S3. 2D image of the surface (X, Y) using bright field (BF) microscopy for a representative aerogel at each stage being (A) raw aerogel, (B) PLA-coated aerogel, (C) oil immersed PLA-coated aerogel and (D) after oil release.

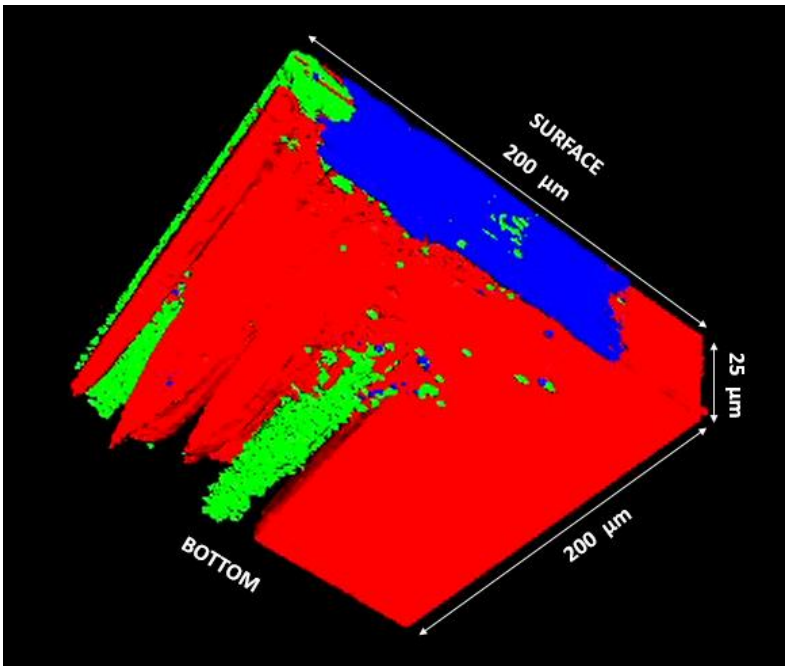

Figure S4. 3D image of the PLA-coated aerogel (NANO F2A 2%) after oil immersion. The cellulosic background is represented in green, PLA in blue and oil in red. SURFACE and BOTTOM marks indicate the orientation of the aerogel.

4.3. Multifunctional cellulosic aerogels from Posidonia oceanica waste biomass with antioxidant properties for meat preservation.

This section is an adapted version of the following published research article:

Benito-González, I., Galarza-Giménez, P., López-Rubio, A. & Martínez-Sanz, M. (2020). Multifunctional cellulosic aerogels from *Posidonia oceanica* waste biomass with antioxidant properties for meat preservation.

International Journal of Biological Macromolecules, 185, 654-663. DOI:

https://doi.org/10.1016/j.ijbiomac.2021.06.192

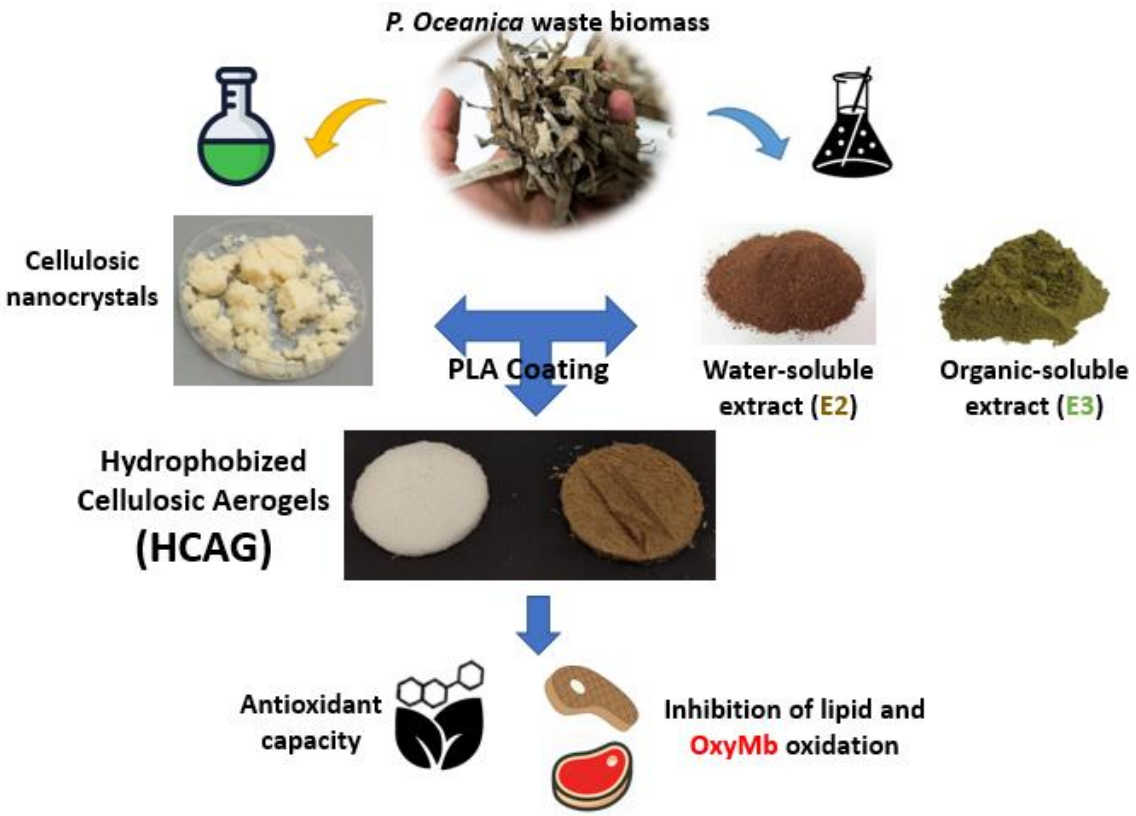

1. Abstract

Posidonia oceanica waste biomass has been valorized to develop bioactive hydrophobized cellulosic aerogels (HCAG) by simpler and greener protocols. Hydrophobization of cellulosic aerogels was achieved through PLA coating, while bioactivity was imparted by the incorporation of water- (E2) and organic-soluble extracts (E3) produced from the same biomass. The incorporation of extracts led to denser aerogels, with less porous structures. These aerogels showed outstanding water and oil sorption capacities (1500-1900%), being able to release the adsorbed liquid almost completely after 7 days. Interestingly, all the aerogels showed a positive inhibition effect (23-91%) on the β-carotene bleaching assay. Moreover, the aerogels loaded with extracts, especially when combining E2 and E3, were able to reduce the oxidation of lipids and oxymyoglobin in red meat after 10 days of storage. This evidences the potential of these aerogels as bioactive adsorbing pads to preserve the quality of fresh packaged foods.

2. Introduction

The valorization of waste biomass, arising from industrial activities or even from natural residues, is an interesting approach for the extraction of biopolymers. Cellulose is one of the most attractive components present in waste biomass, since it is known to present excellent mechanical and barrier performance and as a result, has been extensively used to generate packaging materials, either as the base material or as additive to improve the properties of other biopolymers [56]. Cellulose-based materials can be used to produce different packaging structures, such as films [41], trays [57] or even aerogels [58]. Aerogels are extremely light and porous materials with high surface area and low density, which are useful for a wide range of applications due to their high absorption and adsorption capacities [8-10]. Particularly, cellulose-based aerogels have gained a great deal of interest over the past years due to their interesting properties [14-16]. Furthermore, some studies have reported on the possibility of producing these cellulosic aerogels from waste biomass, such as the residues from the invasive plant *Arundo donax* [6] and the residues from the aquatic plant *Posidonia oceanica* [25, 59], making these aerogels more environmentally-sustainable. One of the main drawbacks of cellulose-based materials is their highly hydrophilic character, which can be detrimental for their application in food packaging. To overcome this issue, sophisticated strategies based on chemical modification, cross-linking and/or coating with hydrophobic non-food grade compounds are typically applied [19, 20], compromising the sustainability of the obtained materials. Interestingly, a recent work reported on the possibility of producing sustainable cellulose-based aerogels, which were hydrophobized simply by dipping the aerogels into PLA solutions [25, 59]. As opposed to the native cellulose-based aerogels, the PLA-

coated specimens maintained their integrity when soaked in water and were able to adsorb large quantities of liquids, both from hydrophilic and hydrophobic nature.

Based on the enormous potential of these aerogels, in this work we wanted to evaluate their suitability to be used as adsorbent pads for the preservation of fresh packaged foods, such as meat. For this particular application, it would be desirable to use materials with antioxidant properties to inhibit the oxidation processes taking place upon storage and which compromise the quality of meat. In this sense, it is expected that the presence of antioxidant compounds in the aerogels will reduce the oxidation of polyunsaturated acids and delay the meat color loss caused by the interaction of oxidation products with myogoblin. The most conventional strategy to achieve this is to incorporate antioxidant compounds into the packaging structure, which are then released or exert their protective function upon contact with food [60-63]. Given their outstanding sorption and desorption capacity, aerogels are excellent candidates for the incorporation and sustained release of a range of bioactive compounds with applications in biomedical and food areas, amongst others. Their performance when used as controlled delivery vehicles depends on different factors, such as the density of the materials composing the aerogels, their sorption capacity, the solubility of the incorporated compounds and the interconnections within the aerogel matrix [64]. Specifically in the food area, bioactive aerogels could be used with a dual function to both act as sorption pads in fresh products, as well as prolonging the shelf-life of food products through the sustained release of antioxidant or antimicrobial compounds [6, 65].

In this work, we propose a complete valorization of *Posidonia oceanica* waste biomass to produce hydrophobized cellulosic aerogels with antioxidant properties. The same waste biomass was used for the extraction of the cellulosic nanocrystals composing the main structure of the aerogels and for the production of hydrophilic and hydrophobic bioactive extracts, according to the methods described in a previous work [66]. The effect of extract incorporation in the morphology and adsorption capacity of the aerogels was investigated and their antioxidant capacity was tested for their application as adsorbing pads.

3. Materials & Methods

3.1 Materials

Posidonia oceanica (P. oceanica) leaves were directly collected from the seashore in Denia, Alicante (Spain) in July 2019. The leaves were washed with water to remove salts and sand and stored under refrigeration conditions (4 °C) until further use.

Sulphuric acid (≥97.5%), 2,2,2-Trifluoroethanol (TFE) (≥99%), potassium sulphate, potassium persulphate (≥99%), potassium chloride (99%) β-carotene (≥97%), linoleic acid (≥99%), Tween®

40, 2Thiobarbituric acid (98%) and phosphate buffered saline tablets were purchased from Sigma-Aldrich (Spain). Sodium chlorite 80% was supplied by Acros organics (Spain).

3.2 Preparation of cellulosic nanocrystals from *P. oceanica* biomass

A simplified purification procedure previously reported for the extraction of cellulosic fractions from *P. oceanica* leaves was applied, generating cellulose-based nanocrystals containing hemicelluloses and lipidic compounds, as described in [41]. These nanocrystals were labelled as NANO F2A. Briefly, *P. oceanica* biomass was subjected to a de-lignification step with $NaClO_2$, obtaining the cellulose-rich fraction, which was then subjected to a hydrolysis treatment with sulphuric acid (30 % v/v) at 50º C, under stirring conditions, for 1.5 h. These cellulosic nanocrystals presented a cellulose content up to 92% (as deduced from the glucose content determined by monosaccharide analysis of the sample subjected to a sulphuric acid hydrolysis [67]), and the extraction yield was 26% (with regards to the raw biomass weight), as previously reported [41]. The nanocrystals were stored in the fridge as partially hydrated materials until further use.

3.3 Production of bioactive extracts from *P. oceanica* biomass

Hydrophilic and hydrophobic extracts were generated from *P. oceanica* leaves using the water-based and organic solvent-based extraction protocols previously described in [66]. Briefly, 10 g of *P. oceanica* biomass (dry weight basis) were added to 200 mL of distilled water and mixed in a blender until a paste was obtained. The material was then heated up to 90 °C and kept at a constant temperature and under stirring for 2 h. After that, the material was centrifuged and the supernatant was separated, placed in an ice bath and the required volume of ethanol (75% with regards to the volume of aqueous supernatant v/v) was slowly added. The material was kept stirring in the ice bath overnight and after that, centrifuged again (12500 rpm, 15 °C, 20 min). The precipitate was collected, re-suspended in distilled water and freeze-dried. The obtained powder extracts were labelled as E2. For the organic solvent-based extraction, the solid residues obtained after the first centrifugation step in the hot water extraction were subjected to a Soxhlet extraction with 800 mL of toluene:ethanol (2:1) for 24h. The liquid phase was then collected, and the solvents were evaporated by distillation on a rotary evaporator (G3 Heidolph, Schwabach, Germany) operating at 60 ºC and vacuum conditions. The dry material was re-suspended in 50 mL of pure ethanol, which was subsequently evaporated at room temperature. The obtained powder extract was labelled as E3. According to a previous study [66], E2 was composed of ca.

29% carbohydrates, 36% protein, 34% ash and 9% phenolics while E3 was composed of 56% lipids, 34% ashes and 8% phenolics. Both extracts were stored at 0% RH until further use.

3.4 Preparation of cellulosic aerogels

Figure 1 shows a schematic representation of the methodology followed to prepare the different cellulosic aerogels. Cellulosic aerogels were prepared by adding 0.075 g of NANO F2A (dry weight) to 15 mL of distilled water (leading to a concentration of 0.5% w/v) and dispersing them by ultra-turrax homogenization until obtaining homogeneous suspensions. These were then poured into Petri dishes (diameter of 6 cm), frozen at −80 °C and subsequently, freeze-dried using a Genesis 35-EL freeze-dryer (Virtis), yielding cellulosic aerogels (CAG). Hydrophobized cellulose aerogels (HCAG) were subsequently produced by coating the cellulosic aerogels with PLA, following a dipping method described in a previous work [59]. Two different concentrations of the PLA dipping solution (1 and 5% (w/v) in TFE) were tested to evaluate the performance of the coated aerogels. The amount of PLA sorbed by the cellulosic aerogels was calculated as follows:

$$\%\ PLA = \frac{Wf\ -W0}{W0}\ x\ 100 \quad (1)$$

where $W0$ refers to the initial weight of the cellulosic aerogel and Wf corresponds to the final sample weight (aerogel + PLA).

For the production of bioactive aerogels, different methodologies were followed to incorporate the hydrophilic and hydrophobic extracts. (i) The hydrophilic extract (E2) was added on the initial homogenization step. The required amount of extract was dispersed in water together with the cellulosic nanocrystals to obtain a final concentration of 75 wt.-% with respect to the cellulosic solid material, prior to the freeze-drying step. This concentration was chosen based on preliminary trials in which the extract concentration was varied between 10 and 75% w/w; this was the range of extract concentration which ensured a sufficient mechanical integrity of the aerogels. The obtained hybrid aerogels were then PLA-coated by following the same dipping method applied to the cellulosic aerogels, using a dipping solution of 1% w/v PLA, yielding the aerogels labelled as HCAG + E2. (ii) The hydrophobic extract (E3) was incorporated into the cellulosic aerogels during the dipping step. The required amount of extract was dissolved into the PLA dipping solution (1% or 5% w/v) to attain a concentration of 75 wt.-% E3, with regards to the amount of PLA incorporated into the aerogels (previously determined). These aerogels were labelled as HCAG + E3. Additionally, bioactive aerogels containing both extracts, labelled as HCAG + E2 + E3, were also prepared by adding E2 during the homogenization step and E3 during the dipping step. All the produced aerogels were stored at 0% RH until further use.

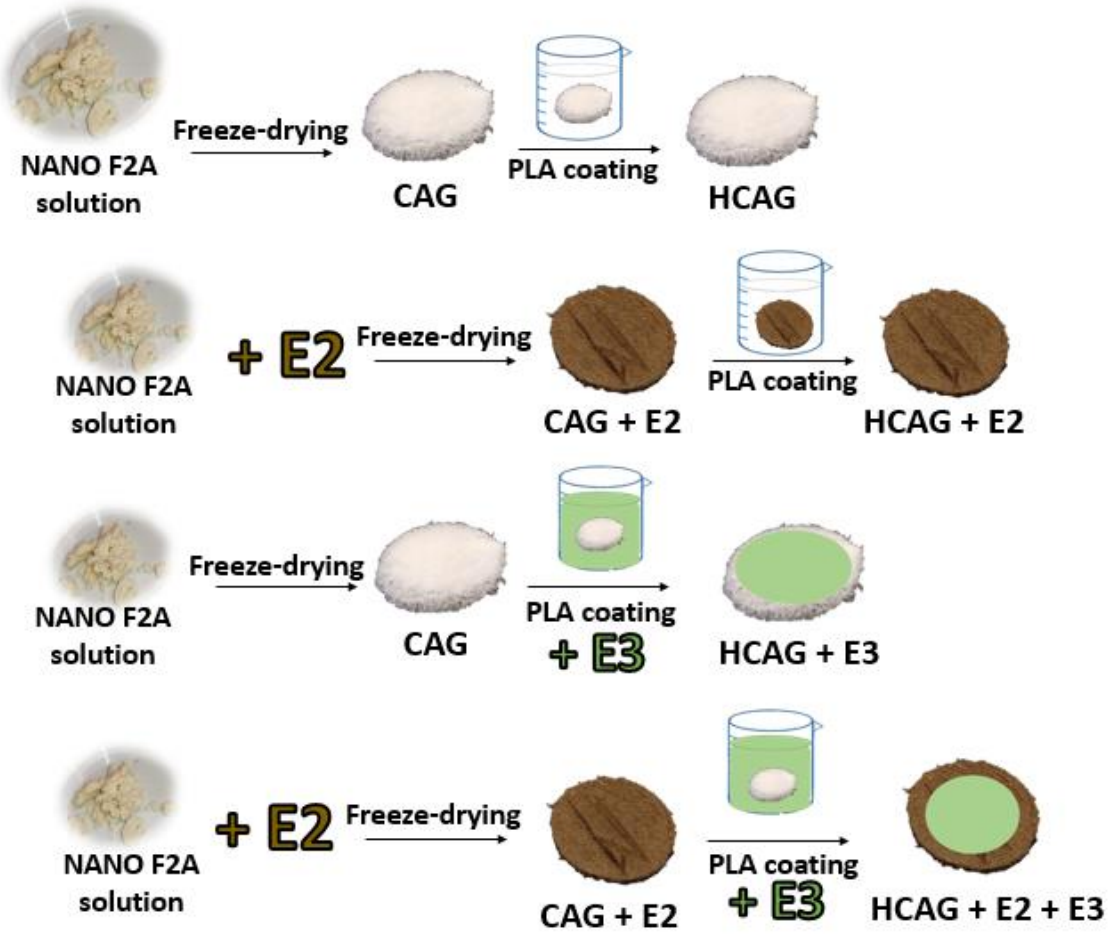

Figure 1. Schematic representation of the methodology followed to prepare the different cellulosic aerogels.

3.5 Fourier Transform Infrared Spectroscopy (FT-IR)

Selected aerogels were analysed by FT-IR in attenuated total reflectance (ATR) mode using a Thermo Nicolet Nexus (GMI, USA) equipment. The spectra were taken at 4 cm^{-1} resolution in a wavelength range between 400-4000 cm^{-1} and averaging a minimum of 32 scans.

3.6 Scanning electron microscopy (SEM)

SEM was conducted on a Hitachi microscope (Hitachi S-4800) at an accelerating voltage of 10 kV and a working distance of 8-16 mm. Small samples (~5 mm^2 area) of the aerogels were cut to observe their surface. The samples were then sputtered with a gold–palladium mixture under vacuum during 3 minutes before their morphology was examined.

3.7 Density of aerogels

Aerogel densities were determined from the weight and volume of each individual aerogel. The weight was determined by an analytical balance (Precisa Gravimetrics AG SERIES320XB, Dietikon, Switzerland) and the dimensions were measured by a digital calliper at three different positions.

3.8 Water and oil sorption

Square aerogel specimens with a total surface area of 1 cm^2 were cut, weighed and immersed in sealed containers containing 15 mL of distilled water or sunflower oil. The samples were periodically taken out of the liquid and weighed after removing the excess liquid. Measurements were taken until the samples were equilibrated and the total weight gain was calculated. After equilibration, the samples were removed from the liquid, placed on top of aluminum foil (in the case of water) and filter paper (in the case of oil) and left drying at ambient conditions, following the methodology described in [59]. The weight was registered periodically, until it was constant (~1 week). The water and oil retention capacity were calculated from the difference between the weight after drying and the initial weight of the samples, before soaking them in the liquids. All the measurements were carried out at least in triplicate.

3.9 β-Carotene-linoleic acid assay

The antioxidant capacity of the aerogels was evaluated by the β-carotene-linoleic acid assay, according to [68], with minor modifications. In brief, 2 mg of β-carotene was dissolved in 10 mL of chloroform. 2 mL of this solution were placed on a rotary evaporator and the chloroform was evaporated. Then, 50 μL of linoleic acid and 400 mg of Tween 40 were added and the content of the flask was mixed with stirring. After that, 100 mL of aerated distilled water was transferred to the flask and stirred vigorously. BHT (0.5 mg/mL), or 0.5 mL of TFE as positive or negative controls (respectively) were transferred to test tubes and then 5 mL of the β-carotene emulsion were added. For testing the bioactive aerogels, 25 mg of sample was transferred to the tubes and 5 mL of the β-carotene emulsion were added. The samples were incubated in a water bath at 50 °C for 120 min. The absorbance of each sample at 470 nm was measured every 30 min using a spectrophotometer. A sample of HCAG (with no added extracts) was used as an additional negative control. The determinations were carried out in duplicate.

3.10 Evaluation of the antioxidant effect of bioactive aerogels on red meat

Bioactive aerogels containing the E2 and E3 extracts and the HCAG control aerogel were tested as absorption pads for the preservation of red meat. The aerogels were placed covering the bottom surface of glass Petri dishes (diameter = 6 cm) and portions of ca. 12 g of minced beef meat were placed on top of the aerogels. The samples were then sealed with a plastic wrap film and stored in the fridge at 4 °C for 10 days. Additional control samples were prepared by using commercial meat pads (COMMERCIAL) and blank samples (CONTROL (-)) were prepared by adding the same amount of meat to Petri dishes with no pads.

3.10.1 Determination of oxymyoglobin and metmyoglobin

The ability of the aerogels to prevent the colour loss in the red meat after storage was evaluated through the determination of the oxymyoglobin and metmyoglobin content proportions in the raw red meat and in the samples after refrigerated storage for 10 days by following the procedure described by Carlez et al. [69]. Briefly, 2 g of minced meat samples were homogenized with 20 mL of 0.04 mol/L potassium phosphate buffer (pH = 6.8). The homogenized samples were kept in an ice bath for 1 h and after that, they were centrifuged at 4200 rpm and 10 °C for 30 min. The supernatant was then filtered using 0.45 μm pore size filters (Nylon, OlimPeak) and the volume of the filtrate was adjusted to 25 mL with the same phosphate buffer. The absorbance of the supernatant was measured at 525, 545, 565 and 572 nm in a spectrophotometer. The concentrations of oxymyoglobin and metmyoglobin were calculated using the following equations, as described in [69]:

$$\%\, MbO2 = (0.882\, R_1 - 1.267\, R_2 - 0.809\, R_3 + 0.361) \times 100 \quad (2)$$

$$\%\, MetMb = (-2.541\, R1 + 0.777\, R_2 + 0.800\, R_3 + 1.098) \times 100 \quad (3)$$

Where R1, R2, R3 are the absorbance ratios A^{572}/A^{525}, A^{565}/A^{525}, A^{545}/A^{525}, respectively. All the determinations were done in triplicate.

3.10.2 Measurement of lipid oxidation

The degree of lipid oxidation in the red meat samples after 10 days of storage was also measured by following the 2-thiobarbituric acid (TBA) distillation method [70]. 10.0 g of meat were homogenized with 30 mL of water. The sample was then transferred to a distillation flask with 65 mL of water and the pH was adjusted to 1.5 with HCl 4N. Ethanolic propyl gallate (10%, 1 mL), 10% EDTA (disodium salt, 1 mL), and a drop of antifoaming agent were added. The flask

was connected to a Soxhlet apparatus and the mixture was boiled until 50 mL of distillate were collected. In a screw capped test tube, 5 mL of the distillate was reacted with 5 mL of TBA reagent (0.02 M TBA in 90% acetic acid) in a boiling water bath for 35 min. A control made up of 5 mL distilled water and 5 mL of TBA reagent was also boiled for 35 min. The tubes were cooled to room temperature and the absorbance was measured at 535 nm in a spectrophotometer. The TBA reactive substances (TBARS) were calculated by multiplying the absorbance readings by a factor of 7.8 and expressed as mg malondialdehyde (MDA)/Kg meat. The inhibition of lipid oxidation was calculated as follows:

$$Inhibition\ (\%) = \frac{(TBARS_{Blank} - TBARS_{Day\ 0}) - (TBARS_{Pad} - TBARS_{Day\ 0})}{(TBARS_{Blank} - TBARS_{Day\ 0})} \times 100 \quad (4)$$

Where $TBARS_{Day0}$ refers to the TBARS in the raw minced meat and $TBARS_{Blank}$ and $TBARS_{Pad}$ correspond to the TBARS in the meat samples after 10 days of refrigerated storage (blank sample and samples with the commercial or the cellulosic aerogel pads, respectively). These determinations were carried out in triplicate.

3.11 Statistical analysis

Analysis of variance (ANOVA) followed by a Tukey-b test were used when comparing more than two data sets, after confirming the homogeneity of variances by the Levene test using IBM SPSS Statistics software v.26. All data have been represented as the average ± standard deviation. Significant differences ($p \leq 0.05$) are denoted by showing the data provided in tables and figures with different letters.

4. Results and Discussion

4.1 Optimization of the formulation of hydrophobized cellulosic aerogels loaded with extracts

A previous work demonstrated the potential of the highly porous aerogels from cellulosic fractions extracted from *Posidonia oceanica* waste biomass to be used as adsorbent materials. In particular, less purified cellulosic nanocrystals showed a great compromise between adsorption capacity and environmental and economical sustainability [59]. To overcome the excessive hydrophilicity and poor mechanical performance of the pristine cellulosic aerogels, a simple PLA dipping method was proven to be an efficient strategy to hydrophobize the aerogels. Previous results indicated that the density of the aerogels was key to enable a proper incorporation of PLA and maximize the hydrophobization effect [59]. The incorporation of the extract E2 into the cellulosic aerogel matrix was expected to affect the structure and density of the uncoated aerogels; this was not the case for E3, which was directly dissolved into the PLA dipping solutions. Thus,

different E2 concentrations (10, 25, 50 and 75% (w/w)) were tested and the density values were determined. All the tested concentrations yielded homogeneous aerogels with good mechanical integrity. As shown in Figure S1, when increasing the extract concentration, the aerogels presented a darker brown coloration (inherent from the extract) and a more compact consistency. Indeed, as deduced from Table 1, increasing E2 concentration led to denser aerogels. These aerogels were then soaked into PLA solutions at two different concentrations (1 and 5% (w/v)) and the amount of PLA adsorbed, as well as the contact angle of the coated aerogels, were determined to evaluate their hydrophobicity (cf. Table 1). As already anticipated, the amount of PLA incorporated into the aerogels diminished when increasing the aerogel's density (i.e. when increasing the amount of E2). On the other hand, increasing 5-fold the PLA concentration in the dipping solutions led to a 3-4-fold increase in the amount of PLA incorporated into the aerogels. Interestingly, the reduced PLA incorporation did not have a strong negative impact on the hydrophobicity of the aerogels, as inferred from the measured contact angle values, which were greater than 80º for all the aerogel formulations. This can be explained by the fact that, as already demonstrated [59], there seems to be an optimum density range allowing the incorporation of PLA not only filling in the pores of the aerogels, but also coating their surface, thus maximizing the hydrophobization effect. According to this, the aerogel prepared by adding 75% (w/w) E2 and subsequently dipped into a 1% (w/v) PLA solution seemed to be the most optimum to conduct further experiments, since it provided a sufficiently hydrophobic behaviour (i.e. it was able to keep its integrity when soaked in water) while maximizing the amount of bioactive extract and minimizing the amount of PLA incorporated into the aerogels. In the case of the E3 extract, the concentration was fixed at 75 wt.-% with regards to the amount of PLA to provide a sufficiently high concentration as to ensure the bioactivity of the extract [66].

Table 1. Density, PLA gain and contact angle of the different tested cellulosic aerogel formulations. Different letters at the same column denote significant differences between samples ($p \leq 0.05$).

		PLA gain (%)		**Contact angle (º)**	
	Density (mg/cm^3)	**1% PLA (w/v)**	**5% PLA (w/v)**	**1% PLA (w/v)**	**5% PLA (w/v)**
CAG	12.8 ± 0.1^{a}	78 ± 2^{a}	249 ± 14^{a}	98 ± 12^{abc}	101 ± 6^{ab}
CAG + 10% E2	13.4 ± 0.4^{a}	67 ± 2^{b}	226 ± 12^{a}	101 ± 6^{ab}	110 ± 9^{a}
CAG + 25% E2	16.7 ± 3.3^{ab}	62 ± 5^{b}	228 ± 14^{a}	108 ± 6^{a}	115 ± 11^{a}
CAG + 50% E2	22.2 ± 2.3^{b}	46 ± 1^{c}	175 ± 10^{b}	92 ± 6^{bc}	95 ± 2^{b}
CAG + 75% E2	29.7 ± 1.2^{c}	38 ± 1^{d}	131 ± 1^{c}	83 ± 6^{c}	97 ± 9^{ab}

Although PLA coating is positive to improve the aerogels' performance at high relative humidity conditions, the porosity of the materials is known to significantly decrease [59]. Since the aim of this work was to develop bioactive aerogels through the incorporation of *P. oceanica* extracts, which could be progressively released upon contact with food products, the release of extracts E2 and E3 in aerogel samples produced by dipping into 1 and 5% (w/v) PLA solutions was estimated gravimetrically after immersing the samples into a 50/50 water/ethanol mixture overnight. Figures 2A and 2B show the visual appearance of aerogel specimens before and after being soaked in the liquid medium. A clear coloration loss occurred in the aerogels loaded with E3, while this was not so evident in the aerogels containing E2. In fact, as seen in Figure 2C, the release values for E3 were much higher than E2, indicating that the hydrophobic extract is more easily released from the aerogel template when using a mixture of water/ethanol. This may also be explained by the fact that while the E2 extract was incorporated into the inner cellulosic structure, the E3 extract was incorporated through the PLA coating, hence forming part of the more superficial layers of the material and therefore, facilitating its release. Furthermore, while the PLA concentration of the dipping solution had a minor effect on the release of E3 (with maximum release values of ca. 99% and 97% for the aerogels dipped into 1% PLA and 5% PLA solutions, respectively), a greater release of the E2 extract was achieved for the aerogel produced from the less concentrated PLA dipping solution (40% release with 1% PLA vs. 15% release with 5% PLA). This highlights the importance of preserving as much as possible the porous aerogel structure to guarantee the release of the bioactive extracts upon contact with liquids. Thus, the less concentrated PLA dipping solution was selected as the optimum for further experiments.

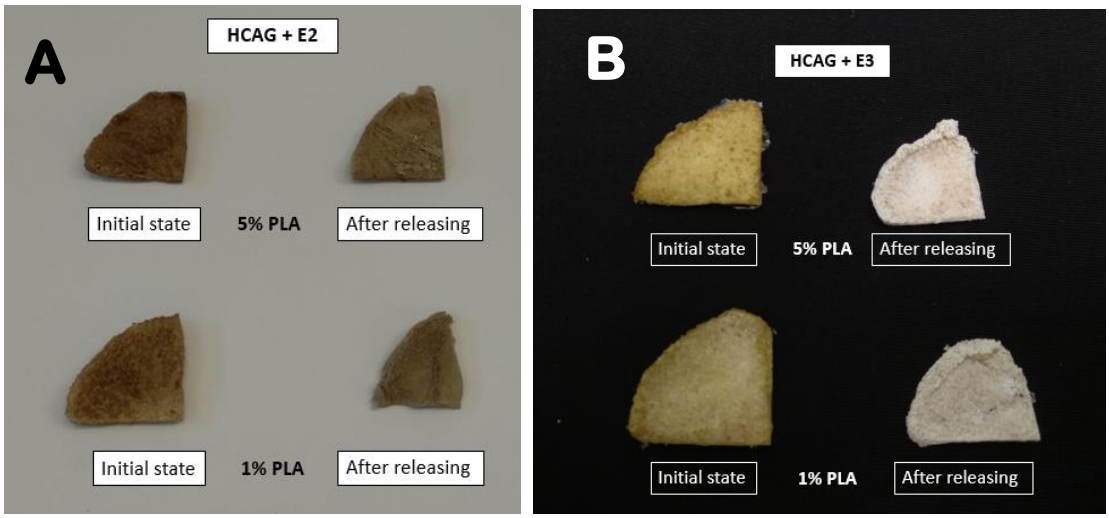

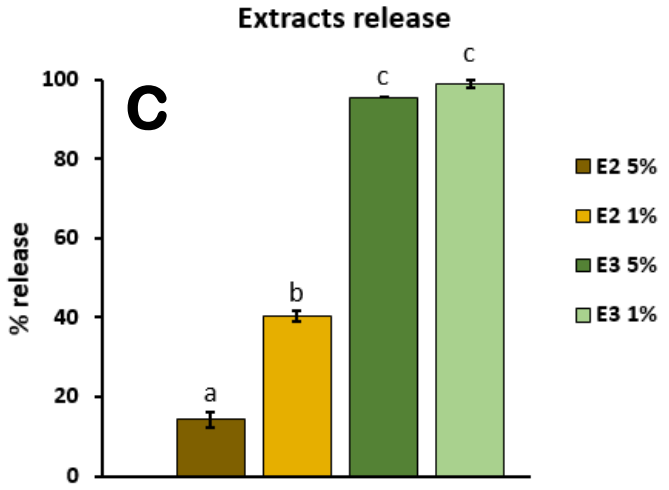

Figure 2. Visual appearance of aerogel specimens containing E2 extract (A) and E3 extract (B) after being soaked into 50/50 water/ethanol solutions overnight. (C) Maximum extract release determined gravimetrically. Different letters in Figure 2C denote significant differences between samples ($p \leq 0.05$).

4.2 Structural characterization of hydrophobized cellulosic aerogels loaded with extracts

After fixing the extract concentrations, as well as the PLA concentration of the dipping solutions, hybrid aerogels were developed by incorporating the E2 and E3 extracts individually (HCAG + E2, HCAG + E3) and simultaneously (HCAG + E2 + E3). FT-IR characterization of the different aerogels was carried out and results are shown in Figure 3A, while the spectra of raw extracts and PLA used for their preparation are shown in Figure 3B. As observed, several cellulose characteristic bands, such as those located at 1103, 1054 and 984 cm^{-1} (corresponding to C-C, C-O, C-H stretching and C-OH bending modes [71, 72]), were intense and defined in all the aerogels, as expected. The incorporation of PLA in all the aerogels could also be confirmed by the appearance of the carbonyl stretching band at around 1750 cm^{-1} [31] (cf. Figure 3B). However, it should be noted that a band was also detected within this region in the FT-IR spectra from E3 (cf. Figure 3B), which has been reported to arise from the presence of lipidic compounds [66]. As a result, this band was more intense in those aerogels containing the E3 extract. Other PLA characteristic peaks were also present at around 1200 and 1080 cm^{-1}, corresponding to the C–O–C stretching peaks [31]. Moreover, for the aerogels containing E3 the bands located at 2918 and 2850 cm^{-1}, corresponding to the CH_2 asymmetrical and symmetrical stretching, were sharper and more intense. These bands are very intense in the FT-IR spectra from the extract (cf. Figure 3B) and have been attributed to the presence of fatty acids [73].

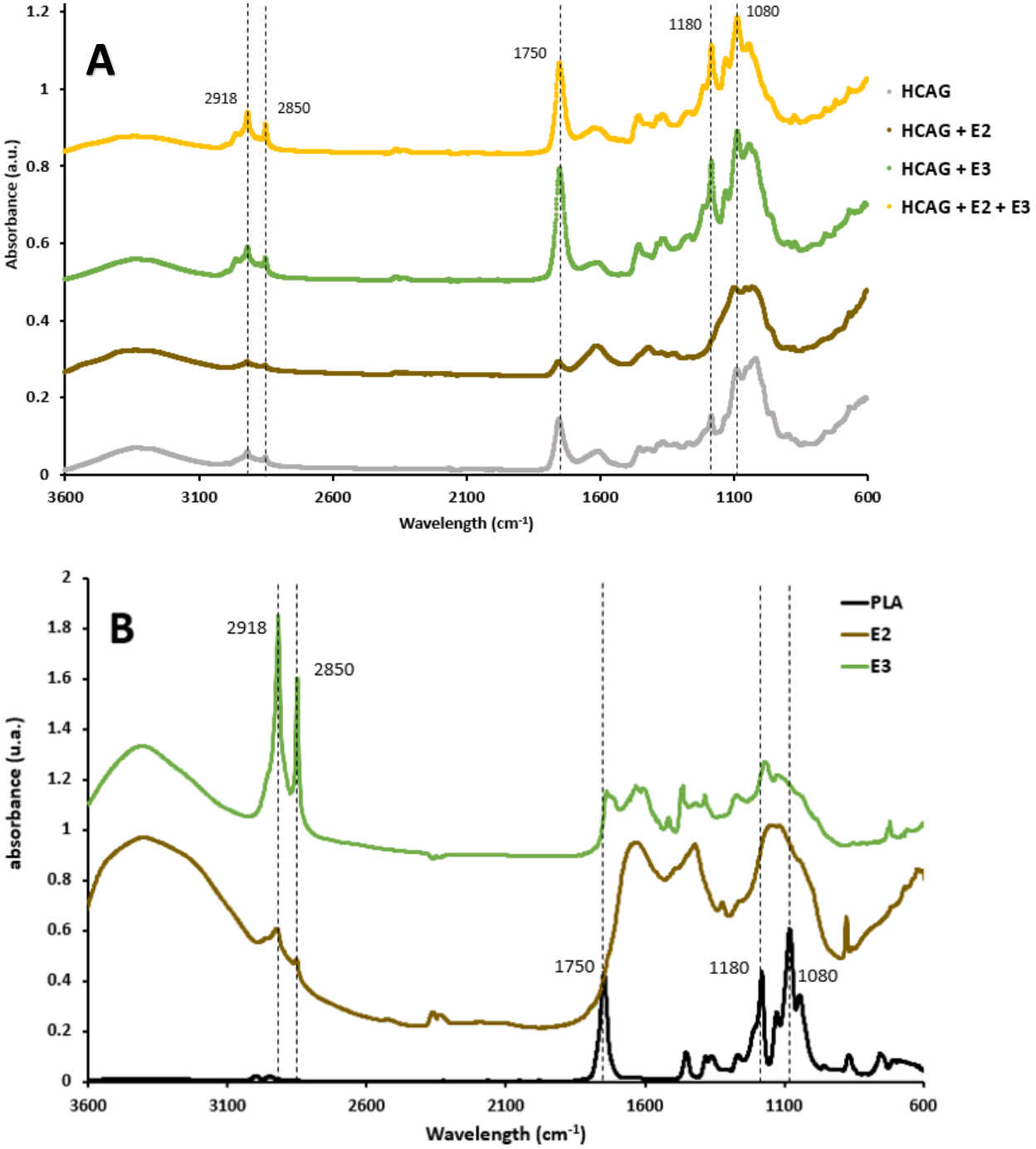

Figure 3. (A) FT-IR spectra of the bioactive aerogels and (B) the hydrophilic (E2) and hydrophobic (E3) antioxidant extracts, as well as the PLA used to hydrophobize the aerogels. Spectra have been offset for clarity.

The morphology of the different aerogels was investigated by SEM to evaluate the effect of the extracts' incorporation and representative images are shown in Figure 4. As expected, PLA coated the cellulosic fibers in HCAG, thus reducing the porosity as compared with an uncoated cellulosic aerogel [59, 74]. The morphology of this aerogel was very similar to that previously reported for hydrophobized cellulosic aerogels dipped into 5% (w/w) PLA solutions [59]. In general, after the incorporation of the extracts the aerogels presented a more continuous surface, with fewer pores. Interestingly, the morphology of the aerogels significantly differed depending on the type of extract incorporated (see insets in Figure 4), which is reasonable given the different method followed for their incorporation into the aerogels. In the case of HCAG + E2, some regions where fine threads of E2 extract covered the cellulosic fibers were visible (Fig. 4B). In this case, since the extract was incorporated together with the cellulosic nanocrystals prior to the freeze-drying step, interactions between the nanocrystals and the extract were expected to take place.

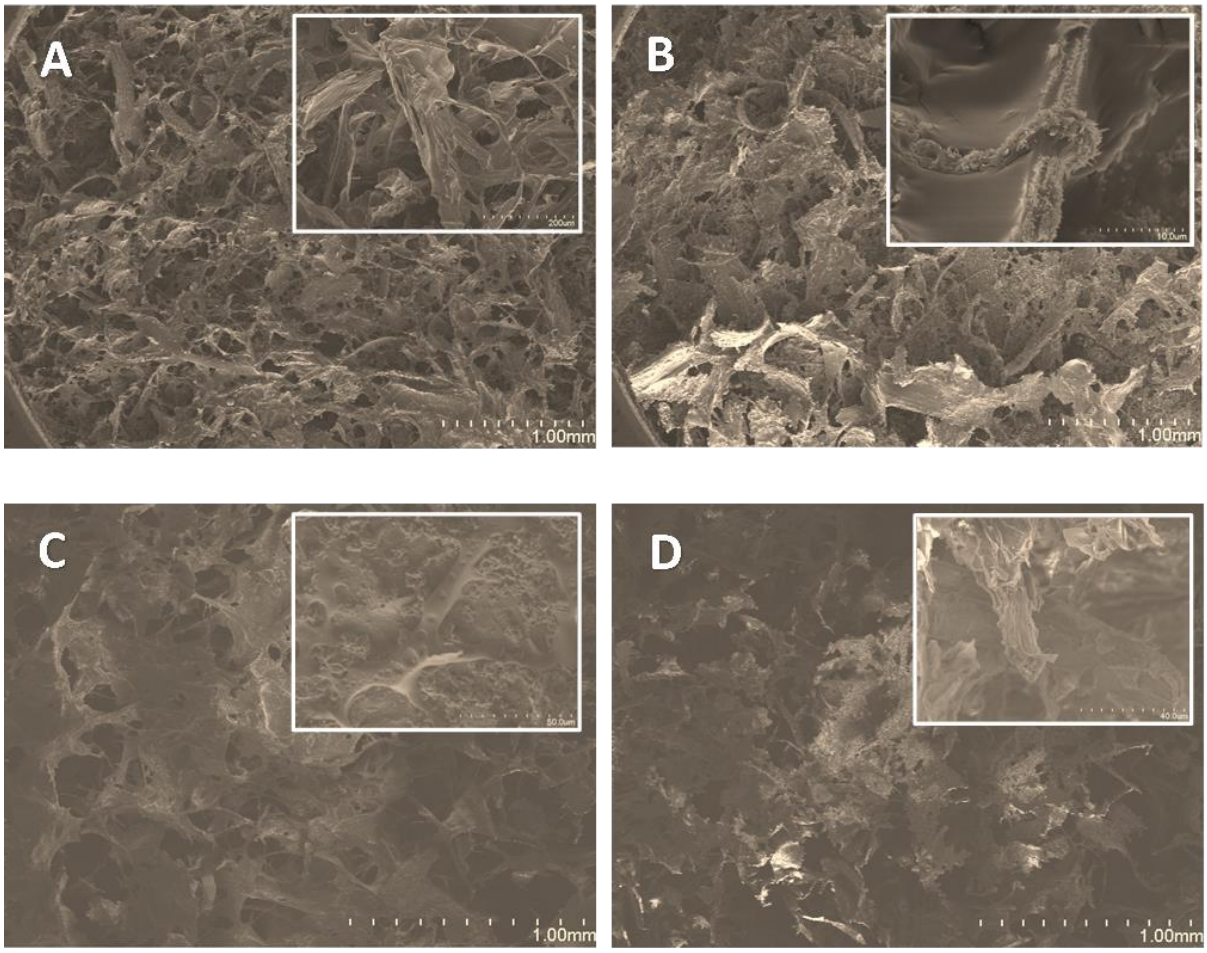

Figure 4. SEM images of the hydrophobized cellulosic aerogels. (A) HCAG, (B) HCAG + E2, (C) HCAG + E3 and (D) HCAG + E2 + E3. Insets correspond to images with higher magnifications (scale markers correspond to 100 μm).

In contrast, in the case of HCAG + E3, the extract was added together with PLA in the dipping phase; hence it affected the coating appearance, which seemed to be more continuous than in HCAG. The combination of both extracts in HCAG + E2 + E3 resulted in a denser material where it was difficult to identify the different components. The densities of all the aerogels were estimated and the results are summarized in Table 2. As observed, the density of the aerogels increased with the incorporation of the extracts, being HCAG + E2 + E3 the densest one (55.8 mg/cm^3). This supports the results from SEM characterization, confirming that more compact and less porous structures were attained when adding the bioactive extracts.

To evaluate the effect of the morphology on the adsorption capacity of the aerogels, sorption experiments were carried out by soaking the aerogels into water and oil. The sorption and desorption kinetics are shown in Figure S2, while the maximum sorption values are gathered in Table 2. For both liquids, the sorption process was much faster than the desorption, reaching the maximum sorption within the first 60 minutes of the experiment. The sorption capacity of the aerogels was clearly correlated with their structure, i.e. density and porous structure. Specifically, the density of the aerogels was a key factor controlling water sorption, with the most porous aerogel (HCAG) reaching water sorption values up to 1500% and the most compact aerogel (HCAG+ E2 + E3) showing the lowest water sorption value of 644%. Notably, all the aerogels were able to completely release water after less than 2 h. As opposed to water sorption, oil sorption could not be directly correlated to the density of the aerogels and instead, the presence of the E3 extract seemed to have a significant impact in reducing the aerogels' oil sorption capacity. While HCAG reached a maximum oil sorption of 1900%, HCAG + E2 + E3 was capable of adsorbing a maximum of 867%. The oil desorption process took place more slowly than water desorption, which agrees well with previous experiments [59] and is reasonable, given the higher viscosity and evaporation temperature of the oil. Approximately 90-100% of the adsorbed oil was released after 7 days. The capacity of the aerogels to release most of the adsorbed oil could be very beneficial in terms of allowing their re-utilization when used as adsorbent pads. These results highlight the outstanding water and oil sorption capacity of the developed aerogels, which was even higher than that reported for hydrophobized cellulosic aerogels prepared using the same PLA dipping method (with maximum sorption values of 670% and 920% for water and oil, respectively) [59], although remained lower to other super-absorbent materials made for oil spilling purposes like those obtained from silanized pomelo peel-based aerogels mixed with filter paper (4800%) [75]. The use of more concentrated PLA dipping solutions (5% (w/v)) improved the mechanical performance of the native cellulosic aerogels to a higher extent (with up to 10-fold increase in the compressive stress, as previously determined by compression tests), but it also diminished the porosity of the coated aerogels, thus reducing their adsorption capacity [59]. The aerogel formulations developed in this work present a great potential to be used as absorbing pads

for food packaging (for instance, under fresh meat or fish fillets), being able to adsorb liquids of both hydrophilic and hydrophobic nature.

Table 2. Density and maximum water and oil sorption capacity of the bioactive cellulosic aerogels. Different letters at the same column denote significant differences between samples ($p \leq 0.05$).

	Density (mg/cm^3) (*)	**Water sorption (%)**	**Oil Sorption (%)**
HCAG	25.4 ± 2.1^a	1515 ± 171^a	1814 ± 117^a
HCAG + E2	39.6 ± 1.4^b	931 ± 62^b	1900 ± 101^a
HCAG + E3	37.2 ± 3.1^b	922 ± 25^b	1141 ± 129^b
HCAG + E2 + E3	55.8 ± 4.9^c	644 ± 53^c	867 ± 80^b

4.3 Evaluation of the bioactive capacity of hydrophobized cellulosic aerogels loaded with extracts

As the final stage of this work, the bioactive properties of the developed aerogels were studied to assess the effect of the incorporation of the antioxidant extracts and evaluate their potential for bioactive packaging applications. The β-carotene bleaching assay was carried out to evaluate the antioxidant capacity of the aerogels and the obtained results are shown in Figure 5 (see Table S1 for the inhibition values corresponding to 120 min). As observed, all the aerogels, including HCAG, showed a positive inhibitory effect. The bleaching inhibition capacity of HCAG (24%) can be explained by the presence of non-cellulosic components, such as hemicelluloses and lipidic compounds, in the less purified cellulosic nanocrystals produced by the applied simplified purification protocol [41]. The presence of these components has been shown to confer antioxidant capacity to similar cellulosic materials, with inhibition values of around 30% for cellulosic films from vine shoots [76] and 6% for cellulosic films from *Arundo donax* waste biomass [6]. The aerogel combining both extracts (HCAG + E2 + E3) showed the highest bleaching inhibition activity (91%), while HCAG + E2 and HCAG + E3 showed inhibition values of 68% and 55%, respectively. A previous study reported inhibition values of 65% for E2 solutions and 83% for E3 solutions (tested at a concentration of 0.5 mg/mL in ethanol) [66]; thus, one would in principle expect a greater inhibition for the aerogel loaded with E3. The greater activity of HCAG + E2 can be explained by the greater solubility of the hydrophilic extract E2 in

the aqueous media used in the β-carotene bleaching assay, as opposed to E3, which is known to be more soluble in non-polar media [66]. In fact, considering the inhibition values previously reported for the extract solutions, the inhibition values estimated for the hybrid aerogels suggest that while the extract E2 was released towards the liquid medium, being at a final concentration of approximately 0.3 mg/mL, E3 could be found at a concentration of ca. 0.2 mg/mL in the liquid medium. These results evidence the antioxidant capacity of these aerogels, especially those combining both extracts.

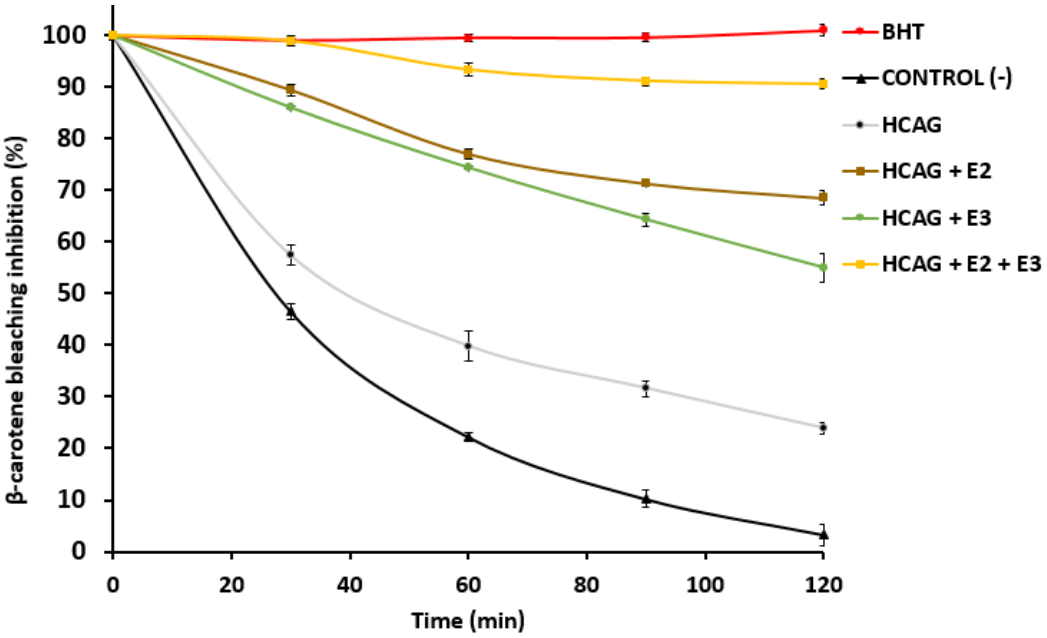

Figure 5. Kinetics of the β-carotene bleaching inhibition of the hydrophobized cellulosic aerogels. CONTROL (-): Negative control with no added aerogel; BHT: Positive control.

As a final bioactivity test, the hydrophobized cellulosic aerogels loaded with extracts were tested as absorption pads to improve the preservation of minced red meat upon refrigerated storage and their capacity to inhibit lipid oxidation and colour loss was evaluated. The capability of the aerogels to prevent lipid oxidation in red meat was evaluated by calculating the TBARS content in the raw minced meat and after storage for 10 days. The percentage of lipid oxidation inhibition with regards to a blank sample (i.e. minced meat stored without any pad) was calculated and the results are summarized in Table 3. It could be observed that, interestingly, the commercial pads were not capable of preventing lipid oxidation. This can be explained by the absence of antioxidant substances in the commercial pads, which act merely as adsorbent materials for the released water and/or fats. Notably, all the developed aerogels, including HCAG, presented a positive effect in preventing lipid oxidation. This again evidences the benefits of using less

purified cellulosic nanocrystals, since not only they are more environmentally and economically efficient, but the presence of non-cellulosic components confers them additional functionalities. Once again, the aerogel loaded with E2 had a more remarkable effect (46% inhibition) than the aerogel loaded with E3 (33% inhibition), probably due to the greater solubility of E2 in the predominantly aqueous media released by minced meat upon storage. Combining both extracts provided a maximum inhibition of ca. 54%, which is greater than the values previously reported for cellulosic aerogels loaded with water-soluble extracts from *Arundo donax* (28-41% inhibition) [6]. This highlights the potential of combining extracts of different nature (both hydrophilic and hydrophobic) through the simple methodology applied in this work to achieve greater inhibition values. The lipid oxidation inhibition of the developed aerogels is even comparable to that achieved by the addition of potent antioxidants, directly applied to foods or incorporated through coatings. For instance, a gelatin coating enriched with antioxidant tomato by-products, applied on pork meat, showed 50% inhibition after 13 days of storage [77]. In another work, 300 mg/kg of two commercial antioxidants (tea catechins and α-tocopherol) were sprayed and mixed with beef meat, showing inhibition values of 51% and 56%, respectively [70].

Table 3. 2-Thiobarbituric acid reactive substances (TBARS) and estimated lipid oxidation inhibition in the raw minced red meat (day 0) and in the meat after 10 days of storage. Different letters at the same column denote significant differences between samples ($p \leq 0.05$).

	TBARS (mg malonaldehyde /Kg meat)	**Lipid oxidation Inhibition (%) VS control (-)**
Day 0	0.49 ± 0.10^{f}	---
Control (-)	7.44 ± 0.13^{b}	---
Commercial pad	8.65 ± 0.34^{a}	---
HCAG	6.51 ± 0.14^{c}	13.3
HCAG + E2	4.90 ± 0.12^{d}	36.6
HCAG + E3	5.97 ± 0.11^{c}	21.2
HCAG + E2 + E3	3.72 ± 0.18^{e}	53.6

Meat discolouration upon storage was also evaluated. This phenomenon is attributed to the process of oxymyoglobin oxidation, giving rise to the formation of metmyoglobin. The proportion of these two myoglobin forms was determined in the raw minced meat and after storage for 10 days and the results are shown in Figure 6. As expected, the fresh meat showed the highest oxymyoglobin and lowest metmyoglobin contents. The commercial pad presented again the worst performance, with the highest metmyoglobin and lowest oxymyoglobin contents after 10 days of storage, i.e. producing the greatest meat colour loss. Despite the variability of the data, a trend of decreased metmyoglobin and increased oxymyoglobin, as compared with the control sample, was observed for the aerogels loaded with extracts. The combination of both extracts (HCAG + E2 + E3) yielded the most significant inhibition of oxymyoglobin oxidation, confirming the great potential of this aerogel to be used as bioactive adsorbent pad in food packaging. These results are better than those previously reported for a cellulosic aerogel derived from *Arundo donax* waste biomass loaded with water-soluble antioxidant extracts, with a maximum OxyMb/MetMb ratio of ≈1/3 [6]. Another work, where the commercial antioxidant amexol was incorporated as a natural antioxidant into a polypropylene film (up to 8% w/w) to design an active packaging system for beef meat, reported a reduction in the oxymyoglobin oxidation up to 33% after 10 days of storage [60], which is significantly lower than the 54% reduction in the oxymyoglobin oxidation achieved with HCAG + E2 + E3.

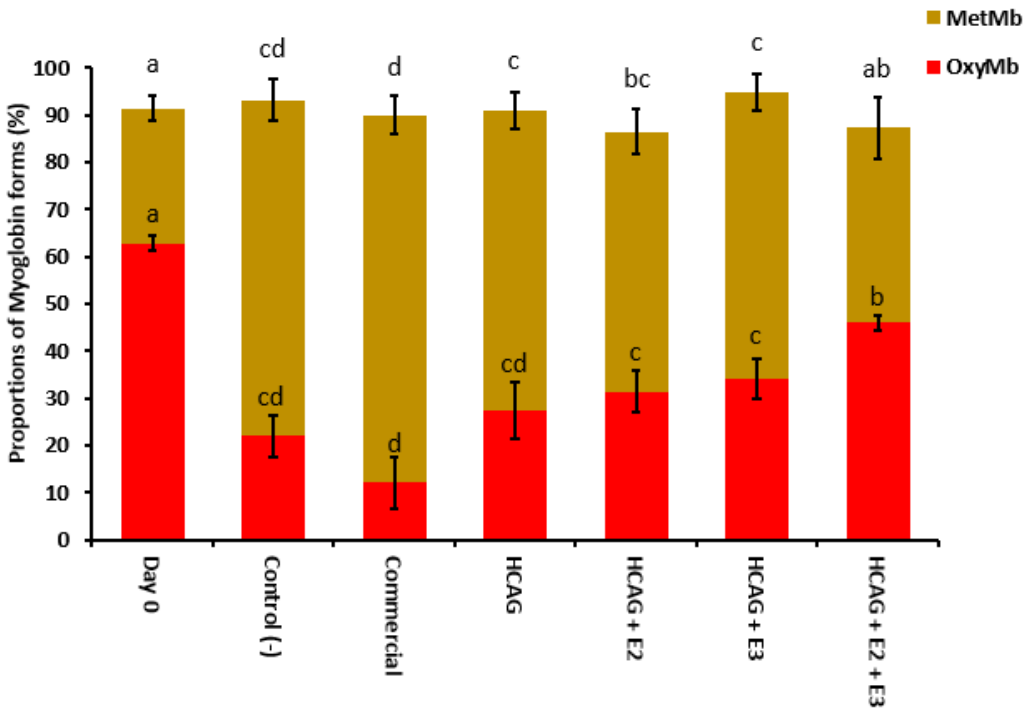

Figure 6. Proportions of oxymyoglobin (%OxyMb) and metmyoglobin (%MetMb) in the raw minced red meat (day 0) and in the meat after 10 days of storage. Different letters denote significant differences between samples ($p \leq 0.05$).

5. Conclusions

P. oceanica waste biomass has been fully valorised to produce hydrophobized cellulosic aerogels (HCAG) with high antioxidant potential. The aerogels were composed of less purified cellulosic nanocrystals extracted by a greener methodology and were hydrophobized by a simple PLA dipping method. Hydrophilic (E2) and hydrophobic (E3) antioxidant extracts were also produced from *P. oceanica* waste biomass and subsequently incorporated into the aerogels through the cellulosic (HCAG + E2) and the PLA phase (HCAG + E3), as well as simultaneously (HCAG + E2 + E3).

The incorporation of the extracts produced more compact and less porous structures, with greater densities than the unloaded aerogel, especially when both of them were combined. All the developed aerogels were capable of adsorbing great amounts of both water and oil, releasing most of the adsorbed liquid after less than 3h (water) and 7 days (oil). The water sorption capability was clearly correlated to the density of the aerogels, with the most porous aerogel (HCAG) adsorbing up to 1500% water. On the other hand, oil sorption was limited by the presence of E3 in the hydrophobic PLA coating phase and a maximum sorption of 1900% was attained with HCAG. Moreover, all the developed aerogels presented an inhibitory effect on the β-carotene bleaching assay (23-91% inhibition), which was a combined effect of the non-cellulosic components present in the cellulosic aerogel and the incorporated extracts. The aerogels loaded with extracts were also capable of reducing lipid and oxymyoglobin oxidation in red meat upon storage, being HCAG + E2 + E3 the one with best performance (60% inhibition of lipid oxidation and 54% reduction in the oxymyoglobin oxidation), proving a synergic effect between extracts. These results highlight the potential of the developed aerogels to be used as bioactive adsorbing pads in packaged fresh foods, such as red meat, being able to adsorb great amounts of hydrophilic and hydrophobic liquids and preserving the quality of red meat upon prolonged storage.

6. Supplementary Material

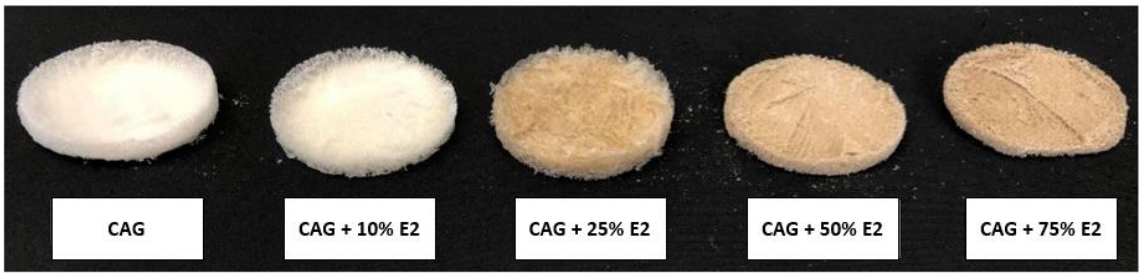

Figure S1. Visual aspect of the cellulosic aerogels loaded with increasing E2 concentrations.

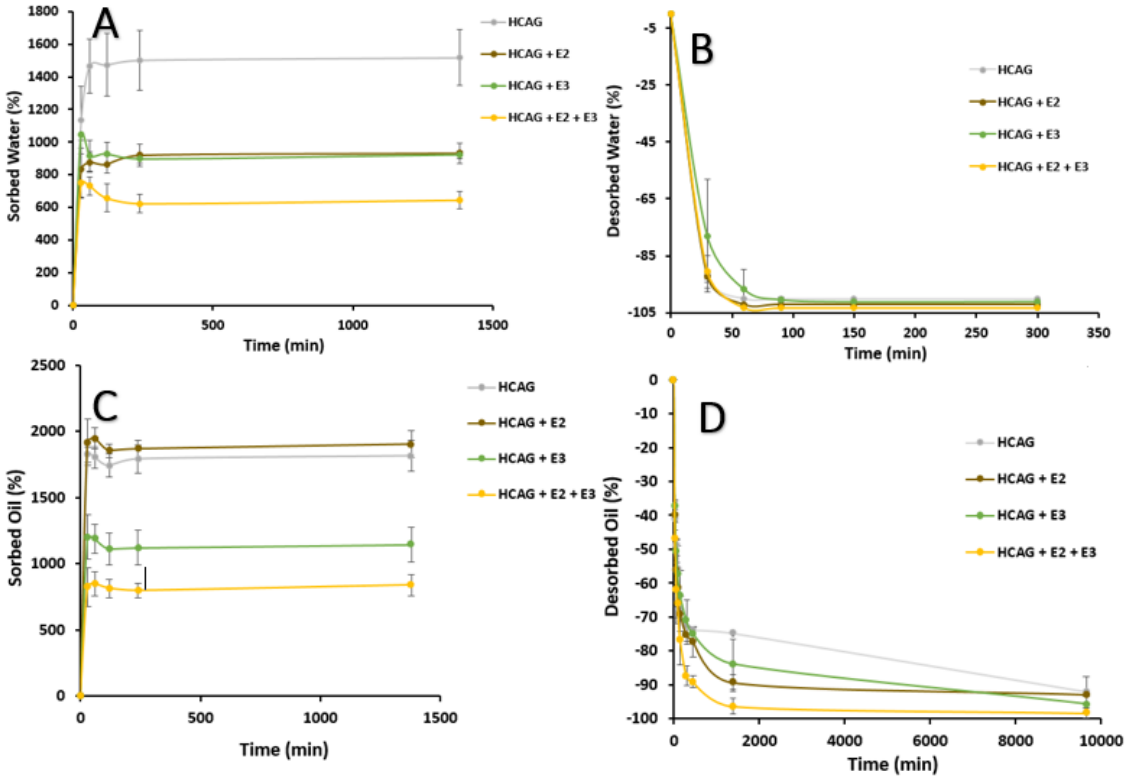

Figure S2. Water (A) and oil (C) sorption and water (B) and oil (D) desorption kinetics of bioactive aerogels.

Table S1. Antioxidant capacity of the hydrophobized cellulosic aerogels, measured from the β-carotene bleaching assay. Different letters within the same column denote significant differences between samples ($p \leq 0.05$).

	β-carotene bleaching inhibition (%)	**Δ β-carotene bleaching inhibition (%) (†)**
HCAG	23.88 ± 0.55^{d}	---
HCAG + E2	68.45 ± 1.39^{b}	44.56 ± 1.04^{b}
HCAG + E3	55.04 ± 3.41^{c}	31.15 ± 2.81^{c}
HCAG + E2 + E3	90.52 ± 1.07^{a}	66.64 ± 0.72^{a}

(†) Calculated by subtracting the HCAG bleaching inhibition.

List of references of Chapter 4

[1] C. Zarfl, D. Fleet, E. Fries, F. Galgani, G. Gerdts, G. Hanke, M. Matthies, Microplastics in oceans, Marine Pollution Bulletin 62 (2011) 1589-1591.
[2] L.G.A. Barboza, A.D. Vethaak, B.R. Lavorante, A.-K. Lundebye, L. Guilhermino, Marine microplastic debris: An emerging issue for food security, food safety and human health, Marine pollution bulletin 133 (2018) 336-348.
[3] M. Carbery, W. O'Connor, T. Palanisami, Trophic transfer of microplastics and mixed contaminants in the marine food web and implications for human health, Environment International 115 (2018) 400-409.
[4] V. Siracusa, P. Rocculi, S. Romani, M. Dalla Rosa, Biodegradable polymers for food packaging: a review, Trends in Food Science & Technology 19(12) (2008) 634-643.
[5] J.-W. Rhim, Potential use of biopolymer-based nanocomposite films in food packaging applications, Food Science and Biotechnology 16(5) (2007) 691-709.
[6] C. Fontes-Candia, E. Erboz, A. Martínez-Abad, A. López-Rubio, M. Martínez-Sanz, Superabsorbent food packaging bioactive cellulose-based aerogels from Arundo donax waste biomass, Food Hydrocolloids 96 (2019) 151-160.
[7] J.P. de Oliveira, G.P. Bruni, M.J. Fabra, E. da Rosa Zavareze, A. López-Rubio, M. Martínez-Sanz, Development of food packaging bioactive aerogels through the valorization of Gelidium sesquipedale seaweed, Food Hydrocolloids 89 (2019) 337-350.
[8] L. Heath, W. Thielemans, Cellulose nanowhisker aerogels, Green Chemistry 12(8) (2010) 1448-1453.
[9] E. Guilminot, F. Fischer, M. Chatenet, A. Rigacci, S. Berthon-Fabry, P. Achard, E. Chainet, Use of cellulose-based carbon aerogels as catalyst support for PEM fuel cell electrodes: Electrochemical characterization, Journal of Power Sources 166(1) (2007) 104-111.
[10] I. Smirnova, S. Suttiruengwong, W. Arlt, Feasibility study of hydrophilic and hydrophobic silica aerogels as drug delivery systems, Journal of Non-Crystalline Solids 350 (2004) 54-60.
[11] M. Schmidt, F. Schwertfeger, Applications for silica aerogel products, Journal of non-crystalline solids 225 (1998) 364-368.
[12] A.S. Dorcheh, M. Abbasi, Silica aerogel; synthesis, properties and characterization, Journal of materials processing technology 199(1-3) (2008) 10-26.
[13] S. Zhao, W.J. Malfait, N. Guerrero-Alburquerque, M.M. Koebel, G. Nyström, Biopolymer aerogels and foams: Chemistry, properties, and applications, Angewandte Chemie International Edition 57(26) (2018) 7580-7608.
[14] J. Feng, S.T. Nguyen, Z. Fan, H.M. Duong, Advanced fabrication and oil absorption properties of super-hydrophobic recycled cellulose aerogels, Chemical Engineering Journal 270 (2015) 168-175.
[15] S.T. Nguyen, J. Feng, S.K. Ng, J.P. Wong, V.B. Tan, H.M. Duong, Advanced thermal insulation and absorption properties of recycled cellulose aerogels, Colloids and Surfaces A: Physicochemical and Engineering Aspects 445 (2014) 128-134.
[16] N. Buchtova, C. Pradille, J.-L. Bouvard, T. Budtova, Mechanical properties of cellulose aerogels and cryogels, Soft matter (2019).
[17] K.J. De France, T. Hoare, E.D. Cranston, Review of hydrogels and aerogels containing nanocellulose, Chemistry of Materials 29(11) (2017) 4609-4631.
[18] Y. Miao, H. Luo, M. Pudukudy, Y. Zhi, W. Zhao, S. Shan, Q. Jia, Y. Ni, CO2 capture performance and characterization of cellulose aerogels synthesized from old corrugated containers, Carbohydrate Polymers (2019) 115380.
[19] R. Baetens, B.P. Jelle, A. Gustavsen, Aerogel insulation for building applications: a state-of-the-art review, Energy and Buildings 43(4) (2011) 761-769.
[20] F. Schwertfeger, D. Frank, M. Schmidt, Hydrophobic waterglass based aerogels without solvent exchange or supercritical drying, Journal of Non-Crystalline Solids 225 (1998) 24-29.
[21] Q.B. Thai, S.T. Nguyen, D.K. Ho, T. Du Tran, D.M. Huynh, N.H. Do, T.P. Luu, P.K. Le, D.K. Le, N. Phan-Thien, Cellulose-based aerogels from sugarcane bagasse for oil spill-cleaning and heat insulation applications, Carbohydrate Polymers (2019) 115365.

[22] M. Chhajed, C. Yadav, A.K. Agrawal, P.K. Maji, Esterified superhydrophobic nanofibrillated cellulose based aerogel for oil spill treatment, Carbohydrate polymers (2019) 115286.
[23] I. Benito-González, A. López-Rubio, R. Gavara, M. Martínez-Sanz, Cellulose nanocrystal-based films produced by more sustainable extraction protocols from Posidonia oceanica waste biomass, Cellulose (2019) 1-18.
[24] M. Martínez-Sanz, A.A. Vicente, N. Gontard, A. Lopez-Rubio, J.M. Lagaron, On the extraction of cellulose nanowhiskers from food by-products and their comparative reinforcing effect on a polyhydroxybutyrate-co-valerate polymer, Cellulose 22(1) (2015) 535-551.
[25] I. Benito-González, A. López-Rubio, M. Martínez-Sanz, Potential of lignocellulosic fractions from Posidonia oceanica to improve barrier and mechanical properties of bio-based packaging materials, International journal of biological macromolecules 118 (2018) 542-551.
[26] M. Martínez-Sanz, I. Benito-González, A. López-Rubio, Procedimiento para la preparación de aerogeles hidrofóbicos, in: CSIC (Ed.) Spain, 2019.
[27] M. Wang, I.V. Anoshkin, A.G. Nasibulin, J.T. Korhonen, J. Seitsonen, J. Pere, E.I. Kauppinen, R.H. Ras, O. Ikkala, Modifying native nanocellulose aerogels with carbon nanotubes for mechanoresponsive conductivity and pressure sensing, Advanced materials 25(17) (2013) 2428-2432.
[28] F. Jiang, Y.-L. Hsieh, Amphiphilic superabsorbent cellulose nanofibril aerogels, Journal of Materials Chemistry A 2(18) (2014) 6337-6342.
[29] S.T. Nguyen, J. Feng, N.T. Le, A.T. Le, N. Hoang, V.B. Tan, H.M. Duong, Cellulose aerogel from paper waste for crude oil spill cleaning, Industrial & engineering chemistry research 52(51) (2013) 18386-18391.
[30] N. Pircher, S. Veigel, N. Aigner, J.-M. Nedelec, T. Rosenau, F. Liebner, Reinforcement of bacterial cellulose aerogels with biocompatible polymers, Carbohydrate polymers 111 (2014) 505-513.
[31] D. Edith, J.-L. Six, Surface characteristics of PLA and PLGA films, Applied Surface Science 253(5) (2006) 2758-2764.
[32] D. Cohn, H. Younes, Biodegradable PEO/PLA block copolymers, Journal of biomedical materials research 22(11) (1988) 993-1009.
[33] L.M. Diamante, T. Lan, Absolute viscosities of vegetable oils at different temperatures and shear rate range of 64.5 to 4835 s− 1, Journal of food processing 2014 (2014).
[34] X. Yang, K. Shi, I. Zhitomirsky, E.D. Cranston, Cellulose nanocrystal aerogels as universal 3D lightweight substrates for supercapacitor materials, Advanced Materials 27(40) (2015) 6104-6109.
[35] M. Xu, W. Bao, S. Xu, X. Wang, R. Sun, Porous cellulose aerogels with high mechanical performance and their absorption behaviors, BioResources 11(1) (2016) 8-20.
[36] J.-s. Fan, Y.-h. Li, Maximizing the yield of nanocrystalline cellulose from cotton pulp fiber, Carbohydrate polymers 88(4) (2012) 1184-1188.
[37] E. Dinand, H. Chanzy, R. Vignon, Suspensions of cellulose microfibrils from sugar beet pulp, Food hydrocolloids 13(3) (1999) 275-283.
[38] F. Grüneberger, T. Künniger, T. Zimmermann, M. Arnold, Nanofibrillated cellulose in wood coatings: mechanical properties of free composite films, Journal of materials science 49(18) (2014) 6437-6448.
[39] S. Han, Q. Sun, H. Zheng, J. Li, C. Jin, Green and facile fabrication of carbon aerogels from cellulose-based waste newspaper for solving organic pollution, Carbohydrate polymers 136 (2016) 95-100.
[40] G. Balata, A. Tola, Cost-opportunity analysis of the use of Posidonia oceanica as a source of bio-energy in tourism-oriented territories. The case of Alghero, Journal of Cleaner Production (2017).
[41] I. Benito-González, A. López-Rubio, R. Gavara, M. Martínez-Sanz, Cellulose nanocrystal-based films produced by more sustainable extraction protocols from Posidonia oceanica waste biomass, Cellulose 26(13-14) (2019) 8007-8024.
[42] I. Benito-González, A. López-Rubio, L.G. Gómez-Mascaraque, M. Martínez-Sanz, PLA coating improves the performance of renewable adsorbent pads based on cellulosic aerogels from aquatic waste biomass, Chemical Engineering Journal 390 (2020) 124607.
[43] M.A. AUTY, M. Twomey, T.P. GUINEE, D.M. MULVIHILL, Development and application of confocal scanning laser microscopy methods for studying the distribution of fat and protein in selected dairy products, Journal of Dairy Research 68(3) (2001) 417-427.

[44] A.B. McKenna, Examination of whole milk powder by confocal laser scanning microscopy, Journal of Dairy Research 64(3) (1997) 423-432.
[45] G.R. Littlejohn, J.C. Mansfield, D. Parker, R. Lind, S. Perfect, M. Seymour, N. Smirnoff, J. Love, J. Moger, In vivo chemical and structural analysis of plant cuticular waxes using stimulated Raman scattering microscopy, Plant physiology 168(1) (2015) 18-28.
[46] J. Huen, C. Weikusat, M. Bayer-Giraldi, I. Weikusat, L. Ringer, K. Lösche, Confocal Raman microscopy of frozen bread dough, Journal of cereal science 60(3) (2014) 555-560.
[47] G.P. Smith, S.E. Holroyd, D.C. Reid, K.C. Gordon, Raman imaging processed cheese and its components, Journal of Raman Spectroscopy 48(3) (2017) 374-383.
[48] N. Gierlinger, T. Keplinger, M. Harrington, Imaging of plant cell walls by confocal Raman microscopy, nature protocols 7(9) (2012) 1694.
[49] A.-S. Jääskeläinen, U. Holopainen-Mantila, T. Tamminen, T. Vuorinen, Endosperm and aleurone cell structure in barley and wheat as studied by optical and Raman microscopy, Journal of cereal science 57(3) (2013) 543-550.
[50] I. Benito-González, A. López-Rubio, M. Martínez-Sanz, High-performance starch biocomposites with celullose from waste biomass: Film properties and retrogradation behaviour, Carbohydrate polymers 216 (2019) 180-188.
[51] M. Martínez-Sanz, I. Benito-González, A. López-Rubio, Patent application number: P201930871. Holder entity: CSIC, 2019.
[52] S.H. Kim, C.M. Lee, K. Kafle, Characterization of crystalline cellulose in biomass: basic principles, applications, and limitations of XRD, NMR, IR, Raman, and SFG, Korean Journal of Chemical Engineering 30(12) (2013) 2127-2141.
[53] G. Kister, G. Cassanas, M. Vert, Effects of morphology, conformation and configuration on the IR and Raman spectra of various poly (lactic acid) s, Polymer 39(2) (1998) 267-273.
[54] B. Muik, B. Lendl, A. Molina-Díaz, M.J. Ayora-Cañada, Direct monitoring of lipid oxidation in edible oils by Fourier transform Raman spectroscopy, Chemistry and physics of lipids 134(2) (2005) 173-182.
[55] K. Czamara, K. Majzner, M.Z. Pacia, K. Kochan, A. Kaczor, M. Baranska, Raman spectroscopy of lipids: a review, Journal of Raman Spectroscopy 46(1) (2015) 4-20.
[56] F. Li, E. Mascheroni, L. Piergiovanni, The potential of nanocellulose in the packaging field: a review, Packaging Technology and Science 28(6) (2015) 475-508.
[57] A. da Silva, L.M. Nievola, C.A. Tischer, S. Mali, P.C. Faria-Tischer, Cassava starch-based foams reinforced with bacterial cellulose, Journal of Applied Polymer Science 130(5) (2013) 3043-3049.
[58] T. Budtova, Cellulose II aerogels: A review, Cellulose 26(1) (2019) 81-121.
[59] I. Benito-González, A. López-Rubio, L.G. Gómez-Mascaraque, M. Martínez-Sanz, PLA coating improves the performance of renewable adsorbent pads based on cellulosic aerogels from aquatic waste biomass, Chemical Engineering Journal (2020) 124607.
[60] C. Nerín, L. Tovar, D. Djenane, J. Camo, J. Salafranca, J.A. Beltrán, P. Roncalés, Stabilization of beef meat by a new active packaging containing natural antioxidants, Journal of Agricultural and Food Chemistry 54(20) (2006) 7840-7846.
[61] K.K. Gaikwad, J.Y. Lee, Y.S. Lee, Development of polyvinyl alcohol and apple pomace bio-composite film with antioxidant properties for active food packaging application, Journal of food science and technology 53(3) (2016) 1608-1619.
[62] M. Belizón, M. Fernández-Ponce, L. Casas, C. Mantell, E.M. De La Ossa-Fernández, Supercritical impregnation of antioxidant mango polyphenols into a multilayer PET/PP food-grade film, Journal of CO2 Utilization 25 (2018) 56-67.
[63] M. Moudache, C. Nerín, M. Colon, F. Zaidi, Antioxidant effect of an innovative active plastic film containing olive leaves extract on fresh pork meat and its evaluation by Raman spectroscopy, Food chemistry 229 (2017) 98-103.
[64] C.A. García-González, A. Sosnik, J. Kalmár, I. De Marco, C. Erkey, A. Concheiro, C. Alvarez-Lorenzo, Aerogels in drug delivery: From design to application, Journal of Controlled Release (2021).
[65] L.M. Fonseca, F.T. da Silva, G.P. Bruni, C.D. Borges, E. da Rosa Zavareze, A.R.G. Dias, Aerogels based on corn starch as carriers for pinhão coat extract (Araucaria angustifolia) rich in phenolic compounds for active packaging, International Journal of Biological Macromolecules 169 (2021) 362-370.

[66] I. Benito-González, A. López-Rubio, A. Martínez-Abad, A.-R. Ballester, I. Falcó, L. González-Candelas, G. Sánchez, J. Lozano-Sánchez, I. Borrás-Linares, A. Segura-Carretero, In-Depth Characterization of Bioactive Extracts from Posidonia oceanica Waste Biomass, Marine drugs 17(7) (2019) 409.
[67] J.F. Saeman, Kinetics of wood saccharification-hydrolysis of cellulose and decomposition of sugars in dilute acid at high temperature, Industrial & Engineering Chemistry 37(1) (1945) 43-52.
[68] H. Miller, A simplified method for the evaluation of antioxidants, Journal of the American Oil Chemists Society 48(2) (1971) 91-91.
[69] A. Carlez, T. Veciana-Nogues, J.-C. Cheftel, Changes in colour and myoglobin of minced beef meat due to high pressure processing, LWT-Food Science and Technology 28(5) (1995) 528-538.
[70] S. Tang, D. Sheehan, D.J. Buckley, P.A. Morrissey, J.P. Kerry, Anti-oxidant activity of added tea catechins on lipid oxidation of raw minced red meat, poultry and fish muscle, International journal of food science & technology 36(6) (2001) 685-692.
[71] R. Khiari, Z. Marrakchi, M.N. Belgacem, E. Mauret, F. Mhenni, New lignocellulosic fibres-reinforced composite materials: A stepforward in the valorisation of the Posidonia oceanica balls, Composites Science and Technology 71(16) (2011) 1867-1872.
[72] S.Y. Oh, D.I. Yoo, Y. Shin, G. Seo, FTIR analysis of cellulose treated with sodium hydroxide and carbon dioxide, Carbohydrate Research 340(3) (2005) 417-428.
[73] N. Abidi, L. Cabrales, C.H. Haigler, Changes in the cell wall and cellulose content of developing cotton fibers investigated by FTIR spectroscopy, Carbohydrate Polymers 100 (2014) 9-16.
[74] I. Benito-González, M. Martínez-Sanz, A. López-Rubio, L.G. Gómez-Mascaraque, Confocal Raman imaging as a useful tool to understand the internal microstructure of multicomponent aerogels, Journal of Raman Spectroscopy 51(10) (2020) 2022-2035.
[75] G. Shi, Y. Qian, F. Tan, W. Cai, Y. Li, Y. Cao, Controllable synthesis of pomelo peel-based aerogel and its application in adsorption of oil/organic pollutants, Royal Society open science 6(2) (2019) 181823.
[76] I. Benito-González, C.M. Jaén-Cano, A. López-Rubio, A. Martínez-Abad, M. Martínez-Sanz, Valorisation of vine shoots for the development of cellulose-based biocomposite films with improved performance and bioactivity, International Journal of Biological Macromolecules (2020).
[77] M. Gallego, M. Arnal, P. Talens, F. Toldrá, L. Mora, Effect of Gelatin Coating Enriched with Antioxidant Tomato By-Products on the Quality of Pork Meat, Polymers 12(5) (2020) 1032.

IV. General discussion of the results

1. Integral valorization of *P. oceanica* waste biomass: Production of cellulosic fractions and nanocrystals and bioactive extracts

In the first chapter of this thesis, the waste biomass constituted by *P. oceanica* dead leaves was proposed as a valuable source of cellulose and bioactive compounds. After a complete characterization of the material, holocellulose content was calculated to be around 60%, being the main component and confirming its potential for the extraction of cellulose. Significant contents of lignin (18%) and ashes (13%) were also detected, while other minor components were lipids (4%) and proteins (7%). A conventional protocol was successfully applied to obtain pure cellulose with an extraction yield of 25%. In addition, less purified fractions were obtained after each of the sequentially applied purification steps: F1 after lipid extraction by Soxhlet (with 80% yield) and F2 after both lipid and lignin removal (with 50% yield), being F3 the pure cellulose obtained after an additional alkaline treatment for the removal of hemicelluloses.

These fractions were then used to generate films by means of vacuum filtration, being the F3 films those with the best mechanical and barrier performance. The fractions were also used as fillers (at a fixed loading of 10% w/w with regards to starch weight) for the production of starch-based biocomposites by melt mixing. In that case, although F3 performed best in terms of mechanical performance, the water vapor barrier was not only substantially increased (up to 43%) with the addition of F3, but also with the less purified fraction F1 (up to 39%). This improvement in the water barrier was linked to the key role of the lignin present in F1 in the starch gelatinization process, preserving the starch structure to a higher extent during melt mixing and thus giving rise to more crystalline composites, as evidenced by SAXS/WAXS. These results evidenced the potential of *P. oceanica* waste biomass for the extraction of cellulose-based fractions with excellent properties for the development of bio-based packaging films (either as matrices or as fillers). Furthermore, they highlighted the potential of less purified cellulosic fractions for developing cost-efficient and more environmentally friendly materials, without compromising their performance, and established a starting point for further investigation on this topic.

The two lignin-free fractions (F2 and F3) were selected for further investigation and, additionally, less purified fractions (named as F2A and F3A) were obtained by skipping the Soxhlet purification step. Furthermore, all these cellulosic fractions were subsequently subjected to a short sulphuric acid hydrolysis to produce nanocrystals (labelled as NANO) by a patented method (PCT/ES2019/070448). As expected, the extraction yield for the less purified nanocrystals was higher (up to 26% for NANO F2A) than that of the pure cellulose nanocrystals (14%). Cellulose-

based films were then obtained by vacuum-filtration of aqueous suspensions from the fractions and nanocrystals. Interestingly, although the more purified fractions (F3 and F3A) performed better in terms of mechanical and barrier performance, the less purified nanocrystals (NANO F2A and NANO F2) showed significantly improved mechanical performance (up to 45% improvement in tensile strength and 2-fold increase in the elongation) and higher water vapor barrier (up to 50%) compared to the more purified ones (NANO F3 and NANO F3A). This suggests a positive effect of the hemicelluloses remaining in NANO F2A and NANO F2, which resisted the sulphuric acid treatment. On the other hand, oxygen barrier was drastically diminished by the presence of lipidic components in NANO F2A and NANO F3A. Once again, these results demonstrate that simpler protocols with less purification steps resulted not only in more cost-efficient cellulosic materials (with higher extraction yields) but were also seen to outperform conventional cellulose nanocrystals due to the presence of minor acid-resistant additional components, being especially relevant the effect of hemicelluloses.

Finally, *P. oceanica* waste biomass was also valorized for the production of bioactive extracts. Conventional protocols based on the use of organic solvents were followed and compared to greener methodologies such as ultrasound-assisted (US) and hot water (H_2O) extractions. In the case of the water-based extractions, extracts were labelled as E1 (soluble in ethanol) and E2 (insoluble in ethanol), while the extracts obtained by the conventional method were labelled as E3. Compositional analyses of the extracts revealed major differences which affected their bioactive properties, being E1 mostly composed of ashes, while E2 consisted of a mixture of ashes, proteins and carbohydrates and E3 contained mainly lipids. Interestingly, although E3 extracts showed the highest antiviral activity, the E2 extract obtained by hot water extraction presented the highest antioxidant capacity (730 µmol TE/g extract). On the other hand, the E2 extracts obtained by ultrasound-assisted extraction displayed the best antifungal activities against several microorganisms. These results evidenced the potential of *P. oceanica* waste biomass for obtaining bioactive extracts by greener and more environmentally friendly methodologies, with possible application in the food industry.

2. Development of high-performance starch-based biocomposites using cellulosic fractions and nanocrystals from *P. oceanica* as fillers

Once the potential of using less purified cellulosic fractions and nanocrystals from *P. oceanica* waste biomass was assessed in the first chapter, the simplified extraction protocols were aimed to be scaled-up in order to confirm the industrial viability of the processes. Moreover, the performance of starch-based biocomposites loaded with the up-scaled cellulosic fillers was evaluated to assess the potential improvements achieved with the incorporation of these reinforcing materials.

Thus, in the first work from this chapter, the effect of incorporating pure cellulose (F3) at different loadings (5, 10, 20 and 40% w/w) in the properties of starch-based biocomposites produced by melt mixing and hot pressing was evaluated. Since humidity conditions were seen to be highly relevant to the final properties of the obtained starch films, starch was pre-conditioned at two different relative humidity conditions (53%, close to common ambient conditions, and 85% RH). Interestingly, pre-conditioning at 85% RH resulted in more amorphous films, as evidenced by XRD. Regarding the composites, although the highest cellulose loading of 40% yielded the best mechanical and barrier improvements, the processability of the blends was greatly compromised due to the high cellulose content. As a result, 20 % was selected as the most optimum loading, showing a 4-fold increase in both the Young's modulus and tensile strength of the films and 33% improvement in the water vapor barrier performance. Additionally, the retrogradation of starch after two months of storage was studied in the pure starch and in the optimum biocomposite films. The results showed that retrogradation was significantly limited by the presence of cellulose, as evidenced by the lower increase in crystallinity and the smaller relative change in the mechanical properties (only 50% increase of the stiffness in the case of the biocomposites vs. 300% increase in the pure starch). Thus, cellulose derived from *P. oceanica* waste biomass was seen to successfully improve the mechanical and barrier performance of starch-based films, as well as increase the stability of the materials upon storage.

The second work from this chapter was devoted to the scaling-up of the process for obtaining cellulosic fractions and nanocrystals from *P. oceanica* waste biomass, as well as to produce biocomposite starch-based packaging structures using industrially relevant technologies such as extrusion and thermoforming. Initially, the purification process of both cellulosic (NANO F3A) and less purified cellulosic (NANO F2A) nanocrystals was upscaled (using 20 L tanks). As a consequence of the lower efficacy of the hydrolysis process when working with greater volumes (probably due to greater heat dissipation and less homogeneous stirring conditions), the extraction yields were slightly increased (ca. 8% increase) and the obtained nanocrystals showed minor differences with respect to the lab-scale ones in terms of composition, morphology and thermal

resistance. Preliminary tests were conducted on lab-scale to produce starch biocomposites containing the less purified cellulosic nanocrystals as fillers (at 10 and 20% w/w). The nanocrystals were seen to be properly dispersed within the starch matrix and the biocomposites showed better mechanical properties (up to 15-fold increase in the Young's Modulus and 10-fold increase in the tensile strength) and water vapor barrier (up to 2-fold increase) as compared to the biocomposites previously obtained using the same loadings of pure cellulose (F3) in the first work of the chapter. This evidences that the reduced size and the more crystalline character of the cellulosic nanocrystals are advantageous to improve the properties of biopolymers when used as fillers. Based on these results, the production of optimized starch biocomposites with cellulosic nanocrystals (10% w/w) was upscaled to obtain films by extrusion. In this case, the formulations needed to be adjusted to ensure a proper processing of the blends. In particular, the composition and amount of plasticizer was adjusted, and blends of sorbitol/glycerol were used. Furthermore, the hygroscopic behavior of the less purified nanocrystals led to the formation of bubbles, which hindered proper processing. In spite of that, the presence of cellulosic nanocrystals improved the mechanical performance (2-fold increase in the Young's Modulus) and water vapor permeability (36% decrease) of the extruded films, with minor differences in the performance of the films containing the less purified (NANO F2A) or the more purified (NANO F3A) cellulosic nanocrystals. These films were finally thermoformed to simulate industrial production processes for obtaining biopolymer-based food packaging structures such as trays. The presence of the cellulosic nanocrystals in the thermoformed trays also led to improved mechanical and water vapor barrier performance when compared with the starch trays. Most importantly, while the starch trays were not able to maintain their shape after prolonged storage, the presence of the cellulosic nanocrystals could significantly improve the dimensional stability of the thermoformed trays.

These results showed the potential of *P. oceanica* waste biomass for developing high-performance starch biocomposites using both cellulose fibers and less purified cellulosic nanocrystals. Cellulosic nanocrystals showed a greater potential to significantly improve the mechanical and water barrier performance of starch biocomposites. Furthermore, the extraction of the cellulosic nanocrystals and the production of biocomposite extruded films and thermoformed trays were successfully upscaled at pilot-plant level, demonstrating the industrial feasibility of the protocols developed at lab-scale.

3. Application of the simpler methodologies for the extraction of cellulosic fractions and nanocrystals to other biomass sources

As it was initially shown in the first chapter, biomass sources such as *P. oceanica* waste, containing a minor amount of lipidic compounds, can be subjected to a simplified extraction protocol, omitting the initial Soxhlet treatment, yielding cellulosic fractions with interesting properties. Furthermore, the presence of hemicelluloses in the fractions and nanocrystals extracted without applying the alkaline treatment step may confer them better mechanical performance while increasing the sustainability and cost efficiency of the materials. In this context, the objective of the works from this chapter was to assess the applicability of the previously developed simplified protocols to other sources of waste biomass.

In the first work from this chapter, vine shoots (one of the most abundant and underutilized terrestrial waste biomass in Spain) were explored as a source of cellulosic nanocrystals. A complete compositional characterization of the biomass confirmed that holocellulose was the main component (>70%), followed by lignin (22%). Lipids (7%), proteins (5%) and ashes (2%) were present in much minor amounts. Given the relatively similar composition of this biomass to that from *P. oceanica* waste, the conventional and simplified protocols for the extraction of cellulosic fractions and nanocrystals were successfully applied, producing similar extraction yields to those noted in chapter 1. Interestingly, monosaccharide analyses revealed the presence of a recalcitrant xylan fraction (resistant to the sulphuric hydrolysis), which had not been previously observed in *P. oceanica* biomass. This fraction of resistant hemicelluloses modified the properties of the resulting cellulosic nanocrystals (NANO F3), yielding structures with higher crystallinity (X_C~89%) than those previously obtained from *P. oceanica* (X_C~77%) but with more heterogeneous aspect ratios. Interestingly, the films produced from the less purified nanocrystals (NANO F2A) performed similarly in terms of mechanical properties and water barrier to those produced from the purified cellulose nanocrystals (NANO F3), which may be explained by their similar crystallinity. These nanocrystals were then used to produce hybrid cellulosic films by blending with agar (at 20, 40 and 80% content with regards to the total film weight). As it has been previously mentioned, the inherent high rigidity of cellulose should be lowered to increase the elongation of the films and make them more suitable for food packaging purposes. In this sense, blending with other biopolymer such as agar was seen to be an efficient strategy, allowing to increase up to 3-fold the elongation of the films without significantly compromising their mechanical resistance and water vapor barrier. These hybrid cellulosic films are, thus, a promising alternative for developing biodegradable films for food packaging using renewable resources.

The second work of this chapter reports on the valorization of white rice agroindustrial by-products to produce biocomposite materials by melt mixing. In this case, the base biopolymer for

the films was obtained from broken rice, which was directly milled to produce rice flour, as well as subjected to a simplified purification protocol to obtain rice starch. The high starch content (~90%) in the rice flour, with only minor amounts of proteins (~7%), lipids (< 2%) and ashes (< 2%), made this material a suitable source of starch without the need of further purification. On the other hand, rice husks (RH) and rice straw (RS), being mainly composed of holocellulose (78% in RH and 71% in RS), were used as the source of cellulosic nanocrystals (CN-RH and CN-RS). Morphological analysis of the nanocrystals by TEM showed greater and more agglomerated structures in the case of CN-RH, which could also affect hydrolysis. The presence of greater amounts of impurities in RH, mainly ashes (19%) and lignin (14%), led to larger cellulosic nanocrystals with a more heterogeneous size distribution. The characterization of the films produced by melt mixing showed that a better mechanical performance was attained for the rice flour films as compared to the rice starch ones (5-fold increase in the TS). Furthermore, the presence of major amounts of additional compounds in the rice flour conferred antioxidant properties to the films. Water vapor permeability was, on the contrary, higher for rice flour films, which was easily counteracted by the addition of cellulosic fillers (promoting a drop of up to 66% in the permeability). It should be noted that the improved dispersion of CN-RS led to enhanced transparency and mechanical performance of the biocomposites. These results evidenced again that less purified materials can not only outperform their more purified counterparts in terms of performance properties, but can also provide additional advantages such as improved yields, cost-efficiency and even bioactivity due to the presence of additional compounds in their formulations. In general, this chapter showed that simpler protocols can be successfully applied to a wide range of waste biomass sources. Although the final performance of the extracted cellulosic materials will be mainly defined by the initial composition of the sources, the simplification of the purification process has been shown to successfully increase the yields and even improve the performance of the resulting materials with regards to the more purified counterparts.

4. Production and characterization of high-performance cellulose-based aerogels

In this final chapter, the development of other type of packaging structures known as aerogels, with outstanding properties such as high porosity and adsorption capacity was explored, using *P. oceanica* cellulosic fractions and nanocrystals as the base materials. Although the cellulose-based aerogels could be produced simply by freeze-drying aqueous suspensions, the obtained aerogels lacked resistance to high-humidity conditions and disintegrated when soaked in water. To overcome this major drawback, a novel, fast and simple hydrophobization methodology based on PLA dipping, was proposed and patented (PCT/ES2020/070607). PLA dipping modified the microstructure of the cellulosic aerogels by coating the cellulosic skeleton, thus increasing the density of the materials up to 3-fold. In addition, PLA dipping was seen to successfully improve up to 10-fold their compression resistance, and most importantly, shifted the behavior of the aerogels from strongly hydrophilic to hydrophobic (>110º contact angle). Moreover, the coated aerogels showed an outstanding sorption capacity of both water (up to 600%) and oil (up to 950%). Interestingly, the aerogels made from less purified nanocrystals (NANO F2A) presented lower density and higher porosity (explained by the presence of hemicelluloses), which enabled them to incorporate greater amounts of PLA, hence leading to greater improvements in the properties of the coated aerogels.

To understand how the PLA coating was distributed within the aerogels' structure, in the second work from this chapter, an in-depth characterization of the internal microstructure of the most optimum aerogels was carried out through a novel approach based on Confocal Raman Microscopy (CRM). Although PLA was seen to be preferentially located on the aerogels' surface, a significant fraction could also penetrate into inner regions of the aerogels, being this favored in the case of the more porous aerogels obtained from the less purified nanocrystals. The different PLA penetration within the aerogel structure also affected oil sorption/desorption capacity, with the aerogels made from the most purified fractions and nanocrystals showing lower oil adsorption (as evidenced by the lower oil presence in depth scans after oil immersion), as well as higher oil retention rates. Overall, CRM was seen to be an efficient methodology for characterizing the inner microstructure of these multicomponent cellulosic aerogels.

In the last work from this chapter, the most promising cellulosic aerogels (in terms of microstructure and cost-efficiency) (NANO F2A) were used as templates for the incorporation of bioactive extracts from *P. oceanica* biomass (characterized in chapter 1) with hydrophilic (E2) and hydrophobic (E3) character. These extracts could be incorporated into the aerogels separately or simultaneously, to generate hybrid aerogels. Lowering the concentration of the PLA dipping solution was seen to maximize the extracts release, which was most likely due to the more porous

structure of the aerogels. The hybrid aerogels incorporating both bioactive extracts provided the best results in terms of antioxidant capacity and were able to reduce oxymyoglobin and lipid oxidation of red meat by 54% and 60%, respectively, when used as adsorbent "pads".

Overall, these works highlighted the potential of the developed PLA dipping methodology to produce high-performance cellulosic aerogels from less purified fractions with excellent adsorption capacities. Furthermore, the production method enables the incorporation of both hydrophobic and hydrophilic compounds which make them attractive for the development of bioactive packaging structures.

V. Conclusions

The present Ph. D. thesis shows a complete valorization of *P. oceanica* waste biomass for the development of more sustainable, high-performance, bio-based food packaging structures based on cellulosic materials, extending the application of the developed methods to other sources of waste biomass. Accordingly, the main conclusions from this thesis are summarized as follows:

1. It was possible to extract cellulose, as well as less purified cellulosic fractions and nanocrystals from *P. oceanica* waste biomass by the application of conventional and simplified purification protocols, in which some of the steps applied in the conventional method were omitted. Interestingly, these less purified cellulosic fractions and nanocrystals, containing minor amounts of hemicelluloses and/or lipids, outperformed more purified cellulose when used directly as film-forming structures or as fillers in starch-based biocomposites.

2. The simplified protocols for the extraction of less purified cellulosic nanocrystals were successfully applied to terrestrial waste biomass sources such as vine shoots, rice straw and rice husks. The biomass composition (especially hemicelluloses and lipids), as well as their carbohydrate profile, were seen to be key factors determining the final properties of the resulting nanocrystals.

3. Starch-based biocomposites with enhanced performance can be produced adding cellulosic fractions and nanocrystals as fillers through melt mixing and hot pressing. Starch pre-conditioning is crucial to determine the behavior of the blends upon processing and the final properties of the films. The maximum filler loading which enabled a good processability was around 20% w/w, with the cellulosic nanocrystals providing greater improvements on the mechanical and water barrier performance than the cellulosic fractions.

4. The simplified purification protocols for the extraction of cellulosic fractions and nanocrystals are industrially applicable, as demonstrated by their successful upscaling to pilot-plant level. The production of starch biocomposites containing these nanocrystals as fillers can be also industrially implemented using processing techniques such as extrusion and thermoforming. However, lab-scale formulations should be modified to ensure a good processability by each specific processing technique.

5. An integral valorization of *P. oceanica* waste biomass was achieved by obtaining bioactive extracts. Interestingly, greener water-based extraction methodologies (such as ultrasound-assisted and hot-water extractions) yielded extracts which showed remarkable antioxidant and antifungal capacities, very similar or even higher than some of those obtained from more conventional extraction techniques based on the use of organic solvents.

6. *P. oceanica* waste biomass can be also used to generate highly porous aerogels, with excellent water and oil sorption capacities, by freeze-drying of cellulosic aqueous suspensions. Interestingly, the presence of other components such as hemicelluloses in the less purified cellulosic fractions and nanocrystals led to more porous and less dense aerogels, which were shown to outperform those obtained from more purified cellulose. Through a novel methodology based on PLA dipping, the highly hydrophilic character of the aerogels, which lost their integrity when soaked in water, was turned into hydrophobic (>110º). Moreover, PLA coating substantially improved the mechanical performance of the aerogels, while maintaining their high water and oil sorption capacities and without compromising their sustainability.

7. The coated aerogels prepared by means of this novel PLA dipping method could be used as templates for the incorporation of both hydrophilic and hydrophobic extracts. These aerogels were tested as bioactive food packaging structures and were able to successfully increase the shelf life of red meat by preventing the oxidation of lipids (60%) and oxymyoglobin (54%) upon storage.

8. Waste biomass has been shown to present enormous potential for developing food packaging structures following zero-waste principles by the extraction of cellulose-based materials, as well as bioactive extracts (obtained by greener methodologies too) which have been shown to increase the shelf life of food products, thus reducing food waste. In addition, simplified protocols have been shown to significantly increase the bioactivity and cost-efficiency of the resulting materials even outperforming pure cellulose in a wide range of packaging applications, from reinforcing fillers in biopolymeric films to cellulosic aerogels, as well as constituting film-forming structures by themselves. Thus, these materials can also represent a feasible solution for the current overuse of synthetic plastics providing a more sustainable alternative which is in line with current circular economy policies.

VI. Annexes

Annex A. List of publications included in this thesis

International Journal of Biological Macromolecules 118 (2018) 542–551

Contents lists available at ScienceDirect

International Journal of Biological Macromolecules

journal homepage: http://www.elsevier.com/locate/ijbiomac

Potential of lignocellulosic fractions from *Posidonia oceanica* to improve barrier and mechanical properties of bio-based packaging materials

Isaac Benito-González, Amparo López-Rubio, Marta Martínez-Sanz *

Food Safety and Preservation Department, IATA-CSIC, Avda. Agustín Escardino 7, 46980 Paterna, Valencia, Spain

ARTICLE INFO

Article history:
Received 14 May 2018
Accepted 11 June 2018
Available online 20 June 2018

Keywords:
Posidonia oceanica
Lignocellulosic fractions
Food packaging
Biopolymers
Starch

ABSTRACT

This work reports on the valorization of residues from *Posidonia oceanica* leaves for the purpose of obtaining lignocellulosic fractions of interest for the development of bio-based materials for food packaging. The lignocellulosic fractions were characterized, thereby confirming the purification of cellulose and showing increases in crystallinity and thermal stability after the consecutive extraction steps. Subsequently, pure lignocellulosic films were obtained and characterized and the pure cellulose film showed the best properties in terms of mechanical performance and water vapor permeability. Finally, composite starch films containing lignocellulosic fractions were developed by melt compounding and characterized. Although the film containing the pure cellulose additive showed the optimum improvement in terms of mechanical properties (with an increase of 85% in the elastic modulus and 38% in the tensile strength), similar water vapor permeability reduction (~40%) was achieved with the least purified fractions, explained by their effect on starch gelatinization, as evidenced by SAXS/WAXS.

Cellulose (2019) 26:8007–8024
https://doi.org/10.1007/s10570-019-02641-4

ORIGINAL RESEARCH

Cellulose nanocrystal-based films produced by more sustainable extraction protocols from *Posidonia oceanica* waste biomass

Isaac Benito-González · Amparo López-Rubio · Rafael Gavara · Marta Martínez-Sanz

Received: 3 May 2019 / Accepted: 18 July 2019 / Published online: 22 July 2019

Abstract Simplified extraction procedures (avoiding Soxhlet treatment and/or hemicellulose removal) were evaluated to valorize waste biomass from *Posidonia oceanica* leaves, obtaining cellulosic fractions and nanocrystals, which were subsequently used to produce films from their aqueous suspensions. Cellulose purification significantly improved mechanical and barrier properties of the films obtained from the fractions, while the extracted nanocrystals yielded films with remarkably improved properties, outperforming most benchmark biopolymers. The lipids initially present in the fractions without Soxhlet treatment were not completely digested by the hydrolysis treatment, having a positive impact on the water vapor permeability of the films (up to 63% drop), although negatively impacting oxygen permeability (increased by 20–30-fold). On the contrary, some hemicelluloses present in the less purified fractions, strongly interacting with cellulose, remained in the extracted nanocrystals leading to enhanced mechanical properties (45% higher tensile strength and 2-fold increase in the elongation at break), but lower water barrier (up to 70% higher permeability than the pure cellulose nanocrystals) due to their hydrophilic character. Films produced from the less purified nanocrystals showed the best compromise between mechanical and barrier performance, while offering a great advantage in terms of sustainability and reduced costs.

marine drugs

MDPI

Article

In-Depth Characterization of Bioactive Extracts from *Posidonia oceanica* Waste Biomass

Isaac Benito-González [1], Amparo López-Rubio [1], Antonio Martínez-Abad [2], Ana-Rosa Ballester [3], Irene Falcó [1,4], Luis González-Candelas [3], Gloria Sánchez [1], Jesús Lozano-Sánchez [5,6], Isabel Borrás-Linares [5], Antonio Segura-Carretero [5,7] and Marta Martínez-Sanz [1,*]

1 Food Safety and Preservation Department, IATA-CSIC, Calle Catedrático Agustín Escardino Benlloch 7, Paterna, 46980 Valencia, Spain
2 Department of Analytical Chemistry, Nutrition and Food Sciences, University of Alicante, San Vicente del Raspeig, 03690 Alicante, Spain
3 Food Biotechnology Department, IATA-CSIC, Calle Catedrático Agustín Escardino Benlloch 7, Paterna, 46980 Valencia, Spain
4 Microbiology and Ecology Department, University of Valencia. Avda. Dr. Moliner, 50. Burjassot, 46100 Valencia, Spain
5 Center of Research and Development of Functional Food. Health Science Technological Park, Avda. del Conocimiento s/n, 18100 Granada, Spain
6 Department of Food Science and Nutrition, University of Granada, Campus Universitario s/n, 18071 Granada, Spain
7 Department of Analytical Chemistry, Faculty of Sciences, University of Granada, 18071 Granada, Spain
* Correspondence: mmartinez@iata.csic.es; Tel.: +34-963-200-022

Received: 14 June 2019; Accepted: 5 July 2019; Published: 9 July 2019

check for updates

Abstract: *Posidonia oceanica* waste biomass has been valorised to produce extracts by means of different methodologies and their bioactive properties have been evaluated. Water-based extracts were produced using ultrasound-assisted and hot water methods and classified according to their ethanol-affinity (E1: ethanol soluble; E2: non-soluble). Moreover, a conventional protocol with organic solvents was applied, yielding E3 extracts. Compositional and structural characterization confirmed that while E1 and E3 extracts were mainly composed of minerals and lipids, respectively, E2 extracts were a mixture of minerals, proteins and carbohydrates. All the extracts showed remarkably high antioxidant capacity, which was not only related to phenolic compounds but also to the presence of proteins and polysaccharides. All E2 and E3 extracts inhibited the growth of several foodborne fungi, while only E3 extracts decreased substantially the infectivity of feline calicivirus and murine norovirus. These results show the potential of *P. oceanica* waste biomass for the production of bioactive extracts.

Keywords: valorisation; antiviral; antifungal activity; antioxidant capacity; ultrasound; hot water extraction

Carbohydrate Polymers 216 (2019) 180–188

Contents lists available at ScienceDirect

Carbohydrate Polymers

journal homepage: www.elsevier.com/locate/carbpol

High-performance starch biocomposites with celullose from waste biomass: Film properties and retrogradation behaviour

Isaac Benito-González, Amparo López-Rubio, Marta Martínez-Sanz*

Food Safety and Preservation Department, IATA-CSIC, Avda. Agustín Escardino 7, 46980 Paterna, Valencia, Spain

ARTICLE INFO

Keywords:
Biopolymers
Retrogradation
Melt compounding
X-ray diffraction
Permeability

ABSTRACT

In this work, the effects of relative humidity (RH) pre-conditioning (53% vs. 85% RH) and incorporation of cellulose fillers (from *Posidonia* waste biomass) on the properties and retrogradation of melt compounded starch biocomposites were investigated. Pre-conditioning at 85% RH promoted starch gelatinization during processing, leading to more amorphous materials with reduced stiffness but better barrier properties. Furthermore, these films were less stable upon storage due to greater starch retrogradation. Cellulose incorporation improved significantly the mechanical and water barrier performance, especially in the films pre-conditioned at 85% RH due to enhanced filler dispersion. Although incomplete gelatinization of the starch pre-conditioned at 53% RH led to films with bigger cellulose aggregates, their mechanical and water barrier properties were better, outperforming starch-cellulose biocomposites typically reported in the literature. Moreover, the presence of cellulose limited the degree of starch retrogradation upon storage, highlighting the potential of *Posidonia* biomass as a cheap source of high-performance fillers.

Food Packaging and Shelf Life 30 (2021) 100730

Contents lists available at ScienceDirect

Food Packaging and Shelf Life

journal homepage: www.elsevier.com/locate/fpsl

Pilot plant scale-up of the production of optimized starch-based biocomposites loaded with cellulosic nanocrystals from *Posidonia oceanica* waste biomass

Isaac Benito-González [a], Gülden Göksen [a,b], Zaida Pérez-Bassart [a], Amparo López-Rubio [a], Rafael Sánchez [c], José María Alonso [c], Rafael Gavara [a], Miriam Gallur [c], Marta Martínez-Sanz [a,*]

[a] *Food Safety and Preservation Department, IATA-CSIC, Avda. Agustín Escardino 7, 46980, Paterna, Valencia, Spain*
[b] *Department of Food Engineering, Mersin University, Ciftlikkoy, Mersin, 33343, Turkey*
[c] *Grupo de Tecnología de Envases y Embalajes, Instituto Tecnológico del Embalaje, Transporte y Logística, ITENE, Unidad Asociada al CSIC, C/Albert Einstein 1, 46980, Paterna, Valencia, Spain*

ARTICLE INFO

Keywords:
Cellulosic nanocrystals
Extrusion
Thermoforming
Pilot plant
Waste biomass
Biopolymers

ABSTRACT

Posidonia oceanica biomass has been valorized to produce cellulosic nanocrystals with different purification degrees at lab- and pilot plant-scale. The cellulosic nanocrystals (10 % and 20 % (w/w)) were incorporated into corn starch, producing biocomposite films by melt mixing and hot-pressing at lab-scale. Biocomposite films showed remarkable improvements on the mechanical and water barrier performance (up to 10-fold increase in the elastic modulus and 2-fold decrease in the water permeability). Biocomposite packaging structures were also produced at pilot plant-scale by extrusion and thermoforming. Adjusting the plasticizer formulation and increasing the nanocrystals' loading up to the maximum enabling good processability (10 % (w/w)) allowed the production of trays with enhanced water barrier and mechanical performance, which, unlike the pure starch, kept their shape upon storage. These results highlight the potential of *P. oceanica* nanocrystals to improve the performance of starch-based packaging structures and demonstrates the potential of the production process to be industrially applied.

International Journal of Biological Macromolecules 165 (2020) 1540–1551

Contents lists available at ScienceDirect

International Journal of Biological Macromolecules

journal homepage: http://www.elsevier.com/locate/ijbiomac

Valorisation of vine shoots for the development of cellulose-based biocomposite films with improved performance and bioactivity

Isaac Benito-González, Carmen M. Jaén-Cano, Amparo López-Rubio, Antonio Martínez-Abad, Marta Martínez-Sanz *

Food Safety and Preservation Department, IATA-CSIC, Avda. Agustín Escardino 7, 46980 Paterna, Valencia, Spain

ARTICLE INFO

Article history:
Received 27 August 2020
Received in revised form 22 September 2020
Accepted 27 September 2020
Available online 3 October 2020

Keywords:
Cellulosic fractions
Bio-based packaging
Vine shoots
Waste biomass
Agar

ABSTRACT

This work reports on the valorization of *Tempranillo* vine shoots for the development of bio-based packaging materials. Cellulose (F3) and nanocellulose (NANO F3) were produced by the conventional method, while less purified cellulosic fractions (F2A) and nanocrystals (NANO F2A) were extracted by simplified protocols (omitting Soxhlet and alkaline treatments) to reduce production costs and environmental impact and evaluate the potential added functionalities of these less purified materials. Although most of the hemicelluloses in F2A were digested upon acid hydrolysis, a small fraction remained in NANO F2A. On the other hand, the presence of a minor xylan fraction in F3 limited the access of sulphuric acid towards the cellulose microfibrils, hindering hydrolysis and producing heterogeneous fibrillar structures in NANO F3. The obtained materials were used to produce cellulosic films, as well as blends with agar, and their performance properties were evaluated. Overall, NANO F2A films showed the best compromise between performance and sustainability and presented additional antioxidant capacity. The properties of the films could be adjusted by the incorporation of agar, improving their ductility and water permeability.

Carbohydrate Polymers

Sustainable biocomposite films fully-based on white rice (Oryza sativa) agroindustrial by-products

--Manuscript Draft--

Manuscript Number:	
Article Type:	Research Paper
Keywords:	Rice flour; cellulosic nanocrystals; melt-mixing; active packaging; XRD; valorization
Corresponding Author:	Marta Martínez-Sanz Instituto de Investigación en Ciencias de la Alimentación: Instituto de Investigacion en Ciencias de la Alimentacion Paterna, Valencia, SPAIN
First Author:	Isaac Benito-González
Order of Authors:	Isaac Benito-González
	María del Mar Ortiz-Gimeno
	Amparo López-Rubio
	Antonio Martínez-Abad
	Agustín Garrido-Fernández
	Marta Martínez-Sanz
Abstract:	In this work, biocomposites fully-based on the valorization of white rice agroindustrial by-products have been produced by melt mixing. The film matrix consisted on rice flour (RF) or rice starch (RS) obtained from broken rice, which was reinforced with cellulose-rich nanocrystals obtained through simplified extraction processes from rice husks (CN-RH) and rice straw (CN-RS). The presence of impurities in RF induced the re-crystallization of starch, producing more crystalline films with better mechanical performance, but greater water vapor permeability than RS. This was overcome by the addition of 15% (w/w) cellulosic nanocrystals. Moreover, the cellulosic nanocrystals increased the stiffness of the films, with the CN-RS yielding better mechanical performance due to their more homogeneous morphology and distribution within the RF matrix. Interestingly, all the RF films showed remarkable antioxidant capacity (>20% inhibition of β-carotene bleaching), highlighting the potential of less purified materials to develop sustainable food packaging with additional functionalities.

Chemical Engineering Journal 390 (2020) 124607

Contents lists available at ScienceDirect

Chemical Engineering Journal

journal homepage: www.elsevier.com/locate/cej

PLA coating improves the performance of renewable adsorbent pads based on cellulosic aerogels from aquatic waste biomass

Isaac Benito-González[a,b], Amparo López-Rubio[a], Laura G. Gómez-Mascaraque[b], Marta Martínez-Sanz[a,*]

[a] Food Safety and Preservation Department, IATA-CSIC, Avda. Agustín Escardino 7, 46980 Paterna, Valencia, Spain
[b] Department of Food Chemistry & Technology, Teagasc Food Research Centre, Moorepark, Fermoy, Co. Cork, Ireland

HIGHLIGHTS

- Sustainable, lightweight, hydrophobic, cellulose-based adsorbent pads were produced.
- *P. oceanica* biomass was valorized for the development of (nano)cellulosic aerogels.
- The least purified nanocellulosic fractions yielded the most porous aerogels.
- PLA dipping highly improved the aerogels' hydrophobicity and mechanical performance.
- Microstructure played a crucial role in both PLA incorporation and aerogels' performance.

GRAPHICAL ABSTRACT

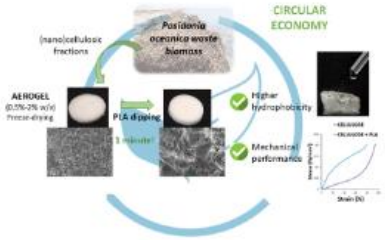

ARTICLE INFO

Keywords:
Porous materials
Posidonia
Seaweed
Biopolymers
Oil sorption
Microstructure

ABSTRACT

Lightweight, hydrophobic, adsorbent pads based on aerogels from different cellulosic and nanocellulosic fractions extracted from *Posidonia oceanica* waste biomass were developed by a simple freeze-drying and PLA dipping method. The pure (nano)cellulosic aerogels presented highly porous structures, capable of adsorbing large amounts of oil (up to ~34 g oil/g aerogel); however, they lost their integrity when soaked in water. The incorporation of PLA hydrophobized the aerogels and improved significantly their mechanical performance (up to 10-fold increase in the compression stress). The most porous aerogel structures, obtained with the lowest (nano) cellulosic concentrations and with the less purified fractions, incorporated greater amounts of PLA upon dipping, which was mostly distributed filling in the pores. All the PLA-coated (nano)cellulosic aerogels presented a hydrophobic behaviour, with contact angles of 95–130° and selectively adsorbing greater amounts of oil (5.9–9.2 g oil/g aerogel) than water (2.8–6.7 g H_2O/g aerogel). These materials present a great potential as adsorbent pads for oil spill cleaning and food packaging applications.

Received: 9 April 2020 | Revised: 9 June 2020 | Accepted: 14 June 2020

DOI: 10.1002/jrs.5936

RESEARCH ARTICLE

Journal of RAMAN SPECTROSCOPY WILEY

Confocal Raman imaging as a useful tool to understand the internal microstructure of multicomponent aerogels

Isaac Benito-González[1] | **Marta Martínez-Sanz**[1,2] | **Amparo López-Rubio**[1,2] | **Laura G. Gómez-Mascaraque**[3]

[1]Food Safety and Preservation Department, IATA-CSIC, Paterna, Spain

[2]Interdisciplinary Platform for Sustainable Plastics towards a Circular Economy, Spanish National Research Council (SusPlast-CSIC), Madrid, Spain

[3]Teagasc Food Research Centre, Fermoy, Ireland

Correspondence
Laura G. Gómez-Mascaraque, Teagasc Food Research Centre, Moorepark, Fermoy. Co. Cork, Ireland.
Email: laura.mascaraque@teagasc.ie

Funding information
European Commission Erasmus+, Grant/Award Number: 2017.121178; Horizon 2020 Framework Programme, Grant/Award Number: ERA-Net SUSFOOD2; Ministerio de Ciencia, Innovación y Universidades, Grant/Award Number: RTI2018-094408-J-I00; European Union; Spanish Ministry of Science, Innovation and Universities

Abstract

This work shows the characterization of (nano)cellulosic aerogels prepared from *Posidonia oceanica* waste biomass by means of confocal Raman microscopy (CRM). For this aim, aerogels were prepared by simple freeze-drying of aqueous dispersions of four (nano)cellulosic fractions with different purification degrees, tested at two different concentrations (0.5% and 2%). These were then coated with polylactic acid (PLA) in order to improve their hydrophobicity and subjected to oil sorption–desorption experiments. Both univariate and multivariate analyses, including an approach based on comparing the spectra with those of reference materials and another one based on automatic detection of components, were compared in terms of the quality and the accuracy of the information provided. Univariate analysis only provided accurate information in the simplest systems (native (nano)cellulosic aerogels), while multivariate analyses facilitated the detection of the different components even for the most complex structures. Automatic identification of components was selected as the optimal methodology, although it also underestimated the abundance of the components with the least intense Raman spectra (cellulosic clusters) in the presence of PLA and oil. Comparison with the reference materials resulted in unrealistic images for the most complex systems. Micron-sized regions of concentrated cellulose were detected using CRM, being more abundant in the denser aerogels. Results also confirmed that PLA was preferentially located close to the surface, while oil could penetrate deeper along the matrix. Overall, the results showed the potential of Raman imaging as a novel approach for the characterization of complex biopolymeric aerogels.

KEYWORDS

cellulose, hyperspectral imaging, multivariate analysis, Raman microscopy, renewable

International Journal of Biological Macromolecules 185 (2021) 654–663

Contents lists available at ScienceDirect

International Journal of Biological Macromolecules

journal homepage: www.elsevier.com/locate/ijbiomac

Multifunctional cellulosic aerogels from *Posidonia oceanica* waste biomass with antioxidant properties for meat preservation

Isaac Benito-González [a,b], Amparo López-Rubio [a,b], Paula Galarza-Jiménez [a], Marta Martínez-Sanz [b,c,*]

[a] Food Safety and Preservation Department, IATA-CSIC, Avda. Agustín Escardino 7, 46980 Paterna, Valencia, Spain
[b] Interdisciplinary Platform for Sustainable Plastics towards a Circular Economy- Spanish National Research Council (SusPlast-CSIC), Madrid, Spain
[c] Instituto de Investigación en Ciencias de la Alimentación, CIAL (CSIC-UAM), Nicolás Cabrera, 9, 28049 Madrid, Spain

ARTICLE INFO

Keywords:
Cellulosic nanocrystals
Aerogels
Antioxidant
Food packaging
PLA
Bioactive extracts

ABSTRACT

Posidonia oceanica waste biomass has been valorized to develop bioactive multifunctional cellulosic aerogels (HCAG) by simpler and greener protocols. Hydrophobization of cellulosic aerogels was achieved through PLA coating, while bioactivity was imparted by the incorporation of hydrophilic (E2) and hydrophobic extracts (E3) produced from the same biomass. The incorporation of extracts led to denser aerogels, with less porous structures. These aerogels showed outstanding water and oil sorption capacities (1500–1900%), being able to release the adsorbed liquid almost completely after 7 days. Interestingly, all the aerogels showed a positive inhibition effect (23–91%) on the β-carotene bleaching assay. Moreover, the aerogels loaded with extracts, especially when combining E2 and E3, were able to reduce the oxidation of lipids and oxymyoglobin in red meat after 10 days of storage. This evidences the potential of these multifunctional aerogels as bioactive adsorbing pads to preserve the quality of fresh packaged foods.

Annex B. List of patents included in this thesis

Patent 1

"Method for obtaining nanocrystals from lignocellulosic biomass by means of acid treatment"

Inventors: Marta Martínez Sanz, Isaac Benito González, Amparo López Rubio

MINISTERIO
DE INDUSTRIA, ENERGIA
Y TURISMO

Oficina Española
de Patentes y Marcas

Justificante de presentación electrónica de solicitud de patente

Este documento es un justificante de que se ha recibido una solicitud española de patente por vía electrónica utilizando la conexión segura de la O.E.P.M. De acuerdo con lo dispuesto en el art. 16.1 del Reglamento de ejecución de la Ley 24/2015 de Patentes, se han asignado a su solicitud un número de expediente y una fecha de recepción de forma automática. La fecha de presentación de la solicitud a la que se refiere el art. 24 de la Ley le será comunicada posteriormente.

Número de solicitud:	P201830650
Fecha de recepción:	29 junio 2018, 12:36 (CEST)
Oficina receptora:	OEPM Madrid
Su referencia:	ES1641.1382
Solicitante:	CONSEJO SUPERIOR DE INVESTIGACIONES CIENTÍFICAS
Número de solicitantes:	1
País:	ES
Título:	PROCEDIMIENTO PARA OBTENER NANOCRISTALES MEDIANTE TRATAMIENTO ÁCIDO A PARTIR DE BIOMASA LIGNOCELULÓSICA

Patent 2

"Process of hydrophobizing biopolymeric aerogels"

Inventors: Marta Martínez Sanz, Isaac Benito González, Amparo López Rubio

MINISTERIO
DE INDUSTRIA, ENERGÍA
Y TURISMO

Oficina Española
de Patentes y Marcas

TRATADO DE COOPERACIÓN EN MATERIA DE PATENTES
NOTIFICACIÓN DE LA RECEPCIÓN DE LOS DOCUMENTOS QUE CONSTITUYEN SUPUESTAMENTE UNA SOLICITUD INTERNACIONAL PRESENTADA DE FORMA ELECTRÓNICA.
(Instrucciones Administrativas del PCT, Parte Séptima)

1.-Se notifica al solicitante que la Oficina Receptora ha recibido en la fecha de recepción indicada más abajo, los documentos que supuestamente constituyen una solicitud internacional.
2.-Se llama la atención del solicitante sobre el hecho de que la Oficina Receptora no ha comprobado aún si estos documentos satisfacen las condiciones del art. 11.1, es decir, si cumple los requisitos para que le sea atribuida una fecha de presentación internacional. En cuanto la Oficina Receptora haya comprobado los documentos, avisará al solicitante.
3.-El número de la supuesta solicitud internacional indicado más abajo ha sido otorgado automáticamente a estos documentos. Se invita al solicitante a mencionar este número en toda la correspondencia con la Oficina Receptora.

Número de presentación	300383053
Solicitud Número PCT	PCT/ES2020/070607
Fecha de recepción	07 octubre 2020
Oficina Receptora	Oficina Española de Patentes y Marcas, Madrid
Referencia del expediente del solicitante o mandatario	PCT1641.1494
Solicitante	CONSEJO SUPERIOR DE INVESTIGACIONES CIENTÍFICAS
Número de solicitantes	1
País	ES
Título de la invención	PROCEDIMIENTO PARA LA PREPARACIÓN DE AEROGELES HIDROFÓBICOS

Annex C. List of publications not included in this thesis

CHAPTER

5

Health Effect of Dietary Fibers

Isaac Benito-González, Marta Martínez-Sanz, Maria José Fabra, Amparo López-Rubio

Food Preservation and Food Quality Department, IATA-CSIC, Valencia, Spain

OUTLINE

Artículos

Valorización de biomasa acuática para el desarrollo de estructuras biopoliméricas de uso alimentario (1): materiales para envases biodegradables

Autores: Isaac Benito-González, Marta Martínez-Sanz, Cynthia Fontes-Candia, Vera Cebrian-Lloret, Antonio Martínez-Abad, Amparo López-Rubio*

Food Safety and Preservation Department, IATA-CSIC, Avda. Agustín Escardino 7, 46980 Paterna, Valencia, Spain

Interdisciplinary Platform for Sustainable Plastics towards a Circular Economy- Spanish National Research Council (SusPlast-CSIC), Madrid, Spain

*amparo.lopez@iata.csic.es

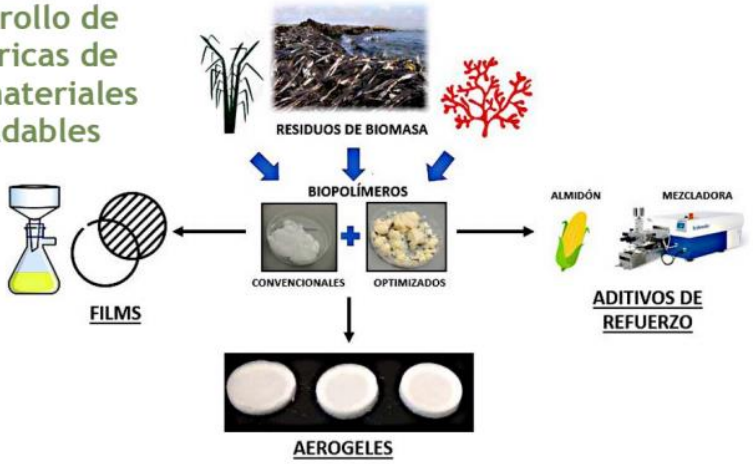

Artículos

Valorización de biomasa acuática para el desarrollo de estructuras biopoliméricas de uso alimentario (2): aplicaciones como texturizantes de alimentos

Autores: Cynthia Fontes-Candia, Marta Martínez-Sanz, Isaac Benito-González, Vera Cebrian-Lloret, Antonio Martínez-Abad, Amparo López-Rubio*

Food Safety and Preservation Department, IATA-CSIC, Avda. Agustín Escardino 7, 46980 Paterna, Valencia, Spain

Interdisciplinary Platform for Sustainable Plastics towards a Circular Economy- Spanish National Research Council (SusPlast-CSIC), Madrid, Spain

*amparo.lopez@iata.csic.es